AD-A285 949

\TION PAGE

1. AGENCY USE ONLY *(Leave blank)*	2. REPORT DATE July 1994	3. REPORT TYPE AND DATES COVERED Technical Report Mar 1990–Jul 1994

4. TITLE AND SUBTITLE

Omega Navigation System Course Book *Vol II*

6. AUTHOR(S)

P.B. Morris, R.R. Gupta, R.S. Warren, and P.M. Creamer

5. FUNDING NUMBERS

DTCG-89-C-20008
Task Orders 90-0002, 91-0002, and 92-0004

7. PERFORMING ORGANIZATION NAME(S) AND ADDRESS(ES)

TASC
55 Walkers Brook Drive
Reading, MA 01867

8. PERFORMING ORGANIZATION REPORT NUMBER

9. SPONSORING/MONITORING AGENCY NAME(S) AND ADDRESS(ES)

U.S. Department of Transportation
U.S. Coast Guard Navigation Center
7323 Telegraph Road
Alexandria, VA 22315

10. SPONSORING/MONITORING AGENCY REPORT NUMBER

2-D-5

11. SUPPLEMENTARY NOTES

DTIC

12a. DISTRIBUTION/AVAILABILITY STATEMENT

NTIS Approved for Public Release
Distribution is Unlimted

12b. DISTRIBUTION CODE

OCT 31 1994

B

13. ABSTRACT *(Maximum 200 words)*

This self-contained book on the Omega Navigation System is intended to provide theoretical and operational information needed by NAVCEN personnel to manage and maintain the Omega System. The book is composed of 13 chapters and seven appendices and can be used as a self-paced learning aid or in a classroom course environment. The course material addresses all major components of the Omega System, with emphasis placed on signal structure and utilization. Topics covered in the book include: Omega background, signal generation, navigation and propagation principles, operations, system performance evaluation, system utilization, and the future role of Omega in conjunction with other radionavigation systems. Several appendices are included to provide further detail on the material contained in the chapters.

14. SUBJECT TERMS

Omega History
Signal Propagation
System Performance
Transmitting Stations
Navigation Principles
Observed Signal Behavior

15. NUMBER OF PAGES 820

16. PRICE CODE

17. SECURITY CLASSIFICATION OF REPORT	18. SECURITY CLASSIFICATION OF THIS PAGE	19. SECURITY CLASSIFICATION OF ABSTRACT	20. LIMITATION OF ABSTRACT
UNCLASSIFIED	UNCLASSIFIED	UNCLASSIFIED	UL

NSN 7540-01-280-5500

Standard Form 298 (Rev 2-89)

GENERAL INSTRUCTIONS FOR COMPLETING SF 298

The Report Documentation Page (RDP) is used in announcing and cataloging reports. It is important that this information be consistent with the rest of the report, particularly the cover and title page. Instructions for filling in each block of the form follow. It is important to *stay within the lines* to meet *optical scanning requirements*.

Block 1. Agency Use Only (Leave blank).

Block 2. Report Date. Full publication date including day, month, and year, if available (e.g. 1 Jan 88). Must cite at least the year.

Block 3. Type of Report and Dates Covered. State whether report is interim, final, etc. If applicable, enter inclusive report dates (e.g. 10 Jun 87 - 30 Jun 88).

Block 4. Title and Subtitle. A title is taken from the part of the report that provides the most meaningful and complete information. When a report is prepared in more than one volume, repeat the primary title, add volume number, and include subtitle for the specific volume. On classified documents enter the title classification in parentheses.

Block 5. Funding Numbers. To include contract and grant numbers; may include program element number(s), project number(s), task number(s), and work unit number(s). Use the following labels:

C -	Contract	**PR** -	Project
G -	Grant	**TA** -	Task
PE -	Program Element	**WU** -	Work Unit Accession No.

Block 6. Author(s). Name(s) of person(s) responsible for writing the report, performing the research, or credited with the content of the report. If editor or compiler, this should follow the name(s).

Block 7. Performing Organization Name(s) and Address(es). Self-explanatory.

Block 8. Performing Organization Report Number. Enter the unique alphanumeric report number(s) assigned by the organization performing the report.

Block 9. Sponsoring/Monitoring Agency Name(s) and Address(es). Self-explanatory.

Block 10. Sponsoring/Monitoring Agency Report Number. (If known)

Block 11. Supplementary Notes. Enter information not included elsewhere such as: Prepared in cooperation with...; Trans. of...; To be published in.... When a report is revised, include a statement whether the new report supersedes or supplements the older report.

Block 12a. Distribution/Availability Statement. Denotes public availability or limitations. Cite any availability to the public. Enter additional limitations or special markings in all capitals (e.g. NOFORN, REL, ITAR).

DOD - See DoDD 5230.24, "Distribution Statements on Technical Documents."
DOE - See authorities.
NASA - See Handbook NHB 2200.2.
NTIS - Leave blank.

Block 12b. Distribution Code.

DOD - Leave blank.
DOE - Enter DOE distribution categories from the Standard Distribution for Unclassified Scientific and Technical Reports.
NASA - Leave blank.
NTIS - Leave blank.

Block 13. Abstract. Include a brief *(Maximum 200 words)* factual summary of the most significant information contained in the report.

Block 14. Subject Terms. Keywords or phrases identifying major subjects in the report.

Block 15. Number of Pages. Enter the total number of pages.

Block 16. Price Code. Enter appropriate price code *(NTIS only)*.

Blocks 17. - 19. Security Classifications. Self-explanatory. Enter U.S. Security Classification in accordance with U.S. Security Regulations (i.e., UNCLASSIFIED). If form contains classified information, stamp classification on the top and bottom of the page.

Block 20. Limitation of Abstract. This block must be completed to assign a limitation to the abstract. Enter either UL (unlimited) or SAR (same as report). An entry in this block is necessary if the abstract is to be limited. If blank, the abstract is assumed to be unlimited.

OMEGA NAVIGATION SYSTEM
COURSE BOOK

Volume II

OMEGA NAVIGATION SYSTEM

A
NORTH DAKOTA

E
LA REUNION

C
HAWAII

F
ARGENTINA

B
LIBERIA

G
AUSTRALIA

A
NORWAY

H
JAPAN

SERVING THE WORLD

94-33696

U.S. COAST GUARD
OMEGA NAVIGATION SYSTEM CENTER

94 10 88 071

CHAPTER 10

OMEGA SIGNAL COVERAGE PRODUCTS

Chapter Overview — This chapter presents the Omega Navigation System signal coverage products that have been developed and published since the early period of the Omega system. Section 10.1 gi̇ . verview of the system and its use. The Omega signal propagation concepts an. ∴ .isms, including the signal usability criteria for reliable navigation, are described in .ction 10.2. The capabilities and limitations of the available Omega coverage products are discussed in Section 10.3. Section 10.4 presents the general characteristics of the coverage provided by an individual station and the full system. The chapter is summarized in Section 10.5. Section 10.6 provides sample problems, including problems to be solved by the reader. Section 10.7 defines the abbreviations and acronyms used in the chapter, and S. cṫon ṭ0.8 contains the references cited in the chapter.

10.1 INTRODUCTION

Omega is a very low frequency (VLF) radio navigation system transmitting radiowave navigational signals at 10.2, 11.05, 11 ⅓, 13.6 kHz and the station-specific "unique" frequencies (in the 10 to 14 kHz range) from a worldwide network of eight ground-based Omega transmitting stations. The system provides worldwide medium-accuracy (two to four nautical miles) position-fixing capabilities. Omega signals propagate outward from the station along great-circle radial paths emanating from the station. The paths lie on the surface of the earth. Like other radio signals, an Omega signal has amplitude* and phase that fully characterize the signal. An Omega navigation user (receiver) determines its position by processing the measured phase of the signals received from three or more Omega stations. Two stations are sufficient if the user has a stable (several parts in ten billion) clock such as a cesium clock.

For the Omega Navigation System to provide the advertised position-fix accuracy, each navigational signal must be "usable" and, furthermore, the signals must arrive at the receiver from diverse directions. A usable signal is one whose amplitude and phase satisfy the appropriate "usable signal access criteria" (see Section 10.2.8) needed to achieve the advertised fix accuracy. Navigational signals arriving at the receiver from diverse directions have a higher potential of providing a "good" accuracy fix (see Section 10.2.7) than the same signals arriving at the receiver from less diverse directions.

---

*The amplitude is the magnitude of the signal; the phase is the fraction of a complete cycle of the sinusoidal Omega signal elapsed as measured from a specified reference point on the signal cycle.

The amplitude and phase of an Omega signal at a point along a signal path (as described in Chapter 5 and Section 10.2) are complex functions of the spatial (location-dependent) and temporal (time-dependent) electromagnetic properties: (1) along the entire signal path between the station and the point, (2) signal frequency, (3) transmitting station antenna characteristics, and (4) receiving antenna characteristics. Local variations in the electromagnetic properties of a path can produce wide variations in the amplitude and phase characteristics of Omega signals. This has a direct impact on the usability characteristics of the signals for Omega navigation. If the mathematical model used in the receiver to compute a position fix could faithfully model all of the spatial and temporal variations in the Omega signal phase, the resulting fix would be very accurate. Unfortunately, such a model is not economically practical. Thus it is necessary to live with some level of phase error and hence the resulting position-fix error.

The phrase "signal coverage" has traditionally described where and when the Omega system signals, based on the specified usable signal access criteria, are expected to provide usable signals for reliable Omega navigation. Recently, for the Omega system and other radionavigation systems such as Loran-C, "signal coverage" has also been used to describe where and when the system signals are *expected* to provide an acceptable position-fix accuracy based on a combination of the specified usable signal access criteria and the expected phase (measurement) errors. The keyword is "expected" because it is virtually impossible to measure and catalog the actual signal coverage or fix accuracy as a function of time at every location on the earth. Furthermore, navigation accuracy is highly dependent on the specific receiving equipment being used. Therefore, to provide a general measure of the signal usability that is independent of specific receiver characteristics, Omega signal coverage is defined in terms of the most fundamental quantity, the expected *signal phase*.

If the signal phase could be predicted exactly (by the receiver) and then measured without error, the comparison of the prediction with measurement would potentially be an error-free position fix. In practice, however, noise (both atmospheric* and receiver installation-induced) limits the measurement accuracy, and complexities of the signal propagation medium severely limit the phase prediction accuracy. Therefore, the signal coverage is characterized by the expected availability of Omega signals with: (1) "acceptable" signal-to-noise ratios,§ the ability to accurately measure the signal phase, and (2) a "small" deviation of the signal phase from the reference phase, the value provided by the receiver's "reference" phase model.

---

*Lightning discharges throughout the world produce atmospheric noise.

§ Signal-to-noise ratio is the ratio of the amplitude of the signal and the amplitude of the envelope of the atmospheric noise fields.

The reference phase model in the receiver is based on an assumed "nominal" (time- and location-independent) signal path where the signal phase at any point along the signal path is a simple linear function of the radial distance from the station. In other words, simply multiply the distance by an appropriate constant to determine the phase. Because the "real-world" propagation path is usually very different than the simple path assumed in the receiver reference model, the measured phase of a signal can significantly differ from the receiver reference phase. This difference causes the fix error. The measured phase can be adjusted (by the user) to account for some of the differences between the measured and the reference phase. The approach taken by most Omega users is to adjust (or convert) the measured phase by applying a predicted offset quantity called the "propagation correction" (PPC) which attempts to account for the propagation differences.* PPCs are thus used in the receiver to "correct" the phase measurement and bring it in closer agreement with the reference phase. Therefore, the fidelity (accuracy) of PPCs determines the realizable navigation accuracy. If the PPCs were "perfect," the phase errors would be zero and Omega signals could be used anywhere in the world, provided the signals are strong enough to provide accurate signal phase measurements. In actuality, it is virtually impossible to capture all of the propagation complexities of the real-world medium in the PPCs. There will be some errors in the PPCs and the resulting usability of a station signal is primarily limited by what is commonly referred to as "modal interference" (see Section 10.2.2) and long-path propagation effects (see Section 10.2.4), and receiver signal-to-noise ratio detection threshold level.

## 10.2   OMEGA SIGNAL PROPAGATION MECHANISMS AND CONCEPTS

Chapter 5 presents a detailed discussion of Omega signal propagation mechanisms and the signal characteristics. This section presents an overview and review of the signal propagation mechanisms and characteristics that are necessary to understand the development and application of Omega signal coverage products.

10.2.1   Propagation Mechanisms

Figure 10.2-1 illustrates a representative great-circle radial path TR from the transmitting station T to the receiver R. This representative signal path over the surface of the earth is composed of land, fresh-water ice, and sea water. Also, the path is a mixed-illumination path with the day illumination

---

* PPCs are similar to the "additional secondary phase factor (ASF)," the spatial corrections, used in Loran-C navigation; however, PPCs also vary substantially over the course of a day — like early Loran-C "skywave corrections."
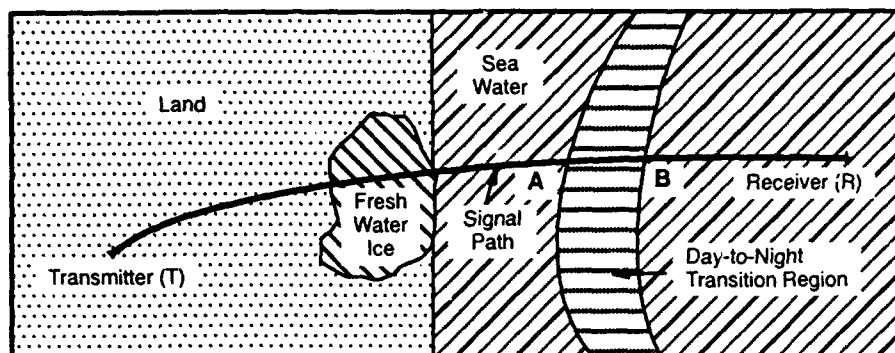
Figure 10.2-1 An Example of Signal Path (TR)

(i.e., χ [solar zenith angle*] $\leq 90°$) condition along the TA segment of the path, night illumination (i.e., $\chi \geq 99°$) condition along the BR segment of the path, and the day to night transition illumination (i.e., $90° < \chi < 99°$) condition along the AB segment of the path. Actual paths may encounter any or all of these specific conditions and characteristics.

Omega signal propagation along a signal path such as path TR actually takes place in the space between the earth's surface and the D-region ionosphere called the "earth-ionosphere" waveguide. Figure 10.2-2 is a side view of the earth-ionosphere waveguide characterizing the signal path TR shown in Fig. 10.2-1. In this waveguide, the lower boundary is the earth's surface and the upper boundary is the D-region ionosphere. The lower boundary is characterized by its ground conductivity and an associated dielectric constant (also called permittivity), which are functions of geographic location. The upper
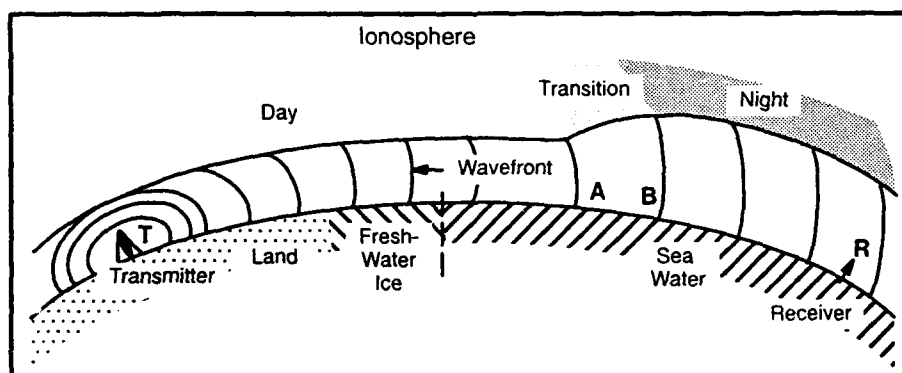
Figure 10.2-2 A Side View of the Earth-Ionosphere Waveguide Formed Along the Signal Path TR Shown in Fig. 10.2-1

---

*Solar zenith angle is the angle of the sun relative to a point on the signal path.

boundary is characterized by the pair of ionospheric parameters: ionospheric reflection height and iono-spheric conductivity gradient. These parameters are functions of tne charged particle density and collision frequency of the D-region ionosphere and solar zenith angle. The signal propagation characteristics in a waveguide are thus functions of the waveguide boundary parameters (i.e., ground conductivity, ionospheric parameters, as functions of solar zenith angle). In addition, the propagation characteristics are functions of the magnitude and direction (relative to the signal path direction) of the earth's magnetic field. The earth's magnetic field makes the ionosphere behave like an anisotropic medium that in turn causes the signal propagation characteristics at a path point to depend on the direction (relative to the earth's magnetic field) of the signal path at the point. The effects of the earth's magnetic field on the signal propagation characteristics at a path point are functions of the dip angle (or, alternatively, the geomagnetic latitude* which is related to the dip angle) and the path azimuth (bearing angle) relative to the geographic north. Dip angle is the angle between the earth's magnetic field and its horizontal component.

In a waveguide, the electric field (or, alternatively, the associated magnetic field, which is linearly related to the electric field) of a signal propagating at a path point is conveniently described using the waveguide-mode theory representation (Refs. 1 and 2). In this representation, the signal in the waveguide is adequately approximated as a sum of significant (i.e., strongest amplitude) "modes" (mathematical functions) excited in the waveguide. A mode has a unique electromagnetic field pattern (i.e., the spatial variations of the electric and magnetic fields); it is like a term in a Fourier expansion of an arbitrary function, such as a sine or cosine term in a sinusoidal Fourier series. The electric/magnetic field of a mode signal is a vector quantity, i.e., the field has a magnitude and direction along which the field is pointed or directed. In the waveguide mode representation, the electric field (or, alternatively, the magnetic field) of a signal at a point along the signal path is obtained by the vector-phasor sum[§] of the vector electric (or vector magnetic) fields of the modes propagating in the waveguide.

The strongest component of an electric field is the vertical component (the one perpendicular to the earth's surface); alternatively, the horizontal component is the strongest component of the magnetic field. For this reason, most Omega receivers measure either the vertical component of the electric field, using a whip antenna (called an E-field antenna), or the horizontal component of the magnetic field, using a crossed-loop antenna (called an H-field antenna). Thus, Omega users need information on the availability and usability characteristics of the vertical component of the electric field or the horizontal component of the associated magnetic field of Omega signals. Since the horizontal component of the

---

*The geomagnetic latitude, θ_m, is related to the dip angle, I, by $\tan \theta = \frac{1}{2} \tan I$.

[§] Vector-phasor sum is a sum of the individual mode phasors, each of which is a complex quantity and has a magnitude and phase associated with it. See Section 10.2.2.

magnetic field can be obtained by multiplying the vertical component of the electric field by an appropriate constant, the Omega signal coverage products provide coverage information (the availability and usability characteristics of the signal) for the vertical component of the electric field of the signals. Throughout this chapter, the terms "signal," "signal field," or "field" are used interchangeably to mean the vertical component of the electric field of an Omega signal.

The waveguide modes are usually classified as either transverse-magnetic (TM) or transverse-electric (TE). A TM (TE) mode signal at any point in the waveguide has its magnetic field (electric field) oriented in the plane which is perpendicular to the direction of the signal path. The propagation characteristics of a mode signal field at a path point in the waveguide are conveniently described by the following four parameters:

- *Attenuation rate* — The spatial rate at which the mode dissipates (reduces) its energy at the path point

- *Phase velocity* — The spatial velocity at which the "wave front" of the mode appears to propagate at the path point

- *Excitation factor* — A measure of the relative efficiency with which the mode is excited by the transmitting antenna, or received by the receiving antenna, at the path point

- *Height-gain function* — The variation of the mode field in the vertical direction (relative to the earth surface) at the path point.

Waveguide modes are generally numbered with an increasing mode index according to the increasing phase velocity associated with the modes in the waveguide. Mode 1 is the lowest phase-velocity TM mode and is the most important mode and it usually has the lowest attenuation rate (consequently it usually is the strongest-amplitude mode) of the signal for navigation purposes; Mode 2, Mode 3, . . . are the higher-order modes. In this type of mode-numbering system, the TM and TE modes are the odd- and even-numbered modes of the waveguide, respectively.

An Omega signal, as mentioned above, consists of many modes. With the following exceptions, the signal amplitude along most worldwide Omega signal paths, at most times of the day, is dominated by its Mode 1 amplitude: (1) certain nighttime westerly-directed signal paths from a station, and (2) station signal paths inside the "near-field" region of the station. The resulting signal is usually referred to as a Mode 1-dominated signal. In other words, the Mode 1 amplitude is much stronger than the amplitude of the phasor sum of the higher-order modes (e.g., Mode 2, Mode 3, etc.). Thus, the presence of the higher-order modes in the signal can be effectively ignored without any noticeable error in the resulting signal

characteristics. The near-field region of a station is a region where the signal is composed of several strong-amplitude modes. The region extends outward from the station up to 500 to 1000 km when the region is in daylight and increases usually to 1000 to 2000 km when the region goes into darkness (night).

Since the phase of Mode 1 varies almost linearly with distance, the phase of a Mode 1-dominated signal also varies almost linearly with distance. See, for example, Figs. 10.2-3(a) and 10.2-3(b). In these figures, the phases of the predicted Mode 1 signal and the total signal are shown by thin and thick dashed lines, respectively. Omega receivers usually assume that the received signals contain only Mode 1. Therefore, the receiver corrects (or adjusts) the measured phase of a received signal using the PPC (which assumes the received signal as a purely Mode 1 signal) so that the resulting PPC-adjusted phase of the signal closely matches the reference phase derived from the mathematical model in the receiver.

10.2.2   Modal Interference Effects

In the near-field region of a station as well as along certain nighttime segment(s) of the westerly directed radial paths from a station, especially from a station located near the geomagnetic equator,* Mode 1 frequently fails to be the dominant mode of the signal (i.e., strongest mode relative to the other modes by a certain margin). Westerly directed paths are typically paths with bearing angles (at the station) between 180 and 360 degrees. Also, along certain mixed-illumination (i.e., part day and part night) paths, Mode 1 may fail to be the dominant mode of the signal. This is especially true along the transition segment of a path where the illumination condition changes from night to day, or day to night. This lack of Mode 1 dominance in a signal at a path point, or along a path segment, is called "modal interference" and the associated signal is referred to as being a "modal" signal. Thus a modal signal displays one of the following characteristics: It is either composed of several competing-amplitude modes, or it is dominated by a single mode other than Mode 1.

If it is composed of several competing-amplitude modes, they may or may not include Mode 1. This may alternately dominate the signal on different segments of the signal path. In this case, because of the differing phase velocity of the modes, the amplitude/phase of the modal signal exhibits an oscillatory behavior with distance along the path. (See Fig. 10.2-4 where Mode 3 is the dominant mode of the signal up to 5000 km from the station and Mode 1 is the dominant mode of the signal along the remainder of the path.)

---

*Note that the geomagnetic equator is a locus of the geographic locations with dip angle of 90°; it is near but not the same as the geographic equator.

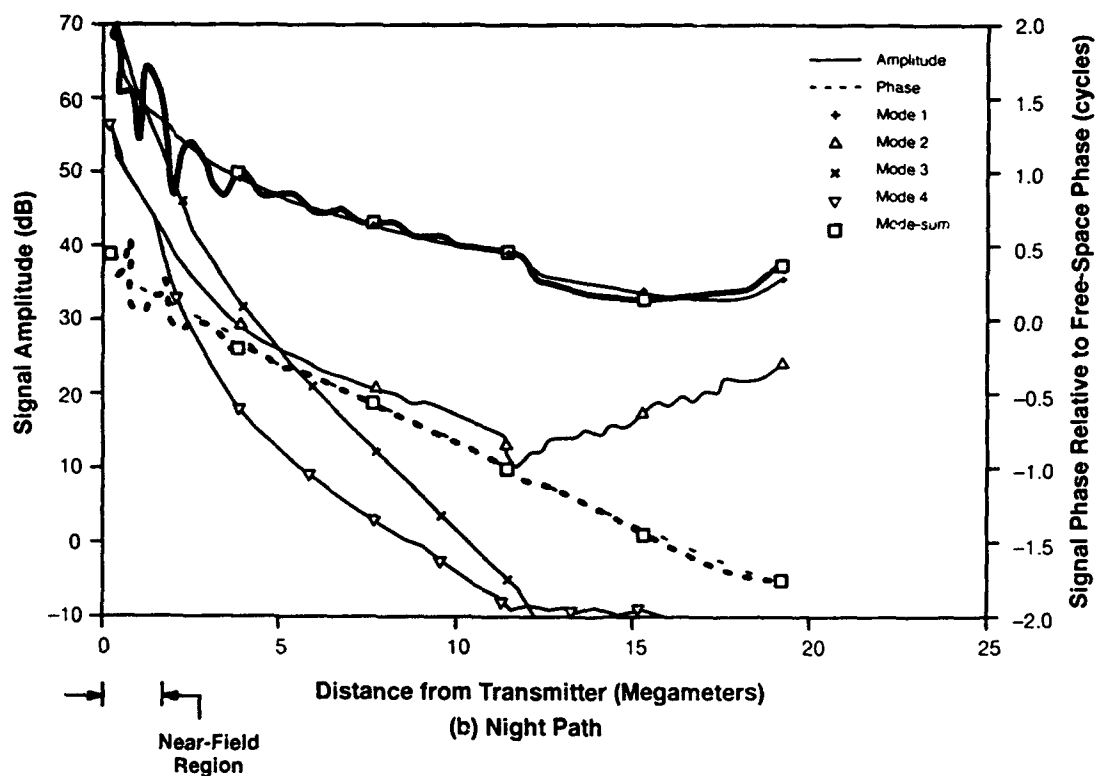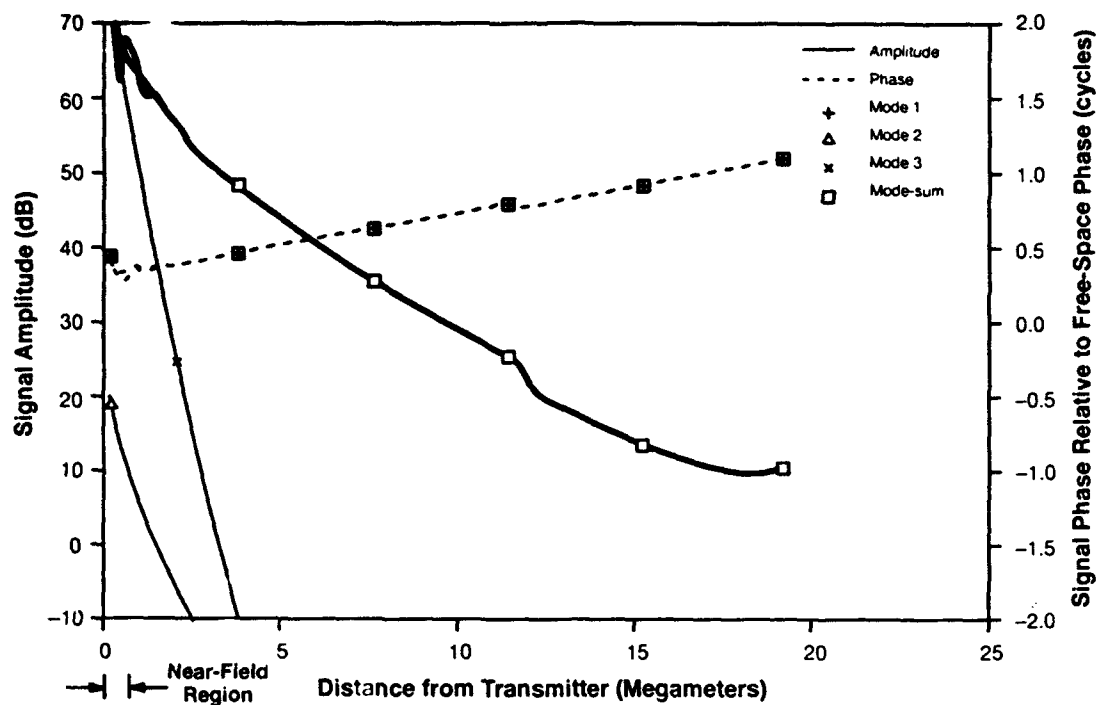**Figure 10.2-3** Examples of Mode 1-dominated Signal Along a Path
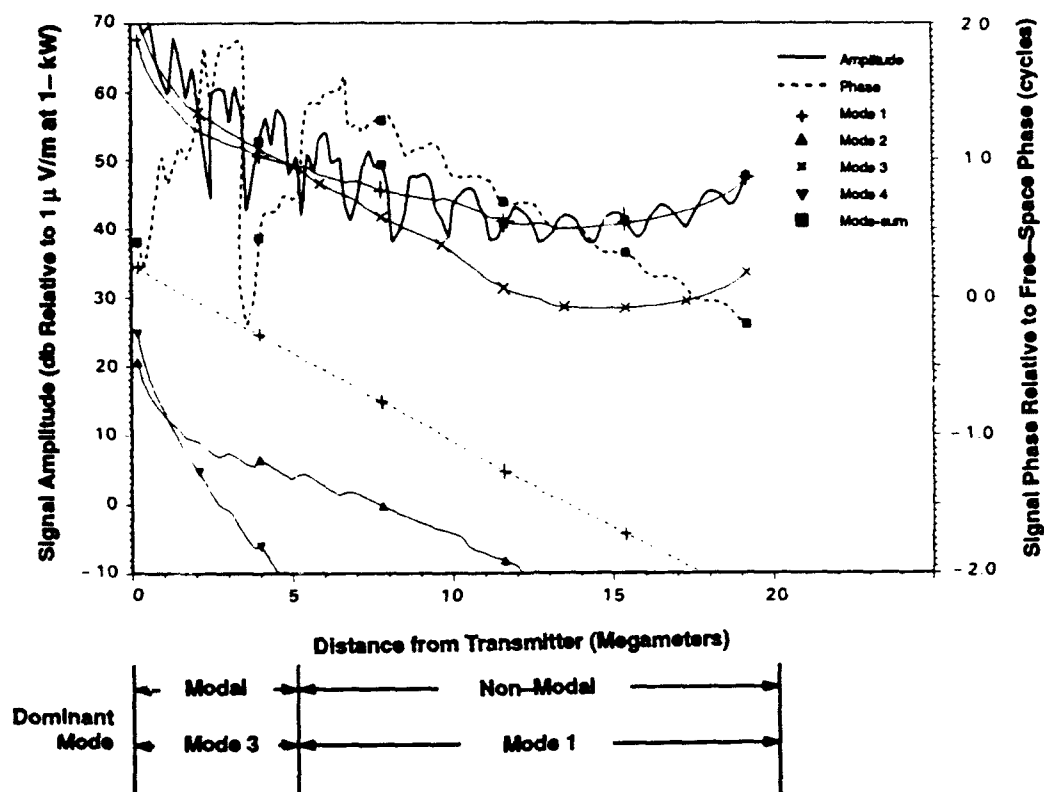
Figure 10.2-4 Example of a Signal Exhibiting Mode Dominance Switch-over

It may be dominated by a single mode other than Mode 1 (e.g., Mode 2 or Mode 3). (See, for example, Fig. 10.2-5, the signal outside the near-field of the station [about 3500 km from the station], a Mode 2-dominated signal.) In this case, the phase of the signal will vary linearly with distance but its proportionality (phase shift per unit distance) can significantly differ from that embodied in the PPCs used by the receiver to adjust the measured phase. This difference can, for example, cause the phase of the received signal to be significantly different from the PPC-adjusted phase of the signal (e.g., causing as much as 2 to 4 cycles of phase change from the Mode 1 phase over a 10 Mm signal path.)

Note that Omega navigation is based on the assumption that the received signal is a Mode 1 signal. However, there is no practical way for a receiver to determine from measurements alone if the signal is, or is not, a predominantly Mode 1 signal. Therefore, *a priori* information is needed on the modal/non-modal characterization of Omega signals prior to their use in Omega position-fix computations; otherwise the computed fix could be in significant error.

An example of the phasor sum of a multi-mode signal is given in Fig. 10.2-6. In this example, the signal field is assumed to be composed of two strong-amplitude modes (Modes 1 and 2). The amplitude
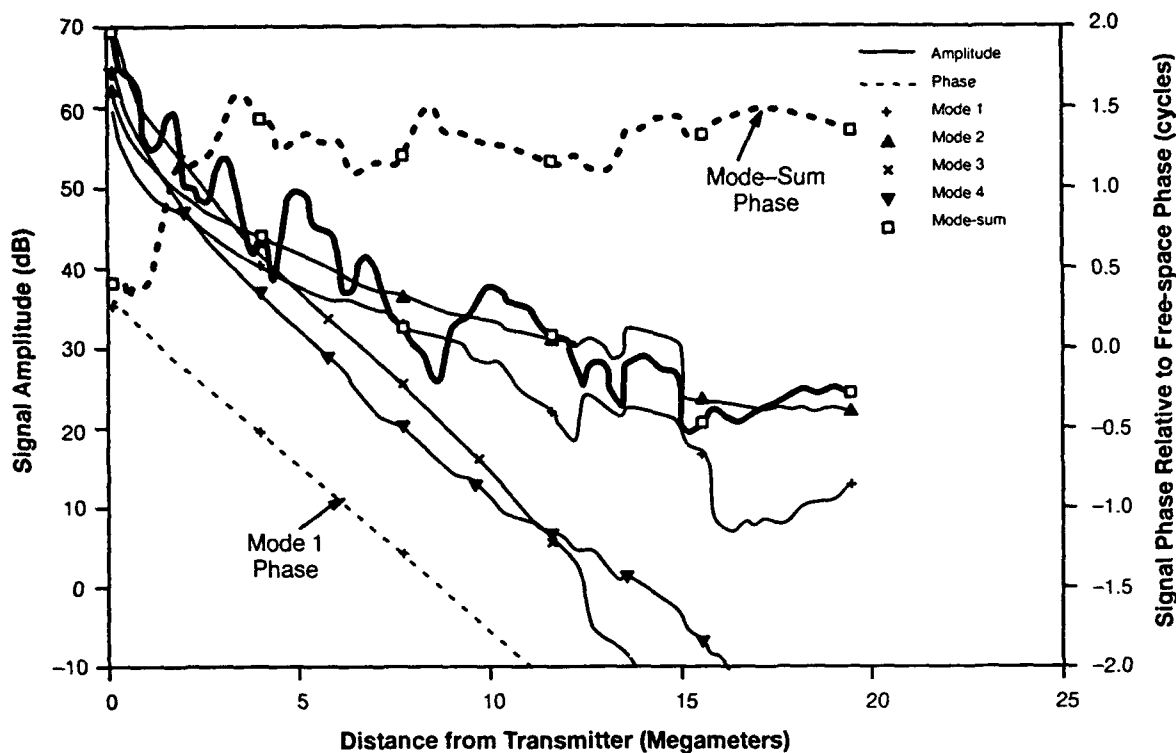
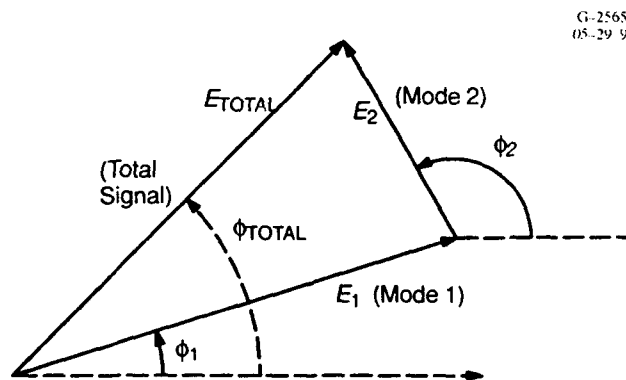**Figure 10.2-5**   Example of Modal Signal Along a Nighttime Path

Figure 10.2-6   An Example of the Phasor Sum of the Signals $E_1 \angle \phi_1$ and $E_2 \angle \phi_2$ of Modes 1 and 2 $(E_{total} \angle \phi_{total} = E_1 \angle \phi_1 + E_2 \angle \phi_2)$

and phase of each mode are E_i and ϕ_i, respectively, where $i = 1, 2$. The amplitude, E_{total}, and phase, ϕ_{total}, of the total (mode-sum) signal are thus given by:

$$E_{\text{total}} = [E1^2 + E_2^2 + 2E,E_2\cos\phi]^{1/2}$$

$$\phi_T = \tan^{-1}\left[\frac{E_1\sin\phi_1 + E_2\sin\phi_2}{E_1\cos\phi_1 + E_2\cos\phi_2}\right]$$

(10.2-1)

where $\phi = \phi_2 - \phi_1$

When the signal is composed of many higher-order (e.g., Mode 2, Mode 3) strong-amplitude modes, the phasor* $E_2 \angle \phi_2$ can be thought of as the phasor sum of the higher-order modes.

Modal interference at a path point is characterized as being "spatial" or "temporal" depending upon the solar illumination condition along the path between the station and the path point. Modal interference during the day or night illumination condition along a path is classified as *spatial* interference if the degree of the interference at each path point is nearly the same during the day or night hours along the entire path (and thus depends only on spatial coordinates). The spatial interference is generally larger in magnitude and persists to longer distances along a signal path during night than day. This can be seen in Figs. 10.2-3(a) and 10.2-3(b) by comparing a theoretically predicted amplitude/phase vs. distance behavior of the daytime and nighttime signals propagating along a path. Furthermore, the spatial modal effects are generally more severe both in magnitude and (spatial) extent along nighttime paths emanating from the Omega stations located at low geomagnetic latitudes. Examples of such stations are Liberia, Hawaii, and Japan. Figure 10.2-5 shows an example of such severe spatial interference effects along a westerly-directed nighttime path from the Hawaii station. In this example, severe modal effects persist along the entire radial path and the signal is Mode 3 dominated out to about 3500 km from the station, and beyond this point the signal is Mode 2 dominated.

Temporal modal interference arises from "mode conversion"§ at the day/night terminator crossing along a mixed path which is subject to "usual" spatial interference when the path is fully dark (i.e., the path is in a nighttime illumination condition). Figure 10.2-7 depicts a mixed-path waveguide where the

---

*The phasor notation "$E_2 \angle \phi_2$" indicates a phasor with the magnitude E_2 and phase ϕ_2.

§ Mode conversion (see Chapter 5) occurs at a point along a signal path whenever any of the path properties (such as ground conductivity, ionospheric parameters) change sharply at or in the close vicinity of the day/night terminator crossing along the path.
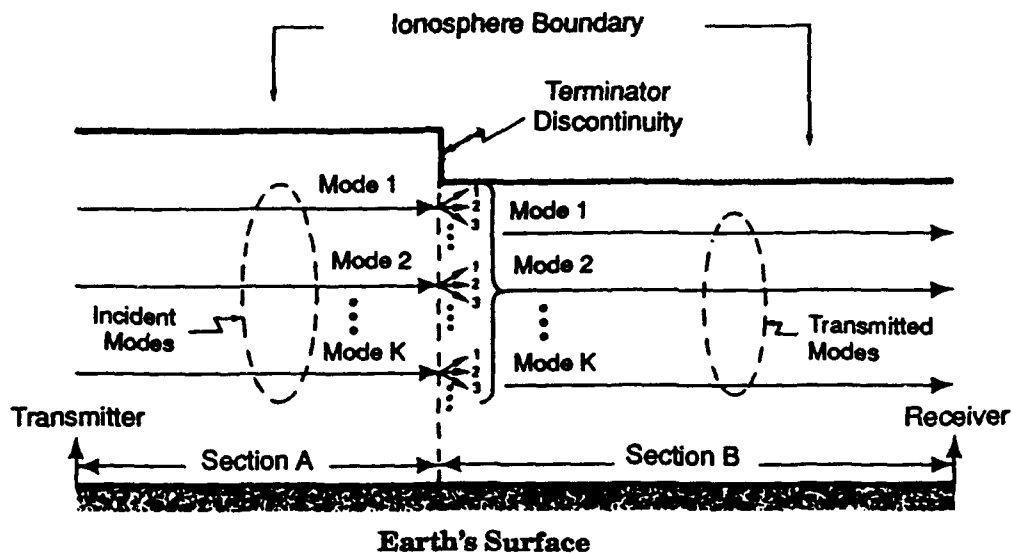
Figure 10.2-7 A Mixed-path Earth-ionosphere Waveguide

night and day segments of the path are assumed to have homogeneous (i.e., constant) path properties. The day/night terminator crossing along the path is assumed to have a zero width and to have caused a step change only in the ionospheric properties (which are the ionospheric reflection height and iono-spheric conductivity gradient, as described in Section 10.2.1) at the crossing. In this waveguide, both the daytime and nighttime signals in the waveguide are assumed to be composed of K number of modes. Due to mode conversion at the terminator crossing, the relative distribution of the signal energy among the modes of the signal, which are incident at the terminator crossing, changes as the signal propagates beyond the terminator. Because the amplitudes of the modes reflected from the terminator are generally insignificant compared to the amplitude of the incident modes, the presence of reflected modes in the total signal calculation is usually neglected without any noticeable error. The degree of temporal inter-ference at a path point generally varies with time in response to the movement of the terminator along the path. An example of the observed temporal modal interference effects in a VLF signal is shown in Fig. 10.2-8 where severe modal effects are observed during the sunrise and sunset hours at the receiver location.

10.2.3 General Guidance for Omega Signal Propagation Effects Determination

This section presents general guidance for assessing the usability and non-usability of the Omega signals for Omega navigation. Some general rules follow.

1. The Omega signal, in general, is a multi-mode signal; however, Mode 1, the lowest-order transverse-magnetic mode, is frequently the strongest-amplitude mode of the signal.

10-12
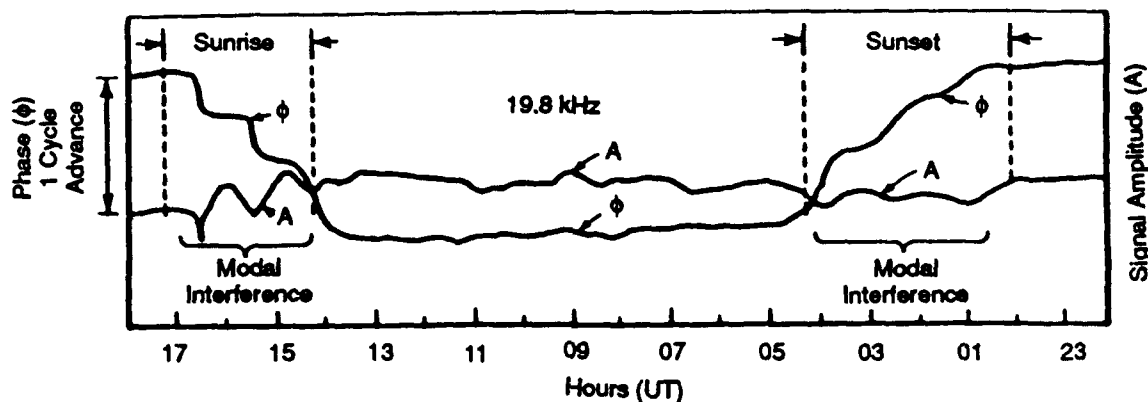
Figure 10.2-8   Phase and Amplitude Variations of the NPM Station
(Lualualei, Hawaii) 19.8 kHz Signal Received at
Boulder, Colorado*

2.   Compared to Mode 1, higher-order modes have greater signal attenuation rate and thus attenuate rapidly with increasing distance from a station, although they are more strongly excited at the station.

3.   Mode 1 is sufficient to approximate a daytime signal outside the station near-field region that typically extends up to 500 to 1000 km from the station.

4.   Mode 1 is sufficient to characterize a nighttime signal at most worldwide locations except for the following locations where the signal is expected to be modal (i.e., strongly multi-mode):

   a.   In the station near-field region that typically extends up to 1000 to 2000 km from the station

   b.   Along westerly-directed paths, i.e., paths with bearing angles (at the station) between 180 and 360 degrees.

5.   Mode 1 signal attenuation rate:

   a.   Is lower at the higher Omega frequencies, i.e., attenuation rate is usually highest at 10.2 kHz and lowest at 13.6 kHz

   b.   Is lower during night than during day, and is in between the day and night values during transition

   c.   Increases greatly with decreasing ground conductivity of the path; it is lowest over sea water (the highest conductivity region) and highest over ice cap (the lowest conductivity region, such as Greenland/Antarctica)

   d.   Higher towards west than towards east

   e.   Higher in the equatorial belt (~ 1000 km on both sides of the geomagnetic equator) along westerly directed paths.

---

*Note that the Lualualei signs are now transmitted at 23.4 kHz; Ref. 3.

6. A modal signal is composed of one or more strong-amplitude higher-order (non-Mode 1) modes; Omega signals are modal:
   a. In a station near-field region
   b. Along westerly-directed nighttime paths emanating from the stations at the low geomagnetic latitudes
   c. At and around the day/night terminator crossing along a path

For accurate Omega navigation, Omega signals must be Mode 1-dominated (i.e., nc. .odal) signals (required by the Omega receivers) with adequate signal-to-noise ratios to provide accurate phase measurements.

10.2.4 Long-path Propagation

A station signal reaches a receiver via both the shorter arc (less than 20 Mm [megameters]) and longer arc (greater than 20 Mm) of the great circle (over an assumed spherical earth) joining the station and receiver. The signals (Fig. 10.2-9) arriving at a receiver via the shorter arc and the longer arc of the great circle are called, respectively, the "short path" and "long-path" components of the signal. Unless special care is exercised by the user to receive only the short-path component of the signal, the signals received may include both the short-path and long-path components of the signal.
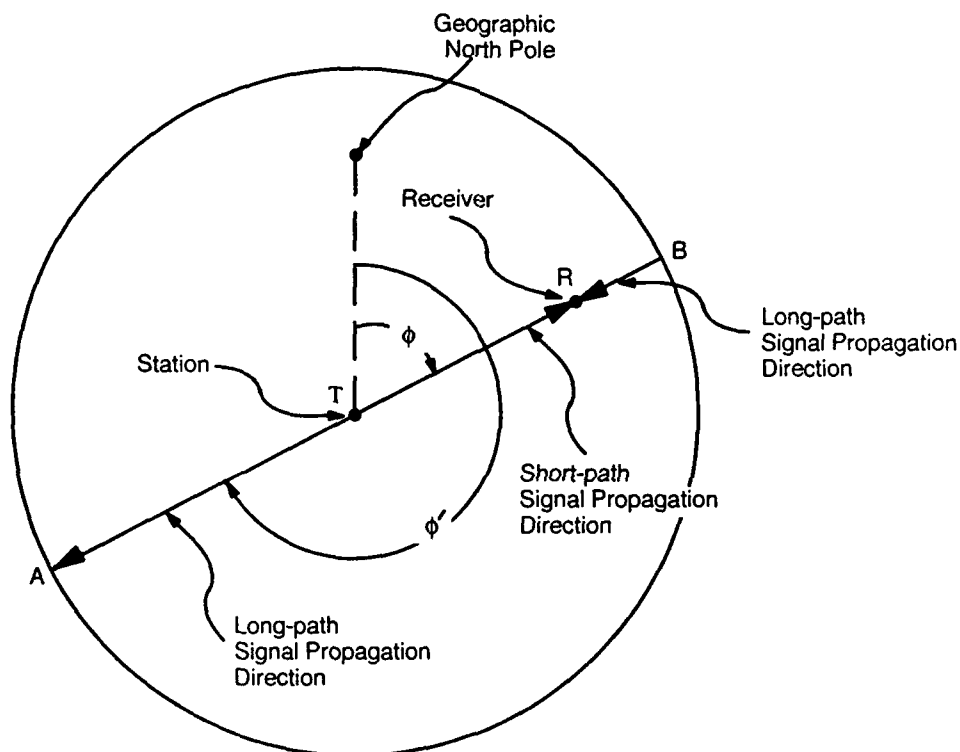

G-11965
2-19-91

Figure 10.2-9 Short Path and Associated Long Path from a Transmitting Station

An Omega station signal is a short-path dominated signal (i.e., short-path component of the signal is stronger than its long-path component) unless:

- The receiver is west of the station

- The long path is composed of mostly high ground conductivity regions (e.g., sea water and land) and the short path includes low-conductivity regions (e.g., Greenland or Antarctica)

- The long path includes the entire nighttime hemisphere and, conversely, the short-path is an all-day path (see Fig. 10.2-10).

Since Omega receivers assume that the received signals are short-path signals, accurate Omega navigation requires that the navigational signals be short-path signals, otherwise the resulting navigation position-fix accuracy could be highly degraded because the phase of the long-path signal significantly differs from that of the short-path signal.

An example of a long-path (i.e., long-path dominated) signal at a fixed receiver site is shown in Fig. 10.2-11 (Ref. 4). The figure shows the predicted and observed patterns of the diurnal variation of the signal phase over the course of the day. The predictions are based on the PPC model (Ref. 5), which assumes the signal to be a purely short-path signal. These predictions are used to correct the received


G-27201
9-09-91
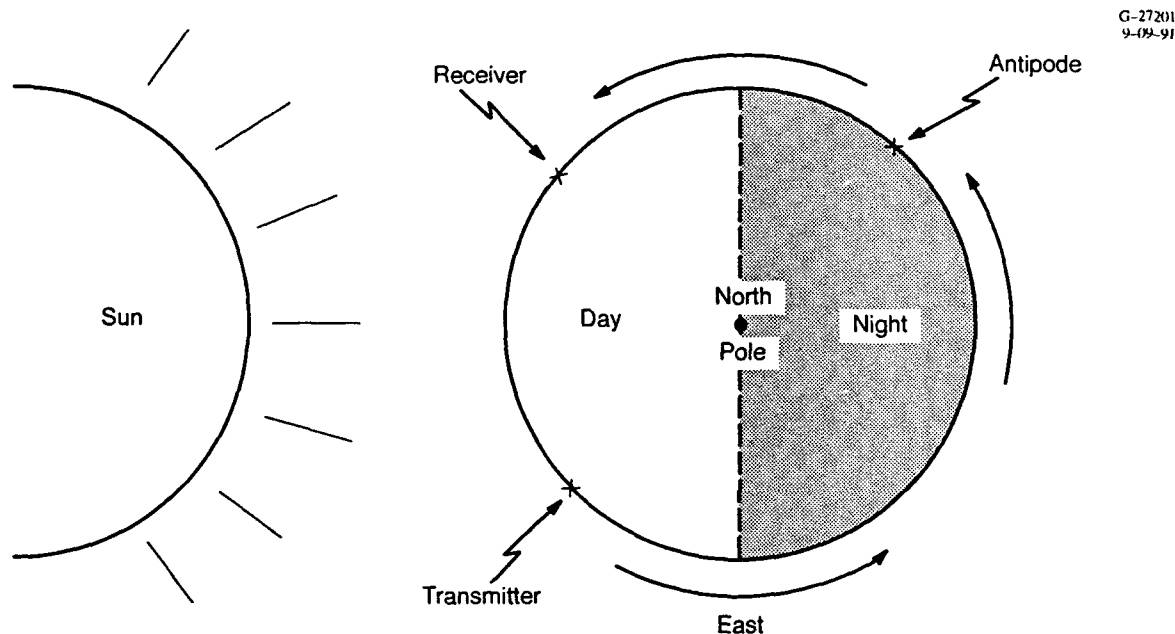
Figure 10.2-10 Ideal Long-Path Situation (transmitter and Receiver on the Equator, and Earth is at Equinox)
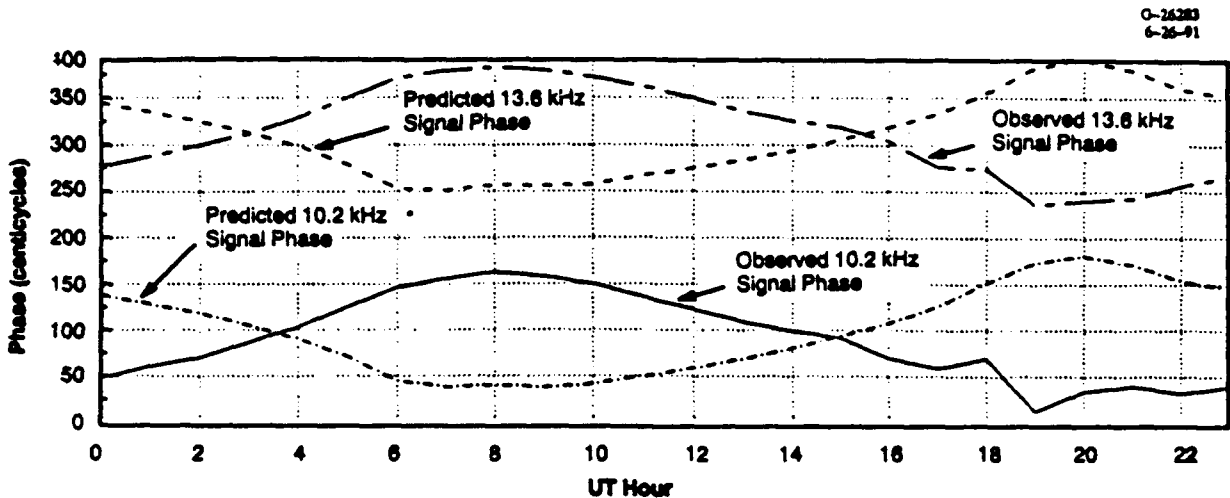
Figure 10.2-11 Example of Long-Path Effects in the Japan (H) Station
Signal Received at the Liberia (B) Monitor Site

(observed) Omega signal phase readings so that the corrected phase will closely match the reference phase embodied in the receivers and thus the expected navigation accuracy can be achieved by the receivers. Note that the observed diurnal variation is exactly opposite that of the predicted diurnal variation. The observations are showing nighttime delays while the predictions correspond to the day-time delays.

An example of the received signal changing from a long-path signal to a short-path signal and then to a long-path signal over the course of the day is shown in Fig. 10.2-12, as recorded by a marine navigator (Ref. 6). The plot of this figure shows phase tracks of the Hawaii station signal recorded on a vessel located at about 10,000 km southwest of the Hawaii station, and the vessel is proceeding towards the station at approximately a constant heading and approximately constant speed. The phase data in Fig. 10.2-12 is plotted on a scale of one Omega "lane" so each discontinuity in the phase track represents a lane change. In this figure, the slope of the phase tracks between 0200 to 1000 UT hours and 1800 to 2400 UT hours and is an increasing phase with decreasing distance from the station, suggesting that the signal is a long-path signal whereas the phase tracks between 1000 and 1800 UT hours show decreasing phase with the decreasing distance from the station, indicating that the signal is a short-path signal.
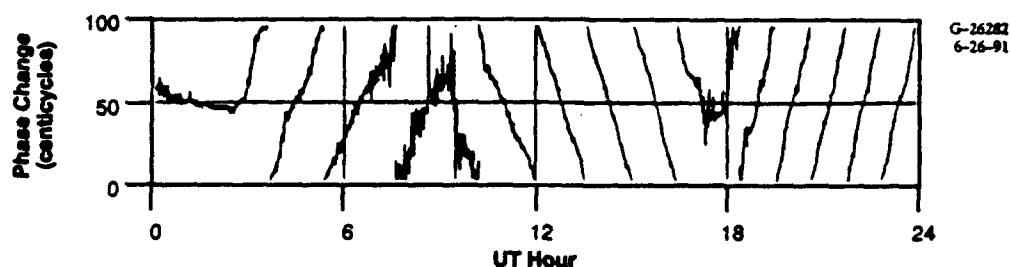
Figure 10.2-12   Moving Vessel Phase Tracks for Hawaii Signals

10.2.5   Path/Terminator Crossing Effects

Analyzing the VLF signal phase instabilities observed on signal paths nearly parallel to the day/night terminator (path/terminator crossing angle <10 degrees), Mannheimer (Ref. 7) has postulated the existence of signal reflections/refractions (see Chapter 5) from the day/night terminator to explain the observed phase behavior (see Fig. 10.2-13). The presence of reflected signals from the terminator (in addition to the direct-path, i.e., short-path, signal) can explain, though not rigorously establish, why transition effects are observed well before the geometrical terminator (the solar zenith angle equal to 90 deg) begins to cross the path. Similarly, reflections can explain why transition effects linger after the
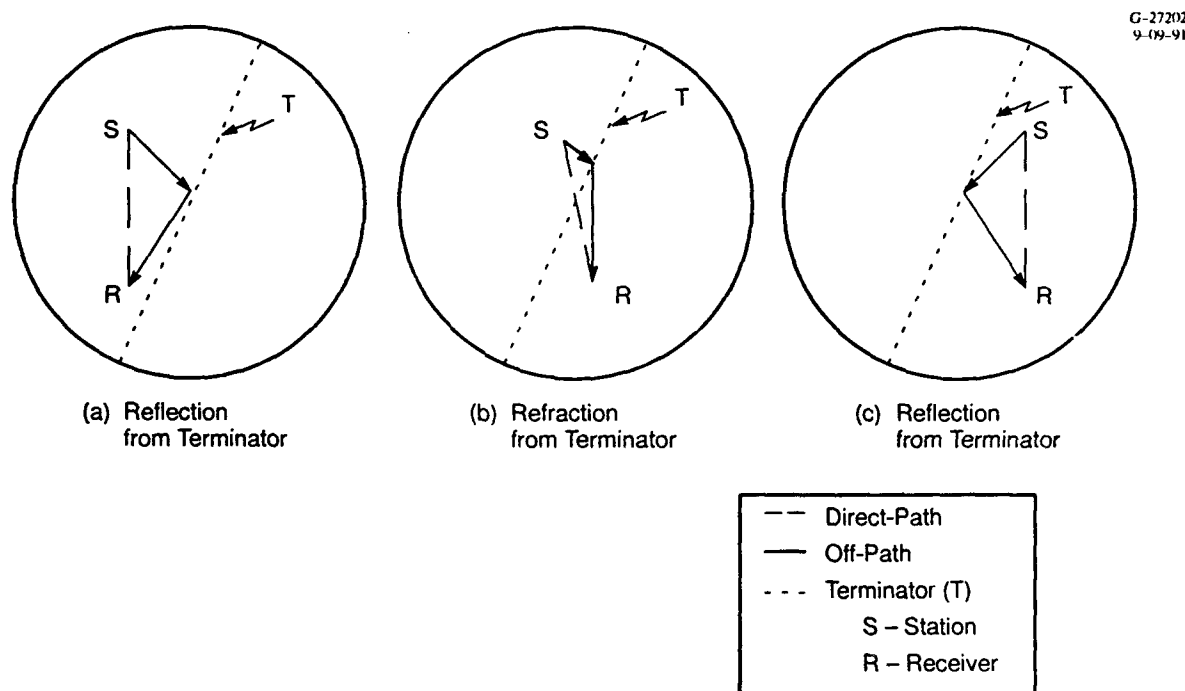

Figure 10.2-13   Terminator-induced Reflections and Refractions

10-17

terminator has crossed the entire path (see Figs. 10.2-13a and 10.2-13c). The signal phase instabilities observed during transition (while the terminator is crossing the path) may be explained as an interference between the refracted signal and the direct-path signal (see Fig. 10.2-13c). Note that mode conversion effects are usually greatest and the refractive effects smallest when the path and terminator are perpendicular to each other. However, mode conversion effects are smallest, while refractive effects are largest when the path/terminator crossing angle is small. Mannheimer's analysis suggests that the terminator-induced reflections/refractions can introduce large phase errors in a received (direct-path) signal when the crossing angle is between 0 and 5 degrees. Therefore, Mannheimer has indicated that signals propagating along paths whose crossing angle is less than five degrees with the day/night terminator should not be used for Omega navigation because these signals have large phase instabilities; their use in a position-fix computation can result in a highly inaccurate position-fix prediction.

10.2.6 Antipodal Signal Exclusion Region

As mentioned in Section 10.1, Omega signals propagate outward from the station with approximately circular signal phase wave fronts as shown in Fig. 10.2-14. The signal propagation direction at a receiver location is along the great-circle radial path joining the station and receiver. The station (great-circle) radial paths converge at both the station and its antipode (the geographic location on a spherical earth geometrically opposite to the station). The signal characteristics at a receiver location are functions of the locally varying bearing (azimuth), one of the properties along the signal path. As a receiver
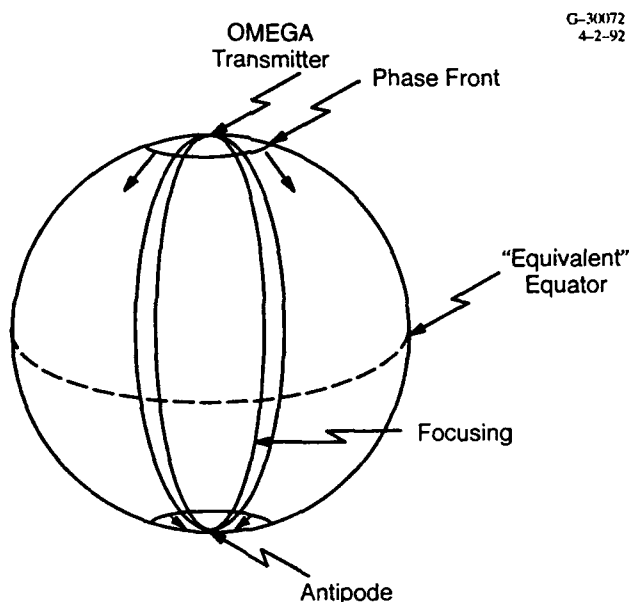
Figure 10.2-14   Station Antipode and the Signal Phase Wave Front

platform track gets closer to the station or its antipode, the tracking of the station signal path bearing becomes more and more error prone. Note that Omega receivers measure the phase of a received signal by averaging the received signal phase over a receiver time constant, typically one to five minutes. Because of the rapidly changing bearing of the signal path along the receiver platform tracks close to a station or its antipode, the measured phase of the signal along such a track could have significant error. Therefore Omega signals should not be used in the close vicinity of a station or its antipode. The non-usable antipodal region of a station is assumed to cover a distance of 1000 to 2000 km from the station antipode.

10.2.7 Geometric Dilution of Precision (GDOP)

The accuracy of Omega navigation is affected by the relative geometry of the navigation signal paths at the position-fix poiːt. GDOP is a measure (figure of merit) of the "quality" of the fix geometry, and is commonly defined as the ratio of the root mean squared (rms) position error to the rms single-station range error (Ref. 8). For a given amount of single-station range error (or, equivalently, the single-station phase error), the two hyperbolic lines of position (LOPs) that cross at right angles will have the smallest position-fix error, while the two LOPs which are nearly parallel will have the largest position-fix error.* In general, for the case of the two LOPs, GDOP decreases as the LOP crossing angle increases. The position fix geometries with lower GDOP values are the preferred fix geometries.

Assuming the standard deviation of the single-station phase errors to be the same for all three stations used in a hyperbolic navigation position-fix geometry (see Fig. 10.2-15), the first-order position-fix error is given by (Ref. 9):

$$\sigma_r = \frac{\lambda \sigma_\phi}{\sqrt{2} \sin \theta} \left[\frac{1}{\sin^2 \frac{(\phi_{12})}{2}} - \frac{2\rho \cos \theta}{\sin \frac{(\phi_{12})}{2} \sin \frac{(\phi_{31})}{2}} + \frac{1}{\sin^2 \frac{(\phi_{31})}{2}} \right]^{1/2} \qquad (10.2-2)$$

where

λ	=	Signal wavelength (km)
σ_r	=	Standard deviation of radial position error (km)
σ_ϕ	=	Standard deviation of single-station phase error (cycle)
ϕ_{12}	=	Angle subtended at the receiver by transmitting station 1 relative to station 2 = $\phi_1 - \phi_2$

---

* Each hyperbolic line of position is a contour of constant phase difference between the two synchronized station signals associated with the line of position; hyperbolic navigation is described in Chapter 4.
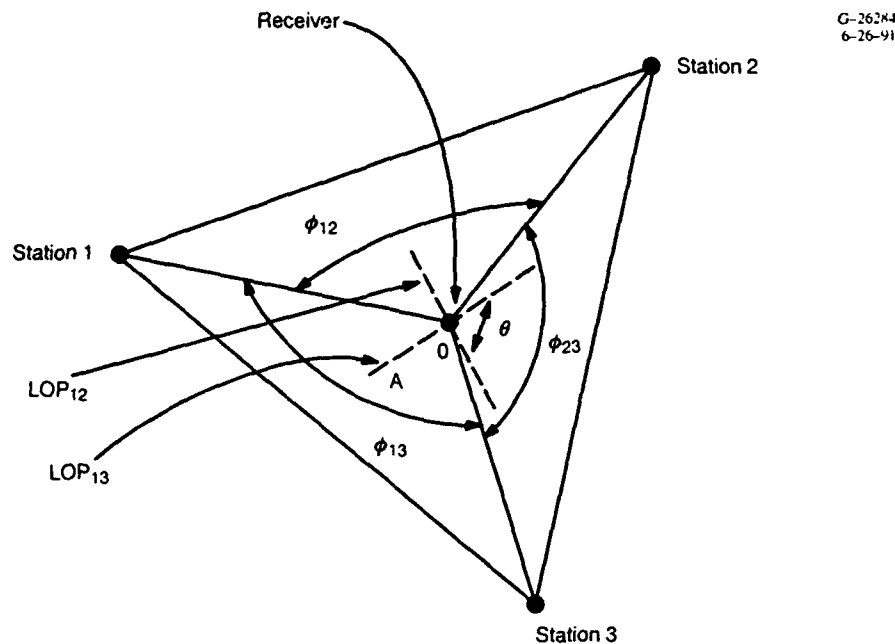
Figure 10.2-15   Position-fix Geometry using Two Hyperbolic LOPs

ϕ_3 = Angle subtended at the receiver by transmitting station 3 relative to
station $1 = \phi_3 - \phi_1$

LOP_{ij} = Line-of-position of constant phase difference between the signals
received from the ith and j^{th} stations*

θ = Crossing angle between LOP_{12} and LOP_{13} = $\dfrac{(\phi_{12} + \phi_{31})}{2} = \dfrac{\phi_3 - \phi_2}{2}$

ϱ = Phase-difference error correlation between LOP_{12} and $LOP_{13} = 0.5$.§

GDOP, the ratio of the radial position error (σ_r) to the single-station range error ($\lambda\sigma_\phi$) is then given by:

$$GDOP = (\sigma_r / \lambda\sigma_\phi) \tag{10.2-3}$$

Note that although GDOP (Eq. 10.2-3) is a *non-dimensioned* or *dimensionless* quantity; in a number of earlier coverage products (Refs. 9, 13, 16, 24, 25, and 26) it is defined and used as a *dimensioned* quantity:

$$GDOP = (\sigma_r / \sigma_\phi) \tag{10.2-4}$$

---

* It can be shown that LOP_{ij} bisects the angle θij; for example, in Fig. 10.2-15, the LOP_{13} (shown as line OA_1) bisects the angle θ_{13}.

§ Value of ϱ is based on the assumption that different station signal paths are uncorrelated.

As a consequence, the dimensioned GDOP (Eq. 10.2-4) has the dimension of km per cycle. It is important to note that the GDOP is affected by both the *spreading* of hyperbolic LOPs and the *crossing angle* between LOPs.

Note that in the above GDOP definitions, the GDOP is a "single-phase GDOP," and σ_ϕ is the single-station phase error. Thus, the rms position error is simply the product of the GDOP and σ_ϕ. In some of the coverage products, such as the coverage diagrams and Omega ACCESS described in Section 10.3.2.4, the dimensioned-GDOP has been referenced relative to the (hyperbolic) phase-difference error. Thus, the hyperbolic-based, dimensioned-GDOP in these specific products will be $\sqrt{2}$ smaller than the value that would be obtained using Eq. 10.2-4.

10.2.8 Usable Signal Criteria

Accurate Omega navigation is based on the availability of an adequate number of usable signals. Most Omega receivers assume that the Omega navigational signals are both short-path dominated and non-modal so that the reference phase model (incorporated in Omega receivers) adequately characterizes the PPC-adjusted phase of the received Omega signals. A station signal is considered usable if it satisfies the following usable signal access criteria:

- The short-path component of the signal exceeds the long-path component (so that the received signal is predominantly a short-path signal, as modeled by the receiver)

- The signal is non-modal (so that the receiver phase model adequately characterizes the received signal phase)

- The signal is strong (so that the received SNR exceeds the receiver detection threshold to provide an accurate phase measurement)

- The signal path/terminator crossing angle is not too small (to avoid reflections/ refractions of the signal that may occur at the day/night terminator crossing along the signal path)

- The signal receiver location is outside the station antipodal region (to avoid rapidly changing signal path bearing which most receivers cannot adequately track).

The typical threshold levels or values of the usable signal criteria parameters are:

- The short-path SNR $\geq$ Receiver detection threshold level

- The ratio of short-path SNR (SPSNR) to long-path SNR (LPSNR) $\geq$ 6 dB

- The short-path is signal non-modal, i.e., the signal is a Mode 1 dominated signal and its "phase deviation" is less than 20 centicycles

- The path/terminator crossing angle $\geq$ 5 degrees.

Note that short-path phase deviation (SPPD) is the magnitude of the deviation (difference) of the phase of the total signal from the phase of the signal's Mode 1 component. For a moderate-performance receiver, the SNR detection threshold level is typically –20 dB (in 100 Hz bandwidth), while it is –30 dB (in 100 Hz bandwidth) for a high performance receiver (Ref. 10).

An alternative and more conservative definition of the non-modal signal based on the signal's Mode 1 Dominance Margin (M1DM) has been used in a recently-developed coverage product (the matrix database, see Section 10.3.2.5). M1DM is the ratio of the amplitude of the signal's Mode 1 component and the amplitude of the signal's Interfering Mode (IM) where IM is the phasor sum of the signal's non-Mode 1 components. A signal with an SPPD value less than 20 centicycles will have an M1DM value greater than about 1 dB. For this product, it is recommended that the signal be considered non-modal if its M1DM exceeds or equals 6 dB; otherwise the signal should be considered modal. The 6 dB threshold value is recommended (Ref. 11) to ensure that an indicated non-modal signal at any path point will remain non-modal at the point in spite of the normal, day-to-day, random, spatial fluctuations experienced by the ionosphere (along the path) which together with the properties of the earth's surface at the path point determine the Omega signal propagation characteristics. These fluctuations can cause as much as 2 to 4 dB fluctuations in the amplitude of each of the component modes (especially the higher-order modes) of the signal, thereby causing potential changes as large as ±6 dB in the M1DM value.

10.3 AVAILABLE COVERAGE PRODUCTS

10.3.1 Need for Coverage Products

As mentioned in Section 10.1, Omega signal propagation characteristics and thus the signal coverage, are a complicated function of the spatially and temporally varying (electromagnetic) properties of the signal path propagation medium and signal frequency. The commonly used descriptors or elements of signal coverage are:

- Short-path SNR which determines the phase measurement accuracy

- Non-modal/modal characterization of the signal (i.e., phase deviation and whether the signal is Mode 1 dominated or not) which relates to the phase stability of the signal and thus adherence to the reference phase model used in the receiver

- Long-path SNR which relates to the reference phase model adherence

- Path/terminator crossing angle which relates to the phase stability.

Based on the desired usable signal access criteria, threshold values are assigned to the coverage elements to permit a quantitative inference of expected signal coverage. Omega signal coverage products are generally used in the following principal applications:

1. Support mission planning prior to establishing a navigation route or departure of a mission

2. Provide real-time navigation receiver support by using coverage information not readily detected or measured by an on-board system

3. Support system performance assessment.

Application 1 generally refers to the use of coverage information by organizations (such as military units or airlines) for selecting a navigation system for specific global region(s). Application 2 is frequently employed by receiver manufacturers who embed in their receivers the appropriate space- and time-dependent coverage information needed to enable the receiver to properly deselect the navigationally unusable signals. Application 3 refers to the system provider (i.e., ONSCEN*) who is interested in assessing regional/global availability of the Omega system for the specified usable signal conditions as a function of space and time, and thus determining the potential impact on the regional/global system availability due to certain changes in the system operational conditions/parameters (e.g., unscheduled station downtime or reduced power operation of a station).

In Application 2, some coverage data can be sensed in real time by the on-board system — other data cannot. For example, SNR is derived (from the measured signal phase stability) by most receivers but non-modal/modal (signal characterization) information must come from *a priori* signal coverage data. The presence of strong long-path signals can be detected and eliminated with a directional antenna (with an asymmetric front-to-back antenna radiation pattern symmetry) but, in most cases, the long-path coverage information is based on *a priori* coverage information. Although SNR is estimated by the receiver, SNR predictions from coverage information are useful for isolating highly anomalous local (installation-dependent) noise sources if the prediction and the measurement significantly differ.

Omega coverage information can also be combined with similar coverage information for other radionavigation sensors. For example, a candidate hybrid navigation system may use Omega as a back-up to a satellite-based system (such as the Global Positioning System [GPS]) and the Omega phase is continuously corrected by the satellite-based system signal receiver. If a significant loss of coverage

---

*Omega Navigation System Center, the U.S. Coast Guard organization responsible for operating, maintaining, and improving the Omega Navigation System. Formerly, ONSCEN was known as the Omega Navigation System Operations Detail (ONSOD).

(i.e., reduction in accuracy or loss of a satellite) is experienced with the satellite system for a particular time interval, Omega coverage information can be used to determine the applicability of the Omega system as a substitute primary navigation system during the interval.

10.3.2 Signal Coverage Products Overview

Table 10.3-1 presents a chronological listing of the known Omega signal coverage products that have been developed and published as of January 1992. A number of derivative products have since been produced and some of the better known derivatives are described herein along with the parent products.

In the list, note that the *contour diagrams* provide coverage information for the specified coverage conditions via the use of contours. Figure 10.3-1 illustrates contour diagrams and is discussed later in this chapter. An individual station contour diagram shows two contours: a constant SNR criterion threshold value (e.g., −20 dB) contour and a constant SPPD* criterion threshold value (e.g., 20 cec) contour.

Table 10.3-1   Overview of Published Coverage Products (As of January 1992)*

| NAME | YEAR PUBLISHED | SIGNAL FREQUENCY (kHz) | COVERAGE TIMES DURING THE YEAR | PRODUCT | |
				USABLE SIGNAL	DISPLAY MEDIUM
1974 Contour Diagrams	1976 (Ref. 12)	10.2	2 local times	Coverage criteria contours	Hard copy
1980 Contour Diagrams	1980 (Ref. 13)	10.2	8 global times	Coverage criteria contours	Hard copy
1983 Matrix Diagrams	1983 (Ref. 14)	10.2	2 local times	Coverage/accuracy ranges	Hard copy
1985 Matrix Diagrams	1985 (Ref. 15)	10.2	8 global times	Coverage/accuracy ranges	Hard copy
1985 Contour Diagrams	1985 (Ref. 16)	13.6	8 global times	Coverage criteria contours	Hard copy
1986 Omega ACCESS	1986 (Ref. 17)	10.2/13.6	8 global times	Coverage criteria contours	Electronic
1991 Matrix Database	1991 (Ref. 18)	10.2/13.6	96 global times	Coverage parameter values	Electronic

Note: an earlier overview of the coverage products is given in Ref. 19.

---

*Since January 1992, several products have been developed including ACCESS II and PACE.

The constant SNR (or SPPD) contour separates the world into two regions: one where the SNR (or SPPD) exceeds the specified threshold value and the other where SNR (or SPPD) does not exceed the threshold value. A station signal is considered usable at a location when the coverage parameters simultaneously satisfy all of the usable signal criteria threshold values. Frequently, the area satisfied by the signal coverage criteria parameters of a station's signal is composed of a large region and few smaller regions (frequently referred to as "islands"). To reduce complexity and clutter, the composite diagrams (each is an overlay of usable-signal region contours of the system's eight stations) show only the largest contiguous region where the criteria are satisfied. That is to say, the coverage parameters are assumed to fail the criteria values in the islands. As a consequence, the contour diagrams provide a conservative estimate of the usable signal region. The composite (full system) contour diagram shows an overlay of the contours bounding the usable-signal regions of each of the eight Omega stations. Electronic display of the 1980/1985 contour diagrams on a personal computer is provided by the Omega ACCESS software package.

The *matrix diagrams* display the ranges of the signal coverage element values for the specified coverage conditions at each of the cells in a matrix of cells covering the globe. The *matrix database*, on the other hand, provides numerical values (rather than the ranges within which the actual value lies) of each of the signal coverage criteria elements as a function of time at each of the cells covering the globe.

Before the Omega system could be declared fully operational[§], the system providers (ONSCEN) needed predicted coverage information for the fully operational Omega system so as to permit the evaluation of the Omega system as a potential replacement for Loran-A and other similar radionavigation systems. In response to this need, in 1974 ONSCEN developed the Omega system coverage diagrams (Refs. 12 and 20) that included a set of the individual Omega station coverage diagrams[†] and a set of the composite diagrams for the full (i.e., planned fully operational) Omega system. These diagrams were produced in hard-copy format for: (1) two representative local times corresponding to potentially "worst" and "best" signal coverage conditions, (2) the primary Omega navigational signal frequency of 10.2 kHz, and (3) the usable signal coverage criteria consistent with the late 1970s Omega receivers.

---

[*] In some coverage products, SPPD has been called $\Delta\phi$, MI (Modal Interference or Possible Significant Modal Interference [PSMI]).

[§] The last of the final configuration Omega system stations, Australia, began operating in 1982.

[†] The individual station diagrams also included diagrams for the Trinidad station which was later decommissioned.

As the Omega system was evolving in the early seventies, there was a marked shift in the Omega user-platform mix, which greatly influenced the types of coverage information produced after the development of the 1974 diagrams. Omega was originally targeted for marine transportation on the high seas. However, the first generation of Omega receivers included bulky, unwieldy units whose operation required the use of Omega PPC tables (hard copy) and hand plotting of data on charts. Thus Omega navigation required slow, tedious, and labor-intensive procedures, leading most marine users to abandon Omega in favor of satellite systems (e.g., TRANSIT, Ref. 21). Aircraft receiver systems, on the other hand, were developed with the second-generation Omega receiver equipment and were specifically tailored for the airborne operating environment. Thus the Omega user community evolved from marine-dominated to airborne-dominated. Consequently, coverage information targeted to the marine users, such as portrayal of local coverage conditions, was reformulated for the airborne users (e.g., coverage under multiple global-time conditions).

Advancing information display technology also changed the format or medium and use of the Omega signal coverage information. The early coverage products were produced in hard-copy format, which was the practical display technology at the time. Because of the complex nature (i.e., a large number of intersecting usable station signal contours) of the diagrams, especially the composite diagrams, users found the hard-copy diagrams difficult to use and/or interpret. As microprocessor development moved forward to make personal computers commonplace, coverage information was developed and disseminated on magnetic media as a software package for use on a personal computer with a color graphics display. This not only allows rapid access and efficient storage but also permits use of the other features, such as toggling among multiple displays and the overlay of displays for different coverage conditions to enhance understanding of the coverage information.

The 1974 diagrams were developed using the best available signal coverage prediction models. Since then, understanding and modeling of the signal propagation medium have significantly improved. Thus, the earlier propagation prediction models have undergone significant improvements over time and now the new models incorporate a physically much more realistic and accurate description of the real-world signal propagation environment.

Due to the changing Omega user population/requirements and improving Omega receiver/display technologies, the later coverage diagrams were developed using the improved coverage prediction models for eight global times and two signal frequencies (10.2 and 13.6 kHz). The eight times were

0600 and 1800 UT hours in the months of February, May, August, and November; they were selected to adequately show the changing coverage with time with a manageable number of diagrams. Signal coverage over the eight global times was found to vary:

- Significantly between the two computed hours for each of the months
- Relatively little between the consecutive coverage months for the same hour.

As a consequence, coverage information for the eight global times was found to be useful, but not adequate to determine coverage between the two computed hours. To fill the substantial gaps in coverage information, a subsequent signal coverage product included all of the 24 UT hours for each of the same four months for which the earlier coverage information had been available.

A detailed discussion of the capabilities and limitations of the coverage products, listed in Table 10.3-1 and derivatives (if any) developed from these products, is given in the following sections. A brief review of the signal coverage prediction models employed to obtain the coverage information for these products is also included.

10.3.2.1 1974 Contour Diagrams* — The diagrams were produced in hard copy and were primarily targeted to marine users. The package of the 1974 diagrams included the individual station diagrams (on the station-centered Azimuthal-Equal-Distance [AED] projection of the world) for each of the eight Omega stations and the composite diagrams (on a Mercator projection of the world) for the full system. The individual station diagrams show the worldwide availability of usable signals from each of the individual Omega stations for the specified coverage conditions, i.e., usable signal criteria and coverage time. The composite diagram is an overlay of the contours bounding the usable signal regions of each system, and displays the worldwide accessibility of the usable signals for the full system for the specified conditions.

The 1974 diagrams were developed for two representative local times and one usable signal access criteria. The two times are local summer noon (LSN) and local winter midnight (LWM) (at each

---

*The diagrams were developed in 1974 and a paper describing them was presented at the Second Omega Symposium of the Institute of Navigation, Washington, DC, on November 5, 1974. Subsequently, the ground conductivity map in the VLF signal propagation prediction code, IPP (Ref. 22), used to develop the coverage information was found to include incorrect values for the low ground conductivity regions of the world. These diagrams were modified in 1975 (Ref. 12) to reflect the correct low ground conductivity values. The paper presented at the symposium (which contains the incorrect diagrams) was subsequently published by the Institute of Navigation in their Spring 1976 volume (Ref. 20).

spatial point in the coverage diagrams). These times correspond to what was then thought to be "worst and best" signal propagation conditions for Omega, in terms of the signal attenuation rate and hence the signal amplitude, and the impact of atmospheric noise on the SNR and signal phase.

In these diagrams, the signal from a station is considered usable at a location and time if the station (assumed operating at the full 10 kW radiated power level) signal satisfies the following signal access criteria:

- Has a short-path SNR $\geq$ –20 dB (in 100 Hz bandwidth)
- Is non-modal; i.e., SPPD (referred to in the 1974 diagrams as PSMI of the short-path signal) is less than or equal to 13 cec.

Note that the 1974 diagrams do not specifically require the usable signal to be either a short-path dominated signal or to satisfy any specific path/terminator crossing angle requirement. Both the SNR and $\Delta\phi$ criteria of the usable signal must be satisfied at every point within a radial path segment at least 1000 km long; the radial segment is along the station radial passing through the desired location. The 1000 km was chosen to assure the availability of usable signals over a reasonable navigation distance/time.

Additionally, the usable signal location is required to be outside the station's antipodal region, which, in these diagrams, is assumed to extend up to 2000 km from the station antipode. This requirement permits reliable tracking of the signal path bearing along the receiver track. In these diagrams, station signals are assumed to be modal for both LSN and LWM conditions in the station near-field region which is assumed to encompass distances of 1000 km from the station.

The computed signal information for the diagrams was developed using a version of the IPP (Ref. 22) algorithm/model/code based on the waveguide-mode theory. IPP provides reliable signal predictions along paths with gradually varying properties. The gradually varying path properties limitation on IPP is due to the fact that IPP ignores mode conversion effects (caused by redistribution of signal energy among the propagating signal's component modes; see Chapter 5) which occur at path points where: (1) either, the path properties have changed abruptly, such as a change from sea water to ice cap along a path transiting through Greenland, or (2) the mode characteristics have changed very rapidly along the path (typically occurring at points along westerly directed paths within the geomagnetic belt* having either a night or transition illumination condition). The atmospheric noise information for the diagrams was obtained from the CCIR noise map (Ref. 23).


*Geomagnetic belt is the geographic region bounded between ±10 deg geomagnetic latitudes.

Note that signal and noise information, as a function of distance (from the station), for each of the individual station diagrams is derived along a minimum of eight station-specific great-circle radial paths (20 Mm long) emanating from the station. This means that the radials have an angular spacing of 45 deg, with additional radials, as necessary, added to provide adequate sampling of the spatially varying ground conductivity around the Greenlandand Antarctic regions, the lowest ground conductivity regions in the world. To exclude the antipodal region of a station from the SNR/$\Delta\phi$-satisfied region, SNR/$\Delta\phi$ is assumed to fail the criteria threshold values inside the antipodal region. The antipodal region in the 1974 diagrams includes radial distances of 2000 km from the station antipode. (A detailed discussion of the methodology and signal coverage prediction models used to develop the diagrams is given in Ref. 12.)

An example of the individual station diagram is shown in Fig. 10.3-1. The example diagram shows four contours, labeled as –20 dB LSN, –20 dB LWM, PSMI-D, and PSMI-N. PSMI-D/N is the "Possible Significant Mode Interference" for all-day (D)/all-night (N) path illumination condition. The –20 dB LSN (or LWM) contour is the contour outside the station antipodal exclusion region, and at any point on the contour the SNR for the LSN (or LWM) condition, is: (1) greater than –20 dB (the SNR criterion value) in the direction towards the station, and (2) less than –20 dB in the direction away from the station. For example, in Fig. 10.3-1, the Liberia Station SNR at the West Coast of the U.S. is less than –20 dB at LSN, and is greater than –20 dB for LWM. The PSMI-D and PSMI-N are the contours separating the modal region from the non-modal region of the station for the indicated local illumination condition: D (Day) and N (Night). For example, the signal at the west coast of the U.S. is modal at nighttime. The usable signal region of a station is the region where the predicted values of both the SNR and PSMI satisfy the usable signal access criteria.

An example of the 1974 composite diagrams is shown in Fig. 10.3-2, which depicts the 10.2 kHz signal coverage of the full Omega system (all eight Omega stations operating at the full 10 kW radiated power level) at the assumed local summer noon illumination condition. In this figure, the combinations of the usable 10.2 kHz stations signals that are accessible at any point at the local summer noon is indicated by the set of letters found in the contours enclosing that point. For example, from the figure it can be seen that at local summer noon, the expected coverage in San Francisco is from Omega stations: C (Hawaii), D (North Dakota), and H (Japan). Some smaller regions just have a number indicating how many usable signal stations can be assessed in that region, but those stations can be readily determined. Each of the contours in the diagrams is labeled with an appropriate station with an arrow in the direction of the accessibility for the usable signal from the indicated station. For example, at the 40°S and 180°W
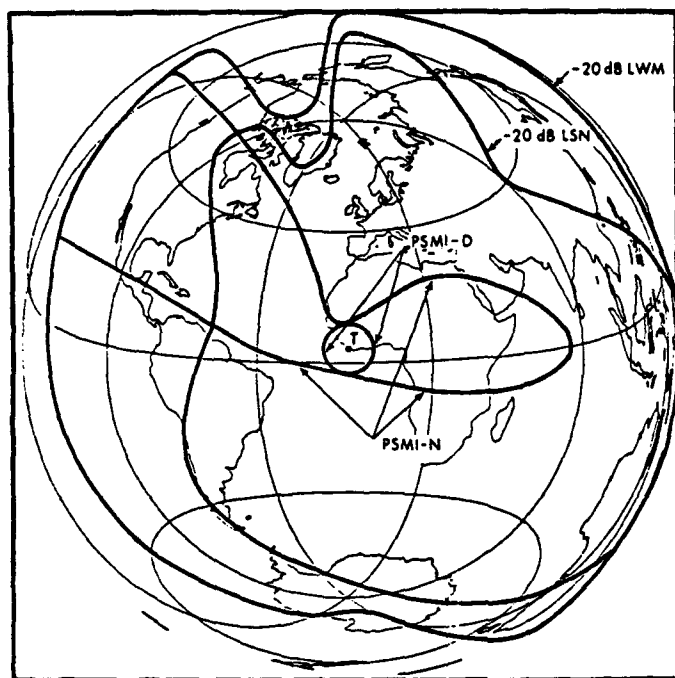
Figure 10.3-1 Example of Individual Station Signal Coverage Diagrams: Liberia (B)
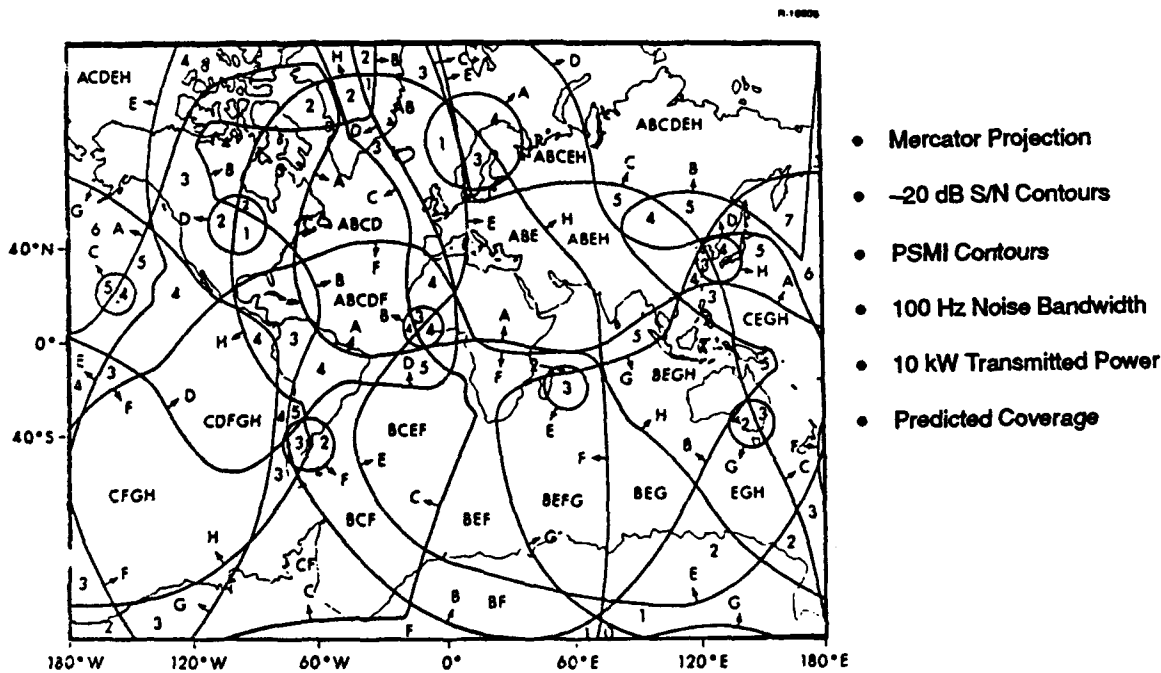
Figure 10.3-2 Example of 1974 Composite Signal Coverage Diagrams: Local Summer Noon

location, there are five usable stations: C, E, F, G, and H. Note that the small circular region around each station is the "near-field" region where the station signals are assumed modal and not usable. Because the composite diagrams include many contours, they have been nicknamed "*spaghetti diagrams.*"

The coverage information in the diagrams has not been validated with observations because the required observations were not available at the time. Although the 1974 contour diagrams were useful to assess the potential coverage capabilities of the Omega system, they did not find wide acceptance among Omega users because of extremely restrictive solar illumination conditions.

10.3.2.2 1980/1985 Contour Diagrams — The 1980 and 1985 sets of the diagrams are the 10.2 and 13.6 kHz Omega signal coverage diagrams developed for ONSCEN in 1980 (Refs. 9, 13, 24, and 25) and 1985 (Refs. 16 and 26), respectively. Because both the 10.2 and 13.6 kHz diagrams have almost the same attributes (e.g., content, display format, coverage times, and usable signal access criteria) and employ similar methodology and models to generate the diagrams, they are discussed here as a group.

The 1980 and 1985 set of diagrams includes individual station and composite diagrams. These diagrams display the worldwide accessibility of the usable 10.2 kHz signals (1980 diagrams) or 13.6 kHz signals (1985 diagrams) from the Omega stations, each operating at the full 10 kW station radiated power level, for: (1) each of eight global times of the year, and (2) usable signal access criteria appropriate for moderate-performance (M-P) receivers. In addition to the M-P receiver usable signal access criteria, the 1980 diagrams also provide the usable 10.2 kHz signal coverage information for the usable signal access criteria appropriate for high-performance (H-P) receivers. The moderate- and high-performance receivers are those with the SNR (in a 100 Hz bandwidth) detection threshold levels of −20 dB and 30 dB, respectively.

For both the 1980 and 1985 sets, the diagrams are provided for 0600 and 1800 UT hours in the months of February, May, August, and November. The total number of times for which the coverage diagrams could be provided was limited due to the high cost of developing the coverage information and also the need to keep the total number of (station and composite) diagrams available to the users to a manageable number. The specific coverage display times were selected to choose the same UT pair (two UT hours spaced 12 hours apart) in each of the four months (spaced three calendar months apart) of the

year, which minimized the adverse effects of the day/night terminator* on the Omega signals. Therefore the terminator had to be as far away as possible from all of the system stations for the selected times. The smallest station-to-terminator distance for the selected eight times was greater than 700 km.

The individual station coverage diagrams (see Fig. 10.3-3) in each of the 1980 and 1985 sets display the station and composite coverages on a Mercator projection of the world. The Mercator diagram shows coverage in the low- and mid-latitude regions from 60°S to 80°N latitude. The individual station coverage in the non-displayed regions (80–90°N, 60–90°S) in a Mercator diagram is easily inferred from the displayed regions of the world. However, since the composite diagrams overlay the contours bounding the individual station's usable-signal regions, they are quite cluttered (many contours) and the coverage in the non-displayed regions cannot be reliably inferred from the coverage shown in the Mercator composite diagrams. Therefore, composite diagrams for both sets were developed for two additional projections of the world. These projections are: (1) a North Pole-centered AED map of the world (see Fig. 10.3-4a) showing the composite coverage of the Omega system in the northern polar region from the North Pole to 55°N latitude, and (2) a South Pole-centered AED map of the world (see Fig. 10.3-4b) showing the composite coverage of the system in the southern polar region from the South Pole to 55°S latitude.

In these diagrams, a signal from an Omega station, operating at the full 10 kW radiated power level, at a location and time is considered usable if the signal satisfied the following usable signal access criteria:

- The short-path SNR (in a 100 Hz bandwidth) exceeds or equals:
    a. −20 dB ("M-P SNR criterion")
    b. −30 dB ("H-P SNR criterion")

- The short-path signal is non-modal, i.e., the short-path signal is Mode 1 dominated and the SPPD ($\Delta\phi$) does not exceed 20 cec.[§]

Furthermore, the signal must satisfy both the SNR and $\Delta\phi$ usable signal criteria at every point within a radial path segment of the specified length containing the point. The length was chosen to be 1000 km

---

* The day/night terminator along a path is defined as the location along the path where the solar zenith angle is 90 degrees.

[§] The 1974 diagrams were developed with $\Delta\phi \leq 13$ cec which was subsequently considered to be very conservative; therefore, the later diagrams (e.g., 1980 and 1985 diagrams; see Table 10.3-1) were developed with $\Delta\phi \leq 20$ cec.

for the 1980 diagrams (same distance as in the 1974 diagrams). This length was later considered to be insufficient to provide reliable navigation over a reasonable distance/time. Therefore, in the 1985 diagrams, the length was increased to 2000 km. In addition, the usable signal location was limited to be outside the station antipodal region which was assumed to extend outward from the station antipode up to 1000 km*. The 1980/1985 diagrams did not specifically require the usable signal to be either a short-path dominated signal or to satisfy any specific path/terminator crossing angle criterion.

The 1980 diagrams were developed for use by both the moderate-performance (M-P SNR criterion) and the high-performance (H-P SNR criterion) receivers. However, because most of the available Omega receivers were designed for –20 dB SNR detection threshold level (the M-P SNR criterion), the 1985 diagrams were produced for only the M-P SNR criterion.

Both the 1980 and 1985 diagrams were generated using the following signal and noise prediction models:

- The amplitude (needed to form the SNR) of a station short-path signal as a function of location and time is based on specially developed 10.2 and 13.6 kHz semi-empirical signal prediction models§ (Refs. 27 and 28).

- Atmospheric noise amplitude (needed for the SNR) as a function of location and time is determined using the WGL/NRL-developed atmospheric noise prediction model[†] code documented in Ref. 29.

---

* In the 1974 diagrams, the antipodal region extended up to 2000 km from the antipode. This distance was later considered to be too conservative (large). Therefore, the 1980 and 1985 diagrams were developed for the antipodal region extending up to 1000 km from the station antipode.

§ The semi-empirical signal amplitude prediction models assume the signal to be a purely Mode 1 signal, which is true at most locations and times. Each model combines the day and night spatial sub-models of Mode 1 signal with an empirically derived diurnal sub-model. The combined 10.2/13.6 kHz model provided the signal amplitude of the 10.2/13.6 kHz signal as a function of location and time. The spatial sub-models incorporate the day and night functional dependencies of the signal amplitude on the signal path properties for the day and night illumination conditions. The diurnal sub-model is a solar zenith angle-dependent sub-model describing the change in signal amplitude with time of day (solar zenith angle).

† The model developed by Westinghouse Geophysics Laboratory (WGL) and the Naval Research Laboratory (NRL) is a semi-empirical model (Refs. 30 and 31) based on a worldwide thunderstorm and lightning activity data and the waveguide-mode theory propagation concepts applied to propagation of noise signals from the centers of thunderstorm and lightning activity in the world. The model has been reported (Ref. 32) to provide much more realistic noise predictions than the CCIR Report (Ref. 23). The CCIR-provided noise information was used in the 1974 diagrams.

- For each station, the modal/non-modal characterization of the short-path signal as a function of location and time is obtained by:
    1. Using the IPP model (Ref. 22) for an assumed worldwide idealized nighttime illumination condition
    2. Applying the "⅓–⅔" empirical rule (Ref. 26) to the nighttime modal/non-modal characterization at each location to provide the time-specific non-modal/modal characterization.

The ⅓–⅔ rule considers the signal from a station (T) at a location (P) and the time t to be modal if: (1) the signal path TP (station T to location P) is more than one third in darkness, and (2) the signal at P is expected to be modal when the entire TP path is in darkness; otherwise the signal at P at the time t is assumed to be non-modal. The signal coverage information for each of the Omega system stations was obtained as a function of radial distance from the station along the station-specific set of radial paths, each 20 Mm long. The set included 24 radials emanating from the station at 0, 15, 30, . . . 345 degrees and several additional radials, interspersed between the 24 radials, to provide adequate sampling of the changing ground conductivity around Greenland and Antarctica. The signal and noise models used for these diagrams were the most realistic models that were available or could be developed from then-available models.

Both the 1980 and 1985 diagrams have been validated with a limited set of the available empirical coverage data collected under ONSCEN's Omega Regional Validation Program (Ref. 33) and some of the data collected by the network of fixed Omega signal monitoring sites maintained by ONSCEN. These diagrams, though sparsely validated with empirical data, have proven to be quite reliable and valuable to Omega users. Their useful and reliable guidance to Omega users in the selection of usable signal stations provides more accurate navigation and position information than had been available in the past. A serious drawback of these diagrams is the limited number of times for which the coverage information is provided (the two UT hours during the day) because this information cannot be reliably interpolated across the coverage hours.

The content and display format of the 1980 (10.2 kHz) and 1985 (13.6 kHz) signal coverage diagrams are the same; therefore, only samples of 1985 individual station and composite diagrams are shown in Fig. 10.3-3, and Figs. 10.3-4a, b, and c. Figure 10.3-3, an individual station diagram, displays the –20 dB SNR threshold level* (and, in addition, the –30 dB SNR threshold level in the 1980 diagrams), and the 20 cec $\Delta\phi$ boundary. The SNR contour in the diagrams is displayed by a solid line while

---

*If the SNR/$\Delta\phi$ threshold level boundary extends inside the antipodal region boundary, the displayed SNR/$\Delta\phi$ threshold level boundary is cut off at the station antipodal region boundary (which begins at 19 Mm from the station).

the $\Delta\phi$ contour is shown by a dashed line. In these diagrams, the predicted SNR is above (or $\Delta\phi$ is below) the indicated threshold level on the side of the contour in the direction of the arrow. For example, in Fig. 10.3-3, north of Rio de Janeiro, the SNR of the Norway station 13.6 kHz signal in February at 0600 UT hour is shown to be greater than –20 dB while south of Rio de Janeiro, the SNR coverage is shown to be less than –20 dB. The SPPD, $\Delta\phi$, of the Norway 13.6 kHz signals (see Fig. 10.3-3) in and around Brazil is shown to be greater than 20 cec. The usable signal coverage regions of a station are the regions where both the SNR and $\Delta\phi$ threshold criteria are satisfied. For example, near the Norway station within the dashed contour (see Fig. 10.3-3), Norway signals are unusable because $\Delta\phi$ is predicted to be greater than the threshold level of 20 cec even though the SNR at this point is predicted to be greater than –20 dB.

The composite diagrams display the worldwide availability of usable signals for the specified coverage conditions. Examples of the composite diagrams in the three map projections are shown in Figs. 10.3-4a, 10.3-4b, and 10.3-4c. In a composite diagram, the combination of usable signals available in a region is indicated by the set of letters within the contour enclosing the region. For example, in the
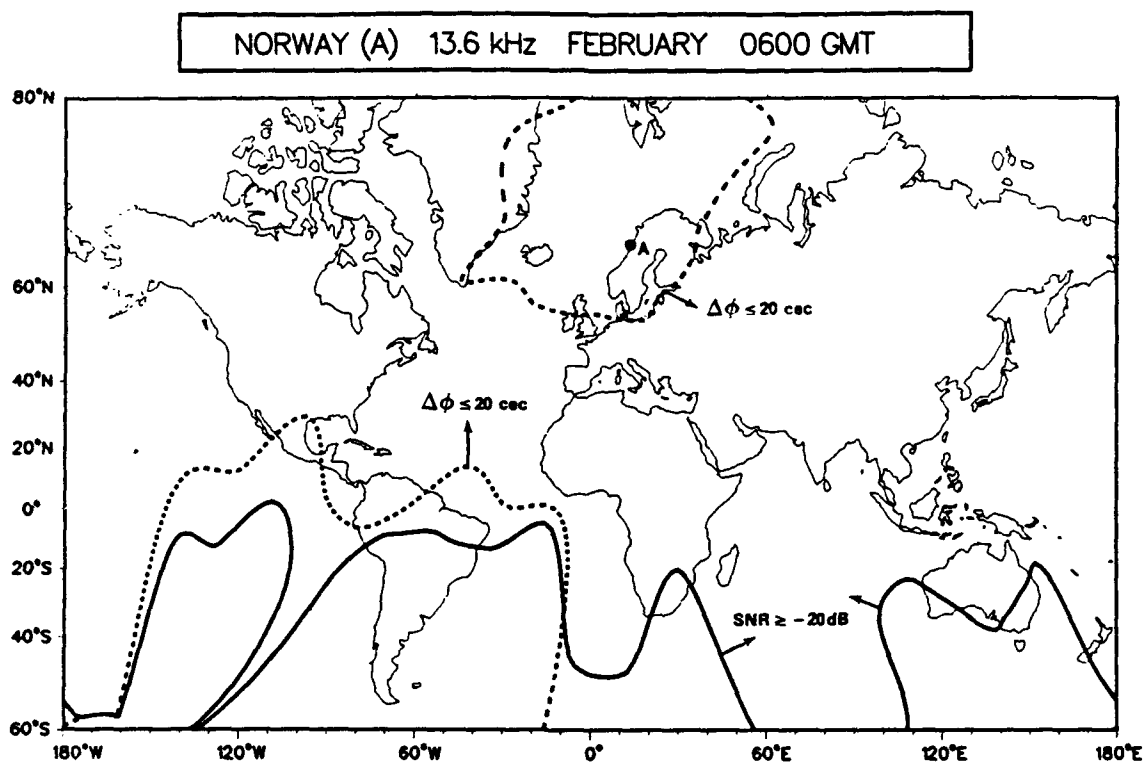
Figure 10.3-3 A Sample of the 1985 Individual Station Coverage Diagram: Norway Station

composite diagram shown in Fig. 10.3-4a, the expected coverage in Iceland is from stations B, C, D, E, F, and H. Like the 1974 diagrams, some regions display a number indicating the total number of usable signals predicted to be accessible in that region. The corresponding stations, are readily determined because each coverage contour is labeled with a station designator and an arrow in the direction of the accessibility of the usable signal from the labeled station. For example, the region bounding the La Reunion station in Fig. 10.3-4a is labeled with a number 5. The coverage in this region is from stations A, B, F, G, and H.

The composite diagrams, in addition to displaying the accessibility of the usable signals from the system, identify regions of the world where none of the three-station combination(s) in the regions having three or four usable signals have a three-station hyperbolic navigation position-fix geometry with an associated GDOP value less than the specified threshold value. These regions are shown as shaded areas in the diagrams. The GDOP threshold level for the 10.2 kHz and 13.6 kHz diagrams were selected to be 1.0 km/cec and 0.5 km/cec, respectively. The GDOP value of 1 km/cec means one kilometer of rms radial position error per centicycle of the standard deviation of the phase-difference error. Note that the GDOP
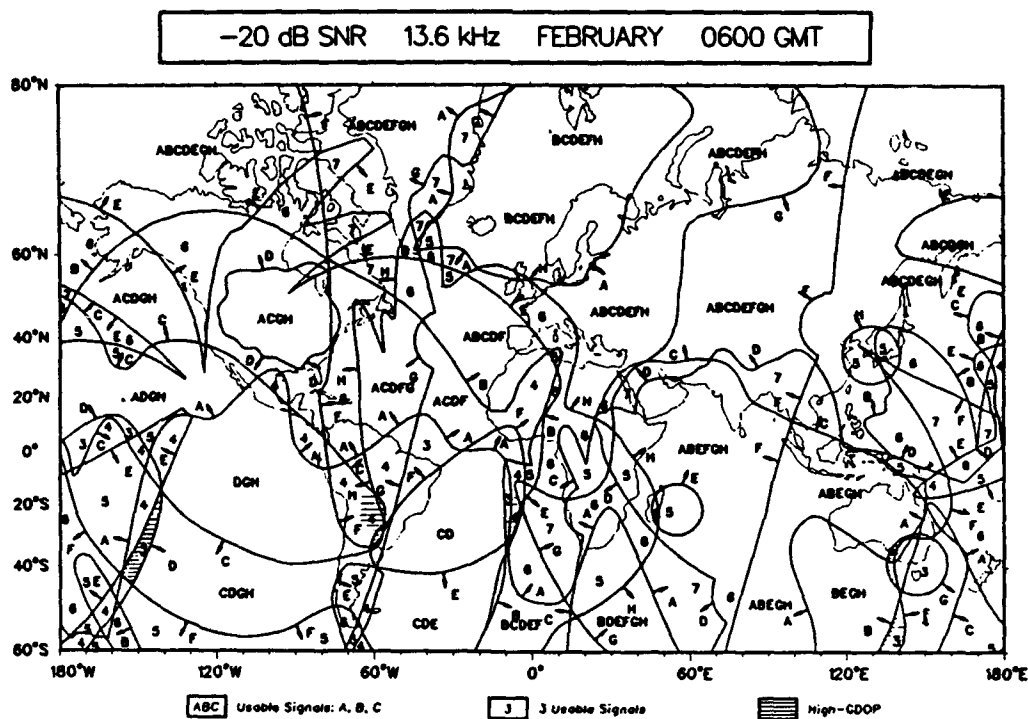
a) Mercator Projection

Figure 10.3-4   Sample 1985 Composite Diagrams
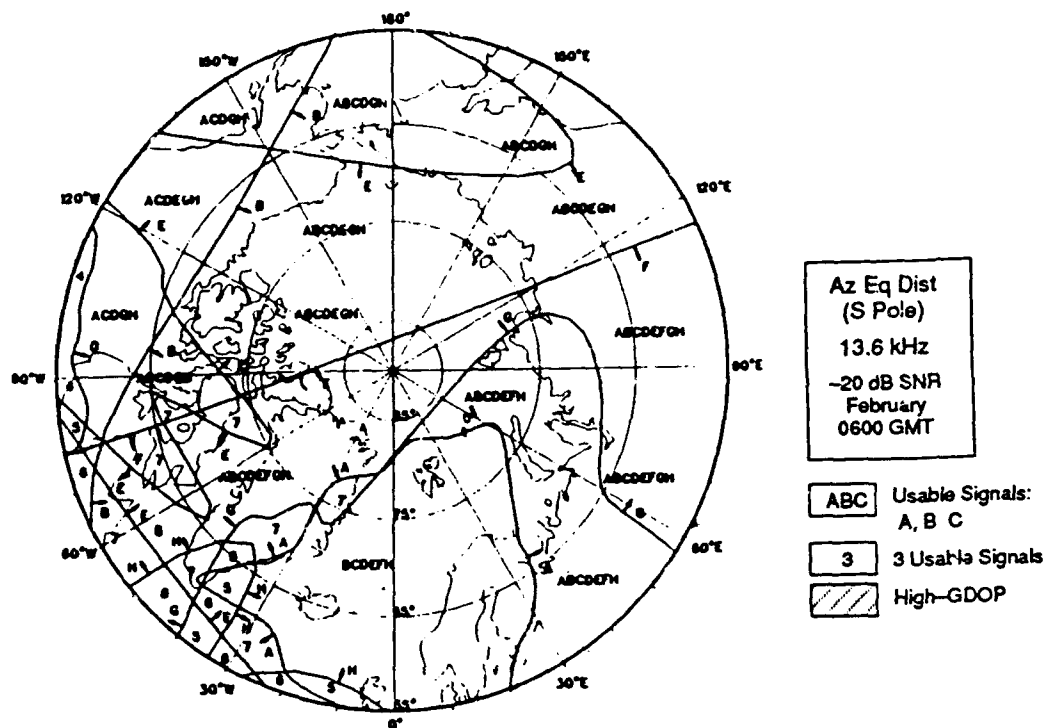
b) North Pole-centered Azimuthal Equidistant Projection
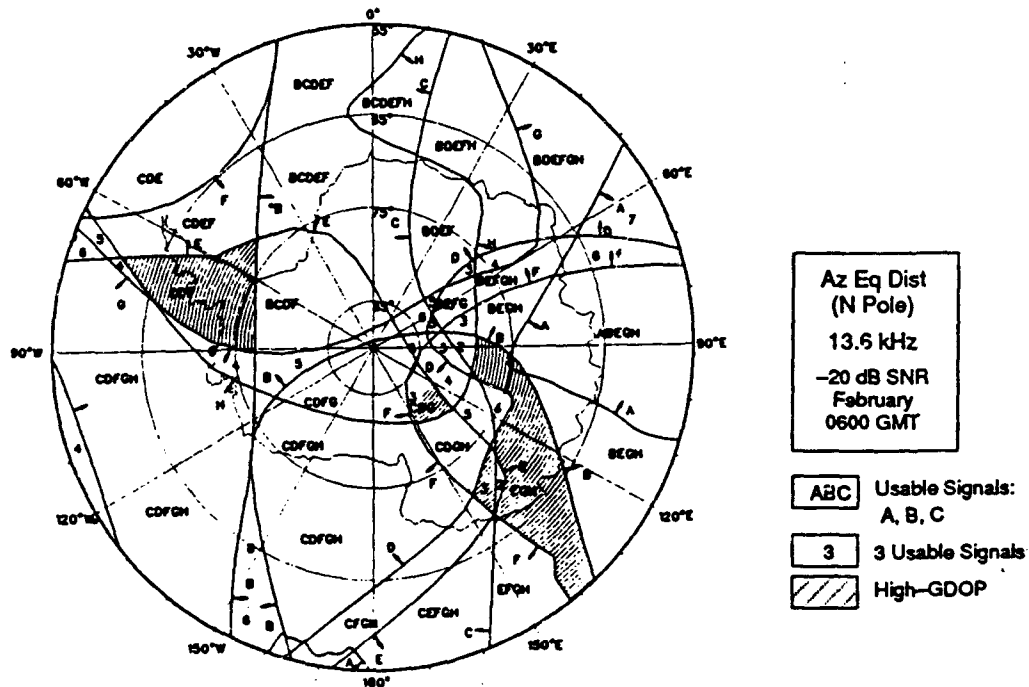
c) South Pole-centered Azimuthal Equidistant Projection

Figure 10.3-4 Sample 1985 Composite Diagrams (Continued)

Table 10.3-2   10.2 kHz Omega Station Deselection Chart

			RECOMMENDED DESELECTIONS						
			WRONG-WAY PATH†			MODERATE INTERFERENCE†		SEVERE INTERFERENCE†	
GEOGRAPHIC LOCATION	PREFERRED STATIONS	POLAR PATHS*	STATION	INTERVAL (GMT)§ SUSPECTED	INTERVAL (GMT)§ REPORTED	STATION	INTERVAL (GMT)§	STATION	INTERVAL (GMT)§
1. Bermuda	A, D, F	H	E	0600–1800	1000–1400	B F	2200–0700 2200–1000	E	1400–1000
2. Boston, MA	C, D, F	A, H	E	0600–1800	1100–1400	B F	2300–0700 2300–1000	B E	0700–1100 1900–2300 1400–1100
3. Eglin AFB, FL	A, C, D	A, H	E	0700–1900	1200–1400	B	2400–0700	B E F	0700–1200 1900–2400 1400–1200 2200–1200
4. Fairbanks, AK	A, D, H	All						F	2200–1600
5. Holloman AFB, NM	C, D, H	A	B E	1300–1900 0700–1900	1300–1400	B	1900–1300	E F	All Times 2200–1300
6. Seattle, WA	C, D, H	A, E	B F	1400–1900 1400–2300		B	0200–0700	B F	0700–1400 1900–0200 2200–1400
7. Buenos Aires, Argentina	C, E, G	G				F	All Times	A B	1700–1000 1900–1000
• • •									
23. Bombay, India	A, B, E	D	C G H	2000–0800 2200–1000 0100–0900	0100–0400			C G	0800–2000 1000–2200
24. Djakarta, Indonesia	B, E, G	A	C	1900–0700	2300–0400			C F H	0700–1900 All Times 0900–2300
25. Midway Island	A, C, H	A	F	1400–0200	1800–2200			B F	All Times 0200–1400
26. Nagasaki, Japan	A, G, E	A	D F	2100–2400 1500–0300	2100–2200	C H	0400–2100 All Times	F	0300–1500

*Deselect only during PCD.
§Times are approximate and vary seasonally (see text).
†All entries for station G are based solely on theoretical predictions.
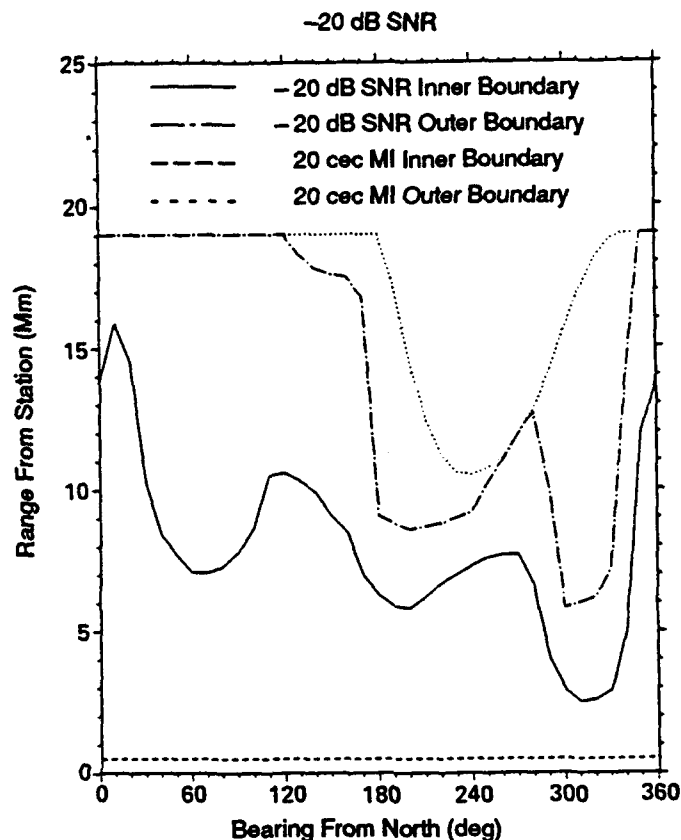
Figure 10.3-5 Range-Bearing Plot of Extreme SNR and MI Contours: 10.2 kHz

This combination reduced the number of the individual station diagrams from 64 to 32 "combined diagrams." The combined diagrams were obtained by overlaying the 1980 individual station diagrams of the appropriate months. For example, the combined April-September/0600 GMT diagram was obtained by overlaying the SNR and $\Delta\phi$ threshold level contours contained in the May/0600 GMT and August/0600 GMT diagrams. Note that in the combined diagrams, e.g., in the April-September/0600 GMT diagram, the SNR or $\Delta\phi$ signal coverage access criterion at a location is satisfied only when the criterion is satisfied both in the May/0600 GMT and August/0600 GMT 1980 diagrams; otherwise, the criterion is considered to be not satisfied.

These diagrams show the accessibility of the usable signals based on both the –20 dB and –30 dB SNR (in 100 Hz bandwidth) threshold criteria and the 20 centicycles modal interference-induced phase deviation criterion. Figure 10.3-6 is an example of the DMAHTC-developed diagram. In this example, the Norway signals in Darwin, Australia, during April-September at 0600 GMT, are shown to have the SNR between –20 dB and –30 dB and the phase deviation less than 20 centicycles.
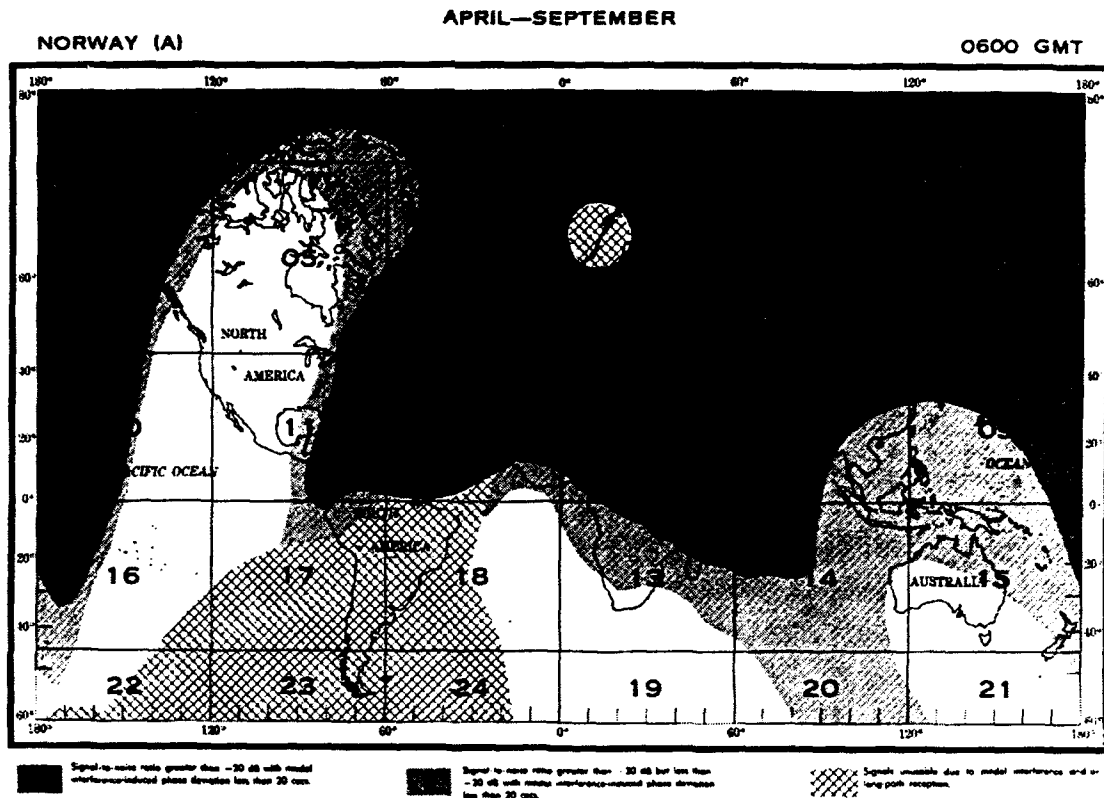
Figure 10.3-6   Example of the DMAHTC-developed Coverage Diagrams

Nighttime Modal Diagrams — The development of the time-specific (96 times) modal/non-modal signal information for the 1980 and 1985 coverage diagrams required development of the night-time modal/non-modal information for the individual Omega stations. This information has since been packaged (in hard copy) separately as the "individual station nighttime modal interference diagrams" (Refs. 9 and 26). The 1980 (10.2 kHz)/1985 (13.6 kHz) nighttime modal interference diagrams identify geographic regions of the world where the specified 10.2 kHz (13.6 kHz) Omega station signals are expected to be non-modal/modal for the assumed worldwide nighttime illumination conditions. Note that the modal/non-modal condition along a path generally varies with the illumination condition along the entire path and it is (usually) more severe when the path has nighttime (full dark) condition. Thus any region identified to be non-modal for a given station signal is likely to remain non-modal for most other conditions along the path. Thus, nighttime modal interference diagrams provide a conservative guidance for deselection of potentially modal signals from the Omega system. Based on these diagrams, in 1985 Gupta *et al.* published the combined 10.2 and 13.6 kHz individual station nighttime modal interference diagrams (Ref. 39). Figure 10.3-7 is an example of the combined 10.2 and 13.6 kHz nighttime modal interference diagram. In this diagram, the signals are predicted to be non-modal everywhere
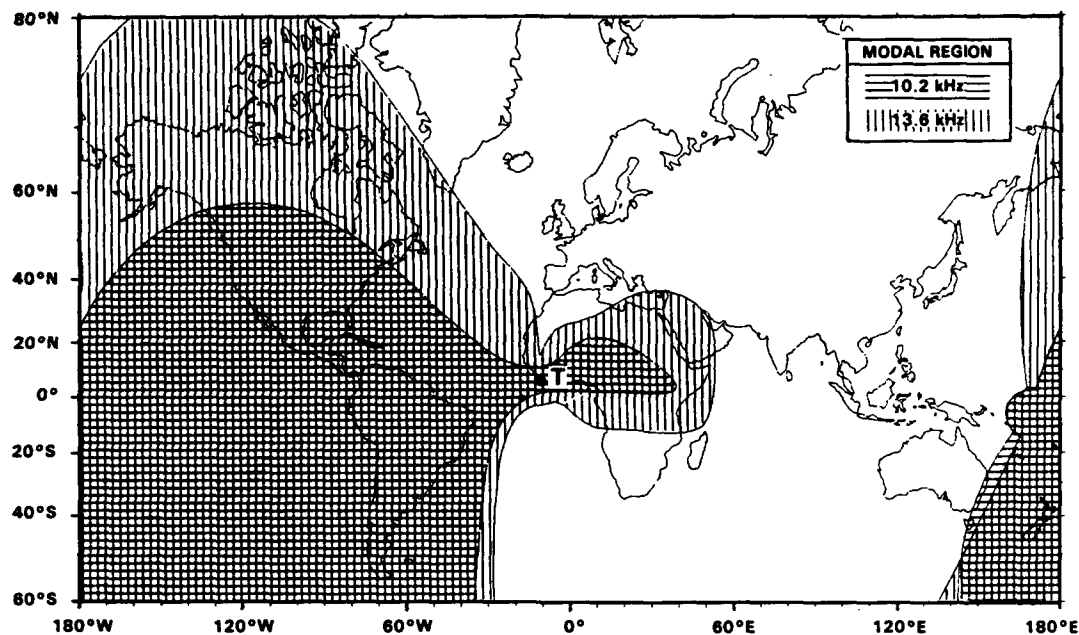
Figure 10.3-7 Example of the Combined 10.2 and 13.6 kHz Nighttime
Modal Interference Diagram: Liberia Station

except in the shaded regions. Note, for example, in Montreal (Canada), the Liberia station 10.2 kHz
signals are non-modal while the 13.6 kHz signals are modal.

Omega Station Deselection Chart — Based on the coverage information contained in the
1980 and 1985 coverage diagrams, Morris *et al.* (Ref. 40) developed a chart (see Table 10.3-2)
containing a guide for deselecting unusable Omega station signals as functions of time of day at 79
locations around the world (see Fig. 10.3-8). Table 10.3-3 shows selected parts of the chart. At each
location, the unusable signal stations are identified along with the potential cause(s) (e.g., long-path,
modal condition) of the signal unusability. In addition, at each location, the table lists the station(s)
whose signal path(s) (to the location) traverse the polar region. The polar paths are recommended to be
deselected during a PCD.

10.3.2.3 1983 Matrix Diagrams — In 1983, Swanson (Ref. 14) published a set of 10.2 kHz
signal coverage/accuracy diagrams for the individual Omega stations and the full Omega system for the
idealized day and night conditions, using a "parametric approach." This approach uses a two-mode
(Modes 1 and 2) parametric model (based on the IPP model; Ref. 22) for signal amplitude and signal
modal condition predictions, and the model has since been extended to provide 10.2 kHz coverage
predictions for the fixed global times (Ref. 15). The parametric model does not fully characterize the
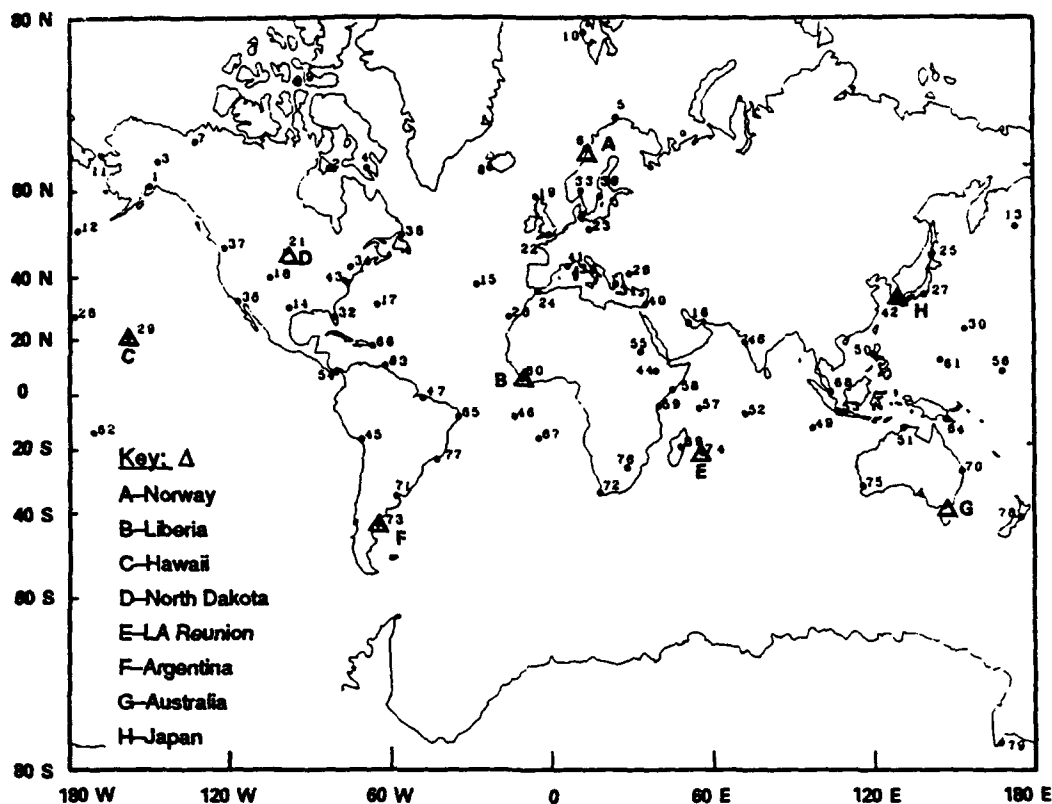
Figure 10.3-8   Geographic Locations of the Sites Contained in Table 10.3-3

nighttime, trans-equatorial propagation effects along westerly paths, as predicted by IPP. Furthermore, the signal phase deviation predictions (and hence modal predictions) ignore mode conversion effects occurring at the path/terminator discontinuity along a mixed path.

Individual station signal coverage information is provided at worldwide (10 deg latitude by 10 deg longitude) grid points (see Fig. 10.3-9) where the notation on each grid point indicates limitations (if any) on the station signal usability due to signal-to-noise ratio, modal interference, long-path interference, and antipodal effect. In this figure, note that the North Dakota signals in Australia are shown to be "perturbed" (i.e., slightly modal) but are indicated to be usable. The individual station coverage information has been combined with the expected random errors (ignoring bias errors) in the signal phase measurements, based on the Morris/Swanson PPC prediction model (Ref. 5), to develop the Omega system accuracy diagrams. The position-fix accuracy available from the full system is indicated at the worldwide latitude-longitude grid points. An example of a system accuracy diagram of this type is

Table 10.3-3   Omega Station Deselection Chart

GEOGRAPHIC				RECOMMENDED DESELECTIONS		
REGION	LOCATION	LAT* (deg)	LON (deg)	POLAR§	NIGHTTIME MODAL	NIGHTTIME MODAL/ DAYTIME LONGPATH
Arctic (LAT > 60 °N)	1. Anchorage, AK, USA	61	−150	A, B, D, E		F
	2. Coral Harbor, Canada	64	−83	A, B, C, D, E, F, G, H	F	
	3. Fairbanks, AK, USA	65	−147	A, D, E, H		B, F
	⋮					
	11. Wales, AK, USA	66	−168	A, B, D, E		F
Northern Mid-Latitude (20° N < LAT < 60 ° N)	12. Adak, AK, USA	52	−177	A, B		F
	13. Attu, AK, USA	53	173	A, B		F
	14. Austin, TX, USA	31	−98		B, F	A, E
	⋮					
	43. Washington, DC, USA	39	−77	A, H	B, D, F	
Equatorial (20° S < LAT < 20° N)	44. Addis Ababba, Ethiopia	9	39	D		B, C, G, H
	45. Arequipa, Peru	−16	−71	H	B, F	E
	46. Ascension, Is., UK	−8	−14	G	A, B, E	
	⋮					
	69. Tananarive, Madagascar	−19	48	D		C, E
Southern Mid-Latitude (20° S < LAT < 60° S)	70. Brisbane, Australia	−27	153	A, B	C, G	F
	71. Buenos Aires,* Argentina	−35	−58	G	B, E, F	A
	72. Cape Town, South Africa	−34	18			C, H
	⋮					
	78. Wellington, New Zealand	−41	175	A, E	C	B, D
Antarctica (LAT > 60° S)	79. McMurdo, USA	−78	167	A, B, C, D, E, F, G, H	E	

*Note that "LAT" denotes the geographic latitude.

§Deselect during PCD.

10-45
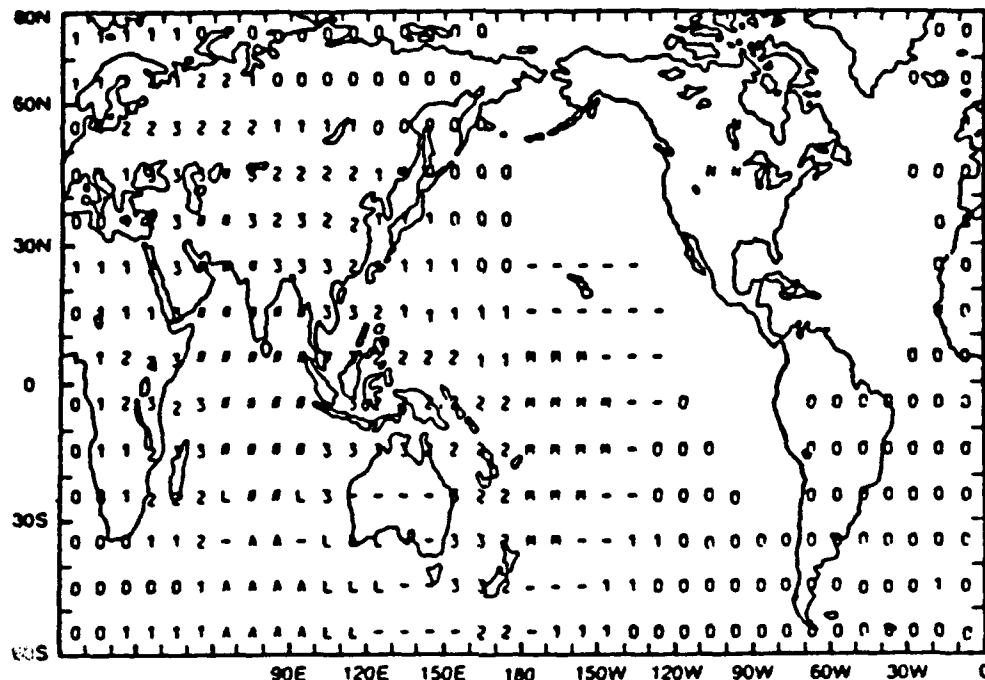
(Key for Coverage Display: M - Modal Interference, L - Long-path Interference, N - Near-field Region, A - Antipodal Region, - - Signal is moderately perturbed by modal/long-path interference but can be used if needed, (Blank) - SNR > 0 dB, 0 - 0 ≥ SNR > -10 dB, 1 - -10 ≥ SNR > -20 dB, 2 - -20 ≥ SNR > -30 dB, 3 - -30 ≥ SNR > -40 dB, # - SNR ≤ -40 dB; note that SNR is in 100 Hz Bandwidth).

Figure 10.3-9 Example of Matrix Diagram showing the Station Coverage for North Dakota at 0600 UT (vernal equinox)

shown in Fig. 10.3-10, in which the system accuracy at 10.2 kHz is predicted to be one nautical mile everywhere in Australia except in the southeast portion of the country where the accuracy is predicted to be two nautical miles.

Swanson's matrix diagrams add a dimension of information not included in the earlier published diagrams (1980 and 1985) because Swanson's diagrams show the presence of (undesired) strong-amplitude long-path signals that may interfere with or dominate the (desired) short-path signals. Although a number of the matrix diagrams displaying the individual station coverage and Omega system accuracy have been published by Swanson for 10.2 kHz signals, a full set of the matrix diagrams is not available to provide worldwide coverage/accuracy guidance as a function of time.

10.3.2.4 Omega ACCESS — Because of the spatial and temporal complexities of system coverage, the extensive information contained in the hard-copy diagrams could not be readily and effectively used for side-by-side comparison of the coverage information for alternative coverage scenarios.
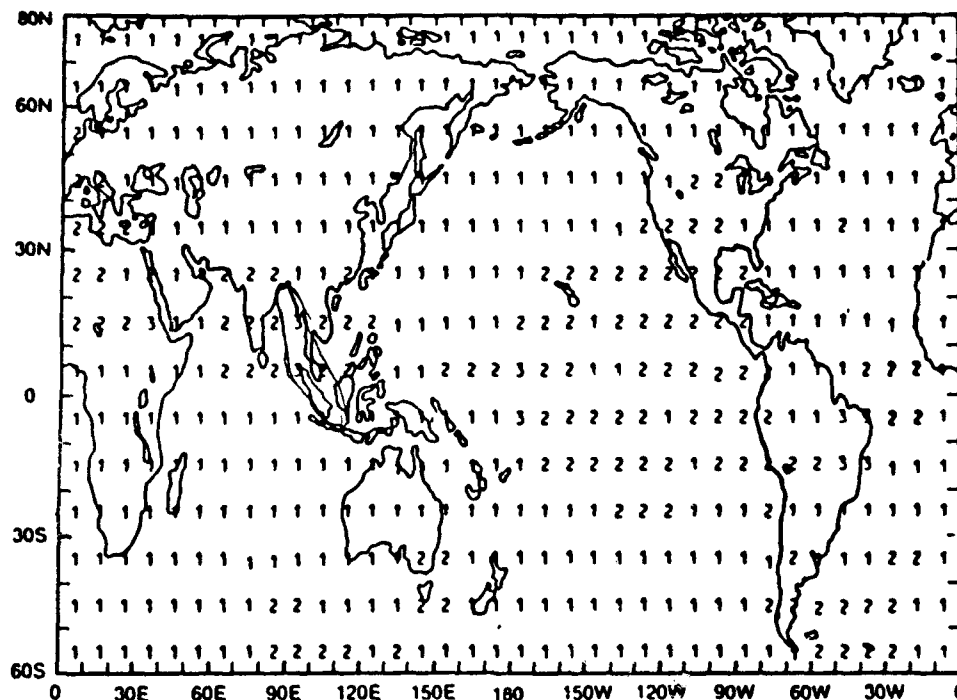
*Numbers show median accuracy in nautical miles, cep.

Figure 10.3-10   Example of Matrix Diagram showing the
24-hour System Accuracy at 10.2 kHz

This led to the development (Ref. 17) of an electronic display for the signal coverage, called Omega ACCESS (Automated Composite Coverage Evaluator of System Signals). Figure 10.3-11 presents an overview of Omega ACCESS. It displays coverage data in several world map projections (Mercator, polar, station-centered AED, etc.), and allows an Omega ACCESS user/analyst to answer a wide variety of "what-if" coverage questions related to changing coverage conditions.

The coverage database incorporated in Omega ACCESS is the same, except for some minor adjustments, as that used by Gupta *et al.* to develop the 10.2 kHz (Ref. 13) and 13.6 kHz (Ref. 16) signal coverage diagrams. These adjustments were applied to 10.2 kHz signal coverage contours in the South Atlantic region to reflect the Omega validation program results in the region. In addition to nominal (10 kW) station radiated power coverage data, Omega ACCESS provides coverage information for reduced station power conditions. Specifically, coverage diagrams are provided for: (1) a 6 dB reduction (from the nominal) in the radiated power level of each Omega station except the Japan station, and (2) reductions of 2, 4, 6, 8, and 10 dB in the Japan station radiated power level.
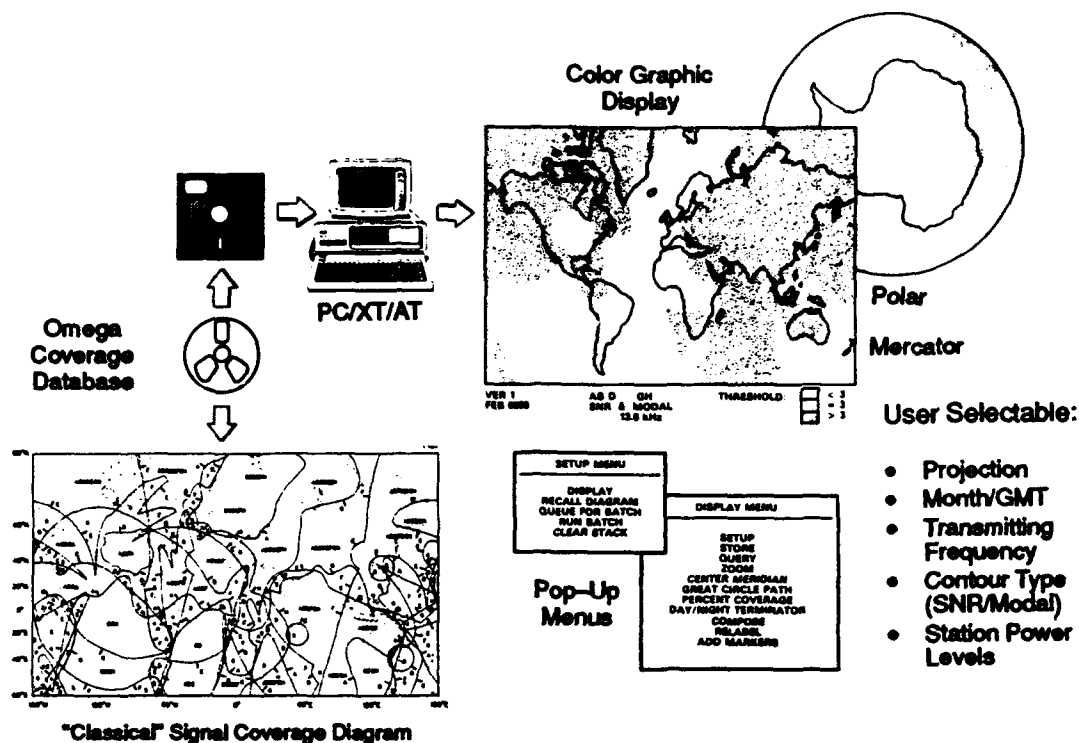
Figure 10.3-11   Overview of Omega ACCESS

10.3.2.5 1991 Matrix Database — The matrix database is a 24-hour/4-month/2-frequency/cell-format database of Omega signal coverage elements needed to establish the usability of the 10.2 and 13.6 kHz Omega system station signals as functions of location (cell) and time (UT hour and month). The database was developed (Ref. 11) for use in the PACE (Performance Assessment and Coverage Evaluation) workstation developed for ONSCEN (Refs. 41 and 42). The workstation assesses the expected availability of the Omega system signals for the globe, a region (group of cells), or cell at a given time (Refs. 41–44).

The database consists of individual station signal coverage elements for each combination of:

- Station (each of the eight Omega stations)

- Time (each of the 96* times)

- Cell (each of the 444 cells covering the entire globe)

- Signal frequency (each of 10.2 and 13.6 kHz).

---

*96 = 24 (UT hours) × 4 (months).

§ SNR in a 100 Hz bandwidth.

The individual station signal coverage elements[§] are:

- Short-path SNR (SPSNR)
- Ratio of SPSNR and long-path SNR (LPSNR)
- Short-path phase deviation (SPPD)
- Mode 1 dominance margin (M1DM)
- Path/terminator crossing angle (PTCA).

Note that PTCA is independent of signal frequency. In addition, at each of the locations (cell-centers), the database contains a set of 219 GDOP values associated with the 219 possible combinations of three or more Omega stations. Because the modal character of a signal can be readily established from the M1DM parameter given in the database (which was not available in the earlier coverage diagrams/ databases), the SPPD parameter is no longer needed to establish the modal character of a signal. The SPPD values in the database are included for information only.

An Omega station signal at a given signal frequency, time, and (cell-center) location (by inference, the entire cell) is considered usable if the following criteria are satisfied:

1. SPSNR exceeds the receiver SNR signal detection threshold (typically –20 dB in 100 Hz noise bandwidth) so that the receiver provides accurate signal phase measurements

2. SPSNR exceeds LPSNR (typically by 6 dB) so that the signal is short-path-dominated signal

3. M1DF exceeds, or equals 6 dB so that the signal is non-modal

4. PTCA exceeds the threshold value (typically 5 deg, Ref. 7) so that any possible terminator-induced signal reflections/refractions are relatively insignificant.

Note that GDOP values are provided to determine the navigation accuracy of the available Omega signals (three or more stations), e.g., station combinations with a GDOP value* of six or less are expected to provide reasonable navigation accuracy at most locations and times, provided the station signals are usable.

Database Attributes — The database contains computed signal quantities required to establish the usability of the 10.2 and 13.6 kHz Omega signals as functions of location and time. The data is spatially referenced to the centers of a worldwide-distributed matrix of 444 cells (Table 10.3-4). Each

---

*The GDOP value is based on the single-phase GDOP formula given in Refs. 44 and 45. For a three-station navigation geometry, Eq. 10.2-4, which is also a single-phase GDOP equation, provides the same GDOP values as that provided by the GDOP formula in Ref. 44.

Table 10.3-4   Latitude/Longitude Sizes of Cells in the Cell Database

LATITUDE RANGE* (deg)	CELL SIZE (deg)		Total number of Cells in both hemispheres
	Latitude	Longitude	
0 to 40	10	10	288
40 to 60	10	15	96
60 to 75	15	15	48
75 to 90	15	60	12
TOTAL NUMBER OF CELLS = 444			

*Same for northern and southern hemispheres

cell is approximately 10 deg in latitude and 10 deg in longitude; latitude/longitude intervals increase with latitude to maintain a nearly constant cell area of about one square megameter. The database times are each of the 24 UT hours in the months of February, May, August, and November. The database locations and times are selected to permit reliable interpolation of the database coverage parameters in both space and time. A subset of the cell grid format of the matrix database is shown in Fig. 10.3-12. This figure also illustrates the various coverage element values contained in the database for each of the combinations of the cell (location) and time in the database.

Database Generation Methodology — The database is composed of 16 station- and frequency-specific sets (8 stations × 2 frequencies). Each set is composed of 42 to 48 station-specific radial paths. The station-specific set of radial paths includes 36 short-path radials emanating from the station at the
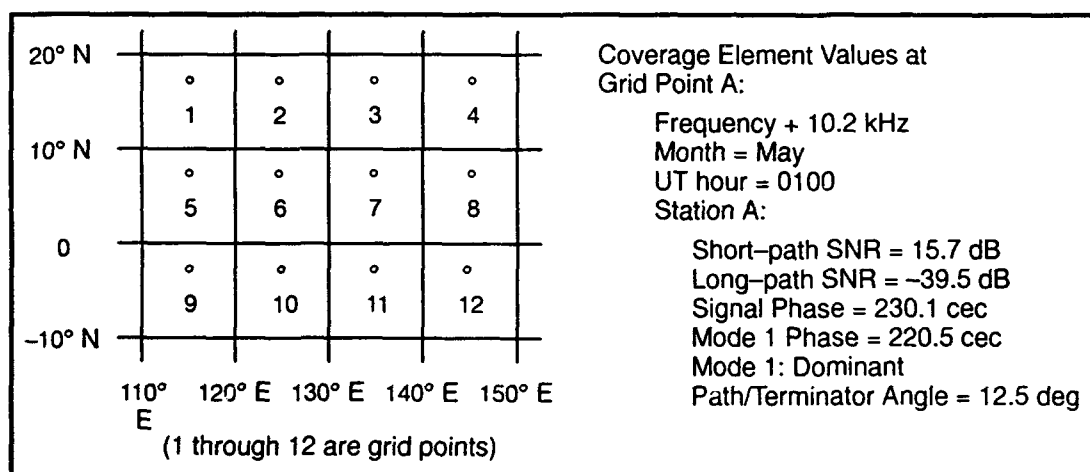
Figure 10.3-12   Example of Coverage Element Values at a Cell Center

10-50

geographic bearing angles of 0, 10, 20, . . . 350 deg, and 6 to 12 additional station-specific radials. The additional radials are specifically chosen so that the combined set of the station-specific set of radials adequately samples the spatially varying ground conductivity regions of the world, especially the low-conductivity regions such as Greenland and Antarctica and the areas immediately surrounding the low-conductivity regions. The signal information, needed for the database, for each radial path of each of the 16 station- and frequency-specific sets was obtained using the best-available state-of-the-art VLF signal and noise prediction models described in Ref. 11. A comparison of the coverage information contained in the matrix database and the coverage information conveyed by the contour diagrams is given in Table 10.3-5.

Table 10.3-5   Comparison of the Matrix Database with the Coverage Information Contained in the Contour Diagrams

COVERAGE	MATRIX DATABASE	CONTOUR DIAGRAMS* (INCLUDING OMEGA ACCESS)
Attributes		
Stations	All eight Omega stations	
Frequencies	10.2 and 13.6 kHz	
Times of year	96 (each of 24 UT hours in months of Feb., May, Aug., and Nov.	8 (0600 nd 1800 UT hours in months of Feb., May, Aug., and Nov.)
Station Radiated Power	Arbitrary	Full (10 kW) and 6 dB below$ full
Parameters		
Short-Path SNR	Yes	Flag indicates if the predicted SNR exceeds the specified SNR threshold level
Modal/Non-Modal Characterization	Yes (Mode 1 Dominance Margin)	Flag indicating whether the signal is modal or non-modal
Antipodal-Region	Not applicable	Excluded from the contours
Long-Path SNR	Yes	No
Small Path-Terminator Crossing-Angle	Yes	No
Spatial Coverage Format	Worldwide latitude-longitude grid	Worldwide
Coverage Prediction Models	Matrix database generated using more realistic models than the contour diagrams	
Coverage Validation with Empirical Data	Matrix database may be validated with much more spatially- and temporally-representative empirical observations than we used to validate the contour diagrams	
Interpolation		
Spatial and Temporal	Matrix database can be more reliably interpolated both in space and time than the contour diagrams	
Power Level Changes	Coverage information can be obtained for arbitrary station power level by proper adjustment of the SNR valuet	Can be reliably interpolated for only the Japan station
Worldwide Coverage Prediction Quality	Matrix database provides more realistic assessment of the Omega system coverage than the existing contour diagrams	

* −20 dB and −30 dB SNR threshold levels (in 100 Hz bandwidth) for 10.2 kHz coverage diagrams (Ref. 13) and −20 dB SNR threshold level (in 100 Hz bandwidth) for 13.6 kHz coverage diagrams (Ref. 16).

$ For the Japan station, the contour diagrams also exists for the station power levels of 2, 4, 8, and 10 dB below the full power.

† Note that SNR (dB) for the power level of X-dB below the full power is equal to the SNR (dB) at the full power minus X-dB.

10.4 GENERAL OMEGA SIGNAL COVERAGE CHARACTERISTICS

This section presents general characteristics of the individual station coverage and gives an assessment of the composite (full system) coverage.

10.4.1 Individual Station Signal Coverage Characteristics

The general station signal coverage characteristics are:

- Due to the higher attenuation rate of the signal in day than in night, the usable signal coverage of a station extends to shorter distances along a day path than along a night path

- Due to geomagnetic field effects, usable signal coverage of a station generally extends to:

  > Longer distances in the easterly direction
  >
  > Shorter distances in the westerly direction
  >
  > Moderate distances in the northerly/southerly direction

- Usable signal coverage does not extend to large distances for paths transiting Greenland/Antarctica due to extremely high signal attenuation rate (especially under daytime conditions) caused by the very low ground conductivity of these regions

- Due to the lower signal attenuation rate of the 13.6 kHz signals and approximately the same atmospheric noise level, the 13.6 kHz SNR coverage extends somewhat farther from a station than the 10.2 kHz SNR coverage

- These stations closest to the geomagnetic equator, such as the Liberia station, generate signals which are modal over the largest areas

- Nighttime modal interference regions extend to the south and west beyond the geomagnetic equator for northern hemisphere stations, and to the north and west beyond the geomagnetic equator for southern hemisphere stations

- Modal interference at 13.6 kHz is generally more extensive (spatially) than at 10.2 kHz.

10.4.2 The Full System Coverage Characteristics

For the most commonly used Omega receivers, the moderate performance receivers (SNR detection threshold level of –20 dB), the predicted Omega coverage is almost worldwide:

- Over 90 percent of the earth's surface receives usable signals most of the time from at least three stations with good GDOP (position-fix geometry)

- Over 80 percent of the earth's surface has usable signals most of the time from four or more stations with good GDOP.

If high-performance receivers are used for Omega navigation, the predicted coverage increases to about 98 percent for three or more usable-signal stations and to 90 percent for four or more usable-signal stations.

Although the percentage of the earth's surface covered is almost the same at each frequency (10.2 and 13.6 kHz), the specific geographic regions covered by the signals could vary significantly due to differing modal characteristics of the 10.2 and 13.6 kHz signals. Also, coverage in several areas of the world is either marginal (i.e., exists for only part of the day) or is inadequate. Some of these areas are the well-known "Winnipeg hole" in central Canada, and certain regions near the geomagnetic equator and in the general coastal regions surrounding Greenland and Antarctica. In the inadequate Omega coverage areas, the Omega coverage is often supplemented with VLF signals from the U.S. Navy/NATO stations, e.g., Annapolis (NSS), Cutler (NAA), Jim Creek (NLK), Lualualei (NPM).

10.5 SUMMARY

Omega signal coverage is spatially and temporally complex, thereby providing the requirement for signal coverage products to support mission planning, etc., by users. System coverage is a function of the system navigational signal frequency, time (UT/month), and usable signal access criteria. The system coverage is almost worldwide, although there are several navigationally important areas of the world (e.g., the Winnipeg hole in central Canada) where Omega coverage is inadequate and assistance from other navigational aids (such as a method or the VLF Communication signals) is required to reliably navigate in these areas.

The first published Omega signal coverage product (contour diagrams) was developed in 1974. This product was developed to find primarily the Omega coverage bounds which would permit the system provider (ONSCEN) to determine if Omega could adequately replace Loran A. During the intervening years, a number of improved coverage products have been produced and made available to Omega users. The improvements have been in the areas of:

- Accuracy/reliability of the Omega signal coverage prediction models/algorithms/ codes due to better understanding of the Omega signal propagation environment/ mechanisms and availability of inexpensive/fast computation capabilities

- Receiver technology due to the advent of inexpensive microprocessors

- Coverage information content due to changing user population/requirements and availability of inexpensive/faster computation/storage capabilities

- Coverage information display medium/format due to user preference and also due to the advent of inexpensive microprocessors

- Signal coverage access criteria/conditions due to the changing user needs/requirements.

Advancements in the area of coverage information content is evidenced in the: (1) matrix diagrams (described in Section 10.3.2.3) which provide the expected worldwide coverage and accuracy of the 10.2 kHz Omega signals for a limited number of times; these diagrams were based on very approximate signal coverage/accuracy assessment models; and (2) matrix (24-hour/4-month/2-frequency/cell-format) database which includes the expected values of the signal coverage elements which are needed to establish usability of 10.2/13.6 kHz Omega signals as a function of time at the centers of the cells of a worldwide matrix of 444 cells. The database is generated using the most reliable and state-of-the-art signal coverage prediction models available. The matrix database was especially developed for incorporation in the Omega system performance workstation called PACE (Performance Assessment and Coverage Evaluation). The database is available from ONSCEN. Another advancement in the coverage content was going from local time (e.g., local noon) to global time (e.g., 1300 UT hour in the month of May) as well as from very few (eight) global times to 96 global times which will now permit reliable interpolation of the coverage information in time (UT and month).

Advancement in the area of coverage presentation format/medium is evidenced by Omega ACCESS (an electronic display system) which displays worldwide coverage information, at eight global times, in a number of useful and user-friendly formats. Also, Omega ACCESS allows a user/analyst to answer a wide variety of "what-if" questions on the system coverage in response to system station operational status. Currently, ONSCEN is developing an improved Omega ACCESS (called Omega ACCESS II) which is planned to provide the coverage criteria threshold level contours as well as the expected values of the signal coverage elements (using the 24-hour/4-month/2-frequency/cell-format matrix database described in Section 10.3.2.5) as functions of location (cell) and time. Omega ACCESS II is also planned to incorporate many new features to aid in a better/faster interpretation of the depicted coverage information.

10.6 PROBLEMS

10.6.1 Sample Problems with Solution:

1. What information does GDOP convey to a user? Using Eqs. 10.2-3 and 10.2-4, compute the non-dimensioned and dimensioned hyperbolic GDOPs for a three-station position-fix geometry where the stations are spaced 120 degrees apart at the user location.

Solution:

GDOP is a relative measure of the quality of the navigation fix geometry. Assuming the individual station signal phase errors are same, the fix accuracy increases as the GDOP of the fix decreases.

10-54

The non-dimensional hyperbolic GDOP, based on Eqs. 10.2-2 and 10.2-3, is given by:

$$\frac{1}{\sqrt{2}\sin\theta}\left[\frac{1}{\sin^2\frac{(\phi_{12})}{2}} - \frac{2\rho\cos\theta}{\sin\frac{(\phi_{12})}{2}\sin\frac{(\phi_{31})}{2}} + \frac{1}{\sin^2\frac{(\phi_{31})}{2}}\right]^{1/2}$$

where (see Fig. 10.2-15)

ϕ_{12} = Angle subtended at the receiver by station 1 relative to station 2 = $\phi_1 - \phi_2 = 0° - 120° = 120°$

ϕ_{31} = Angle subtended at the receiver by station 3 relative to station 1 = $\phi_3 - \phi_1 = 240° - 0° = 240°$

θ = Crossing angle between LOP$_{12}$ and LOP$_{31}$
$$\frac{\phi_{12} + \phi_{31}}{2} = \frac{(\phi_1 - \phi_2) + (\phi_3 - \phi_1)}{2} = \frac{\phi_3 - \phi_2}{2} = \frac{240° - 120°}{2} = 60°$$

ρ = Phase-difference error correlation coefficient between LOP$_{12}$ and LOP$_{31}$ = –0.5

$$\therefore \left.\begin{array}{l}\text{Non-dimensional}\\\text{Hyperbolic GDOP}\end{array}\right\} = \frac{1}{\sqrt{2}\left(\sqrt{\frac{3}{4}}\right)}\left[\frac{1}{\frac{3}{4}} - \frac{2\left(-\frac{1}{2}\right)\left(\frac{1}{2}\right)}{\left(-\sqrt{\frac{3}{4}}\right)\left(\sqrt{\frac{3}{4}}\right)} + \frac{1}{\frac{3}{4}}\right]^{1/2}$$

$$= \frac{1}{\sqrt{2}\sqrt{\frac{3}{4}}}\left[\frac{4}{3} - \frac{1}{2}\left(\frac{4}{3}\right) + \frac{4}{3}\right]^{1/2}$$

$$= \frac{1}{\sqrt{2}\sqrt{\frac{3}{4}}}\left[\sqrt{2}\right] = \sqrt{\frac{4}{3}}$$

2. Based on the 1985 composite diagrams shown in Figs. 10.3-4(a), 10.3-4(b), and 10.3-4(c), list the usable signal stations at 60°N and 170°W, North Pole, and South Pole.

Solution:

Location	Usable-Signal Stations
60° N and 170° W	A, B, C, D, G, H
North Pole	All eight stations
South Pole	B, C, D, F, G

3. Is Omega navigation expected to be reliable in the shaded regions of the 1985 composite diagram shown in Figs. 10.3-4(a)? Why?

Solution:

In the 1985 composite diagrams, the shaded regions have:

(1) Three usable-signal stations available for the fix computation, but the associated GDOP is above the required threshold value of 0.5 km per centicycle of the phase-difference error, or

(2) Four usable-signal stations available for the fix computation, but the smallest 3-station-based GDOP from the available stations in the region is greater than the required threshold value of 0.5 km per centicycle of the phase-difference error.

10.6.2 Problems to be Solved by Reader:

1. What is the difference between a station's short path and long path? What is the maximum value of the short-path length?

2. Explain differences between the dimensioned and non-dimensioned GDOP definitions.

3. List the usable signal coverage criteria parameters and their nominal threshold values, along with rationale for choosing these values. Which parameter tends to be the most important (restrictive) in determining coverage?

4. What is the minimum number of signal stations needed for reliable hyperbolic navigation? Is the minimum number always sufficient? Why?

5. Based on the Healy *et al.* station deselection chart shown in Table 10.3-2, which Omega stations should be deselected at Boston, MA, during a PCD event? Why?

6. Based on the DMAHTC-developed composite diagram shown in Fig. 10.3-6, at the southern tip of Australia what are the values of the SNR and mode interference-induced phase deviation?

7. Which direction from a station (east or west) is coverage generally the greatest? Why?

8. What is the primary source of noise at Omega frequencies and what time (local) of the day is it the greatest?

10.7 ABBREVIATIONS/ACRONYMS

ACCESS	Automated Composite Coverage Evaluator of System Signals
AED	Azimuth Equal Distance
cec	Centicycle (one-hundredth of a cycle)
CCIR	International Radio Consultative Committee
cep	Circular Error Probable
CGA	Color Graphics Adaptor

dB	Decibel
DMAHTC	Defense Mapping Agency Hydrographic/Topographic Center
f	Frequency
GDOP	Geometric Dilution of Precision
GPS	Global Positioning System
hr	Hour
Hz	Hertz
IM	Interfering Mode
IPP	Integrated Propagation Prediction (Program for VLF Signal Predictions)
kHz	Kilohertz
km	Kilometer
LOP	Line-of-Position
LPSA	Long-Path Signal Amplitude
LPSNR	Long-Path SNR
LSN	Local Summer Noon
LWM	Local Winter Midnight
M1DM	Mode 1 Dominance Margin
Mm	Megameter
NATO	North Atlantic Treaty Organization
NELC	Naval Electronics Laboratory Center (now NOSC)
NOSC	Naval Ocean Systems Center (formerly NELC)
NRL	Naval Research Laboratory
ONSCEN	Omega Navigation System Center (formerly ONSOD)
ONSOD	Omega Navigation Operations Detail (now ONSCEN)
PACE	Performance Assessment and Coverage Evaluation
PCD	Polar Cap Disturbance
PPC	Propagation Correction
PSMI	Possible Significant Mode Interference
PTCA	Path/Terminator Crossing Angle
rms	Root-Mean-Square
2-drms	Twice the Two-dimensional Root-Mean-Square Value
SID	Sudden Ionospheric Disturbance

SNR	Signal-to-Noise Ratio
SPPD	Short-Path Phase Deviation
SPSA	Short-Path Signal Amplitude
SPSNR	Short-Path SNR
TASC	The Analytic Sciences Corporation
TE	Transverse Electric
TM	Transverse Magnetic
WGL	Westinghouse Geophysics Laboratory
VLF	Very Low Frequency
UT	Universal Time

10.8 REFERENCES

1. Watt, A.D., *VLF Radio Engineering*, Pergamon Press, Oxford, 1967.

2. Wait, J.R., *Electromagnetic Waves in Stratified Media*, Second Edition, Pergamon Press, 1970.

3. Crombie, D.D., Periodic fading of VLF signals received over long paths during sunrise and sunset, *Radio Science Journal of Research NBS/USNC-URSI*, Vol. 68D, No. 11, November 1964.

4. Wenzel, R.J., and Kugel, C., Mediterranean Sea Omega Validation Analysis, U.S. Department of Transportation, United States Coast Guard/Omega Navigation Syste Center, Report No. CG-ONSCEN-06-91.

5. Morris, P.B., and Swanson, E.R., New Coefficients for the Swanson Propagation Correction Model, *Proc. of the Fifth Annual Meeting*, International Omega Association Meeting (Bergen, Norway), August 1980.

6. Tanana, S., Ajato, K., and Suenaga, M., Omega Synchronization Process and Propagation Evaluation at Deep Sea, *Proc. of the Twelfth Annual Meeting*, International Omega Association (Honolulu, Hawaii), 19–23 October 1987.

7. Mannheimer, D., Twilight bending effects on Omega navigation, *Proc. of the Eighth Annual Meeting*, International Omega Association (Lisbon, Portugal), July 1982.

8. Swanson, E.R., Omega Coverage in India: A Case Study, Naval Electronics Laboratory Center, NELT/TR1974, January 1976.

9. Gupta, R.R., Donnelly, S.F., Creamer, P.M., and Sayer, S., Omega Signal Coverage Prediction Diagrams for 10.2 kHz, Volume I: Technical Approach, TASC Technical Report TR-3077-1 (ADA 092741), October 1980.

10. Morris, P.B., Omega System Performance Assessment, TASC Technical Report TR-5351-8-1, (Report No. CG-ONSCEN-01-89/ADA-210342), March 1989.

11. Gupta, R.R., Omega/VLF Signal Coverage Database Development, TASC Technical Information Memorandum TIM-5834-3-1 (Report No. CG-ONSCEN-03-91), January 1991.

12. Gupta, R.R., Evaluation of Coverage and Anomalous Propagation Effects for Alternative G Transmitter Sites, TASC Technical Report TR-343-14, June 1974.

13. Gupta, R.R., Donnelly, S.F., Morris, P.B., and Vence, R.L., Jr., Omega System 10.2 kHz Signal Coverage Diagrams, *Proc. of the Fifth Annual Meeting*, International Omega Association (Bergen, Norway), August 1980.

14. Swanson, E.R., A New Approach to Omega Coverage Diagrams, *Proc. of the Eighth Annual Meeting*, International Omega Association (Lisbon, Portugal), July 1983.

15. Swanson, E.R., Omega Coverage Accuracy at Specified Times, *Proc. of the Ninth Annual Meeting*, International Omega Association (Seattle, Washington), August 1984.

16. Gupta, R.R., Morris, P.B., and Doubt, R.J., Omega Signal Coverage Prediction Diagrams for 13.6 kHz, *Proc. of the Tenth Annual Meeting*, International Omega Association (Brighton, England), July 1985.

17. Warren, R.S., Tench, K.A., Gupta, R.R., and Morris, P.B., Omega ACCESS: A Microcomputer Display of Omega Signal Coverage Diagrams, *Proc. of the Forty-Second Annual Meeting*, The Institute of Navigation (Seattle, Washington), June 1986. (Also published in *Proc. of the Eleventh Annual Meeting*, International Omega Association (Quebec, Canada), August, 1986.)

18. Gupta, R.R., and Morris, P.B., A New Database of Signal Coverage Predictions for Omega, *Proc. of Sixteenth Annual Meeting*, International Omega Association (Bali, Indonesia), September 1990.

19. Gupta, R.R., and Morris, P.B., Overview of Omega Signal Coverage, *Navigation: Journal of Institute of Navigation*, Vol. 33, No. 3, Fall 1986.

20. Bortz, J.E., Sr., Gupta, R.R., Scull, D.C., and Morris, P.B., Omega signal coverage prediction, *Navigation: Journal of the Institute of Navigation*, Vol. 23, No. 1, Spring 1976.

21. Perlowski, W., User Acceptance of Omega in the Marine Community, *Proc. Omega Workshop*, Sponsored by FAA Technical Center of the U.S. Department of Transportation (Atlantic City, NJ), 11-13 May 1982.

22. Ferguson, J.A., Report on the Integration Prediction Program with Nuclear Environment (IPP-2), NELC Technical Note TN 1980, July 1971.

23. International Radio Consultative Committee, World Distribution and Characteristics of Atmospheric Radio Noise, International Telecommunications Union, CCIR Report 332, 1964.

24. Gupta, R.R., Donnelly, S.F., Creamer, P.M., and Sayer, S., Omega Signal Coverage Prediction Diagrams for 10.2 kHz, Volume II: Individual Station Diagrams, TASC Technical Report TR-3077-2 (ADA 092742), October 1980.

25. Gupta, R.R., Donnelly, S.F., Creamer, P.M., and Sayer, S., Omega Signal Coverage Prediction Diagrams for 10.2 kHz, Volume III: Composite Diagrams, TASC Technical Report TR-3077-3 (ADA 092743), October 1980.

26. Gupta, R.R., Omega Signal Coverage Prediction Diagrams for 13.6 kHz, TASC Technical Report TR-4418-6, August 1985.

27. Gupta, R.R., Griffiths, B.E., and Creamer, P.M., An Extended Omega Amplitude Prediction Model, TASC Technical Report TR-1319-2, December 1979.

28. Reynolds, R.A., and Gupta, R.R., Omega signal amplitude model computer program documentation, TASC Technical Report TR-4418-5, August 1985.

29. Preliminary Noise Program Documentation, U.S. Coast Guard, Omega Navigation Systems Operations Detail, October 1979.

30. Maxwell, E.L., Stone, D.L., Croghan, R.D., Ball, L., and Watt, A.D., Development of a VLF Atmospheric Noise Prediction Model, Westinghouse Georesearch Laboratory Report No. 70-1H2-VLFNO-R1, June 1970.

31. Stone, D.L., Croghan, R.D., and Crail, A.C., Computer Program Operational Manual for Atmospheric Noise Predictions, Westinghouse Geophysics Laboratory Report No. 70-1H2-VLFNO-R2, June 1970.

32. Hauser, J.P., and Rhoads, F.J., Analysis of a VLF atmospheric noise prediction model, Paper presented at *USNC/URSI Meeting*, Commission VIII, Session I, August 21-24, 1973.

33. CDR Kay, W.K., Omega: A System Operator's Perspective, *Proceedings of the Ninth Annual Meeting*, International Omega Association (Seattle, Washington), August 1984.

34. Gupta, R.R., Creamer, P.M., and Morris, P.B., Assessment of Omega Phase-Difference Errors, *Proc. of the Seventh Annual Meeting*, International Omega Association (Arlington, VA), October 1982.

35. Creamer, P.M., Gupta, R.R., and Morris, P.B., Omega Navigation System Position-Fix Accuracy Assessment, *Proc. of the Ninth Annual Meeting*, International Omega Association (Seattle, WA), August 1984.

36. Healy, R.D., Gupta, R.R., and Morris, P.B., Updated Station Deselection Procedures to Support Automatic Omega Receiver Operation, *Proc. of NEACON* (Dayton, OH), May 1981.

37. Gupta, R.R., and Warren, R.S., Omega Station 10.2 kHz Signal Selection Made Easy, *Proc. of National Meeting of Aerospace*, Institute of Navigation (Trevose, PA), April 1981.

38. Omega Coverage Diagrams: 10.2 kHz, Defense Mapping Agency Hydrographic/Topographic Center DMA Stock No. OMPUB224COVDIAG, 1983.

39. Gupta, R.R., and Morris, P.B., Omega Modal Interference Maps, *Proc. of the Eighth Annual Meeting*, International Omega Association (Lisbon, Portugal), August 1983.

40. Morris, P.B., and Gupta, R.R., Omega navigation signal characteristics, *Navigation: Journal of Institute of Navigation*, Vol. 33, No. 3, Fall 1986.

41. Desrochers, G.R., Performance Analysis and Coverage Evaluation (PACE) workstation: User's Manual, TASC Technical Information Memorandum TIM-5834-2-1, December 1990.

42. Desrochers, G.R., Omega System Performance and Coverage Evaluation (PACE) workstation: design and implementation, TASC Technical Information Memorandum TIM-5834-2-2, February 1991.

43. Morris, P.B., Omega System Availability as Global Measures of Navigation Accuracy, TASC Technical Information Memorandum TIM-5834-5-2, September 1990.

44. Morris, P.B., Analysis and Evaluation of Selected PACE Applications, TASC Technical Information Memorandum TIM-5834-4-1, April 1991.

CHAPTER 11

SYSTEM PERFORMANCE ASSESSMENT

Chapter Overview — The overall assessment, evaluation, and quantification of Omega system performance is presented in this chapter. Section 11.1 discusses the motivation for seeking an overall measure of Omega performance in terms of system availability. This section also includes a brief sketch of the model used to quantify system availability and the computer workstation (PACE), which implements the model calculations. Section 11.2 provides further detail on specifying system performance; both historical measures of system performance and alternative measures of system availability are considered. The System Availability Model is presented in terms of its four model components in Section 11.3. Section 11.4 explains how the model components are meshed into a coherent, probabilistic model of system availability. This section also includes a summary of the model synthesis and sample results. Section 11.5 provides an overview of PACE, including a description of the databases employed, execution options, and operation. Section 11.6 contains a probabilistic treatment of the station reliability/availability component. Section 11.7 describes the enhanced version of the System Availability Model which treats one of the signal coverage parameters as a random variable. An augmented version of the model is described in Section 11.8; in this version of the model, the system availability index characterizes the probability of attaining a certain accuracy with Omega rather than the probability of accessing three or more usable signals. Problems, including worked-out examples and those to be solved by the reader, are included in Section 11.9. Abbreviations and acronyms used in the chapter are given in Section 11.10 and references cited in the chapter are found in Section 11.11.

11.1 INTRODUCTION

11.1.1 Rationale for Omega System Performance Assessment

Omega is generally considered to be a highly reliable radionavigation system whose signals are nearly always available, or accessible, to the system users worldwide. This characterization is supported by typical monthly station reliability figures of 99 percent (defined as the percentage of time the station is on the air) and global signal coverage estimates of 95 percent (Ref. 1). However, it is widely recognized that Omega performance varies considerably over the dimensions of space and time. Any measure of system performance, therefore, must account for these variations and their effect on the users of the system.

Most radionavigation systems (e.g., Loran) are characterized by the size or location of their coverage area, i.e., the approximate geographic region served by their signals. This area can be increased or

decreased by changing the transmitted signal power or frequency(ies), and, in general, the area serviced by the propagated signals changes little over time (on scales of hours/days/months). For Omega, however, the service area is the entire globe and the patterns of coverage* change significantly with time, especially over a 24-hour period. This suggests that coverage itself (the fraction of the earth's surface covered) should be included in any meaningful measure of system performance. Omega signal coverage diagrams (see Chapter 10) that portray global coverage at specific global times provide an estimate of "average" system performance and its variation over time. From the viewpoint of signal coverage, system performance is governed by signal propagation considerations that are not under the control of the system provider. Certain aspects of signal coverage, such as those which depend on signal strength, are affected by significant system modifications, such as changes in transmitting station power levels or receiver sensitivity thresholds.

From the viewpoint of an Omega user, Omega System performance can be at least partly characterized by the dependability and reliability of the user's receiving system. For example, a navigator with an inoperable receiver would be in the same position as if several stations were off-air or a severe signal coverage deficiency existed while the receiver was operational. The Omega user is often unaware of whether an Omega "problem" is due to the transmitting station, signal propagation, or malfunctioning of the user's receiver. As in the case of signal coverage, the system provider has no control of the operational status of a user's receiving system, although it is clearly an element that must be included in the overall definition of system performance.

Historically, the managers of Omega System operations (since 1972, ONSOD/ONSCEN, a Coast Guard Headquarters unit) have considered Omega system performance in terms of the reliability of the transmitting stations. This emphasis has followed from the system manager's primary responsibility for the construction, engineering maintenance, and operation of the Omega transmitting stations. Following a long period of station acquisition and construction (ending in 1982), the principal focus of the system manager shifted to maintenance and operation of a highly reliable network of transmitting stations. From the viewpoint of the station reliability, system performance, to a large degree, depends on the efficient management of each station, e.g., stocking of spare parts, following equipment maintenance schedules, regular training of station personnel, etc.

---

*Signal coverage is defined and described more extensively later in the chapter; here it is simply defined as the geographic region in which the system signals are usable for navigation.

Individually, none of these indicators of system performance (coverage, receiver reliability, or station reliability) furnishes a proper accounting of total Omega system performance from the viewpoint of the user or system provider. However, if properly combined, signal coverage, receiver reliability, and station reliability (in addition to other system features such as user geographic priority) can be used to appropriately describe Omega system performance.

11.1.2 The Omega System Availability Model

To tie together the several aspects of Omega system performance mentioned, the Omega System Availability Model was developed. This probabilistic model considers four aspects of Omega system performance which, when appropriately combined, answer the question:

> What is the probability that an Omega user can utilize three or more Omega signals with a properly functioning Omega receiving system at any location (within a region or the entire globe) and at any time?

The probability figure sought by this question is called the *system availability index* and is denoted as P_{SA}. This probability figure is defined from a user's perspective but, since its scope is global, it can also serve as a suitable figure of merit for the Omega system manager.

The four aspects, or components, of Omega system performance addressed by the original version of the System Availability Model are:

(1) Transmitting station reliability/availability

(2) Signal accessibility/coverage

(3) Receiver reliability/availability

(4) User geographic regional priority.

An overview of the Omega System Availability Model/Algorithm is given in Fig. 11.1-1. This figure illustrates how the various components of the System Availability Model are integrated into an algorithm to compute P_{SA}. Computation of P_{SA} is quite extensive and is facilitated through the use of a workstation that provides global and regional displays of areas with P_{SA} above or below a certain threshold.

Since the overall model is probabilistic, random events associated with one or more of the components listed above form the basis for the calculation of P_{SA}. Certain combinations of these random events may make the Omega system unavailable to a user at a given location/time. The System Availability Model establishes a procedure for finding the *a priori* probability that these random events will cause the Omega system to be available/unavailable at a given location/time.
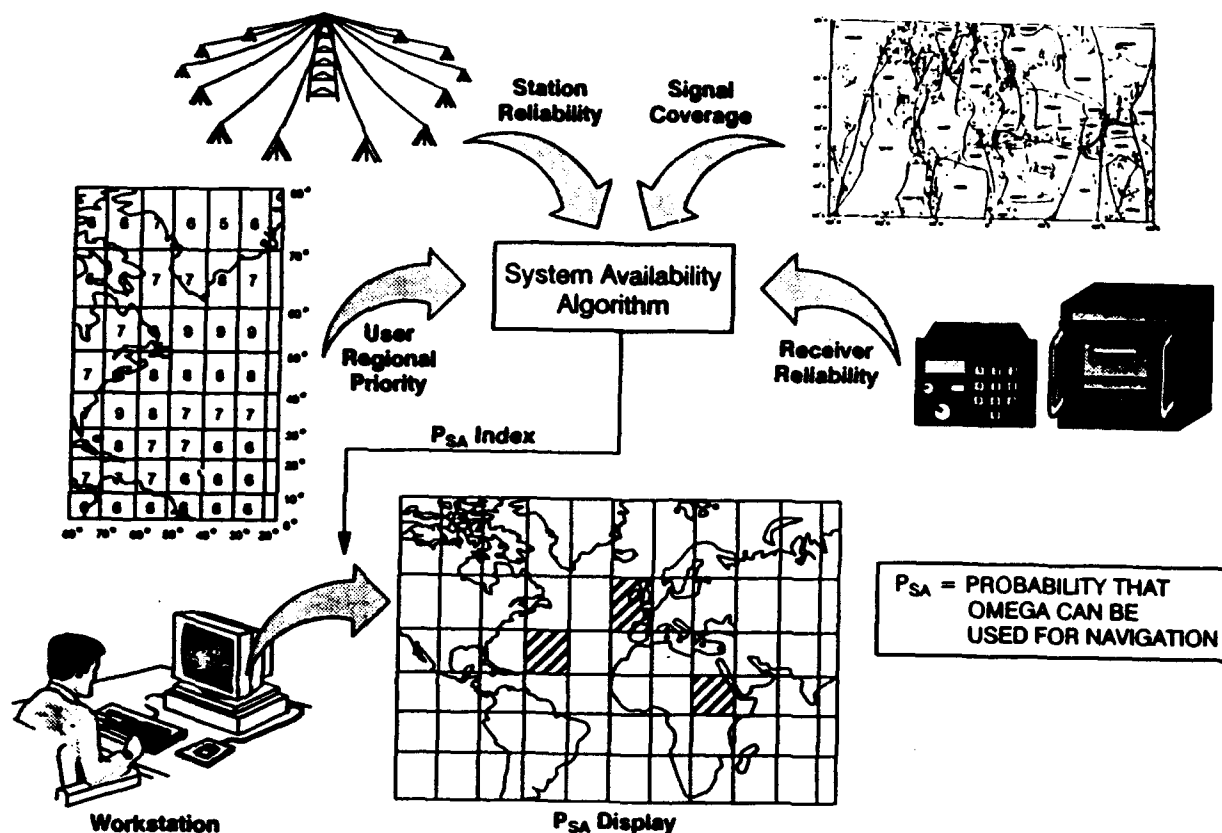
Figure 11.1-1 Overview of the Omega System Availability Model/Algorithm

Before proceeding, it is helpful to clarify the meaning of a random event as used in a probabilistic model. Consider the toss of a uniformly weighted coin having heads on one side and tails on the other. Clearly, a flip of heads is a random event, i.e., it is unpredictable before the flip. The *probability* of this event taking place (i.e., a flip of heads) is a definite number (0.5), which is fixed as long as the procedural rules are not changed. Some events are more probable than others; e.g., consider the simultaneous flips of two identical coins. The event that, after the flip, one coin is heads and one coin tails is more probable than the event that both coins are heads. In certain limiting cases, or, by definition, events may become "less" random (i.e., more probable) and eventually the outcomes may become certain, or *deterministic*. For example, the probability that one million consecutive flips will *not* produce all heads is very nearly 1.0. Also, the event that a flipped coin will yield either heads *or* tails is deterministic, i.e., the event probability is 1.0.

In the case of station reliability/availability (component (1) above), an unscheduled station off-air is clearly a random event with historically established statistics. As explained below, scheduled off-airs are subdivided into two categories: those with long-term advance notice and those with short-term (a few days) advance notice. In looking ahead over a time period much longer than a few days, a scheduled off-air with short-term advance notice has the characteristics of a randomly occurring event. Scheduled off-airs with long-term advance notice are clearly not random events and are said to be *deterministic*. For unscheduled off-air events and scheduled off-air events with short-term advance notice, both the occurrence and the duration are random quantities. Although a station off-air may occur anytime during a month, the duration of the off-air (which depends on the station and the month) is typically one to two hours.

Signal coverage (component (2)), with its complex dependence on space and time, may appear random, but the predicted quantities which make up this component may be treated as deterministic. This may seem contradictory at first, but recall that random events, by their very nature, cannot be predicted. Many of the quantitative features which make up signal coverage can, to an acceptable degree of accuracy, be predicted (see Chapter 10). As prediction models are improved, signal coverage predictions appear less random when compared with operational Omega experience. Actual measurements of signals, however, are corrupted by electromagnetic noise, a random quantity (defined by several parameters) that can never be predicted. To accommodate the most uncertain of the predicted signal coverage quantities, an enhanced version of the System Availability Model has been developed. The particular attributes of the enhanced version are discussed in Section 11.7.

Omega receivers, which are addressed in component (3), have well established statistics for their random failures, much like transmitting station equipment. As with unscheduled station off-airs, receiver failures have random occurrence times and random durations (repair times).

Inherent in the definition of P_{SA} is the projected use of Omega at *any* location/time. This implies a randomness (defined in component (4)) on the part of the user regarding the worldwide location and time required for the use of Omega. Since most Omega users operate in limited regions, a pattern of regional weighting may be employed to define the non-uniform probability of Omega usage throughout the world.

Since its original development, the System Availability Model has been extended to increase its accuracy and applicability. Two versions of the extended model have been produced: (1) the enhanced version, and (2) the augmented version. These versions are briefly described in Sections 11.4, 11.7, and 11.8. The analytical basis of the augmented system availability model is presented in Appendix B.

11.1.3 Implementation of the Omega System Availability Model

The System Availability Model is implemented by calculating the System Availability Index (P_{SA}). In the original development of this model (Ref. 2), P_{SA} was computed by using a fractional coverage database (hard copy) and an *ad hoc* computer program. With the advent of the 24-hour/ 4-month/ 2-frequency signal coverage database (Ref. 3), a much more elaborate method of calculation and user interaction has been implemented on a workstation known as PACE (Performance Assessment and Coverage Evaluation). PACE is an essential tool for the practical application of the System Availability Model due to the complexity and computationally intensive nature of the P_{SA} calculation. The PACE workstation is designed for the system operator who wishes to evaluate the total impact of various system options, such as station off-airs, transmitter power reductions, or annual maintenance scheduling changes.

Simply stated, PACE implements the calculation of P_{SA} based on the System Availability Model. Because PACE is a workstation, it has an interactive user interface to facilitate user input and to support interpretation of the output. It also has special features to permit global comparison of system availability for alternative system configurations/options.

PACE can be used to compute P_{SA} over all space (surface of the earth) and time (hour/month) or over any restricted domain(s) of space and time. A minimum-tolerable P_{SA} threshold value must be input by the user for comparison with the computed P_{SA} value. With regard to the transmitting station network, the PACE user must input the station on-air/off-air status, relative power, and station reliability statistics. For signal coverage, inputs of usable signal and noise thresholds are required as well as indicators of preferred navigation geometry. Receiver reliability/availability statistics are not used in PACE so that the receiver is effectively assumed to have 100 percent reliability. Omega user regional priority is input as a weight attached to a spatial unit* (for the globe or specified region). Further discussion of PACE is given in Section 11.5.

11.2 SPECIFICATION OF SYSTEM PERFORMANCE

11.2.1 Historical Measures of Omega System Performance

The interpretation of Omega system performance depends on the way one interacts with the system. Thus, an analyst responsible for system synchronization is likely to measure/interpret system per-

---

*In PACE, the spatial unit is the *cell*, a "square-shaped" region of approximately 10 degrees (latitude) by 10 degrees (longitude) in the low-latitude regions; in the higher-latitude regions, its definition and shape change to maintain a nearly constant area.

formance differently than an Omega user in a fishing vessel off the coast of South America. Although these various measures of system performance are not always precisely defined, they do reflect the intended interpretation.

As mentioned in Section 11.1, station reliability has been used as an historical measure of system performance by Omega system management. Station reliability is measured by the fraction of time a station is on-air — usually over the period of a month. For reporting purposes, the monthly statistics are often aggregated over periods of three months or a year. The month is a natural time period for measuring station reliability because station annual maintenance is typically scheduled within monthly intervals. When station reliability statistics are reported, a distinction is usually made between *planned* (scheduled) off-airs and *unplanned* (unscheduled) off-airs. This is important in the sense that scheduled off-airs are, in principle, known in advance by all users so that appropriate contingency plans can be made. Unscheduled off-airs, on the other hand, immediately affect most signal users and thus represent an unexpected "failure" of a portion of the system. Unscheduled off-airs of less than a minute duration ("momentary off-airs") are not reported since their duration is generally much less than the "time constant" of an Omega receiver; the receiver essentially "coasts" through the momentary outage.

In building a measure of system performance, the monthly reliability figure for a single station has historically been reported as either (or both):

- On-air probability $= 1 - \dfrac{\text{total off-air time}}{\text{total time in month}}$

- Expected on-air probability $= 1 - \dfrac{\text{total unscheduled off-air time}}{\text{total time in month}}$

From these individual station figures, the total system performance has been reported as: (1) the average of the eight station reliability figures, (2) the maximum/minimum station reliability figure, (3) the number of stations achieving a monthly reliability figure of 100 percent (or greater than 99 percent), etc. The actual off-air time included in the reported reliability figures is normally only for the 10.2 kHz transmission frequency. Occasionally, a station's 10.2 kHz signal will cease transmission while one or more other frequencies continue to be transmitted. This suggests that a more meaningful indicator of system performance would include some dependence on the actual frequency transmitted (and, presumably, duty cycle; Ref. 4).

As measured by station reliability (according to the prescriptions given above), system performance is subject to control by system management. This means that station reliability may be

increased through greater attention to existing safety and maintenance procedures, improved procedures, more frequent equipment/site inspections, modified equipment, etc. As measured by signal coverage alone, however, system performance is not subject to active control by system management, except, perhaps, by major (expensive) modifications, such as transmitter/antenna upgrade. In this sense, signal coverage is a passive indicator of system performance.

In terms of signal coverage, system performance has been characterized by the fraction of the earth's surface served by three or more usable signals at a specified time(s). As the availability and efficiency of computer-based signal coverage prediction tools have evolved over the years (see Chapter 10), the number of specific global (or local) times for which spatial coverage is computed and presented has increased. Because the number of coverage times was small (fewer than ten) in the first few generations of signal coverage information development, the system performance (fractional coverage, assuming all stations on-air) was often specified for each coverage time (Ref. 1). The smallest of these fractional coverage figures was generally emphasized, since system performance could be said to be "better" than that number, at least over those times for which spatial coverage was given. As an example, suppose the minimum coverage fraction is 0.95 over the eight hour/month coverage times (0600 and 1800 UT in the months of February, May, August, and November). Then system performance is better than (or the same as) 0.95.

The original idea for combining receiving equipment reliability/availability and signal coverage was inspired by later review of an early U.S. Navy Specific Operational Requirement (Ref. 5, Section II) for Omega which stated, in part, that ". . . overall system availability shall be 95%. MTBF* of the receiving system shall be at least 1000 hours. MTTR§ shall not exceed 30 minutes . . ." In supporting documentation (Ref. 5, Section XIII), system availability is defined as the probability that at any point in time and at any point on the earth's surface, an Omega user's receiver is properly functioning and three or more Omega signals can be effectively utilized for successful navigation/position-fixing.

11.2.2 Definitions and Measures of System Availability

In the original version of the System Availability Model (Ref. 2), system availability, as measured by the system availability index, P_{SA}, is defined as the probability that, at any time and at any point on the earth's surface, an Omega user's receiver is properly functioning and three or more usable Omega signals are available to permit successful navigation, position fixing, or other use of the system. For

---

*Mean Time Between Failure.
§ Mean Time To Repair.

example, a P_{SA} value of 0.8 means that in 80 percent of the cases having the specified conditions (location, time, frequency, etc.), a user has a functioning receiver and access to three or more usable signals. With this definition and the fact that receiver reliability/availability is independent of station signal access, P_{SA} may be expressed as:

$$P_{SA} = P_R P_A$$

where P_R is the probability that the receiver operated by the Omega user is reliable and available and P_A is the probability that three or more usable signals (in space) are available. The probabilities are multiplied because of the independence assumption mentioned above. P_R is generally computed using a simple model for receiver reliability/availability. Calculation of P_A for any time and location on the globe requires at least three model components:

- Transmitting station reliability/availability
- Signal accessibility/coverage
- User geographic regional priority.

These model components are described in Section 11.3.

As noted in Section 11.1, system availability is a probabilistic indicator of system performance and thus assumes a certain amount of randomness in each of the model components. In the original version of the System Availability Model, random quantities are modeled in three of the components as shown in Table 11.2-1. Although a simple model of Omega receiver reliability/availability was included in the original version of the System Availability Model, this model was not included in PACE; PACE assumes a perfect, 100 percent reliable Omega receiver. Station off-air occurrence and duration probabilities are derived from historical station reliability figures for both scheduled and unscheduled off-airs. Databases of reliability figures have been developed for specific years (e.g., 1985–1987), from

**Table 11.2-1   Random Quantities Included in the Components
of the System Availability Model (Original Version)**

System Component	Random Quantities
(1) Transmitting station reliability/availability	Off-air occurrence times; off-air durations
(2) Signal accessibility/coverage	None
(3) Receiver reliability/availability	Failure occurrence rate; repair time duration
(4) User geographic regional priority	Cell occupied by user

composite averages over a number of years (e.g., 1985–1987), or as default/projected figures. Randomness in the user cell occupation is governed by the cell weights assigned. In PACE, station reliability figures (in file format) and cell weights ⌐   ' ⌐d inputs.

Notably absent from the list of model components with random quantities for the original version of the System Availability Model is the signal coverage component. This simplifying assumption means that the signal and noise parameters used in the model are assumed to be deterministic functions of time and space. Here, deterministic is used in an approximate sense; i.e., a random quantity whose measure of uncertainty (e.g., the standard deviation) is negligibly small relative to the mean. The signal parameter (for example, signal amplitude) is well defined and exhibits relatively little variation about its mean value. On the other hand, VLF electromagnetic noise in a 100 Hz bandwidth at Omega frequencies is a distinctly random quantity with a reasonably well-established probability distribution. However, when the noise power (in a bandwidth of 100 Hz) is averaged over a few minutes (corresponding to a receiver time constant), a sample is obtained which is approximately the same as 10 to 20 additional samples consecutively measured over the period of an hour. Thus, mean/median noise power (or a related measure, known as noise level) is the parameter used to represent the noise in a deterministic model. This, of course, ignores any (day-to-day) variation of the noise level about the mean value for the given hour.

11.2.3 Index of System Availability

As defined in Section 11.2.2, the system availability index is the probability (and therefore has a value between 0 and 1) that at any given time/location an Omega user's receiver functions properly and the signals accessible to the user permit successful system utilization. For most applications, the Omega system is utilized for navigation but it is also used for time recovery, frequency control, or vehicle tracking. Within the framework of navigation, successful system utilization normally means that, at a minimum, three usable signals are accessible. With a supplementary precise frequency reference (e.g., a cesium standard), an Omega receiver can supply reliable navigation information with access to as few as two usable station signals. As also discussed in Section 11.2.2, an additional requirement for successful system utilization is that the navigation/positioning accuracy of the collective set of individually usable signals must be within a user-desired specification (e.g., a maximum RMS error of 3 nm). Alternative definitions/ requirements of successful system utilization would presumably be needed for other applications.

The system availability index (denoted as P_{SA}) is defined above as a measure of Omega system performance from the viewpoint of a single user. This measure of performance applies to the entire system if the users are homogeneous (similar) in terms of receiver reliability statistics and user operating

area distribution. If the population of users appears inhomogeneous but is basically homogeneous within defined user classes (see Section 11.3.1), then the characterization is essentially the same (in terms of a "composite" user). This characterization is permissible because the service to a single user (user class) is independent of the total number of other users (user classes).

From the viewpoint of the system manager, P_{SA} also provides useful information. As a single figure of merit, the system availability index ties together the most important aspects of overall system performance. Regular monitoring of this index can furnish important information to those responsible for Omega operations. Changes in the index serve to indicate: (1) short-term station equipment problems or propagation anomalies, (2) longer-term problems common to a number of stations or receiver types, or (3) exceptional diligence on the part of a station crew to maintain high reliability. The index can be computed weekly, monthly, or quarterly depending on reporting schedules or review cycles.

11.3 SYSTEM AVAILABILITY MODEL

In this section, the four components of the original System Availability Model are described. A probabilistic treatment of the station reliability/availability component is given in Section 11.6. The probabilistic description of the signal coverage component, as extended by the enhanced version of the model, is presented in Section 11.7. The two supplementary model components that are needed for the augmented version of the System Availability Model are treated in Section 11.8. Figure 11.3-1 provides an overview of the System Availability Model in terms of its components.

11.3.1 Receiver Reliability/Availability Component

The original definition of P_{SA} includes two independent types of events: the proper functioning of an Omega receiver and the presence of three or more usable signals. Thus, by definition

$$P_{SA} = P_R P_A$$

where P_R is the probability that the user's Omega receiver is both functioning normally and being operated correctly at the fixed point in time and space; P_A is the probability that three or more usable signals are accessible. P_R is considered to have a long-term time dependence as successive generations of receivers are expected to exhibit improved reliability. As an example of the calculation of P_R, consider a uniform failure interval and repair time model that is characterized by two parameters: a mean time between failure (MTBF) and a mean time to repair (MTTR). In terms of these parameters, the receiver reliability is:

$$P_R = 1 - \frac{MTTR}{MTBF}$$
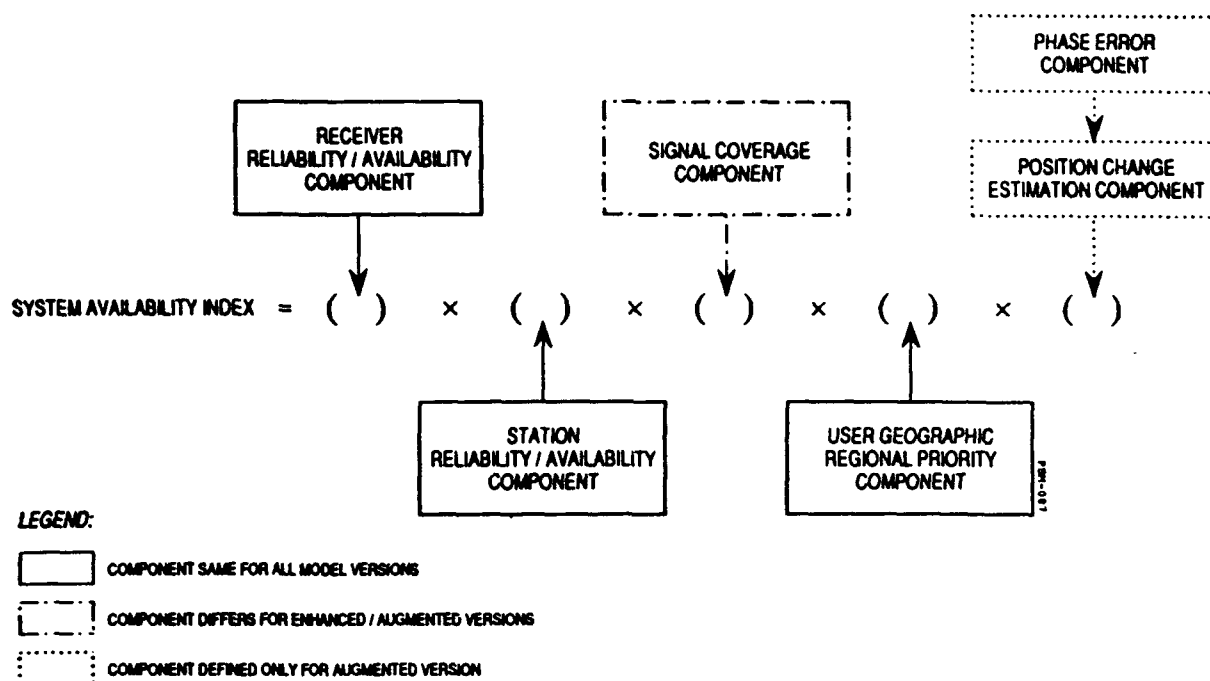
Figure 11.3-1 *Overview of System Availability Index Calculation in*
Terms of System Availability Model Components

In general, the MTBF and MTTR depend on the specific Omega receiver system (manufacturer/model) including the antenna installation, but for receivers within the same generic class (as discussed in the following section), these two parameters are approximately constant.

Classes of Omega Receiver Systems — Omega receiver systems are manufactured for a variety of applications including airborne, surface (marine/land), and special sensors. Receiver systems within each application area can differ markedly (e.g., those marine receivers that are used for surface ships and those used for submarines). For most applications, two classes of receiver systems are distinguished:

1) Modern airborne/marine Omega systems

2) Omega sensors/early-generation systems.

A brief description of each of these receiver systems follows using terminology given in Chapter 12.

Airborne systems for airliners and high-performance military aircraft are usually quite sophisticated and include VLF* signal processing, rate aiding from true air speed and heading sensors, electronically steerable crossed loop H-field antennas, and coupling into the autopilot and mission computer.

11-12

Omega systems for general aviation aircraft are less sophisticated and generally feature E-field antennas (e.g., vertical whip) because there is less degradation in signal-to-noise ratio associated with the closer proximity to the engine. Surface marine systems include rate aiding (speed through water and magnetic heading) and E-field antennas but do not process VLF signals. Receivers on board submerged vessels process signals in the hyperbolic mode to eliminate the highly variable antenna to sea-surface segment of the propagation path. Omega sensors include repeating units for meteorological balloons or airborne drones. In many cases, these sensors are "throw-aways," used only once. Early-generation systems refer to first- or second-generation receiver systems (introduced for service in the early 1970s) that are still in use.

Reliability and availability parameters, e.g., MTBF, for receivers in the above classes vary widely. In some cases, these parameters have been established for individual components of the receiver equipment, e.g., MTBF for the antenna coupler unit or control display unit. For class (1) systems, the MTBF figures range from 3000 to 6000 hours and MTTR[§] of about 2 hours. The MTBF figures for class (2) systems (excluding throw-away sensors) are generally shorter, e.g., 1000 to 2000 hours, with MTTR values somewhat less than 2 hours.

For multiple receiver classes, a more general form for the system availability index, P_{SA}, is given by:

$$P_{SA} = \frac{1}{N} \sum_{i=1}^{n_c} n_i \, P_{R_i} \, P_{A_i}$$

where:

n_i = number of receivers of class i ($i = 1, 2, \ldots, n_c$)

n_c = number of receiver classes

N = total number of receivers = $\displaystyle\sum_{i=1}^{n_c} n_i$

P_{R_i} = reliability/availability for a class i receiver

P_{A_i} = probability that three or more usable signals are accessible by a class i receiver

Unlike the reliability/availability probability, P_{R_i}, the dependence of P_{A_i} on receiver class is not so obvious. P_{A_i} depends on the signal coverage parameters and on the specific signal access criteria

---

[*] Here, VLF refers to those communication signals broadcast by the U.S. Navy/NATO communication stations at frequencies between 16 and 30 kHz.

[§] An alternative measure (to MTTR) that is sometimes used is *mean time for unit replacement.*

employed for assigning/defining coverage. In particular, the signal access criterion threshold for SNR is chosen based on estimates of conventional Omega receiver sensitivity and other parameters (see Ref. 2, Appendix B). Because these receiver parameters are roughly the same for a given receiver class, the SNR threshold criterion may be keyed to receiver class. PACE is not structured for analysis of multiple receiver classes, and since there is no universally accepted "average" reliability/availability figure for Omega receiver systems, P_R is set to 1.0 for PACE applications.*

11.3.2 Transmitting Station Reliability/Availability Component

Omega station reliability is clearly central to the calculation of system availability and has some important operational features that critically influence the development of this component. One of the most important features of station reliability is that all station off-air occurrences are classified as either:

- Unscheduled — random occurrence/duration
- Scheduled — deterministic occurrence/duration.

These types of off-airs are discussed in the following subsections.

Unscheduled Off-air Conditions — Unscheduled off-airs occur as the result of unforeseen circumstances — usually equipment failure. Their individual occurrence may be considered random but occurrence statistics can be compiled that are characteristic of a particular Omega station. This characterization arises because of antenna type, environmental factors, and component replacement history. The off-air occurrence statistics are naturally derived from historical reliability figures for a particular Omega station. The statistics are best compiled on a month/year/station basis because the month (as a unit of time) is:

- Equal to or shorter than any climatically important interval such as winter, summer, wet season, dry season, typhoon season, etc.; thus, the monthly statistics can be examined for climatic trends
- Long compared to the time required to resolve a problem causing an emergency/ unscheduled off-air condition; as a result the off-air probability assigned based on historical figures is more meaningful.

Based on average off-air times for a given month/year (compiled from historical figures), it can be shown (Ref. 2 and Appendix B) that for simple yet reasonably general off-air occurrence/duration probability functions, the probability that a particular station is in an unscheduled off-air condition at any

---

*For a typical, high-quality airborne Omega receiver, P_R is at least 0.999.

given time during a specified month is approximately T_{OA}/T_{TOT}. Here, T_{OA} is the average total off-air time (usually in minutes) for the specified month/station (based on compiled data for the same month/station) and T_{TOT} is the total time in the specified month (same units).

Scheduled Off-air Conditions — Scheduled off-airs are, as the name implies, planned conditions under which a station ceases operation. In this case "planned" refers to both the time at which the off-air begins and the off-air duration. The planning usually includes an advance notification to users of the scheduled off-air conditions, although the amount of advance notice may vary considerably depending on the urgency of the work to be done during the off-air.

Typical advance notice for scheduled off-airs (excluding annual maintenance, see below) is one to two weeks. From a user's viewpoint, these types of scheduled off-airs may be considered to have random occurrence times in terms of predictability on time scales longer than the advance off-air notice. Thus, a scheduled off-air probability is defined for the entire month for each station, similar to that for unscheduled off-airs, assuming no advance knowledge of the off-air at the beginning of the month.* Note that the probability is assumed constant throughout the month, independent of whether or not an off-air occurred previously in the month.

Annual maintenance periods are a rather special type of scheduled off-air having two main features:

- The maintenance off-air period for maintenance and/or repair must occur in a specific, distinct month for each station (see Fig. 11.3-2); any antenna, electronics, or structural maintenance/repair which is not of an urgent nature must be scheduled during the station's annual maintenance period.

- The scheduled off-air period for annual station maintenance is planned well in advance and users are generally given one to two months' notice.

Because of the long lead time, these types of scheduled off-air events are deterministic for a monthly prediction interval. Deterministic events may be incorporated in a probabilistic model by assuming an "impulse-type" probability density function (see Ref. 2, Appendix A). Thus, the different probability distributions followed by unscheduled off-airs and both types of scheduled off-airs may be incorporated into a single probabilistic model of system availability.

Probabilistic Relationships between Unscheduled and Scheduled Off-air Events — Several important operational features concerning station off-airs are also incorporated into this model

---

*If advance notice is received by the first of the month, the scheduled off-air will likely occur in the first few days of the month, thus leaving the off-air probability figure (based on historical records) to apply for the remainder of the month.

Month	Station							
	A	B	C	D	E	F	G	H
January								
February								
March								
April								
May								
June								
July								
August								
September								
October								
November								
December								

G–13553
11–20–91

Figure 11.3-2   Omega Station Annual Maintenance Months

component. From a probabilistic viewpoint, these features may be grouped in two categories that identify exclusive events and independent events:

Exclusive Events:

- An unscheduled off-air event at a given station cannot be concurrent with a scheduled off-air event at the same station, i.e., an off-air is either scheduled or unscheduled, not both.

- A scheduled off-air event at a given station cannot be concurrent with a scheduled off-air event at any other station; this operational doctrine is imposed to stop the preventable loss in system coverage occurring with simultaneous station off-airs.

Independent Events:

- An unscheduled off-air event at a given station is independent of a concurrent unscheduled off-air event at any other station; this is due to the random nature of unscheduled off-airs.

- An unscheduled off-air event at a given station is independent of a concurrent scheduled off-air at any other station; this is again due to the unpredictable nature of unscheduled off-air events.

These types of off-air events and their interrelationships are described quantitatively in Section 11.6.

Historical Station Reliability Statistics — Monthly Omega station off-air times have been compiled for a number of years. As an example, Table 11.3-1 lists the scheduled and unscheduled

Table 11.3-1 Station off-air Probabilities (Unscheduled and Scheduled) $\times 10^4$ for the Months of February, May, August, and November during the Years 1985, 1986, and 1987

Station	Unsched(U) or Sched(S)	1985				1986				1987			
		Feb	May	Aug	Nov	Feb	May	Aug	Nov	Feb	May	Aug	Nov
A	U	1.2	1.9*	1.6	1.9*	1.9*	1.9*	0.7	2.1	1.2*	9.0	1.9*	1.9*
	S	26.9§	26.9§	697.6	26.9§	26.9§	26.9§	564.3	26.9§	26.9§	26.9§	2055.1	26.9§
B	U	29.5	16.4	6.7	13.0	250.2	8.1	49.7	8.1	23.4	33.6	0.4	6.9
	S	2981.1	3.7§	3.7§	3.7§	4205.1	3.7§	47.7	3.7§	3184.5	3.7§	3.7§	3.7§
C	U	1.0	2.8*	0.7	1.9	2.8*	2.8*	4.7	11.3	2.8*	2.8*	11.9	1.9
	S	207.3	360.4§	360.4§	360.4§	360.4§	360.4§	360.4§	360.4§	360.4§	9999.9†	17.2	360.4§
D	U	3.7*	3.7*	6.7	3.0	0.5	1.6	3.7	5.1	1.5	3.7*	6.3	3.7*
	S	2.4§	2.4§	2.4§	2.4§	2.4§	2.4§	2.4§	2.4§	2.4§	2.4§	2.4§	2.4§
E	U	3.7	2.5	0.9	1.2	1.2	1.8	258.8	0.7	9.2	2.2	7.2	21.8
	S	16.3§	16.3§	282.3	16.3§	16.3§	16.3§	16.3§	16.3§	16.3§	16.3§	16.3§	16.3§
F	U	6.8*	6.3	6.9	4.6	1.5	0.9	4.7	0.5	43.2	6.8*	20.6	4.6
	S	3.0§	3.0§	3.0§	3.0§	3.0§	3.0§	3.0§	3.0§	3.0§	3.0§	3.0§	3.0§
G	U	3.5	1.2*	17.0	1.2*	1.5	1.2*	1.2*	3.0	1.2	1.2*	1.2*	1.6
	S	6.1§	6.1§	6.1§	294.7	6.1§	6.1§	6.1§	207.9	6.1§	6.1§	6.1§	15.3
H	U	1.5	0.9	0.2	1.4	0.5	2.5	2.2*	0.5	2.2	4.5	9.0	2.2*
	S	0.7	0.9	0.9	0.5	1.0	0.9	0.9	0.9	1.0	0.5§	0.5§	0.5§

* No unscheduled off-air for the indicated month; value shown is default based on station's average unscheduled off-air for years 1985–1988.

§ No scheduled off-air for the indicated month; value shown is default based on station's average schedule off-air (excluding annual maintenance month) for years 1985–1988.

† No scheduled on-air for the indicated month; value shown is default adjustment.

station off-air probabilities ($\times 10^4$) for the months of February, May, August, and November in the years 1985 to 1987. For example, in February 1987, the unscheduled off-air probability for Station F (Argentina) was 0.00432. The data shown in the table does not strictly report the actual unscheduled and scheduled off-air fraction, but rather projects off-air probabilities for each station/month in future years based on historical records. As the notes at the bottom of the table indicate, in many cases, no unscheduled and/or scheduled off-air was reported for a particular month/year/station. A strict projection of this data into the future would imply that the corresponding probabilities are also zero. Since this projection is unrealistic (and also violates some of the mathematical foundations of the model), *default* values are substituted for these zero probabilities based on off-air fraction averages over the years 1985 to 1988 for the given station and month. For scheduled off-airs, the averaging excludes annual maintenance periods, since these are considered deterministic over monthly cycles, whereas the occurrence of scheduled off-airs is assumed to be random at the beginning of a month. Based on reasoning similar to that for off-air defaults, a fixed *on-air* default of 10^{-5} is used to indicate a finite on-air probability for the station/ month (assuming that an entire month's off-air is not a certainty at the beginning of the month).

Any set of station off-air statistics may be used in PACE, but a default set is provided which is recommended for most applications. These default statistics specify an unscheduled off-air probability of 0.001* for all stations and months. The default scheduled off-air (excluding annual maintenance) event probabilities are assumed to be station-specific but are constant for each month over the year (all default off-air probabilities are assumed independent of year). These values are obtained by averaging observed scheduled off-air times (excluding annual maintenance) over three recent years (data obtained from Ref. 6) for each station. Scheduled off-air probabilities for annual maintenance are computed by averaging the off-air times for each station's maintenance month over three recent years (Ref. 6). The resulting data are shown in Table 11.3-2. In this table, the first entry (for a given month/station combination) is the fixed unscheduled off-air event probability, the second is the scheduled off-air (excluding annual maintenance) event probability, and the third is the scheduled annual maintenance event probability. Note that the scheduled off-air (excluding annual maintenance) event probability is specified even for the months corresponding to a station's annual maintenance. This is because a scheduled off-air event (with a few days advance notice) may occur during the month, before or after the annual maintenance period with approximately the same relative probability as during the other months. Unscheduled off-air events at one or more stations may also occur, but scheduled events differ probabilistically in that they are never concurrent.

11.3.3 Signal Coverage Component

In descriptions of Omega signal coverage, the word "coverage" is usually defined in terms of the usability of a single signal for position/navigation. Although the usability is broken down into categories, the essential idea is that the signal phase must be an approximately linear, regularly varying, increasing function of distance from a transmitting station (for a fixed time/time interval).

The original presentation of the System Availability Model (Ref. 2) utilized the 2-hour/4-month 10.2 kHz signal coverage information developed in 1980 (see Chapter 10) to obtain sample numerical results. Since that time, however, implementations of the System Availability Model have used the much more comprehensive 24-hour/4-month/2-frequency signal coverage database. This database is conveniently described in terms of how it is generated. The 24-hour/4-month/2-frequency signal coverage database is generated in two stages as described below.

In the first stage, signal amplitude and phase are computed (from theoretical models) for both the total (mode-sum) signal and its Mode 1 component. These two components are separately specified

---

*This has the approximate meaning that for any selected (short) interval of time, Δt, (e.g., $\Delta t \sim 1$ minute), the probability that the station is off-air between t and t+Δt.

Table 11.3-2   Station Reliability/Availability Parameters for PACE*

MONTH	STATIONS							
	A	B	C	D	E	F	G	H
JAN	.00100 .00269 .00000	.00100 .00037 .00000	.00100 .03604 .00000	.00100 .00024 .00000	.00100 .00163 .00000	.00100 .00030 .00000	.00100 .00061 .00000	.00100 .00005 .00000
FEB	.00100 .00269 .00000	.00100 .00037 .34569	.00100 .03604 .00000	.00100 .00024 .00000	.00100 .00163 .00000	.00100 .00030 .00000	.00100 .00061 .00000	.00100 .00005 .00000
MAR	.00100 .00269 .00000	.00100 .00037 .00000	.00100 .03604 .00000	.00100 .00024 .00000	.00100 .00163 .00000	.00100 .00030 .20511	.00100 .00061 .00000	.00100 .00005 .00000
APR	.00100 .00269 .00000	.00100 .00037 .00000	.00100 .03604 .00000	.00100 .00024 .00000	.00100 .00163 .00000	.00100 .00030 .00000	.00100 .00061 .00000	.00100 .00005 .00000
MAY	.00100 .00269 .00000	.00100 .00037 .00000	.00100 .03604 .00000	.00100 .00024 .00000	.00100 .00163 .00000	.00100 .00030 .00000	.00100 .00061 .00000	.00100 .00005 .00000
JUN	.00100 .00269 .00000	.00100 .00037 .00000	.00100 .03604 .28628	.00100 .00024 .00000	.00100 .00163 .00000	.00100 .00030 .00000	.00100 .00061 .00000	.00100 .00005 .00000
JUL	.00100 .00269 .00000	.00100 .00037 .00000	.00100 .03604 .00000	.00100 .00024 .07895	.00100 .00163 .00000	.00100 .00030 .00000	.00100 .00061 .00000	.00100 .00005 .00000
AUG	.00100 .00269 .11057	.00100 .00037 .00000	.00100 .03604 .00000	.00100 .00024 .00000	.00100 .00163 .00000	.00100 .00030 .00000	.00100 .00061 .00000	.00100 .00005 .00000
SEP	.00100 .00269 .00000	.00100 .00037 .00000	.00100 .03604 .00000	.00100 .00024 .00000	.00100 .00163 .61490	.00100 .00030 .00000	.00100 .00061 .00000	.00100 .00005 .00000
OCT	.00100 .00269 .00000	.00100 .00037 .00000	.00100 .03604 .00000	.00100 .00024 .00000	.00100 .00163 .00000	.00100 .00030 .00000	.00100 .00061 .00000	.00100 .00005 .32515
NOV	.00100 .00269 .00000	.00100 .00037 .00000	.00100 .03604 .00000	.00100 .00024 .00000	.00100 .00163 .00000	.00100 .00030 .00000	.00100 .00061 .01726	.00100 .00005 .00000
DEC	.00100 .00269 .00000	.00100 .00037 .00000	.00100 .03604 .00000	.00100 .00024 .00000	.00100 .00163 .00000	.00100 .00030 .00000	.00100 .00061 .00000	.00100 .00005 .00000

* First entry is the unscheduled off-air event probability; second entry is the scheduled off-air (excluding annual maintenance) event probability; third entry is the scheduled annual maintenance off-air event probability.

because the Mode 1 component is assumed to adequately represent the total signal for navigation purposes, although the Mode-sum signal is actually received. The first-stage database contains the signal amplitude for the short-path/long-path (shorter or longer of the two great-circle paths between a transmitter and receiver) and phase for the short-path only. The amplitude for the short- and long-paths is separately specified because most navigation models assume that the received signal is propagated via the short-path whereas in some cases the long-path signal may actually dominate the total received signal amplitude. The signal parameters stored in this database are specified for:

- Signal frequencies of 10.2 and 13.6 kHz
- Each of the eight Omega stations
- Radial paths at bearing intervals of approximately 10 degrees from each station
- Distance intervals of 500 km along each path
- Each of the 24 UT hours
- The months of February, May, August, and November.

In the second stage of the database generation, the signal parameters defined above are interpolated from the station radial path-based grid to a coarser-scale matrix/cell format for use with PACE. The parameters in the first-stage database are transformed into parameters specified by the signal coverage access criteria. The resulting database is known as the PACE database. Specifically, the parameters of the propagated Omega signal stored in the PACE database are, for a given path (Omega transmitting station and receiver location), time (hour/month), and frequency (10.2 or 13.6 kHz):

- Short-Path Signal-to-Noise Ratio (100 Hz BW) [SPSNR]
- Ratio of SPSNR to Long-Path signal-to-noise ratio (100 Hz BW) [SP/LP]
- Mode 1 Dominance Margin (invoked as a criterion if Dominant Mode selector ON; not invoked if Dominant Mode selector OFF) [M1DM]
- Path-Terminator Crossing Angle (invoked as a criterion only if terminator crosses short path) [PTCA]
- Geometric Dilution Of Precision [GDOP].

In the above, SP and LP refer to the shorter and longer arcs, respectively, of the great-circle path connecting transmitting station and receiver locations over the (assumed spherical) earth. In most cases, Mode 1 is the Omega signal's transverse magnetic (TM) modal component with the lowest phase velocity and attenuation rate; mode-sum refers to the sum of all modal components, i.e., the total signal. The Mode 1 dominance margin is the ratio of the amplitude of the Mode 1 amplitude to the interfering mode (IM)

amplitude. The IM is the phasor sum of all modal components excluding Mode 1. When M1DM has small positive values or is negative, the phase deviation is likely to be large and a navigation user may experience a cycle slip or jump. Also, when the angle between the short (great-circle) path and the terminator (great-circle boundary between day and night on the surface of the earth) is small, the day-to-night transition may occur too quickly for signal phase tracking by the receiver. Thus, the path/terminator angle is computed to test for conditions leading to a possible cycle slip or jump. The analytical form of the GDOP is based on a navigation data processor model representative of a typical airborne Omega receiver (Ref. 7).

Spatially, the signal parameter data is referenced to propagated paths from each transmitting station to 444 receive points distributed uniformly throughout the globe. Located at the center of "cells" (the unit of spatial resolution of the database), the receive points are assumed to adequately represent signal reception from a given station throughout the cell. The cells are 10 degrees (latitude) by 10 degrees (longitude) near the equator but are redefined in the higher latitudes to maintain an approximately constant area of one square megameter (10^6 km^2). Table 11.3-3 defines the cell latitude and longitude dimensions as a function of latitude.

Temporally, the data is referenced to signal paths (defined by transmitting station/cell combinations) at fixed global times. The signal path calculations are made on the hour for each of the 24 UT hours. Since for a given hour, the signal propagation parameters show definite change from month-to-month but little change day-to-day within a month, the signal calculations are made for the 15th day in each of four months: February, May, August, and November. Moreover, since the month-to-month change in the hourly signal propagation parameters is not too large, the signal data can be reliably interpolated over the two months separating "neighboring" coverage months. Thus, the information in the PACE database is referenced to 24 hours and 12 months.

Table 11.3-3   Latitude/Longitude Dimensions of Cells for Signal Coverage Database (Matrix Format)

LATITUDE RANGE*	DIMENSION OF CELL		NUMBER OF CELLS IN BOTH HEMISPHERES
	LATITUDE	LONGITUDE	
0° to 40°	10°	10°	288
40° to 60°	10°	15°	96
60° to 75°	15°	15°	48
75° to 90°	15°	60°	12
TOTAL NUMBER OF CELLS = 444			

*Same for northern and southern hemisphere.

Data from the database and models described above do not solely determine coverage. Signal coverage access criteria, together with the corresponding thresholds, are applied to the data to determine the usability of the given signal in the presence of the given noise. Application of an access criterion yields a "yes" (presence of coverage) or a "no" (absence of coverage). Default signal coverage access criteria (as recommended for use with PACE) are given as follows:

1) $SNR \geq -20$ dB (100 Hz BW)
2) $M1DM \geq 6$ dB
3) $SP/LP \geq 6$ dB
4) $PTCA \geq 5°$
5) $GDOP \leq 6$.

Signals that satisfy the deterministic signal coverage access criteria for a given location/time are said to constitute the *coverage set*. Table 11.3-4 shows a cell coverage example in which the coverage set is composed of signals CGH. The shaded entries indicate those parameters that fail the default signal coverage access criteria.

11.3.4   User Geographic Regional Priority Component

The user geographic regional priority component of the System Availability Model incorporates a type of spatial dependence different from that for the signal coverage parameters described in Section 11.3.3. Through the use of relative weights, this component specifies the probability of Omega usage in different geographical regions. The system availability index, P_{SA}, is first computed for individual cells and then combined into an overall P_{SA} using the weights.

Table 11.3-4   Cell Coverage Example

STATION SIGNALS	SNR (dB)	M1DM (dB)	SP/LP (dB)	PTCA (deg)
A	−25	7.2	+85	47
B	−11	0.02	+09	58
C	+10	10.3	+122	61
D	+45	−1.1	+156	81
E	−16	6.6	−22	36
F	−22	−4.4	+93	06
G	−10	7.9	+88	41
H	−15	6.2	+52	14

The probability obtained in combining probabilities governing separate spatial cells must be carefully interpreted. The overall P_{SA} is not, for example, the probability that receivers are functioning and three or more signals are accessible (or that the position accuracy exceeds some threshold) simultaneously in all cells on the globe. It is also not the probability that these same conditions exist in at least one of the 444 worldwide cells. The resulting P_{SA} is the probability that a single user is in any particular cell on the globe at any given time, the user's receiver is functioning, and three or more signals are accessible (or the position accuracy exceeds some threshold). In practice, the time and space domains may be restricted, e.g., one or more hours in a month and/or a certain region of the globe, but this restriction is properly handled by normalized weights and does not affect the basic theory. Because P_{SA} is targeted to the individual user, the probability of his location in space and time is therefore important to the calculation. If a given Omega user is no particular predisposition for any cell/time, the probabilities are all equal (uniform weighting) and is proportional to the sum of the P_{SA} components computed at each cell and time. Most users do have geographical preferences/needs, however, so that the probability of utilizing Omega in a given cell varies from cell to cell. Preferences in time are much less common, although some user classes may exhibit more local daytime usage than local nighttime.

The probability of utilizing Omega in each of the 444 global cells is specified by a cell weighting matrix. For PACE applications, the weights associated with each cell are chosen as integral values between 0 and 10. To represent utilization probabilities, a selected set of weights is normalized over the globe. A region may be selected for evaluation of by assigning non-zero weights to the appropriate cells and zero weights to all other cells. An example of cell weighting for the North Pacific region is shown in Fig. 11.3-3. The figure shows a weights display screen from PACE which indicates non-zero weights for cells in the North Pacific region and zero weights elsewhere.

To quantify the above discussion, define event D as follows:

D ≡ event that, at a given time, an Omega user has a functioning receiver and:

a) has access to at least three usable signals (original and enhanced System Availability Model)

b) experiences a radial position error less than a pre-established threshold error (augmented model).

Notice that in this event definition, condition (b) presumes that condition (a) is satisfied. Now define event L_i as:

L_i ≡ event that, at the given time, the user is located in cell i.
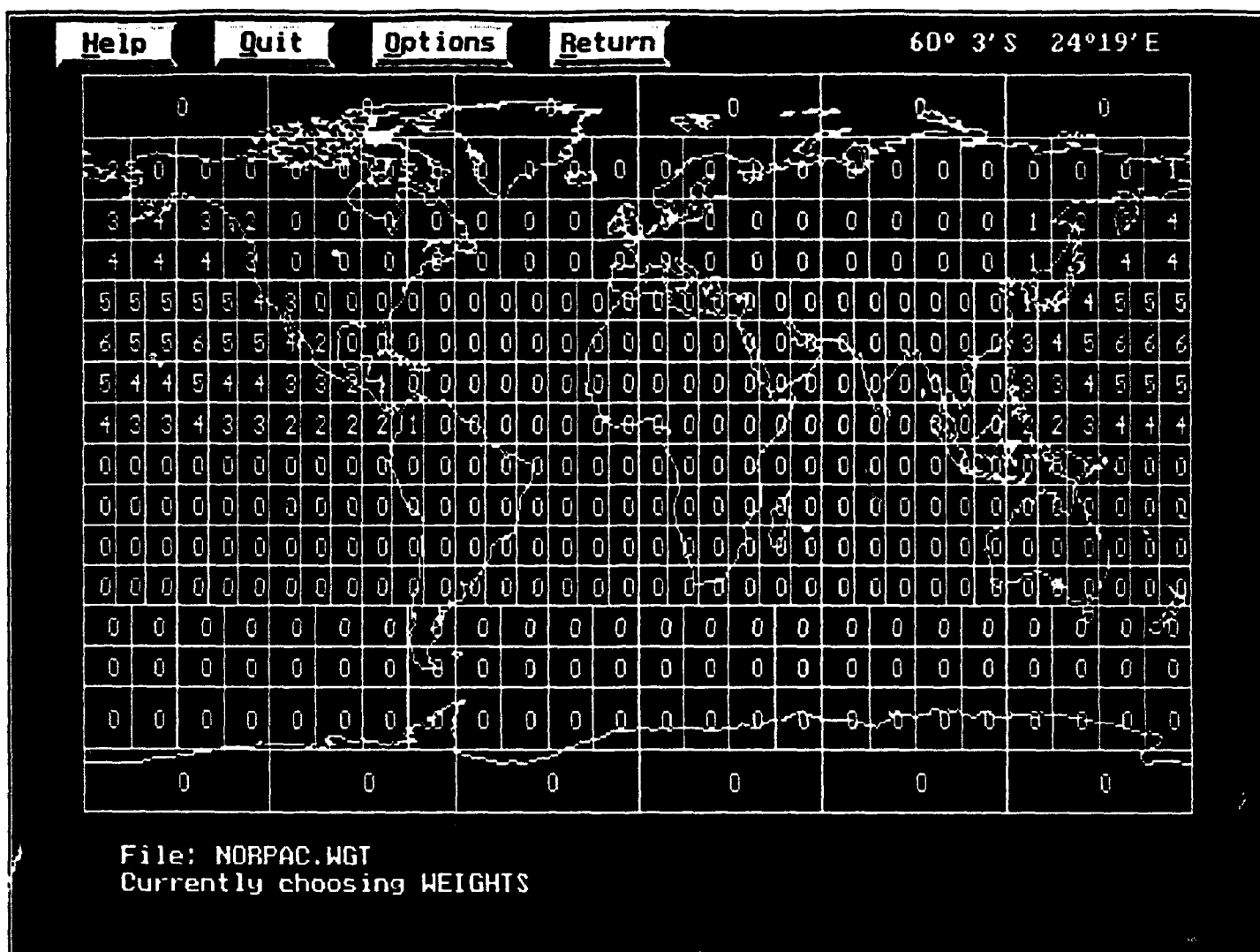
Figure 11.3-3 PACE "Weights" Screen showing Weights Assigned to Cells in the North Pacific (all other cells are weighted zero)

The events, L_i, $i = 1, 2, \ldots 444$ are mutually exclusive, since the single user can only be in one cell at a given time. Using this property, it can be shown (Ref. 6) that:

$$P(D) = \sum_{i=1}^{444} P(DL_i).$$

In this expression, the indicated "product" means the set intersection of the two events. In terms of conditional events, this may be written:

$$P(D) = \sum_{i=1}^{444} P(D \mid L_i) P(L_i) = \sum_{i=1}^{444} P(D_i) P(L_i) = \sum_{i=1}^{444} w_i P(L_i)$$

where event D_i is the event D subject to the condition that the user is located in cell i and $w_i = P(D_i)$ is the "weight" assigned to cell i to indicate the user's *a priori* probability of being located in cell i. Since $P(D_i)$ is normalized over the entire space of cells, the weights, wi, must also be normalized, so that:

$$\sum_{i=1}^{444} w_i = 1$$

11.4 CALCULATION OF SYSTEM AVAILABILITY INDEX

In this section, the probabilistic results obtained for each of the System Availability Model components described in Section 11.3 are combined to construct an analytical form for the system availability index, P_{SA}. The enhanced and augmented versions of System Availability Model are also briefly described in this section. More complete treatments of these versions are found in Sections 11.7, 11.8, and Appendix B. Because the synthesis of the model components into a full probabilistic model is somewhat complex, the development in this section focuses briefly on the overall procedure and uses examples to illustrate the concepts. Most of the analytical details are contained in Sections 11.6, 11.7, and 11.8. Advanced readers may wish to pursue the formal development of the analytical form for P_{SA}, which is contained in Ref. 7 and Appendix B.

11.4.1 P_{SA} in Terms of Receiver Reliability/Availability and Coverage Probability

Recall from Section 11.3.1 that P_{SA} may be expressed as a product of probabilities:

$$P_{SA} = P_R P_A \tag{11.4-1}$$

where P_R is the probability that a user's receiver is operational, e.g.,

$$P_R = 1 - MTTR/MTBF$$

for a uniform failure model of receivers with reliability/availability parameters MTTR (mean time to repair) and MTBF (mean time between failure). This can be further generalized by allowing for multiple receiver classes as explained in Section 11.3.1.1.

P_A is the access probability, i.e., the probability that three or more signals are accessible. Accessibility is defined in terms of the coverage criteria applied to single or collective signals.

First, assume that the user is confined to a single "cell" (two-dimensional spatial unit) so that P_A is defined locally. Once P_A is determined analytically for a single cell, the user geographic regional priority component is used to specify P_A (and P_{SA}) for the entire globe.

Also, in the following development, it is assumed that the time (month and hour) is fixed. Using the resulting analytical expression, P_A can be determined for each time and/or averaged over a desired set of hours/months (as permitted in PACE).

11.4.2 Calculation of P_A in Terms of Accessible Signals

To simplify the development and make the discussion more concrete, the example of signal coverage given in Table 11.3-4 is used. Except for GDOP, the table lists the signal parameters specified in the signal coverage access criteria. GDOP is a collective signal access criterion and thus depends on the set of signals satisfying the individual signal access criteria. Although the coverage parameters listed in the table do not correspond to real data, they are representative of data which might be obtained in a southeastern U.S. cell at a time in local late afternoon. For this example, the default signal coverage access criteria introduced in Section 11.3.3 are used, i.e.,

1) SNR $\geq$ –20 dB (100 Hz BW)
2) M1DM $\geq$ 6 dB (Dominant Mode selector ON)
3) SP/LP $\geq$ 6 dB
4) PTCA $\geq$ 5°
5) GDOP $\leq$ 6.

Coverage is determined simply by applying each of the coverage criteria to the corresponding signal parameters for each station signal. A station signal then "covers" the cell/time assumed by the table if *all* of the signal access criteria (except GDOP) are satisfied. Inspection of the table shows that station signals C, G, and H satisfy the individual signal access criteria. The resulting GDOP for these three signals is 5.6, which meets the GDOP criterion. Thus, for the default signal access criteria, signals C, G, and H cover the cell at the given time.

In determining signal coverage above, it is implicitly assumed that the station signals are always on-air. Thus, when a station undergoes an unscheduled or scheduled off-air, the coverage pattern changes and the cell may be "uncovered" for the cell/time. The probability of stations being concurrently off-air is addressed by the transmitting station reliability/availability component in Section 11.3.2. These results are combined with the signal coverage component to determine system availability.

11.4.3 Calculation of P_A for Deterministic Coverage Parameters

Define X as the event that three or more station signals are both on-air and are accessible to (cover) the cell/time of the example discussed in Section 11.3.3. Then:

$$P_A = P(X)$$

It can be shown (Ref. 6 and Appendix B) that $P(X)$ may be expressed as:

$$P(X) = P(XB_0) + P(XB_1) + \ldots + P(XB_{12}) + \ldots + P(XB_{123}) + \ldots + P(XB_{45678}) \ [219 \text{ terms}]$$

$$(11.4\text{-}2)$$

where B_0 is the event that no stations are off-air, B_1 is the event that station 1 is off-air, B_2 is the event that station 2 is off-air, etc. Similarly, B_{12} is the event that stations 1 and 2 are off-air, B_{13} is the event that stations 1 and 3 are off-air, etc. In the same way, B_{123}, B_{1234}, and B_{12345} are examples of 3, 4, and 5 station concurrent off-air events, respectively. The sum does not include events with more than five concurrent station off-airs, since, in that case, fewer than three station signals would be on-air, thus violating the definition of event X. $P(X)$ may be written as a sum of probabilities because the B-events are all mutually exclusive.

In terms of conditional probabilities (written as Q), the probabilities of the intersection of the X and B events appearing in Eq. 11.4-2 may be written:

$$P(XB) = P(X/B) \, P(B) \qquad \text{[For each type of B-event]}$$
$$= Q \, P(B)$$

where Q* has subscripts to match B's subscripts, e.g., $Q_0 = P(X/B_0)$. To illustrate the meaning of the conditional probabilities, recall that in the deterministic example given in Section 11.3.3, stations C, G, and H (or, equivalently 3, 7, and 8) are accessible, so that, for example,

$$P(X/B_1) = Q_1 = 1 \; ; \; Q_7 = 0$$
$$Q_{12} = 1 \; ; \; Q_{23} = 0$$
$$Q_{125} = 1 \; ; \; Q_{458} = 0$$
$$\ldots\ldots\ldots \qquad \ldots\ldots\ldots\ldots$$

Thus, in the deterministic case, $P(X)$ is just the sum over the probabilities for those B-events which do not specify any of the stations 3, 7, or 8 as off-air. In this case, only 31 of the original 219 terms are non-zero. The probabilities for the B-events are obtained using the methods outlined in Section 11.3.2.

11.4.4 Enhanced Version of the System Availability Model

As used in this report, system availability is a probabilistic indicator of system performance and thus assumes a certain amount of randomness in each of the model components. In the original version

---

*For a particular location and time, the Q's, i.e., Q_0, Q_1, $\ldots$ Q_{123}, are known as the *local coverage elements*.

of the System Availability Model, the signal coverage component is assumed to be completely deterministic, i.e., none of the signal coverage parameters are assumed to be random. The enhanced version of the System Availability Model incorporates random signal and noise variation from the signal coverage component into the probabilistic structure of the model. Thus the system availability index, P_{SA}, retains its probabilistic definition when computed with the enhanced version and the numerical value of P_{SA} should be more representative of Omega usage probabilities actually experienced. This increase in model realism is balanced by an increase in model complexity.

As explained above, the original System Availability Model treats the signal amplitude from the Omega signal coverage database and the noise level from the WGL/NRL noise model/algorithm (Ref. 8) as deterministic quantities. This restriction is removed in the enhanced version of the System Availability Model which considers signal amplitude and noise level as random quantities. Specifically, signal amplitude and noise level are assumed to be lognormally distributed (Ref. 9) with mean values obtained, respectively, from the signal coverage database and the WGL/NRL model/algorithm. Standard deviations for the signal amplitude distribution are available from an algorithm based on empirical data (Ref. 9). The noise level standard deviation data may be generated by use of the WGL/NRL model/algorithm for the specified cells and times.

In the case of assumed deterministic coverage variables (e.g., path/terminator angle), application of an access criterion yields a "yes" (presence of coverage) of a "no" (absence of coverage). For assumed random coverage variables (e.g., noise level), the criterion threshold furnishes a limit for a probability distribution function so that satisfaction of the criterion is determined in a probabilistic sense. The default signal coverage access criteria given in Section 11.3.3 are repeated as follows:

1) SNR $\geq$ –20 dB (100 Hz BW)
2) M1DM $\geq$ 6 dB (Dominant Mode selector ON)
3) SP/LP $\geq$ 6 dB
4) PTCA $\geq$ 5°
5) GDOP $\leq$ 6.

All the above- cited criteria are considered deterministic from the viewpoint of the original System Availability Model. For the enhanced version of the Model, default criteria (2) and (3) are considered deterministic, since:

- Criterion (2) addresses only the relative distribution of energy (among the modes
- Criterion (3) involves only the signal amplitude which is less variable than the noise.

Criterion (4) is deterministic for all versions of the model. The signal amplitude and noise level which make up the SNR specified in Criterion (1) are actually the mean values of these (assumed random) variables.

Signals that satisfy the deterministic signal coverage access criteria for a given location and time are said to compose the *maximal coverage set*. The maximal coverage set is so named because all signals of the set "cover" the point in question if the random quantities (e.g., signal amplitude and noise level) simultaneously satisfy the appropriate coverage access criterion. In the same sense, there is a finite probability that the actual coverage set could be empty if all random quantities simultaneously failed to satisfy the appropriate access criteria. Table 11.4-1 shows a cell coverage example identical to the example given in Table 11.3-4 except that the shaded entries indicate those *deterministic* parameters which fail the default signal coverage access criteria. In this example, then, the maximal coverage set comprises signals ACGH.

The calculation of the local coverage elements for the random SNR case is not as straightforward as for the deterministic case. Because the calculation is somewhat involved, it is presented in Section 11.7.

11.4.5   Augmented Version of the System Availability Model

Since its original development, the System Availability Model has been augmented to incorporate an expanded definition of signal coverage. Instead of asking whether three or more individual signals are accessible at a given location/time, the augmented version of the model seeks to know if the

Table 11.4-1   Cell Coverage Example for Random SNR

STATION SIGNALS	SNR (dB)	M1DM (dB)	SP/LP (dB)	PTCA (deg)
A	−25	7.2	+85	47
B	−11	0.02	+09	58
C	+10	10.3	+122	61
D	+45	−1.1	+156	81
E	−16	6.6	−22	36
F	−22	−4.4	+93	06
G	−10	7.9	+88	41
H	−15	6.2	+52	14

collection of individually accessible signals is likely to provide a minimum acceptable position accuracy. Thus, for the augmented version, the accessibility question is rephrased to ask:

> What is the probability that an Omega user can utilize three or more Omega signals with a properly functioning Omega receiving system *to achieve an acceptable navigation/ position accuracy (less than some maximum error threshold)* at any location (within a region or the entire globe) and at any time?

This definition of coverage is consistent with some other navigation/location systems (e.g., NAVSTAR GPS, a satellite-based positioning system for air and surface users) that define system coverage in terms of *position accuracy* instead of signal accessibility. This is especially true for systems (unlike Omega) in which signal accessibility is not generally a problem. Because of the concern for signal usability and the fact that a variety of positioning/navigation algorithms were used in Omega receivers, position accuracy was not incorporated into earlier definitions of Omega coverage. As airborne receivers began to dominate the Omega market in the 1980s, however, the different types of navigation/positioning algorithms began to converge. As a result, a single generic navigation algorithm, typical of aircraft-based Omega receivers and reasonably representative of the performance realized by a majority of current Omega users, can be analyzed to determine typical airborne Omega receiver navigation performance.

Based on the above ideas, the augmented version of the System Availability Model (Ref. 7) was developed to provide a more comprehensive (and, hopefully, more meaningful) representation of system availability. In this version, P_{SA} is defined as the probability that, at any location/time, a user's receiver is properly functioning and the position indicated by the receiver is in error by less than a pre-determined threshold. A model based on this definition of P_{SA} requires signal phase error and position change estimation components in addition to the four components composing the basic System Availability Model.

The signal phase error component addresses Omega signal phase error that arises from uncertainties involved in transforming the received signal phase to a two-dimensional position on (or near) the earth's surface. This procedure is performed in the normal course of navigating with Omega. To make this transformation, a propagation correction (PPC) is added to the received signal phase measurement to properly relate the phase measurement to position. Some error is incurred in the receiver measurement process, but most of the error is found in the predicted PPCs. The error in the predicted phase (or, equivalently, the PPC) is obtained from measurements made at specially instrumented Omega monitoring sites around the world. The phase errors are characterized by two parameters of the phase error probability distribution: (1) the mean error for a given hour over a month or half-month (also known as bias error), and (2) the standard deviation of error for a given hour over a month or half-month (also known as random error).

The position change estimation component describes the transformation of the phase error into position error based on a generic navigation processor model characteristic of airborne Omega receivers. The transformation involves parameters such as bearing angles to the stations and the update interval used to process Omega signal phase measurements.

The calculation of P_A for the augmented version is complex since it involves the integration of a radial error probability density function up to the threshold (maximum tolerable) error. Because of the complexity involved, further details regarding the calculation of P_A are given in Section 11.8.

11.4.6 Summary of P_{SA} Calculation

Because the calculation of P_{SA} is complex and involves a number of components, it is useful to review the computational procedure, the sequence in which the components are invoked, and the inputs required at each stage. Figure 11.4-1 illustrates the procedure as a computational flow through the model components for each of the three versions of the System Availability Model. The nomenclature is consistent with that introduced in this section, Section 11.3, and Sections 11.6–8.
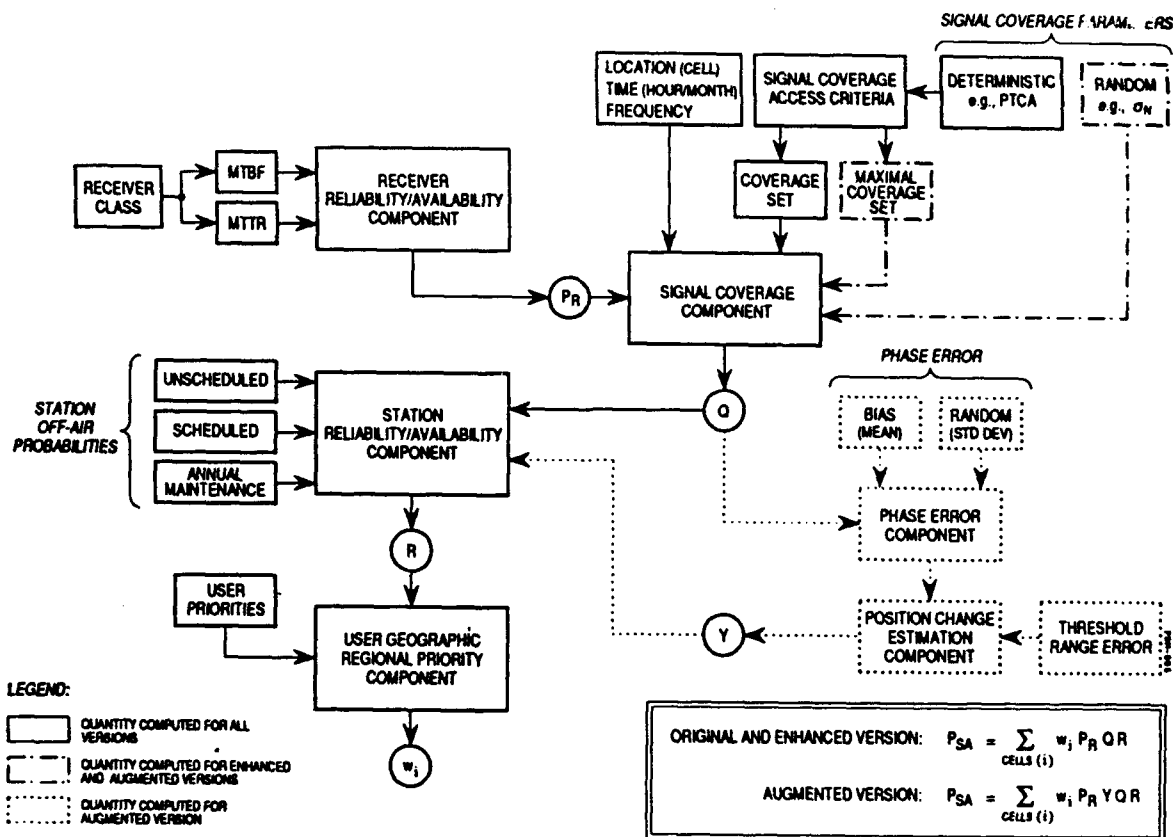
Figure 11.4-1 Computational Flow for P_{SA} in terms of the Model Components for the Original, Enhanced, and Augmented Versions of the System Availability Model

The receiver reliability/availability component is usually first invoked since it is generally independent of other components (although it does have indirect ties to the coverage component as noted in Section 11.3.1). If invoked, this component requires a MTBF and MTTR for one or more receiver classes. The result of the component calculation is the probability that the receiver is properly functioning (P_R) at the time it is required for service.

The signal coverage component requires the approximate position (to within ~ 300 nautical miles) and time (hour and month). This component also requires input of the signal coverage access criteria as discussed in Section 11.3.3. The signal coverage parameters (available from the 24-hour/4-month/2-frequency signal coverage database) are placed into one of two groups depending on the version of the System Availability Model considered:

1) The deterministic coverage parameters: For the original version of the System Availability Model, these include all the coverage parameters; for the enhanced and augmented versions, these include M1DM, SP/LP, and PTCA (GDOP is a collective signal access criterion used in the original and enhanced versions but not in the augmented version).

2) The random coverage parameters (only for the enhanced and augmented versions): These include the standard deviations of signal amplitude and noise level.

In the original version, the signal parameters that satisfy the signal coverage access criteria make up the coverage set that is used in the signal coverage component to compute Q. For the enhanced and augmented versions, station signals for which the *deterministic* coverage parameters satisfy the signal coverage access criteria make up what is known as the maximal coverage set. With these data, the signal coverage component specifies the probability of coverage (Q), given that a certain combination of stations is on-air.

The phase error component is invoked only by the augmented version of the System Availability Model. This component requires inputs of phase error bias (obtained from the mean value of phase measurements over a month or half-month at a given hour) and random (day-to-day standard deviation at a fixed hour) components. These phase error data are available only at Omega monitor sites, thus severely limiting the spatial application of this component. However, if a satisfactory spatial model of phase error becomes available, this component would have unrestricted global application.

The position change estimation component describes how the phase error probability distribution is transformed to position error density and distribution functions. The transformation is based on a least squares estimation technique that is reasonably similar to that employed in the navigation filters of conventional aircraft Omega receiver systems. The position error density function can be used to calcu-

late conventional error measures (e.g., RMS error) or converted to a radial error distribution function. As input, the component requires a threshold range error, which is measured with respect to the "true" position or the fix bias position. This component computes the conditional probability that the radial error is less than some threshold value (Y), given that a certain combination of stations are accessible.

The station reliability/availability component computes the network reliability factors (R), the joint off-air/off-air probabilities associated with each possible combination of stations. The calculations of R are based on historical (or otherwise specified) records of station reliability figures for unscheduled, scheduled, and annual maintenance off-airs. Each R-value associated with a specific subset of off-air stations is multiplied by the Q-value for the corresponding signal subset to obtain the complete probability that the signals in the maximal coverage set are available. The sum is then taken over all possible subsets. For the augmented version, the resulting probabilities are combined with the Y-values (evaluated for the desired threshold range error) and summed over all subsets of the maximal coverage set.

Finally, the user geographic regional priority component is invoked to compute P_{SA} over all cells of the globe, or a region. User preferences/priorities regarding Omega usage are input to this component and normalized weights (w_i) for one or more cells are produced. The resulting weights are multiplied by the previously computed probabilities (including P_R) for each cell and summed to obtain the final value for P_{SA}. At the bottom of Figure 11.4-1, a heuristic form is given for P_{SA} for the original/enhanced and augmented versions in terms of the output probabilities for each of the components.

11.4.7   Sample P_{SA} Results

In this section, two applications of the original version of the System Availability Model using the 24-hour/4-month/2-frequency signal coverage database are presented. These applications show how P_{SA} can be used to evaluate system options. The calculations made in these applications are based on a 1991 PACE database. More recent versions of PACE have a revised database so that current PACE results for the same scenario may differ somewhat from those presented here.

The P_{SA} values for these applications are computed using PACE. The inputs and conditions for the calculation are listed below for each model component.

1) Receiver reliability/availability component: assume a perfectly functional receiver, i.e., $P_R = 1$.

2) Signal coverage component: use the PACE default signal coverage access criteria given in Section 11.3.3; assume a signal frequency of 10.2 kHz. [Space/time conditions are given for each application.]

3) Phase error component: not invoked.

4) Position change estimation component: not invoked.

5) Station reliability/availability component: off-air/on-air probabilities given as PACE default values specified in Section 11.3.2.4.

6) User geographic regional priority component: assume equally weighted cells over the globe.

The results of the P_{SA} calculations are illustrated as diurnal plots, i.e., spline curve fits to P_{SA} values at each of the 24 UT hours for a given month. These plots show the sizable variation of P_{SA} over any 24-hour day in a given month.

In the first application, system options regarding the operating power level of a single station are to be evaluated. The hypothetical system options may be imagined to arise from a corroding antenna span at a station which must eventually be replaced or removed. Temporarily, the station can continue at full power (10 kW), but after several months, the station must operate at reduced power (2.5 kW) after the span is removed. If the reduced power operation proves untenable, the station will be disestablished. To assist the system manager in evaluating alternatives, system availability is to be computed for the following three conditions:

1) All transmitting stations at full power (10 kW effective radiated power at 10.2 kHz)

2) All transmitting stations at full power except for Station C (Hawaii) at 2.5 kW (6 dB power reduction)

3) All transmitting stations at full power except for Station C (Hawaii) at 0 kW Hawaii permanently off-air).

Diurnal P_{SA} plots for two months (corresponding to "best" and "worst" P_{SA}) are to be analyzed.

Figures 11.4-2 and 11.4-3 illustrate the effect on global P_{SA} of Hawaii power reduction during February and August. The February plot shows that a 6 dB reduction in Hawaii power has little effect on P_{SA} during the hours 0100 to about 1500 UT although the P_{SA} difference between Hawaii off-air and on-air is largest during this period (especially 0100 to 0900 UT). After 1500 UT, the P_{SA} diurnal curve for Hawaii at 2.5 kW begins to approach the off-air Hawaii curve, because between 0100 to about 0700 UT, signals on westerly paths from Hawaii provide maximum coverage because the paths are generally fully illuminated (up to their SNR range cutoff) and therefore non-modal. Thus, they are important contributors to coverage in this region and, when absent, P_{SA} is likely to drop substantially. Also, the average daytime attenuation rate for westerly paths from Hawaii is about 4 to 5 dB/Mm, so that a 6 dB reduction in Hawaii power (corresponding to a 3 dB reduction in signal amplitude) implies less than a 1 Mm reduction in the path SNR range cutoff, giving rise to little change in coverage. From about 0700 to 1600

11-34
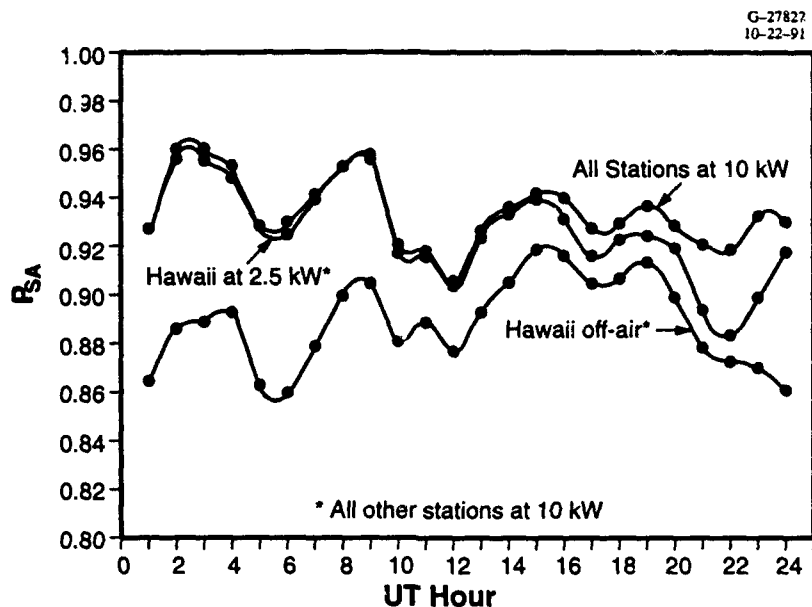
Figure 11.4-2 Effect of Hawaii Power Reduction on Global P_{SA} Diurnal Behavior in February using Default PACE Signal Coverage Access Criteria
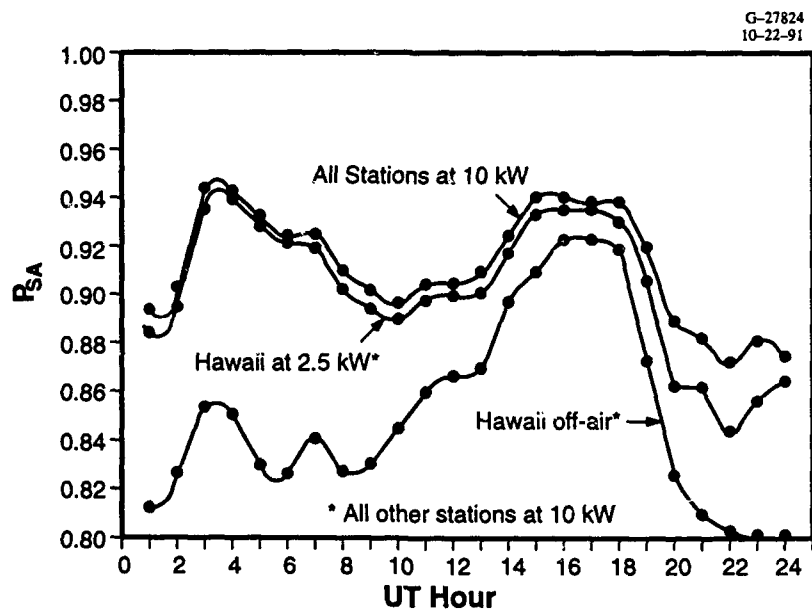
Figure 11.4-3 Effect of Hawaii Power Reduction on Global P_{SA} Diurnal Behavior in August using Default PACE Signal Coverage Access Criteria

UT, the westerly paths from Hawaii are in darkness giving rise to modal signals so that coverage is less affected by Hawaii's power level. This explains why the 10 kW and 0 kW curves become closer in Fig. 11.4-2. After about 1600 UT, Hawaii signals propagate through a daytime hemisphere to the east (many continue easterly into the nighttime hemisphere) in which the average attenuation rate is much lower. This leads to a greater dependence on Hawaii power level as reflected in the P_{SA} diurnal curves. Although the underlying P_{SA} diurnal curves are different, most of the same features described in connection with Fig. 11.4-2 appear in Fig. 11.4-3.

These results show that P_{SA} is little affected by a 6 dB Hawaii power reduction, relative to Hawaii off-air. Thus, a system manager may conclude it worthwhile to continue operating Hawaii at reduced power (assuming full-power operation is prohibitively expensive), even if some additional costs are incurred.

The second application considers evaluation of options to increase/decrease *all* station power levels, or equivalently, to increase/decrease minimum receiver sensitivity. This equivalence arises through the SNR coverage parameter which increases in direct proportion (in dB) to the station power level. Thus, for example, consider a user with a receiver having a minimum detection SNR of -20 dB operating along a route in which the SNR (for a given signal) decreases below -20 dB at some point and the receiver no longer tracks the signal. If the user follows the same route with a new receiver and is able to track the given signal in the previously excluded regime, the user cannot tell whether the station power level increased or the new receiver exhibited a similar increase (in dB) in sensitivity.

To analyze these options, diurnal plots of P_{SA} are constructed for four different sets of signal coverage access criteria. In each set, the coverage access criteria remain the same (equal to the PACE default signal coverage access criteria) except for the SNR criterion. Four threshold values for the lower-bound SNR in a 100 Hz bandwidth are considered: -10 dB, -20 dB (default), -30 dB, and -40 dB.

Figure 11.4-4 shows the global P_{SA} diurnal behavior in May for the four different SNR thresholds. The P_{SA} diurnal curve parameterized by an SNR threshold of -10 dB is substantially lower than the other curves. This indicates that a significant fraction of the globe includes signals with SNR between -10 and -20 dB. Fortunately, most Omega receivers on airborne platforms are designed with a minimum signal detection threshold corresponding to an SNR of -20 dB in a 100 Hz bandwidth. Other studies indicate that actual SNR thresholds may be 5 to 10 dB lower (Ref. 2, Appendix B). Figure 11.4-4 indicates that the P_{SA} diurnal curve for an SNR threshold of -20 dB, although much higher than the curve for -10 dB, is significantly lower (1 to 8%) than the curve for -30 dB. The exception occurs at about 0300 UT when P_{SA} values for SNR thresholds of $-20, -30,$ and -40 dB are within about 2% of each
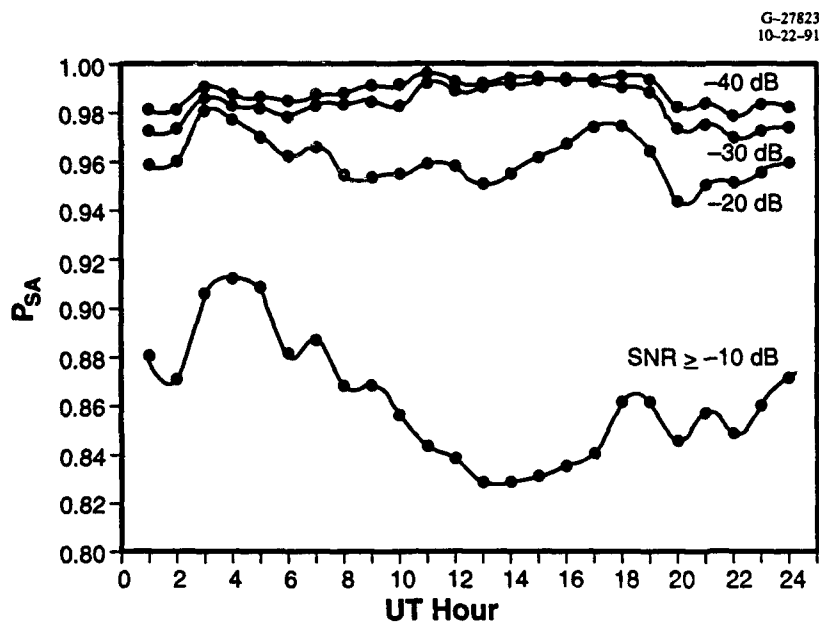
Figure 11.4-4 Global P_{SA} Diurnal Behavior in May for Four SNR Thresholds using Default PACE Signal Coverage Access Criteria for all other Criteria/Thresholds

other. During this time, it is presumed that modal (especially in connection with the Liberia signal) and other non-SNR effects are the principal sources of signal coverage exclusion. Finally, the figure shows little difference in P_{SA} between SNR thresholds of −30 and −40 dB at all hours.

If the current minimum SNR threshold for most receivers is assumed to be −20 dB, then a reduction of 10 dB in the power level of all Omega stations would result in a substantial, certainly unacceptable, drop in system availability. On the other hand, an increase of 10 dB in all station power levels (or a corresponding increase in receiver sensitivity) does increase system availability significantly (up to about 8%) for most hours. Another increase of 10 dB in station power level at all stations (or a corresponding increase in receiver sensitivity) increases P_{SA} very little. With this information, a system manager might very well leave station power at current levels, given that a 10 dB power level increase at all stations is extremely expensive. At the same time, receiver manufacturers may be persuaded that another 10 dB increase in receiver sensitivity is not warranted in view of the system availability differences.

11.5 PACE OVERVIEW

The Performance Assessment and Coverage Evaluation (PACE) workstation implements the System Availability Model described in detail in Sections 11.3 and 11.4. This graphical tool may be used interactively to:

- Extensively analyze of Omega system performance under user-selected conditions and criteria

- Selectively evaluate the effectiveness of the Omega system based upon spatial and temporal signal variations

- Analyze computational results with the use of features such as a summary global presentation of Omega signal availability and space- and time-dependent signal parameter displays

- Assess changes in Omega system performance based on specific operational assumptions using visual displays and comparison utilities.

In this section, a brief description of PACE structure and utilization is given, including databases, execution options, displays, and analysis procedures. Additional information on PACE and its more recent versions is found in Appendix C and Ref. 10.

11.5.1 PACE Top-level Description/Utilization

PACE is generally based on the original version of the System Availability Model with two major exceptions:

1) The receiver reliability/availability component is effectively ignored since PACE assumes the receiver 100% reliable and thus always available for use

2) GDOP is included directly in the calculation of P_{SA} rather than serving only as a criterion for the coverage (or maximal coverage) set.

The second exception above may be clarified further by recalling from Section 11.4.3 that the local coverage element (for the deterministic case) is one or zero, depending on whether:

- Three of more station signals are accessible (Q=1)

- Fewer than three station signals are accessible (Q=0)

when the appropriate off-air signals are deleted. In this case, accessible means satisfying the *individual* signal coverage access criteria (see Section 11.3.3.1). PACE has expanded the definition of accessibility by including GDOP as a collective signal access criterion to determine the value (zero or one) of each local coverage element.

The PACE workstation consists of software and database information hosted on any DOS-based IBM personal computer or compatible with the following minimum hardware configuration:

- 30 MBytes of hard disk space
- 1.44 MByte floppy disk drive
- 1 MByte of RAM
- EGA/VGA color monitor.

The PACE workstation software calcul..te   ?stem availability index (P_{SA}) for user-selected times, geographical areas, and signal coverage . . . The PACE workstation database includes pre- dicted signal parameters for each of the eight Omega transmitters. The PACE user interacts with the workstation through a set of on-screen selectors and controls, using a pointing device (mouse) and key- board to make selections. The P_{SA} calculation results are pr-c-nted both graphically and numerically using color displays to provide the overall "big picture" and quer, capability to provide detailed numerical P_{SA} and signal information. The use of color graphics to represent scenario results allows the quick identification of problem areas and/or times that warrant further investigation. PACE also facili- tates in-depth analysis of Omega system operation by providing access to intermediate P_{SA} calculation results as well as detailed signal database information.

One of the primary uses of PACE is to assist in the evaluation of different Omega system opera- tion/management options. System operation issues that can be addressed with PACE include the devel- opment of user guidance for properly using the Omega signals, the evaluation of signal coverage condi- tions for given operational scenarios and the investigation of Omega signal degradation due to geographical/temporal variation. System management options that can be evaluated include alternative station maintenance schedules, alternative station power levels, station disestablishment, and setting goals for station performance in terms of scheduled and unscheduled off-air periods. In summary, PACE provides Omega system operators and managers with a tool for investigating, assessing, and predicting Omega system performance for a wide range of operational conditions.

11.5.2 PACE Databases

PACE contains several databases that are used for computing coverage and system availability. Primarily, the signal parameter database and the station reliability database (also called the QR database) are used in the computation of system availability. Other PACE utility/support databases are discussed in Appendix C.

Signal information in the PACE signal database consists of predicted values for M1DM, SPSNR, long-path SNR, SPPD, and PTCA (see Section 11.3.3 for a description of these parameters). This signal information is used to compute signal coverage, which is an input into the coverage component of the system availability Model implemented by PACE.

The PACE signal parameter database contains spatially and temporally referenced signal information for all eight Omega transmitting stations and for two transmission frequencies (10.2 and 13.6 kHz). The spatial and temporal resolution of the data, i.e., the cell and the hour/month, respectively, is described in Section 11.3.3. With this resolution, the signal database contains 2,045,952 records of signal information (8 stations $\times$ 2 frequencies $\times$ 444 cells $\times$ 24 hours $\times$ 12 months). Each database record contains the signal information for the cell, hour, month, station, and frequency associated with that record.

Station reliability information and partially computed system availability indices (QR products; see Fig. 11.4-1) are contained in the PACE reliability database. In this database, each of the eight Omega stations is assigned a probability of a scheduled off-air event, a probability of an unscheduled off-air event, and an annual maintenance off-air probability for each month of the year. Essentially, these probabilities represent the fraction of the month that a station will be off-air due to one of the three defined off-air conditions. There are 96 records of reliability information in the reliability database (8 stations $\times$ 12 months). The QR products are pre-computed for all possible station combinations (256)* for each month and stored in the reliability database. The coverage set is merely a station combination which is used as an index to access the appropriate QR value. Once the coverage set and month of interest have been established during PACE operation, the corresponding QR value is retrieved to compute P_{SA}.

Annual maintenance at an Omega station typically occurs over a consecutive period during the month specified for annual maintenance at that station. The station reliability/availability component specifies this type of scheduled off-air as deterministic. However, these annual maintenance periods can be incorporated into the model as a uniform off-air probability distribution over the annual maintenance month. PACE employs this annual maintenance off-air algorithm in the "nominal station reliability model (SRM)." PACE offers two additional interpretations of the annual maintenance off-air probability: best SRM, and worst SRM. For the best SRM option, it as assumed that no station will be off-air due to annual maintenance for the time of interest. The worst case option assumes that a station with a non-zero maintenance probability for a given month will be off-air for the time of interest. For the reliability database, QR values for the best and nominal SRM are computed and stored for each signal coverage/month combination. The worst SRM QR values are not stored; these are handled at PACE execution time by

---

*As noted earlier, only 219 of these combinations include three or more stations.

selectively excluding station signals from the coverage set. The reliability database, then, contains 96 records of reliability information (8 stations × 12 months) and 6,144 records of QR values (256 station combinations × 12 months × 2 best/nominal SRM selections).

11.5.3 PACE Inputs

User input to the computation of a P_{SA} scenario fall into three general categories: the P_{SA} computation parameters, the signal coverage criteria thresholds, and thresholding and display parameters that control how PACE results are presented. The significance of the three parameter categories and how they contribute to PACE operation as a whole is discussed below. Table 11.5-1 lists the various PACE inputs according to category.

P_{SA} computation parameters are defined in PACE as those quantities that form the basic input to the P_{SA} algorithm. These parameters are the station off-air probabilities and the QR values in the reliability database, and the SRM selection. These inputs are transformed and combined according to the other user selections to produce the primary P_{SA} output of PACE.

Table 11.5-1   PACE User Input Parameters

	PARAMETER	DESCRIPTION	RANGE
P_{SA} Computation Parameters	Reliability	Station Reliability Set	Any file name
	SOM	Station Off-air Model	Best, nominal, worst
Signal Coverage Parameters	SNR	Short Path Signal to Noise Ratio	−99 dB to 99 dB
	S/L	Short/Long Path Signal Ratio	−198 dB to +198 dB
	ANG	Path Terminator Crossing Angle	0 deg to 90 deg
	σ_N	Standard Deviation of Noise Level	0 dB to 10 dB
	MDM	Mode 1 Dominance Margin	−99 dB to +99 dB
	A-H	Station Power Level	off, on, −99 dB to 99 dB
	GDP	Geometric Dilution of Precision	0 to 25
	FRQ	Frequency	10.2 kHz, 13.6 kHz, AND, OR
Thresholding and Display Parameters	P_{SA}	P_{SA}, P_{AC}, P_{AT} Threshold	0 to 0.999
	Month	Months of Interest	Jan to Dec
	Hour	Hours of Interest	0100 to 2400
	CCR	Cell Coloring Rule	Minimum, Mean, Maximum
	Weights	Weights and Region Definitions	0 to 9, on, off

Signal coverage criteria thresholds fix the criteria that are used to determine Omega signal coverage. In PACE, the coverage criteria thresholds established by user input are compared against the signal coverage database information to determine whether or not a particular cell/location is covered. Signal coverage criteria threshold values exist for all of the signal database quantities as well as the collective coverage parameter, GDOP.

After the system availability quantities have been computed by PACE, the thresholding and display parameters govern how the results will be presented on the display screen. These inputs include the display threshold for graphically displaying P_{SA} values, the specification of the months and hours of interest in the calculation, time-integrated P_{SA} statistics, and weight and/or special region definitions for specific cell areas of interest. The time-integrated Psa statistics indicate how spatial cells pass/fail the P_{SA} criterion:

- *Minimum* — Minimum P_{SA} over all times of interest for the cell
- *Maximum* — Maximum P_{SA} over all times of interest for the cell
- *Mean* — Mean P_{SA} over all times of interest for the cell.

11.5.4 PACE Execution and Results

PACE has several execution options that enable the user to observe various forms of time statistics for individual cells as well as global statistics. On the cell level, it is possible to select either the minimum, mean, or maximum time-integrated statistics for the times of interest within a cell. In the basic System Availability Model, the mean P_{SA} over the times of interest at a particular cell is used to represent the system availability value index for that cell. In PACE, however, additional user selections allow the user to choose either the minimum or the maximum value of the time-specific system availability values to represent the overall value for a cell. For the Minimum selection, PACE reports the most conservative or worst-case time-specific P_{SA} values for the cell. The Maximum selection reports the least conservative or best-case P_{SA} values. These selections allow the user to bound the range of P_{SA} attainable at any cell for a given set of input combinations.

11.5.5 PACE Display/Operation

The results of PACE computations are presented to the user in a variety of graphical and numerical displays. The primary capabilities include spatial and temporal representations of the P_{SA} results, comparison displays and utilities, and a scenario archive/retrieval subsystem. The various displays and controls allow the user to assess and further investigate the P_{SA} computation results.

The cell display is the primary display output for graphical system availability results. The display of P_{SA} computation results is shown at the cell level, with each cell's individual system availability

value compared against the user-selected P_{SA} threshold to obtain the appropriate cell color. The display is useful as a quick, visual means of assessing the overall impact of specific Omega system operational conditions.

Following processing and display of a scenario at the cell level display, more detailed information about the temporal nature of the P_{SA} result may be obtained. The summary cell query display shows a month/hour color coded matrix that indicates the hourly/monthly behavior of the time-specific P_{SA} values relative to the user selected threshold. Further information about time-dependent coverage and signal information may also be displayed numerically for any hour/month combination. Finally, single-station spatial coverage information is available for display in a cell format for a specific hour/month/frequency combination and user-selected threshold values.

The fundamental method available in PACE for assessing the difference between two P_{SA} scenarios is the split-screen display. In this display, the user is allowed to simultaneously view two scenario cell displays in side-by-side windows on the display screen. With this utility, the user can visually assess the impact of changes in the scenario input parameters.

To assist the user in managing a set of specific P_{SA} scenarios and the computed results, PACE incorporates an archive manager for saving and retrieving specific information concerning a scenario. The PACE archive contains any number of archived scenario files. A scenario file consists of a complete record of the parameters and results of a scenario as well as a descriptive comment about the scenario. The archive facility is useful for constructing scenario permutations and for performing scenario comparisons in conjunction with the split-screen feature.

11.5.6   PACE Utilization

This section presents several examples of the kinds of analyses that can be performed using PACE. The general steps that must be taken and the kinds of analyses that should be performed are explained. The examples address the effects of alternative operation for a single station including permanent disestablishment, changes in the annual maintenance months/durations, and the identification of low system availability conditions in specific geographic regions.

The first example explores the effects of: (1) reducing the transmitted power at a particular station and (2) permanently disestablishing that station. As a basis for comparison, a nominal scenario is first computed with all stations transmitting at nominal power and with default/baseline signal coverage access criteria thresholds. For the baseline scenario, it is also desirable to select all hours and months so

that the initial assessment is made on a spatial basis only. Once the baseline scenario has been computed, the split-screen option of PACE can be used to compare the baseline and reduced power scenario. For the reduced power case, the edit screen should be used to reduce the power level of the station of interest by the desired margin, or to turn off the transmitter entirely. After the reduced power/off-air scenario has been run, the split-screen view will visually indicate where P_{SA} changes from the baseline to the reduced power/off-air scenario. By changing the P_{SA} threshold value for both the baseline and the reduced power/off-air scenario (i.e., setting it to the same value in both scenarios) the sensitivity of the change can be observed. For example, if selecting a slightly lower P_{SA} threshold value (for both scenarios) causes large numbers of cells to fall below the threshold in the reduced power/off-air scenario, then P_{SA} is very sensitive to the power level for the station of interest.

After the spatial analysis outlined above has been performed, the next step is to select and explore a particular geographic area of interest for time-dependent P_{SA} behavior. For example, P_{SA} diurnal behavior for a small group of cells (e.g., $\leq$ 10 cells) may be desired for a particular region (e.g., North Atlantic air routes). To explore the region, a cell of interest is selected that brings up the hour/month matrix of the cell query display. On the cell query display, diurnal effects are recognized by groups of hour cells on the display indicating periods of time during the day that P_{SA} falls above or below the selected threshold. Monthly variations are indicated by changes in size/position of hour cell blocks where P_{SA} falls below the selected threshold. Further investigation into the source of the signal deficiency can be made by activating the detailed cell query window to display the database information and coverage for a particular station. For example, it may be useful to observe the SNR at a particular cell/hour/month combination for the reduced power station for both the baseline and the reduced power/off-air scenarios. In summary, the utilization of the user input parameters, split-screen display, and cell query capabilities of PACE provide the mechanisms to assess the effect of reducing the power or disestablishing any of the eight Omega stations.

The second example of PACE analysis is the assessment of alternative annual maintenance schedules in terms of overall system performance. For this example, it is necessary to build two different reliability databases, each reflecting the appropriate probability of station off-air due to annual maintenance in the desired annual maintenance month. Specifically, this example considers the effect of shifting the annual maintenance month/duration for station A from its default value (equivalent to approximately 3.5 days in August) to 15 days in April. The revised off-air probability for station A's annual maintenance is then 0.5 (= 15 days maintenance/30 days in the month of April). This can be accomplished using the QRBUILD program supplied with PACE. PACE can then be executed using the nominal reliability set (with default off-air probabilities for station A) for one scenario and using the revised

reliability set (with station A scheduled for maintenance in April) for the other. Further investigation can then be performed to isolate the effects of the change in month and duration of the off-air by executing additional scenarios for a 15-day annual maintenance period in August and a 3.5-day period in April. The results can then be compared using the split-screen mode to observe spatial and temporal changes using the procedure outlined in the reduced power/off-air case described above. Additionally, it may be beneficial to compare the results for the originally scheduled maintenance month (August) for both the normal and revised reliability sets by selecting only August for the display of P_{SA} results. A similar analysis can be performed for the revised annual maintenance month. The overall effect of changing station A's annual maintenance month/duration is given by the revised global P_{SA} value or P_{SA} difference (default – revised) for all hours and months.

The final example considers the evaluation of system availability for a specific region. This example is a useful application of the System Availability Model to users operating in a specific geographical area. A case in point would be aircraft equipped with Omega receivers flying regular routes over the North Pacific. In this case, the overall system availability should reflect the emphasis of Omega system performance in the North Pacific over Omega performance in all other regions (e.g., Antarctica). With the PACE cell weighting facility, the cells in the North Pacific can be assigned relatively more importance than the other global cells. Also, individual cells within the North Pacific region can also be ranked relative to one another. An example of a weighting scheme for the North Pacific region is shown in Figure 11.3-3. Using this cell weighting, a P_{SA} scenario can be processed. To detect specific problem areas/times, the Minimum time-integrated statistics should be used with this scenario. The use of Minimum statistics will cause the worst-case P_{SA} value for all hours/months of interest to be the reported P_{SA} value for each cell. This has the effect of bringing all of the "show stoppers" to the base cell display so that problem cells can be immediately identified. After the scenario is processed, the same type of spatial and temporal analysis described for the reduced power/off-air case can be performed.

11.6 APPENDIX: PROBABILISTIC DESCRIPTION OF STATION RELIABILITY/AVAILABILITY COMPONENT

11.6.1 Definitions and Properties of Off-air Events

Several important operational features concerning station off-airs are incorporated into the Transmitting Station Reliability/availability component. From a probabilistic viewpoint, these features may be grouped in two categories which identify exclusive events and independent events.

Exclusive Events:

- An unscheduled off-air event at a given station cannot be concurrent with a scheduled off-air event at the same station, i.e., on off-air must be either scheduled or unscheduled, not both.
- A scheduled off-air event at a given station cannot be concurrent with a scheduled off-air event at any other station; this operational doctrine is imposed to stop the preventable loss in system coverage occurring with simultaneous station off-airs.

Independent Events:

- An unscheduled off-air event at a given station is independent of a concurrent unscheduled off-air event at any other station; this is due to the random nature of unscheduled off-airs.
- An unscheduled off-air event at a given station is independent of a concurrent scheduled off-air at any other station; this is again due to the unpredictable nature of unscheduled off-air events.

To quantify these features as they apply to a probabilistic model, the various types of off-air events and their interrelationships are defined below. In operations with events, the following conventions (as with sets) are assumed in this and the following appendices:

- Sum indicates set union, i.e., $A + B = A \cup B$.
- "U" labels the universe, i.e., the set of all possible events.
- The complement of a set or event (denoted with a bar over the event label) means the collection of all possible events *exclusive* of the labeled event, i.e., for any event, $A, A \cup \overline{A} = U$.
- Difference indicates intersection with complement, i.e., $A - B = A \cup \overline{B}$.
- Product indicates intersection, i.e., $A\,B = A \cap B$.

Also, a probability function (denoted by $P()$) is assumed to be uniquely associated with each event, so that for event A, $P(A)$ is the probability that A will occur.

If $\overline{T}_i$ is defined as the event that station i $(i = 1, 2, \ldots 8)$ is off-air, then from the discussion above, this event may be decomposed as

$$\overline{T}_i = \overline{T}_i^u + \overline{T}_i^s \; ; \quad i = 1, 2, \ldots 8$$

where the superscript u labels an unscheduled off-air event and superscript s labels a scheduled off-air event. As noted above, the u- and s-events are mutually exclusive, so that

$$\overline{T}_i^u \, \overline{T}_i^s = 0 \; ; \quad i = 1, 2, \ldots 8$$

where "0" means the empty set. Another kind of exclusive event pair noted above arises from the operational exclusion of two concurrent scheduled off-airs, i.e.,

$$\bar{T}_i^s \, \bar{T}_j^s = 0 \; ; \; i,j = 1, 2, \ldots 8 \; ; \; i \neq j$$

Whereas mutually exclusive event pairs are defined in terms of set intersection and union as above, event *independence* is expressed in terms of the probability function defined on the event, i.e., the independence of events A and B is expressed as P(AB) = P(A)P(B). Thus, the independence of unscheduled off-air events at different stations is expressed as

$$P(\bar{T}_i^u \, \bar{T}_j^u) = P(\bar{T}_i^u) \, P(\bar{T}_j^u) \; ; \; i,j = 1, 2, \ldots, 8 \; ; \; i \neq j$$

Also, the independence of an unscheduled off-air event at any one station and a scheduled off-air event at any different station is expressed as

$$P(\bar{T}_i^u \, \bar{T}_j^s) = P(\bar{T}_i^u) \, P(\bar{T}_j^s) \; ; \; i,j = 1, 2, \ldots, 8 \; ; \; i \neq j$$

Note that the probability of the intersection of two s-events is zero, since the resulting event is operationally excluded.

11.6.2 Calculation of the Network Reliability Factors

In general, the network reliability factors are probabilities of intersections of eight on-air/off-air events, e.g.,

$$R_{35} = P(T_1 T_2 \bar{T}_3 T_4 \bar{T}_5 T_6 T_7 T_8)$$

where the T-events are defined in Section 11.6.1. A quantity such as R_{35} cannot be directly computed from the station reliability statistics, which are typically reported as single station values. Moreover, the historical off-air data is usually separately reported in terms of unscheduled and scheduled off-air statistics. Thus, the network reliability factors must be decomposed into probabilities of single station on-airs/off-airs.

The general decomposition of the network reliability factors into probabilities is complex and will not be given here. A thorough treatment is given in Ref. 2 and Appendix B. A brief glimpse of some of the properties of the T-events is given to give the reader an appreciation of the methods used. In this development, repeated use is made of the mutual exclusively and independence of the unscheduled and scheduled off-air events at the same or different stations which is presented in Section 11.6.1.

Consider for a moment the decomposition of the network reliability factor R_{12}. Thus,

$$R_{12} = P(\overline{T}1\overline{T}_2T_3T_4T_5T_6T_7T_8)$$
$$= P[(\overline{T}_1^u + \overline{T}_1^s)\,(\overline{T}_2^u + \overline{T}_2^s)\,T_3T_4T_5T_6T_7T_8]$$
$$= P[\overline{T}_1^u\overline{T}_2^u V + \overline{T}_1^u\overline{T}_2^s V + \overline{T}_1^s\overline{T}_2^u V]$$

where $V = T_3T_4T_5T_6T_7T_8$ and the fourth term vanishes because of the exclusion of simultaneous scheduled off-airs. Since the terms inside the brackets are mutually exclusive, R_{12} may be written

$$R_{12} = P(\overline{T}_1^u\overline{T}_2^u V) + P(\overline{T}_1^u\overline{T}_2^s V) + P(\overline{T}_1^s\overline{T}_2^u V)$$

Since unscheduled off-airs are independent of all other events, the three terms may be decomposed as

$$R_{12} = P(\overline{T}_1^u)P(\overline{T}_2^u)P(V) + P(\overline{T}_1^u)P(\overline{T}_2^s V) + P(\overline{T}_2^u)P(\overline{T}_1^s V)$$

Terms such as $P(TV)$ are decomposed using iterative methods explained in Ref. 2 and Appendix B. The result is that R_{12} can be expressed in terms of probabilities of unscheduled and scheduled off-air events.

To demonstrate the dependence of the on-air events, consider just two on-air events at stations 1 and 2. Thus,

$$P\,(T_1) = P(T_1U) = P(T_1\,(T_2 + \overline{T}_2)) = P(T_1T_2) + P(T_1\overline{T}_2)$$

where U is the set universe having the property that $AU = A$ and $U = A + \overline{A}$ for all sets A. The last equality above follows because the events inside the parenthesis are mutually exclusive (since $T_1T_2T_1\overline{T}_2 = 0$ (empty set)). Now the off-air events are decomposed into the mutually exclusive unscheduled and scheduled off-air events, i.e., $\overline{T} = \overline{T}^u + \overline{T}^s$. Hence, using the above equation to obtain $P(T_1T_2)$ yields

$$P(T_1T_2) = P(T_1) - P(T_1\overline{T}_2) = P(T_1) - P(T_1(\overline{T}_2^u + \overline{T}_2^s)) = P(T_1) - P(T_1\overline{T}_2^u + T_1\overline{T}_2^s)$$
$$= P(T_1) - P(T_1\overline{T}_2^u) - P(T_1\overline{T}_2^s) = P(T_1)\,(1 - P(\overline{T}_2^u)) - P(T_1\overline{T}_2^s)$$

where the mutually exclusive property of unscheduled and scheduled off-air events at the same station is used as well as the independence of unscheduled off-air events. The last term is decomposed in the same way that $P(T_1T_2)$ was decomposed above, i.e.,

$$P(T_1\overline{T}_2^s) = P(\overline{T}_2^s) - P(\overline{T}_1\overline{T}_2^s) = P(\overline{T}_2^s) - P((\overline{T}_1^u + \overline{T}_1^s)\overline{T}_2^s) = P(\overline{T}_2^s) - P(\overline{T}_1^u\overline{T}_2^s + \overline{T}_1^s\overline{T}_2^s)$$
$$= P(\overline{T}_2^s) - P(\overline{T}_1^u\overline{T}_2^s) = P(\overline{T}_2^s)\,(1 - P(\overline{T}_1^u))$$

11-48

where the exclusion of two concurrent scheduled off-air events is used. Substituting this result into the expression for $P(T_1T_2)$ gives

$$P(T_1T_2) = P(T_1)(1 - P(\overline{T_2''})) - P(\overline{T_2^s})(1 - P(\overline{T_1''}))$$

Now, by definition,

$$P(T_1) = 1 - P(\overline{T_1}) = 1 - P(\overline{T_1''} + \overline{T_1^s}) = 1 - P(\overline{T_1''}) - P(\overline{T_1^s})$$

and thus,

$$1 - P(\overline{T_1''}) = P(T_1) + P(\overline{T_1^s})$$

with the same result for T_2. Substituting these forms into the expression for $P(T_1T_2)$ yields

$$P(T_1T_2) = P(T_1) \, (P(T_2) + P(\overline{T_2^s})) - P(\overline{T_2^s}) \, (P(T_1) + P(\overline{T_1^s}))$$

$$= P(T_1) \, P(T_2) - P(\overline{T_1}^s) \, P(\overline{T_2^s})$$

This result (which exhibits the required symmetry for interchange of stations 1 and 2) shows explicitly the departure of events T_1 and T_2 from independence. Clearly, if the scheduled off-air probabilities are small, then the on-air events T_1 and T_2 are approximately independent as expected. However, if the scheduled off-air probabilities are significant (based on historical figures), then the inter-dependence of T_1 and T_2 is substantial. Finally, as noted before, this dependence arises because of the mutual exclusion of concurrent scheduled off-airs.

11.7 APPENDIX: PROBABILISTIC DESCRIPTION OF SIGNAL COVERAGE COMPONENT

11.7.1 Probabilistic Description of Random Coverage Variables

Consider the signals in the maximal coverage set at a given location/time. For these signals, define the following events involving the random variables making up the SNR:

$$A_i \equiv \text{event that } S_i/N \geq a \; ; \; \overline{A_i} \equiv \text{event that } S_i/N < a$$

where S_i is the signal amplitude for the signal from station i, N is the noise level, and a is the selected SNR lower bound threshold. By definition of the maximal coverage set, all other (deterministic) coverage access criteria are satisfied so that if event A_i occurs, signal i is accessible (or usable) to the space/time point; if $\overline{A_i}$ occurs, it is not.

If the probability density function for the SNR is defined to be p_{R_i}, then the probability of event A_i is

$$P(A_i) = \int_a^\infty dx\, p_{R_i}(x) \quad ; \quad P(\overline{A}_i) = 1 - P(A_i) \tag{11.7-1}$$

Since the signal and noise random variables making up the SNR are lognormal, it is convenient to define the SNR as $S_i - N$, where S_i and N are defined logarithmically (in dB). Then $p_{R_i}(x)$ is expressed in terms of the joint probability density function of S_i and N, subject to the constraint that $R_i = S_i - N$. Since the random signal and noise levels are assumed independent, the SNR density function, $p_{R_i}(x_i)$, may be written as

$$p_{R_i}(x_i) = \int_{-\infty}^{+\infty} dn\, p_{S_i}(n + x_i)\, p_N(n) \tag{11.7-2}$$

In this relation, p_{S_i} is the probability density function for the amplitude of the signal from station i and p_N is the probability density function for the noise level common to all signals. The above relation says simply that the probability of a given SNR value is just the sum (integral) over all possible noise levels of the probability of a signal level times the probability of the noise level such that the difference of the signal level and the noise level is just the given SNR value.

Since the signal and noise levels are assumed to be lognormal, the density functions may be written

$$p_{S_i}(s_i) = \frac{e^{-(s_i - \overline{s}_i)^2/2\sigma_{S_i}^2}}{\sigma_{S_i}\sqrt{2\pi}}$$

$$p_N(n) = \frac{e^{-(n - \overline{n})^2/2\sigma_N^2}}{\sigma_N\sqrt{2\pi}}$$

As noted above, the amplitude for signal i and the local noise level are independent random variables. Moreover, the amplitudes for each signal i are assumed to have independent variation since they are generally received over paths having a relatively wide range of electromagnetic environments. The noise envelope amplitude, n, is that which would be sampled over a period comparable to a receiver time constant (approximately 2–5 minutes). This noise level is thus common to the SNR for each signal, i, processed by an Omega receiver.

Substituting the expressions for the signal and noise level probability density functions into Eq. 11.7-2 yields for the SNR density function

$$p_{R_i}(x_i) = \frac{e^{-(x_i - (\bar{s}_i - \bar{n}))^2/2(\sigma_{S_i}^2 + \sigma_N^2)}}{\sqrt{2\pi(\sigma_{S_i}^2 + \sigma_N^2)}}$$

The SNR density function is thus also lognormal with mean value equal to the difference of the mean signal and noise levels and variance equal to the sum of the variances of the signal and noise levels. Substituting this result into Eq. 11.7-1 and performing the integration gives

$$P(A_i) = 1 - (1/2)erfc\left[((\bar{s}_i - n) - a)/\sqrt{2(\sigma_{S_i}^2 + \sigma_N^2)}\right]$$

The function labeled "efrc" in this expression is the complementary error function. This function is related to the more commonly used error function (erf) by $erfc(x) = 1 - erf(x)$.

For comparison, the probability of event A_i for the deterministic coverage component assumed in the original version of the System Availability Model (and PACE) is

$$P(A_i) = 1 \text{ if } \bar{s}_i - \bar{n} \geq a$$
$$= 0 \text{ if } \bar{s}_i - \bar{n} < a$$

The two expressions for $P(A_i)$ are plotted and compared in Fig. 11.7-1. The plots become more similar as σ_{S_i} and σ_N become smaller, since the uncertainty in the random variation becomes smaller and therefore more closely approximates a deterministic situation.

The joint probability distribution function for multiple A-events is more complex since these events are not independent. This dependence arises from the common noise level accompanying the processing of each signal during the period of a receiver time constant. The resulting joint probability density function (derived in Ref. 9) is given by

$$P(A_{i_1} A_{i_2} ... A_{i_m}) = \int_{-\infty}^{+\infty} F_{i_1}(n) F_{i_2}(n) ... F_{i_m}(n) p_N(n) \, dn \qquad (11.7-3)$$

where

$$F_{i_q}(n) = (1/2)erfc[(a - (\bar{s}_{i_q} - n))/(\sigma_{S_{i_q}}\sqrt{2})]$$

$$q = 1, 2, ... m$$

$$m = \text{number of signals in the maximal coverage set.}$$
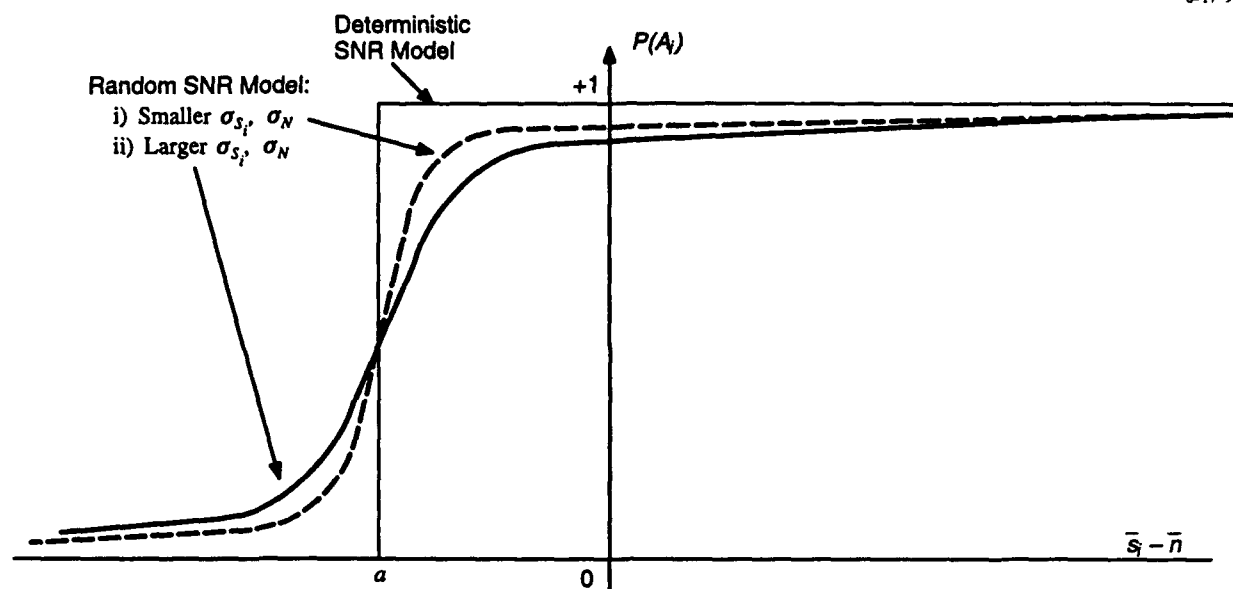
Figure 11.7-1   Probability that SNR for Station i $(\bar{s}_i - \bar{n})$ Exceeds Threshold a for the Deterministic SNR Model and the Random SNR Model (Two Cases)

The single integral over noise level in this expression must, in general, be evaluated numerically. The signal amplitude parameters (mean and standard deviation) as well as the threshold parameter, a, occur in the functions F_{iq}. The noise level parameters are contained in the noise level probability density function, p_N. In the deterministic case, the noise is also common to the multi-signal processing, but, since all quantities are deterministic, the calculation of the joint SNR distribution function is much simpler, i.e.,

$$P(A_{i_1} A_{i_2} \ldots A_{i_m}) \;=\; 1 \;\; if \, \bar{s}_{i_q} - \bar{n} \geq a \;\; for\, all\, i_q, q = 1, 2, \ldots m$$
$$=\; 0 \;\; \text{otherwise}$$

11.7.2   Calculation of P_A for Random SNR

For the random SNR case, calculation of the conditional probabilities is not as straightforward as for deterministic SNR. To simplify the development and make the discussion more concrete, the example of signal coverage given in Table 11.7-1 is used. Except for GDOP, the table lists the signal parameters specified in the signal coverage access criteria. GDOP is a collective signal access criterion and thus depends on the set of signals satisfying the individual signal access criteria. Although the coverage parameters listed in the table do not correspond to real data, they are representative of data that might be

obtained in southeastern U.S. cell at a time in local late afternoon. For this example, the default signal coverage access criteria are used, i.e.,

1) SNR $\geq$ –20 dB (100 Hz BW)

2) M1DM $\geq$ 6 dB

3) SP/LP $\geq$ 6 dB

4) PTCA $\geq$ 5°

5) GDOP $\leq$ 6.

Table 11.7-1   Example of Cell Coverage for Random SNR

STATION SIGNALS	SNR* (dB)	M1DM§ (dB)	SP/LP§ (dB)	PTCA§ (deg)
A	–25	7.2	+85	47
B	–11	0.02	+09	58
C	+10	10.3	+122	61
D	+45	–1.1	+156	81
E	–16	6.6	–22	36
F	–22	–4.4	+93	06
G	–10	7.9	+88	41
H	–15	6.2	+52	14

*Parameter is deterministic for original version; random for enhanced and augmented versions.
§Parameter is deterministic for all versions.

If all the signal coverage parameters are regarded as deterministic, coverage is determined simply by applying each of the coverage criteria to the corresponding signal parameters for each station signal. A station signal then "covers" the cell/time assumed by the table if *all* of the signal access criteria (except GDOP) are satisfied. Inspection of the table shows that station signals, C, G, and H satisfy the individual signal access criteria. The resulting GDOP for these three signals is 5.6, which meets the GDOP criterion. Thus, for deterministic signal coverage parameters and the default signal access criteria, the signals C, G, and H cover the cell at the given time.

If the SNR is regarded as random and all other signal parameters deterministic, then the *maximal coverage set* must be first established. By definition, the maximal coverage set includes those signals for which the *deterministic* coverage parameters satisfy the corresponding signal coverage access criteria. From the table it is seen that signals from stations A, C, G, and H satisfy signal access criteria (2) through (5) and thus make up the maximal coverage set.

First, consider $P(X/B_0) = Q_0$ and since the maximal coverage set contains A, C, G, and H (1, 3, 7, and 8), the definitions introduced in Section 11.7.1 may be used to show that

$$Q_0 = P[A_1A_3A_7\overline{A}_8 + A_1A_3\overline{A}_7A_8 + A_1\overline{A}_3A_7A_8 + \overline{A}_1A_3A_7A_8 + A_1A_3A_7A_8]$$

The first four terms in the brackets are the four mutually exclusive events describing which three of the four signals in the maximal coverage set are accessible, i.e., having an SNR that exceeds the minimum threshold. The fourth term is the event that all four signals of the maximal coverage set are accessible. Since the events are mutually exclusive, Q_0 may be written

$$Q_0 = P(A_1A_3A_7\overline{A}_8) + P(A_1A_3\overline{A}_7A_8) + P(A_1\overline{A}_3A_7A_8) + P(\overline{A}_1A_3A_7A_8) + P(A_1A_3A_7A_8)$$

The five probability terms in this expression cannot be further simplified because the A-events are *not* independent. This mutual dependence arises because of the noise level common to the measurement of each signal phase. The first term above may be written

$$P(A_1A_3A_7A_8) = P(A_1A_3A_7) - P(A_1A_3A_7A_8)$$

since $A_1A_3A_7U = A_1A_3A_7(A_8+\overline{A}_8) = A_1A_3A_7A_8 + A_1A_3A_7\overline{A}_8$ where U is the set universe and the last two events are mutually exclusive. Making this type of substitution for the first four terms in the expression for Q_0 yields

$$Q_0 = P(A_1A_3A_7) + P(A_1A_3A_8) + P(A_1A_7A_8) + P(A_3A_7A_8) - 3P(A_1A_3A_7A_8)$$

Each of the terms in this expression can be evaluated using Eq. 11.7-3. Note that

$$Q_0 = Q_2 = Q_4 = Q_5 = Q_6 = Q_{24} = Q_{25} = Q_{26} = Q_{45} = Q_{46} = Q_{56} = Q_{245} = \dots ,$$

i.e., Q_0 is the same as any Q whose indices do not include 1, 3, 7, and 8 — the station signals in the maximal coverage set.

Conditional probabilities that include just one of the maximal coverage set signals are easier to calculate since only three signals remain. Thus, for example, Q_1 is given by

$$Q_1 = P(A_3A_7A_8)$$

11-54

which again may be calculated by means of Eq. 11.7-3. Similarly,

$$Q_3 = P(A_1A_7A_8) \; ; \; Q_7 = P(A_1A_3A_8) \; ; \; Q_8 = P(A_1A_3A_7)$$

Furthermore, it is clear that

$$Q_{13} = Q_{17} = Q_{18} = Q_{37} = Q_{38} = Q_{78} = Q_{137} = Q_{138} = Q_{178} = Q_{378} = Q_{1378} = 0$$

since, in these cases, fewer than three station signals in the maximal coverage set remain on-air.

Thus, the calculation of each of the conditional probabilities (Q's) in the expression for $P(X)$ in the example being considered has been reduced to either one or zero in the deterministic case and to the integral formula (Eq. 11.7-3) or zero for the random SNR case. It is instructive to note that the formula for the probability of the intersection of A-events yields (after integrating over all noise levels) a value which depends on the mean value and standard deviation of the noise level, the mean and standard deviation of amplitude for each signal identified by the A-event index, and the lower-bound threshold SNR given by signal access criterion (1). Table 11.7-1 does not list any of these parameters, since the table reflects deterministic coverage parameters.* The parameters required for the random SNR case (except for the standard deviation of signal amplitude) are computed in the first stage of the 24-hour/ 4-month/2-frequency signal coverage database generation and are available in the most recent version of PACE (Ref. 10).

Thus, the expression of P_A, for either the deterministic or random case, is given by

$$
\begin{aligned}
P_A = P(X) = \; & Q_0R_0 \\
& +Q_1R_1+\ldots+Q_8R_8 \\
& +Q_{12}R_{12}+Q_{13}R_{13}+\ldots+Q_{78}R_{78} \\
& +Q_{123}R_{123}+Q_{124}R_{124}+\ldots+Q_{678}R_{678} \\
& +Q_{1234}R_{1234}+Q_{1235}R_{1235}+\ldots+Q_{5678}R_{5678} \\
& +Q_{12345}R_{12345}+Q_{12346}R_{12346}+\ldots+Q_{45678}R_{45678}
\end{aligned}
$$

where R (sometimes called the network reliability factor) labels the probability of the various B-events, i.e.,

$$R = P(B) \qquad \text{[For each type of B-event]}$$

and the subscripts of B match the subscripts of R.

---

*Recall that the SNR listed in Table 11.7-1 is actually $\bar{s} - \bar{n}$, i.e., the mean signal amplitude (dB) minus the mean noise level (dB), which are deterministic parameters.

11.8 APPENDIX: AUGMENTED SYSTEM AVAILABILITY MODEL COMPONENTS

In addition to the four components of the original System Availability Model — i.e., receiver reliability/availability, station reliability/availability, signal coverage, and user geographic regional priority — the Augmented System Availability Model contains a phase error and position change estimation component in order to compute a system availability index that incorporates position accuracy. These two model components are described in this Appendix, as well as the access probability, P_A, in terms of these model component parameters.

11.8.1 Phase Error Component

The phase error component is introduced in the augmented version of the System Availability Model since the system availability index for this version addresses position accuracy which is directly affected by phase errors. The station reliability and signal coverage components are structured to determine the probability that station signals are on-air and usable. The phase error component is used to find the distribution of phase errors for the the the on-air/usable station signals at a location and time.

To understand what phase error means, it is necessary to explain briefly how the received signal phase is used in a typical Omega navigation receiver system. In most of these systems, a correction known as the propagation correction (PPC), is added to the "raw" phase detected by the receiver. The PPC is *intended* to remove the complexities of signal phase behavior due to the long paths over which the signal is guided between the spatially varying earth's surface and the space- and time-varying ionosphere. When the PPC is added to the measured phase, the resulting phase obeys a so-called "nominal" model of signal phase dependence on distance from the station, which is independent of time, direction of propagation, and the multitude of other parameters on which the PPC depends. Thus, the nominal model (common to most receiver navigation algorithms) linearly relates the signal phase at a given frequency to distance from the transmitting station. However, the PPC itself depends on geographic location as well as time, station, frequency, etc. Thus, the reasoning may seem circular in the sense that the position must be known in order to apply the correct PPC value, which is used (together with the corrected phase values for two or more other stations) to determine the receiver location! The key point is that the PPC is *relatively* insensitive to position compared to the position dependence of the nominal value. The PPC is applied using only a *rough approximation* to the position (nearest 50 to 100 nautical miles) and the resulting corrected phase value is accurate to a few (1 to 4) nautical miles, depending mostly on the accuracy of the PPC value.

Thus, by definition, the PPC and the nominal model together determine the predicted phase for a given station, signal frequency, position, and time. The relationship is simply given by

$$\text{Predicted Phase} = \text{Nominal Phase} - \text{PPC}$$

In this relation, the nominal phase is the "dominant" term in the sense that it contains approximately 99 percent of the cumulative phase from the signal source, i.e., the distance between the transmitting station and the receiver in units of wavelength. Measured in cycles of signal wavelength (somewhat larger than a free-space wavelength at 10.2 kHz), the nominal phase is 100 to 500 for typical paths whereas the PPC is usually between −3.00 and +3.00, with a resolution of 0.01 cycle (a unit referred to as a centicycle). The predicted phase has a typical diurnal variation of 1 to 2 cycles, amounting to about 0.2 to 2 percent of the nominal phase.

Since the PPCs are predicted quantities, they contain errors, known as prediction errors which are given by (using the above equation for predicted phase)

$$\text{Prediction Error} = \text{Observed Phase} - \text{Predicted Phase}$$
$$= \text{Observed Phase} + \text{PPC} - \text{Nominal Phase} \qquad (11.8\text{-}1)$$

Two difficulties arise in determining the observed phase. The first is that a highly stable frequency standard (e.g., a cesium standard) must be used in connection with an Omega signal phase monitoring receiver synchronized to Coordinated Universal Time (UTC) (as are the Omega stations). Such standards are available at only a few Omega monitor sites. Monitor sites associated with each transmitting station may be conveniently used for this purpose, since they record a distant (remote) signal phase with respect to the local station phase. For these monitor sites, the cumulative phase from the local station (approximately one wavelength) is time-invariant (signal does not interact with the ionosphere) and can thus be precisely measured. The second difficulty is that the total cumulative phase cannot be measured with a single frequency phase comparison system alone. In principle, direct measurement of cumulative phase is possible with a time-of-arrival measurement of the leading edge of the one-second Omega pulse envelope or phase measurement of two synchronized, transmitted tones, separated in frequency by about 100 Hz. Since these methods are impractical, the usual procedure is to assume the nominal phase is correct to the nearest cycle.

Prediction error is composed of bias and random components. The bias error component is obtained by averaging the observed phase for a given station signal/frequency/monitor/hour over a two- to four-week period, i.e., from Eq. 11.8-1,

$$\text{Bias Error} = <\text{Observed Phase}> + \text{PPC} - \text{Nominal Phase}$$

where < > indicates average value.

This averaging procedure is permissible because the PPCs are roughly constant over a two- to four-week duration. The associated random component is computed as the standard deviation of the prediction error over the same period. For signals in the maximal coverage set, bias errors, both positive and negative, typically range from 0 to more than 20 centicycles (cecs) at 10.2 kHz; random error standard deviations (always positive) for the same signals typically range from 3 to 10 cecs. For the shorter wavelength Omega signal at 13.6 kHz, spatial displacements of the ionosphere will affect a greater fraction of the signal's wavelength, thus leading to larger centicycle errors at 13.6 kHz than 10.2 kHz. Although its wavelength is intermediate in length, $11^1/_3$ kHz Omega signals generally have larger prediction errors than the other two frequencies because of the smaller database from which the PPC model coefficients were computed (Ref. 11). In general, prediction errors are large for:

- Mixed paths (paths containing both day and night segments)
- Nighttime paths
- Transequatorial paths
- Westerly paths
- Longer paths (but the shorter of the two great-circle paths).

Before attempting to model prediction errors probabilistically, the sources of these errors must be investigated. In considering possible sources of error, noise is usually first proposed as the cause of random (zero-mean) error. The relatively long processing times (i.e., narrow processing bandwidths) common to Omega receivers, however, greatly reduce the impact of external atmospheric noise.

For example, consider a very marginal accessibility condition for a signal received in the presence of noise: a signal-to-noise ratio (SNR) of –20 dB in a 100 Hz bandwidth using a typical receiver on board an aircraft whose dynamics limit the designed receiver time constant to about 100 seconds. Since the duty cycle (fraction of time on-air) for one of the four common Omega signals is about 10 percent, the effective integration time is approximately 10 seconds. Now, it can be shown that for a receiver with an exponential filter (generally true for phase lock loop-type receivers) having a time constant of $1/a$, the noise equivalent bandwidth (Ref. 7) is $a/4$. Thus, for a time constant of 10 seconds, the effective bandwidth is 0.025 Hz. Since the noise referred to in the definition of SNR is noise power per unit bandwidth, the SNR increase realized in reducing the bandwidth from 100 Hz to 0.025 Hz is

$$10 \log_{10} (100/0.025) = 36.02 \text{ dB}$$

Hence, the effective SNR at the receiver output is $-20 + 36 = 16$ dB. Furthermore, using a phasor model of signal phase error due to noise (see, for example, Ref. 7, Appendix A), the standard deviation of phase error for a SNR of 16 dB is 1.8 centicycles. Even at the lowest threshold usually considered for phase detection, a SNR of -30 dB in a 100 Hz bandwidth, the phase error for the above example is only 5.8 cec. Since the great majority of usable signals have SNRs better than -20 dB (100 Hz bandwidth), the phase error due to random atmospheric noise is nearly always less than 2 cec. Except for the worst case (-30 dB) noted above, the phase errors arising from SNR considerations are significantly smaller than the observed day-to-day variation of signal phase recorded at Omega signal monitors.

The random phase error component associated with the SNR is defined over a receiver time constant (typically, 1 to 5 minutes). Thus, for this component, the phase error is due to VLF atmospheric noise (in a 100 Hz bandwidth) that corrupts the signal being detected during the period of a receiver time constant. The fact that the day-to-day variation in phase is larger than the SNR-induced phase error suggests that the day-to-day variation is not attributable to noise, even allowing for possible errors in the receiver's SNR calibration curve. Day-to-day variations in the signal phase are presumably due to day-to-day differences in the ionosphere which serves as an upper boundary for the signal propagation path. Although the Omega signal wavelengths are long (approximately 30 km at 10.2 kHz), and thus insensitive to small changes in the ionosphere, the paths are also long (typically, 100 wavelengths), which means they are subject to several different sources of variation, e.g., latitude-dependent magnetosphere-ionosphere interactions. These sources are presumably the same as those which give rise to the signal amplitude variations which are described in the enhanced version of the System Availability Model (Ref. 9). As treated in the signal coverage component (enhanced version) the signal amplitude variations are lognormally distributed with mean value given by the theoretical prediction (from the signal coverage database). Thus, the signal amplitude "errors" (actual value − prediction) that result are symmetrically distributed (with respect to a logarithmically defined signal amplitude) about zero mean. Moreover, since amplitude errors and phase errors are logarithmically related (Ref. 12), the day-to-day random phase error (associated with the signal amplitude error) is expected to be normally distributed with a standard deviation determined by measurements.

The phase bias error results from errors in the coefficients or functional forms associated with the semi-empirical PPC model. This error component is particularly important for Omega signals since most measurement data shows that the bias error substantially exceeds the random error in magnitude. The phase bias error is independent of the random phase error since the prediction uncertainties are, for the most part, unrelated to the sources of day-to-day variation. As with the standard deviation of the random error component, the phase bias error is difficult to model and is best obtained from measurement.

Thus, neglecting the relatively small phase error component associated with the SNR, the phase errors are taken to be normally distributed with mean given by the phase bias error (measured) and standard deviation given by the random day-to-day variation (measured). In terms of a probability density function, the phase errors are distributed according to

$$P_{\Delta\phi}(\delta\phi) = \frac{e^{-(\delta\phi - \overline{\delta\phi})^2/2\sigma_\phi^2}}{\sigma_\phi\sqrt{2\pi}}$$

where $\delta\phi$ is the bias error and σ_ϕ is the random error standard deviation. This equation describes the density function for a single station signal at a given location and at a given time (month or half-month at a given hour). In the absence of a general model specifying the spatial dependence of phase error, the density function is strictly valid only at monitor sites where $\overline{\delta\phi}$ and σ_ϕ are available from measurements. In the time domain, measurement of $\overline{\delta\phi}$ and σ_ϕ for a given hour/month/monitor site during a year or set of years presumably establishes the density function for the next year for the same hour/month/monitor site. However, recent studies (Refs. 13 and 14) suggest that projection of the phase error statistics from year to year may have a large uncertainty.

Calculation of the probability density function for position accuracy requires the joint phase error probability density function for multiple station signals (at a fixed frequency) received at a given monitor site. The joint probability density function is constructed from the individual probability density functions through a known or assumed interdependence of signal phase errors. Since, in this case, the time and space dependence of signal phase error sources is not adequately known, the interdependence of multiple signal phase errors is also not known. Clearly, however, paths that are nearly identical will exhibit nearly identical phase errors. As the paths become more differentiated, the interdependence weakens, leading to eventual path independence. At the station monitors, some paths from remote stations have similar bearings, but large portions of the paths will not overlap. Thus, to a good approximation, signal phase errors (at the monitor sites) on multiple signals may be considered independent and the joint phase error probability density function may be written (for the signals in the maximal coverage set)

$$P_{\Delta\phi_1,\Delta\phi_2,...\Delta\phi_m}(\delta\phi_1,\delta\phi_2,...\delta\phi_m) = \frac{e^{-(1/2)\sum_{i=1}^{m}\left(\frac{\delta\phi_i - \overline{\delta\phi}_i}{\sigma_{\phi_i}}\right)^2}}{(2\pi)^{m/2}\sigma_{\phi_1}\sigma_{\phi_2}...\sigma_{\phi_m}}$$

where $\delta\phi_i$ is the phase error for station signal i, $\overline{\delta\phi_i}$ is the bias error for signal i, σ_{ϕ_i} is the standard deviation of the day-to-day variation of the phase of signal i, and m is the number of signals in the maximal coverage set. In practice, the phase error domain is limited to a few cycles (depending on the monitor receiver information output to the recorder).

11.8.2 Position Change Estimation Component

Because the great majority of present-day Omega navigation users are from the air transportation community, the position estimation algorithm used for the position change estimation component of the augmented version of the System Availability Model parallels (as far as possible) the position estimation techniques implemented in aircraft receiver systems. Although aircraft Omega receiver mechanizations differ between manufacturers, a generic scheme is described, which is considered common to a large class of aircraft receiver navigation algorithms. Some background is presented in this subsection to motivate this method. The generic scheme must be defined in order to show how phase errors are converted to position errors in the normal course of navigation.

Both Omega users (with first-generation Omega receivers) and receiver manufacturers (in later-generation equipment) have employed a number of schemes to convert phase measurements to two-dimensional position on the surface of the earth. Before the advent of microprocessor-based receivers, hyperbolic techniques (mostly for surface applications) were used in which phase differences (measured by the receiver) identified lines-of-position (LOPs) plotted on special charts. These LOPs are actually segments of hyperbolas defined on the surface of a sphere. The user's position (initially fixed by the intersection of two or more LOPs) is assumed known to within the resolution of a "lane" (distance interval corresponding to a full cycle of phase difference) and navigation is performed by tracking the changing position and noting any lane changes. This method was primarily used because it eliminated the need for an expensive, on-board frequency standard and because most of the early users (marine craft) moved sufficiently slowly so that multiple fixes occurred within a lane. With more than two LOPs available, manual methods were also used in estimating position, although with considerably less precision than analytical/numerical methods now implemented in microprocessor-controlled receivers.

The great velocity and maneuvering differences in air and marine vehicle motions lead to correspondingly different navigation/positioning schemes for Omega receiver systems on these two kinds of platforms. One important difference is that the faster airborne vehicle speed permits sensing the change in single-station phase using a relatively inexpensive precision crystal oscillator. In a relatively short

time, spatially separated measurements (which can be treated as quasi-independent quantities) are made which can be used to obtain position and Omega "epoch"* when the signal propagation path is at an essentially fixed global time. For example, an aircraft traveling toward a station at 200 knots using a receiver with a 2-minute time constant will effectively make two independent measurements during each 16-nautical-mile lane (at 10.2 kHz). Hence, three independent measurements are made in a period of 6 minutes, a time interval during which the ionosphere over a typical path changes very little. Moreover, the distance between measurement updates (approximately 7 nautical miles in this example) is short compared to the curvature of the earth so that a "flat-earth" approximation can be used. This property also permits linearizing the range equations (see below) so that position updates can be rapidly and efficiently processed from the phase measurements.

Thus, navigation of the airborne receiver can proceed from an initial known position by processing phase change measurements from several stations using the linearized range equations. A minimum of two station phase measurements is required because at least two unknown quantities appear in the linearized range equations: position change along two orthogonal surface coordinates (e.g., north/east or latitude/longitude). Accurate phase change measurements are possible if the receiver's internal clock on-board the aircraft is sufficiently stable within successive updates. A typical requirement is that the oscillator "drift" between successive updates be less than one microsecond (approximately one centi-cycle at 10.2 kHz). For a two-minute time constant receiver, this requirement translates into a stability of approximately 8 parts in 10^9, which is well within the capability of most modern precision crystal oscillators. In an operational airborne receiver, the initial position (e.g., coordinates of the point of departure) is known but, once en route, relatively few precision updates (obtained by external means) are available. Thus, between precision updates, the position error may grow, but not monotonically, since the phase errors have a complex (non-systematic) space/time dependence on the signal paths. The receiver's clock/oscillator "drift" between precision updates is usually well-approximated as a linear function of time (drift rate constant) and thus systematically grows between precision updates. For these and other reasons, most receiver implementations include the clock drift offset as a state variable. In this case, a minimum of three station signals are required. These ideas are quantified in the following development.

The phase change, $\Delta\phi$, between updates on a given station signal with respect to a receiver's clock/oscillator is

$$\Delta\phi = (\partial\phi/\partial a)\Delta a + (\partial\phi/\partial T)\Delta T \qquad (11.8\text{-}2)$$

---

*In this context, Omega epoch is defined as the time at which the signal is in a zero-crossing, positive-going condition at the station antenna.

where α is the signal path length over the great circle between the transmitting station and the receiver and ΔT is the time between updates. Since PPCs are added to the phase measurement to remove space and time dependence (transformation to the nominal model), the first partial derivative in the above equation is given as

$$\frac{\partial \phi}{\partial \alpha} = k_0$$

where k_0 is the frequency-dependent nominal wave number.* Since the clock drift between updates is assumed linear, the second term partial derivative in Eq. 11.8-2 is

$$\frac{\partial \phi}{\partial T} = \gamma$$

where γ is the constant clock drift rate. Thus, Eq. 11.8-2 becomes

$$\Delta \phi = k_0 \, \Delta \alpha + \gamma \Delta T \qquad (11.8\text{-}3)$$

Since $\Delta \phi$ is measured by the receiver and ΔT is just the elapsed time between updates, the unknowns in Eq. 11.8-3 are $\Delta \alpha$ and γ.

The path length (α (radians)) on a spherical earth is obtained as the scalar product of unit position vectors for the receiver ($\hat{r}_R$) and transmitter ($\hat{r}_T$) in a geocentric coordinate system, i.e.,

$$\hat{r}_R \cdot \hat{r}_T = \cos \alpha$$

If the small change in $\hat{r}_R$ between updates is denoted as $\Delta \hat{r}_R$ then, to first order in $\Delta \hat{r}_R$ and $\Delta \alpha$, Eq. 11.8-3 implies (recall $\hat{r}_T$ is fixed)

$$\Delta \hat{r}_R \cdot \hat{r}_T = -\sin \alpha \Delta \alpha \qquad (11.8\text{-}4)$$

Expanding $\Delta \hat{r}_R$ in local north and east coordinates (in the earth's tangent plane at $\hat{r}_R$), i.e.,

$$\Delta \hat{r}_R = \Delta N \hat{n} + \Delta E \hat{e}$$

where $\hat{n}$ and $\hat{e}$ are unit vectors along north and east, respectively, and ΔN, ΔE are north and east components of the change in receiver position. Substituting this expression into Eq. 11.8-4 can be shown to result in

$$\cos \beta \Delta N + \sin \beta \Delta E = -\Delta \alpha$$

---

*For example, at 10.2 kHz, k_0 is about 0.034 cycle/km.

where β is the local station bearing (with respect to geographic north). Substituting this form for the change in signal path length (between updates) into Eq. 11.8-3 yields

$$\Delta\phi = -k_0(\cos\beta\Delta N + \sin\beta\Delta E) + \gamma\Delta T \qquad (11.8\text{-}5)$$

Equation 11.8-5 contains three unknowns (ΔN, ΔE, and γ) and thus three signal phase measurements are required to determine position change. When more than three signals are available, the redundant data are used to provide increased position accuracy, since the errors on each signal path (to each monitor) are assumed independent. For more than one signal, phase change relations (similar to Eq. 11.8-5) may be written in matrix form, viz.

$$\Delta\phi = H \Delta X' + v$$

where: $\Delta\phi$ is a vector whose components, $\Delta\phi_i$, $i = 1, 2, \ldots 8$, are the changes in phase for station signal i (for a given frequency) between successive navigation updates, H is the measurement matrix whose components are given by

$$H_{i1} = k_0\cos\beta_i, \quad H_{i2} = k_0\sin\beta_i, \quad H_{i3} = \Delta T, i = 1, 2, \ldots 8,$$

β_i is the geographic bearing to the ith station, $\Delta X'$ is a three-component vector in which $(\Delta X')_1 = \Delta N$, $(\Delta X')_2 = \Delta E$, and $(\Delta X')_3 = \gamma$, the minus sign is absorbed in k_0, and v is the zero-mean measurement noise vector.

In most receiver systems, position change and clock drift are estimated from redundant phase data using a least squares method. For this technique, estimates of ΔN, ΔE, and γ are sought, which minimize $E(v^T W v)$ where W is a symmetric weighting matrix which permits inter-channel measurement noise coupling and $E()$ indicates expectation over the noise statistics. The resulting estimates are given in terms of the measurements by

$$\Delta\hat{X}' = (H^T W H)^{-1} H^T W \Delta\phi \qquad (11.8\text{-}6)$$

In conventional systems these position change and clock drift estimates are filtered in software (e.g., a Kalman filter) to minimize the possibility of large, sudden excursions in position and clock drift. Many systems also include algorithms to deselect signals which are expected to contain dominant long-path or modal components. Thus, a reasonable working assumption is that signals actually processed for navigation are those in the maximal coverage set.

To structure the position change estimation component for the System Availability Model, a relation is needed between the signal phase errors and the resulting position errors assuming the Omega signals are processed by a generic aircraft receiver system. In particular, the least-squares position change/clock drift estimate (Eq. 11.8-6) based on measured phase changes is used but other assumptions are necessary to make the probabilistic model tractable. The principal assumptions for the model component are summarized as follows:

1) The position change/clock drift corresponding to the measured phase change is based on the least-squares estimate, Eq. 11.8-6.

2) The initial position is assumed correct so that errors incurred in the final position are due to phase change errors transformed through the position change estimate.

3) Initially, the receiver clock offset (with respect to the Omega epoch) is zero so that the receiver clock is precisely synchronized with Omega time at the beginning of the update cycle.

4) No filtering or weighting of position estimates is performed.

Assumptions (2) through (4) are necessary to make the model scenario-independent. In a typical flight scenario, the known airport position is entered at departure and successive position updates are computed based on Omega phase measurements and other information; occasionally, precision updates are made en route when, for example, the aircraft overflies a known, surveyed position. Clearly, errors in position grow as the flight departs its initial position, although the error growth is not necessarily monotonic and is nearly always bounded. In a similar way, errors in the estimated clock drift can accumulate following flight departure. Thus, the error at a given update point along the flight route depends to a degree on the flight history (e.g., departure time and location). To remove this scenario dependence, the initial position and clock synchronization, at any point in the flight, are assumed to be correct. Similarly, filtering and weighting are processes that depend on previous measurement/update states and thus, also have a flight history dependence. As a result, no filtering or weighing is assumed. Assumption (2) is clearly optimistic in the sense that no errors are assumed to be carried over from the previous update cycle. This assumption is partially compensated for by assumption (3) which specifies no filtering or weighting. This means that successive position estimates (which incur error over only one update cycle) tend to "jump" around the true position and noisy signals are weighted the same as strong signals.

The phase change measured by the receiver (and modified by the PPC) may be separated into two components, i.e.,

$$\Delta\phi = \Delta_0\phi + \delta\phi$$

11-65

where $\Delta_0\phi$ is the "true" phase change and $\delta\phi$ is the phase change error. The least-squares estimate expression, Eq. 11.8-6, is linear, so that insertion of the above expression (in vector form) for $\Delta\phi$ into Eq. 11.8-6 yields (no weighting implies W is an identity matrix)

$$\Delta\hat{X}' = (H^TH)^{-1} H^T\Delta_0\phi + (H^TH)^{-1}H^T\delta\phi$$

The first term on the right-hand side of the above expression is the true position change since no errors are involved and redundant LOPs pass through the single intersection point. Thus, the second term is the position change/clock drift error, which may be written as

$$\delta X' = (H^TH)^{-1}H^T\delta\phi \tag{11.8-7}$$

This expression is used to transform the phase error probability density function to an intermediate probability density function over position error and clock drift error. This intermediate density function is integrated over clock drift error to obtain the position error probability density function (Ref. 7).

11.8.3 Calculation of P_A in Terms of Navigation Accuracy

If the definition of coverage is generalized to be the event that the radial position error incurred using three or more accessible (usable) signals is less than some pre-determined threshold, then the general procedure used to compute P_A for the original System Availability Model may be applied except that each previously defined coverage event becomes a precondition for the new (generalized) coverage event. If Y is defined to be the generalized coverage event, then, the previous statement is heuristically expressed as

$$P_A = P(Y) = \sum_{\text{all } X} P(Y/X) \sum_{\text{all } B} P(X/B)P(B)$$

where X is the event that three or more usable station signals are accessible at a given point in space and time. B is the event whose subscripts indicate which stations are off-air. Consider an example in which signals from stations 1, 3, 7, and 8 are in the maximal coverage set. Then, the local coverage element, $Q_o \equiv P(X/B_o)$, is given by

$$Q_o = P[A_1A_3A_7\overline{A}_8 + A_1A_3\overline{A}_7A_8 + A_1\overline{A}_3A_7A_8 + \overline{A}_1A_3A_7A_8 + A_1A_3A_7A_8]$$

where A_i is the event that the SNR for station signal i is greater than the threshold SNR (typically –20 dB in a 100 Hz bandwidth) and $\overline{A}_i$ is the complement of A_i.

Thus, Q_0 is the sum of the probabilities of five mutually exclusive events, each of which specifies a configuration of three or more station signals (in the maximal coverage set) with individual SNR values exceeding the pre-selected threshold. Consider the first event probability, i.e,

$$P(A_1 A_3 A_7 \overline{A}_8) \equiv P(V_{137})$$

which serves to define event V_{137}. To calculate the generalized coverage event probability, this probability is multiplied by the probability of event Y, given that signals 1, 3, 7, and 8 are accessible, i.e.,

$$P(Y/V_{137})\ P(V_{137})$$

The conditional probability $P(Y/V_{137})$ is obtained through the following steps:

- Construct the phase error probability density function (see Section 11.8.1) from the phase error statistics (mean (bias) and standard deviation) measured at the point of interest (or nearby location) for the specified time (hour/month)

- Construct the position error probability density function (in local north and east coordinates) by transforming the phase error probability density function using the linear, unweighted least-squares transformation (Eq. 11.8-7) dictated by the position change estimation component (see Section 11.8.2)

- Transform the position error probability density function into polar coordinates (two-dimensional) centered on either the "true" position or mean value (coordinates of the fix bias error)

- Integrate the polar form of the position error probability density function over the radial coordinate from zero to R_T, the pre-selected radial error threshold.

These steps are not explicitly performed for each term in the calculation, since they have been reduced to an algorithm (Ref. 7 (Appendix B)). Evaluation of the algorithm may be lengthy, however, since it involves numerical integration.

A major issue involved in the first step of the procedure listed above is the determination of the phase error statistics. In the example being used to illustrate this development, the location of the user/receiver is simply identified as a cell. This specification is sufficient for coverage parameters, which are assumed to change little over the dimensions of a cell. Prediction errors, however, are likely to change noticeably over a cell, since the PPCs in most modern receivers are calculated by means of a path integral algorithm which has a minimum spatial resolution of about 64 km. Thus, the PPC (for a given signal) usually shows a definite change over a cell and the resulting accuracy is likely to change also. A more important problem from the implementation viewpoint is that phase error statistics are available only from data at high-quality monitor sites which are located at relatively few sites throughout the world.

11-67

Thus, the procedure for determining $P(Y)$ can only be performed at a few cells. If a reliable, global model of signal phase error is ultimately developed, then the procedure for computing $P(Y)$ could be applied globally, much like $P(X)$.

To complete the example for $P(Y)$, the conditional probabilities are computed for each set of signals corresponding to the indices of event V. Thus, for example, the second term in the expression for Q_0 would be

$$P(Y/V_{138}) \, P(V_{138}) \; ; \; V_{138} = A_1 A_3 \overline{A}_7 A_8$$

Like $P(V_{137})$, the calculation of $P(V_{138})$ is described in Section 11.7 and $P(Y/V_{138})$ is computed according to the procedure outlined above. The other terms in the expression for Q_0 are treated in the same way. Similar comments apply to the calculation of Q_1, Q_3, Q_7, and Q_8 (each of which have only one term). It is also true here that

$$Q_{13} = Q_{17} = Q_{18} = Q_{37} = Q_{78} = Q_{138} = Q_{178} = Q_{378} = Q_{1378} = 0$$

since fewer than three station signals are specified by these quantities.

11.9 PROBLEMS

11.9.1 Sample Problems

1. Suppose there are two Omega receiver classes with the following properties:

	Number of receivers	Receiver MTBF (hours)	Receiver MTTR (hours)
Class I	2000	3500	2
Class II	3000	2000	1

Find the receiver reliability/availability (P_R) for each of these two receiver classes.

Solution: Using the expression $P_R = 1 - \text{MTTR/MTBF}$, one finds that

Class I: $P_R = 0.999429$

Class II: $P_R = 0.999500$.

2. For the coverage scenario given in Problem 5, assume all coverage parameters are deterministic and apply the PACE default signal coverage access criteria to determine:

   a) Q_0

Solution: Since no stations are off-air, the coverage is the same as that for Problem 5(a), i.e., stations B, D, and E are accessible. Since three stations are accessible, $Q_0 = 1$.

b) Q_1

Solution: Since station 1's off-air does not affect signals from stations B, D, and E, $Q_1 = 1$.

c) Q_{23}

Solution: Since station 2 is off-air, only signals from stations D and E are accessible and hence $Q_{23} = 0$.

d) Q_{13678}

Solution: Since signals from stations B, D, and E remain unaffected,

$$Q_{13678} = 1.$$

3.   Perform a comparison of two scenarios with and without Liberia on-air and find the percentage change in global system unavailability. Also find the cells where system unavailability changes by more than 5%.

Solution: Compute two scenarios using nominal parameters and turn Liberia off for one of the scenarios. Calculate the percent change in $1-P_{SA}$, based on the P_{SA} results from each scenario. Use the difference display and select a -0.05 value for the lower limit, zero value for the upper limit and the $\Delta(1 - P_{SA})$ control.

11.9.2   Problems to be Solved by the Reader

1.   For the example in Sample Problem 1, what is the percentage increase in the *unreliability* $(1 - P_R)$ of a Class II receiver if the MTBF is decreased by 100 hours?

2.   Using Table 11.3-1, find the probability that station B is in an unscheduled off-air condition and station F is in a scheduled off-air condition during August of 1986.

3.   Suppose that following unscheduled off-air probabilities for stations C and E are projected for a given month:

$$P(\overline{T}_3{}^u) = 0.025 \; ; \; P(\overline{T}_5{}^u) = 0.104$$

Find the probability that at least one of these two stations is in an unscheduled off-air condition for the month.

4. Assume the following signal coverage parameters are given for a specific cell/time:

Station Signals	SNR (dB)	SPPD (cec)	M1DM (dB)	SP/LP (dB)	PTCA (deg)
A	−15	10	4.4	52	34
B	−18	4	7.3	21	11
C	+6	5	6.1	34	3
D	−4	1	9.8	19	29
E	+2	6	6.5	8	90
F	−24	2	8.3	94	51
G	−12	5	7.0	1	44
H	−27	1	7.7	66	7

GDOP > 6 only for those three- and four-station combinations containing both F and G.

To determine coverage, apply the PACE default signal coverage access criteria.

    a) For the deterministic case, what signals are in the coverage set?

    b) For the random SNR case, find the signals in the maximal coverage set.

5. For the example in Problem 4 and using the notation in Section 11.7, compute, for the deterministic case:

    a) $P(A_1 A_2 A_3)$

    b) $P(A_2 A_4 A_5)$

    c) $P(A_4 A_5 A_6 A_8)$

    d) How would the answer to part (c) above qualitatively differ in the random SNR case?

6. Consider the following group of cells:

```
        +---+
        | 1 |
    +---+---+
    | 2 | 3 |
    +---+---+
    | 4 | 5 |
    +---+---+
    | 6 |
    +---+
```
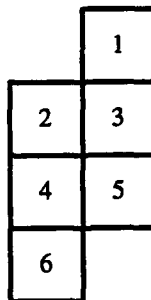
with the following associated weights and signal access probabilities:

$$w_1 = 2 \qquad w_4 = 5 \qquad P_{A_1} = 0.85 \qquad P_{A_4} = 0.93$$

$$w_2 = 4 \qquad w_5 = 6 \qquad P_{A_2} = 0.80 \qquad P_{A_5} = 0.78$$

$$w_3 = 7 \qquad w_6 = 3 \qquad P_{A_3} = 0.72 \qquad P_{A_6} = 0.87$$

Find P_{SA} for this group of cells assuming $P_R = 0.9$.

7. Consider the following receiver (R)/station (T) configuration

T_1

$N\uparrow$

T_4 R T_3

T_3
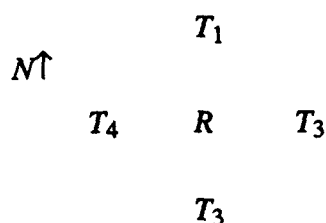
in which $\beta_1 = 0°$, $\beta_2 = 90°$, $\beta_3 = 180°$, $\beta_4 = 270°$

Assume the single-station phase errors are given (in cycles) by

$$\delta\phi_1 = 0.02; \quad \delta\phi_2 = -0.05;$$
$$\delta\phi_3 = 0.08; \quad \delta\phi_4 = -0.04$$

Using an update interval of $\Delta T = 2$ min and $k_0 = 0.034$ cycle/km at 10.2 kHz, find the north and east error components (in km) and the error in the oscillator drift rate (cycle/minute).

8. Use the coverage scenario given in Problem 4. Apply the PACE default signal coverage access criteria but modify the SP/LP criterion so that

$$SP/LP \geq 0 \text{ dB}$$

Determine:

    a) the coverage set for the deterministic case

    b) the maximal coverage set (random SNR case)

    c) Q_0

    d) Q_{23} (deterministic case)

    e) Q_{128} (random SNR case) in terms of the probabilities of joint A-events (do not evaluate the probabilities themselves).

9. Assume the coverage scenario of Problem 8. For the deterministic case (see Problem 8a).

    a) How many of the coverage probabilities for single station outage (i.e., Q_1, Q_2, .. Q_8) are non-zero?

    b) How many of the coverage probabilities for dual station outage (e.g., Q_{12}, Q_{45}, . . .) are non-zero?

    c) Find P_{SA} if:

$$P_R = 0.9 \qquad\qquad P(B_0) = 0.732$$

$$P(B_i) = 0.010 \text{ for all } i = 1, 2, \ldots 8$$

$$P(B_{ij}) = 0.001 \text{ for all } i, j = 1, 2, \ldots 8; \ i \neq j$$

$$P(B_{ijk}) = P(B_{ijkl}) = P(B_{ijklm}) = 0 \text{ for all } B \text{ subscripts}$$

10. Consider any two of the Omega stations. In comparison to the case in which concurrent scheduled off-airs are allowed, does the requirement that no two stations have concurrent scheduled off-air periods increase or decrease the joint probability that the two stations are simultaneously on-air? Why?

In the following problems, the reader need only describe the *procedure* for obtaining the desired result. If a PACE workstation is available, the reader will gain additional understanding by actually using PACE to find the quantities specified in the problems.

11. You wish to assign stations A and B the same annual maintenance month (say January) with A off-air during the first part of the month and B off-air during the latter part of the month. Assess the effect of this schedule.

12. A P_{SA} scenario with reduced power at both Hawaii and Liberia has been computed and you want to see the composite coverage (not the P_{SA}) given this situation.

13. Find all geographical locations where the GDOP for stations A, E, and H is large (> 6).

11.10 ABBREVIATIONS/ACRONYMS

BW	Bandwidth
cec	Centicyle(s)
CCIR	International Radio Consultative Committee
dB	Decibel(s)
GDOP	Geometric Dilution of Precision
Hz	Hertz
IM	Interfering Mode(s)
kHz	Kilohertz
km	Kilometer(s)
kW	Kilowatt
LOP	Line of Position
MIDM	Mode 1 Dominance Margin
Mm	Megameter(s)
MTBF	Mean Time Between Failures
MTTR	Mean Time To Repair
ONSCEN	Omega Navigation System Center (formerly ONSOD)
NAVSTAR GPS	NAVSTAR (Satellite) Global Positioning System
PACE	Performance Assessment and Coverage Evaluation
PPC	Propagation Correction
P_{AC}	P_{SA} at a cell (averaged over all specified times)
P_{AT}	P_{SA} for a given cell/time
P_{SA}	System availability index
PTCA	Path/Terminator Crossing Angle
QR	Pre-stored values of P_{SA} in PACE; values are accessed by an 8-bit coverage vector
QRBUILD	Program which computes QR (executed prior to running PACE)
RMS	Root Mean Squared
SNR	Signal-to-Noise Ratio
SP/LP	Short-Path to Long-Path Ratio
SPPD	Short-Path Phase Deviation
SPA I	System Performance Assessment: Phase I
SPA II	System Performance Assessment: Phase II
SPSNR	Short-Path SNR
SRM	Station Reliability Model
VLF	Very Low Frequency
UT	Universal Time
UTC	Coordinated Universal Time
WGL/NRL	Westinghouse Georesearch Laboratory/Naval Research Laboratory

11.11 REFERENCES

1. Gupta, R., Donnelly, S., Morris, P., and Vence, CDR R., Jr., Omega System 10.2 kHz Signal Coverage Diagrams, *Proceedings of the Fifth Annual Meeting of the International Omega Association*, Bergen, Norway, August 1980.

2. Morris, P., Omega System Performance Assessment, Report No. CG-ONSCEN-01-89, March 1989.

3. Gupta, R., Omega/VLF Signal Coverage Database Development, Report No. CG-ONSCEN-03-91, January 1991.

4. Thomson, LT R., Omega Navigation System Performance Statistics, International Omega Technical Commission Conference, 1988.

5. Project Office/PM-9, *Project Master Plan for Omega Navigation System*, Chief of Naval Materiel, Department of the Navy, April 1966.

6. Omega Station Performance Statistics, Omega Navigation System Center, U.S. Coast Guard, Letter Correspondence to TASC, August 1988.

7. Morris, P., Omega System Availability as a Global Measure of Navigation Accuracy, Report No. CG-ONSCEN-05-90, September 1990.

8. Maxwell, E., Stone, D., Croghan, R., Ball, L., and Watt, A. Development of a VLF Atmospheric Noise Prediction Model, Westinghouse Georesearch Laboratory, Repor: No. 70-1H2-VLFNO-R1, Office of Naval Research, Washington, DC, 30 June 1970.

9. Morris, P., Enhancement of the Omega System Availability Algorithm, Report No. CG-ONS CEN-01-90, March 1990.

10. Hansen, A., Omega System Performance Assessment and Coverage Evaluation (PACE) Workstation Design and Implementation, TASC TIM-6993-4, May 1994.

11. Morris, P., and Swanson, E., New Coefficients for the Swanson Propagation Correction Model, *Proceedings of the Fifth Annual Meeting of the International Omega Association*, Bergen, Norway, August 1980.

12. Watt, A., *VLF Radio Engineering*, International Series of Monographs in Electromagnetic Waves, Vol. 14, Pergamon Press, 1967.

13. Swanson, E., Long-term Variations in Omega Signals, *Proceedings of the Fourteenth Annual Meeting of the International Omega Association*, Long Beach, CA, October 1989.

14. Wenzel, CAPT R., McManus, H., Casswell, R., and Vannicola, V., The 1980 Omega PPC Model time term should not be used, *Proceedings of the Fifteenth Annual Meeting of the International Omega Association*, Sanur, Bali, Indonesia, September 1990.

15. Gupta, R. and Hansen, A., PACE Analyst's Guide, TASC TIM-6993-5, May 1994.

CHAPTER 12

OMEGA RECEIVING SYSTEMS

Chapter Overview — This chapter provides a top-level description of the most common types of Omega signal receiving systems, both in current use and of major historical interest. Most of the systems in use support navigation and positioning, although a few sample non-navigation applications are briefly addressed. Section 12.1 discusses Omega receivers and traces their evolution throughout the system's history. The general techniques of signal processing used in Omega receivers are qualitatively reviewed in Section 12.2. These techniques include pre-processing, signal detection, and signal tracking. Section 12.3 describes signal post-processing methods commonly employed, including signal synchronization, PPC adjustment, signal selection/de-selection, and navigation processing. Typical navigation receiver performance is also addressed. Integration with other systems is discussed in Section 12.4. Problems, including worked-out examples as well as those to be solved by the reader, are found in Section 12.5. Abbreviations and acronyms used in the chapter are given in Section 12.6, followed by the cited references listed in Section 12.7.

12.1 INTRODUCTION

12.1.1 Overview of Omega Receiving Systems

The Omega *system* is often treated in terms of three general categories: signal generation, signal propagation, and signal reception. Chapters 3, 7, and Appendix G, as well as portions of Chapters 2, 8, 11, and Appendices B and C focus on the signal transmission process. The complexities of signal propagation are treated in Chapters 5, 6, 9, 10, and Appendix A, in addition to parts of Chapters 2, 8, 11, and Appendices B and C. Signal reception is principally covered in this chapter although related material can be found in Chapters 4, 6, 8, and 11. The importance of the signal-receiving process is illustrated by noting that the inability to navigate, as the result of an Omega receiver failure or operator problem, is often interpreted as an *Omega system* failure, even if the stations operate flawlessly and signals propagate as predicted. The point is that receiver characteristics must also be understood so that signal transmitting procedures and policy can be appropriately formulated and signal propagation parameters and thresholds can be properly selected.

Today, most Omega receivers are automated, although some older receivers currently in use are manually operated. The automated receivers perform much of the processing previously handled by navigators as part of the "art of navigation." Many of today's Omega receiver and processing modules are intelligently combined with other navigation sensors to provide integrated systems that are more accurate than any single constituent system. Interoperable navigation systems apply the sensor integration at a more basic level, providing "pseudo-range" data from a variety of systems to establish position/track. Thanks to technology innovations, modern systems are less expensive and more reliable than their predecessors. Even stand-alone Omega systems are more accurate nowadays because of more sophisticated processing techniques and improved propagation corrections.

12.1.2   Historical Overview of Omega Receiving Systems

Omega, as conceived by the U.S. Navy when it authorized implementation of the system, was primarily intended for marine users, both surface and sub-surface. Omega was seen as a navigation aid in the open ocean, far from coastal areas where existing radionavigation systems could be used. Moreover, the fact that Omega signals could be detected some tens of meters below the surface of the ocean (depending on the signal-to-noise ratio at the surface) made it attractive as a navigation aid for submarines. The system was never considered accurate enough for weapons delivery from a submarine platform but was looked upon as an alternative navigation system for underwater patrol craft.

As a consequence, the first operational Omega receivers were designed for shipboard platforms. These were large bulky units with a long whip antenna, analog phase-difference measuring circuitry, and a strip-chart recorder to track lanes. This equipment was given mixed reports from the (mostly U.S. Navy) users. Although some found them accurate and reliable, others did not and nearly all agreed that the units required considerable time to operate. Manual synchronization to the Omega pattern (using blinking lights or headphones) was difficult and error-prone. Thick books of tables were consulted to obtain propagation corrections (PPCs; known in the late 1960s as skywave corrections) for the appropriate station and frequency signals. The displayed phase-difference values were manually corrected by these PPCs and the results plotted on large navigational charts overprinted with Omega lines of position. The chart recorders also had to be routinely checked to verify the correct lane identity.

Because of the inordinate amount of operator attention required, their comparatively low reliability, and the relatively few stations available in the late 1960s and early 1970s, Omega marine receivers were not popular, especially in the civil marine sector, during this period. Instead, marine users turned to satellite navigation systems employing the TRANSIT satellite signals in which fixes were obtained through Doppler measurements (i.e., measurements of the apparent signal frequency shift due to

the relative velocity of the user and the satellite). The TRANSIT satellites provided accurate fixes (a few hundred meters for the two-frequency units) although the time between fixes ranged from 2 to 6 hours. Thus, by the time combined Omega/TRANSIT units (which were accurate, reliable and required little operator attention) appeared in the late 1970s, the navigation system of choice for the marine transportation community was TRANSIT. Subsurface use of Omega has fared somewhat better since: (1) the military provide a "captive" user population, and (2) the first operational units were based on an innovative aircraft design. Although expensive to produce, submarine Omega receivers have generally performed well over the past 20 years.

In contrast to marine receivers, the use of Omega receiver systems for aircraft grew rapidly during the second generation of Omega receiver development. From the outset, airborne Omega receivers enjoyed the reputation of little operator attention, high reliability, and reasonably good accuracy. Supplemented with signals from the VLF communications stations and enhanced with signal selection/ deselection algorithms and improved PPCs, airborne systems grew to dominate the Omega receiver markets by the 1980s. Following FAA certification of Omega on certain routes, many of these systems were acquired by air carriers for their overseas routes. The systems were less popular on general aviation aircraft, possibly because their operating areas are largely confined to continental regions, where more accurate systems, such as VOR/DME or loran are in place. Except for certain U.S. Army applications (Ref. 1) and commercial operations in Canada and China (Ref. 2), rotary wing aircraft saw limited use of Omega receivers.

One non-navigational application of Omega signals, probably not foreseen during the early system implementation, was the tracking of meteorological balloons, which developed rapidly in the 1980s. In these systems, balloon-borne radiosondes repeat Omega signals to a ground controller that tracks the balloon position and computes a wind speed profile with altitude. By using Omega signals, these units are made inexpensively using expendable components and can be used practically anywhere on the globe. Recent figures (Ref. 3) indicate that about 200,000 of these units are deployed each year.

12.2 SIGNAL PROCESSING IN OMEGA RECEIVING SYSTEMS

12.2.1 Principal Types of Omega Receiving Systems

Omega receiver systems are manufactured for a variety of applications including airborne, surface (marine/land), and special sensors. Receiver systems within each application area can differ markedly. For example, marine receivers used for surface ships differ from those used for submarines in terms of antennas, signal processing, mechanization, and many other respects.

Airborne Omega receiver systems for airliners and high-performance military aircraft are usually quite sophisticated and include VLF signal processing, rate aiding from true air speed and heading sensors, electronically steerable crossed loop H-field antennas, and coupling into the autopilot and mission computer. Omega systems for general aviation aircraft are less sophisticated and generally feature E-field antennas because of the closer proximity to the engine. Figure 12.2-1 illustrates the assembled components of a typical airborne Omega receiver of the mid-1980s. Note that the antenna is "flat," i.e., flush-mounted to minimize drag or turbulent flow over the airframe surface.

Surface marine systems normally do not include VLF signal processing since the speed of the platform is such that propagation-induced phase changes between successive VLF "lanes" may be significant. Rate aiding (speed through water and magnetic heading) and E-field antennas are found on most marine Omega systems.

Receivers on board submerged vessels process signals in the hyperbolic mode to eliminate the highly variable antenna to sea-surface segment of the propagation path. Such systems use both loops and long horizontal wire antennas.
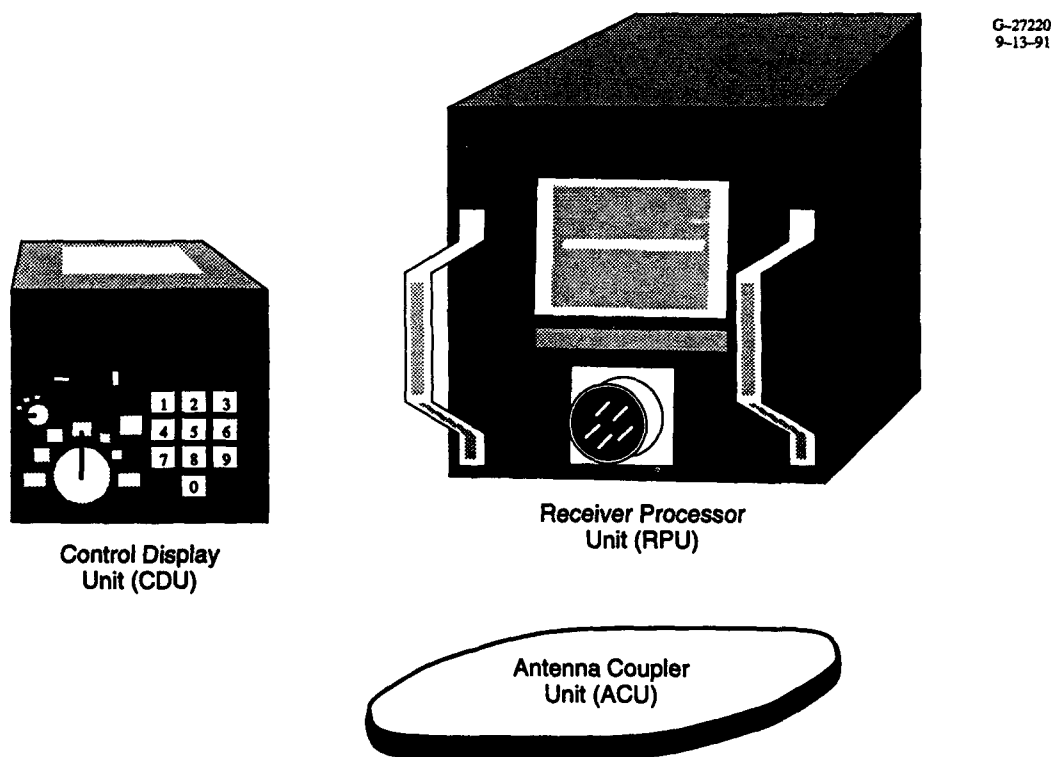
Figure 12.2-1 Assembled Components of a Typical Omega Airborne Receiver

Omega sensors are used in a number of applications including windfinding and remote tracking of unmanned craft. Because of the large number required for a given application, Omega sensor design emphasizes simplicity and low cost. Compared to high-performance aircraft receiver systems, these sensors use rudimentary detection schemes and perform minimal signal processing.

Most modern navigation systems that include the processing of Omega signals are equipped with several other navigation system receiver/sensors and processors, e.g., inertial, GPS, and Loran-C. Virtually all external information processing, such as propagation correction (PPC) algorithm implementation, is automated in these receivers. Some manual, stand-alone Omega receivers are still in use, but no known manual receivers are currently being manufactured (as of 1994).

The VLF windfinding radiosondes developed by Vaisalo Oy measure upper-air winds using Omega and VLF transmitting stations (Refs. 20 and 21). The radiosonde includes a VLF receiver and retransmitter. The signals are relayed to the ground station simultaneously with pressure, temperature and humidity information. The relayed Omega signals are then passed to a correlation processor to derive their relative phases from which movements of the sonde can be calculated. The processing software includes segments for control of the correlation and coherent integration processes, phase detection, data quality control and wind computation using a general solution for all available VLF transmitters. Automatic synchronization is based on the specific frequencies transmitted by each Omega station.

12.2.2 Noise Sources

In essence, any radionavigation receiver detects and processes two electromagnetic entities: the desired signal and the unwanted signal. We usually identify the unwanted signal as "noise," even though it might be relatively "clean" (e.g., a coherent interferer). In describing the effects of noise on Omega receiving systems (especially those on airborne platforms), it is convenient to define three categories of noise types, or sources:

- Atmospheric
- Precipitation static
- Artificial.

Each of these sources is briefly discussed in the following paragraphs.

Atmospheric noise refers to electromagnetic energy in the VLF band propagated from distant sources. These distant sources radiate VLF energy as the result of natural mechanisms, such as lightning discharges or magnetospheric "hiss." Because these sources are numerous and VLF energy propagates

to very long ranges, the superposition of the source radiations at any given point on the earth leads to a lognormal distribution of noise levels.* Lightning discharges associated with thunderstorms that are "nearby" (~ 100 to 1000 km) contribute very high-amplitude, short-duration levels, which are collectively known as "impulsive" noise. Because the strength of these noise impulses is very high (up to 10 V/m) a ,ceeds the limiter level of most receivers, the statistics of impulsive noise address features such as the impulse frequency.

Precipitation static is noise caused by the rapid discharging of free charges that build up on geometrically narrow or "pointed" conducting structures. This type of noise is a severe problem mainly for aircraft, including helicopters and meteorological balloons. As shown in Fig. 12.2-2, charge buildup on these platforms occurs in three ways:

- Frictional charging — results when aircraft pass through ice crystals and/or dense clouds

- Engine charging — stems from ionization in engine exhaust that produces outflowing positive ions, thus leaving negative charge on vehicle

- Exogenous charging — occurs when aircraft pass through the electric field set up between two oppositely charged clouds.

The free charge carried by precipitation particles causes noise when it interacts with the aircraft surfaces. Dielectric surfaces, such as windshields, which become charged as the result of impinging particles, can discharge to nearby metal structures ("streamering") thereby producing noise in the VLF band. Charged airborne particles moving with respect to the antenna induce noise fields directly on the antenna.

"Artificial" sources refer to electrical and electronic devices that produce relatively strong wideband or discrete emissions that lie in the VLF band. These sources are usually categorized as incoherent or coherent. Incoherent sources include arc welding torches and power generators, which produce very strong fields, but over a wide bandwidth, so that spectral noise density is usually tolerable if the devices are not too close to a user's receiver. Coherent noise normally refers to power line harmonics that are very close or within the nominal receiver front-end bandwidth (100 Hz) about any of the Omega frequencies. Some 400 Hz power sources in aircraft are so poorly controlled that the harmonics appear to drift randomly across the receiver bandwidth, resulting in effectively incoherent noise.

---

*A lognormal distribution of noise levels is just a normal or Gaussian distribution of of the levels expressed logarithmically, i.e., in decibels (dB) relative to some level, e.g., one microvolt/meter.
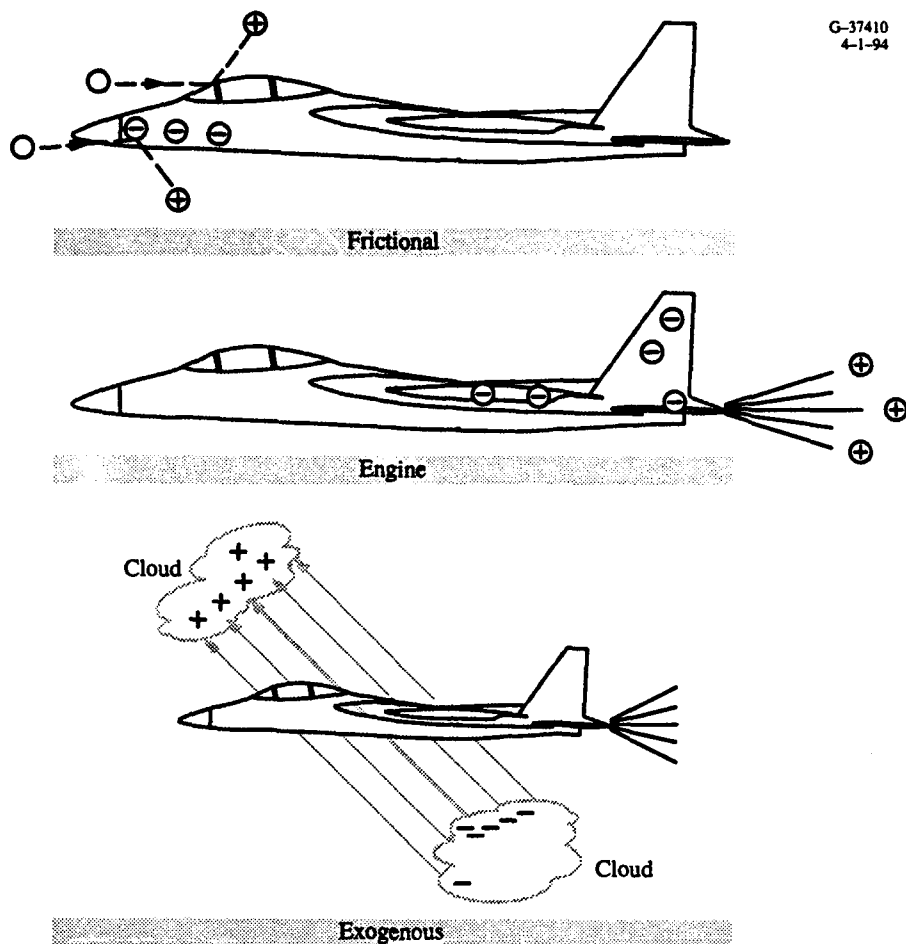
Figure 12.2-2 Aircraft Charging Processes

12.2.3 Signal Pre-processing

Pre-processing of the signal refers to the initial stages of signal acquisition at the antenna and the coupling unit, or pre-amplifier. Figure 12.2-3 schematically portrays the important functions of a typical aircraft Omega receiver system. Without the loop steering section and some of the input/outputs, this diagram also describes Omega receiver systems for many other applications.

Narrowband Omega signals and noise from all sources (including harmonic interference) are received at the E-field (probe) or H-field (loop) antenna having a bandwidth of about 4 kHz. The E-field probe is effectively a straight-wire antenna that senses the vertically polarized electric field of the Omega signal. Because of an omnidirectional pattern in the plane normal to the wire, this antenna requires no "steering." However, the E-field probe is highly susceptible to precipitation static primarily through induction discharging (described in Section 12.2.2). An H-field antenna is composed of one or more loops of
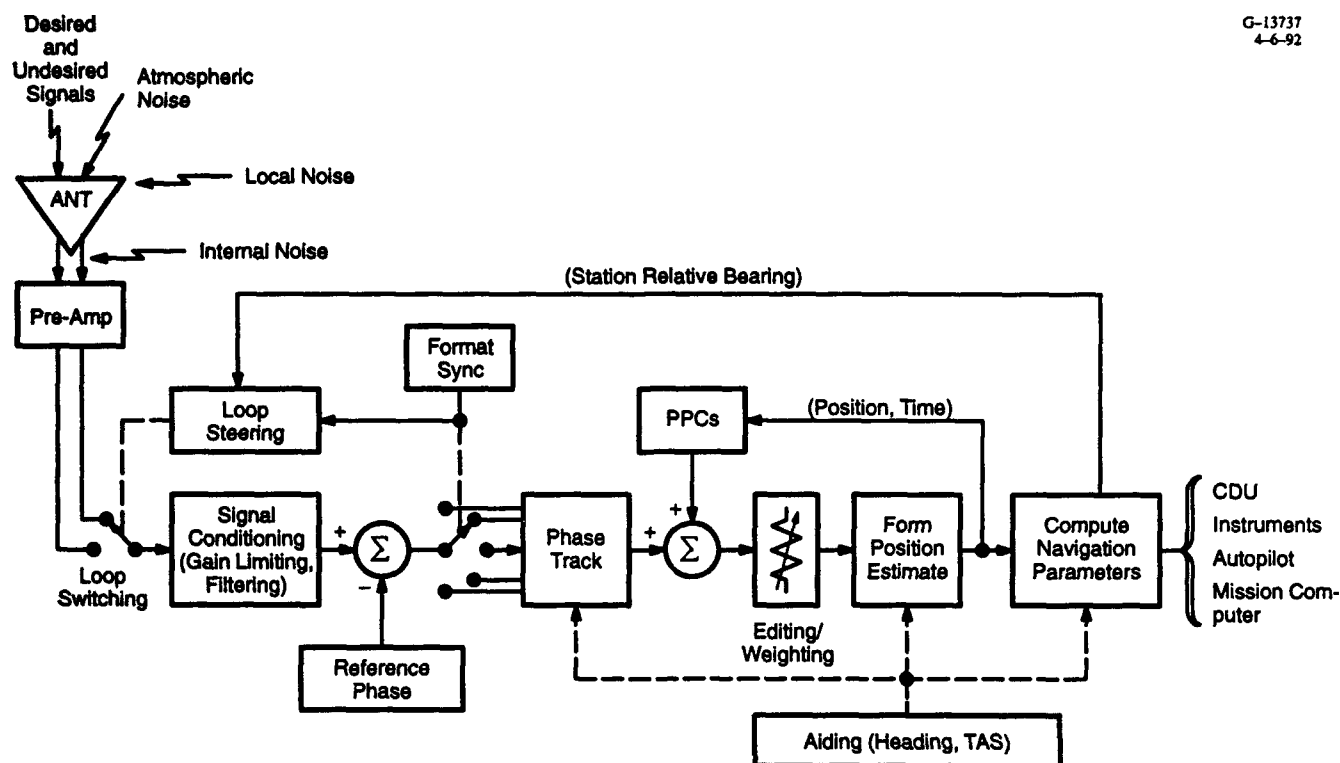
Figure 12.2-3 Functional Block Diagram for Conventional Airborne
Omega Navigation Receiver System

wire in which a current is induced by the horizontally polarized magnetic field component of the Omega signal normal to the plane of the loop. When properly oriented with respect to the Omega signal field, the antenna gain is higher than for the E-field probe. Because it is not subject to the electrostatic Coulomb field of the free charges, the H-field antenna is also much less sensitive to precipitation static than the E-field antenna. For these reasons, most aircraft receiver systems employ H-field antennas, configured as electronically steered crossed loops. The current outputs of these loops are phased so that the effective antenna pattern achieves maximum gain for each Omega station signal received.

Figure 12.2-4 gives a simplified view of H-field crossed-loop antenna patterns in the horizontal plane for a typical airborne Omega receiver. In the left panel of the figure, the lobe labeled "e_1" is the pattern for a loop in the plane containing the aircraft wings and the local vertical whose normal points along the direction of motion of the craft (forward and backward). Similarly, lobe "e_2" describes a pattern from an orthogonal loop whose normal is in the horizontal plane and points left or right. In each case, the minus sign attached to the back lobe indicates that the phase of a signal arriving from this direction must be shifted by 180° for correct processing. The outputs of each of the loops are phased and combined so that the lobes
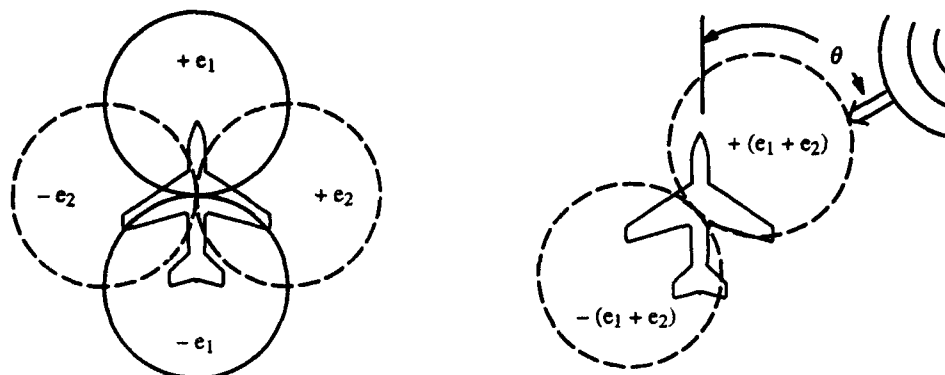
G-37409
3-31-94

Figure 12.2-4 Crossed-loop H-field Antenna Patterns
for an Airborne Omega Receiver

are maximized in the direction of the arriving signal. The right panel of Fig. 12.2-4 shows an equal phasing of the loops and the resulting lobe structure which has maximum gain at an angle of 45°, approximating θ, the bearing (with respect to the fuselage axis) of the desired station signal.

In most receivers, the antenna coupler unit (ACU) contains a relatively wideband pre-amplifier that boosts the signal and noise levels received by the antenna. This amplification is necessary because of the comparatively weak signals being detected as well as the additional loss in the cable connecting the ACU to the receiver processing unit (RPU; see Fig. 12.2-1).

Because of the wide variation in electromagnetic currents and fields over the airframe, location of the ACU must be carefully chosen. This process, known as "skin-mapping," seeks to avoid spiky noise in aircraft system direct-current electrical loads, harmonics of power system frequencies in the Omega band, and strong power system fields that may saturate the ACU. In this procedure, a spectrum analyzer (or, sometimes, an Omega sensor) is used to measure noise sources at or near Omega frequencies at all candidate ACU sites throughout the aircraft. Skin-mapping is performed both when all aircraft systems are energized and when they are turned off.

12.2.4   Signal Processing and Noise Reduction Techniques

At the end of the pre-processing stage, the signal is effectively captured, but often is buried in the noise also sensed by the antenna. The main objective of the signal processing stage is to isolate the desired signal from the noise. Referring to Fig. 12.2-3, the electromagnetic energy (composed of signals and noise) is passed from the ACU to the signal conditioning, or detector, stage of the Omega receiver processor unit. The loop steering switch shown in the figure indicates that signals from the two crossed loops are gated sequentially during each time segment.

Filtering is performed at the front-end of the detector, reducing the bandwidth to about 100 Hz. The 100 Hz figure represents a design tradeoff between Gaussian-distributed and impulsive noise levels (Ref. 9). The fast rise and decay times of impulsive noise yield a rather broad spectrum. Thus, a wider bandwidth is better for impulsive noise identification and rejection. On the other hand, a wide bandwidth admits a greater amount of Gaussian amplitude noise, which has an essentially flat narrow-band spectrum.

At this stage, the signal is amplified and then amplitude limited to prevent swamping from large impulsive noise spikes. Typical limiter levels which are equivalent to electric fields of 1 to 100 mV/m are also the result of trade-off between lower impulsive noise and phase-corrupting intermodulation products resulting from excessive limiting. Intermodulation products are essentially unwanted signals, the result of incoming electromagnetic energy that is subject to the non-linear limiting process. Some early receivers produced in the late 1960s and early 1970s had no envelope limiting function and hence were linear in the sense that the ratio of input and output levels is constant. For this type of receiver, the measured phase is free of intermodulation noise but the detection circuitry is easily saturated by in-band noise bursts. Unlike modern receivers, these units could measure signal amplitude directly, using a calibrated antenna.

In subsequent processing, the signal is referenced to an internal or external clock/oscillator and properties of the waveform are measured. Two methods of processing are in common use in these stages of the detection process: tuned RF and heterodyning. In the tuned RF method, the signal is processed at its original frequency, which does not require elaborate circuit design since the signal frequency (VLF) is low. An even lower-frequency signal, obtained by mixing the original signal with a reference signal, is used for processing in the heterodyning method. Since the signal passes through fewer devices, RF processing results in less internally generated noise than heterodyning but can sometimes suffer from cross-channel interference.

In either case, the signal to be processed is compared with a reference signal at the same frequency having sufficient stability over one or more ten-second Omega time frames. The phase drift of the reference signal must be small over at least a ten-second time frame so that referencing to all Omega signals in the time-frame is on the same basis. For most receivers, the actual *epoch* of the reference signal is not critical, since it "drops out" in the navigation processing algorithms.

For many of the older Omega receivers which employed analog signal processing methods, quadrature detection was used to measure and track signal phase. In this scheme, samples of the signal are shifted by 90° to give sinusoidal (in-phase) and cosinusoidal (quadrature) components. To obtain the tangent of the phase, the component levels are concurrently sampled, averaged, and divided. The sum of

the squared component levels is formed for use in later stages. Matched filters, which were used in the detection stages of some analog receivers, have been superseded by digital matched filters, found in some current receiving systems [See Ref. 4 for an explanation of matched filters].

In most modern Omega receivers, the signal is acquired and tracked by means of digital techniques. With these techniques, phase is usually measured as the interval between a reference clock pulse and the next zero-crossing of the input signal in units of clock cycles*. In most cases, the signal is tracked by means of a phase-locked loop (PLL) which is illustrated in Fig. 12.2-5 for both digital and analog implementations (Ref. 5). The phase detector compares the phases of the input and reference signals and produces an error signal that passes through a loop filter. For the analog case, the loop filter is a suitable low-pass filter and for the digital implementation, the filter truncates the error signal pulse if longer than one cycle of the reference signal. The digital clock reference is shifted by an amount equal to the error signal (or its negative). In the analog case, a voltage-controlled oscillator (VCO) responds to the error signal in a similar way. In either case, the PLL circuitry serves to synchronize the reference oscillator to the input signal.

For the digital case, the action of the PLL is to shift the reference phase by an amount which depends on the following two quantities:

- The previous phase measurement
- The time-averaged phase computed at the previous measurement time.
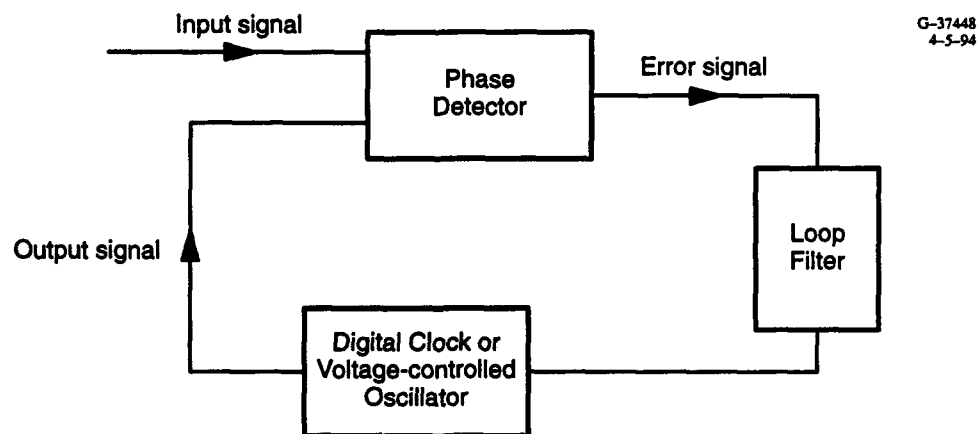
Figure 12.2-5   General Diagram of a Phase-locked Loop

---

*The reference clock/oscillator commonly has a frequency of 1 to 5 MHz but may be down-converted to a lower frequency.

Here, the time-averaging refers to a moving average that differs from the average at the previous loop cycle by a weighted value of the previous measurement. The weight value is inversely proportional to the effective time constant of the PLL. The PLL error is the RMS difference between the moving average and the current measurement, computed over a suitable number of loop cycles. This loop error is a measure of the input SNR and may be temporarily stored/displayed as an indicator of the signal "quality." For systems with adaptive time constants, the weight attached to the previous phase measurement is directly related to the RMS loop error or SNR estimate. Thus, a large RMS loop error means that the input SNR is low so that the weight assigned to the previous phase measurement is small. As a result, the effective time constant for receiver processing is long. Conversely, a small RMS loop error implies a high input SNR and a short effective time constant. A second-order PLL is designed to track the time rate of change of phase in a manner similar to that described above for a first-order loop (Ref. 5). Second-order PLLs have better response to rapid phase changes that occur in high-dynamics vehicle motions.

Like most signal-tracking circuitry, a basic function of the PLL is to reduce the effective bandwidth (inversely proportional to the effective time constant) so as to best reproduce the desired signal. Since the Omega signal has a very narrow bandwidth, virtually all bandwidth reduction performed by the receiver will be realized as signal gain. For aircraft receivers, time constants typically range from 100 to 200 seconds. Shorter time constants do not provide sufficient averaging or noise rejection and longer time constants may exceed the time required for aircraft maneuvers, such as sharp turns. Since the duty cycle (fraction of time on-air) for each of the common frequency Omega signals is 10 percent, the effective phase measurement time constant is 10 to 20 seconds. Using standard assumptions, these time constants correspond to noise-equivalent bandwidths (see Ref. 5 for a definition of noise-equivalent bandwidths) of 0.025 to 0.013 Hz. When compared to the input bandwidth of 100 Hz, these narrow output bandwidths correspond to gains of better than 35 dB. Thus, signals with SNRs as low as –20 to –30 dB in the 100 Hz receiver input bandwidth can be effectively utilized in aircraft Omega receivers.

In many receivers, the limiter level is chosen near the median atmospheric noise level in a 100 Hz bandwidth multiplied by the gain of the pre-amplifier. Thus, the receiver is in a limiting condition much of the time and large noise impulses are cut off. If the limiter level is above the median noise level, then the median SNR is unchanged, both internal and external to the receiver (the *mean* SNR, however, is lower internally than externally). However, if the median noise level is *above* the limiter level, then the median SNR is reduced relative to its pre-limiter value and a processing gain is realized. This gain depends on the pre-amplifier gain, atmospheric noise statistics, and pre-detection bandwidth and may be

as large as 10 to 15 dB (Ref. 6). In practice, not all this gain is realized with respect to *predicted* SNR levels, since local, platform-generated VLF noise of as much as 10 dB is commonly measured during skin-mapping on vehicle installations (Ref. 6).

For Omega-based radiosondes, phases are detected by a digital technique known as polarity cross correlation. Two separate channels are used:

- The local channel is used for monitoring, testing and synchronization of the system; it is also utilized for corrections when the differential mode of computation is desired.
- The remote channel receives the relayed signals, which are used for computation of upper-air winds.

Signals received from the remote and local channels pass through pass-band filter circuits. Narrow-band analog circuits, being prone to ringing when subjected to pulse type interference, are not applied.

The VLF correlator uses a high-stability oscillator as the system time base. The synthesizer circuits produce accurate, clean copies of the Omega frequency and pulse format. The relayed signals are compared with those internally generated references by polarity cross correlation for detection of phase shift. For each transmitting station, the phase of each frequency used is detected during the transmission sequence. The phase is calculated from station-unique frequency signals and from $11\frac{1}{3}$ and 13.6 kHz navigational signals, resulting in 24 station-frequency combinations. The polarity correlation principle is efficient for periodic signals of known frequency in a high-noise environment. The process is digital in nature and requires no critical level settings. Consequently, it is stable over time and insensitive to environmental variations. Various error sources due to anomalous signal propagation are avoided by extensive consistency checking of signals at various frequencies for several different VLF transmitting stations.

If the noise level accompanying the sampled signal is approximately constant over several sampling times, a corresponding phase error occurs during the detection process. This leads to a simple relation between SNR and phase error which is valid when the SNR is sufficiently high, i.e., in those cases when the noise is small enough to act as a *perturbation* of the signal. Figure 12.2-6 shows a sinusoidal waveform representing an Omega signal perturbed by a mean noise level, $N(0)$, near the signal's reference zero crossing point, $\phi = 0^*$. Thus, in this simple example, a phase value of zero would be measured in the absence of noise. The mean noise level near the zero phase point shifts the zero crossing at $\phi = 0$ to $\phi' = -\Delta\phi$. Here, the phase, ϕ, refers to the *signal* phase, which has a one-to-one relationship with time, e.g., at 10.2 kHz, a phase interval of 2π corresponds to about 100 μsec. Thus, for simplicity, we can take $\phi = 0$ to correspond to $t = 0$, where t is time.
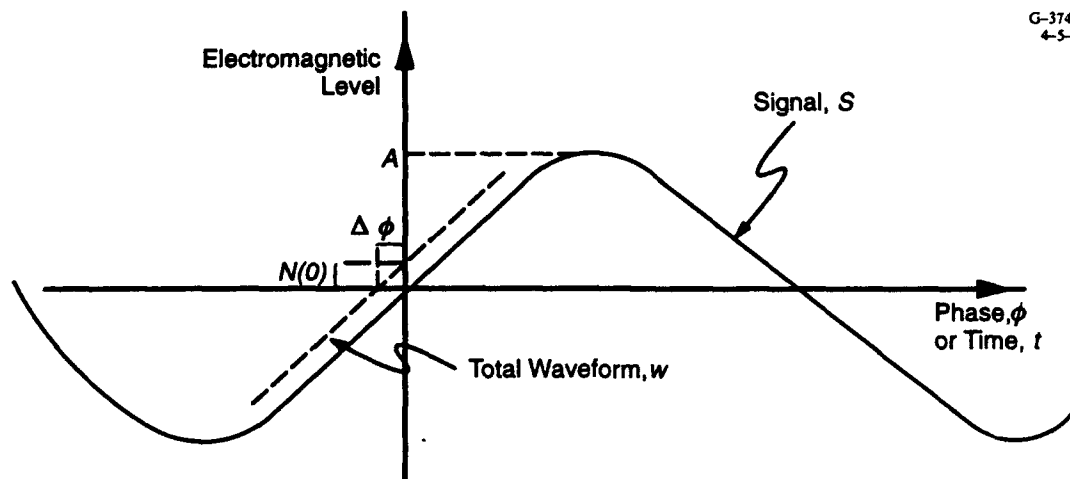
Figure 12.2-6   Signal Phase Error ($\Delta\phi$) Caused by Non-zero Noise Level
Near $\phi = 0$ in Narrow Band about Signal Frequency

Defining the total waveform processed by the receiver as $w(t) = S(t) + N(t)$, we note that $w(0) = N(0)$. Further, since the noise level is assumed constant over the interval $\Delta\phi$, the time derivative of w near $t = 0$ is approximated by

$$\frac{N(0)}{\Delta\phi} = \frac{dw}{d\phi}\bigg|_{\phi = 0} \qquad (12.2\text{-}1)$$

Since N is constant over $\Delta\phi$ and $S = A \sin\phi$, where A is the amplitude, then $dw/d\phi = A$ at $\phi = 0$. Solving Eq. 12.2-1 for $\Delta\phi$ yields

$$\Delta\phi = \frac{N(0)}{A} \qquad (12.2\text{-}2)$$

Finally, the average power, P_s, developed by a sinusoidally varying signal is easily shown to be proportional to $A^2/2$ while the power, P_N, developed by the constant noise level over $\Delta\phi$ is just $N^2(0)$ to within the same proportionality constant. Thus, in terms of signal and noise power levels, Eq. 12.2-2 becomes

$$\Delta\phi = \frac{1}{\sqrt{2P_S/P_N}} \qquad (12.2\text{-}3)$$

where $\Delta\phi$ is the phase error in radians and P_S/P_N is the signal-to-noise ratio for a given bandwidth.

---

* Recall that the phase is measured as the "time" interval between the signal zero crossing and a reference signal zero crossing.

12.3 POST-PROCESSING IN OMEGA RECEIVER SYSTEMS

12.3.1 Synchronization to Omega Signal Format

Signal processing in Omega receivers normally includes the detection, measurement, and tracking of signal phase. As explained in Section 12.2, the processing makes use of a reference signal having the same frequency as the signal being detected. However, in the signal acquisition mode (used, for example, at receiver startup), the receiver has no *a priori* knowledge of the incoming signal frequency or pulse length. Thus, in this mode, the signals undergo special processing (see Fig. 12.2-3) so that the receiver can synchronize itself to the Omega signal transmission format.

To determine the Omega pattern, some modern receivers employ digital techniques to measure the properties of the received signals (and noise) within "time slices" (typically of about 100 ms duration and repeated every 10 seconds). Zero-crossing intervals are measured within the time slices to determine frequency and quantized waveform energy. The measured signal energy is compared to a threshold to provide an estimate of whether the time slice lies in the 200 ms interval between the time/frequency transmission segments or within a segment. Similar tests are performed with adjacent time slices and the process is repeated to determine the width/boundary of each segment and its associated frequency. Because low SNR in some time segments may mimic a "silent" interval, the procedure may have to be repeated several times. Correlation schemes are also used in which a replica of the time/frequency format is successively shifted in time and compared to the received pattern. In performing these format synchronization procedures, the effective duty cycle is normally less than the 10 percent figure used in the tracking mode. As a result, the effective bandwidth is wider so that the SNR requirements are more stringent than in the tracking mode. The acquisition time may become lengthy if too many signals have low SNR.

For radiosonde Omega sensors, the ground station processor synchronizes to the Omega transmission sequence prior to launch by using the station-unique frequencies. If the signal pattern cannot be acquired prior to launch, the synchronization is performed immediately after an adequate signal is available from the radiosonde. After start-up, the VLF correlator is automatically synchronized to the Omega format using transmission time and frequency of the signals received from the local VLF antenna. The process is invisible to the user and takes about one minute.

12.3.2 PPC Algorithm Implementation

After the signal phase measurements are made in the signal processing stage of the receiver, the phase must be "corrected" for the expected variations from linearity due to the spatially and temporally

varying electromagnetic environment of the earth-ionosphere waveguide (see Chapter 5). These phase corrections, known as propagation corrections (PPCs), are computed using a U.S. Coast Guard-authorized model/algorithm (see Chapter 9) which is coded into the RPU software. The PPCs are added to the measured phase to produce an "idealized" phase value which can be readily used in the subsequent navigation and positioning calculations. It is important to recognize that although the PPCs require receiver position as an input, the PPCs are not sensitive to precise position, i.e., they vary less than 0.05 cycle over ranges of 50 to 100 km. Thus, the PPCs can be accurately computed from only *approximate* knowledge of position. Because the PPCs depend quite sensitively on time (year, month, day, hour, and minute), the operator must initially insert this time data into the receiver. The other quantities on which the PPC depends, including station, frequency, and approximate receiver location, are available from other storage locations in the RPU.

The more recent PPC models, including the 1980 and 1993 algorithms may be too large or time-consuming in their standard forms (Chapter 9) for inclusion into the receiver software. As a result, manufacturers often make approximations, shortcuts, deletions, and simplifications to the basic model/algorithm. The most common approximation is to transform the ten-level conductivity map into a three-level map, i.e., low, middle, and high conductivity. Interestingly, the 1993 PPC Model uses a reduced seven-level map in its treatment of mid-path sub-models. Most other modifications made in developing the receiver software are less severe and include simple approximations to the functional forms and/or larger path segment sizes.

PPCs are usually applied to *all* signals that can be tracked. Thus, phase-corrected signals are passed to the next stage of processing even if the basic signal is anomalous and contains little or no information. This is because the PPC algorithm is based on a Mode 1 model of signal propagation and thus assumes all received signals contain no higher-order modes.

12.3.3   Signal Weighting and Deselection

After PPCs have been added, the signal is potentially usable for navigation. However, some signals are more "usable" than others and some signals cannot be used under any conditions. Signal usability is evaluated using both internal (i.e., measured) and external information.

Internal to the receiver, usability of the (idealized) signal phases is determined by an assigned weight based on the expected relative accuracy of the phase measurement. This accuracy is most commonly taken to be the estimated SNR which, for phase-locked loop receivers, is closely related to the

RMS loop error, as discussed in Section 12.2.4. Thus, for example, averaging the cosine of the loop error yields, for small, non-zero loop error (Ref. 6), the following estimate of SNR:

$$(S/N)_{estimate} = \frac{1}{4(1- <\cos\phi>)}$$

where $<\cos\phi>$ is the averaged cosine of the loop error angle. Note that as the loop error becomes larger, the estimated SNR is smaller. SNR estimates for multiple signals are compared by forming normalized weights. Thus, if 5 signals are tracked and $(SNR)_i$ is the SNR for signal i, then the relative weight attached to the phase of this signal is given by

$$w_i = \frac{SNR_i}{\sum_{j=1}^{5}(SNR)_j}$$

If the estimated SNR is below a preset threshold, signal phase is usually excluded for use (given zero weight) in the navigation solution.

In addition to the weighting and exclusion procedures that are based on internally derived SNR data, modern Omega receiver systems invoke external information to assist in evaluating the signals. External data provides general guidance for identifying path-times that may exhibit the following anomalous conditions for a given frequency:

- Modal interference — measured by the Mode 1 Dominance Margin
- Long-path domination — measured by the short-path-to-long-path amplitude ratio
- Cycle slip/jump geometry — measured by the path-terminator crossing angle.

The actual anomalous/normal assignment depends on the thresholds selected for each of the measurable parameters listed above. In other words, the external coverage data provides the measurable parameter values; criteria and thresholds must be applied to actually determine acceptability. These thresholds vary from manufacturer to manufacturer and sometimes within the same receiver, depending on navigation conditions. External information is necessary because some signal anomalies, e.g., modal interference, cannot be reliably ascertained from measurements of the received signal alone. External information, such as signal deselection data, is generally extracted from ONSCEN-supplied coverage products, including modal "maps" and data on the occurrence of long-path signals (see Chapter 10). The available information is coded into the receiver software as digitized maps or algorithms. For example, if the

external data indicates that signals from a given station at a specific frequency* are subject to modal interference or long-path domination at the receiver's location and time, then the signals are deselected unless an insufficient number of signals are otherwise available; in the latter case, the signal selection algorithm chooses one of the following options:

- Temporarily enter a dead reckoning mode
- Include one or more non-Omega VLF stations (if receiver has VLF option)
- Tentatively include one or more anomalous signals and monitor position change estimate uncertainty.

Only recently have modal exclusion products become available at all 24 UT hours (Ref. 7). Prior to that time, the modal data was published for only two UT hours (0600 and 1800 UT) and for all-night path conditions. At intermediate times (say, 0312 UT) receiver algorithms employed a crude "$\frac{1}{3}$ – $\frac{2}{3}$" rule (Ref. 8) in which the path-night modal information is used when the path is more than $\frac{1}{3}$ dark.

Some coverage information and deselection guidance has also been published for operation during temporal anomalies that occur as the result of ionospheric disturbances (Refs. 7 and 8). For example, polar cap disturbances (PCDs; see Chapter 6) result from solar-terrestrial interactions that cause excess ionization in the northern and southern polar caps (regions bounded by the north/south auroral zones). During PCD events, paths that cross these regions should be deselected. For users inside the polar regions, less navigational error is generally incurred (depending on the mix of signals) than for users outside the region. Some receiver processing algorithms "de-weight" rather than deselect transpolar paths during PCD events. Compared to the usual yes/no deselection algorithms, receivers with these algorithms run less risk of signal "starvation" and provide better tracking continuity during passage into and out of disturbed polar regions.

The collective set of signals that survives the deselection/exclusion process are further screened for acceptable navigation geometry. Acceptable geometry depends on the type of navigation mode employed by the receiver (e.g., rho-rho) and the threshold selected. In most cases, the Geometric Dilution of Precision (GDOP) is used as a specific measure of navigation accuracy, even though the GDOP strictly applies only to those rare cases in which the phase errors for all signals are equal. Limits of geometry acceptability, otherwise known as GDOP thresholds, may vary depending on the algorithm design philosophy or need for a minimum signal set.

---

*Most coverage products apply to only two frequencies:10.2 and 13.6 kHz (see Chapter 10).

Virtually all modern navigation receivers process 13.6 kHz signals for navigation/positioning. Most receivers also process 10.2 and 11⅓ kHz signals on the same basis, although one known manufacturer uses these two frequencies for pattern synchronization/acquisition. Other systems utilize 11⅓ kHz estimated SNRs or "quality numbers" together with those of other frequencies to compile a figure-of-merit which serves as a signal selection criterion. The remaining common frequency, 11.05 kHz, and the unique frequencies are used either as VLF signals in the navigation solution or to calibrate the receiver clock in the rho-rho-rho navigation mode. In some receiver mechanizations, all three common frequency (excluding 11.05 kHz) signals from a station must be acceptable to be used in the navigation fix. In these mechanizations, the phase value at each frequency is often treated as an independent estimate of the phase of a signal reduced to a common frequency (e.g., 1.1⅓ kHz). This contrasts with other earlier difference-frequency receiving systems which assume a high degree of correlation between the signal phases at different frequencies on the same path. Other receiver mechanizations permit the use of one or more acceptable signal frequencies from a station for inclusion in the fix algorithm. This procedure provides much more flexibility and greatly reduces the probability of insufficient signals.

12.3.4 Signal Utilization and Navigation Processing

At this stage, the phase values for all trackable signals (out of all possible stations/frequencies) are measured, corrected, and weighted, using both receiver-internal and receiver-external data. These values provide the basis for navigation or positioning.

Originally, Omega was proposed only as a navigation system because of the lane ambiguity problem (see Chapter 4). However, the maximum lane width expanded considerably with the addition of multiple frequencies, so that positioning, in the usual sense, became more meaningful. However, Omega has been most successful as a navigation system, since navigation relies on the accurate transformation of incremental phase changes to incremental position changes. For most paths, Omega signal phase can be characterized as having large bias errors, but relatively small random errors. Thus, once the large phase bias errors have been removed (such as at initialization), Omega position accuracy can be extremely high.

A number of schemes have been employed to convert phase measurements to two-dimensional position on the surface of the earth. Before the advent of microprocessor-based receivers, hyperbolic techniques (mostly for surface applications) were used in which phase differences provided by the receiver could be used to identify charted lines of position (LOPs). These LOPs are actually segments of hyperbolas defined on the surface of a sphere. The user's position is assumed known to within the resolution of a "lane" (distance interval corresponding to a full cycle of phase difference) and navigation is

performed by tracking the changing position and noting any lane changes. This method was primarily used because it eliminated the need for an expensive, on-board frequency standard and because most of the early users (marine craft) moved sufficiently slowly so that multiple fixes occurred within a lane.

The great differences in air and marine vehicle motions lead to different navigation/positioning schemes for Omega receiver systems. One important difference is that the faster aircraft speed permits sensing the change in single-station phase using a relatively inexpensive precision crystal oscillator. Thus, in a relatively short time, spatially separated measurements are made that can be treated as quasi-independent expressions for the phase when the propagation path is at an essentially fixed global time. For example, an aircraft traveling toward a station at 200 knots using a receiver with a 2-minute time constant will effectively make two independent measurements during each 16 nautical mile lane. Hence, three independent measurements are made in a period of 6 minutes, a time interval during which the ionosphere over a typical path changes very little. Moreover, the distance between measurement updates (approximately 7 nm for this example) is short compared to the curvature of the earth so that a "flat-earth" approximation can be used. Under these conditions, the range equations can be linearized so that position updates can be rapidly and efficiently processed from the phase measurements.

For radiosondes using Omega sensors, the wind vector is computed based on the rate of change of the signal phases (phase derivatives) which are caused by the movement of the radionsonde. The rate of change of the phase depends on movement of the radionsonde relative to the VLF transmitters and on the change of the distance between the radiosonde and the ground station. Signals from east three transmitters are needed to locate the radiosonde, to compensate for the drift of the local oscillator and the change in the distance between the radiosonde and the ground station. Computed wind vectors are passed through a quality control program to assure that incorrect vectors are rejected.

The wind computation consists of the following steps:

- Phase detection using polarity correlation

- Phase editing (quality control) and deviative computation with residual variances

- Composition of phase derivatives from different frequencies to produce a single phase derivative for each Omega transmitting station

- Wind vector computation

- Consistency checking

- Wind value quality control.

12-20

The variances and derivatives of the VLF signals are determined by fitting a straight line to the phases in a 2- to 4-minute time window. Phase values that do not fit the line well enough are dropped and the procedure is repeated until a good fit is obtained. If too many phases are dropped or the remaining variance is too large, the corresponding transmitting station is ignored. The rejection limits and the length of the time window are adjustable. Any station is unconditionally excluded if anomalous behavior in the corresponding signal is suspected. The derivative composition is a weighted average of computed phase variances. The final weight is the sum of individual weights. Before composition of phase derivatives of the $11\frac{1}{3}$ kHz signal and a station-unique frequency are compared with 13.6 kHz derivative which is used as a reference; derivatives with substantial deviations are rejected.

The phase editing process yields a phase derivative vector and a weighting matrix which is inversely proportional to residual variances. Because the solution is overdetermined, the consistency of the phase derivatives can be verified each time a wind vector is computed. If predictions indicate the signal may arrive via the long path, the sign of the arrival direction vector of the signals of the suspected transmitting station is changed and the wind vector recomputed. Stray wind values are rejected by using a procedure to determine whether the largest or smallest observed value belongs to the same population as the other observations. The rejection procedure is applied to a sliding window of wind values separately for speed and direction. At each moment of time the window is subjected to an iterative application of the procedure for rejection of faulty values. A cubic spline is fitted to accepted points in two phases. In the first phase, the spline is made to accurately traverse through all wind values. For this spline, a value indicating its smoothing capacity is sought which fits the wind values as closely as possible.

Since current use of Omega involves predominantly airborne platforms, aircraft navigation will be emphasized in the following development. Although aircraft Omega receiver mechanizations differ between manufacturers, a generic scheme, common to a large class of aircraft receivers, is described. Some background material is presented. The generic scheme also indicates how phase errors are converted to position errors in the normal course of navigation.

Navigation of the airborne receiver proceeds from an initial known position by processing phase change measurements from two or more stations using the linearized range equations. A minimum of two station phase measurements is required because two unknown quantities appear in the linearized range equations: position change along two orthogonal surface coordinates (e.g., north/east or latitude/longitude). Accurate phase change measurements are possible if the receiver's internal clock on board the aircraft is sufficiently stable within successive updates. A typical requirement is that the oscillator "drift" between successive updates be less than one microsecond (approximately one centicycle at

10.2 kHz). For a two-minute time constant receiver, this requirement translates into a stability of approximately 8 parts in 10^9, well within the capability of most modern precision crystal oscillators. In an operational airborne receiver, however, the initial position (e.g., coordinates of the point of departure) is known but, once en route, relatively few precision updates (obtained by external means) are available. Thus, a clock/oscillator with a precision about 2 to 3 orders of magnitude better than a crystal oscillator is required to perform navigation with as few as two station signals. Receiving systems with highly stable clocks, such as rubidium or cesium frequency standards that have the required stability, are said to operate in the rho-rho navigation mode, so-named for the fact that only two range measurements are required.

Between precision updates, the position error may grow, but not monotonically, since the phase errors have a complex (non-systematic) space/time dependence on the signal paths. The drift between precision updates for lower-stability clocks such as temperature-controlled crystal oscillators is usually well-approximated as a linear function of time (drift rate constant) and thus systematically grows between precision updates. Since the constant drift rate must be determined in addition to the two surface coordinates, a minimum of three station signals is required. Because crystal oscillators are far less expensive than the highly stable clocks, most receiver implementations include the clock drift offset as a state variable and are said to operate in the rho-rho-rho navigation mode (three or more range measurements required). These ideas are quantified in the following development.

The phase change, $\Delta\phi$, between updates on a given station signal with respect to a receiver's clock/oscillator is given as

$$\Delta\phi = \frac{\partial\phi}{\partial a}\Delta a + \frac{\partial\phi}{\partial T}\Delta T \qquad (12.3\text{-}1)$$

where a is the signal path length over the great circle between the transmitting station and the receiver and ΔT is the time between updates. Since PPCs are added to the phase measurement to remove space and time dependence (transformation to the nominal model), the first partial derivative in Eq. 12.3-1 is just k_0, the frequency-dependent nominal wave number (see Chapter 9). Since the clock drift between updates is assumed linear, the second term partial derivative in Eq. 12.3-1 is a constant, labeled γ. Thus, Eq. 12.3-1 becomes

$$\Delta\phi = k_0\Delta a + \gamma\Delta T \qquad (12.3\text{-}2)$$

Since $\Delta\phi$ is measured by the receiver and ΔT is just the elapsed time between updates, the unknowns in Eq. 12.3-2 are Δa and γ.

The path length, a (in radians) on a spherical earth is obtained as the scalar product of unit position vectors for the receiver ($\hat{r}_R$) and transmitter ($\hat{r}_T$) in a geocentric coordinate system, i.e.,

$$\hat{r}_R \cdot \hat{r}_T = \cos a \qquad (12.3\text{-}3)$$

If the small change in $\hat{r}_R$ between updates is denoted as $\Delta\hat{r}_R$, then, to first order in $\Delta\hat{r}_R$ and Δa, Eq. 12.3-3 implies (recall $\hat{r}_T$ is fixed)

$$\Delta\hat{r}_R \cdot \hat{r}_T = -\sin a \Delta a \qquad (12.3\text{-}4)$$

Expanding $\Delta\hat{r}_R$ in local north and east coordinates (in the earth's tangent plane at $\hat{r}_R$), i.e.,

$$\Delta\hat{r}_R = \Delta N \hat{n} + \Delta E \hat{e} \; ; \; \begin{array}{l} \hat{n} = \textit{north unit vector} \\ \hat{e} = \textit{east unit vector} \end{array} \qquad (12.3\text{-}5)$$

where ΔN and ΔE are the distance changes between updates along north and east, respectively. Substituting Eq. 12.3-5 into 12.3-4 can be shown to result in

$$\cos\beta\Delta N + \sin\beta\Delta E = -\Delta a$$

where β is the local station bearing (with respect to geographic north). Substituting this form for the change in signal path length (between updates) into Eq. 12.3-2 yields

$$\Delta\phi = -k_0(\cos\beta\Delta N + \sin\beta\Delta E) + \gamma\Delta T \qquad (12.3\text{-}6)$$

Equation 12.3-6 contains three unknowns (ΔN, ΔE, and γ) and thus three signal phase measurements are required. When more than three signals are available, the redundant data are used to provide increased position accuracy, since the errors on each signal path (to each monitor) are assumed independent. For more than one signal, relations similar to Eq. 12.3-6 may be written in matrix form, viz.

$$\Delta\phi = H\Delta X' + v$$

where: $\Delta\phi$ is a vector whose components, $\Delta\phi_i$, $i = 1, 2, \ldots 8$, are the changes in phase for station signal i (for a given frequency) between successive navigation updates, H is the measurement matrix whose components are given by

$$H_{1i} = k_0\cos\beta_{2i} \; ; \; H_{3i} = k_0\sin\beta_i \; ; \; H_i = \Delta T \; ; \; i = 1, 2, \ldots 8$$

where β_i is the geographic bearing to the station i, $\Delta X'$ is a 3-component vector in which $(\Delta X')_1 = \Delta N$, $(\Delta X')_2 = \Delta E$, and $(\Delta X')_3 = \gamma$, the minus sign is absorbed in k_0, and v is the zero-mean measurement noise vector.

In most receiver systems, position change and clock drift are estimated from redundant phase data using a least squares method. For this technique, estimates of ΔN, ΔE, and γ are sought which minimize $E(v^TWv)$, where W is a symmetric weighting matrix which indicates inter-channel measurement noise coupling and E( ) indicates expectation over the noise statistics. The resulting estimates are given in terms of the measurements by

$$\Delta \hat{X}' = (H^TWH)^{-1}H^TW\Delta\phi \qquad (12.3\text{-}7)$$

In conventional systems these position change and clock drift estimates are filtered in software (e.g., a Kalman filter) to minimize the possibility of large, sudden excursions in position and clock drift. Since Eq. 12.3-7 specifies the phase measurement processing required to obtain the estimated position change, it also provides the recipe for determining position errors from the input phase errors.

The Omega-based calculation of position change is combined with the aircraft-supplied true air speed (TAS) and heading information to furnish the best fix estimate. Note that, in the absence of Omega signal information, dead reckoning depends on TAS and heading information. Since successive Omega fixes supply ground-track information and the aircraft heading indicates direction of motion with respect to the surrounding air, wind vector data is easily derived and is available on most Omega receiver control display units (CDU). Because it is derived from data which is averaged over one or more receiver time constants, the displayed wind vector data is also averaged over past data and thus does not characterize the instantaneous winds.

From the updated position estimate, navigation commands and parameters are computed and sent to the CDU and other aircraft instruments. The mission computer compares the new position data to the stored flight plan track and determines cross-track deviations. Steering correction information is then computed and sent to the autopilot. The updated station bearing information (based on the new position estimate) is combined with the aircraft heading data and fed back to adjust the loop steering as shown in Figure 12.2-3.

12.4 INTEGRATION WITH OTHER SYSTEMS

12.4.1 Use of VLF Communication Signals

Because signals from the network of VLF Communication Stations make up perhaps the most common external radionavigation source integrated with Omega signals in hybrid aircraft receiver systems, use of signals from these stations merits separate mention.

The carrier signals from the VLF Communication Stations (listed in Table 12.4-1) are modulated with a minimum shift keying (MSK) format utilizing signals separated by 50 Hz. This small frequency separation yields a 3000 km phase difference "lane" that practically eliminates lane ambiguity. Unlike the Omega stations, the VLF communication stations are not synchronized, so that only phase *changes* from each station can be processed in a navigation mode. This means that VLF signal processing is used to supplement Omega navigation rather than acting as a substitute. Moreover, these communication signals are broadcast for national/international security purposes, so that stations can switch frequency, change modulation, or temporarily cease operation with no advance warning. Thus, although VLF signals serve a very useful supplementary function in many (mostly airborne) modern Omega receivers, they are not intended for navigation and thus cannot play a primary navigational role.

Table 12.4-1   VLF Communications Stations*

STATION ID	LOCATION	LATITUDE	LONGITUDE	FREQUENCY (kHz)	RADIATED POWER (kW)
GBR[§]	Rugby, U.K.	52°22'N	1°11'W	16.0	45
JXZ[§]	Noviken, Norway	66°58'N	13°53'E	16.4	45
NDT[†]	Yokosuka, Japan	34°58'N	137°01'E	17.4	38
GQD[§]	Anthorne, U.K.	54°55'N	3°16'W	19.0	42
ICY[§]	Tavolara, Italy	40°55'N	5°45'W	20.27	43
NSS[†]	Annapolis, Maryland, U.S.	38°59'N	76°27'W	21.4	213
NWC[†]	Exmouth, Australia	21°49'S	114°10'E	19.8	1800
NPM[†]	Lualualei, Hawaii, U.S.	21°25'N	158°09'W	23.4	502
NAA[†]	Cutler, Maine, U.S.	44°39'N	67°17'W	24.0, 17.8	1200
NLK[†]	Jim Creek, Washington, U.S.	48°12'N	121°55'W	24.8	245
NAU[†]	Aguada, Puerto Rico (U.S.)	18°23'N	67°11'W	28.5	100

* This table lists most of the VLF stations whose signals are utilized by conventional Omega/VLF receiving systems; a complete list of VLF stations is given in Ref. 12.

§ Operated by the North Atlantic Treaty Organization (NATO).

† Operated by the U.S. Navy (USN).

Since the 1970s, navigational receivers have been built to demodulate the MSK signal and extract the navigational information from the carrier waveform (Refs. 10 and 11). However, since the signals are intended for communication, accompanying signal propagation information, such as propagation correction (PPCs) and signal deselection algorithms (Ref. 8), is not generally accessible to the user or receiver manufacturer. In fact, global theoretical or empirical data on VLF modal interference (above 14 kHz) and short-path/long-path amplitude ratios has not been systematically computed or measured.

One important feature of Omega/VLF receivers is the difference in the algorithms that guide the processing of Omega and VLF signals. Some of these distinctions arise from inherent differences in the two transmitting systems. For example, since the stations in the VLF network are not synchronized (although the carrier signals are synthesized from precise standards), no receiver acquisition of a time-frequency pattern is required as for Omega signals. This also means that signal phase from different stations cannot be compared to determine position as for other radionavigation systems such as Omega and Loran-C. Because the received VLF signal is generally time-stable (in the absence of propagation anomalies), VLF navigation begins with an initial calibration (where known coordinates are fed to the receiver) and subsequent phase tracking of the signals from selected VLF stations. Accurate phase tracking requires an on-board precise frequency standard or an estimate of the frequency/time offset of the receiver's internal clock relative to each VLF station's transmission epoch. This estimate is usually obtained by techniques similar to Omega signal processing in the rho-rho-rho mode (see Section 12.3.4).

In addition to internal differences in signal processing, signals from the two systems are processed differently regarding external data/information. For example, all known Omega/VLF receivers use externally supplied PPCs to correct the measured Omega phase prior to navigation use whereas few, if any, currently operational receivers correct VLF signal phase measurements. A simple algorithm for VLF PPCs has been developed (Ref. 13), although its operational validity is not known. This means that, for most receivers, the received VLF signal phase is not accurately related to distance over the ground, a problem which is not necessarily ameliorated by redundant measurements. Modal signal deselection tables and algorithms are another type of external data used to process signals difference found in most receivers. Deselection data regarding modal and long-path signals are available for Omega (based on U.S. Coast Guard-supplied information) but not for VLF (due to lack of sufficient information). Failure to deselect modal signals is potentially a more serious problem for navigation than the lack of VLF PPCs since modal phase excursions can be large and sudden, often resulting in cycle slips/advances.

As a result of these signal processing differences, receiver processing algorithms treat Omega and VLF signals differently. Once acquired (synchronized to the Omega format) and initialized, Omega signal processing alone is robust and will fail only under unusual circumstances (e.g., cycle shifts or fewer than three signals above the minimum SNR). VLF signal processing schemes generally rely on the presence of Omega signals and other aids in the receiver's navigation filter. In most receivers, VLF signals are closely monitored with frequent cross-consistency checks. Normally, Omega/VLF receivers are programmed to exclude initialization with VLF signals alone, since this represents a "degraded" state, similar to the DR mode. In fact, current FAA certification procedures require that an Omega/VLF receiver system operate satisfactorily with Omega signals alone (see also Chapter 13).

In summary, VLF signals are intended for high-priority communication with undersea craft and are only incidentally used for navigation. Differences in Omega and VLF signal processing are partly due to this difference in the reliability of signal generation. These differences, coupled with the lack of system synchronization and signal propagation information, insure that VLF signals are generally treated as backup support to Omega signals in the navigation algorithms. Although VLF signals often provide useful supplementary navigation data, they are usually not considered sufficiently reliable to be used *alone on more than just a temporary basis*.

12.4.2 Integration with Other Systems

Instead of processing signals from a single type of system, modern aircraft navigation suites employ "hybrid" systems that combine outputs from several navigation sensors to provide more accurate and reliable navigation. The most common of these are "integrated systems" that combine position estimates from two or more navigation aids, such as Omega, Loran-C, or inertial systems so as to produce an estimated position more accurate than that supplied by each system acting alone.

Ideally, the integration makes use of the complementary features of each system. For example, a continuous system, such as Omega, is effectively periodically calibrated by a more accurate but not continuously available source, such as the signal from the TRANSIT satellite system. Another example is an inertial system, whose position errors grow monotonically, combined with an error-bounded system, such as Omega or Loran-C.

More recently, the concept of "interoperable systems" have been introduced in which measurement parameters developed by multiple sensors are combined prior to computing a position fix (Ref. 14). In effect, "pseudoranges" are provided by each sensor to a master processor that applies appropriate weights and editing in computing the resulting navigation/positioning information.

12.4.3 General Performance Characteristics

Specifying the position determination accuracy obtained from the use of Omega signals is very complex for a variety of reasons. First, it must be kept in mind that Omega is a navigation system so that accuracy must be measured on either an incremental basis (given that one point is correctly located, determine the error in the succeeding position update) or an integrated basis, i.e., the error incurred between precision updates. Neither of these bases of measurement are particularly amenable to analysis and only the integrated basis has benefited from any data collection (see e.g., Ref. 19). Position error data at fixed sites has been collected and analyzed (Ref. 15), but it is difficult to translate this information to navigation errors, where the space- and time-dependence of position errors is mixed.

Omega position error can be traced to a variety of sources, including station synchronization offset, receiver dysfunction (e.g., lane slip/jump), operator mistakes (e.g., initialization coordinate insertion error), and temporal anomalies (e.g., a PCD). The predominant error source, however, is the propagation correction (or PPC). As explained in Section 12.3.2, the PPC is an external, predicted quantity obtained from a set of tables or algorithms, and is applied to the measured phase to transform from the highly complex, "real" phase variation to an idealized phase which varies linearly with distance.

The PPCs are obtained from a semi-empirical model/algorithm of Omega signal phase behavior, which is calibrated largely from phase measurements at globally distributed fixed Omega monitor sites. Analysis of these measurements can thus reveal important features of Omega phase behavior as well as provide insights into Omega PPC and position error. A basic property indicated by these measurements is that, at a fixed site, Omega phase (and phase error) generally varies more over 24 consecutive hours (diurnally) than over a year at a fixed hour. Thus, the observed phase and the predicted phase (based on the PPCs) show little systematic change over 15 consecutive days (measurements) at a fixed hour. Superimposed on this general trend are random (non-systematic) day-to-day variations in the observed phase on the order of 1 to 5 cecs. Since these random variations (which are due to ionospheric fluctuations) are not reflected in the PPCs, they make up the random component of PPC error. A more important error component is the PPC bias error, which is the difference between the predicted phase and the observed phase for a given hour averaged over 15 days. Bias error varies in magnitude from 0 to 30 cecs, and is usually larger than the random variation. The measurements also indicate that the random phase error due to ionospheric fluctuations is usually much larger than the phase error due to interfering noise in the signal processing bandwidth of the receiver.

12-28

When converting phase measurements to position, the bias and random components of phase error produce corresponding bias and random components of position error. As seen in Section 12.3.4, the transformation of the phase error components to position error components is complex and depends upon the individual phase errors of all signals received and the geometrical configuration of the receiver and stations corresponding to the received signals. If the magnitude of the random phase errors is assumed to be the same for all signals received and the bias error is assumed to be zero, then the radial position error standard deviation can be obtained by multiplying the phase error standard deviation by a scalar factor known as the Geometric Dilution of Precision (GDOP). For a least-squares method of position determination when multiple redundant signals are present, a dimensionless expression for GDOP is obtained in closed form (see Ref. 16 and Chapters 11 and 4). The GDOP becomes very large if no more than two stations have substantially different bearings. Another interesting property of the GDOP is that the GDOP for q station signals is never greater than the GDOP for any subset (≥ 3 stations) of q.

For moving vehicles performing navigation, the bias error is removed at initialization, leaving only phase error due to noise (typically less than 1 cec) during the initial segment of the journey (30 minutes to one hour). However, the paths from the station to the receiver eventually change (both in space and time) enough so that the initial correction, usually implemented as a PPC correction, becomes invalid. From this de-correlation time until the next precision update, the Omega receiver is subject to PPC errors and the effect of GDOP. Omega-only accuracies are measured when the aircraft comes under radar control at the termination of the flight. In these cases, accuracy figures of 2.7 to 3.3 nautical miles, 95 percent of the time have been reported (Refs. 17 and 18).

When integrated with navigation aids other than true air speed and heading, Omega accuracy differs considerably from that obtained in a stand-alone mode. In the usual case, Omega is combined with a sensor having an intrinsically higher absolute position accuracy, but providing data at discrete times. As a continuous navigation aid, Omega data provides incremental position data between the discrete times. In these cases, the resulting accuracy of the integrated system (averaged over all times) depends on the length of the intervals between the discrete times.

12.5 PROBLEMS

12.5.1 Sample Problems

1. Consider an Omega signal field propagating in the TM mode, i.e., the electric field vector is vertical (with respect to the earth's surface) and the signal's magnetic field vector is parallel to the earth's surface and perpendicular to the direction of propagation. For a receiver with an E-field probe antenna, what is the best orientation of the antenna to maximize gain? Similarly for a receiver with an H-field loop antenna, what is the best antenna orientation?

Answer:

Since the TM mode signal is present, the signal electric field is vertical and thus the E-field probe should also be vertical to maximize gain (i.e., greater induced voltage in the antenna by the signal). For the loop antenna, maximum gain is achieved when the signal's magnetic field is perpendicular to the loop (maximum induced current by Ampere's Law). Since the magnetic field is parallel to the ground and perpendicular to the propagation vector, the loop must lie in a plane containing the propagation vector and the local vertical. For a pair of orthogonal "crossed-loop" antennas, the second loop is perpendicular to the first, rotated 90° about the vertical axis.

2. A transmitting station is at a bearing of 30° (measured clockwise with respect to geographic north) relative to a receiver on an aircraft moving *away* from the station (assume a windless day). What relative phasing of the two crossed-loop antennas will maximize antenna gain? Can the presence of long-path signals be detected/eliminated using this phasing with no external knowledge?

Answer:

Since the aircraft is moving away from the station and no wind is present, the station is at an angle of 210° measured clockwise from the nose of the aircraft. Thus, according to the convention of Fig. 12.2-4, the appropriate phasing for maximum gain is

$$-\left(\sqrt{3/2}\right) e_1 - (1/2) e_2 \tag{12.2-1}$$

Since this phasing gives rise to a pattern which is symmetric with respect to a plane perpendicular to the receiver-to-station unit vector, the long-path signal, if present, would be received with gain equal to that of the short-path signal. Successive processing of long-path signals, however, would reveal an *increase* in phase, rather than a decrease in phase as expected for a receiver moving away from the station.

12.5.2 Problems to be Solved by Reader

1. Consider an aircraft receiver with a time constant of 150 seconds.

   a. What is the duty cycle and effective averaging time associated with processing any of the four common Omega frequencies?

   b. What is the duty cycle and effective averaging time associated with processing any of the unique Omega frequencies?

Assume the noise equivalent bandwidth is $1/(4\tau)$ where τ is the effective averaging time. Assume a receiver input bandwidth of 100 Hz.

c. For case a. above, find the noise equivalent bandwidth and processing gain (relative to the input bandwidth).

d. For case b. above, find the noise equivalent bandwidth and processing gain (relative to the input bandwidth).

2. Find the phase error in radians for a signal-to-noise ratio of +12dB. If the signal frequency is 13.6 kHz, what is the phase error in μsec?

3. For a phase-locked loop receiver, what is the estimate of SNR for each of four signals if the averaged cosine of loop error is

> 0.82 for Station A
> 0.77 for Station C
> 0.61 for Station G
> 0.94 for Station H

If these signals are weighted by SNR in the navigation solution, find the weight given to each.

12.6 ABBREVIATIONS/ACRONYMS

ACU	Antenna Coupler Unit
CDU	Control Display Unit
dB	Decibel
DME	Distance Measuring Equipment
DR	Dead Reckoning
FAA	Federal Aviation Administration
GDOP	Geometric Dilution of Precision
GPS	Global Positioning System
Hz	Hertz
kHz	Kilohertz
km	Kilometer
LOP	Line of Position
m	Meter
ms	Milliseconds
mV	Millivolt(s)
MHz	Megahertz
MSK	Minimum Shift Keying

nm	Nautical mile
ONSCEN	Omega Navigation System Center
PCD	Polar Cap Disturbance event
PLL	Phase-locked loop
PPC	Propagation Correction
RF	Radio frequency
RMS	Root-mean-squared
RPU	Receiver Processing Unit
SNR	Signal-to-Noise Ratio
TAS	True Air Speed
TRANSIT	U.S. Navy Satellite Navigation System using Doppler Measurements
UT	Shortened form of UTC
UTC	Coordinated Universal Time
V	Volt(s)
VCO	Voltage-controlled Oscillator
VLF	Very low frequency
VOR	VHF Omnidirectional Radionavigation

12.7   REFERENCES

1.   Litchford, G., and Saganowich, J., An Omega/transponder display system, *Proceedings of the Eleventh Annual Meeting of the International Omega Association*, Quebec City, P.Q., Canada, August 1986.

2.   McLennan, R., Omega usage in helicopter operations, *Proceedings of the Ninth Annual Meeting of the International Omega Association*, Seattle, WA, August 1984.

3.   Stratton, A., Report on Omega Users Survey Project, *Proceedings of the Fifteenth Annual Meeting of the International Omega Association*, Sanur, Bali, Indonesia, September 1990.

4.   Wozencraft, J., and Jacobs, I., *Principles of Communication Engineering*, John Wiley & Sons, Inc., 1965.

5.   Blanchard, A., *Phase-locked Loops: Application to Coherent Receiver Design*, John Wiley & Sons, Inc., 1976.

6.   Morris, P., Omega System Performance Assessment, CG-ONSCEN-01-89, TASC TR-5351-8-1, DTIC Accession No. AD-A-210342, March 1989.

7.   Casswell, R., Gupta, R., Desrochers, G., and Warren, R., Omega ACCESS II: An improved signal coverage prediction tool, *Proceedings of the Eighteenth Annual Meeting of the International Navigation Association*, Orlando, FL, October 1993.

8. Morris, P., and Gupta, R., Omega Navigation Signal Characteristics, AGARDOgraph No. 314, Analysis, Design, and Synthesis Methods for Guidance and Control Systems, Ed. Leondes, C., Advisory Group for Aerospace Research and Development, North Atlantic Treaty Organization, June 1990.

9. Lanoue, J., Omega/VLF receiver design and signal processing, *Proceedings of the Ninth Annual Meeting of the International Omega Association*, Seattle, WA, August 1984.

10. deBuda, R., Coherent demodulation of frequency-shift keying with low deviation ratio, IEEE Transactions on Communication (Concise Papers), Part I, Vol. COM-20, pp. 429–435, June 1972.

11. Mathwich, H.R. Balcewicz, J.F., and Hecht, M., The effect of tandem band and amplitude limiting of the E_b/N_0 performance of minimum (frequency) shift keying (MSK), *IEEE Transactions of Communication*, Vol. COM-22, pp. 1525–1540, October 1974.

12. Kleinhans, C., Fixed VLF/LF Database, Technical Document 1965, Naval Ocean Systems Center, San Diego, CA, October 1990.

13. Levine, P., Tests of a simple Omega phase model including solar flare effects, *Proceedings of the Fifth Annual Meeting of the International Omega Association*, Bergen, Norway, August 1980.

14. Schlachta, H. and Studenny, J., Interoperability versus integration, *Proceedings of the Fourteenth Annual Meeting of the International Omega Association*, Long Beach, CA, October 1989.

15. Morris, P., Calibration of the 1992 PPC Model at 10.2 kHz, TASC TIM 5915-2-2, March 1993.

16. Morris, P., Omega System Availability as a Global Measure of Navigation Accuracy, Report. No. CG-ONSCEN-05-90, NTIS Accession No. AD-A 229-492.

17. Reynolds, P., Pan American World Airways Omega experience, *Proceedings of the Fourth Annual Meeting of the International Omega Association*, San Diego, CA, September 1979.

18. Sakran, C., U.S. Navy flight test results with the LTN-211 ONS, *Proceedings of the Sixth Annual Meeting of the International Omega Association*, Montreal, P.Q., Canada, August 1981.

19. Wenzel, CAPT R., and Kugel, C., Mediterranean Sea Omega Validation Analysis, Report, No. CG-ONSCEN-01-91, May 1991.

20. Kostamo, P., World-wide use of Omega for balloon tracking, *Proceedings of the Fourteenth Annual Meeting of the International Omega Association*, Long Beach, CA, October 1989.

21. Karhunen, P., private communication, January 1994.

CHAPTER 13

EXISTING/FUTURE GLOBAL
RADIONAVIGATION SYSTEMS

Chapter Overview *— The Federal Radionavigation Plan states that Omega operation will continue at least until GPS can meet requirements for the oceanic en route phase of flight, effectively linking the future of Omega closely with the future of GPS. Section 13.1 reviews the FRP policy statement regarding Omega and introduces a potential long-term role for Omega as an augmentation to GPS for civil aviation. Section 13.2 explores GPS/Omega integration for aviation use in more detail. Also described are the more traditional integrated uses of Omega, specifically, differential Omega (Section 13.3), integration with other VLF signals (Section 13.4), and Omega/inertial integration (Section 13.5). Abbreviations/acronyms used in the chapter are defined in Section 13.6 and the chapter references are listed in Section 13.7.*

13.1 INTRODUCTION

The Federal Policy and Plans for the Future Radionavigation Systems Mix 1992 included in the 1992 Federal Radionavigation Plan (Ref. 1) includes the following statement regarding the outlook for Omega:

> *Omega is currently the only operational radionavigation system that provides global coverage and serves maritime and aviation users. The civil aviation requirements for Omega will remain in effect until GPS is approved to meet the Required Navigation Performance (RNP) criteria for the oceanic en route phase of flight. This is expected to occur in 1995. The U.S. does not expect to end Omega operations before the year 2005. However, the U.S. operates Omega with six partner nations (Norway, Liberia, France, Argentina, Australia, and Japan); therefore, the system is dependent upon continued participation by these nations under bilateral agreements with the U.S. · Continued operation after this date would depend on identifying navigation requirements or non-navigation requirements that are not met by other systems. The DoD requirement for Omega will end December 31, 1994; however, limited use is expected as long as the system remains operational.*

Clearly, the future of Omega is closely tied to the future of GPS, particularly the future of GPS as used for civil aviation. The above statement specifically mentions the potential of GPS to replace Omega for the oceanic en route phase of flight. Current FAA plans also call for GPS to be used for phases of flight where Omega is not currently used, including domestic en route and non-precision approach. It is in these phases of flight, where requirements for availability and integrity are more stringent, that GPS may find a "new life" as an integral part of the aviation navaid mix.

In the domestic en route and non-precision approach phases of flight, the planned constellation of 24 GPS satellites alone will not provide sufficient integrity and availability to meet FAA requirements. The FAA is currently pursuing augmentation schemes based on geostationary satellites broadcasting some combination of ranging signals, correction messages, and integrity messages. This is a very active and high-visibility project within the FAA, and, in all likelihood, satellite-based augmentations will be the implemented solution. Alternative solutions based on a combination of GPS and Omega signals have been proposed, but to date have been studied in much less depth. Nevertheless, early research suggests that such solutions are technically feasible (Ref. 4). If the current emphasis on satellite augmentations should change (whether for technical, political, or financial reasons) Omega could take a central role in aviation navigation.

The primary focus of this chapter will be on the potential use of Omega in conjunction with GPS for aviation use, as this is the application most likely to extend the lifetime of Omega significantly beyond the year 2000. In addition, the traditional integrated uses of Omega will be described, specifically, differential Omega, integration with other VLF signals, and Omega/inertial integration.

13.2 GPS/OMEGA INTEGRATION FOR AVIATION USE

13.2.1 Background

The Global Positioning System (GPS) comprises a Space Segment, a User Segment, and a Control Segment, as shown in Fig. 13.2-1. When completed, the Space Segment will contain 24 satellites equally distributed in six planes. The User Segment comprises all surface and air users and the Control Segment includes the Master Control Station and the monitor stations. Additional information on GPS is given in Appendices E and F.

The drive to integrate GPS in the National Airspace System has resulted in a process of redefinition of the navigation requirements for the various phases of flight — a process that continues at the present time (March 1994). The navigation system requirements for the oceanic, domestic en route, and non-precision approach phases of flight that will be applied in the year 2000 are therefore not known at this time. The new requirements will be in terms of Required Navigation Performance (RNP), which is "a statement of the navigation performance necessary within a defined airspace. RNP is intended to define the navigation performance of each individual aircraft within the airspace commensurate with the navigation requirements of that airspace" (Ref. 1). The key   of the RNP approach is that requirements are specified in terms of total system performance; requirements for components such as

Constellation

- 6 Planes
- 4 Satellites each Plane
- 55° Inclination

Space Segment

Uplink Data

- Satellite Ephemeris (Position) Constants
- Clock Correction Factors
- Atmospheric Data
- Almanac

Downlink Information

- Coded Ranging Signals
- Carrier Signals
- Navigation Message (Satellite Clock and Ephemeris, Almanac, Atmosphere)

Monitor Stations

User Segment

Ground Antenna

Master Control Station

Control Segment

Figure 13.2-1 The GPS System and Its Component Segments

navigation systems and flight technical error are not broken out separately; ". . . airspace requirements are satisfied independent of the means by which they are achieved." (Ref. 1). Thus, in principle, a user who can demonstrate that RNP is achieved for any phase of flight using a system that combines GPS and Omega (or any other combination) will have every right to fly that system.

In January 1993, the International Civil Aviation Organization (ICAO) All-Weather Operations Panel (AWOP) 14 specified the following RNP parameters for the approach and landing phases of flight (Ref. 2):

- Accuracy is the ability of the total system to maintain the aircraft position within a total system error (TSE) with a 95 percent probability (called the inner tunnel) and to stay within the outer tunnel which defines the obstacle clearance, terrain avoidance, or aircraft separation criteria for the intended operation. The TSE is based on the 95 percent probability combination of aircraft and non-aircraft sensor errors, display errors, and flight technical errors at each point along the specified procedure.

- Integrity is that quality which relates to the trust that can be placed on the correctness of the information supplied by the total system. Integrity risk is the probability of an undetected [latent] failure of the specified accuracy. Integrity includes the ability of a system to provide timely warnings when the system should not be used for the intended operation.

- Continuity is the ability of the total system to perform its function without the non-scheduled interruptions during the intended operation. The continuity risk is the probability that the system will be unintentionally interrupted and not provide the guidance information for the intended operation.

- Availability is the ability of the total system to provide the required guidance at the initiation of the intended operation. Availability risk is the probability that the required guidance will not be present at the initiation of the intended operation.

Although these definitions were made specifically for the approach and landing phases of flight, there is no reason to believe that they will change significantly when applied to the en route and oceanic phases.

The Radio Technical Commission for Aeronautics (RTCA) Special Committee 159 has the responsibility to write performance standards for airborne equipment using GPS. The committee published the "Minimum Operational Performance Standards [MOPS] for Airborne Supplemental Navigation Equipment Using the GPS" in 1991; this MOPS document focused only on supplemental-mode use of GPS. At this time, the committee realized that GPS could not meet either availability or integrity requirements as a stand-alone system (Ref. 3). Since that time, the focus of the committee has been on augmentations to GPS as a means to improve availability and integrity, with emphasis on satellite-based means.

13.2.2 Potential for Omega Augmentation of GPS

Stratton (Ref. 4) has investigated the "synergistic" combination of GPS and Omega to address the GPS availability and integrity problem for aviation. In the evaluated system, the Omega clock is used as the means to isolate a failure in a set of five satellites. Following detection of the failure, the system "coasts" using Omega relative navigation until GPS service is restored. From Ref. 4, the concept for GPS fault isolation is:

The drift stabilized Omega clock is synchronized to GPS time at each GPS fix. It is then used for comparison with GPS clock drifts measured by sets of four satellites and by substitution in each set of three satellites to compare GPS velocities and positions from the usable satellites at various PDOPs.* This should enable the faulty satellite in five to be isolated.

---

*PDOP is position dilution of precision, a measure of the impact of satellite geometry on three-dimensional position accuracy.

13-4

Following isolation of the faulty satellite, it is possible to either coast on GPS plus the Omega clock (i.e., the Omega clock measurement is substituted for the faulty satellite range measurement in the GPS position and time solution) or to swap completely to the Omega relative navigation solution. Stratton's investigation of the second option concludes that it can improve sole-means system availability from approximately 50 percent for GPS alone to 99.8 percent for the synergistic combination.

Stratton's conclusions are based on several key assumptions concerning the accuracy of Omega coasting. Among these are:

- Maximum temporal phase variation of 11 ns/sec
- Receiver clock drift rate stabilized to the range of 0.2 to 0.5 ns/sec
- Modeling reduces temporal errors by a factor of 10 or better from maximum levels.

To make a synergistic system of this type a reality, some significant work is required to verify these key assumptions. Stratton's own list of recommendations for further in-depth study includes (Ref. 4):

- Investigation of 30 minute phase change statistics
- Investigation of accuracy of PPC model during transition and modal interference
- Investigation of the accuracy of Omega clock stabilization
- Investigation of SID and PCA statistics as they would impact coasting
- Quantification of the potential to reduce SID and PCA effects through multi-frequency techniques.

To qualify a synergistic Omega/GPS system for sole-means aviation use, these investigations would need to be conducted rigorously. It is not anticipated that any in-depth investigations of this type will be initiated by the FAA unless the current satellite-based augmentation plans meet with major setbacks.

13.3 DIFFERENTIAL OMEGA

Like the differential subsystems associated with many large-scale radionavigation systems, differential Omega systems provide a way to enhance the position accuracy in a local region through the transmission of local corrections. The corrections are obtained from a central monitoring facility which compares observed signal phase readings from each of the Omega stations with the "correct" phase (using a nominal model of signal phase and distance; see Chapter 9) based on the location of the monitor and the signal frequency. The accuracy of the correction depends on the spatial correlation/coherence of

the Omega signal phase between the position of the monitor and the user's position. Within a radius of about 50 km from the monitor, the correlation peak is within about 1 centicycle (for typical time constant receivers); for greater distances, the degree of correlation slowly degrades. These corrections can be effectively applied only to "usable" signals, i.e., those that are short-path and Mode 1-dominated with SNRs above the receiver's tracking threshold.

Operational differential Omega systems currently in place (1994) are tailored primarily to marine users, although a number of experimental differential systems for aircraft have been tested. The correction information for marine use is normally broadcast to all users in the local area (having a typical radius of 200 to 500 nm) using a 20 Hz modulation of LF beacon signals with frequencies between 285 and 415 kHz. Measured position accuracies vary from 0.3 nm (100 nm from the monitor station) to about 1 nm (500 nm from the monitor station), 95 percent of the time (Ref. 12). As of 1990, 30 differential Omega systems were in operation throughout the world, including the Atlantic coasts of Europe and Africa, the Mediterranean Sea, the Caribbean, eastern Canada, India, and Indonesia (Ref. 13).

13.4   OMEGA AND OTHER VLF SIGNALS

13.4.1   Overview

The 1992 Federal Radionavigation Plan (Ref. 1) includes the following statement regarding the joint use of Omega and VLF communications signals:

> *Receiver innovations have led to the use of VLF communications transmissions to augment the Omega network and improve overall system redundancy and reliability; however, the U.S. Navy has emphasized that VLF communication signals are not intended for navigation purposes and that the use of these signals for navigation is at the risk of the user.*

Integration of Omega and VLF communications signals currently appears almost exclusively in aviation receiver systems. As noted in Section 13.2, a series of in-depth investigations would be required to qualify a joint Omega/GPS system for sole-means use in the aviation environment. These investigations could be extended to explore the potential additional benefit to be gained from the use of additional VLF signals.

Navy policy on the use of VLF communications signals for navigation is reviewed in Section 13.4.2. Section 13.4.3 summarizes FAA policy. Finally, Section 13.4.4 describes GLONASS and the joint use of Omega and the Russian VLF navigation system, Alpha.

13.4.2 U.S. Navy Policy on the Use of VLF Station Signals for Navigation

The VLF Communications Network includes both stations which are operated by the U.S. Navy and stations operated by the North Atlantic Treaty Organization (NATO). Table 13.4-1 lists the VLF communications stations, including identification code, location, coordinates, transmitting frequency, and radiated power.

Table 13.4-1 U.S. Navy/NATO VLF Communications Stations

IDENTIFICATION	LOCATION	LATITUDE (deg)	LONGITUDE (deg)	FREQUENCY (kHz)	RADIATED POWER (kW)
GBR	Rugby, England	52.37N	1.19W	16.0	45
JXZ	Noviken, Norway	66.97N	13.89E	16.4	45
NDT	Yosami, Japan	34.97N	137.02E	17.4	38
GQD/GBZ	Anthorne, England	54.92N	3.27W	19.0	42
NWC	Exmouth, Australia	21.80S	114.15E	19.8	1800
NSS	Annapolis, MD, USA	39.00N	76.50W	21.4	213
NPM	Lualualei, HI, USA	21.42N	158.15W	23.4	502
NAA	Cutler, ME, USA	44.63N	67.28W	24.0	1200
NLK	Jim Creek, WA, USA	48.20N	121.92	24.8	245
NAU	Aguada, Peurto Rico, USA	18.38N	67.18W	28.5	100

In 1972, the U.S. Department of Transportation began negotiations with the U.S. Department of Defense (DoD) on the use of VLF signals transmitted by the U.S. Naval Communication Stations (NAVCOMMSTAs) for navigation. The negotiations intensified as airborne use of Omega rapidly developed in the early 1970s and manufacturers became aware of the supplementary value of the VLF NAVCOMMSTA signals. At that time Omega was financed by the U.S. Navy (USN) although the system was intended for navigation use by both the civil and military sectors. The mission of the VLF NAVCOMMSTAs, however, remained focused on providing high-priority communications to submerged vessels. Thus, for reasons of national security, USN reserved the right to turn stations on and off, change frequencies and modulation rates, and schedule maintenance periods without advance public notice. These issues apparently did not overly concern military users since, presumably, many had access to advance notification messages. Civil users, of course, did not have such advance notice and although VLF signals were generally used for back-up, concern was expressed for the uncertain availability of

VLF signals. The concern was generally limited to the airborne navigation sector since marine navigation was dominated by TRANSIT satellite use as a result of general dissatisfaction with first-generation Omega receivers. Consequently the Federal Aviation Administration (FAA) became involved with the issue through the need to certify Omega/VLF receivers for civil aviation use. This set the stage for a formal request in 1975 (Ref. 5) by the FAA Administrator that the USN adopt a navigation mission for the VLF stations, specifically requesting

> ". . . scheduled outages, output variations, and signal format changes be kept to a minimum."

and

> ". . . all outage information be made available to the international NOTAM system in a timely manner."

A few months later, DoD declined the FAA request (Ref. 6) citing

> ". . . fundamental inconsistencies between a communication system intended for contingency communication purposes and a communication system intended for navigation purposes."

In subsequent correspondence, DoD clarified its position, acknowledging the navigational use of VLF signals but urging that VLF users be cautioned about unannounced changes in signal format, modulation, and frequency. In the late 1970s the U.S. Naval Observatory (USNO) was given the responsibility of providing information for a joint Omega/VLF Notice to Airmen (NOTAM) which included scheduled maintenance periods, planned changes in transmission frequency(ies) and emission levels, scheduled repair periods, and "after-the-fact" outages of more than 10 minutes. This information is currently supplied in addition to the routinely reported phase/time data on the VLF and Omega signals recorded at USNO. The advance information now carried in the Omega/VLF NOTAMs probably covers the great majority of the actual anomalous VLF station events which occur but the USN still reserves (and occasionally exercises) the right to make unannounced changes in the VLF transmitted signals.

13.4.3   FAA Policy on the Use of VLF Station Signals for Navigation

The USN policy on the use of VLF station signals outlined above limits the policy options of the FAA regarding the use of these signals. Use of multiple, independent navigation aids is a fundamental precept of prudent navigation. Thus, the addition of VLF signals to those of Omega* is considered

---

*The two systems' signals are not independent since they are both affected by certain types of ionospheric phenomena, e.g., sudden ionospheric disturbances (SIDs)

advantageous to the user. The FAA, however, cannot certify for commercial use a receiver that critically depends on signals from a system that apparently does not meet some or all of the requirements for a navigation aid. The approach that the FAA has adopted is to accept Omega/VLF receivers for certification but ensure that the receiver systems satisfy certification requirements using *Omega signals alone*. An FAA Advisory Circular (Ref. 7) states that

> "The Omega/VLF navigation system, while it may use VLF communications stations to supplement and enhance the Omega system (increase areas of coverage, improve performance, etc.), should be capable of accurate navigation using Omega signals alone."

This statement succinctly summarizes FAA policy on the use of VLF station signals for navigation and the policy is not likely to change in the immediate future.

13.4.4   GLONASS and the Joint Use of Omega and Alpha

The Alpha system is the VLF radionavigation system operated by the Commonwealth of Independent States (CIS). The system includes five VLF transmitting stations, listed in Table 13.4-2. Each Alpha station transmits VLF signals at three common frequencies (11.905, 12.649, and 14.881 kHz).

The CIS also operates a satellite-based navigation system known as GLONASS (GLobal NAvigation Satellite System). Table 13.4-3 summarizes the GLONASS technical characteristics and compares them to GPS. Like GPS, the GLONASS constellation will nominally consist of 24 satellites, defined as having 21 operational satellites and three working spares. The planned GLONASS constellation has three planes of eight satellites each. The planes are inclined with respect to the equator by almost 65°, presumably to enhance coverage of more northerly latitudes. Individual GLONASS satellites are at slightly lower altitudes than GPS satellites, and thus have shorter orbital periods (GLONASS satellites execute 17 revolutions in eight sidereal days).

Table 13.4-2   Alpha System Station Specifications

IDENTIFICATION	LOCATION (NEAREST CITY)	LATITUDE (deg)	LONGITUDE (deg)	FREQUENCY (kHz)	RADIATED POWER (kW)
ASH	Ashkhabad	39.46 N	62.72 E	11.905, 12.649, 14.881	50
KOM	Komsomolskamur	50.06 N	136.60 E		
KRA	Krasnodar	45.46 N	38.17 E		
MUR	Murmansk	68.03 N	34.68 E		
NOV	Novosibirsk	55.75 N	84.45 E		

Table 13.4-3 GPS/GLONASS Technical Characteristics

CHARACTERISTICS	GPS	GLONASS
First Launch/Operational	1978/93	1982
Constellation (Nominal)	24	24
Active (as of March 1994)	27	10
Geometry	6 Planes	3 Planes
Inclination (deg)	55	64.8
Altitude (nm)	10,900	10,300
Period (hr:min)	11:56.9	11:15
Carrier Frequency (MHz)	1575	$1602+0.5625n*$
Chip Rate (MHz)	1.023	0.511
Coordinate System	WGS-84	SGC-85
System Time Reference	UTC-USNO	UTC-SU

$*n = 0, 1, 2, \ldots, 23$

In terms of signal structure, each GLONASS satellite broadcasts at two frequencies, analogous to the GPS L_1 and L_2 (only the "GLONASS L_1" is shown in Table 13.4-3). Similarly, the GLONASS employs two pseudorandom codes, corresponding to the GPS C/A- and P-codes. The chipping rates for the GLONASS codes are one-half those for their GPS counterparts. Whereas the GPS "separates" satellite signals by code-division multiplexing (CDM, all satellites broadcast on the same frequency but use different codes), GLONASS separates satellite signals by frequency division multiplexing (FDM, all satellites broadcast the same code but on different frequencies).

Vladimir I. Denisov, Deputy Chairman-Director of the Internavigation Interdepartmental Commission Research and Technical Center of Russia and Radionavigation Intergovernmental Council of the CIS, wrote in June 1993 (Ref. 8):

> *The Alpha system will be in use until the GLONASS system meets air and maritime user requirements and will be operated in combined mode with the Omega system.*

Published efforts to date to integrate the Omega and Alpha systems are dominated by the work of the U.S. Coast Guard Academy, in which several working prototype Alpha/Omega receivers have been built (Refs. 9 and 10). Capt. Benjamin Peterson of the Coast Guard Academy has written (Ref. 9), "Integration of the Russian system with Omega and the availability of integrated receivers could substantially improve VLF navigation availability and accuracy worldwide." At present, no comprehensive assessment of the potential accuracy and availability gains has been published. The technical issues involved in Omega/Alpha integration are minor (e.g., time synchronizations of the systems), and the CIS has been forthcoming with technical information regarding the Alpha system (Ref. 11). However, no commercial development of joint Alpha/Omega systems is currently known to be underway; commercial viability of such a system certainly depends directly on the future of GPS and GLONASS.

13.5 Omega/Inertial Integration

Avionics navigation systems based on Omega/inertial integration are used in a small number of military aircraft (the E-3 AWACS is one example); such systems are virtually nonexistent in the commercial world. With the coming of GPS, it is unlikely that significant future examples of Omega/inertial integration will arise. Nevertheless, the technology exists and has proven its utility.

An inertial navigation system (INS) is a self-contained navigation system typically consisting of gyroscopes, accelerometers, and a computer. Unaided INS position accuracy is influenced by various sensor and environmental errors. The nature of these error sources is such that INS error behavior displays a time-increasing characteristic. System performance is usually characterized in terms of position error growth/unit time, e.g., nm/hr; a nominal accuracy specification on a commercial-quality INS is 1 nm/hr.

Although the long-term error behavior displays time-increasing characteristics, the short-term stability of the position and velocity information available from an INS is excellent. Omega errors have the complementary advantage of being bounded over the long term. Proper integration of Omega and inertial system outputs can provide the advantages of each while eliminating many of the respective disadvantages. The important complementary characteristics of the two systems are given in Table 13.5-1.

Table 13.5-1 Pertinent System Characteristics

OMEGA	INS
Bounded long-term	Time-increasing long-term errors
Noisy short-term position output	Stable short-term position output
Good relative navigation	Good absolute navigation
Requires velocity input	Provides velocity data

13.6 ABBREVIATIONS/ACRONYMS

AWOP	All-Weather Operations Panel
cec	Centicycle
CIS	Commonwealth of Independent States
deg	Degrees
DoD	Department of Defense
FAA	Federal Aviation Administration
GLONASS	Global Navigation Satellite System
GPS	Global Positioning System
hr	Hour
Hz	Hertz
ICAO	International Civil Aviation Organization
INS	Inertial Navigation System
kHz	Kilohertz
km	Kilometer
kW	Kilowatt
LF	Low Frequency
MOPS	*Minimum Operational Performance Standards*
NAVCOMMSTA	Naval Communications Stations
nm	Nautical mile
NOTAM	Notification to Airmen
PCA	Polar Cap Anomaly
PDOP	Position Dilution of Precision
PPC	predicted Propagation Correction
RNP	Required Navigation Performance
RTCA	Radio Technical Commission for Aeronautics
SID	Sudden Ionospheric Disturbance
SNR	Signal-to-Noise Ratio
TSE	Total System Error
USN	U.S. Navy
USNO	U.S. Naval Observatory
VLF	Very Low Frequency

13.7 REFERENCES

1. 1992 Federal Radionavigation Plan, Department of Defense, Report No. DoD-4650.4, Department of Transportation, Report No. DOT-VNTSC-RSPA-92-2, 1992.

2. Davis, J.M., RNP Tunnel Concept for Precision Approach with GNSS Application, Proc. ION, Cambridge, MA, June 1993.

3. VanDierendonck, A.J., and Enge, P., RTCA Special Committee 159 Definitions of the GNSS Integrity Channel (GIC) and Wide Area Differential GNSS (WADGNSS), ION GPS-93, Salt Lake City, September 1993.

4. Stratton, A., Omega: A Synergistic Solution to the Integrity Problem of Satellite Navigation, *Proceedings of the Sixteenth Annual Meeting of the International Omega Association*, Vancouver, British Columbia, Canada, August 1991.

5. Letter correspondence from Honorable James E. Dow, Acting Administrator, Federal Aviation Administration (FAA) to Honorable Frank A. Schrontz, Department of Defense (DoD) Representative to FAA, 25 April 1975.

6. Letter correspondence from Honorable Frank A. Schrontz, Chairman, DoD Advising Committee on Federal Aviation, to Honorable James E. Dow, Acting Administrator, FAA, 30 June 1975.

7. FAA Advisory Circular No. 20-101C, *Airworthiness Approval of Omega/VLF Navigation Systems for Use in the U.S. National Aerospace System (NAS) and Alaska*, U.S. Department of Transportation, September 1988.

8. Denisov, V., Navigation Planning in the CIS, Proc. ION, Cambridge, MA, June 1993.

9. Peterson, B., Gross, K., and Chamberlin, E., Integrated CIS VLF/Omega Receiver Design, *Proceedings of the Seventeenth Meeting of the International Omega Association*, Amsterdam, The Netherlands, August 1992.

10. Peterson, B., Gross, K., and Chamberlin, E., Remotely Controlled, Integrated Alpha/Omega Monitor, *Proceedings of the Eighteenth Meeting of the International Navigation Association*, Orlando, FL, October 1993.

11. Boloshin, S.B., and Guzman, A.S., Synchronization of Stations in the Alpha RNS and Features of Synchronization with the Omega RNS, *Proceedings of the Eighteenth Meeting of the International Navigation Association*, Orlando, FL, October 1993.

12. Nard, G.P., 1980s Differential Omega Navigation and Equipments, *Proceedings of the Fourth Annual Meeting of the International Omega Association*, San Diego, CA, September 1979.

13. Bourasseau, S., Differential Omega in Indonesia, *Proceedings of the Fifteenth Annual Meeting of the International Omega Association*, Sanur, Bali, Indonesia, September 1990.

APPENDIX A

VLF SIGNAL/NOISE PREDICTION MODELS

A.3 VLF/OMEGA SIGNAL PROPAGATION APPROACHES

VLF/Omega signals propagate in the space bounded between the earth's surface and the D-region of the ionosphere, known as the earth-ionosphere (EI) waveguide (see Figs. A.1-1a and A.1-1b). The electromagnetic field characteristics of a signal propagating in the EI waveguide formed along a signal path are derived from solutions of Maxwell's equations applied to the waveguide* modeling the signal path (Refs. 1 through 4). The exact electromagnetic field solutions are extremely difficult to obtain because of the spherical shape of the waveguide and electromagnetic properties along the waveguide that vary both spatially and temporally. The electromagnetic properties are the: (1) spatially varying ground conductivity of the earth's surface, (2) spatially and temporally varying conductivity of the ionosphere boundary, and (3) spatially varying magnitude and orientation[§] of the earth's magnetic field. The earth's magnetic field (geomagnetic field) makes the ionosphere boundary medium appear as anisotropic with respect to VLF signal propagation, i.e., the presence of a geomagnetic field makes the signal propagation depend upon the path direction.

The following full-wave approaches[†] to determining VLF signal propagation characteristics have appeared in the literature:

1. Wave-hop or hop theory (Refs. 5 and 6)
2. Zonal harmonic series approach (Ref. 7)
3. Mode theory (Refs. 1 through 4).

---

*In this appendix, "waveguide," "path," and "signal path" are used interchangeably to refer to the earth-ionosphere waveguide bounding the signal path.

[§] Orientation relative to the signal path direction.

[†]The full-wave approach means that Maxwell's equations have been applied to determine the electromagnetic fields accounting for the varying electromagnetic properties of the wave propagation medium (Ref. 4). These properties can vary significantly for Omega/VLF signals over a distance of the signal wavelength. If, however, the path properties do not vary significantly over a wavelength, as is usually the case for the low- and high-frequency signal propagation, the conventional (non-full-wave) ray or geometrical optics theory can be used.

G–24117a
6–24–92
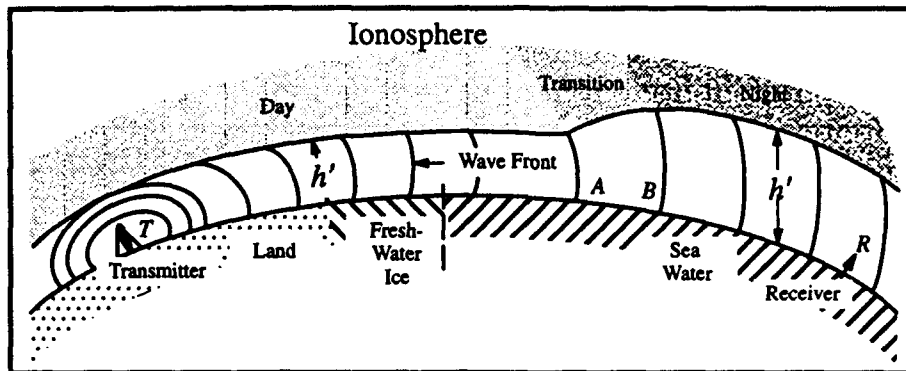
a) Side View of the EI Waveguide Formed Along
the Path TR Shown in Fig. A.1-1b

G–24117
7–3–92
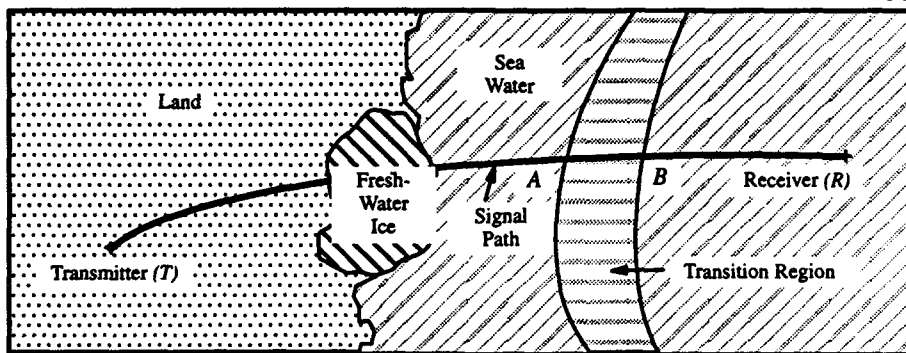
b) An Example of Signal Path TR

Figure A.1-1 Signal Path TR

The first two approaches lend themselves to clear visualization of the signal propagation mechanism in the waveguide, while the third approach, mode theory, provides a useful model for certain characteristics of VLF propagation, such as the "modal interference" (Chapter 5). Of these approaches, mode theory is the most frequently used.

In the *wave-hop theory* (Ref. 5), a signal at a point (receiver) is a sum of the groundwave (i.e., the wave that results in the absence of ionosphere, as in the Loran-C system) and a series of "wave-hops" (also called skywaves) reflected from the ionosphere and earth's surface by successive wave-hops, as shown in Fig. A.1-2. The wave propagation is described by wave-hops that are reflected according to the rules of geometric optics. In the figure, the received signal is composed of the groundwave (not shown) and three wave-hops ($j = 1, 2,$ and 3). Note that wave-hop "j" is reflected j times from the ionosphere and ($j - 1$) times from the earth's surface. This description is of particular interest when the distance (ϱ) between the transmitter and receiver is relatively short, e.g., $\varrho < 1000$ km. For these short distances, it is

A-2
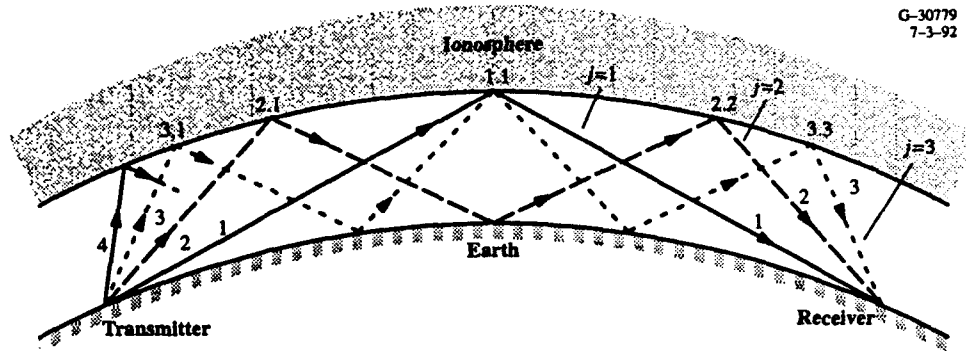
Figure A.1-2 Diagrammatic Representation of Wave-Hops

usually enough to consider the wave-hops that have been reflected from the ionosphere two or three times. The number of wave-hops needed to represent a signal increases as ϱ increases. Because Omega and VLF systems are long-range navigation systems where signals propagate over distances of 10 to 15 thousand kilometers, the currently available propagation algorithm based on wave-hop theory (Ref. 6) is not computationally practical for Omega/VLF signal predictions.

In the *zonal harmonic series* approach (Ref. 7), a signal propagating in the waveguide is decomposed into a zonal harmonic series, which is then reformulated into a more rapidly converging geometric series. The geometric series terms corresponds to "radial" waves originating at the signal source (transmitter) and propagating radially between the earth and ionosphere. The series is slowly convergent, but is useful well below 10 kHz. Typically, several thousand terms are needed at VLF. The zonal harmonic series has been reformulated as a geometric series to improve convergence, but it still is computationally not suited for Omega/VLF signal predictions.

In the *mode theory* (Refs. 1 through 4, 8, and 9), a signal propagating along a path is expressed as a sum of the "characteristic" modes (i.e., specific electromagnetic field patterns) of the earth-ionosphere waveguide formed along the path. A sketch of the electric field pattern of the signal propagating away from a VLF transmitting station is shown in Fig. A.1-3. At short distances (500 to 2000 km) from a transmitting source, the signal is generally very complex as the sum of a large number of competing, strong-amplitude modes. As the distance from a source increases, fewer competing, strong-amplitude, lower-order modes are needed to adequately approximate the signal, as the higher-order modes are attenuated much more rapidly than the lower-order modes. The number of modes needed to approximate a signal, and hence the associated computational time needed for this approach, generally decreases as the signal computation point moves away from the signal source. The mode theory approach has therefore been computationally preferred for Omega/VLF signal predictions at long ranges from a station.

G-30678
6-18-92
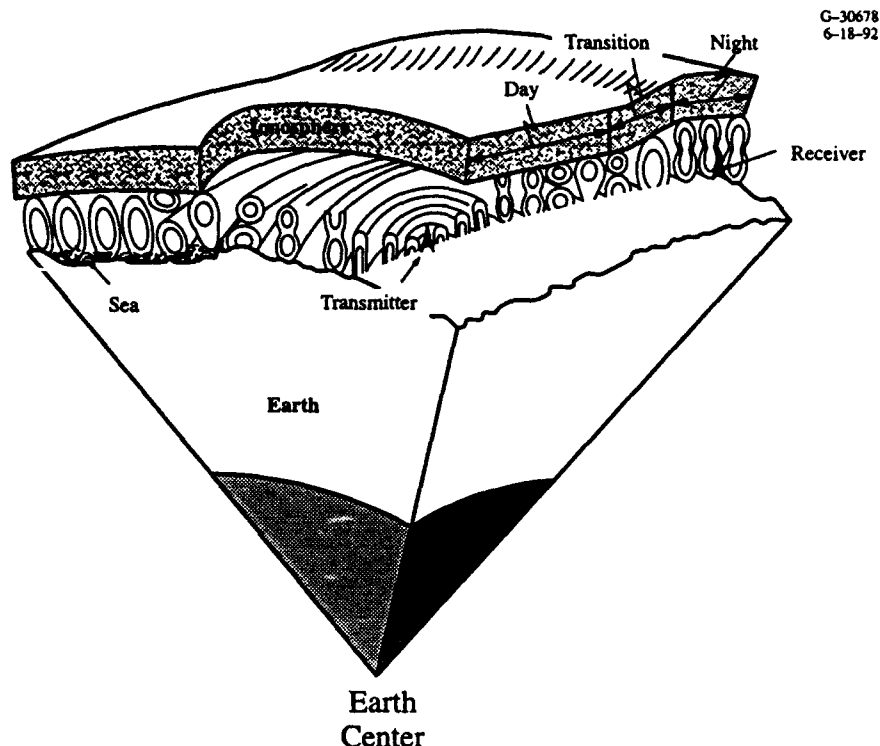
Figure A.1-3 Approximate Electric Field Pattern Within
the Earth-Ionosphere Waveguide

The above considerations led to the use of mode theory-based models for developing Omega signal coverage products. Most of these models have been developed by the Naval Command, Control, and Ocean Surveillance Center (NCCOSC), formerly the Naval Ocean Systems Center (NOSC). In the next section we review the mode theory signal propagation fundamentals and discuss the mode theory-based models used to calculate the signal information for the coverage products.

A.2   MODE THEORY FUNDAMENTALS

In a *homogeneous* waveguide (Refs. 1 through 4), the waveguide modes are either transverse electric (TE) or transverse magnetic (TM). The total signal in a waveguide is the sum of the TM and TE modes excited by the transmitting source antenna in the waveguide. A TE mode has a magnetic field component, but no electric field component, in the direction of signal propagation. A TM mode, on the other hand, has an electric field component, but no magnetic field component, in the direction of signal propagation.

Each mode is uniquely characterized by an eigenangle or eigenvalue (a complex quantity) which is a function of the electromagnetic properties of the signal path and signal frequency. The propagation characteristics (i.e., amplitude and phase) of a mode propagating along a signal path are determined by four mode-specific signal parameters, signal frequency, distance from transmitter, and transmitter characteristics. The four mode-specific parameters are:

- *Attenuation Rate* — the rate at which the mode attenuates along a path.
- *Phase Velocity* — the velocity at which the phase wavefront of the mode appears to propagate along a path.
- *Excitation Factor* — a measure of the relative efficiency with which the mode of the transmitted (received) signal couples into (out of) the EI waveguide.
- *Height-gain Function* — a function describing the variation of the mode field along the local vertical (to the earth surface) perpendicular to the path direction.

Modes are conveniently numbered with an increasing mode number according to the increasing phase velocity. The mode with the lowest phase velocity is called Mode 1. Increasingly higher phase-velocity modes are called Mode 2, Mode 3, etc. In this mode-numbering system, odd-numbered modes (e.g., Modes 1, 3) are TM modes and even-numbered modes (e.g., Modes 2, 4) are TE modes. The signal attenuation rate of a TE or TM mode usually increases with the increasing mode number as well as with the increasing signal frequency. The number of modes needed to approximate a VLF signal increases as the: (1) signal path illumination condition changes from an "all-day" to "all-night" condition, and (2) station signal frequency increases. Signals at Omega frequencies (10 to 14 kHz) are usually well-approximated by a single mode (Mode 1) for an all-day path, and two to three lower-order modes for an all-night path. The number of modes needed to approximate a VLF (14 to 30 kHz) signal is about two to three modes for all-day paths and six to twelve modes for all-night paths.

Note that the VLF station signal path is, in general, inhomogeneous since path properties vary both spatially and temporally along the path. Thus, a conventional mode-eigenvalue determination approach, applicable to a homogeneous waveguide, is not directly usable for VLF signal predictions. The following approach typifies the calculation of signal propagation characteristics along an *inhomogeneous path* (Ref. 8).

1. Use a spatially and temporally varying model for the ionospheric conductivity, and a ten-level map (see Ref. 10) for the spatially varying ground conductivity.

2. Approximate the inhomogeneous path as a concatenation of homogeneous segments. As a consequence, the properties along the approximated path are uniform within each segment and these properties change discontinuously (a step change) at each interface between the adjoining homogeneous segments of the path.

3. Apply the conventional (i.e., homogeneous waveguide) mode theory to find eigen-values of the significant modes in each of the homogeneous segments of the approx-imated path.

4. Compute the mode conversion effects (i.e., the signal energy exchanges among the modes whose eigenvalues are found in Step 3) occurring at the path-segment inter-faces; incorporate these effects into the resultant total (i.e., mode-sum) signal cal-culations.

The most frequently used ionospheric conductivity model in the VLF signal prediction models assumes that the ionospheric conductivity increases exponentially with height above the earth's surface. The ionospheric model parameters, in Wait's notations (Ref. 9), are the ionospheric reflection height (h') and the ionospheric conductivity gradient (β). The ionospheric parameters are, in general, a function of frequency, geomagnetic dip angle, and solar zenith angle (χ). The most recently published ionospheric conductivity model, such as the one embodied in the LWPC (Refs. 12 and 13) and LWPCN (Ref. 14) packages of the NCCOSC-developed VLF signal prediction codes, includes a dip angle dependence for both h' and β and uses the all-day, all-night, or transition values for h' and β at a segment based on the all-day (i.e., $\chi \leq 90°$), all-night (i.e., $\chi \geq 98°$), or transition ($90° < \chi < 98°$) illumination condition at the segment.

In the approximation of an inhomogeneous path by a concatenated series of homogeneous seg-ments, two different path segmentation schemes have been employed in the literature to determine the length of the individual homogeneous segments forming the approximated path. In the first scheme (implemented in IPP, Ref. 11), the prediction path is divided into small segments of equal length (100 to 200 km) such that the path properties along the approximated path would closely approximate the prop-erties along the actual path. In the second scheme (implemented in LWPC and LWPCN), a prediction path is divided into differing-length homogeneous segments such that the computed mode-eigenvalues along the approximated path closely approximate the spatially varying mode-eigenvalues along the pre-diction path. The eigenvalue of a mode is a non-uniformly varying function of local path properties and hence the segment length in the second scheme depends on segment properties. Since the generally longer segments of the second scheme are more consistent with the waveguide-mode model (segment lengths on the order of h tanθ, where h = ionospheric reflection height and θ = real part of the mode-eigenvalue, are needed to set up modes), the second scheme is more realistic. Furthermore, the second scheme leads to fewer path segments and thus requires fewer signal calculations and hence less comput-er time (about 25 to 50 percent of the first scheme), with the attendant signal prediction accuracy being same or better than the first scheme. Therefore, the second scheme is the preferred path segmentation scheme.

Two different procedures have been employed to calculate mode conversion effects at a path segment interface. In the first procedure, developed in the early 1970s and implemented in IPP, mode conversions are assumed to be negligible and are thus ignored in the computation of the total (mode-sum) signal transiting through the interface. Thus, in the first procedure, the signal energy of each of the component modes (and therefore the resulting mode-sum signal) is conserved when the mode transits an interface. The first procedure is described as a WKB-type* approximation in IPP (Ref. 11). As a result of this approximation, the first procedure can be reliably used to compute VLF signal propagation characteristics along paths with gradually varying properties such as those along most all-day and some all-night signal paths.

The second procedure, developed by NCCOSC in 1980, rigorously models the mode conversion effects occurring at a segment interface. In this procedure, the energy of the total signal, and not the energy of each individual mode as in the first procedure, is conserved when the signal transits an interface. The computer implementation of the rigorous mode conversion effects computation algorithm is the FULLMC computer program developed by NCCOSC (Ref. 15). This program is computationally very intensive and is thus useful as a tool for research and development, and not for production. Therefore, NCCOSC developed a much less computation-intensive algorithm to calculate approximate mode conversion effects; the computer implementation of the approximate algorithm is the FASTMC computer program (Ref. 16). Typically, FASTMC requires about one percent of the computation time needed by FULLMC. Furthermore, FASTMC provides reasonably accurate mode conversion effects at the segment interfaces along most all-day paths, and many of the all-night paths that do not transit through the "equatorial belt," defined as the geographic region between ±10° geomagnetic latitudes. For all-night paths with segments inside the equatorial belt as well as for the transition paths, the rigorous algorithm is recommended for computing mode conversion effects.

A.2.1 Mode Theory-Based VLF Signal Prediction Models

The first mode theory-based computer model/program available for calculating VLF signal propagation characteristics was the Integrated Propagation Prediction (IPP) developed by NCCOSC (Ref. 11). IPP was developed to provide VLF signal predictions along signal paths with gradually varying path properties. However, it has been sometimes used to calculate signal predictions along paths with arbitrarily varying properties.

---

*Wenzel-Kramers-Brillioun, the composite names of the three researchers who pioneered the technique.

In 1985, NCCOSC developed a set of computer programs, called the Long Wavelength Propagation Capability (LWPC, Refs. 12 and 13), to calculate mode theory-based VLF signal predictions along paths with arbitrarily varying path properties. This removed the serious drawback of IPP which, strictly speaking, is usable only for the gradually varying properties paths. In addition, LWPC is a significant improvement over IPP as it employs: (1) physically much more realistic models for both the signal path environment and mode conversion phenomenon, and (2) computationally much more efficient signal computation algorithms.

All of the Omega signal coverage products developed prior to 1987 used the IPP model; those developed after 1987 use LWPC, LWPCN, or some derivative of LWPC/LWPCN. An overview of the major modules (programs) and algorithms of IPP and LWPC/LWPCN follows.

IPP — A detailed discussion of the IPP modules follows as LWPC and LWPCN (discussed later) include the derivatives of these modules with different names. The major sub-models and algorithms of IPP are GCPATH, WVGUID, and MODESUM. Signal calculations along a path are done by IPP using the following four-step procedure:

1. GCPATH approximates the signal prediction path as a concatenated series of homogeneous segments, each of a fixed length. The segment length is a user input and the path segmentation is based on the first scheme described earlier. This scheme partitions a path into homogeneous segments of equal length. Next GCPATH assigns to each of the segments a set of the homogeneous properties that are local values of the path properties at the beginning of the segment. The segment properties are: (1) ground conductivity obtained from a ten-level ground conductivity map (see Table A.2-1) which has a spatial resolution of 1/2° in latitude and 1/2° in longitude, (2) magnitude of the earth's magnetic field and dip angle, (3) path azimuth (i.e., path direction clockwise from geomagnetic north), and (4) all-day (for $\chi < 90°$) or all-night (for $\chi > 90°$) values for the ionospheric parameters. Table A.2-2 lists the all-day and all-night values of the ionospheric parameters used in the development of pre-1987 Omega signal coverage products.

Table A.2-1   Ten-Level Ground Conductivity Map (Ref. 17)

CONDUCTIVITY		RELATIVE DIELECTRIC CONSTANT
LEVEL	VALUE (mho/m)	
1	10^{-5} (Ice Cap)	10
2	3×10^{-5}	10
3	10^{-4}	15
4	3×10^{-4}	15
5	10^{-3}	15
6	3×10^{-3}	15
7	10^{-2}	20
8	3×10^{-2}	20
9	10^{-1}	45
10	4 (Seawater)	81

**Table A.2-2   Typical Ionospheric Values Used in the
Pre-1987 Coverage Products**

ILLUMINATION CONDITION	SOLAR ZENITH ANGLE, χ (deg)	IONOSPHERIC PARAMETERS	
		h' (km)	β (km^{-1})
All-Day	$0 \leq \chi \leq 90$	70	0.3
All-Night	$90 < \chi \leq 180$	87	0.5

2.   WVGUID formulates and solves the mode-eigenvalue equation for the user-selected modes in each of the homogeneous segments of the path. WVGUID employs an iterative mode-eigenvalue solution procedure, which needs the starting (guessed) eigenvalues of the selected modes to begin the procedure. The starting mode-eigenvalues for the first segment that contains the transmitter are user-provided. The remaining segments of the path, however, use the mode-eigenvalues found in the preceding segment as the starting mode-eigenvalues. The mode-eigenvalue solutions are quite sensitive to small changes in path properties, especially at night. Furthermore, the path properties can experience large changes such as those encountered in ground conductivity by a path crossing from seawater/land to ice/tundra (e.g., transiting into or out of Greenland). Because the mode-eigenvalue solutions dramatically differ between seawater/land, ice, and tundra segments, WVGUID is often unable to find the correct mode-eigenvalue solutions if the preceding segment has significantly different properties (especially the ground conductivity) from those of the current segment.

3.   Whenever WVGUID fails to find the mode-eigenvalue solutions of the desired modes in a segment, the signal calculations are restarted at the segment where WVGUID failed by inputting the new starting eigenvalues for the segment. The new starting eigenvalues for such a segment are obtained from the NCCOSC-developed MODESRCH routine program (Ref. 18), which is computationally much more burdensome than WVGUID but always finds the correct mode-eigenvalues of all of the desired modes for the segment.

4.   Finally, using the mode-eigenvalue solutions found in the last two steps, MODE-SUM computes the amplitude and phase of the signal propagating along the path. MODESUM performs two functions: first, it computes the signal parameters (i.e., attenuation rate, phase velocity, excitation factor, and height-gain function) of each component mode of the signal, and then it calculates the total (mode-sum) signal propagating along the path as a vector-phasor sum of the individual mode signals. The mode-sum computations use a WKB-type approximation that neglects the mode conversion effects occurring along the path. The output of MODESUM is the amplitude and phase of the signal as well as those of its component modes.

LWPC/LWPCN — The generic names of the four important computer modules of the LWPC/ LWPCN are: PRESEG, SEGWVGD, MODEFNDR, FASTMC, and FULLMC. The signal predictions along a signal path by LWPC/LWPCN are made using the following three-step procedure. First, PRESEG is run to partition the prediction path into a concatenated series of homogenous segments. Second, the combination of SEGWVGD and MODEFNDR* is run to calculate the mode-eigenvalues (and associated parameters needed to compute the mode conversion effects) for each of the segments. MODEFNDR provides the starting (initial) eigenvalues for use in the iterative mode-eigenvalue solution algorithm in SEGWVGD, whenever SEGWVGD deems it necessary. Third, FASTMC (in LWPC), or FASTMC or FULLMC (in LWPCN) is run to calculate: (1) the mode conversion coefficients, and (2) the total signal along the prediction path. The salient features of each of the four modules follow.

1. PRESEG is a path segmentation program based on the second path segmentation scheme discussed earlier. It approximates a signal path as a concatenated series of homogeneous segments of differing lengths. The homogeneous properties of a segment are the values of the local properties at the beginning of the segment. PRESEG employs a physically more realistic, spatially and temporally varying model for the ionospheric conductivity parameters than that used in IPP. To reduce computational burden, PRESEG segments a given signal prediction path into the fewest reasonably homogeneous segments. The length of each homogeneous segment is chosen such that the use of the mode-eigenvalues based on homogeneous path properties, in place of the locally varying mode-eigenvalues based on actual local path properties, will have no noticeable effect on the associated mode signal parameters. Because of the greatly varying sensitivity of the individual mode-eigenvalues to the local path properties, the PRESEG-approximated path is composed of differing length segments. Usually, the mode-eigenvalue sensitivity to the path properties is much less: (1) during day than night, (2) in a high- or mid-latitude region than a low-latitude region, and (3) along a path segment with an easterly path azimuth than a westerly path azimuth. As a result, a signal path has far fewer homogeneous segments for the day portion of the path than for the transition or night portion of the path.

The ionospheric conductivity parameters in PRESEG (Ref. 19) are a function of solar zenith angle (χ), signal frequency, and location (via the geomagnetic dip angle, D). Table A.2-3 lists the PRESEG-provided values of the ionospheric conductivity parameters (h' and β) at 13.6 kHz as a function of χ and D. Figures A.2-1a and A.2-1b show examples of the PRESEG-provided values for ionospheric parameters at 13.6 kHz along a nighttime (all-night), trans-polar path, and a non-polar path undergoing day-to-night transition (i.e., crossed by the day/night terminator).

---

*MODEFNDR is an improved MODESRCH routine.

Table A.2-3   Values of Ionospheric Parameters at 13.6 kHz (Ref. 19)

ILLUMINATION CONDITION	SOLAR ZENITH ANGLE, χ RANGE (deg)	DIP ANGLE, D (deg)	IONOSPHERIC PARAMETERS	
			h' (km)	β (km^{-1})
Day	$0 \leq \chi < 90$	$|D| \leq 90$	74.0	0.30
Transition	$90 < \chi < 91.8$		76.2	0.31
	$91.8 \leq \chi < 93.6$		78.3	0.31
	$93.6 \leq \chi < 95.4$	$|D| \leq 90$	80.5	0.32
	$95.4 \leq \chi < 97.2$		82.7	0.32
	$97.2 \leq \chi < 99$		84.8	0.33
Night		$|D| < 70$	87.0	0.34
		$70 \leq |D| < 72$	84.8	0.33
	$\chi \geq 99$	$72 \leq |D| \leq 74$	82.7	0.32
		$|D| > 74$	80.5	0.32

2. SEGMWVGD (Ref. 20) is an improved version of WVGUID (an IPP module). The improvement consists of including the "Brewster" modes, as part of the signal's component modes which are not included in WVGUID. The Brewster modes are required to correctly characterize the signal along a very low ground conductivity path. Like WVGUID, SEGMWVGD formulates and solves the mode-eigenvalue equation at each of the path segments and then it uses an iterative procedure to find the mode eigenvalues. The output of SEGMWVGD is a set of eigenvalues of the user-selected modes and associated mode parameters needed to compute the mode conversion effects at each of the homogeneous segment interfaces along the path.

3. MODEFNDR (Ref. 21), as mentioned earlier, is an improved version of MODESRCH. It aids SEGMWVGD to find mode-eigenvalues by providing a set of starting (guessed) values for the mode-eigenvalue solution algorithm whenever SEGMWVGD: (1) is trying to solve the waveguide-mode equation at a segment whose ground conductivity is different from the previous segment, or (2) fails to find all the desired modes at a segment and needs a better set of starting mode-eigenvalues to restart the waveguide-mode solution calculations at the segment.

4. FASTMC and FULLMC, as mentioned earlier, are the approximate and rigorous mode conversion computation routines, respectively, developed to calculate the mode conversion parameters and incorporate these parameters into the signal calculations to provide the amplitude and phase of the mode-sum signal along the

entire signal prediction path. FASTMC is used in LWPC to calculate the mode conversion effects at each path segment interface. However, the mode conversion effects at a path segment interface are computed in LWPCN using: FASTMC or FULLMC, based on the degree of mismatch between the path properties across the interface. If the mismatch is small, FASTMC is used; otherwise, FULLMC is used.

G-24112
03-12-91

| $h' = 87.0$ | 84.8 | 82.7 | 80.5 | 82.7 | 84.8 | 87.0 |
| $\beta = 0.34$ | 0.33 | 0.32 | 0.32 | 0.32 | 0.33 | 0.34 |

| D = | 70 | 72 | 74 | 90 | 74 | 72 | 70 |

Non-Polar Region ($D < 70$) ◄──► Temperate-to-Polar Transition ◄──► Polar Region ◄──► Temperate-to-Polar Transition ◄──► Non-Polar Region ($D < 70$)

◄─────────── $\chi \geq 99$ ───────────►
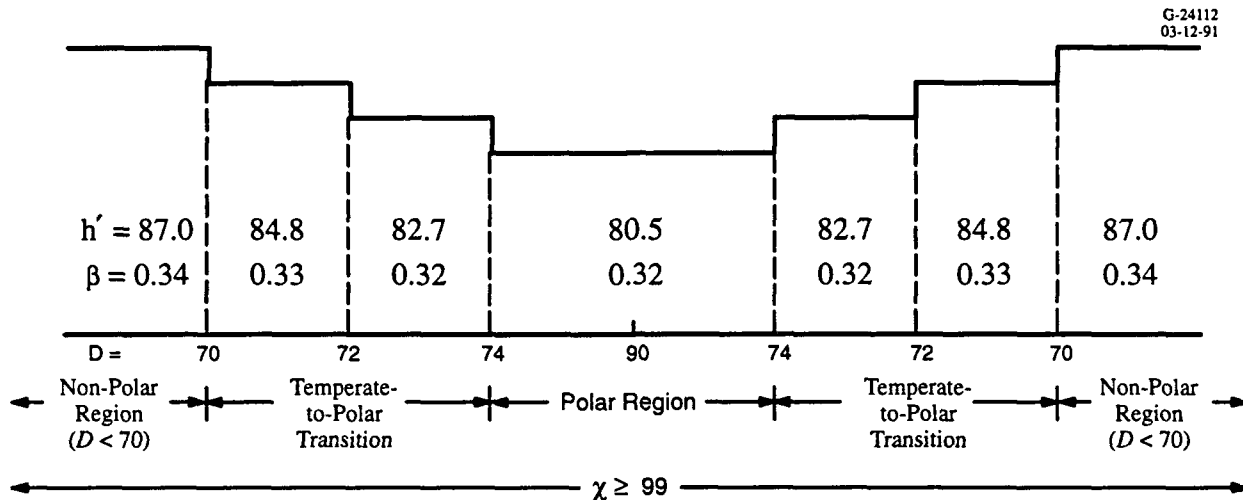
a) h' (km) and β (km^{-1}) as a Function of Solar Zenith Angle, χ (deg), and Dip Angle, D (deg) Along a Nighttime Trans-Polar Path

G-24113
03-12-91

Day ($\chi < 90$) ◄─── Day-to-Night Transition ───► Night ($\chi \geq 99$)

| $h' = 74.0$ | 76.2 | 78.3 | 80.5 | 82.7 | 84.8 | 87.0 |
| $\beta = 0.3$ | 0.31 | 0.31 | 0.32 | 0.32 | 0.33 | 0.34 |

| $\chi =$ | 90.0 | 91.8 | 93.6 | 95.4 | 97.2 | 99.0 |
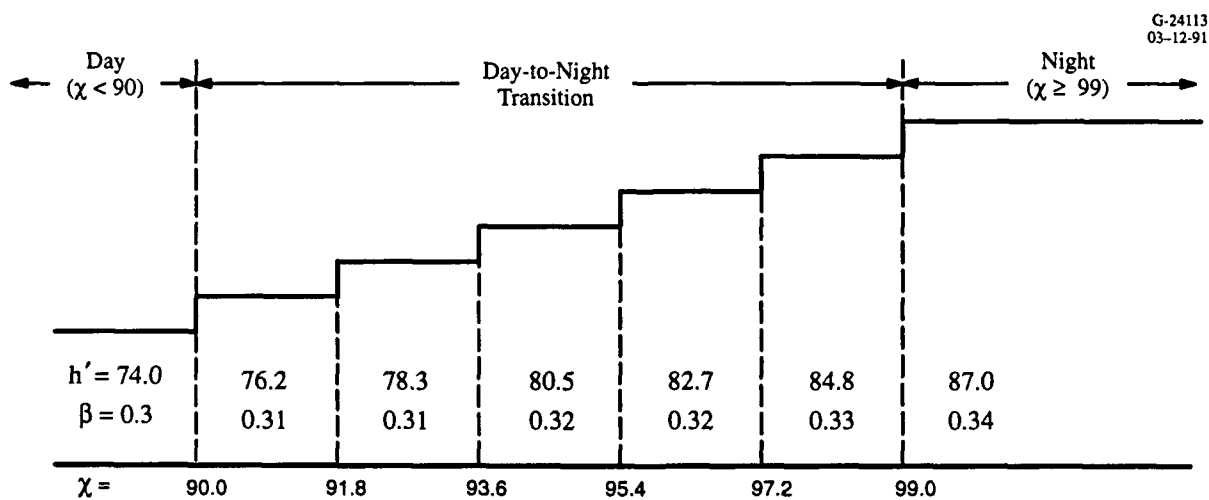
b) h' (km) and β (km^{-1}) as a Function of Solar Zenith Angle, χ (deg), along a Non-Polar Signal Path Undergoing Day-to-Night Transition

Figure A.2-1   Ionospheric Parameters at 13.6 kHz

A-12

Summary — Based on physical realism embodied in the available mode theory-based VLF signal prediction models or packages, LWPCN and LWPC are the preferred packages for calculating the Omega/VLF signal propagation characteristics along a signal path. The two packages differ only in the way mode conversion effects are calculated at the segment interfaces along a path. LWPC uses the approximate (FASTMC) algorithm at each interface along a path, while LWPCN employs the approximate algorithm if the mismatch between the path properties across the interface is small; otherwise, it uses the rigorous algorithm. The rigorous algorithm requires about 100 times more CPU time than the approximate algorithm.

A.3 VLF ATMOSPHERIC NOISE PREDICTION MODELS

A.3.1 VLF Noise Characteristics

Natural electromagnetic emissions in the VLF band that originate in the earth-ionosphere waveguide are called atmospheric noise. The primary sources of this noise (which dominates the total electromagnetic noise in the VLF band) are worldwide lightning discharges from thunderstorm activity. For time scales on order of one second, atmospheric noise is characterized by a random process with large, rapid fluctuations. However, when the noise is observed over a period of several minutes, the average/ rms (root-mean-square) noise voltage level value is found to be nearly constant (within ± 2 dB) for successive observations during a given hour, except during local sunrise or sunset or when there are local thunderstorms (Ref. 22).

Although nearly constant within a given hour, atmospheric noise statistics are a function of geographic location, frequency, season (month), hour, and receiver processing bandwidth. In addition, the average and rms noise level value in a given hour varies from day to day due to changes in thunderstorm activity and propagation conditions. The following statistics measures are commonly used to describe this noise level variation in an hour/month time block (i.e., several consecutive hours during one or more consecutive months):

- Mean value (the mean of the hourly value within the time block)
- Median or 50th percentile value (the hourly value which is exceeded 50% of the time within the time block)
- 90th percentile value (the hourly value which is exceeded 10% of the time within the time block)
- 10th percentile value (the hourly value which is exceeded 90% of the time within the time block).

The VLF atmospheric noise levels, expressed in dB, are roughly log-normally distributed, and therefore, the mean value is nearly the same as the median value. Furthermore, the standard deviation of an hourly noise value is approximately 80 percent of the upper decile value (Ref. 3). The upper decile value for a time block is the value of the average noise power exceeded 90 percent of the time within the time block, i.e., it is the value in dB above the median value for the time block. Table A.3-4 gives an expected range of the upper decile values of the hourly averaged noise power in the VLF band as a function of season.

Table A.3-4   Upper Decile Value Ranges for the VLF Atmospheric Noise Level (Ref. 3)

SEASON	UPPER DECILE RANGE (dB)		
	10 kHz	20 kHz	30 kHz
Spring/Fall	4–5	5–8	6–11
Summer	5–6	4–6	5–8
Winter	3–4	4–7	5–11

The Arctic and Antarctic regions usually have the smallest noise levels since local lightning discharges are locally almost nonexistent and the noise signals which reach these regions from distant sources are highly attenuated by the local low ground conductivity. Lightning is more prevalent in tropical land regions and hence noise levels are usually highest in these regions. Also, since thunderstorm activity is usually most severe at local noon/afternoon and signals are propagated preferentially to the east, the noise levels at most latitudes are highest during local later afternoon and early evening hours.

A.3.2   VLF Noise Prediction Models

It is convenient to categorize the available noise prediction models as: (1) the CCIR group of models, (2) the WGL group of models, and (3) the LNP model. The CCIR models are empirical models, i.e., the model predictions are based strictly on noise measurement data. The WGL group of models as well as the LNP model are semi-empirical models, i.e., the models are developed based on combination of propagation physics and thunderstorm activity observations. A discussion of each of the models within each of the CCIR and WGL groups as well as the LNP model follows.

CCIR Group of Models — The first CCIR (International Radio Consultative Committee) model is contained in CCIR Report 322 (Ref. 22) published in 1964. The report is based on the average noise power measurements made by a worldwide network of 16 data collection sites over several years.

The report provides VLF/LF/MF noise level predictions as a function of location, frequency, and *local time block*. The local time block is a local four-hour time interval during a local season (three consecutive months).* The predictions given in the report are derived by interpolating worldwide noise measurements in space (latitude/longitude), time block, and frequency. The predictions are displayed as contour maps of the *median* value of the noise level (given in the report in terms of the effective noise antenna figure, F_{am}, at 1 MHz frequency) for each of the 24 local time blocks. The report contains 24 maps for the 24 time blocks of the year, one for each combination of season (three months) and four-hour period. In addition to the maps, the report ‑ · ·pporting graphs that display statistical variations of F_{am} for each time block and contain curves .r · illow conversion of the 1 MHz F_{am} value to the F_{am} value at a frequency between 10 kHz and 200 MHz. The report also provides a formula for computing the median value of the rms noise level at a specific frea·ency and receiver bandwidth based on the corresponding F_{am} value.

Since F_{am} maps are displayed in local time (i.e., local four-hour time block in a local season), the F_{am} contours in CCIR Report 322 maps exhibit discontinuities in the F_{am} values at the equator. This is due, for example, to the six-month separation between the northern and southern hemisphere summer seasons. In addition to the seasonal discontinuities at the equator, the maps have some inconsistency in the F_{am} values across the equator (Ref. 3) and also at both the north and south poles. The local time-based F_{am} maps have also been transformed into the Universal Time (UT)-based F_{am} maps each displaying a set of worldwide contours of constant F_{am} values at 10 kHz for each four-hour and three-month UT time blocks. The 10 kHz, universal time F_{am} maps, along with the graph to convert the 10 kHz-based F_{am} value to the F_{am} value at another frequency between 10 kHz and 10 MHz, are contained in Reference 3.

A numerical representation of the data contained in CCIR Report 322 is published as CCIR Report 322-1 (Ref. 23). In 1983, CCIR Report 322 was reprinted as CCIR Report 322-2 (Ref. 24) with a revised text and title, but with the same atmospheric noise information. When additional noise measurement data became available from ten new CIS (the former Soviet Union) sites, the Report 322 was updated to include the additional measurement data; the updated report is called CCIR Report 322-3, (Ref. 25), published in 1986. After publication of CCIR Report 322-3, the data collected at the high-latitude sites, Thule in Greenland and Byrd Station in Antarctica, have been found to be affected by manmade noise (Ref. 26), In addition, the procedure employed to generate noise predictions for Report 322-3 has used incorrect noise data at the high latitude data sites (Refs. 26 and 27). As a result,

---

*For example, 0000–0400 UT hours during the months of December, January, and February.

the noise predictions provided by all CCIR Reports are in error in the northern and southern high-latitude regions. A computer implementation of Report 322-3 is the NTIA noise model which has incorporated an hourly interpolation scheme to provide noise predictions for a one-hour (UT) and three-month time block, instead of the local four-hour season time block as in Report 322-3. NTIA is one of the computer programs in the LWPC (Ref. 13)/LWPCN (Ref. 14) package of VLF signal and noise prediction programs.

WGL Group of Models — In 1970, Westinghouse Georesearch Laboratory (WGL) developed a semi-empirical noise model based on a combination of signal propagation physics and observational data on lightning discharges. The WGL model (Refs. 28 and 29) provides the *mean* value of the rms noise level as a function of location and frequency (10 to 30 kHz) for a one-hour (UT) and one-month time block. The model assumes that lightning discharges are the sole source of the atmospheric noise. Lightning discharge physics is used to convert lightning occurrences (inferred from worldwide thunderstorm activity data) into the electromagnetic energy radiated from a set of 15° (latitude) by 15° (longitude) regions covering the earth's surface. Each region is treated by the WGL model as an effective transmitter of VLF noise which propagates in the earth-ionosphere waveguide (in the same manner as a VLF transmitting station signal) according to the principles of waveguide-mode theory. At the receiver location, the combined energy from all noise transmitters yields the predicted atmospheric noise level. Noise statistics are calculated using measured thunderstorm-day data. Because of the scarcity of lightning flash occurrence rates concurrent with thunderstorms, the model also infers the flash rates from records of thunderstorm days.

The 1970 WGL model was refined by the Naval Research Laboratory (NRL) to allow the use of alternative spectra for the noise pulses resulting from the lightning discharges as well as to include other refinements (Refs. 30 and 31). The WGL/NRL-developed computer code (Ref. 32) for the refined model was found to contain several code errors, which have subsequently been corrected (Ref. 33). The resulting algorithm model is referred to as the DECO model and is contained in both the LWPC and LWPCN packages.

LNP Model — LNP is a semi-empirical ELF/VLF/LF noise prediction model developed by the Pacific-Sierra Research Corporation (Ref. 34). The model provides the *median* value of the rms noise level as a function of location, frequency, and one-hour (UT)/three-month time block. Like the WGL model, it is based on observational data of worldwide thunderstorm occurrences, and the use of physical models for both lightning discharges and propagation of noise energy from the thunderstorm centers to the receiver location. The observations consist of both satellite and ground-based data on lightning

flashes as a function of location, time of day, and season. The use of lightning flash data to form the LNP model circumvents the need to infer lightning flash occurrence statistics from thunderstorm-day maps, as is done in applying the WGL model. Also, the LNP model uses a more sophisticated VLF signal propagation theory than that employed in the WGL model. The LNP prediction capability is currently (1993) being improved to increase the time resolution from the three-month to a one-month time block.

Summary — The NTIA (CCIR Report 322-3) model is empirical, while the DECO and LNP models are semi-empirical. NTIA and LNP predict of the *median* value of the rms noise level in a one-hour and three-month time block, while WGL/DECO gives the *mean* value of the rms noise level in a one-hour and one-month time block. Since the noise level in dB is approximately log-normally distributed, the mean and median values differ very little from each other. Thus, the three models differ only in their temporal prediction capabilities, as listed in Table A.3-5. Because of the reported corruptions introduced in the NTIA model by the man-made noise in the high latitude regions, the NTIA model predictions are questionable in these regions. The results of an evaluation of the prediction performance of the NTIA, DECO, and LNP models is presented in the next section.

Table A.3-5   Temporal Prediction Capabilities of Models

MODEL	TEMPORAL PREDICTION CAPABILITIES
NTIA	• Four-hour/three-month time block • One-hour/three-month time block values computed by interpolation between adjacent four-hour intervals in the same three-month period
DECO	• One-hour/one-month time block
LNP	• One-hour/three-month time block

A.4   NOISE MODEL PREDICTION PERFORMANCE EVALUATION RESULTS

Recently, the prediction performance (i.e., CPU time and accuracy) of the NTIA, DECO, and LNP models (Ref. 35) has been evaluated relative to the VLF atmospheric noise measurement data available in the published literature. The evaluation data includes noise measurements made at 25 worldwide distributed data recording sites over one-hour/three-month as well as four-hour/three-month time blocks. The data include noise measurements made for almost all 24 hours and 12 months, and cover most of the VLF band (10 to 25 kHz). The data site locations are shown in Fig. A.4-1 and the data attributes are summarized in Table A.4-1. The results of CPU time evaluation of the algorithms implementing the models are given in Table A.4-2.

Site Category	Site Name	Site No.
Stanford	Arrival Heights	25
	Dunedin	24
	Kochi	16
	L'Aquila	10
	Sondre Stromfjord	2
	Stanford	14
	Thule	1
CCIR/ESSA	Balboa	20
	Boulder	13
	Cook	23
	Enkoping	5
	Kehaha	19
	New Delhi	18
	Ohira	12
	Pretoria	22
	Rabat	17
	Singapore	21
CCIR/ Russian	Ashkhabad	15
	Khabarovsk	6
	Kiev	8
	Moscow	7
	Mumansk	3
	Simferopol	9
	Sverdlovsk	4
	Tbilisi	11

Legend:
- ■ Standford Data Sites
- ▽ CCIR/ESSA Data Sites
- ● CCIR/Russian Data Sites

Figure A.4-1 Model Evaluation Noise Measurement Data Collection Sites: Names/Locations

G-3370/7 5-10-93

A-18

Table A.4-1 Model Evaluation Database Attributes

SOURCE*	GEOGRAPHIC REGION	FREQUENCY (kHz)	NO. OF DATA VALUES	BANDWIDTH (Hz)	TIME BLOCK	STATISTIC	DATUM
CCIR 322-3	Russia	12.0	48		Four-Hour/ Three-Month	Median Value	Rms Noise Level
		12.5	120	250			
		25.0	144				
ESSA§	Mainly Northern Hemisphere	13.0	480	1000	One-Hour/ Three-Month		
Stanford	Mainly Northern Hemisphere	10.2	150	510	Four-Hour/ Three-Month	Mean Value	Average Noise Level

*See Fig. A.4-1 for the database site locations/names.

§Environmental Science Services Administration, United States Government.

Table A.4-2 Approximate Computer Time Needed to Generate Signal Coverage Noise Data on VAX 6310 Computer

MODEL	TIME BLOCK	CPU TIME* PER PREDICTION
NTIA	One-Hour/Three-Month	0.01 sec
LNP	One-Hour/Three-Month	30 sec
DECO	One-Hour/One-Month	0.5 sec

* The NTIA and DECO codes are designed to run on a VAX computer; LNP is designed to run on a PC; the LNP-indicated time on VAX 6310 is the estimated computer time.

Tables A.4-3 and A.4-4 present the prediction errors of the three models over the one-hour/ three-month and four-hour/three-month evaluation data sets, respectively. The model prediction error in the tables is defined as the measurement data minus the model-based value. The temporal bases of the models differ from each other. Furthermore, the temporal bases of the data differ from the models' temporal bases. The model predicted values for the three models are derived as follows. Denote the three months included in a three-month block as m_1, m_2, and m_3, and the four hours included in a four-hour block as h_1, h_2, h_3, and h_4. For the one-hour/three-month evaluation data: (1) the NTIA/LNP model is consistent with the one-hour/three-month time block and thus NTIA/LNP-provided noise predictions are directly usable to form prediction errors; and (2) the DECO model is inconsistent with the evaluation data set time block and thus the DECO-provided predictions are averaged over months m_1, m_2, and m_3, of the evaluation data time block to form one-hour/three-month noise predictions. Similarly, for the

A-19

four-hour/three-month evaluation data, noise predictions are derived from: (1) the NTIA/LNP model as the average of the four one-hour/three-month model-predicted values associated with the hours h_1, h_2, h_3, and h_4 of the four-hour/three-month time block; and (2) the DECO model as the average of 12 one-hour/one-month DECO model-predicted values associated with the four hours (h_1, h_2, h_3, and h_4) and three months (m_1, m_2, and m_3) of the four-hour/three-month time block.

Table A.4-3   Noise Model Prediction Errors: One-Hour/Three-Month Data

MODEL	NO. OF DATA* VALUES	RMS ERROR (dB)
NTIA		3.6
LNP	480	4.6
DECO		3.8

*13.0 kHz ESSA data.

Table A.4-4   Noise Model Prediction Errors: Four-Hour/Three-Month Data

DATA ATTRIBUTES			RMS ERROR (dB)		
FREQUENCY (kHz)	SOURCE	NO. OF DATA	NTIA	LNP	DECO
10.2	Stanford	150	7.6	6.0	4.4
13.0	ESSA	120*	3.4	4.4	3.6
12.0		48	4.4	5.5	4.7
12.5	CCIR	120	6.5	7.9	8.5
25		144	5.9	8.4	9.4
10.2–25	ALL	582	6.0	6.7	6.6

* Each value is the average of the appropriate four one-hour/one-month ESSA measurements.

Relative to CPU time, NTIA is the best model. Relative to prediction accuracy, there are no significant differences between the models. From this result and considerations of CPU time, NTIA and DECO appear to be the best and next-best models, respectively. However, since NTIA has been reported to provide unreliable predictions in the high latitude regions, DECO is considered the best of the available noise models for predicting VLF atmospheric noise levels.

REFERENCES

1. Wait, J.R., *Electromagnetic Waves in Stratified Media*, Second Edition, Pergamon Press, Oxford, 1970.

2. Galejs, J., *Terrestrial Propagation of Long Electromagnetic Waves*, Pergamon Press, New York, 1972.

3. Watt, A.D., *VLF Radio Engineering*, Pergamon Press, Oxford, 1967.

4. Budden, K.G., *The Propagation of Radio Waves*, Cambridge University Press, 1985.

5. Berry, L.A., Wavehop theory of long distance propagation of low frequency radio waves, *National Bureau of Standards, Journal of Research, Section D, Radio Science*, vol. 68, 1964.

6. Berry, L.A., and Herman, J.E., A wave hop propagation program for an anistropic ionosphere, Institute of Telecommunications, *Telecommunications Research Report OT/ITS RR11*, April 1971.

7. Johler, J.R., Spherical wave theory for MF, LF, and VLF propagation, *Radio Science*, vol. 5 no. 12, December 1970.

8. Pappert, R.A., Gossard, E.E., and Rothmuller, I.J., A numerical investigation of classical approximations used in VLF propagation, *Radio Science*, vol. 2, no. 4, April 1967.

9. Wait, J.R., and Spies, K.P., Characteristics of the earth-ionosphere waveguide for VLF radio waves, National Bureau of Standards, NBS Technical Note No. 300, December 1964.

10. Morgan, R.P., Preparation of a worldwide effective conductivity map, Westinghouse Electric Corporation, Reports 80133F-1 and 80133F-2, January 1968.

11. Donnelly, S.F., Integrated propagation prediction program documentation, TASC, Technical Report TR-343-4, November 1973.

12. Ferguson, J.A., Longwave-propagation capability, full fortran release: version 1.0, Naval Ocean Systems Center, Technical Document 1847 (AD-B147582), July 1990.

13. Ferguson, J.A., and Synder, F.P., Computer programs for assessment of long wavelength radio communications, version 1.0: Full FORTRAN Code User's Guide, Naval Ocean Systems Center, Technical Document 1773 (AD-B144839), April 1990.

14. Ferguson, J.A., The long wavelength propagation capability with nuclear option, Naval Command, Control, and Ocean Surveillance Center, Technical Note, February 1993.

15. Pappert, R.A., and Sheckley, L.R., Mode conversion program for an inhomogeneous anosotropic ionosphere, Naval Electronics Laboratory Center, NELC Interim Report No. 722, May 1972.

16. Ferguson J.F., and Snyder, F.P., Approximate VLF/LF waveguide mode conversion model, Naval Ocean Systems Center, NOSC Technical Document No. 400, November 1990.

17. Morris, P., and Cha, M., Omega propagation corrections: Background and computational algorithm, Report No. ONSOD 01-74, December 1974.

18. Morffitt, D.C., and Shellman, C.H., MODESRCH, An improved computer program for obtaining ELF/VLF/LF mode constants in an earth-ionosphere waveguide, Naval Electronics Laboratory Center, NELC Interim Report No. 721, October 1976.

19. Ferguson, J.A., Snyder, F.P., Morffitt, D.C., and Shellman, C.H., Software program for long-wave propagation capability and documentation, Naval Ocean Systems Center, NOSC Technical Document No. 1518, March 1989.

20. Ferguson, J.A., Snyder, F.P., The segmented waveguide program for long-wavelength propagation calculation, Naval Ocean Systems Center, NOSC Technical Report No. 1071, December 1986.

21. Shellman, C.H., A new version of MODESRCH using interpolated values of the magnetronic reflection coefficients, Naval Ocean Systems Center, NOSC Technical Report No. 1473, October 1986.

22. International Radio Consultative Committee, world distribution and characteristics of atmospheric radio noise, International Telecommunications Union, CCIR Report 332, 1964.

23. Lucas, D.L., and Harper, J.D., A numerical representation of CCIR Report 322: high frequency (3-30 Mc/S) atmosphere-radio data, U.S. Department of Commerce, Washington, DC, NBS Technical Note 318, 1965.

24. International Radio Consultative Committee, Characteristics and applications of atmospheric radio noise data, International Telecommunications Union, CCIR Report 332-2, Geneva, Switzerland, 1983.

25. International Radio Consultative Committee, Characteristics and applications of atmospheric radio noise data, International Telecommunications Union, CCIR Report 332-3, Geneva, Switzerland, 1988.

26. Spaulding, A.D., and Washburn, J.S., Atmospheric radio noise worldwide levels and other characteristics, (U.S.) National Telecommunications and Information Administration, NTIA Report 85-173, April 1985.

27. Sailors, D.B., A Discrepancy in the CCIR Report 322-3 radio noise model, Naval Command, Control, and Ocean Surveillance Center, Presented at the Longwave Noise Program (LNP) and Atmospheric Noise Working Group Meeting at Pacific-Sierra Research Corporation, Los Angeles, CA, 3 February 1983.

28. Maxwell, E.L., Stone, D.L., Croghan, R.D., Ball, L., and Watt, A.D., Development of a VLF atmospheric noise prediction model, Westinghouse Georesearch Laboratory, Report No. 70-1H2-VLFNO-R1, June 1970.

29. Stone, D.L., Croghan, R.D., and Crail, A.C., Computer program operational manual for atmospheric noise predictions, Westinghouse Georesearch Laboratory, Report No. 70-1H2-VLFNO-R2, June 1970.

30. Hauser, J.P., and Rhoads, F.J., Analysis of a VLF atmospheric noise prediction model, USNC/URSI Meeting, Commission VIII, Session I, August 21–24, 1973.

31. Kelly, F.J., Hauser, J.P., and Rhoads, F.J., Computer program model for predicting horizontally and vertically polarized vlf atmospheric noise at elevated receivers, Naval Research Laboratory, NRL Report 8479, December 1981.

32. Preliminary noise program documentation, U.S. Coast Guard, Omega Navigation System Operations Detail, October 1979.

33. WGL-NRL: Revision II, VLF atmospheric noise prediction computer program, TASC, Engineering Memorandum EM-2691, July 1988.

34. Warber, E.C., and Field, E.C., Jr., Long wave noise prediction, vol. 1, Physical basis of the model; and vol. 2, User's guide to the computer code LNP version 2.0, Pacific-Sierra Research Corporation, PSR Report 2137, September 1991.

35. Gupta, R.R., and Frank, D.P., Prediction performance of VLF noise models, TASC, Technical Information Memorandum, TIM-5919-3, June 1993.

APPENDIX B

ANALYTICAL BASIS OF THE SYSTEM AVAILABILITY MODEL

B.1   INTRODUCTION

The Omega System Availability Model is an analytical description of certain random and deterministic features of the entire Omega system, including the transmitting stations, signals in space, users, and receivers. The model serves as a means for computing the System Availability Index (P_{SA}), which is a probabilistic measure of system performance.

This appendix explains the basic tenets of the System Availability Model as part of the derivation of P_{SA}. Other features of the model emerge in describing calculation of the station reliability parameters. P_{SA} is explicitly defined in Section B.2 and an analytical expression is developed to show how the calculation depends on measurable system parameters. Section B.3 explains the basic assumptions regarding scheduled and unscheduled station off-air events and derives the corresponding station off-air time probability distributions.

The system availability index, P_{SA}, is the probability that, for any location on the earth at any time or time-interval, an Omega user's receiver will be properly functioning and three or more Omega signals can be effectively used for navigation. Expressed analytically, P_{SA} is given in terms of event probabilities as

$$P_{SA} = P(D)$$

where D is the event that an Omega user (with operational receiver) located anywhere on the earth's surface (up to and including aircraft altitudes) can effectively utilize three or more Omega signals at any given time. Strictly speaking, P_{SA} is computed for a specified time but, in some applications, it is averaged over selected hour/month combinations.

The definition of P_{SA} given above is the one generally used for evaluating system performance (Ref. 1) and is the algorithm implemented in the PACE workstation (Ref. 2). A generalized formulation of P_{SA} has been developed (Ref. 3), however, which addresses the probability of achieving a certain accuracy threshold.

B.2   DEVELOPMENT OF THE SYSTEM AVAILABILITY INDEX

B.2.1   User Regional Priority Sub-model

The geographic preferences of the Omega user enter the calculation of the system availability index by specifying the probability that a single user is in a certain region or cell. To find an expression for this probability, first define the spatial "universe" as the union of all events that a user is located in any two-dimensional cell on the globe. Here, a "cell" is defined as that area (approximately 600 nm × 600 nm) over which Omega signal accessibility (the ability to use any given set of Omega signals) changes very little. Thus, the spatial universe is expressed as:*

$$U^s = L_1 + L_2 + \ldots + L_{444}$$

where L_i is the event that a user is located in cell i (444 such cells cover the globe). By definition of the set universe, the probability of event D is given as

$$P(D) = P(DU^s) = P\left(D \sum_{i=1}^{444} L_i\right) = P\left(\sum_{i=1}^{444} DL_i\right)$$

Now, the events $DL_1, \; DL_2, \ldots$ are mutually exclusive since the single user being considered can only be located in one of the cells. Thus,

$$P(D) = \sum_{i=1}^{444} P(DL_i)$$

Using Bayes' Law, this expression may be written in terms of the conditional probability as

$$P(D) = \sum_{i=1}^{444} P(D|L_i) \, P(L_i) = \sum_{i=1}^{444} P(D_i)P(L_i)$$

where D_i is the event that an Omega user (with operational receiver) effective utilizes three or more Omega signals at a specific time given that the user is located in cell i. $P(L_i)$, the probability that the user is located in cell i, is usually written as w_i, where $\{ w_i \}$ is a normalized set of weights indicating Omega user preference or experience.

---

*In the following development with sets and events, sum indicates set union and product indicates set intersection.

Thus,

$$P(D) = \sum_{i=1}^{444} w_i \, P(D_i) \qquad ; \sum_{i=1}^{444} w_i = 1 \qquad\qquad \text{(B.2-1)}$$

B.2.2 Receiver Reliability/Availability Sub-model

To include the receiver reliability/availability sub-model, two additional events (G_i and F) are defined by the expression

$$D_i = G_i \, F$$

where G_i is the event that an Omega user in cell i effectively processes three or more Omega signal at a given time and F is the event that the user's Omega receiver functions properly at the given fixed time. As before, the probability of event D_i may be written

$$P(D_i) = P(G_i|F) \, P(F)$$

To determine $P(F)$, assume that all users are grouped into n_c receiver classes and define E_j as the event that the given user is in receiver class j. A receiver "class" is that group of receivers which have approximately the same reliability and detection sensitivity characteristics. As above, the universe of events E is the sum (union) $E_1 + E_2 + \ldots + E_{n_c}$ and thus F may be written

$$F = F(E_1 + E_2 + \ldots + E_{n_c}) = FE_1 + FE_2 + \ldots + FE_{n_c}$$

The events FE_1, FE_2, ... are all mutually exclusive since the single user being considered can only be in one class. Thus

$$P(F) = P\left(\sum_{j=1}^{n_c} FE_j\right) = \sum_{j=1}^{n_c} P(FE_j) = \sum_{j=1}^{n_c} P(F|E_j) \, P(E_j)$$

The probability, $P(E_j)$, that the user has a receiver in receiver class j is

$$P(E_j) = \frac{n_j}{N_u}$$

where n_j is the number of receivers in receiver class j and N_u is the total number of users in all receiver classes, i.e.,

$$N_u = \sum_{j=1}^{n_c} n_j$$

The conditional probability $P(F|E_j)$ is usually referred to as the receiver reliability figure for receiver class j and is often written P_{R_j}. Using a uniform failure interval and repair time model, it can be shown that the reliability figure for a receiver in receiver class j is

$$P_{R_j} = \frac{\text{MTTR}_j}{\text{MTBF}_j}$$

where MTTR_j is the mean time to repair figure for receiver class j and MTBF_j is the mean time between failures figure for receiver class j.

Thus,

$$P(F) = \frac{1}{N_u} \sum_{j=1}^{n_c} n_j P_{R_j}$$

and

$$P(D_i) = \frac{P(G_i|F)}{N_u} \sum_{j=1}^{n_c} n_j P_{R_j} \tag{B.2-2}$$

B.2.3   Signal Coverage Sub-model

The signal coverage sub-model is next invoked by first defining

$$C_i \equiv G_i|F$$

where C_i is the event that an Omega user utilizes three or more Omega signals in cell i given that the user's receiver functions properly. The signals that the user's receiver might possibly use in navigating with Omega in cell i at the given fixed time make up what is known as the *maximal coverage set*. The actual signals in this set depend on the thresholds selected for the access criteria applied to the coverage data. Typical signal access criteria are given as follows:

- Mode 1 Dominance Margin (ratio of Mode 1 amplitude to the interfering mode amplitude) must be greater than 6 dB

- Ratio of total short-path signal amplitude to total long-path signal amplitude must be greater than 6 dB

- Angle between the propagation path and the terminator (if any) which cuts the short path must be greater than 5°

- Geometric dilution of precision (GDOP) for the rho-rho-rho navigation mode must be less than 3.

All signals in the maximal coverage set, i.e., those that satisfy the above access criteria at a given cell and time (hour/month) are not necessarily usable by conventional receivers because of the random variations in the signal amplitude and noise level. A signal with random amplitude is said to be usable if, in addition to the above criteria, the following non-deterministic criterion is satisfied:

> Ratio of total short-path signal amplitude to noise level (assumed mean value   rement) in a 100 Hz BW must be greater than a certain threshold (typically, –20 dB).

If the random variation of the signal amplitude and noise level is ignored, so that the SNR becomes a ratio of median values (over an hour/month), then the last criterion (now deterministic) becomes simply another signal access criterion and the maximal coverage set merges into the coverage set.

The maximal coverage set is so named because if all signals in the maximal coverage set happen to satisfy the non-deterministic criterion, then the usable subset of signals has its "maximal" value. On the other hand, it is possible (but not likely) that all signals in the maximal coverage set could simultaneously fail the non-deterministic criteria, meaning that no signals would be usable.

Of the signals in the maximal coverage set, the universe, U^v, of usable signal combinations are those subsets which contain at least three signals, i.e.,

$$U^v = V_{i_1 i_2 i_3} + V_{i_1 i_2 i_4} + \ldots + V_{i_{m-2} i_{m-1} i_m}$$
$$+ V_{i_1 i_2 i_3 i_4} + V_{i_1 i_2 i_3 i_5} + \ldots + V_{i_{m-3} i_{m-2} i_{m-1} i_m}$$
$$+ \ldots$$
$$+ V_{i_1 i_2 i_3 \ldots i_m}$$

where $V_{i_1 i_2 \ldots i_q}$ is the event that signals labeled $i_1, i_2, \ldots i_q$ are usable in cell i at the given fixed time. From their definition, the component events making up U^v are mutually exclusive. Thus

$$P(C_i) = P(C_i U^v) = P\left(C_i V_{i_1 i_2 i_3} + C_i V_{i_1 i_2 i_4} + \ldots\right)$$
$$= P\left(C_i V_{i_1 i_2 i_3}\right) + P\left(C_i V_{i_1 i_2 i_4}\right) + \ldots$$

In terms of conditional probabilities, the above expression becomes

$$P(C_i) = P\left(C_i | V_{i_1 i_2 i_3}\right) P\left(V_{i_1 i_2 i_3}\right) + P\left(C_i | V_{i_1 i_2 i_4}\right) P(V_{i_1 i_2 i_4})$$
$$+ \ldots$$

(B.2-3)

The event $C_i | V_{i_1 i_2 \ldots i_q}$ describes the situation in which an Omega user with operational receiver in cell i effectively utilizes three or more signals given that Omega signals $i_1, i_2, \ldots i_q$ are in the maximal coverage set. The probability of the V-events is calculated through use of the station reliability/availability sub-model as well as the signal coverage sub-model.

B.2.4   Station Reliability/Availability Sub-model

To show how the calculation of $P(V_{i_1 i_2 \ldots i_q})$ proceeds, it is instructive to consider two simple examples before addressing the general case. The first example is the case in which the maximal coverage set contains only three station signals. The second example considers a maximal coverage set with 4 station signals. Both the station reliability/availability and signal coverage sub-models are required for the calculations in these examples.

First, define the events A_i and $\overline{A}_i$ as follows:

$A_i \equiv$ event that the SNR for signal i exceeds the threshold, a

$\overline{A}_i \equiv$ event that the SNR for signal i is less than a.

The A-events are governed by the random fluctuations of signal and noise levels and do not account for the uncertainty in generating the signal itself. If the random variation of the signal and noise levels is ignored, the A-events are deterministic.

The events which describe the on-air/off-air status of the Omega stations are defined as follows:

$T_i \equiv$ event that station i is on-air

$\overline{T}_i \equiv$ event that station i is off-air.

A station off-air is either scheduled (short advance notice or long advance notice (annual maintenance)) or unscheduled.

A maximal coverage set consisting of three station signals obviously contains only one subset of three or more station signals (a minimum of three station signals is assumed necessary for Omega navigation). For convenience, the signals are labeled 1, 2, 3 (not necessarily corresponding to the usual Omega station number/letter convention). The event that the three signals are usable is given by

$$V_{123} \equiv (A_1 T_1)(A_2 T_2)(A_3 T_3)$$

B-6

The events in parentheses indicate that the station is on-air *and* the signal SNR is above threshold. The probability of event V_{123} is written

$$P(V_{123}) = P\left(A_1 A_2 A_3 T_1 T_2 T_3\right) = P\left(A_1 A_2 A_3\right) P\left(T_1 T_2 T_3\right) \quad, \qquad \text{(B.2-4)}$$

since the *A*-events and *T*-events are independent.

The events A_1, A_2, A_3, however, are *not* independent since the noise level is common to the SNR associated with the three signals in the Omega receiver. For lognormally distributed signal amplitude and noise level, the result (derived in Ref. 4) is

$$P\left(A_1 A_2 A_3\right) = \int_{-\infty}^{+\infty} F_1(n)\ F_2(n)\ F_3(n)\ \frac{e^{-(n-\bar{n})^2/2\sigma_N^2}}{\sigma_N \sqrt{2\pi}}\ dn \qquad \text{(B.2-5)}$$

where

$$F_i(n) = (1/2)\ \text{erfc}\left(\frac{a-(\bar{s}_i-n)}{\sigma_{s_i}\sqrt{2}}\right) \quad,$$

$\bar{s}_i$ is the mean signal amplitude (from the coverage database) for signal i, σ_{s_i} is the standard deviation of signal amplitude for signal i (from a special algorithm; see Ref. 4), $\bar{n}$ is the mean signal noise level and σ_N the noise level standard deviation (both included with the coverage database), and a is the SNR threshold. The function labeled "erfc" is the complimentary error function. These space/time-dependent parameters are specified for cell i at the given time.

The events T_1, T_2, T_3 are also not independent but for a more subtle reason. The off-air event $\overline{T}$ may be separated into mutually exclusive components, viz.,

$$\overline{T}_i = \overline{T}_i^u + \overline{T}_i^s$$

where:

$\overline{T}_i^u \equiv$ event that station i is in an *unscheduled* off-air status

$\overline{T}_i^s \equiv$ event that station i is in a *scheduled* off-air status.

An unscheduled off-air event at a given station is independent of unscheduled or scheduled off-air events at other stations. However, Omega operational doctrine bars the simultaneous occurrence of scheduled off-airs at different stations, i.e.,

$$\overline{T}_i^s \overline{T}_j^s = 0 \quad; \ i,j = 1,2,\ \ldots\ 8 \ ; \ i \neq j$$

This last relation leads to a dependence between events T_i and T_j. It is shown in Ref. 1 that

$$P(T_1 T_2 T_3) = P(T_1 T_2)\left(1 - P(\overline{T}_3^u)\right) - P(\overline{T}_3^s)\left(1 - P(\overline{T}_1^u)\right)\left(1 - P(\overline{T}_2^u)\right) \qquad \text{(B.2-6)}$$

where:

$$P(T_1 T_2) = P(T_1)P(T_2) - P(\overline{T}_1^s)P(\overline{T}_2^s)$$

which also shows explicitly the non-independence of T_1 and T_2. The individual off-air event probabilities $P(\overline{T}_i^u)$, $P(\overline{T}_i^s)$ are obtained from historical station reliability figures as explained in Ref. 1. Thus, Eqs. B.2-5 and B.2-6 are used in Eq. B.2-4 to compute $P(V_{123})$.

The second example considers a maximal coverage set of four station signals which contains four three-signal subsets and one four-signal subset. If the stations are labeled 1, 2, 3, 4 (similar to the previous example), then the first event subset may be written

$$V_{123} = (A_1 T_1)(A_2 T_2)(A_3 T_3)\left(\overline{A}_4 T_4 + \overline{T}_4\right)$$

where the last event in parentheses means that signal 4 is not usable because either the SNR for that signal is below threshold (with the station on-air) *or* the station is off-air. The above expression for V_{123} may be written as the union of two mutually exclusive events:*

$$V_{123} = (A_1 A_2 A_3 \overline{A}_4)(T_1 T_2 T_3 T_4) + (A_1 A_2 A_3)(T_1 T_2 T_3 \overline{T}_4)$$

Since the two events are mutually exclusive, the probability of event V_{123} is

$$P(V_{123}) = P\left[(A_1 A_2 A_3 \overline{A}_4)(T_1 T_2 T_3 T_4) \right] + P\left[(A_1 A_2 A_3)(T_1 T_2 T_3 \overline{T}_4) \right]$$

and since the A-events and T-events are independent,

$$P(V_{123}) = P(A_1 A_2 A_3 \overline{A}_4)P(T_1 T_2 T_3 T_4) + P(A_1 A_2 A_3)P(T_1 T_2 T_3 \overline{T}_4) \qquad \text{(B.2-7)}$$

To calculate $P(A_1 A_2 A_3 \overline{A}_4)$, note that the set universe (for A-events) is $A_4 + \overline{A}_4$. Thus,

$$P(A_1 A_2 A_3) = P(A_1 A_2 A_3 (A_4 + \overline{A}_4))$$
$$= P(A_1 A_2 A_3 A_4) + P(A_1 A_2 A_3 \overline{A}_4)$$

Hence,

$$P(A_1 A_2 A_3 \overline{A}_4) = P(A_1 A_2 A_3) - P(A_1 A_2 A_3 A_4) \qquad \text{(B.2-8)}$$

---

*The events are mutually exclusive because T_4 intersects one event and $\overline{T}_4$ the other event.

B-8

where $P(A_1A_2A_3A_4)$ is given by

$$P(A_1A_2A_3A_4) = \int\limits_{-\infty}^{+\infty} F_1(n)\ F_2(n)\ F_3(n)\ F_4(n)\ \frac{e^{-(n-\bar{n})^2/2\sigma_N{}^2}}{\sigma_N\sqrt{2\pi}}\ dn \qquad \text{(B.2-9)}$$

and all quantities were defined in connection with Eq. B.2-5. Similarly, $P(T_1T_2T_3\bar{T}_4)$ can be written as

$$P(T_1T_2T_3\bar{T}_4) = P(T_1T_2T_3) - P(T_1T_2T_3T_4) \qquad \text{(B.2-10)}$$

where $P(T_1T_2T_3T_4)$ is computed from $P(T_1T_2T_3)$ using the recursion formula (Ref. 1)

$$P(T_1T_2T_3T_4) = P(T_1T_2T_3)\left(1-P(\bar{T}_4^u)\right) - P(\bar{T}_4^s)\left(1-P(\bar{T}_1^u)\right)\left(1-P(\bar{T}_2^u)\right)\left(1-P(\bar{T}_3^u)\right) \qquad \text{(B.2-11)}$$

With the use of Eqs. B.2-8, B.2-11, B.2-5, B.2-10, and B.2-6, $P(V_{123})$ may be calculated by means of Eq. B.2-7. In the same way, the probabilities of the other usable 3-signal subset events, $P(V_{124})$, $P(V_{134})$, $P(V_{234})$, can be calculated. The final event probability to be computed in this example is $P(V_{1234})$, i.e., the probability that all signals in the maximal coverage set are usable. Based on the previous procedure, the probability is given by

$$\begin{aligned} P(V_{1234}) &= P\big[\ (A_1T_1)(A_2T_2)(A_3T_3)(A_4T_4)\ \big] = P\big[\ (A_1A_2A_3A_4)(T_1T_2T_3T_4)\ \big] \\ &= P(A_1A_2A_3A_4)P(T_1T_2T_3T_4) \end{aligned}$$

Thus, this probability is computed with the aid of Eqs. B.2-9, B.2-11, and B.2-6.

For the general case of m signals in the maximal coverage set, the expression for the probability of a usable signal subset event for an arbitrary number of signals is very complex. To simplify the analytic form, an expression for the general event will be given in terms of a sum (union) of mutually-exclusive events. Because of the exclusive event sum and the independence of the A- and T-events, the probability of the general event is readily obtained as in the examples above. In order to obtain an expression for the event $V_{i_1i_2\ldots i_q}$ that the signals $i_1, i_2,\ \ldots\ i_q$ are usable within a maximal coverage set composed of signals $i_1, i_2, i_q, i_{q+1},\ \ldots\ i_m$, the events Z_i, Y_i, and W are first defined, viz.,

$$Z_i = A_iT_i\ ;\quad Y_i = \bar{A}_iT_i = T_i - Z_i\ ;\quad W = Z_{i_1}Z_{i_2}\ldots Z_{i_q}$$

In terms of these (and previously defined) events, the event $V_{i_1 i_2 \ldots i_q}$ is expressed as

$$V_{i_1 i_2 \ldots i_q} = W \prod_{\substack{k=q+1}}^{m} Y_{i_k} + W \sum_{j=q+1}^{m} \overline{T}_{i_j} \prod_{\substack{k=q+1 \\ k \neq j}}^{m} Y_{i_k} + W \sum_{j_1=q+1}^{m-1} \sum_{j_2=j_1+1}^{m} \overline{T}_{i_{j_1}} \overline{T}_{i_{j_2}} \prod_{\substack{k=q+1 \\ k \neq j_1; k \neq j_2}}^{m} Y_{i_k}$$

$$+ \ldots + W \sum_{j_1=q+1}^{m-r+1} \sum_{j_2=j_1+1}^{m-r+2} \cdots \sum_{j_r=j_{r-1}+1}^{m} \overline{T}_{i_{j_1}} \overline{T}_{i_{j_2}} \cdots \overline{T}_{i_{j_r}} \prod_{\substack{k=q+1 \\ k \neq j_1, j_2, \ldots j_r}}^{m} Y_{i_k}$$

$$+ \ldots + W \prod_{k=q+1}^{m} \overline{T}_{i_k} \tag{B.2-12}$$

B.3 OFF-AIR PROBABILITY FUNCTIONS

B.3.1 Off-air Occurrence Probability Functions

A reasonable description of unscheduled (random) off-air occurrence is given by the probability density function shown in Fig. B.3-1(a). The probability density describes the situation in which an off-air occurs at time $t = 0$ and the probability per unit time of the next off-air occurrence is indicated by the plot. The probability following the off-air is zero and gradually increases to a peak at time $1/\lambda$ which represents the average interval between off-air occurrences (based on empirical data). The probability density then gradually decreases for all longer time intervals. The normalized probability density function may be expressed as

$$p_{OAO}(t) = \lambda^2 t e^{-\lambda t} \tag{B.3-1}$$

For scheduled off-airs the process is entirely deterministic so that the probability density function is given by the Dirac-delta function $\delta (t-T)$ where T is the known time of off-air occurrence referenced to a convenient initial point (such as the beginning of a month). This distribution is illustrated in Fig. B.3-1(b).
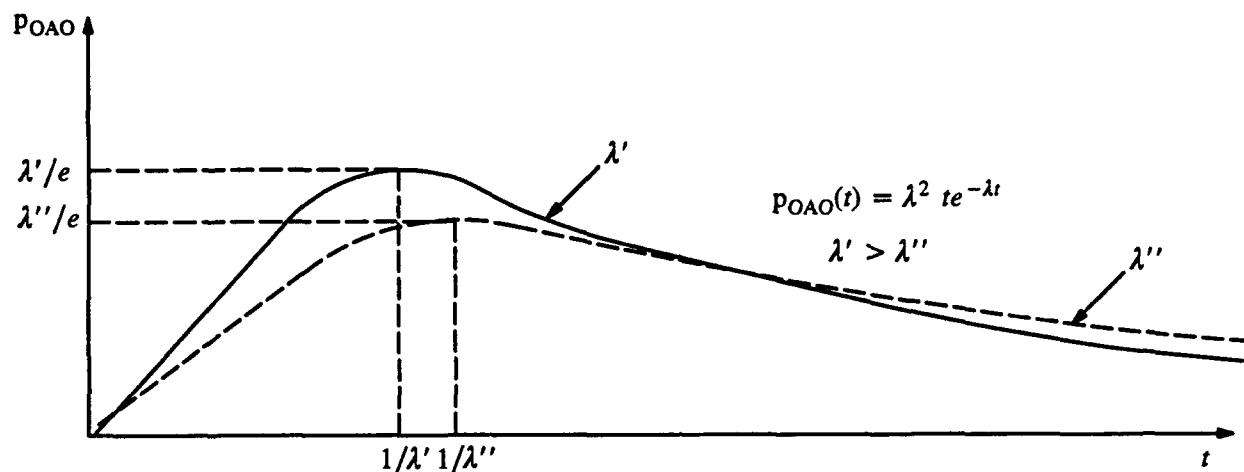
a) Unscheduled (random) Off-Air Occurrence Probability Density Function
for Two Values of the Average Time Between Off-Airs (1/λ)
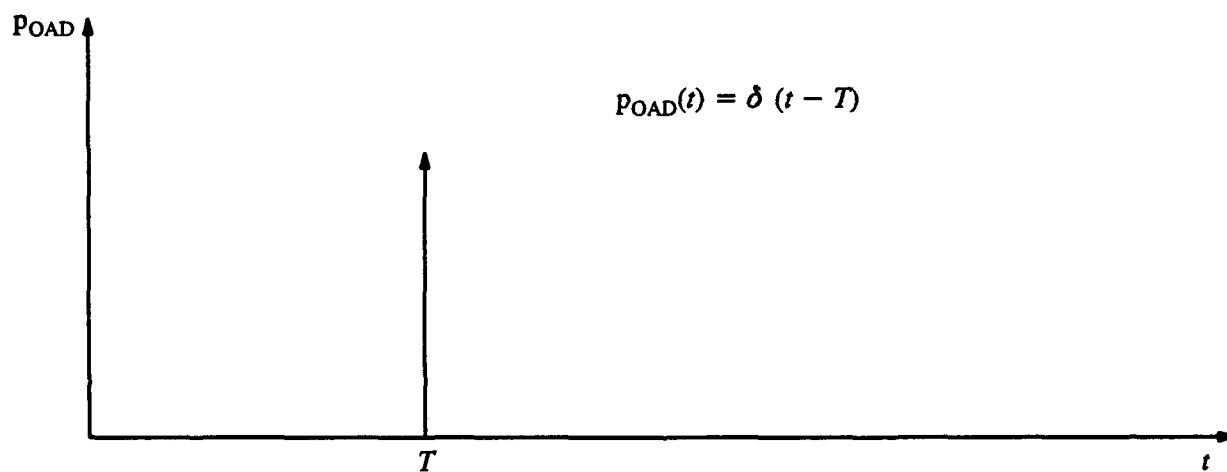
b) Scheduled (Deterministic) Off-Air Occurrence Probability Density Function

Figure B.3-1   Off-air Occurrence Probability Density Function for Unscheduled (random) and Scheduled (deterministic) Off-air Conditions

B.3.2 Off-air Duration Probability Functions

In this case of unscheduled off-airs, the off-air duration may be described by a simple exponential probability density function, which, in its normalized form is given by

$$p_{OAD}(t) = \mu e^{-\mu t} \tag{B.3-2}$$

where $1/\mu$ is the average off-air duration, obtained from empirical data. Figure B.3-2(a) shows a plot of this function and Fig. B.3-2(b) illustrates the corresponding distribution function (integral of the density function) which describes the probability that the off-air duration is less than some value, T.

This density function differs from the off-air occurrence density function (aside from normalization constants) by a factor of t. This factor occurs in the expression for $p_{OAO}(t)$ to explicitly exclude very short intervals between off-air occurrences (e.g., before the station achieves an on-air condition). An unscheduled off-air condition may be indefinitely short, however, since immediate action is always taken to restore the on-air condition. Thus, the exponential factor appears alone (leading to a monotonically decreasing density function) in the expression for $p_{OAD}(t)$.

Since the duration of scheduled off-airs is a deterministic quantity, the probability density function has the same form as for off-air occurrences, i.e., $\delta (t - \Delta T)$ where ΔT is the known off-air duration. This density function is similar to the one shown in Fig. B.3-1(b).

B.3.3 Probability that a Station is Off-air at an Arbitrary Time

Assuming that the time of off-air occurrence is independent of the duration of the corresponding off-air period, the probability that a station is off-air at some arbitrary time t is

$$P_{OA}(t) = \int\limits_{t' < t} dt' p_{OAO}(t') \int\limits_{t-t' < t''} dt'' \, p_{OAD}(t'')$$

$$p_{OAD}(t) = \mu e^{-\mu t}$$
$$\mu'' > \mu'$$
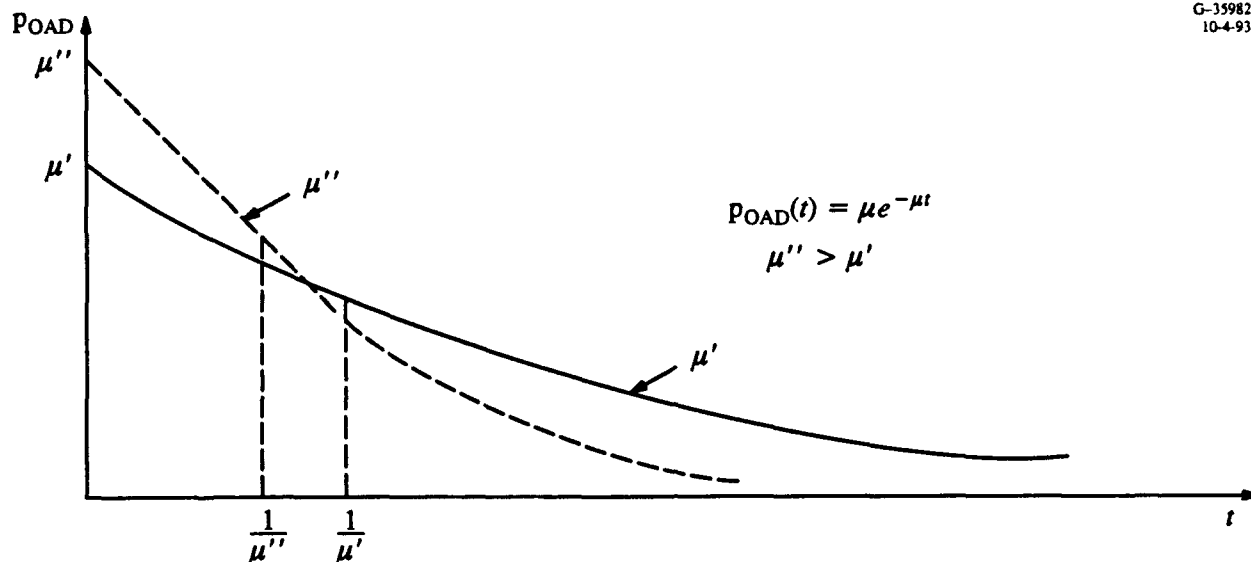
a) Off-Air Duration Probability Density Function for Two Values
of the Average Off-Air Duration (1/μ)

$$P_{OAD}(T) = 1 - e^{-\mu T}$$
$$\mu'' > \mu'$$
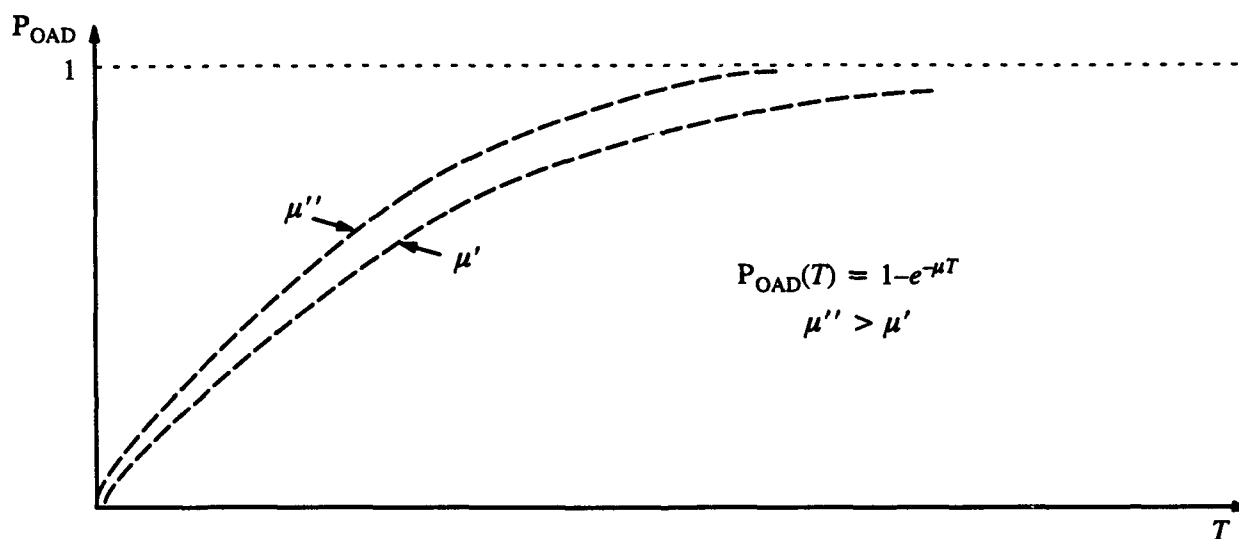
b) Off-Air Duration Probability Distribution Function for Two Values
of the Average Off-Air Duration (1/μ)

Figure B.3-2   Off-air Duration Probability Density and Distribution Functions
for Unscheduled (random) Off-air Conditions

B-13

In words, this says that in order that a station be off-air at time t, the off-air (beginning at t') must begin before t *and* the off-air duration (t'') must be longer that the current elapsed time since the off-air occurrence $t - t'$. This reasoning is illustrated in Fig. B.3-3. With an arbitrary zero-time reference, the above may be written

$$P_{OA}(t) = \int_0^t dt' \; p_{OAO}(t') \int_{t-t'}^\infty dt'' \; p_{OAD}(t'') \qquad (B.3\text{-}3)$$

For the case of unscheduled off-airs, Eqs. B.3-1 and B.3-2 are used for the off-air occurrence and off-air duration probability density functions, respectively. When inserted in Eq. B.3-3, the off-air probability becomes

$$P_{OA}(t) = \mu\lambda^2 \int_0^t dt' \; t'e^{-\lambda t'} \int_{t-t'}^\infty dt'' e^{-\mu t''}$$

This integral is easily evaluated to give

$$P_{OA}(t) = \frac{\lambda^2}{\mu-\lambda} \left[\frac{e^{-\mu t}}{\mu-\lambda} + te^{-\lambda t} - \frac{e^{-\lambda t}}{\mu-\lambda} \right] \qquad (B.3\text{-}4)$$

To evaluate this quantity, the assumption is made that the average time interval between successive off-airs is much larger than the average off-air duration, i.e.,

$$\frac{1}{\lambda} >> \frac{1}{\mu} \quad \text{or} \quad \lambda << \mu$$

Thus, for $t \neq 0$, $e^{-\lambda t} >> e^{-\mu t}$ and the first term in brackets in Eq. B.3-4 can be neglected in comparison to the second and third terms. Since $\mu >> \lambda$, the exponential in the third term in brackets in Eq. B.3-4 is essentially multiplied by $1/\mu$. Thus, for $t >> 1/\mu$ (i.e., for times large compared to an off-air duration), the third term in brackets in Eq. B.3-4 may be neglected in comparison to the second term. Thus with t large compared to the average off-air duration, the off-air probability at time t may be written

$$P_{OA}(t) = \frac{\lambda^2}{\mu-\lambda} te^{-\lambda t} \cong \frac{\lambda^2}{\mu} t \, e^{-\lambda t}$$

Off-Air Occurrence Time = t′
Off-Air Duration, t″ = T′ − t′
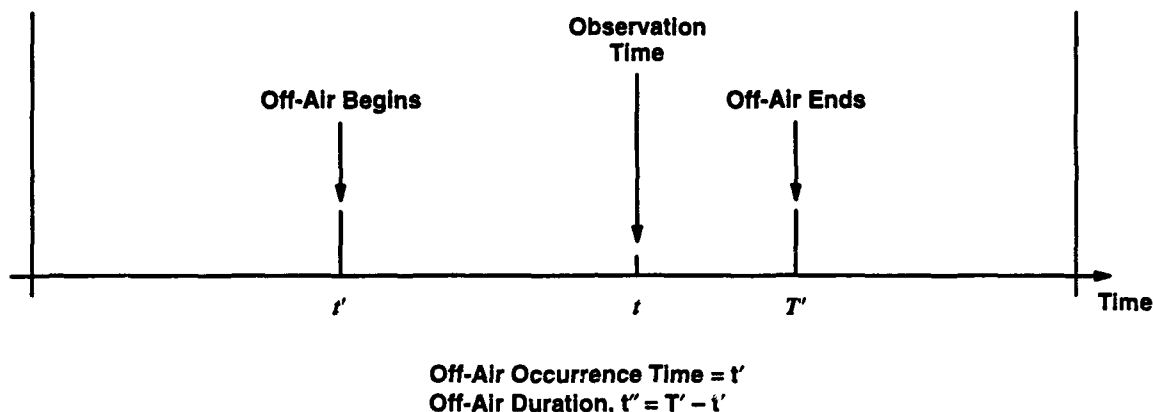
Condition that Station is Off-Air at Time t: t′ < t < T′ = t′ + t″
Or, Equivalently: t′ < t and t − t′ < t″

Figure B.3-3   Conditions Under Which a Station is Off-air at Time t

since $\mu > > \lambda$. Defining the month to begin at $t = 0$ and end at $t = T$, the average value of $P_{OA}(t)$ over the month may be computed as follows:

$$< P_{OA}(t) > \; \equiv \; \frac{1}{T} \int_{0}^{T} P_{OA}(t) \; dt$$

$$= \frac{\lambda^2}{\mu T} \left[\frac{1}{\lambda^2} (1 - e^{-\lambda T}) - \frac{T}{\lambda} e^{-\lambda T} \right] \tag{B.3-5}$$

Now, assuming an average of about three off-air occurrences per month (i.e., $3/\lambda \approx T$)*, the exponential terms occurring inside the brackets in Eq. B.3-5 may be dropped in comparison to the non-exponential term. Thus,

$$< P_{OA}(t) > \; \cong \; \frac{\lambda^2}{\mu T} \left(\frac{1}{\lambda^2} \right) = \frac{1}{\mu T} = \frac{1/\mu}{T} = \frac{T_{OA}}{T} \tag{B.3-6}$$

where T_{OA} is the average off-air duration and T is the total time in the month.

---

*This assumption is based on a sampling of off-airs (>1 min) in four separate months during 1988.

"Scheduled" off-airs that are not planned until after the beginning of the month can be modeled using the *a priori* probability functions (occurrence/duration) treated above with λ, μ given by historical reliability figures* for each station. Once the scheduled off-air is planned/announced, the randomness vanishes (for that particular kind of off-air) and the problem becomes deterministic. Equation B.3-6 may still be used as an approximation to the off-air probability, however, since it is valid except for those intervals during which advance information is known. For the completely deterministic cases/intervals, Eq. B.3-6 simply becomes a fractional off-air figure subject to the exclusion of concurrent scheduled off-airs from different stations.

B.4 REFERENCES

1. Morris, P., Omega System Performance Assessment, Report No. CG-ONSCEN-01-89 (TASC TR 5351-8-1), Available from the National Technical Information Service (NTIS), Accession No. ADA-210342, March 1989.

2. Desrochers, G., and Hansen, A., Omega System Performance Assessment and Coverage Evaluation (PACE) Workstation Design and Implementation (Version 4.1), (TASC TIM 5919-2), May 1993.

3. Morris, P., Omega System Availability as Global Measure of Navigation Accuracy, Report No. CG-ONSCEN-05-90, (TASC TIM 5834-5-2), Available from the National Technical Information Service (NTIS), Accession No. AD-A-229492, September 1990.

4. Morris, P., Enhancement of the Omega System Availability Algorithm, Report No. CG-ONSCEN-01-90 (TASC TIM 5834-1-1), Available from the National Technical Information Service (NTIS), Accession No. AD-A-224814, March 1990.

---

* Excluding scheduled off-airs for annual maintenance which are known well before the month begins and are thus completely deterministic.

APPENDIX C
PACE UTILIZATION

C.1 INTRODUCTION

The Performance Assessment and Coverage Evaluation (PACE) workstation is an interactive, microcomputer-based tool developed by ONSCEN for planning and managing performance (navigation capability) of the Omega system. PACE also evaluates system performance of a "combined system" consisting of selected stations from the Omega, VLFCOM, and Alpha systems. In PACE, the VLFCOM system includes ten VLF communications stations operated by the U.S. Navy and NATO. The Alpha system is a VLF radionavigation system operated by the CIS (Commonwealth of Independent States, the former Soviet Union republics) and consists of five transmitting stations located in CIS territory. ONSCEN's interest in evaluating the performance of a combined system stems from two considerations: (1) Omega system signals are frequently supplemented with VLFCOM system signals for improved navigation capability in regions where the stand-alone Omega performance is marginal or inadequate, and (2) the Alpha system providers have shown interest in a potential navigation use of a combined Omega/Alpha system.

This appendix provides an overview of PACE capabilities and features and presents the Omega/combined system's performance limitations that can be evaluated and analyzed by PACE. A detailed discussion of the PACE capabilities and features and their uses can be found in the PACE User's Manual (Ref. 1), the PACE Analyst's Guide (Ref. 2), and published papers (Refs. 3 through 5). Section C.2 provides an overview of the PACE capabilities and features. It also presents a discussion of the various system performance measures provided by PACE and a discussion of the input information needed to model a system scenario to be assessed by PACE. The types of system performance outputs that can be obtained from PACE are listed in Section C.3. The types of system performance assessment problems that can be assessed and analyzed by PACE are described in Section C.4. Finally, a discussion of how PACE was used for planning of an Omega station maintenance during a five-month loss of Omega station Liberia signal is provided in Section C.5. A summary of PACE capabilities and potential uses is given in Section C.6.

C.2 PACE OVERVIEW

Section C.2.1 presents capabilities and features of PACE. The attributes of the PACE signal coverage database used to calculate system performance are given in Section C.2.2. Section C.2.3 discusses the system performance assessment parameters, conditions, and criteria, which are collectively referred to as the system scenario, or just a scenario. All information input to and output from PACE has a spatial resolution (called a PACE cell) of approximately 1000 km in latitude and 1000 km in longitude, and a temporal resolution of one UT hour in each day of each of the 12 months of the year. As a result, the earth's surface is resolved in a matrix of 444 PACE cells and the year is resolved into 288 times (hour-month time blocks).

C.2.1 PACE Capabilities and Features

PACE is designed to provide one of the following:

- A probabilistic assessment of system performance, called the *system availability,* when the system station off-air occurrences are treated by the system performance assessment model in PACE as probabilistic (random) events

- A deterministic assessment of system performance, called the *system accessibility,* when the system station off-air occurrences are treated by the system performance assessment model in PACE as deterministic events, such as the case with the stations of a combined system.

The system availability, as defined in PACE, is the probability that a navigation user with a perfectly operating receiving system can receive and utilize three or more station signals* at any location on the earth's surface and at any time included in the system scenario. The system availability is calculated using the system availability algorithm described in Chapter 11. Figure C-1 shows a conceptual overview of the major inputs to the system availability algorithm, and illustrates the user inputs to PACE and the major PACE output displays.

The system accessibility is identical to the system availability when all of the system scenario stations remain on-air over the scenario system performance assessment times. Thus, the system accessibility for a system scenario is the accessibility of three or more navigationally usable stations with acceptable station/receiver geometry. The current PACE can provide system accessibility assessment for both the Omega and combined systems, but system availability for only the Omega system. PACE

---

* This defines minimum usability requirements for those users operating in hyperbolic or rho-rho-rho navigation modes; nearly all current Omega navigation use is confined to these modes.

Figure C-1 Conceptual Overview of the PACE System Availability Algorithm

does not provide a probabilistic assessment of a combined system performance since: (1) the system availability calculation model in PACE is currently limited to the Omega system stations, and (2) unlike Omega, no station off-air occurrences information is currently available for the VLFCOM and Alpha system stations.

The system performance (i.e., either system availability or system accessibility) is calculated and displayed by PACE at the local, regional, and global levels. The local system performance (P_{AT}) is the system performance at a specific location and time. The regional system performance (Reg P_{SA}) is the system performance at *any* location within a specified region at *any* of the scenario assessment times. The global system performance (P_{SA}) is the regional system performance when the region is the entire globe. Note that P_{SA} (Reg P_{SA}) is the weighted average of all P_{AT}'s over all PACE cells covering the globe (region) and all scenario assessment times.

PACE is designed to also provide information on where and when the local system performance of the assessed system is unacceptable (i.e., below a certain threshold level). This information is provided in terms of the so-called system performance "show-stoppers." A system performance show-stopper is a specific location (PACE cell) and time (hour and month combination) for which the system performance is below some acceptable threshold level. The temporal information on the system performance is provided by PACE via the color-coded time-panel displays. The time-panel is a matrix of 288 squares, each corresponding to a unique time of the year. A red square in a cell time-panel indicates the cell is a show-stopper; otherwise it appears as a blue square.

The spatial information on the global system performance is provided by PACE via a color-coded map of 444 PACE cells. In this map, a cell is red or blue depending upon the combination of the user-selected cell coloring rule (CCR) option and user-specified system performance threshold. The three CCR options available to a user in PACE are: minimum, mean, and maximum. The use of *minimum* (*maximum*) option colors a cell red, if the lowest (highest) value of the local system performance for the cell over the assessment times is below the specified system performance threshold; otherwise, the cell is colored blue. On the other hand, the use of the *mean* option colors a cell red if the mean value of the local system performance values over the assessment times is below the specified system performance threshold; otherwise, it is colored blue. The minimum option is useful when the PACE user wants to identify cells where the local system performance over the assessment times is never below the specified threshold value. The use of the maximum option is of interest when the user wants to highlight cells where the system performance is more than the specified threshold value at least at one of the assessment times. The most frequently used CCR option is the minimum option.

PACE includes a number of support features and utilities to query, analyze, compare, difference, plot, and document the system performance results. Table C-1 summarizes the frequently used PACE features and utilities. The analysis features and utilities are designed to help the PACE user identify

Table C-1 Overview of PACE Support Features/Utilities*

FEATURE/UTILITY	PURPOSE
Station Signal Path Display	View geophysical environment along a signal path
Day/Night Terminator Display	Observe illumination condition changes along signal paths
Geomagnetic Latitude Contour Display	View geomagnetic-latitude variations along signal paths
Tundra/Ice-cap Region Display	Determine if and where a path transits the tundra/ice-cap region
Signal Coverage Parameters Query	View individual station signal coverage parameter values as well as signal path bearing at a cell and time combination
Signal Coverage Parameters Plot	Observe diurnal and monthly variations in the station signal coverage parameters at a cell
Split-Screen Display	Side-by-side comparison of the system performance displays of two scenarios
Difference Display	View differences in the system performance show-stoppers for two scenarios
QRBUILD Utility†	Construct Omega system station off-air probability file for use by PACE
MAKESSDB Utility†	Generate database of spatial and temporal attributes of the Omega system show-stoppers associated with a scenario, or produced as a result of changes in the scenario elements
Paradox Utility†	Prepare Omega system show-stoppers summary tables/reports

*Path refers to both the short-path and long-path from a station.
†Omega system-specific utility.

probable underlying geophysical and propagation reasons for the system performance results. They include station great-circle path overlay, day/night terminator overlay, tundra/ice-cap region overlay, and geomagnetic contours overlay.

C.2.2 PACE Signal Coverage Database

The coverage database includes signal coverage parameters for the individual station signals in the Omega, VLFCOM, and Alpha systems. The Omega system (see Chapter 2) in PACE is composed of eight worldwide stations, each transmitting signals at 10 kW, and each of four common frequencies (10.2, 11.05, $11^1/_3$, 13.6 kHz) and at a station-unique frequency (10 to 14 kHz). The Omega system signal coverage database in PACE is currently limited to 10.2 and 13.6 kHz frequency signals. As a result, PACE can assess Omega system performance based only on the system navigation at these two frequencies. In PACE, the VLFCOM system (see Table C-2) is composed of ten stations, each transmitting signals at a unique frequency. The Alpha system stations (see Table C-3) are similar to the Omega system stations in that each station transmits signals at several common frequencies. The Alpha system station signal coverage information is currently included in PACE at only the primary navigational frequency of 11.905 kHz.

C-5

Table C-2   VLFCOM System Station Specifications

IDENTIFICATION	FREQUENCY (kHz)	RADIATED POWER (kW)	LOCATION	LATITUDE (deg)	LONGITUDE (deg)
GBR	16.0	45	Rugby, England	52.37 N	1.19 W
JHZ	16.4	45	Noviken, Norway	66.97 N	13.89 E
NDT	17.4	38	Yosami, Japan	34.97 N	137.02 E
GQD*	19.0	42	Anthorne, England	54.91 S	3.27 E
NWC	19.8	1800	Exmouth, Australia	21.80 N	114.15 W
NSS	21.4	213	Annapolis, MD, USA	39.00 N	76.50 W
NPM	23.4	502	Lualualei, HI, USA	21.42 N	158.15 W
NAA	24.0	1200	Cutler, ME, USA	44.63 N	67.28 W
NLK	24.8	245	Jim Creek, WA, USA	48.20 N	121.92 W
NAU	28.5	100	Aguada, Puerto Rico, USA	18.60 N	67.18 W

*Also identified as GBZ.

Table C-3   Alpha System Station Specifications

IDENTIFICATION	FREQUENCY* (kHz)	RADIATED POWER (kW)	LOCATION (NEAREST CITY)	LATITUDE (deg)	LONGITUDE (deg)
ASH			Ashkhabad	39.46 N	62.72 E
KOM			Komosomolsk	50.06 N	136.60 E
KRA	11.905, 12.649, 14.881	50	Krasnodar	45.46 N	38.17 E
MUR			Murmansk	68.03 N	34.68 E
NOV			Novosibirsk	55.75 N	84.45 E

*PACE currently includes signal information at 11.905 kHz.

The coverage database in PACE is composed of the individual station coverage data sets. Each station data set includes a set of five station signal coverage parameters as a function of location (each of 444 PACE cells), time (each of 288 hour-month time blocks), and frequency. For the Omega system, each station has a data set for each of the 10.2 and 13.6 kHz signal frequencies, while for the VLFCOM and Alpha system stations, each station has a single coverage data set. The five station signal coverage parameters are:

- Median value of signal-to-noise ratio (SNR) in decibels, which determines whether the SNR is high enough so that the signal can be reliably tracked for accurate phase measurement

- Short-to-long-path signal amplitude ratio (S/L) in decibels, which determines the extent of contamination of the desired short-path component of the signal by the long-path component

- Signal path/terminator crossing angle (PTCA) in degrees, which indicates the extent of the potential interference of the desired (directly propagating) signal from the undesired (indirect) signals that have been reflected or refracted by the day/night terminator

- Mode 1 dominance margin* (M1DM) in decibels for Omega signals or the scaled wave number gradient§ (WNG) in cec/km for the VLFCOM/Alpha station signals, which determines the extent of expected signal phase instability due to the modal interference effects

- Standard deviation of the atmospheric noise, which allows PACE to calculate any general percentile value using Equation C-1.

Although both signal amplitude and noise level exhibit variation when measured at the same hour for each day of the month, the noise level variation is generally much larger (2 to 12 dB, Ref. 6) than that for the signal amplitude (1 to 3 dB, Ref. 6). As a result, SNR is considered a random quantity, while M1DM and S/L, which involve signal parameters, are treated as deterministic. The database contains the median value (i.e., 50th percentile) of the daily SNR levels at a fixed location for a given hour and month. The median SNR is calculated as the difference in dB of the median value of the signal level and the median value of the noise level, based on the fact that both signal and noise levels are lognormally distributed (Ref. 6). The median SNR value in the database is based on a 100 Hz receiver processing bandwidth.

---

* The ratio of the signal's Mode 1 component amplitude and the interfering mode amplitude, where interfering mode is the phasor-sum of the higher-order modes of the signal.

§ The scaled wave number gradient is the absolute value of the wave number gradient (cec/km^2) multiplied by the earth's radius (km).

Propagation Corrections (PPCs), needed to correct the signal phase measurements prior to their use in a navigation solution, are currently available only for the Omega system signals. As a result, navigation receivers process Omega signals differently from the VLFCOM/Alpha signals so that M1DM and WNG are needed to determine the modal characters of Omega and VLFCOM/Alpha station signals, respectively.

The station signal coverage parameters in the database are used to calculate performance of those system scenarios in which the system performance assessment criteria (see Section C.2.3) is stated in terms of the median SNR value. PACE also allows system performance assessment of scenarios in which the performance criteria are stated in terms of a general percentile SNR level. To accommodate this type of assessment, the database includes σ_N (the standard deviation of the daily noise levels) as a function of frequency, location, hour, and month. The procedure for calculating the desired percentile SNR value is described in the next section.

C.2.3 PACE Input Parameters

The system performance calculations performed by PACE are governed by the PACE set-up (i.e., system scenario constructed by the PACE user). All PACE inputs needed to construct a system scenario have default values. To construct a new scenario, the PACE user alters the nominal scenario values via the PACE graphical user interface. The system scenario, as mentioned earlier, is composed of three system components: (1) system operational parameters, (2) system assessment conditions, and (3) system assessment criteria. This section discusses the user inputs needed to configure a system scenario and describes the system components in more detail.

The *system operational parameters* are:

- *Time-dependent* station power level for each of the eight Omega stations as a function of UT hour of day and month of the year
- *Time-independent* station power levels for the VLFCOM and Alpha system stations
- Omega system station off-air probabilities.

The station off-air probabilities are needed to calculate the system availability of the Omega system. The station off-air probability information, specified for each Omega station on a per-month basis, is made up of three components: scheduled, unscheduled, and annual maintenance. Each of the three probability components represents the fraction of the month that the station will be off-air for the indicated reason. The annual maintenance component is the probability that the station will be off-air due

to planned annual maintenance during an indicated month. All other foreseen interruptions in transmission of a station signal during a month are incorporated into the station's scheduled off-air component for the indicated month. The unscheduled off-air component of a station is the probability that the station will be off-air due to unforeseen events during the indicated month. Included in the PACE workstation is a default set of empirically derived station off-air probabilities. During the formation of an Omega system scenario, the default values of the Omega station off-air probabilities may be modified using the QRBUILD utility, which is a part of the PACE workstation.

The *system assessment parameters* are:

- Assessment times (hours and months)
- Individual station transmitting status: on-air or off-air
- Geographic region/priority file
- Station off-air model (SOM) setting: best, worst, or nominal
- Omega station frequency utilization option: 10.2, 13.6, AND, or OR
- Cell coloring rule (CCR) option: minimum, maximum, or mean
- Station signal phase error statistics.

The geographic region/priority file has two functions: (1) designate geographic priority information in the form of an integer weight assigned to each PACE cell, and (2) store indices for cells that specify the region to be used in the regional coverage and system availability/accessibility computations. PACE's default set of weights are uniformly one. The weights can be modified by the PACE user with the scenario region/priority file editor included in the PACE workstation. In particular, a cell's weight may range in integer values from zero to nine, where zero indicates no navigational significance of the cell to the user and nine represents the highest relative significance. A region consisting of any combination of the 444 PACE cells may also be defined by the PACE user with the editor.

Usually, the Omega system availability is desired for the "nominal" case of the station off-air probabilities in which each station off-air probability is composed of all three off-air components. However, it may be required by a scenario to remove the effect of particular component(s) in the system availability computations. PACE accommodates these possibilities in the system availability assessment calculations via the use of the station off-air model (SOM). The SOM has three settings: best, nominal, and worst. The *best* setting is appropriate when assessing the Omega system availability on days of the month for which no planned annual maintenance is expected for the station whose annual maintenance is scheduled for that month. On the other hand, the *worst* setting assumes that the annual

maintenance of each of the stations is continuous throughout the maintenance-designated month and thus the station will be off-air for the entire maintenance-designated month. Note that the best and worst settings provide the most optimistic and pessimistic assessments of the system availability of an Omega system scenario. The *nominal* setting assumes no *a priori* knowledge of the scheduled station off-air or planned station annual maintenance occurrences, and the resulting system availability is the system availability on any day over scenario-included times.

The frequency utilization option is used to emulate different types of Omega receivers in use. To consider a station to be a usable-signal station, most Omega receivers require availability of usable signals from the station at both 10.2 and 13.6 kHz. This corresponds to the use of the AND option for the Omega station signal frequency utilization selection. However, some Omega receivers require the stations to be used in the navigation solution to have usable signal(s) at: (1) 10.2 kHz only (10.2 option), (2) 13.6 kHz only (13.6 option), or (3) either 10.2 or 13.6 kHz (OR option).

The individual station phase errors statistics (bias and random components) are used to calculate the system navigation accuracy at a specified location and time. PACE has default values for the phase error statistics as a function of station (each of the 23 Omega/VLFCOM/Alpha system stations), Omega signal frequency (10.2 or 13.6 kHz), and signal path illumination condition (day, night, or transition). The default phase error statistics in PACE can be altered via the phase error editor.

The *system assessment criteria* include:

- System navigation criteria
- The system availability/accessibility criterion.

The system navigation criteria consist of the usable signal access criteria and collective signal access criterion. A station signal at a given frequency, location, and time is considered usable if the associated signal coverage parameters satisfy the user-specified usable signal access criteria. The usable signal parameters of a station signal are:

- Signal-to-noise ratio (SNR)
- Short-to-long-path ratio (S/L)
- Mode 1 dominance margin (M1DM) for Omega signals, or scaled wave number gradient (WNG) for VLFCOM/Alpha signals
- Signal path/terminator crossing angle (PTCA).

The collective signal access criterion demands availability of three or more usable-signal stations whose geometric dilution of precision (GDOP) of the stations/receiver geometry satisfies the user-specified

collective signal access criterion. The system availability/accessibility threshold is the minimum value for the system availability/accessibility index for a cell and time combination.

PACE calculates performance of a system scenario based on the user-specified set of threshold levels for the system assessment criteria. Note that the parameters M1DM, PTCA, and GDOP are labeled in the PACE status display as MDM, ANG, and GDP, respectively. Table C-4 lists two sets (a liberal set and a conservative set) of the frequently used system assessment threshold levels. The liberal and conservative sets comprise the less stringent and most stringent threshold levels, respectively. These sets bracket the: (1) performance range of most Omega/combined system receivers, and (2) system availability/accessibility requirements of most Omega/combined system users. The table also gives the rationale for the listed threshold levels. The conservative levels are representative of airborne users, while the liberal levels characterize typical marine users.

The SNR threshold in the navigation criteria is frequently stated for the median SNR value, e.g., as stated in Table C-4. In the navigation criteria based on the median SNR threshold, a station signal at a location for a given hour and month is defined to be navigationally usable if it satisfies the usable signal criteria for at least fifty percent of the days in the specified month. For system scenarios in which the usable signal is defined as one that satisfies the usable signal criteria for at least a specified arbitrary percentage of the days in a month, PACE calculates the system scenario performance using the SNR value appropriate for the specified month-days percentage. For such scenarios, the appropriate value in decibels of the SNR parameter (SNR_{PACE}) is obtained from the associated median value of the SNR parameter in decibels (SNR_{MED}) and the standard deviation of the SNR parameter in decibels (σ_{SNR}) using the following algorithm:

$$SNR_{PACE}\ (S, F, L, M, H, M_P) = SNR_{MED}\ (S, F, L, M, H) - C(P)\ \sigma_{SNR}\ (F, L, M, H) \qquad \text{(C-1)}$$

where the variables in the above equation are: S for station, F for frequency, M for month, H for UT hour, and M_P for month-days percentage; and

$\sigma_{SNR} = (\sigma_N^2 + \sigma_S^2)^{1/2}$

σ_N = standard deviation of the daily noise level (in dB) for a given F, L, M, and H combination

σ_S = standard deviation of the daily signal amplitude (in dB) for a given S, F, L, M, and H combination

P = SNR percentile level = $100 - M_P$

C = standard normal deviate (see Table C-5).

Table C-4 Threshold Levels for Frequently Used System Assessment Criteria

PARAMETER	CONSERVATIVE CRITERIA		LIBERAL CRITERIA	
	THRESHOLD	BASIS	THRESHOLD	BASIS
SNR (median value)	−20 dB*	Minimum SNR required for aircraft navigation; consistent with current receivers	−30 dB*	Minimum SNR for non-maneuvering aircraft assuming some signal processing gain due to receiver limiting
S/L	6 dB	Consistency with M1DM threshold	1 dB	Consistency with M1DM threshold
M1DM	6 dB	Reasonable M1DM for which maximum phase deviation is about 8 cec and which provides sufficient margin for Mode 1 signal to avoid lane slip/jump due to random ionospheric fluctuations	1 dB	Minimum M1DM for which maximum phase deviation is about 18 cec; consistent with previous thresholds and provides 5 cec margin over possible lane slip/jump conditions
WNG	14 cec/km[†]	Maximum absolute value of WNG for which point-to-point range-only type navigation is possible without high probability of lane slip	14 cec/km	Same rationale as for the conservative criteria
PTCA	5 deg	Minimum PTCA needed to exclude extremely rapid day-to-night transition along a path in which lane slip/jump is likely to occur	5 deg	Same rationale as for the conservative criteria
GDOP	3	Maximum GDOP needed to exclude 2-drms position errors greater than 14 km based on about 8 cec PPC error	6	Maximum GDOP threshold needed to exclude 1-drms position errors greater than 14 km based on 8 cec PPC error
P_{TH}	0.99	Minimum P_{TH} for airborne users (Ref. 8)	0.95	Minimum P_{TH} for marine users (Ref. 9)

*100 Hz receiver processing bandwidth.
[†]Centicycles/per kilometer.

The required SNR_{MED} and σ_N values are contained in the PACE coverage database. Because σ_S is much smaller* than σ_N, and is relatively less sensitive to frequency, location, month, and hour, PACE uses a fixed value for σ_S, the default value of which is 2 dB. The above algorithm is based on the fact that both

---

*σ_S varies between 1 and 3 dB, while σ_N varies between 2 and 12 dB (Ref. 6).

σ_S and σ_N (and hence σ_{SNR}) are lognormally distributed parameters. To illustrate the SNR_{PACE} parameter sensitivity to M_p, Table C-5 presents SNR_{PACE} values for several representative M_P values in a hypothetical case where at a given location, month, and hour the SNR_{MED} is -15 dB and σ_N is 8 dB. As an example of the SNR parameter values that are used by PACE to calculate the system performance for this case (see Table C-5), the SNR parameter value is: (1) -15 dB i: the SNR threshold is stated for the median SNR value, i.e., the value associated with $M_P = 50$, and (2) -28.57 dB if the SNR threshold is stated for the 5th percentile SNR value; i.e., the value associated with $M_P = 95$.

Table C-5 SNR_{PACE} Values as a Function of M_P

M_P	P	c	SNR_{MED} (dB)	σ_N (dB)	σ_S (dB)	SNR_{PACE} (dB)
25	75	−0.675				−9.44
50	50	0.000				−15.00
90	10	1.285	−15	8	2	−25.60
95	5	1.645				−28.57
99	1	2.326				−34.18

C.3 SUMMARY OF PACE OUTPUTS

This section summarizes the types of system performance assessment outputs that can be generated using PACE. These outputs include system availability, system accessibility, and navigation accuracy assessments. However, the system availability assessment can be obtained for only the Omega system scenarios, whereas the other outputs can be generated for any of the stand-alone Omega, VLFCOM, and Alpha systems, as well as for any combined system. Specifically, the outputs include:

1. Numerical and graphical displays showing the global, regional and local system availabilities as well as the spatial and temporal features of the system availability show-stoppers for an Omega system scenario.

2. Numerical and graphical displays showing the global and regional system accessibilities as well as the spatial and temporal features of system accessibility show-stoppers of

    •   An Omega, VLFCOM, or Alpha system scenario

    •   A combined system scenario.

3. Numerical values of the station signal coverage parameters at a specified location and time for the selected Omega/VLFCOM/Alpha system stations.

4. Individual station signal coverage diagram for any of the selected Omega/VLFCOM/Alpha system station; the diagram displays worldwide accessibility of navigationally usable signals from the station at a specified time for the selected station attributes and signal usability criteria.

5. Individual station signal coverage parameter plots showing hourly/monthly variations of the parameters.

6. Composite (full-system) signal coverage diagram for the Omega or combined system scenario; the diagram shows worldwide accessibility of navigationally usable signals from three or more stations (with acceptable station/receiver geometry) of the scenario at a specified time.

7. Navigation accuracy at a specified location and time from

    •   The system scenario being assessed

    •   A hypothetical network of stations selected from the Omega, VLFCOM, and Alpha systems, where all selected stations are assumed (without any *a priori* signal usability test done by PACE) to provide navigationally usable signals.

In addition, PACE can be used to compare and difference the system availability and accessibility assessment results of any two system scenarios, thus determining the impact on the system availability and accessibility caused by the differences in the two scenarios.

C.4 PACE USES

This section presents the types of Omega/combined system performance assessment problems and issues that can be evaluated and analyzed by PACE. The typical problems and issues include:

1. What is the system availability for a given Omega system scenario?

2. What is potential impact on the Omega system availability in response to a "what-if" question on the Omega system operational and programmatic issues such as:

    •   Are all Omega stations necessary for continued operation at an acceptable level of Omega system availability for the projected life of the system?

    •   Can some of the Omega stations be operated at reduced power level during certain hours/months to lower the overall system operational cost while maintaining certain level of system availability?

    •   What is the best set of hours during certain month(s) to perform urgent repairs on specified station(s) with minimal impact on the system availability?

    •   Can the station annual maintenance schedule (i.e., the maintenance duration and maintenance month) of certain Omega system station(s) be revised to improve the system availability?

3. What is the system accessibility for a given combined system scenario?

4. What is the impact on the system accessibility of a given combined system scenario in response to addition or deletion of certain station(s) from the scenario?

5. What is the navigation accuracy at a given location and time from

   - A given Omega/combined system scenario?

   - A hypothetical network of user-selected stations from the Omega, VLFCOM, and Alpha system stations where all selected stations are assumed to provide navigationally usable signals?

6. What are the probable geophysical and propagational reasons underlying the PACE-computed system availability/accessibility results at certain locations/times?

Note that the system availability/accessibility results include the global, regional, and local values of system availability and accessibility as well as the spatial and temporal information on the system availability and accessibility show-stoppers.

C.5 OPERATIONAL PLANNING WITH PACE

With PACE, ONSCEN can now rapidly analyze possible system configuration scenarios and manage station performance for maximum system availability. Recent examples best illustrate the power of this capability and its meaning to the navigator.

When Omega station Liberia was forced off-air by civil war in October 1992, the Omega system was left in a seven-station configuration for almost six months. This in itself did not significantly impact the worldwide system coverage, since the Omega system is robust enough to compensate for any one station off-air. By November, however, Omega station La Reunion had suffered a casualty to the power transformer supplying one of the transmitters and required off-air time to reconfigure the remaining transformer to serve either transmitter. Since VLF coverage dominates the area east of each station, the combined effect of both the Liberia and La Reunion station off-airs created the potential of a gaping Omega system availability "hole" over the Indian Ocean and Southeast Asia. Figure C-2 shows the PACE-provided assessment of the Omega system availability for the scenario when both Omega stations Liberia and La Reunion are continuously off-air during the month of interest.

Note that red and blue colors in the actual PACE screen displays are shown in Figure C-2 through Figure C-5 as gray and black colors, respectively. As expected, Omega system availability in the Indian Ocean was shown to be significantly diminished. By opening the time-panel of a cell in this

Figure C-2   Omega System Availability Display for November 0100-2400 UT:
Liberia (B) and La Reunion (E) Off-air

impacted area, however, the PACE analyst quickly saw that while the 24-hour coverage of the area was reduced, a "window" of time existed within each day when the combination of season, geography, and relative location of day/night terminator along signal paths allowed other Omega stations to effectively cover the area. This is clearly illustrated in Figure C-3. Consequently, if Omega station La Reunion could "tailor" scheduling of its maintenance, significant Omega coverage impact could be avoided.

With this in mind, ONSCEN began working with the La Reunion station to plan their needed off-air. Local engineering considerations were taken into account, and a four-hour "window" was targeted for the off-air period. The Omega station La Reunion personnel successfully reconfigured their transmitter/transformer combination during the prescribed off-air, with minimal impact on Omega coverage. Figure C-4 shows the impact of both Liberia and La Reunion station off-airs during this "managed" four-hour off-air period. For comparison, Figure C-5 shows just the Liberia station off-air for that same four-hour period (the baseline condition at that time). The result of this "PACE managed" off-air was an improved equipment redundancy posture at Omega station La Reunion, which was accomplished with minimal worldwide impact.

C-16

Figure C-3   Omega System Availability Display for November 0100-2400 UT with Super-imposed Time-panel for Cell #249: Liberia (B) and La Reunion (E) Off-air

In a similar scenario in June 1993, Omega station North Dakota suffered lightning damage to their main power switch gear. This switch gear is provided to switch the station from commercial power to the emergency generator power, in the event of loss of the commercial power. While the station continued to operate on commercial power, summer thunderstorm activity made eventual power failure a virtual certainty. Omega station North Dakota immediately requested several hours off-air time in order to secure high voltage and repair the switch gear. Unfortunately, Omega station Hawaii was off-air for annual maintenance and could not resume operations for several days. Both Omega stations Hawaii and North Dakota provide critical Omega coverage for Atlantic Ocean air traffic routes, so the effect of their combined off-airs would have been significant. Again, PACE was employed to analyze the scenario, and again a "window" of time when alternate stations covered the Atlantic region was determined. Omega station North Dakota used this "window" to affect the station repairs. System integrity was maintained during the station repair time without impacting overall system coverage. Although we will never know for certain, the total absence of reports of Omega signal availability problems in this highly traveled region seems to indicate that ONSCEN was successful in preventing the disruption of Omega system availability.
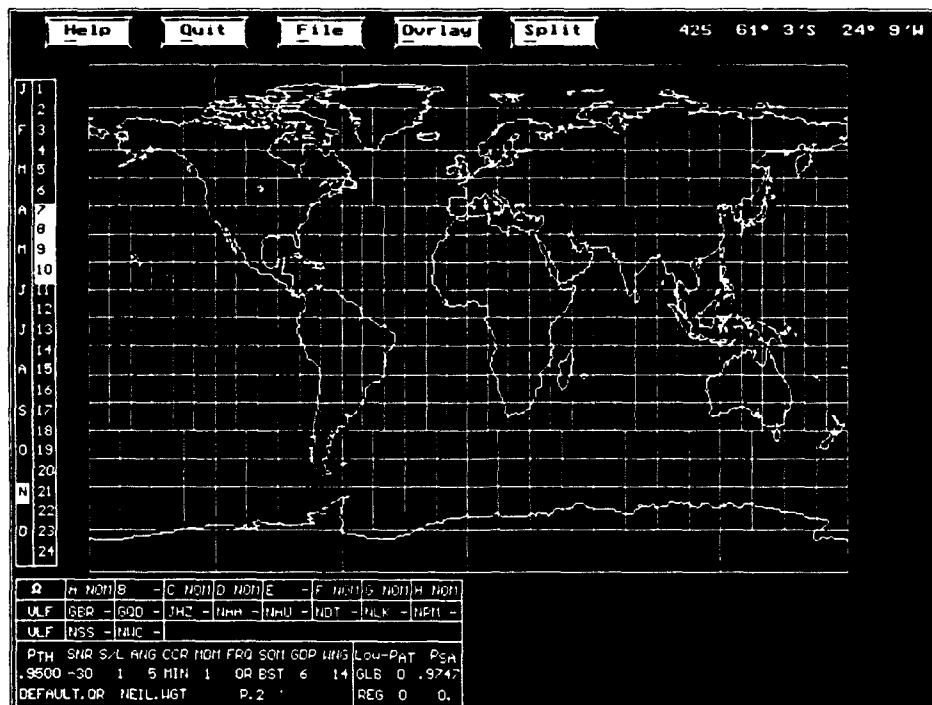
Figure C-4   Omega System Availability Display for November 0700-1000 UT: Liberia (B) and La Reunion (E) Off-air
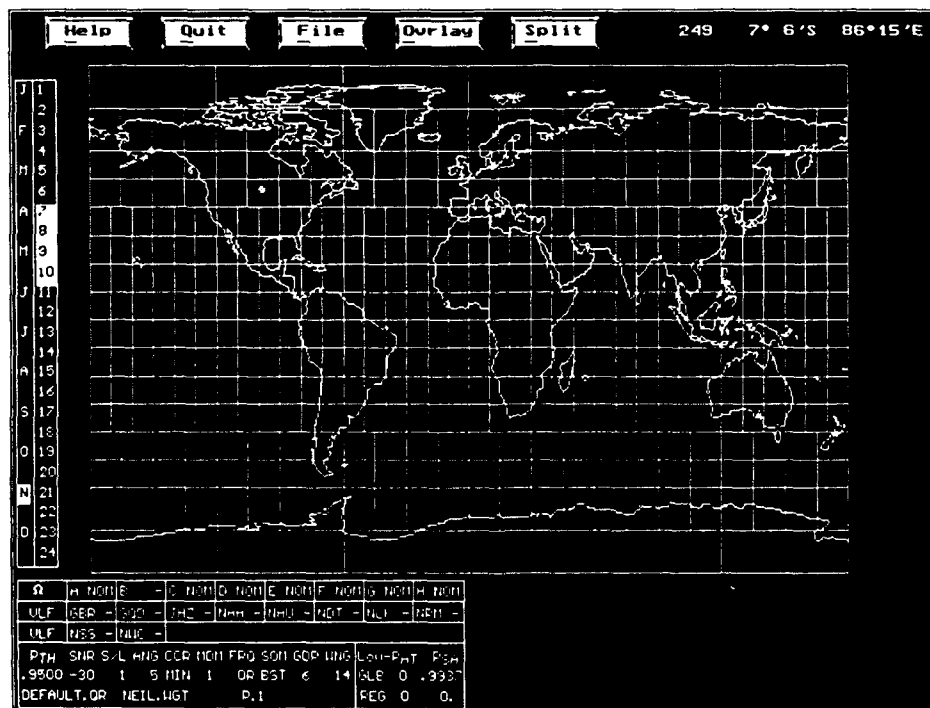
Figure C-5   Omega System Availability Display for November 0700-1000 UT: Liberia (B) Off-air

C-18

Managing Omega Navigation System performance with such finesse was neither a reasonable nor an effective alternative before the advent of PACE. Now, PACE sees extensive use by ONSCEN throughout the year and has almost certainly improved the worldwide Omega availability. A Station Power Level Assignment Algorithm (SPLAA) has been recently developed to be used as a companion to PACE. SPLAA is a microcomputer-based utility for determining the individual Omega station power level necessary to minimize the Omega system power level cost function while maintaining a minimum required global system availability. The algorithm uses analytical, rule-based, and exploratory techniques to adjust the eight Omega station power levels using the signal coverage database contained in PACE.

C.6 SUMMARY

PACE represents what is probably the most powerful tool ever developed for managing and improving the Omega system performance. Based on an extensive database of refined VLF signal coverage information, PACE can take a prescribed system configuration (with selected stations off-air or at reduced power), look at a specific time/location, and calculate the probability that a user, with properly operating receiver, has at least three usable-signal stations with adequate stations/receiver geometry. Issues of the self and short/long path signal interference effects, signal-to-noise ratio, position-fix geometry, and signal path/terminator crossing angle are considered in the calculation of system availability. While this same general information could be derived or intuited from manual calculations in the past, the speed and accuracy of PACE predictions have moved the management of the Omega system into a new era. The PACE workstation will become an increasingly powerful tool in the Omega system management, and thus permit the international Omega partnership to work smarter, and not harder, to improve the system performance.

C.7 REFERENCES

1. Hansen, A.J., Performance Assessment and Coverage Evaluation (PACE) Workstation: User's Manual, Version 5.1. TASC Technical Information Memorandum TIM-6993-3, July 1994.

2. Gupta, R.R., PACE Analyst's Guide, TASC Technical Information Memorandum TIM-5911-6, March 1994.

3. Neill, S.M., Dubay, C.L., and Gupta, R.R., Omega operations planning with the Performance Assessment and Coverage Evaluation (PACE) workstation. In *Proceedings of the Eighteenth Annual Meeting, International Navigation Association*, Orlando, FL, October 1993.

4. Warren, R.S., Morris, P.B., Gupta, R.R., and Desrochers, G.R. Omega system performance assessment. In *Proceedings of the Position, Location, and Navigation Symposium, IEEE Aerospace and Electronics Systems Society*, Monterey, CA, March 1992.

5. Morris, P.B., and Gupta, R.R. Omega system availability assessment. In *Proceedings of the Sixteenth Annual Meeting, International Omega Association*, Vancouver, Canada, October 1991.

6. Morris, P.B., Effect of random signal and noise levels on the system availability index. TASC Technical Information Memorandum TIM-5911-2-1, March 1992.

7. Gupta, R.R., Omega system show-stopper assessment methodology development. TASC Technical Information Memorandum TIM-5911-3, April 1992.

8. U.S. Department of Transportation DRT-1 and U.S. Department of Defense (ASD/C³I), 1990 Federal Radionavigation Plan, Report DoD-4650.4/DOT-VNTSC-RSPA-90-3.

9. Project Office/PM-9, Project Master Plan for Omega Navigation System; Chief of Naval Material, Department of the Navy, April 1966.

APPENDIX D

KALMAN FILTER OVERVIEW

D.1 INTRODUCTION

All practical systems are subject to random disturbances and all measurements of system behavior contain random errors. Briefly stated, the Kalman filter is a recursive data processor that uses knowledge of the system dynamics, measurements of the system outputs, known or assumed statistics of the system and measurement errors, and system initial condition information to estimate the most probable state of a linear system. The system and filter signal flow for this estimation process is illustrated in Fig. D.1-1. Given a linear system with state vector x, and (vector) measurements of its behavior, z, the Kalman filtering algorithm processes the measurement data to obtain a state vector estimate, $\hat{x}$, which is optimum in the sense that the error in the state estimate is statistically minimized. Note that the Kalman filter also requires statistical models that characterize the system and measurement errors, and initial condition information on the state of the system.
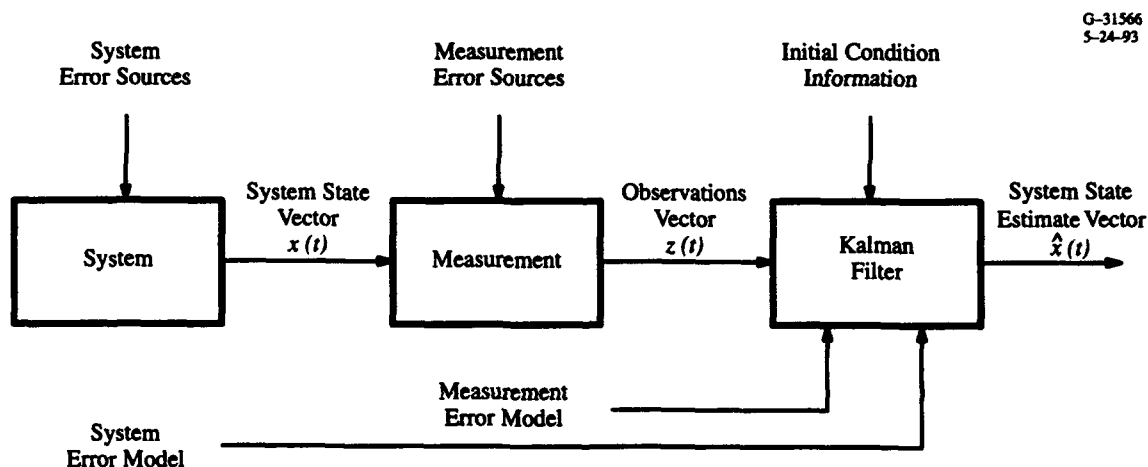
Figure D.1-1   Kalman Filter System and Filter Signal Flow

Kalman filtering forms the basis for most modern multisensor system integration algorithms. Navigation is one of the earliest, and certainly one of the most successful, application of Kalman filtering; data from multiple sensors such as an inertial navigation system (INS), Doppler velocity sensor and

loran and/or Omega radio navigation receivers, etc., are combined in a complementary manner to obtain the "best" overall estimate of vehicle position, velocity and attitude. The optimal use of external measurements, together with data supplied by the INS, can provide an overall accuracy better than that obtainable from either the measurements or the navigation system alone. Kalman filtering also forms the basis for the SYNC2 Omega clock synchronization algorithm (Chapter 7).

Underlying mathematical and statistical concepts needed to understand Kalman filtering are reviewed in this appendix. First, deterministic least-squares and elements of random variable theory are briefly examined in Section D.2. The section ends with a discussion of statistical least-squares estimation and random process theory. Next, Section D.3 presents the multi-dimensional state-space formulation of dynamical systems and gives examples of random processes using this formulation. Section D.4 presents the equations of Kalman filtering and gives heuristic plausibility arguments for their validity. The appendix ends with some simple, but interesting Kalman filter examples.

This appendix is neither comprehensive nor mathematically rigorous. The intent is to present the fundamental theory and to give the reader an appreciation for the power and utility of Kalman filtering. A more complete exposition of both the theory and application of Kalman filtering can be found in Ref. 1.

D.2   REVIEW OF UNDERLYING MATHEMATICAL CONCEPTS

It is assumed that the reader has a working familiarity with linear algebra and, in particular, elementary operations with vectors and matrices. A review of this material can be found in Chapter 2 of Ref. 1.

D.2.1   Deterministic Least-Squares

The development of processing methods for handling noisy data can be traced to Gauss (circa 1800), who invented the technique of deterministic least-squares and used it in a relatively simple orbit determination problem. It is shown in Section D.4 that there is a strong connection between Kalman filtering and deterministic least-squares.

Polynomial curve fitting is a specific example of linear least-squares estimation where one wishes to find the coefficients of a polynomial of chosen order that best fit a given set of measurements in a least-squares sense. That is, find the set of polynomial coefficients that minimize the sum-of-squares differences between the measurements and the chosen functional form for the data.

Figure D.2-1 shows shows the results of a simulation representing the measured phase difference between a cesium beam standard and good quality crystal oscillator. In this example, differential phase measurements are made every two hours over a period of 200 hours. Relative to the standard, the crystal clock is known to have an initial phase offset, a frequency offset and an aging rate or frequency drift, which together result in a parabolic divergence of crystal oscillator phase over time relative to the atomic standard. The measured phase differences are scattered about a parabolic trend due to measurement errors. The functional form to be fit to the data is:

$$\delta\phi(t) = \delta\phi_0 + \delta f_0 t + \delta f_0' t^2/2 \qquad (D.2\text{-}1)$$

where

$\delta\phi(t)$ = clock phase error at time t

$\delta\phi_0$ = initial oscillator phase offset

δf_0 = oscillator frequency offset

$\delta f_0'$ = oscillator aging rate

t = time in hours
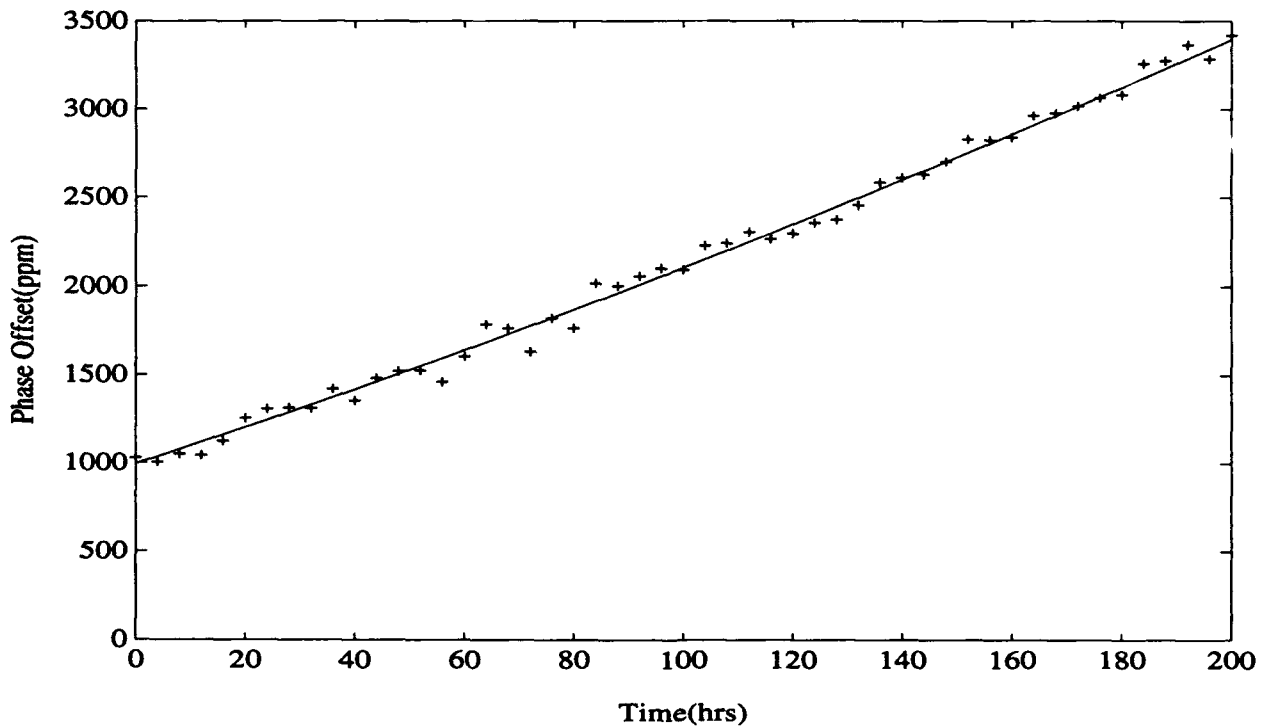
Figure D.2-1 Oscillator Phase Measurements and Least-Squares Fit to Data (solid line)

D-3

Given N noise-corrupted phase measurements, z_k, at discrete instants, t_k, we wish to find values for $\delta\phi_0$, δf_0, and $\delta f_0'$ which minimize

$$\sum_{k=1}^{N} (z_k - \delta\phi(t_k))^2 = \sum_{k=1}^{N} (z_k - \delta\phi_0 - \delta f_0 t_k - \delta f_0' t_k^2/2)^2 \qquad \text{(D.2-2)}$$

This problem and its solution are easily cast in compact vector-matrix notation. First note that the phase measurements, z_k, can be modeled as

$$z_k = \delta\phi_0 - \delta f_0 t_k - \delta f_0' t_k^2/2 + v_k \qquad \text{(D.2-3)}$$

where v_k represents a random measurement error. Then a sequence of N measurements can be written in vector-matrix form as

$$\begin{bmatrix} z_1 \\ \vdots \\ z_N \end{bmatrix} = \begin{bmatrix} 1 & -t_1 & -t_1^2/2 \\ \cdot & \cdot & \cdot \\ \cdot & \cdot & \cdot \\ 1 & -t_N & -t_N^2/2 \end{bmatrix} \begin{bmatrix} \delta\phi_0 \\ \delta f_0 \\ \delta f_0' \end{bmatrix} + \begin{bmatrix} v_1 \\ \vdots \\ v_N \end{bmatrix} \qquad \text{(D.2-4)}$$

or

$$z = Hx + v \qquad \text{(D.2-5)}$$

where z and v are column vector quantities and x denotes the 3-vector of oscillator phase error parameters to be estimated. Ignoring the additive noise term for the moment, Eq. D.2-5 represents an over-determined set of linear equations. The least-squares solution to D.2-5 constitutes an estimate of the oscillator drift model parameters. The solution is given by

$$\hat{x} = (H^TH)^{-1}H^Tz \qquad \text{(D.2-6)}$$

where $\hat{x}$ is the 3-vector of parameters estimates, $(:)^{-1}$ denotes the inverse of a matrix and $(:)^T$ denotes the matrix transpose.

The simulated phase measurements shown in Figure D.2-1 (a total of 101) are generated by adding random phase errors with an rms value of 50 ppm to an oscillator phase drift model with parameters

$$\delta\phi_0 = 1000 \text{ ppm}, \quad \delta f_0 = 10 \text{ ppm/hr and } \delta f_0' = .01 \text{ ppm/hr}^2$$

Solving Eq. D.2-6 using the simulated measurements to obtain the clock model parameter estimates yields

$$\delta\hat{\phi}_0 = 994.6 \text{ ppm}, \quad \hat{\delta f}_0 = 10.18 \text{ ppm/hr} \quad \text{and} \quad \hat{\delta f}_0' = .00914 \text{ ppm/hr}^2$$

The solid line in Figure D.2-1 represents the fit to the measured data using the above parameter estimates. With this fit, the mean and standard deviation of the residual oscillator phase error over the 200-hour period are 1.2 ppm and 53 ppm, respectively. We will return to these results in Section D.4.

D.2.2 Probability and Random Variables

Probability and random variable theory play an important role in the development of Kalman filtering. A random variable X is a variable that takes on values at random. It may be thought of as a function of the outcomes of some random experiment. The probability with which the different values of the random variable occur is specified by the probability *distribution* function $F(x)$, defined as

$$F(x) = Prob(x \leq X) \tag{D.2-7}$$

or the probability density function

$$f(x) = dF(x)/dx \tag{D.2-8}$$

Following the definition of the derivative, $f(x)dx$ can be interpreted as

$$f(x)dx = Prob(x < X \leq x + dx) \tag{D.2-9}$$

Thus $F(x)$ is the probability that the random variable X takes on a value equal to or less than x, while $f(x)dx$ is the probability that X lies in the differential region between x and $x + dx$. A typical distribution function and its corresponding density function are shown in Fig. D.2-2. From the inverse of Eq. (D.2-8),

$$F(x) = \int_{\infty}^{x} f(u)du \tag{D.2-10}$$

From the above definitions it is clear that

$$F(\infty) = 1 \quad \text{and} \quad \int_{-\infty}^{\infty} f(u)du = 1 \tag{D.2-11}$$

D-5
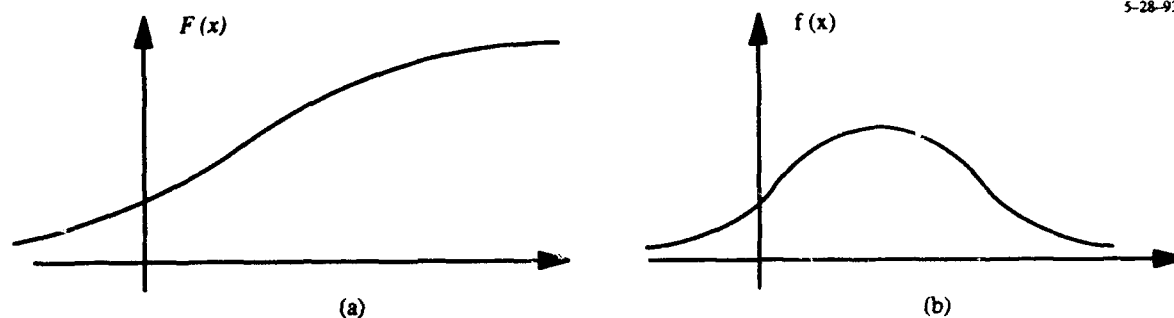
Figure D.2-2　A Typical Probability Distribution (a) and
its Corresponding Density Function (b)

That is, the probability that X is equal to or less than infinity is one and X must lie somewhere on the real line.

Because the estimation problem deals with two sets of random variables, the measurements, z, and the parameter vector (or state), x, one must consider distributions involving multiple random variables. In the case of two random variables, the probability of the joint occurrence of pairs of values is prescribed by the *joint probability distribution function*

$$F_2(x,y) \;=\; Prob(X \leq \text{ and } Y \leq y) \tag{D.2-12}$$

where X and Y are the two random variables under consideration. The corresponding *joint probability density function* is

$$f_2(x,y) \;=\; \partial^2 F_2(x,y)/\partial x \partial y \tag{D.2-13}$$

The individual distribution and density functions can be derived from the joint distribution and density functions. For the X random variable

$$F(x) \;=\; F_2(x, \infty) \tag{D.2-14}$$

and

D-6

$$f(x) = \int\limits_{-\infty}^{\infty} f_2(x, y)dy \qquad (D.2\text{-}15)$$

Corresponding relations give the distribution of Y. The above equations extend directly to the description of the joint behavior of multiple random variables.

Random variables X and Y are said to be independent if the events $(X \leq x)$ and $(Y \leq y)$ are independent. In this case the probability of the joint occurrence of these events is the product of the probabilities for the individual events, i.e.,

$$F_2(x, y) = F_x(x)F_y(y) \qquad (D.2\text{-}16)$$

and

$$f_2(x, y) = f_x(x)f_y(y) \qquad (D.2\text{-}17)$$

Subscripts x and y emphasize the fact that the distributions are different functions of different random variables.

Expectations and Statistics of Random Variables

The *expectation* of a random variable is defined as the sum of all values it may take, each value weighted by the probability with which the value is taken. In this context, expectation may be thought of as a generalized averaging process. This discussion is limited to random variables that take on a continuous range of values. For these variables the summation is done by integration. Thus the expected value (or average value) of x, denoted by $E[X]$ is

$$E[X] = \int\limits_{-\infty}^{\infty} xf(x)dx \qquad (D.2\text{-}18)$$

This is also called the *mean value* of X, the mean of the distribution of X or the *first moment* of X. For simplicity of notation, the expected value of X is often written as m or $\bar{x}$. Another important statistical parameter descriptive of the distribution of X is its *mean-squared value*. This expectation is given by

$$E[X^2] = \int\limits_{-\infty}^{\infty} x^2f(x)dx \qquad (D.2\text{-}19)$$

$E[X^2]$ is also called the *second moment* of X. The root-mean-squared (rms) value of X is the square root of $E[X^2]$. The *variance* of a random variable is the mean-squared deviation of the random variable from its mean. It is often denoted by σ^2 where

$$\sigma^2 = \int_{-\infty}^{\infty} (x - E[X])^2 f(x)dx = E[X^2] - E[X]^2 \qquad \text{(D.2-20)}$$

the square root of the variance, σ, is the *standard deviation* of X. The rms value and the standard deviation of X are equal if X is a zero-mean process.

One consequence of statistical independence that we shall need later involves the expectation of sums of random variables. If X and Y are independent then

$$E[X + Y] = E[X] + E[Y] \qquad \text{(D.2-21)}$$

this result extends to any number of independent random variables.

A very important concept, at the heart of a statistical approach to estimation, is that of *statistical correlation* between random variables. A partial measure of the degree to which two random variables are related is given by the *covariance*, which is the expectation of the product of the deviations of two random variables from their means,

$$E[(X-E[X])(Y-E[Y])] = \int_{-\infty}^{\infty} \int_{-\infty}^{\infty} (x - E[X])(y - E[Y])f_2(x,y)dydx \qquad \text{(D.2-22)}$$

$$= E[XY] - E[X]E[Y]$$

The covariance, normalized by the standard deviations of X and Y is called the *correlation coefficient* and is given by

$$\varrho_{xy} = \frac{E[XY] - E[X]E[Y]}{\sigma_x \sigma_y} \qquad \text{(D.2-23)}$$

The correlation coefficient measures the degree of linear dependence between X and Y. If X and Y are independent, ϱ is zero (the inverse is generally not true, although it is true for normally distributed random variables.). If Y is a linear function of X, e.g., $y = \pm |a|x$ ($a = constant$), then ϱ is ± 1.

D-8

The Uniform and Normal Probability Distributions

Two important probability distributions are the uniform and normal distributions. The uniform distribution is characterized by a constant probability density over a finite interval. The magnitude of the density function is equal to the reciprocal of the interval so as to make the integral of the density function equal unity. This function is shown in Fig. D.2-3a. The normal distribution shown in Fig. D.2-3b, has the analytic form

$$f(x) = \frac{1}{\sqrt{2\pi}\sigma} \exp\left[-\frac{(x-m)^2}{2\sigma^2}\right] \qquad (D.2\text{-}24)$$

where m and σ are the mean and standard deviation of X. Note that the normal distribution is completely specified by its mean and variance. $N(m, \sigma)$ is shorthand notation for the normal distribution. The interval $\pm 1\sigma$ about m represents the 67 percent confidence interval for a normal random variable.

Two jointly normal random variables are described by a *bivariate normal* distribution or density. For zero-mean random variables the normal joint probability density function is

$$f(x_1, x_2) = \frac{1}{2\pi\ \sigma_1\sigma_2\sqrt{1-\varrho^2}} \exp\left[\frac{\frac{x_1^2}{\sigma_1^2} - 2\varrho\frac{x_1}{\sigma_1}\frac{x_2}{\sigma_2} + \frac{x_2^2}{\sigma_2^2}}{2(1-\varrho^2)}\right] \qquad (D.2\text{-}25)$$
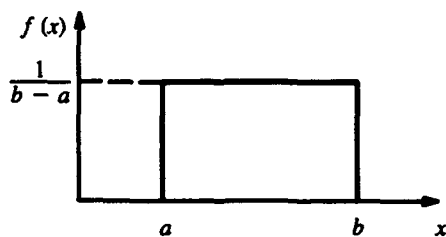
(a) Uniform Probability Density Function　　(b) Normal Probability Density Function
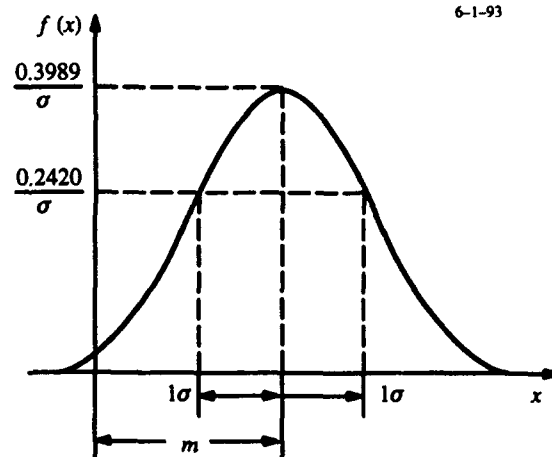
Figure D.2-3　Two Useful Probability Density Functions

D-9

For n random variables, the *multidimensional* or *multivariate* normal density function can be written compactly using vector-matrix notation.

$$f_n(x) = \frac{1}{\sqrt{(2\pi)^{n/2} |P|^{1/2}}} \exp\left[-\frac{1}{2}(x-m)^T P^{-1}(x-m)\right] \qquad \text{(D.2-26)}$$

with

$$x = \left(x_1 \; x_2 \ldots x_n\right)^T, \; m = E[x], \; P_{xx} = E[(x-m)(x-m)^T], \; P_{xx} \text{ an } n \times n \text{ matrix}$$

$$\text{(D.2-27)}$$

The quantities m and P are the mean and covariance of the vector x. Note that the expected value of a vector or matrix is just the vector or matrix containing the expected values of their individual elements. For the case where $n = 2$, the covariance matrix has the form

$$P_{xx} = \begin{bmatrix} E[(x_1-m_1)^2] & E[(x_1-m_1)(x_2-m_2)] \\ E[(x_2-m_2)(x_1-m_1)] & E[(x_2-m_2)^2] \end{bmatrix} = \begin{bmatrix} \sigma_1^2 & \sigma_{12} \\ \sigma_{21} & \sigma_2^2 \end{bmatrix} \qquad \text{(D.2-28)}$$

Because $\sigma_{12} = \sigma_{21}$, P_{xx} is a symmetric matrix. Notice also that the diagonal elements of P are just the mean-square values of the individual components of x. The covariance matrix is important to the development of the Kalman filter equations.

Correlation and Statistical Least-Squares

With the above concepts from probability and random variable theory we can now examine an elementary example in statistical least-squares estimation. If two random variables are correlated, then knowledge of one variable tells something about the other. Consider two zero-mean, jointly distributed random variables, X and Z, with *known* second-order statistics. Assume that x and z are the joint outcomes of an experiment, but only the z outcome is observed. Given z, what is a "good" estimate of x? Since $E[XZ]$ is a measure of the linear dependence between X and Z, a linear estimate is appropriate. Letting $\hat{x}$ denote an estimate for x one has

$$\hat{x} = Kz \qquad \text{(D.2-29)}$$

Defining the error in estimating x as $\tilde{x} = x - Kz$ one obtains

$$\tilde{x}^2 = x^2 + K^2 z^2 - 2Kxz \qquad \text{(D.2-30)}$$

The mean-square estimation error is

$$P_{\tilde{x}\tilde{x}} = E[\tilde{x}^2] = E[x^2] + K^2 E[z^2] - 2KE[xz] \qquad \text{(D.2-31a)}$$

$$= \sigma_x^2 + K^2 \sigma_z^2 - 2K\sigma_{xz} \qquad \text{(D.2-31b)}$$

K is now be selected to minimize the mean-square error in estimating x. This is done by setting the partial derivative of $P_{\tilde{x}\tilde{x}}$ with respect to K equal to zero and solving the resulting equation for K.

$$\partial P_{\tilde{x}\tilde{x}}/\partial K = 2K\sigma_z^2 - 2\sigma_{xz} = 0 \qquad \text{(D.2-32a)}$$

or

$$K = \sigma_{xz}\,\sigma_z^{-2} \qquad \text{(D.2-32b)}$$

Substituting this value for K into Eq. D.2-31b, the mean-squared estimation error becomes

$$P_{\tilde{x}\tilde{x}} = \sigma_x^2 - \sigma_{xz}^2 \sigma_z^{-2} = \sigma_x^2 - \sigma_{xz}\sigma_z^{-2}\sigma_{zx} = \sigma_x^2(1-\varrho^2) \qquad \text{(D.2-33)}$$

The scalar estimation problem can be generalized to the multidimensional or vector case. The details of the derivation will not be given here, but a plausible argument can be made by first drawing the following correspondences between scalar and vector correlations in the form of $P_{\tilde{x}\tilde{x}}$ following the second equals sign in Eq. D.2-33. Let x and z be n and m dimensional vectors, re ctively, and let

$$P_{xx} \sim \sigma_x^2; P_{zz} \sim \sigma_z^2; P_{xz} \sim \sigma_{xz} \text{ and } P_{xz}^T = P_{zx} \sim \sigma_{zx} \qquad \text{(D.2-34)}$$

where P_{xx}, P_{zz} and P_{xz} are n by n, m by m and n by m covariance matrices, respectively. Then

$$\hat{x} = Kz \qquad \text{(D.2-35a)}$$

where the n by m optimum gain matrix, K, is given by

$$K = P_{xz}P_{zz}^{-1} \qquad \text{(D.2-35b)}$$

Again defining the estimation error $\tilde{x}$ as $x - Kz$ one has

$$P_{\tilde{x}\tilde{x}} = E[\tilde{x}\tilde{x}^T] = P_{xx} - P_{xz}P_{zz}^{-1}P_{zx} \qquad \text{(D.2-35c)}$$

Let's carry this process one step further. Suppose the measurement, z, is a known to be of the form of Eq. D.2-5, that is, a linear combination of x corrupted by noise v, where $v = N(0, R)$. Then

$$P_{zz} = E[(Hx + v)(Hx + v)^T] = HP_{xx}H^T + R \text{ and } P_{xz} = E[xz^T] = E[x(hx + v)^T] = P_{xx}H^T$$

$$(D.2\text{-}36)$$

so that

$$K = P_{xx}H^T[HP_{xx}H^T + R]^{-1} \qquad (D.2\text{-}37a)$$

and

$$P_{\tilde{x}\tilde{x}} = P_{xx} - P_{xx}H^T[HP_{xx}H^T + R]^{-1}HP_{xx} = [I - KH]P_{xx} \qquad (D.2\text{-}37b)$$

Eq. D.4-37 will show up again in the derivation of the Kalman filter in Section D.4.

Random Processes

So far we have considered only static random variables. For example, we assumed the oscillator drift parameters in Section D.2.1 to be unknown constants. A random (or stochastic) process brings in the element of time. As shown in Fig. D.2-4, a random process may be visualized as a collection, or *ensemble*, of functions of time, any one of which may be observed on a given trial of an experiment. The value of the process at time t_1 is a random variable. On repeated trials of the experiment, $x(t_1)$ takes on different values at random. Thus the probability distribution or density is a function of time, i.e.,

$$F(x_1, t_1) = Prob[x(t_1) \le x_1] \qquad (D.2\text{-}38)$$

and

$$f(x_1, t_1) = dF(x_1, t_1)/dx_1 \qquad (D.2\text{-}39)$$
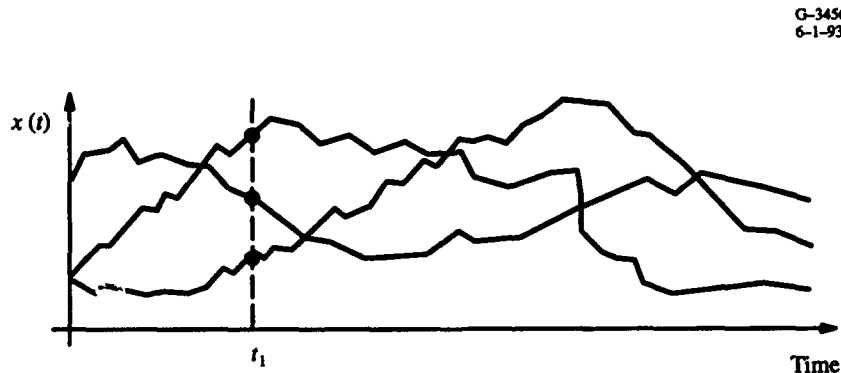
G-34562
6-1-93

Figure D.2-4 An Ensemble of Random Processes

These functions define, in a probabilistic sense, the range of amplitudes a random process undergoes. To gain a sense of how the process is likely to vary over time one must examine a member of the ensemble at two or more times. The probability of the occurrence of a pair of values is given by the second-order joint probability distribution or density

$$F(x_1, t_1; x_2, t_2) = Prob(x(t_1) \leq x_1 \text{ and } x(t_2) \leq x_2) \qquad \text{(D.2-40)}$$

and

$$f(x_1, t_1; x_2, t_2) = \partial^2 F(x_1, t_1; x_2, t_2)/\partial x_1 \, \partial x_2 \qquad \text{(D.2-41)}$$

In practice the distributions of random processes are rarely measured. Only the first and second moments of these distributions are commonly used. For a single random process this moment, called the autocorrelation function, is defined as

$$R_{xx}(t_1, t_2) = E[x(t_1)x(t_2)] = \int_{-\infty}^{\infty} \int_{-\infty}^{\infty} x_1, x_2 \, f(x_1, t_1; x_2, t_2) dx_1 dx_2 \qquad \text{(D.2-42)}$$

If the random process is wide-sense stationary a further simplification of Eq. D.2-42 is possible. A wide-sense stationary random process is one whose first- and second-order statistical properties do not change with time. For this case $f(x, t)$ is independent of t and $f(x_1, t_1; x_2, t_2)$ is a function only of the *time difference*, $\tau = t_2 - t_1$. Thus

$$R_{xx}(\tau) = E[x(t)x(t + \tau)] \qquad \text{(D.2-43)}$$

As in the case of random variables, if there is significant correlation between $x(t)$ and $x(t + \tau)$, it should be possible to estimate the latter with some knowledge of the former. Thus one can predict the future of a random process with knowledge of its current value and its autocorrelation function.

Some Simple Random Processes

Gaussian Random Process — A Gaussian random process is one in which all joint density functions are multivariate normal. The process is thus completely defined by its mean and variance. "Gaussian" here refers to the amplitude distribution of the process and says nothing about its time variation. As a direct consequence of the Central Limit Theorem, Gaussian random processes accurately describe many natural phenomena.

White Noise — White noise is a random process with constant power at all frequencies. Its autocorrelation function has value only at $\tau = 0$. There is zero correlation between any two non-coincident time points of a white noise process. Thus present knowledge of a white noise process tells us nothing about its future. Although an idealized concept, white noise is a very useful approximation in situations where the disturbing noise is wideband compared to the system bandwidth. Also, many useful band-limited random processes can be simulated by passing white noise through a suitable filter. Figure D.2-5a shows a sample from a white noise process.

Gauss-Markov Random Processes — Gauss-Markov (G-M) random processes are a special class of random processes which can be modeled and simulated by passing Gaussian white noise
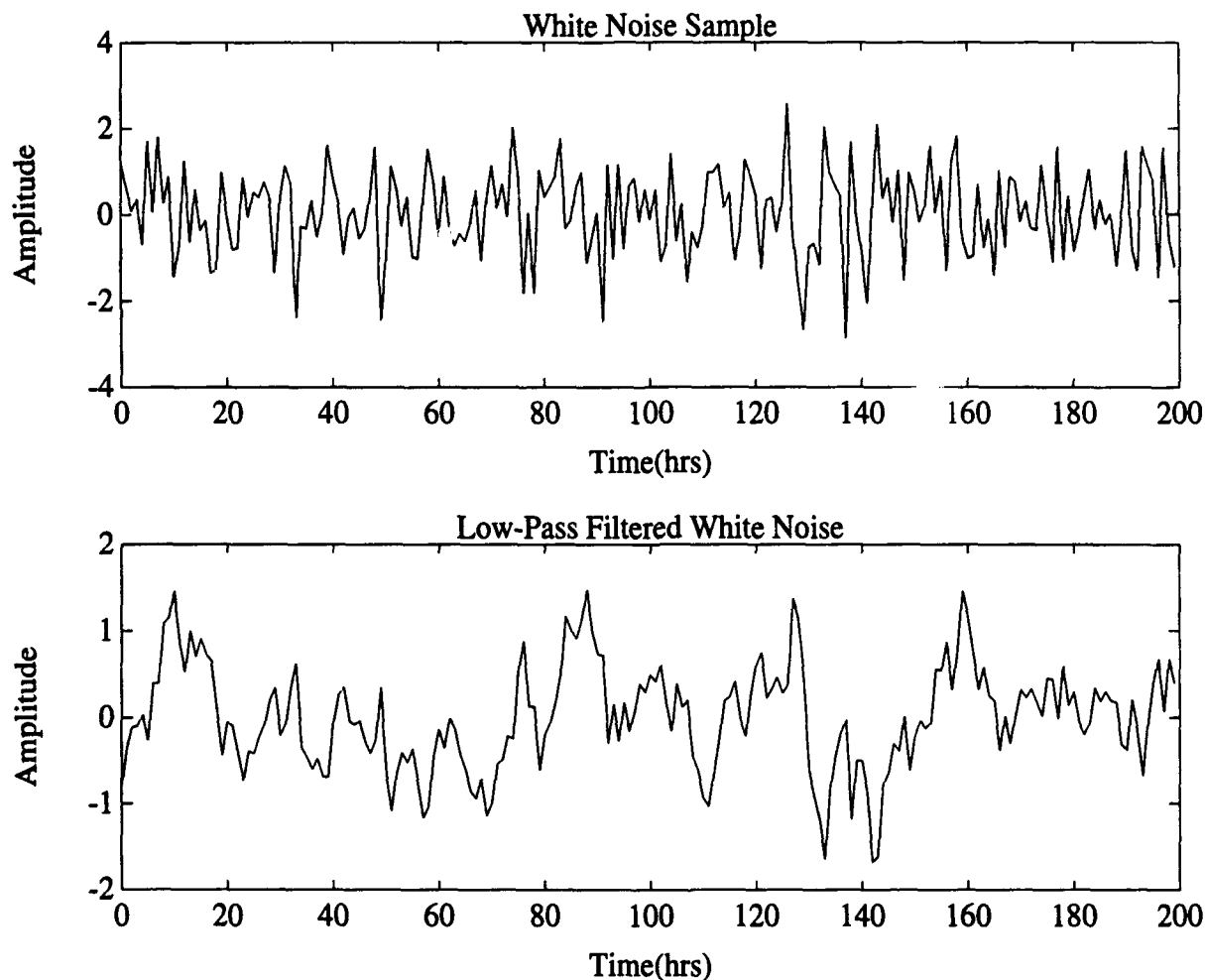
Figure D.2-5   Sample White Noise (a) and Gauss-Markov (b) Random Processes

D-14

through filters. For a first-order G-M process, the probability distribution for the process at time t_k depends only on the value at one point immediately in the past, t_{k-1}. A wide-sense stationary continuous-time first-order Markov process, $x(t)$, obeys the differential equation

$$dx/dt + \beta x = w \qquad \text{(D.2-44)}$$

where w is white noise. If w is Gaussian, x is a Gauss-Markov random process. The autocorrelation function for a zero-mean first-order G-M process is

$$R(\tau) = \sigma^2 \exp(-\beta|\tau|) \qquad \text{(D.2-45)}$$

where σ^2 is the mean-square value of x. The correlation dies away exponentially in time shift, τ. The *correlation time* of the process, the $1/e$ point, is $1/\beta$. Knowledge of the present value of x tells us much about future values less than $1/\beta$ time units away. A typical sample from a first-order G-M process is shown in Figure D.2-5b. It was obtained by passing the white noise sample of Figure D.2-5a through a first-order low-pass filter. Notice that the G-M process is much smoother and shows a much slower variation with time.

D.3   LINEAR DYNAMICAL SYSTEMS AND STATE-SPACE

Kalman filtering applications require that the system under consideration be described by differential or difference equations. These equations describe the time-evolution of a system in response to initial conditions and random disturbances. Because of the high dimensionality of modern systems a compact notation for these equations is needed. That notation is the vector-matrix or *state-space* formulation. The dynamics of a linear, lumped-parameter system excited by random disturbances can be represented by a first-order vector-matrix equation

$$\underline{\dot{x}} = F(t)\underline{x} + G(t)\underline{w}(t) \qquad \text{(D.3-1)}$$

where $x(t)$ is the $(n \times 1)$ system *state vector*, $w(t)$ is an $(m \times 1)$ vector of random forcing functions and F and G are conformable matrices arising in the formulation. Figure D.3-1a illustrates the equation. The state vector, x, is not unique, but is any set of quantities sufficient to describe the unforced motion of the system.

Any n^{th}-order linear differential equation can be written as a set of first-order differential equations. Consider the simple system illustrated in Figure D.3-2. It consists of a rolling mass-spring-dashpot within an enclosure which is being accelerated by a force, $w(t)$. It represents the model for a simple

D-15
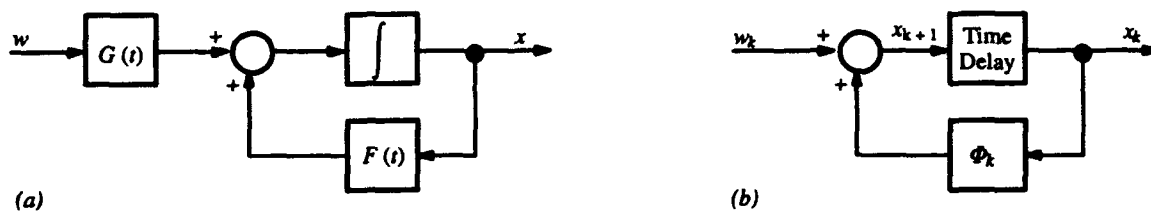
Figure D.3-1   Block Diagram of Continuous-(a) and Discrete
(b) Time Linear Dynamic Systems
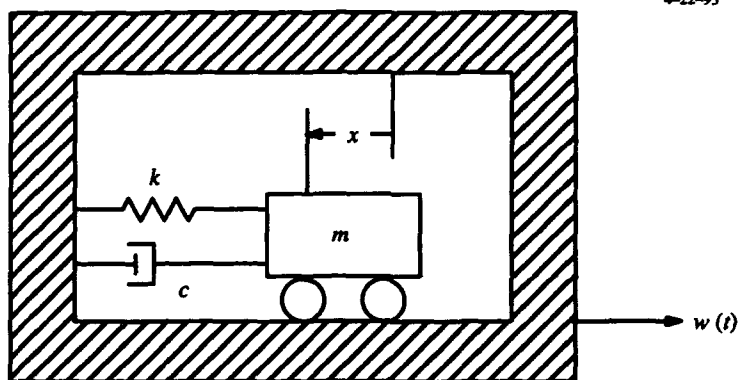
Figure D.3-2   A Simple Second-Order Physical System

accelerometer. x is the displacement of the proof mass, m, from its unforced rest position. The second-order differential equation governing the time evolution of x is

$$m\ddot{x} + c\dot{x} + kx = mw(t) \qquad (D.3-2)$$

Defining a state vector $x^T = [x_1 \ x_2]$, the equation for the system dynamics is

$$\begin{bmatrix} \dot{x}_1 \\ \dot{x}_2 \end{bmatrix} = \begin{bmatrix} 0 & 1 \\ -k/m & -c/m \end{bmatrix} \begin{bmatrix} x_1 \\ x_2 \end{bmatrix} + \begin{bmatrix} 0 \\ 1 \end{bmatrix} w(t) \qquad (D.3-3)$$

The solution to Eq. D.3-1 can be written in the form

$$x(t) = \Phi(t, t_0)x(t_0) + \int_{t_0}^{t} \Phi(t, \ell)G(\ell)w(\ell)d\ell \qquad (D.3-4)$$

where $x(t_0)$ is the initial value of the state vector at time t_0 and $\Phi(t, t_0)$ is the state transition matrix which satisfies the differential equation

$$\dot{\Phi}(t, t_0) = F(t)\Phi(t, t_0); \quad \Phi(t_0, t_0) = I \text{ (the identity matrix)} \tag{D.3-5}$$

The first term on the right-hand side of Eq. D.3-4 represents the unforced system response to initial conditions, while the second term is the system response to the forcing or driving term, $w(t)$. For stationary systems F is constant and Φ is a function only of the time difference $t - t_0 = \Delta t$. Then

$$\Phi(\Delta t) = \exp(F\Delta t) = I + F\Delta + (F\Delta t)^2/2 + (F\Delta t)^3/3! + \ldots \tag{D.3-6}$$

Equation D.3-4 may be used to relate the state at two instants of time, t_k and t_{k+1}. The resulting difference equation takes the form

$$x_{k+1} = \Phi_k x_k + w_k \tag{D.3-7}$$

where $\Phi_k = \Phi(t_{k+1}, t_k)$ and $w_k = \displaystyle\int_{t_k}^{t_{k+1}} \Phi(t, \ell)G(\ell)w(\ell)d\ell$.

An Example: Consider the spring-mass-dashpot system of Eq. D.3-3. Assign the follow values to the model parameters: $m = 1$ Kg; $k = 1$ N/m; $c = 0.5$ N/m/sec and $\Delta t = 0.1$ sec. Then

$$\Phi(0.1) = \exp\begin{bmatrix} 0 & 1 \\ -1 & -0.5 \end{bmatrix} 0.1 = \begin{bmatrix} 0.9951 & 0.0974 \\ -0.0794 & 0.9464 \end{bmatrix}$$

Figure D.3-3 shows the response of this system to initial position offset of 10 cm.

If $w(t)$ is a random process then $x(t)$ is also a random process. If $w(t)$ is a continuous white Gaussian random process w_k is a discrete time Gaussian white sequence and

$$E[w_k w_j] = \begin{cases} Q_k; & k = j \\ 0; & k \neq j \end{cases} \tag{D.3-8}$$

where

$$Q_k = \int_{t_k}^{t_{k+1}} \Phi(t, \ell)G(\ell)Q(\ell)G^T(\ell)\Phi^T(t, \ell)d\ell \tag{D.3-9}$$
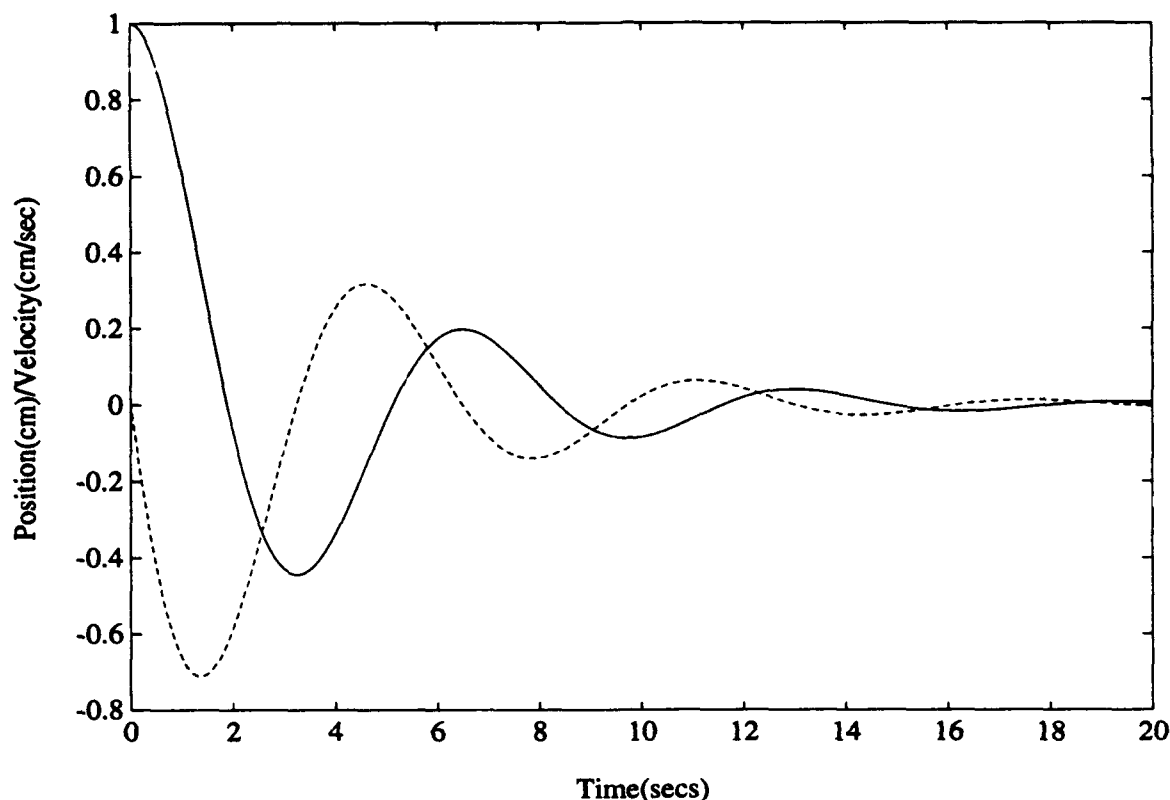
Figure D.3-3   Second-Order System Response to Initial Position Offset;
Position (solid line) Velocity (dotted line)

Notice that the $E[x_k w_k^T] = 0$, i.e., the present state is uncorrelated with the present forcing term because $w(t)$ acts over the interval (t_k, t_{k+1}), the limits on the integral in Eq. D.3-9. If $w(t)$ is zero-mean, w_k and x_k are also zero-mean. The discrete time version of the state equations is very useful for computer simulation and essentially mandatory for Kalman filter implementation.

Some Simple Random Process Models — We have already seen one simple random process, the exponentially correlated random process. In this section we examine three additional simple random processes that find wide use in modeling primitive system error sources; the random constant, the random walk and the random ramp.

Random Constant — The random constant is actually a static random variable. It obeys the state differential and difference equations

$$\dot{x} = 0 \quad \text{and} \quad x_{k+1} = x_k \tag{D.3-10}$$

The random constant can be viewed as the output of an integrator that has no input but does have a random initial condition. [See Figure D.3-4.]

Random Walk — A random walk is generated by integrating white noise. The differential and difference equations for the random walk are

$$\dot{x} = w \quad \text{and} \quad x_{k+1} = x_k + w_k \tag{D.3-11}$$

where w is a stationary continuous white noise random process and w_k is a white noise sequence. The random walk model is illustrated in Figure D.3-4. Recognizing that $\Phi_k = 1$ for the scalar random walk, the covariance for this process is

$$P_{k+1} = P_k + Q \tag{D.3-12}$$

The covariance is seen to grow linearly in time without bound.

Random Ramp — As with the oscillator phase error model of Section D.2, random errors often exhibit growing trends with time. A linear growth trend can be represented by a random ramp. The growth rate of a random ramp is itself a random variable. A random ramp is described by two random variables

$$\dot{x}_1 = x_2 \quad \text{and} \quad \dot{x}_2 = 0 \tag{D.3-13}$$

The state, x_1, is the random ramp process; x_2 is an auxiliary variable whose initial condition represents the slope of the ramp. The initial covariance of x_2 quantifies our uncertainty in the value of that slope. The extension to parabolic and higher-order growth rates is straightforward. Figure D.3-4 shows a three-state model with combined outputs of a random bias, random walk, random ramp, and random parabola that will model the oscillator phase error discussed in Section D.2.

G-34560
5-24-93
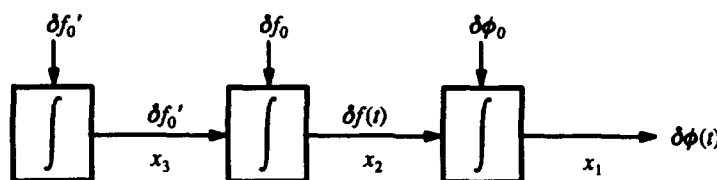
Figure D.3-4   Three-State Model for Oscillator Phase Error

Propagating System Estimates and Covariance — Consider the random process described by Eq. D.3-7 where w_k is a zero-mean Gaussian white random sequence with covariance Q_k. Suppose that an estimate of the state at time t_k is known with an uncertainty expressed by the error covariance matrix

$$P_k = E\left(\tilde{x}_k \tilde{x}_k{}^T\right) \tag{D.3-14}$$

where the error, $\tilde{x}_k = x_k - \hat{x}_k$, is the *difference* between the true state and the estimate, $\hat{x}_k$. An unbiased estimate of x_{k+1} is desired; that is, one for which $E[\tilde{x}_{k+1}] = 0$. A plausible estimate for x_{k+1} is obtained by taking the expected value of both sides of Eq. D.3-7.

$$\hat{x}_{k+1} = E[x_{k+1}] = E[\Phi_k x_k + w_k] = \Phi_k E[x_k] + E[w_k]$$

$$= \Phi \hat{x}_k \tag{D.3-15}$$

where the expected value of the sum is the sum of the expected values because x_k and w_k are independent and the expected value of w_k is zero. To show that the estimate is unbiased, subtract Eq. D.3-15 from D.3-7 to obtain

$$\tilde{x}_{k+1} = \Phi_k \tilde{x}_k + w_k \tag{D.3-16}$$

Taking the expected value of both sides of Eq. D.3-16 yields

$$E[\tilde{x}_{k+1}] = \Phi_k E[\tilde{x}_k] + E[w_k] = 0 \tag{D.3-17}$$

where it is assumed that the previous estimate, $\hat{x}_k$, is unbiased also. Equation D.3-16 can be used to develop an expression for projecting the covariance matrix from time t_k to t_{k+1}.

$$\tilde{x}_{k+1}\tilde{x}_{k+1}{}^T = (\Phi_k \tilde{x}_k + w_k)(\Phi_k \tilde{x}_k + w_k)^T \tag{D.3-18}$$

$$= \Phi_k \tilde{x}_k \tilde{x}_k{}^T - \Phi_k \tilde{x}_k w_k{}^T - w_k \tilde{x}_k{}^T \Phi_k{}^T + w_k w_k$$

Taking expected values on both sides of Eq. D.3-18 and recognizing that x_k and w_k are uncorrelated, the equation for extrapolating the estimation error covariance is

$$P_{k+1} = \Phi_k P_k \Phi_k{}^T + Q_k \tag{D.3-19}$$

D.4 THE DISCRETE-TIME KALMAN FILTER

Recursive Filters — The least-squares estimator of Eq. D.2-6 requires that all measurements be processed simultaneously. If an additional measurement becomes available, all data, past and present, must be reprocessed to obtain a new estimate. Recursive filters do not need to store all past measurements. They use only the new data to make an incremental correction to the prior estimate. An example best illustrates this concept.

Consider the problem of estimating an unknown scalar constant, x, based on k noise-corrupted samples, $z_i = x + v_i$ ($i = 1, 2, \ldots k$). Here v_i is a measurement noise assumed to be a white sequence. A simple averaging of the z_i will produce a minimum variance, unbiased estimate, $\hat{x}$, of x.

$$\hat{x}_k = \frac{1}{k} \sum_{i=1}^{k} z_i \qquad (D.4\text{-}1)$$

When a additional measurement is made a new estimate is formed

$$\hat{x}_{k+1} = \frac{1}{k+1} \sum_{i=1}^{k+1} z_i \qquad (D.4\text{-}2)$$

This estimate can be rewritten to bring out the prior estimate

$$\hat{x}_{k+1} = \frac{k}{k+1} \left[\frac{1}{k} \sum_{i=1}^{k} z_i \right] + \frac{1}{k+1} z_{k+1} = \frac{k}{k+1} \hat{x}_k + \frac{1}{k+1} z_{k+1} \qquad (D.4\text{-}3)$$

Thus, by using the prior estimate, $\hat{x}_k$, past data can be discarded. Only the new data is required to make an incremental correction to x. This is emphasized by writing Eq. D.4-3 in the alternative recursive form

$$\hat{x}_{k+1} = \hat{x}_k + \frac{1}{k+1} (z_{k+1} - \hat{x}_k) \qquad (D.4\text{-}4)$$

where the new estimate is given as linear combination of the prior estimate plus an appropriately weighted *difference* between the new measurement and its expected value, the prior estimate. The quantity $(z_{k+1} - \hat{x}_k)$ is called the measurement *residual*. The residual may also be written as $[z_{k+1} - \hat{z}_{k+1}(-)]$ to emphasize that $\hat{z}_{k+1}(-)$ is our best estimate z_{k+1} *before* the (k+1)[th] measurement is available.

The above example deals with scalar quantities, but the generalization to time varying vectors proceeds directly. Consider a discrete time system governed by the vector difference equation

$$x_k = \Phi_k x_{k-1} + w_{k-1} \qquad \text{(D.4-5)}$$

where x_k is the ($n \times 1$) state vector and w_k is an ($n \times 1$) vector of zero mean white noises with covariance Q_k. Measurements are taken of linear combinations the system state variables, corrupted by additive white noise uncorrelated with the state. The measurement equation is thus written as

$$z_k = H_k x_k + v_k \qquad \text{(D.4-6)}$$

where z_k is a set of m scalar measurements arranged into vector form

$$z_k = [z_{1k}, z_{2k}, \ldots z_{mk}]^T \qquad \text{(D.4-7)}$$

v_k is an ($m \times 1$) vector of zero-mean white noise with covariance R_k and H_k is the ($m \times n$) measurement matrix at time t_k which describes the linear combinations of state variables that make up z_k is the absence of noise.

Given a *prior* estimate of the state at time t_k, denoted $\hat{x}_k(-)$, an updated estimate, $\hat{x}_k(+)$, is sought based on the new measurement z_k. Analogous to Eq. D.4-4, this estimate will have the recursive form

$$\hat{x}_k(+) = \hat{x}_k(-) + K_k[(z_k - H_k \hat{x}_k(-)] \qquad \text{(D.4-8)}$$

where $H_k \hat{x}_k(-)$ is the best estimate of the measurement z_k before it is available. (Note: If we "guess" the measurement perfectly based on all the previous data as embodied in $\hat{x}_k(-)$, the measurement residual, $[(z_k - H_k \hat{x}_k(-)]$, will be zero and the measurement has no new information about x)

The Kalman Filter Update — An expression for the Kalman filter gain, K_k, is obtained by requiring the gain to be selected so as to minimize the mean-square error in estimating the state, x. Using the tilde (~) to denote estimation error, the errors before and after an update are

$$\hat{x}_k(-) = x_k + \tilde{x}_k(-) \text{ and } \hat{x}_k(+) = x_k + \tilde{x}_k(+) \qquad \text{(D.4-9)}$$

Subtracting the state, x_k, from both sides of Eq. D.4-8 and using definitions D.4-9 yields

$$\tilde{x}_k(+) = \tilde{x}_k(-) + K_k H_k \tilde{x}_k(-) + K_k v_k = (I - K_k H_k)\tilde{x}_k + K_k v_k \qquad \text{(D.4-10)}$$

An expression for the mean-square estimation error is obtained by first computing the error covariance, $P_k(+)$ in terms of $P_k(-)$ and the measurement error covariance R_k. The post-update error covariance is given by

$$P_k(+) = E[\{(I - K_k)\quad\quad K_k v_k\}\{(I - K_k H_k)\tilde{x}_k(-) + K_k v_k\}^T]$$

$$= (I - K_k H_k)P_k(-)(I - K_k H_k)^T + K_k R_k K_k^T \qquad (D.4\text{-}11)$$

where we have used the fact that $E[\hat{x}_k(-)v_k^T] = E[v_k \hat{x}_k^T(-)] = 0$.

Recall that the diagonal terms of P_k are simply the variances of the estimation error for each component of x. The total variance of the state estimation error, J_k, is therefore

$$J_k = \sum_{i=1}^{n} x_{ik}^2(+) = \text{trace}[P_k(+)] \qquad (D.4\text{-}12)$$

Taking the partial derivative of J_k with respect to K_k and setting the result to zero yields

$$J_k = -2(I - K_k H_k)P_k(-)H_k^T + 2K_k R_k = 0$$

or

$$K_k = P_k(-)H_k^T[H_k P_k(-)H_k^T + R_k]^{-1} \qquad (D.4\text{-}13)$$

Substituting Eq. D.4-13 into Eq. D.4-11 gives, after some manipulation,

$$P_k(+) = P_k(-) - P_k(-)H_k^T[H_k P_k(-)H_k^T + R_k]^{-1}H_k P_k(-) = [I - K_k H_k]P_k(-)$$

$$(D.4\text{-}14a)$$

Notice that Eqs. D.2-13 and D.2-14 are identical to Eqs. D.2-37a and b. So far in this section we have described the change in the state estimate and the estimation error covariance that occurs across a measurement *update*. The *extrapolation* of the state estimate and error covariance between measurements is given by Eqs. D.3-15 and D.3-19.

Discrete time Kalman filtering is seen to comprise a repetitive sequence of update-extrapolate-update-extrapolate ... operations. Figure D.4-1 shows a timing diagram of the quantities involved in the discrete Kalman filter. The discrete Kalman filter equations are summarized in Table D.4-1. The covariance calculations alone provide K_k. There is no feedback from the state equations to the covariance equations. Thus the gain and covariance can be computed *prior* to the actual filtering operation. We shall return to this point in the examples.
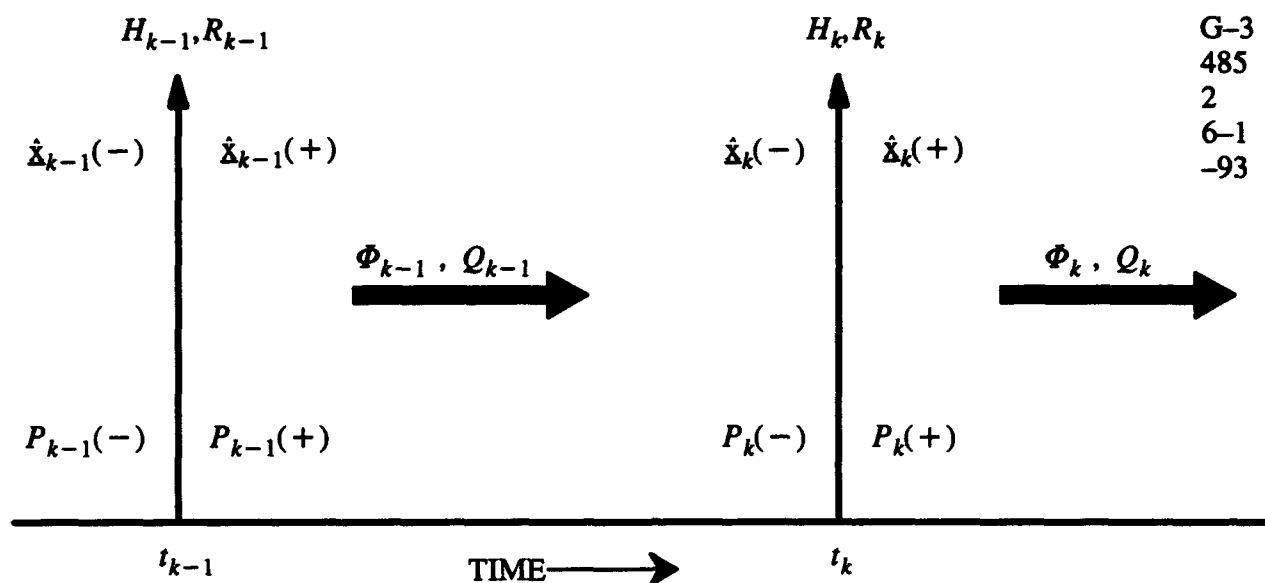
Figure D.4-1   Schematic of Kalman Recursion

Table D.4-1 Summary of Discrete Kalman Filter Equations

System Model	$x_k = \Phi_{k-1} x_{k-1} + w_{k-1}$, $w_k \sim N(0, Q_K)$
Measurement Model	$z_k = H_k x_k + v_k$, $v_k \sim N(0, R_K)$
Initial Conditions	$E[x(0)] = \hat{x}_0$, $E[(x(0) - \hat{x}_0)(x(0) - \hat{x}_0)^T] = P_0$
Other Assumptions	$E[w_k v_j{}^T] = 0$ *for all j, k*
State Estimate Extrapolation	$\hat{x}_k(-) = \Phi_{k-1}\, \hat{x}_{k-1}(+)$
Error Covariance Extrapolation	$P_k(-) = \Phi_{k-1} P_{k-1}(+)\, \Phi_{k-1}{}^T + Q_{k-1}$
State estimate Update	$\hat{x}_k(+) = \hat{x}_k(-) + K_k[z_k - H_k \hat{x}_k(-)]$
Error Covariance Update	$P_k(+) = [I - K_k H_k]\, P_k(-)$
Kalman Gain Matrix	$K_k = P_k(-)\, H_k{}^T [H_k P_k(-) H_k{}^T + R_k]^{-1}$

The Kalman gain, K, can be written in a in terms of $P_k(+)$. After some matrix algebraic manipulation one obtains

$$K_k = P_k(+) H_k{}^T R_k{}^{-1} \tag{D.4-14b}$$

In this form we see that the gain is directly proportional to the uncertainty in x and inversely proportional to the measurement quality. Thus if knowledge of the state is poor relative to the measurement accuracy a heavy weighting in placed on the measurement. If the reverse is true the new measurement will be downgraded relative to the prior estimate of x.

Some Kalman Filter Examples

Example D.4.1: Let's look again at the problem of estimating a random constant in the Kalman filtering context. The scalar equations describing the situation are

System: $x_{k+1} = x_k$

Measurement: $z_k = x_k + v_k \; ; \quad v_k \sim N(0, r_0)$

For this problem $\Phi_k = H_k = 1$ and $Q_k = 0$ so that the covariance extrapolation and measurement update equations are

Extrapolation: $p_{k+1}(-) = \overset{\bullet}{p}_k(+)$

and

Update: $p_{k+1}(+) = p_{k+1}(-) - p_{k+1}(-)[p_{k+1}(-) + r_0]^{-1} p_{k+1}(-)$

$$= \frac{p_{k+1}(-)}{1 + p_{k+1}(-)/r_0} = \frac{p_k(+)}{1 + p_k(+)/r_0} \tag{D.4-15}$$

Given an initial uncertainty in the random constant, say p_0, Eq. D.4-15 can be solved to yield

$$p_k(+) = \frac{p_0/r_0}{[1 + (p_0/r_0)k]} \tag{D.4-16}$$

The discrete optimal filter then becomes

$$\hat{x}_{k+1} = \hat{x}_k + \frac{p_0/r_0}{[1 + (p_0/r_0)k]} [z_k - \hat{x}_k] \tag{D.4-17}$$

The optimum gain is a function of the *ratio* of p_0, the initial uncertainty in x, to r_0, the uncertainty or variance in the measurement. If p_0 is large compared to r_0 the gain is large and the measurement is heavily weighted relative to the prior estimate. Comparing Eq. (D.4-17) to Eq. (D.4-4), the gain in both cases is seen to converge to $1/k$ for large k. Thus simple averaging is asymptotically optimum. For

small k, however, the Kalman filter will provide a smaller estimation error when the statistics, p_0 and r_0, are known.

Example D.4.2: Consider the continuous-time first-order Gauss-Markov process of Eq. D.2-44. The discrete-time system and measurement equations for this process are

System: $\qquad\qquad x_{k+1} = \Phi_k x_k + w_k; \ w_k \sim N(0, q_k)$ $\qquad\qquad$ (D.4-18a)

Measurement: $\qquad z_k = x_k + v_k \ ; \ v_k \sim N(0, r_0)$ $\qquad\qquad$ (D.4-18b)

Assuming $w(t)$ is a quasi-stationary white random process and $t_{k+1} - t_k = \Delta t = const.$, then $\Phi = \exp[-\beta \Delta t] = B$ and $w_k \sim N(0, q_0)$ and the Kalman filter equations become

Extrapolation: $\qquad \hat{x}_{k+1}(-) = B\hat{x}_k(+)$

$$p_{k+1}(-) = B^2 p_k(+) + q_0$$

Update: $\qquad\qquad K_k = \dfrac{p_k(-)/r_0}{1 + p_k(-)/r_0}$

$$\hat{x}_k(+) = \hat{x}_k(-) + \frac{p_k(-)/r_0}{[1 + (p_k(-)/r_0)k]} [z_k - \hat{x}_k(-)] \qquad \text{(D.4-19)}$$

and

$$p_k(+) = \frac{p_k(-)}{1 + p_k(-)/r_0}$$

The update equations are identical to those for example D.4-1. Only the extrapolation equations change to reflect the difference between the random constant and the Gauss-Markov process. The covariance of the random constant estimation error will ultimately decay to zero and the x will be determined with no error. For the G-M process, the covariances $p(+)$ ' $p(-)$ will reach constant, positive values because the system is continually excited by random . . . The steady-state values will depend upon the values for P, q and r_0.

Clock Calibration Revisited — Figure D.3-4 presented a three-state dynamic model for the oscillator drift first discussed in Section D.2. This model may be used in a recursive Kalman filter based oscillator calibration. The state equations for the oscillator drift model are:

$$\dot{x}_1 = x_2 \, , \quad \dot{x}_2 = x_3 \quad \text{and} \quad \dot{x}_3 = 0 \tag{D.4-20}$$

where: $x_1(t) = \phi(t)$, $x_1(0) = \phi_0$, $x_2(t) = \delta f(t)$, $x_2(0) = \delta f_0$ and $x_3(t) = \delta f_0'$. The least-squares oscillator calibration fit a polynomial with three *static* coefficients to the phase drift after collecting 200 hrs of data. In the Kalman filter approach, the oscillator coefficients are initial conditions on the state. These initial values decay over time as the Kalman filter tracks the current phase and frequency values of clock error. In order to compare Kalman filter and least-squares results, we must add two extra initial condition states to the clock error model. These states are the unknown constants

$$\dot{x}_4 = 0; \quad x_4(0) = \phi_0 \quad \text{and} \quad \dot{x}_5 = 0; \quad x_5(0) = \delta f_o' \tag{D.4-21}$$

The system and measurement equations in vector-matrix form are now

$$\dot{x} = Fx \quad \text{and} \quad z = Hx + v \tag{D.4-22}$$

where

$$F = \begin{bmatrix} 0 & 1 & 0 & 0 & 0 \\ 0 & 0 & 1 & 0 & 0 \\ 0 & 0 & 0 & 0 & 0 \\ 0 & 0 & 0 & 0 & 0 \\ 0 & 0 & 0 & 0 & 0 \end{bmatrix} \; ; \quad \Phi(t) = \begin{bmatrix} 1 & t & t^2/2 & 0 & 0 \\ 0 & 1 & t & 0 & 0 \\ 0 & 0 & 1 & 0 & 0 \\ 0 & 0 & 0 & 1 & 0 \\ 0 & 0 & 0 & 0 & 1 \end{bmatrix} = \begin{bmatrix} 1 & 2 & 2 & 0 & 0 \\ 0 & 1 & 2 & 0 & 0 \\ 0 & 0 & 1 & 0 & 0 \\ 0 & 0 & 0 & 1 & 0 \\ 0 & 0 & 0 & 0 & 1 \end{bmatrix} \text{ for t=2hrs}$$

$$H = [1 \; 0 \; 0 \; 0 \; 0] \quad \text{and} \quad v = N(0, r_0) = N(0, (50\text{ppm})^2) \tag{D.4-23}$$

Assuming we have no prior knowledge of the oscillator drift parameters, set the initial state estimate to zero and the initial covariance to some large value, i.e.,

$$\hat{x}_0 = 0 \text{ and } P_0(-) = 100 \begin{bmatrix} (100)^2 & 0 & 0 & (100)^2 & 0 \\ 0 & (10)^2 & 0 & 0 & (10)^2 \\ 0 & 0 & (.01)^2 & 0 & 0 \\ (100)^2 & 0 & 0 & (100)^2 & 0 \\ 0 & (10)^2 & 0 & 0 & (10)^2 \end{bmatrix} \tag{D.4-24}$$

Setting the initial covariances to 100 times the values used in the simulation of Section D.2 tells the filter that there is no prior knowledge of the oscillator coefficients and is equivalent to the static least-squares

fitting process. Notice that the (4,1) and (1,4) off-diagonal terms of P_0 are equal to their on-diagonal values. This tells the filter algorithm that x_1 and x_4 are unity correlated at time t_0. This is the "trick" one must play to get the Kalman algorithm to estimate initial conditions. It is, in effect, a fixed point smoothing process. The (2,5) and (5,2) terms of P_0 are set to their on-diagonal values for the same reason.

Figure D.4-2 shows the the time history of the Kalman filter oscillator phase offset estimate over the 200-hour period. Unlike the smooth polynomial fit of Figure D.2-1, the Kalman filter tends to track the measurements more closely in the early phase of the calibration period, before it has fully "learned"
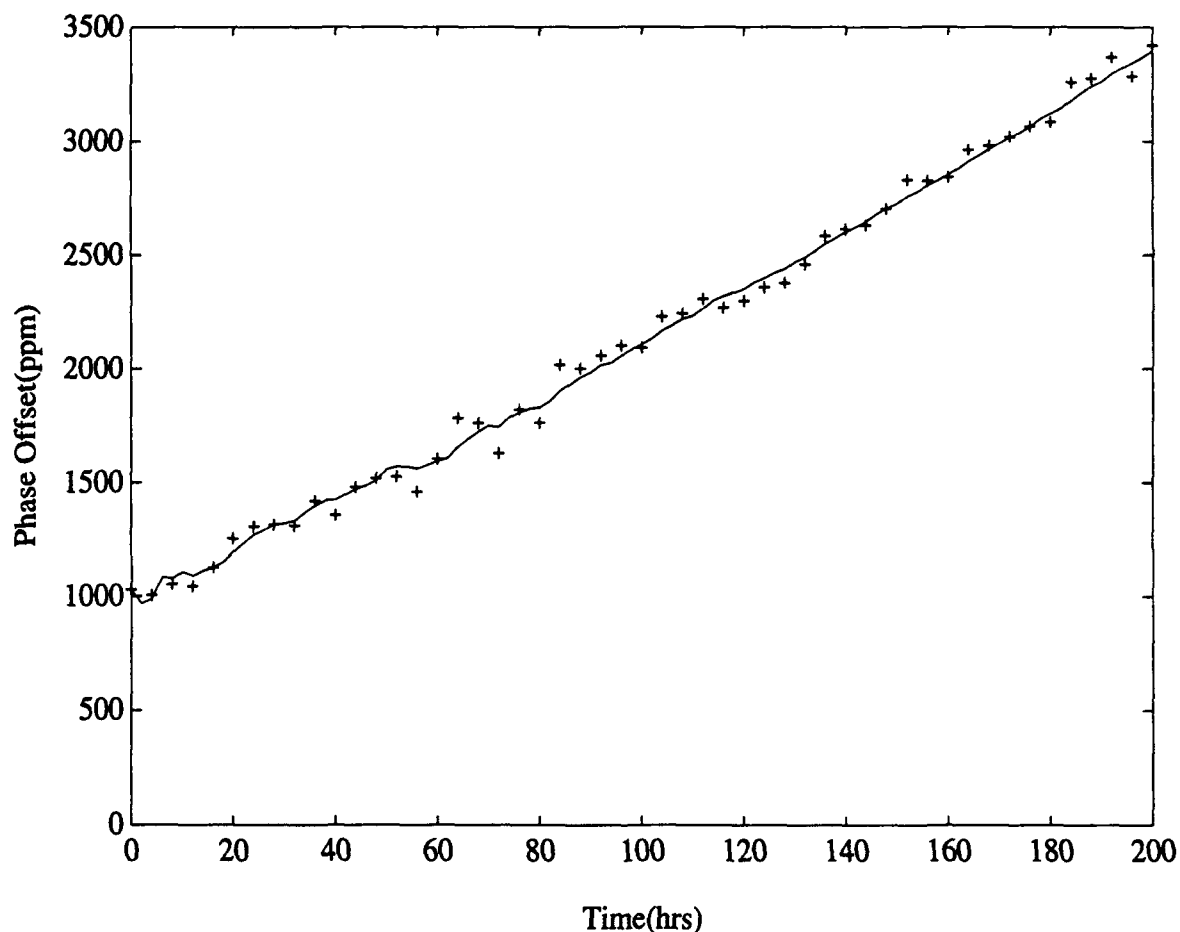
Figure D.4-2   Oscillator Phase Measurements and Kalman Filter
Fit to Data (solid line)

the oscillator parameters. Table D.4-2 presents a numerical comparison of the least-squares and Kalman oscillator calibrations. At the end of 200 hours the oscillator parameter estimates are almost identical and there seems to be little advantage for Kalman filtering (except for recursive processing) over batch least-squares for this simple problem. However, if the oscillator should experience a "break" where there is change in the nominal drift rate, the Kalman filter will tend to capture this effect better than the least-squares algorithm.

**Table D.4-2 Comparison of Least-Square and Kalman Filter Estimates
of Oscillator Drift Parameters**

PARAMETER	KALMAN FILTER	LEAST-SQUARES	TRUE VALUE
$\delta\phi_0$ (ppm)	994.5	994.6	100.0
δf_0 (ppm/hr)	10.18	10.18	10
$\delta f_0'$ (ppm/hr^2)	0.00913	0.00914	0.01

Figure D.4-3 presents a more complete picture of the Kalman filtering process. This figure shows time histories of the Kalman filter estimation *errors* for the oscillator initial phase, frequency and aging parameters. These plots also show the one-sigma confidence bounds for these parameters computed from the square roots of the diagonal terms of $P_k(+)$. From the figure it is clear that all errors have stabilized well within their 1 σ confidence bounds about 125 hours into the calibration. The advantage of the Kalman filter for this simple problem lies in the fact that the estimation error covariance does not depend on the data. It can be computed prior to the calibration and used to determine how long the calibration procedure should be to reach a desired accuracy level.
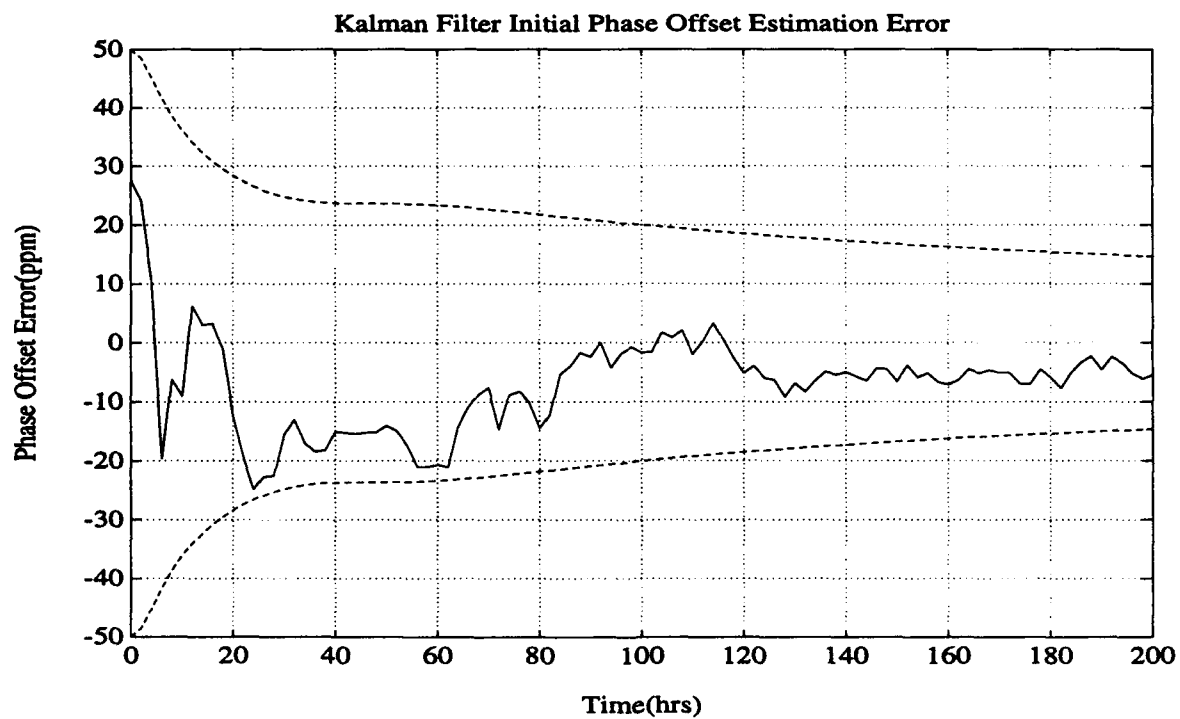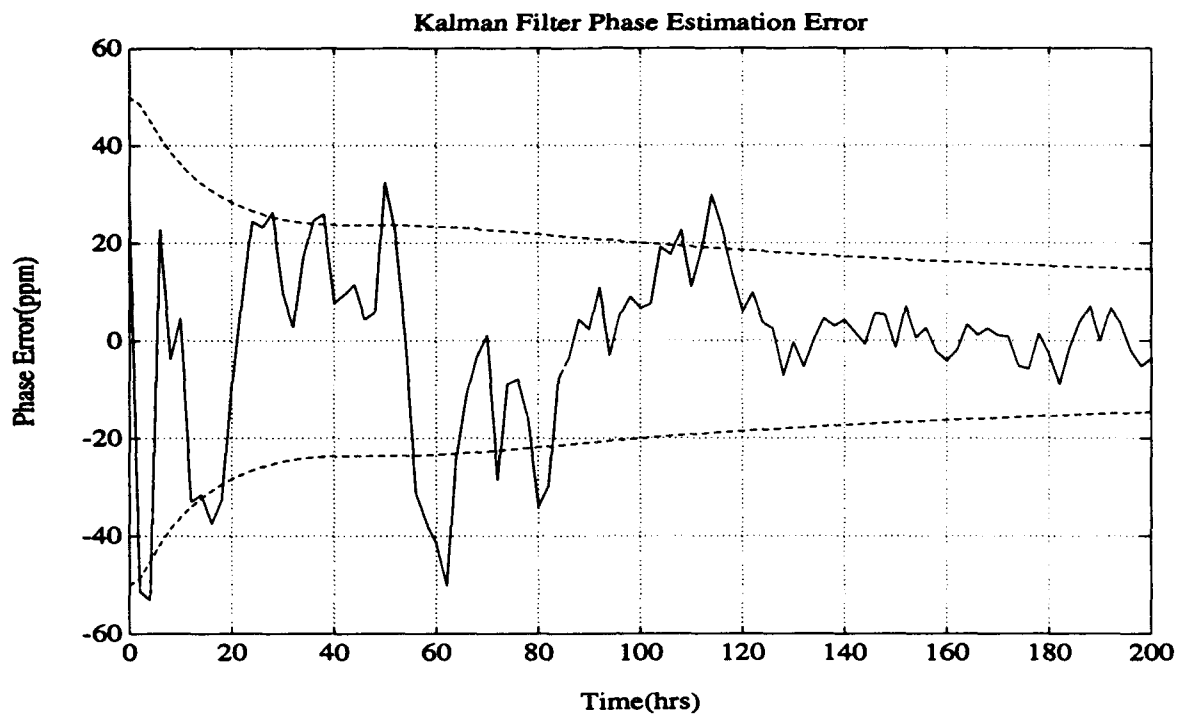
Figure D.4-3   Kalman Filter Estimation Errors and 1σ Bounds (dashed lines)
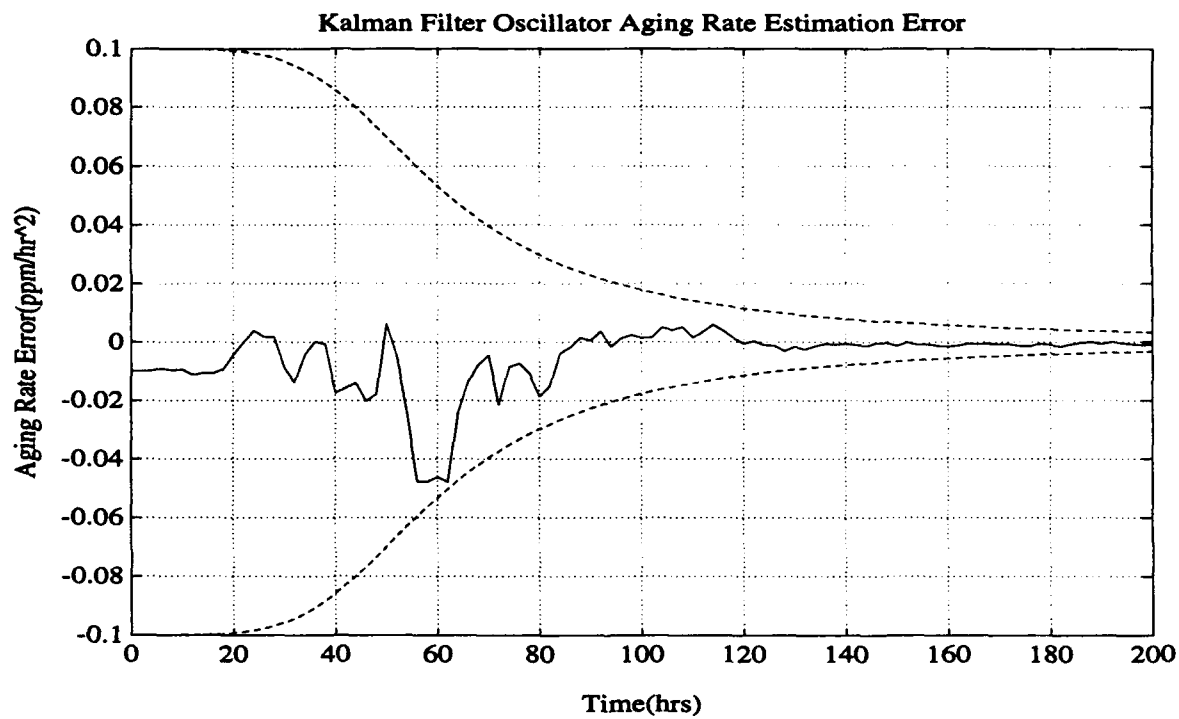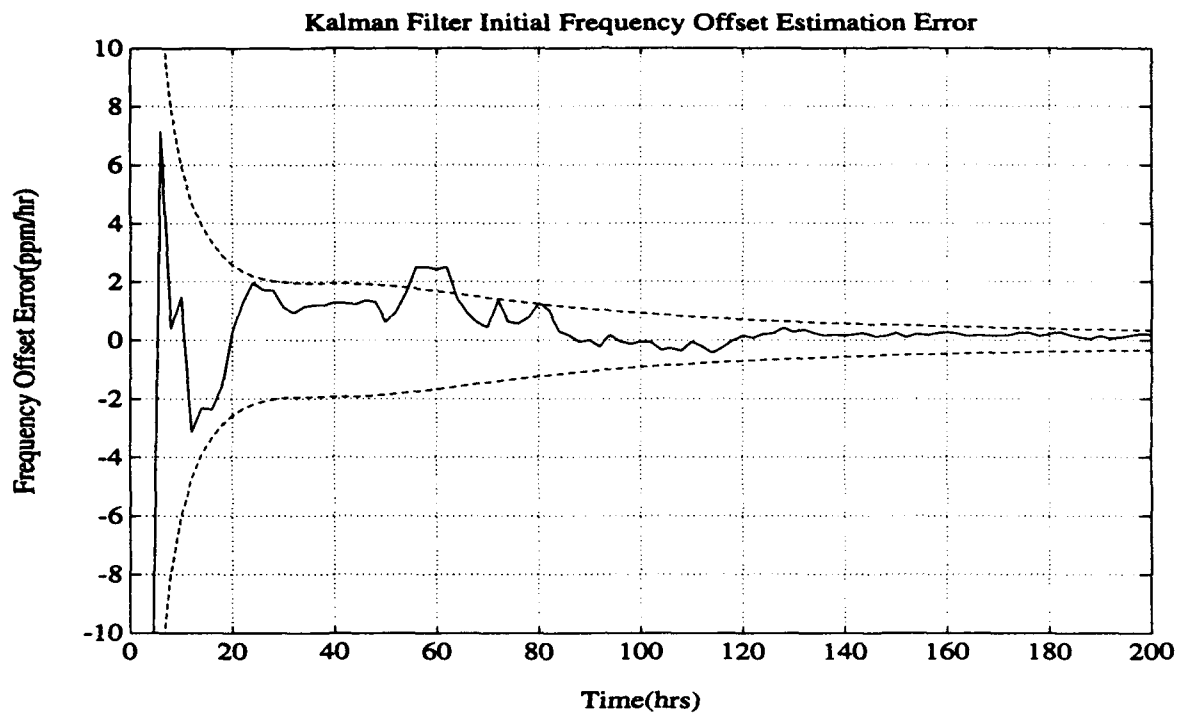
Figure D.4-3 Kalman Filter Estimation Errors and 1σ Bounds (dashed lines) (continued)

REFERENCES

1. A. Gelb (Ed.), *Applied Optimal Estimation*, The M.I.T. Press, Cambridge, MA, 1974.

APPENDIX E

GPS SYSTEM ACCURACY AND AVAILABILITY

E.1 INTRODUCTION

The NAVSTAR Global Positioning System (GPS) is a satellite-based system designed to provide capabilities for worldwide three-dimensional position fixing and precise timing on a nearly continuous basis. The basic technical principle underlying GPS is multilateration, in which the user measures the distances to several known transmitter locations (satellite locations in the GPS case). In a three-dimensional system such as GPS, each distance measurement, or "slant range," reduces the possible user locations to a sphere centered on the satellite involved. If three or more measurements are available, then the user's location may be visualized as the intersection of spheres. The basic GPS configuration consists of three "segments": space, control, and user. The roles of the three segments in the overall GPS system concept are summarized in Fig. E.1-1.

The GPS program began in 1973 with the effective merging of the Navy's Timation program and the Air Force's 621B program. GPS is a multi-service DoD program administered from the Joint Program Office (JPO) at Los Angeles Air Force Station; the Air Force is designated as the lead service for GPS. Associate program managers from other DoD services and Government agencies are located at the JPO. A Coast Guard officer serves as the DOT representative.

The DoD has defined two classes of GPS users: Authorized and Non-authorized. Non-authorized users only have access to the so-called Standard Positioning Service (SPS) that guarantees accuracy of 100 m, 2 DRMS (the 2 DRMS statistic is approximately equivalent to a 95 percent horizontal radial error). Authorized users have access to the Precise Positioning Service (PPS) where guaranteed accuracy is 30 m SEP (spherical error probable, the radius of a sphere containing 50 percent of position errors).

Many factors impact the accuracy actually realized by both Authorized and Non-authorized users at any time and location. The geometric configuration of the satellites used for multilateration plays a critical role in determining position accuracy; because the satellites are in constant motion relative to the earth, GPS "geometry" is constantly changing for all users. GPS geometry is also influenced by satellite down time (which will be scheduled for all satellites on a routine basis) and the very real possibility of unexpected satellite failures. Many factors also impact the accuracy with which slant ranges

Constellation

- 6 Planes
- 4 Satellites each Plane
- 55° Inclination

Space Segment

Uplink Data

- Satellite Ephemeris (Position) Constants
- Clock Correction Factors
- Atmospheric Data
- Almanac

Downlink Information

- Coded Ranging Signals
- Carrier Signals
- Navigation Message (Satellite Clock and Ephemeris, Almanac, Atmosphere)

User Segment

Monitor Stations

Ground Antenna

Master Control Station

Control Segment

Figure E.1-1   The GPS System and Its Component Segments

are determined, including the use of techniques such as "Differential GPS" that have been developed to improve the accuracy of slant ranges.

Within this appendix, a framework is presented in which the many factors impacting GPS accuracy may be quantified. The basis of this framework is the recognition that, because GPS geometry constantly changes, GPS accuracy is a time-variant quantity. Availability, defined as the percentage of time that a specified level of accuracy is provided to users, is therefore a more meaningful measure of GPS performance than accuracy alone. A methodology is presented herein which permits availability to be estimated for any required level of GPS accuracy. The methodology is applicable to both the SPS and PPS and either the nominal "stand-alone" or differential modes of operation.

Section E.2 summarizes GPS basics, including overviews of the three component system "segments" (space, control, and user), and the GPS signal format. Techniques are then described in Section E.3

for static prediction of GPS accuracy, i.e., prediction of accuracy for a fixed satellite geometry. Finally, Section E.4 describes a methodology for estimating the availability of any given level of accuracy.

E.2   GPS BASICS

This section provides a brief overview of basic GPS concepts and terminology, beginning with the basic GPS principle of operation and signal structure (Sections E.2.1 and E.2.2). It then describes the three component system "segments": space (Section E.2.3), control (Section E.2.4), and user (Section E.2.5).

E.2.1   GPS Principles of Operation

As described in Section E.1, a GPS position fix may be visualized as the intersection of spheres defined by slant ranges from satellites. Each slant range is calculated by comparing the time that energy is transmitted by a satellite to the time that it is received by the user. Conceptually, slant range could be measured directly if both the GPS satellite and user carried extremely accurate synchronized clocks. However, while GPS satellites do carry highly accurate atomic clocks, such clocks are prohibitively expensive for most users. As a result, most GPS users require a minimum of four satellite signal measurements to form a position solution. Each of these measurements is the range to a satellite biased by the offset between "GPS time" (to which all satellites are synchronized) and the user receiver's time base. Using the four measurements, the user receiver is able to solve for the four "unknowns": latitude, longitude, altitude, and the offset from GPS time. GPS time is therefore provided as a valuable by-product of the position solution.

E.2.2   The GPS Signal Structure

The basic characteristics of the GPS broadcast signals are summarized in Fig. E.2-1. Each satellite transmits on two L-band frequencies: $L_1 = 1575.42$ MHz and $L_2 = 1227.60$ MHz. Sinusoidal carriers at each of the frequencies are modulated by binary sequences that change polarity in accordance with mathematical formulas termed pseudorandom codes. Two families of codes are used: the "C/A code" (coarse/acquisition) and the "P code" (precision). The C/A code is transmitted only on L_1

E-3
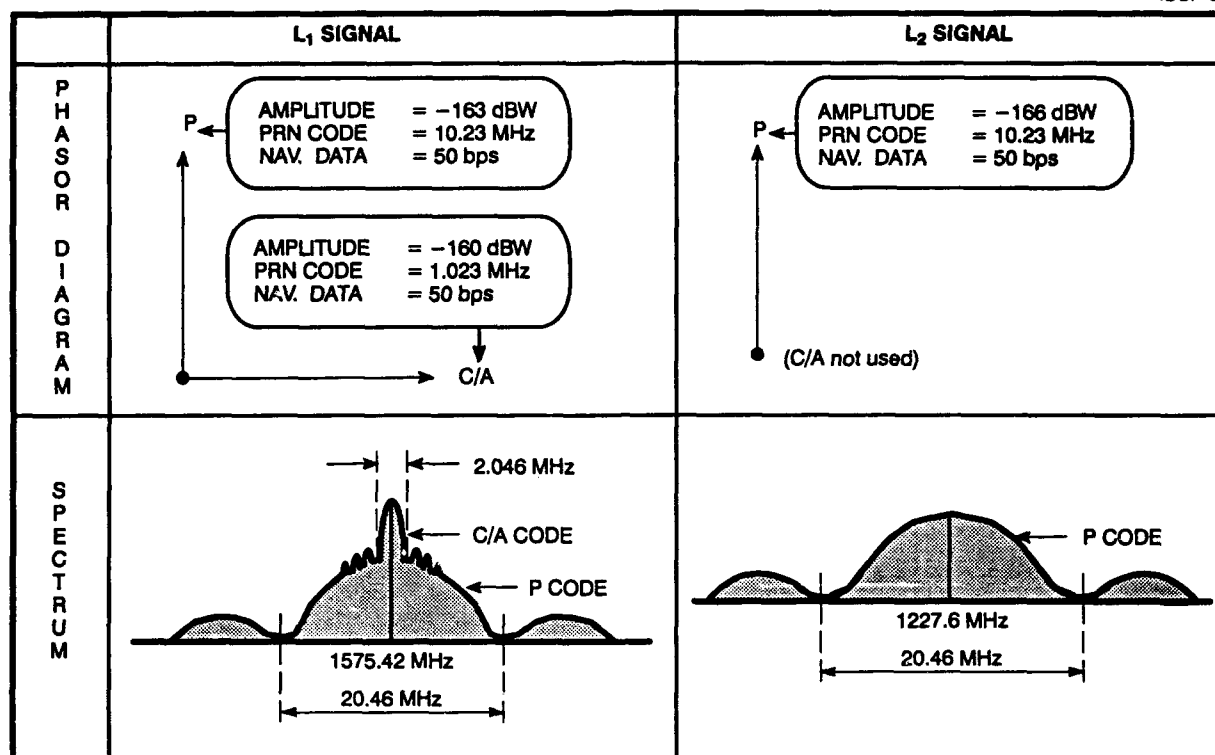
Figure E.2-1   Overview of GPS Signal Structure

and has a bit rate of 1.023 MHz and a length of 1,023 bits (thus it repeats every 1 msec). The C/A code for each satellite is unique and is intended to remain unchanged over the life of the satellite. The C/A code is public information; available to any GPS user. The P code is intended only for use by authorized users and is not officially made public. However, the P code is not closely guarded and has been implemented in some commercial GPS receivers. The P code is changed every seven days for each satellite; users must know the current code in order to use it for navigation.

A Navigation Data message is modulated "on top of " each of the three broadcast pseudorandom codes at the rate of 50 bits/sec. The navigation data contain information that the user needs to compute a navigation solution, most critically, the satellite orbital (or "ephemeris") parameters, and satellite clock corrections.

The distinction between Authorized and Non-authorized users of GPS was introduced in Section E.1. The PPS and SPS services intended for Authorized and Non-authorized users are summarized in Table E.2-1.   The DoD has determined that a capability to deny the PPS level of service to Non-authorized users (which may include potential adversaries) is necessary to preserve the military utility

E-4

of GPS. The newer generation of GPS satellites (termed "Block II," as discussed in the next section) has therefore been designed with features that are intended to enforce the SPS level of service for Non-authorized users. Specifically, the Block II satellites include two key features not present in the earlier Block I satellites, "Selective Availability" (SA) and "Anti-Spoofing" (A-S). SA is the intentional degradation of the satellite signal quality to reduce user navigational accuracy. A-S involves encryption of the P code; the resulting code is termed the "Y code." When SA and A-S are active, the PPS level of service is available only to Authorized users who have access to classified cryptographic equipment and keys.

Table E.2-1   Overview of SPS and PPS

Standard Positioning Service (SPS)
• Access to L_1 C/A-Code and navigation message
• P-codes on L_1 and L_2 may be accessible but are not part of SPS
Precise Positioning Service (PPS)
• Access to C/A-Code on L_1, P-code on L_1 and L_2 and navigation message (ability to remove ionospheric delay)
• Access to Y-Code and ability to compensate for manipulation of orbit data and clock frequency (KYK-13 cryptographic device)

SA is implemented through two mechanisms: intentional mis-statement of the broadcast satellite ephemeris data (sometimes called the "epsilon term" of SA) and intentional jittering of the satellite clock (the "delta term"). The epsilon term results in a relatively low-frequency error contribution to satellite ranging errors (time constant on the order of several minutes); the delta term is associated with high-frequency errors (time constant on the order of a few seconds).

The set of Authorized GPS users is restricted to the U.S. military services, certain other U.S. Government agencies (e.g., the Defense Mapping Agency), NATO nation military services, and Australian Defense Forces. Requests for special-purpose use of the PPS by other organizations or individuals are reviewed on a case-by-case basis.

E.2.3   The GPS Space Segment

Simply stated, the Space Segment consists of all orbiting GPS satellites. The primary mission of the Space Segment is to provide continuous, worldwide transmissions of GPS signals. (The satellites

also have military missions, such as detection of nuclear explosions, which are not relevant here.) This section describes the types of GPS satellites and their current status, and the planned constellation.

Satellite Types and Current Status — Table E.2-2 summarizes the characteristics of the members of the GPS satellite family. The status of the satellite constellation as of December 1992 is summarized in Fig. E.2-2. As of December 1992, the GPS constellation consisted of both Block I developmental series satellites and Block II production series satellites. The Block I series consists of 11 satellites that were launched during the 7.6 years from February 28, 1978 to October 1, 1985. As of December 1992, four Block I satellites remained in a healthy status.

Table E.2-2   GPS Satellite Family

NAVSTAR NO.	DESIGNATION	ON-ORBIT WEIGHT	DESIGN LIFE	COMMENTS
1–11	Block I	960 lb	—	11 launches. One booster failure. 4 operating as of December 1992.
12	Block II Ground Qualification Unit	—	—	Never intended for flight.
13–21	Block II	1850 lb	7.5 yr	1st delivery January 1987. 9 operating as of December 1992.
22–40	Block IIA	2050 lb	7.5 yr	Heavier Block II's. 6 operating as of December 1992.
41–60	Block IIR	2370 lb	10 yr	Replenishment satellites. 1995 delivery date.

During the mid-1980s, U.S. national policy assigned the Space Shuttle as the sole launch vehicle for GPS satellites. The Challenger disaster delayed the initial launch of Block II satellites and led to the selection of alternative launch vehicles. The first Block II satellite (designated PRN 14) was launched on February 14, 1989 using a Delta II unmanned rocket. (Several GPS satellite numbering systems are in use. The NAVSTAR number refers to the satellite construction sequence. The more frequently used PRN number refers to a scheme for labeling the C/A code broadcast by each satellite). During the ensuing 21 months, eight additional Block II satellites were launched — a significant technical and programmatic achievement.

The first of the Block IIA satellite series, which incorporates relatively small design changes to the basic Block II design, was launched on November 26, 1990. Shortly thereafter, this satellite (PRN 23) exhibited problems with control electronics associated with a solar panel. Subsequent Block IIA

E-6

Calendar Year

PRN ID	82	83	84	85	86	87	88	89	90	91	92	93	94	95
11														
13														
12	Block I (Remaining healthy)													
3														
14	Block II (13–21): 1/day upload, additional uploads based on UERE													
2														
16														
19														
17														
18														
20														
21														
15														
23	Block IIA (22–40): Incorporates extended navigation feature													
24														
25														
28														Block IIR
26														
27														
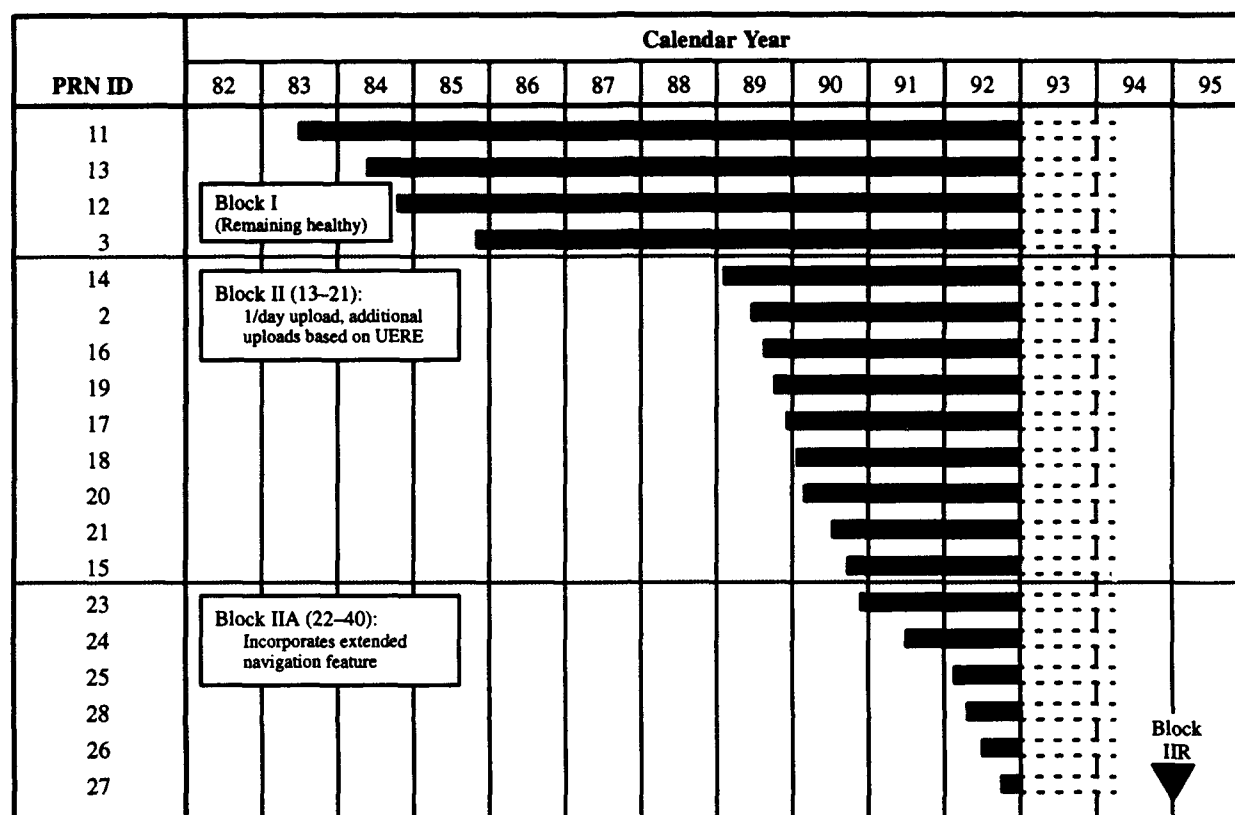
Figure E.2-2   GPS Satellite Constellation Status (December 1992)

launches were postponed while satellites in storage were modified. The second Block IIA satellite (PRN 24) was successfully launched on July 3, 1991.

During the summer of 1991, technical problems associated with a reaction wheel were observed in a satellite undergoing factory testing; similar problems were apparent in PRN 20. Launches were again delayed while satellites in storage were modified. Launches were resumed in early 1992 with PRN 25 (February 23) followed by three additional satellites during FY'92. As of December 1992, 19 operating GPS satellites were in orbit — 15 Block II and 4 Block I. Current plans call for launching six additional satellites during FY'93. The initial operational capability (IOC) of GPS will be declared when a total of 24 satellites (combined Block I and Block II) are in place and operational; this is expected to occur in the summer of 1993. Full operational capability will be declared when 24 Block II satellites are in place; this is expected to occur in the spring of 1994. For all practical purposes, IOC

will mark the beginning of the GPS operational phase for non-DoD users. The transition to FOC will be completely transparent to the civilian GPS community.

The primary differences between the different satellite types that are important to civilian users are the capabilities available only on the Block II satellites to implement Selective Availability (SA) and Anti-spoofing (A-S), as discussed in Section E.2.3. In essence, both SA and A-S are intended to allow DoD to control the level of GPS accuracy available to potential adversaries.

Figure E.2-3 illustrates a typical Block II satellite and identifies several important features of its design. The satellite body is located between the two solar arrays. The body is attitude controlled in a manner that causes the antenna elements shown in the figure to always point toward the center of the earth. In contrast, the solar panels on either side of the body are always pointed toward the sun. A 12-element array of L-band antennas is mounted on the body; this array radiates navigation signals to the users. A single-element S-band antenna appears to the lower left of the L-band array and is used for navigation data uploads and other uplink/downlink data communications with the Control
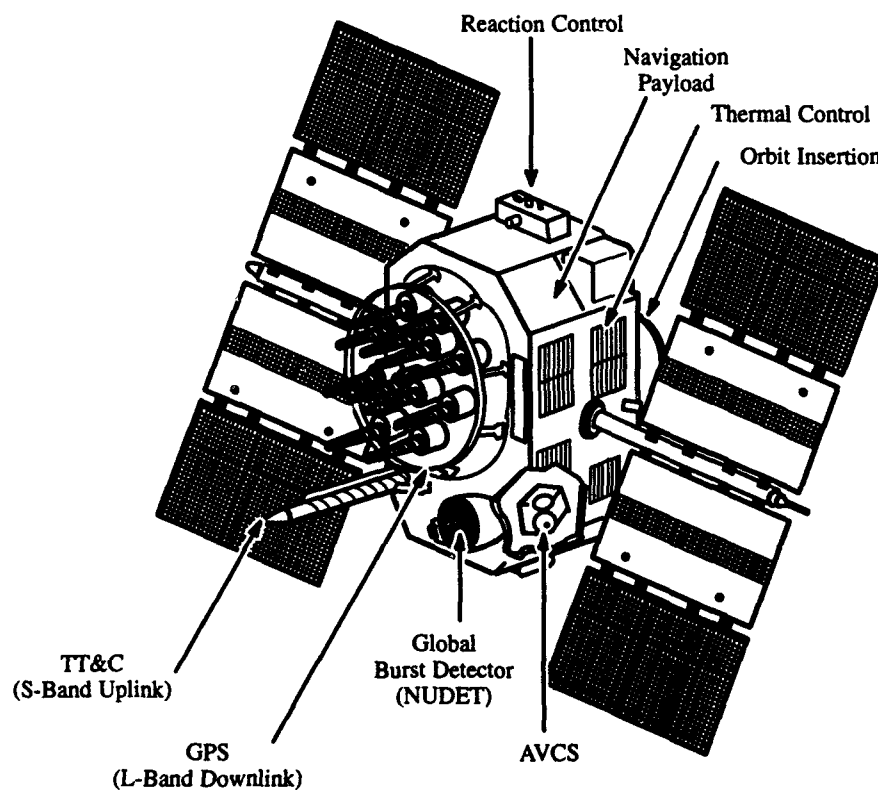
Figure E.2-3   NAVSTAR GPS Satellite

Segment. The solar panels recharge three 35 amp-hr nickel cadmium batteries for primary electrical power. Two cesium and two rubidium atomic clocks are housed within the satellite body.

Planned Constellation — The planned operational Block II satellite configuration is commonly referred to as the "21 Primary Satellite Constellation." This constellation, in fact, will nominally have 24 satellites in orbit, employing six equally spaced orbital planes inclined 55 deg with the equator. The terminology "21 Primary Satellites" is intended to convey the JPO's commitment to have 21 or more satellites fully usable almost all the time. Those working satellites in excess of 21 are said to be operating spares, although the difference between spares and non-spares will not be apparent to users.

Figure E.2-4 illustrates the global network of GPS satellite orbits. The orbits of all GPS satellites are essentially circular. The satellite altitude, 10,898 nm, was selected because it provides a one-half geosynchronous orbit period of 11 hr 55 min 59.3 sec, i.e., a one-half sidereal day period. (A sidereal day — 23 hr 55 min 56.6 sec — is the time it takes for the earth to complete one full rotation relative to an inertially fixed reference frame.) This orbital period allows GPS satellites
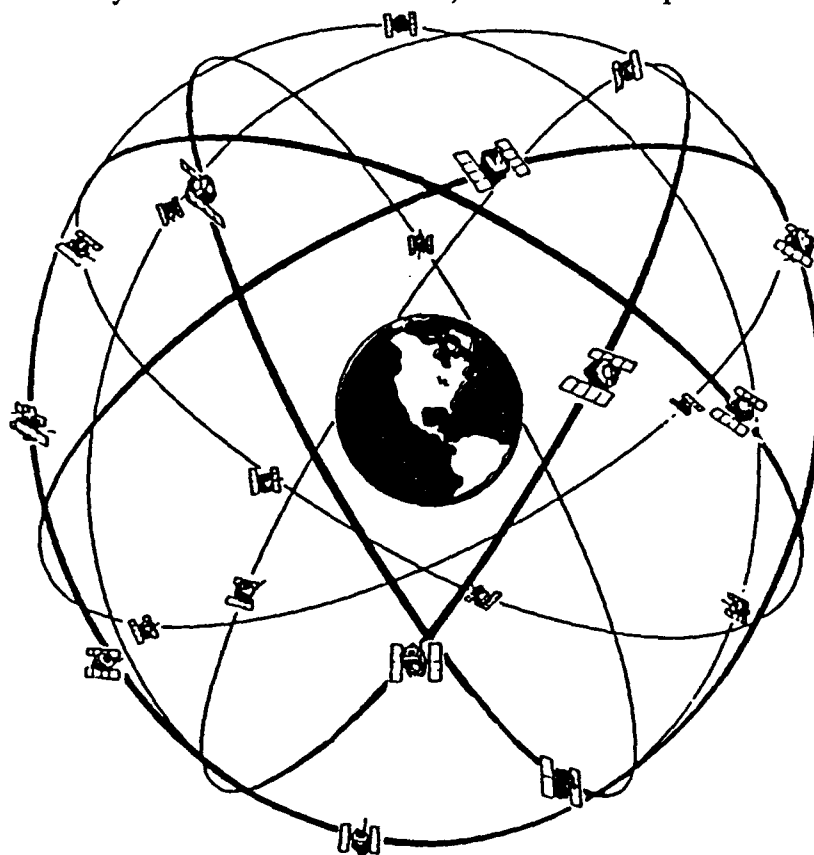
Figure E.2-4 GPS Operational Satellite Constellation

to complete exactly two orbits while the earth completes one rotation, ensuring that satellites overfly the same locations on the earth every day. The strategy behind this orbital plan is to allow each satellite to be viewed by a single control station at least once each day, thus minimizing dependence on stations outside of United States territorial control. Since the GPS orbit periods are synchronized with sidereal days rather than solar days (24 hr), the rise and set times for each satellite advance approximately four minutes each day with respect to local time.

Because each GPS user obtains a navigation solution through multilateration, the geometric relationship of the satellites to the user is a critical factor in determining navigation accuracy. For a full GPS solution, four or more satellites must be visible to the user. Moreover, the satellite locations must not lie in a plane or a cone with the apex at the user for a navigation solution to be found. Wide separation of satellites — e.g., three near the horizon separated by 120 deg in azimuth and one near the vertical — results in more accurate navigation solutions. Geometric considerations such as these led to the selection of the relatively complex orbital structure suggested in Fig. E.2-4.

Figure E.2-5 illustrates the geometric relationship between a single GPS satellite and the earth. The GPS orbital altitude allows 42 percent of the earth's surface to "see" any satellite at any time (users
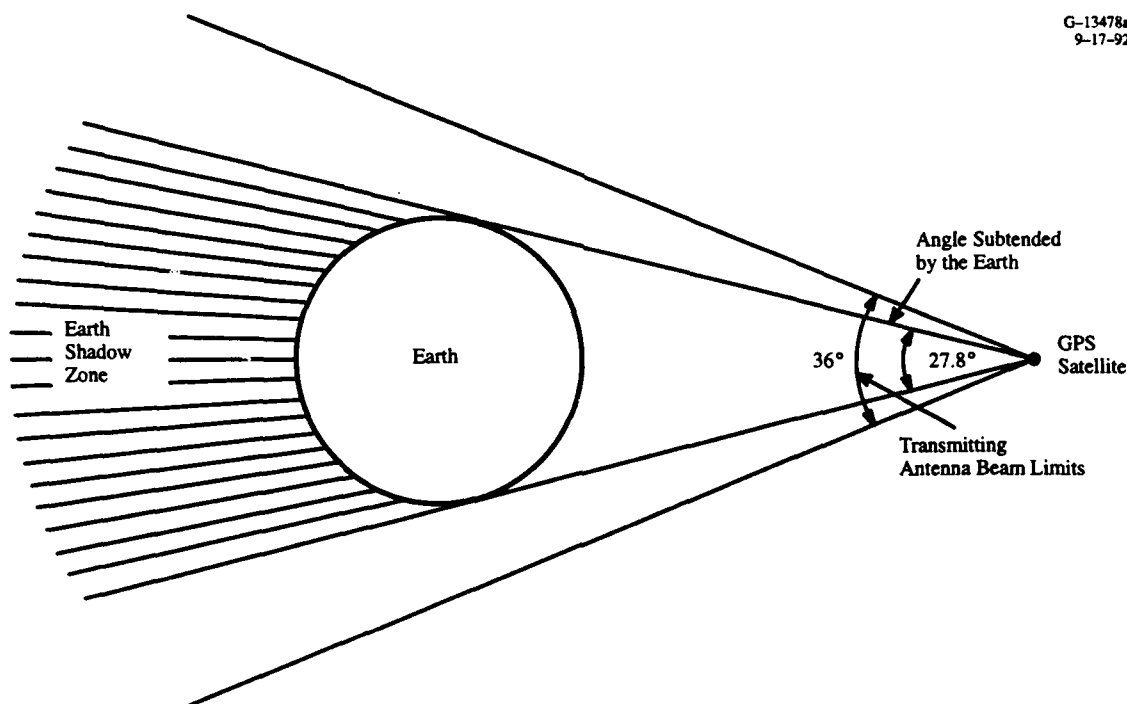
Figure E.2-5 Simplified Geometrical Diagram of GPS Earth Coverage

on the earth's surface seeing the same satellit. may be separated by up to 8000 nm). Moreover, GPS provides signals to users not in the earth's shadow to an altitude of at least 990 nm.

E.2.4 The GPS Control Segment

The purpose of the Control Segment is to provide nearly continuous worldwide mon.toring, tracking, and communications relative to the GPS satellites, and to update each satellite's navigation message.

The functions of the GPS Control Segment are implemented in the Operational Control System (OCS) centered at the Consolidated Space Operations Center (CSOC) at Falcon AFS, Colorado Springs, Colorado. The OCS became operational in 1985 and assumed functions performed by the earlier Initial Control System (ICS). The OCS consists of the Master Control Station (MCS) at Falcon AFS, five Monitor Stations (MS) dispersed around the globe, and three Upload Stations (ULS) collocated with selected MS locations for uplink communications. Figure E.2-6 shows the global locations of these stations. Selection of these geographical locations is such that the longitudinal separation

G-11832a
11-24-92

Sunnyvale

Colorado Springs

Hawaii

Kwajalein

Ascension

Diego Garcia

■ Master Control Station
● Monitor Station
▲ Upload Station
◆ Backup Control Station
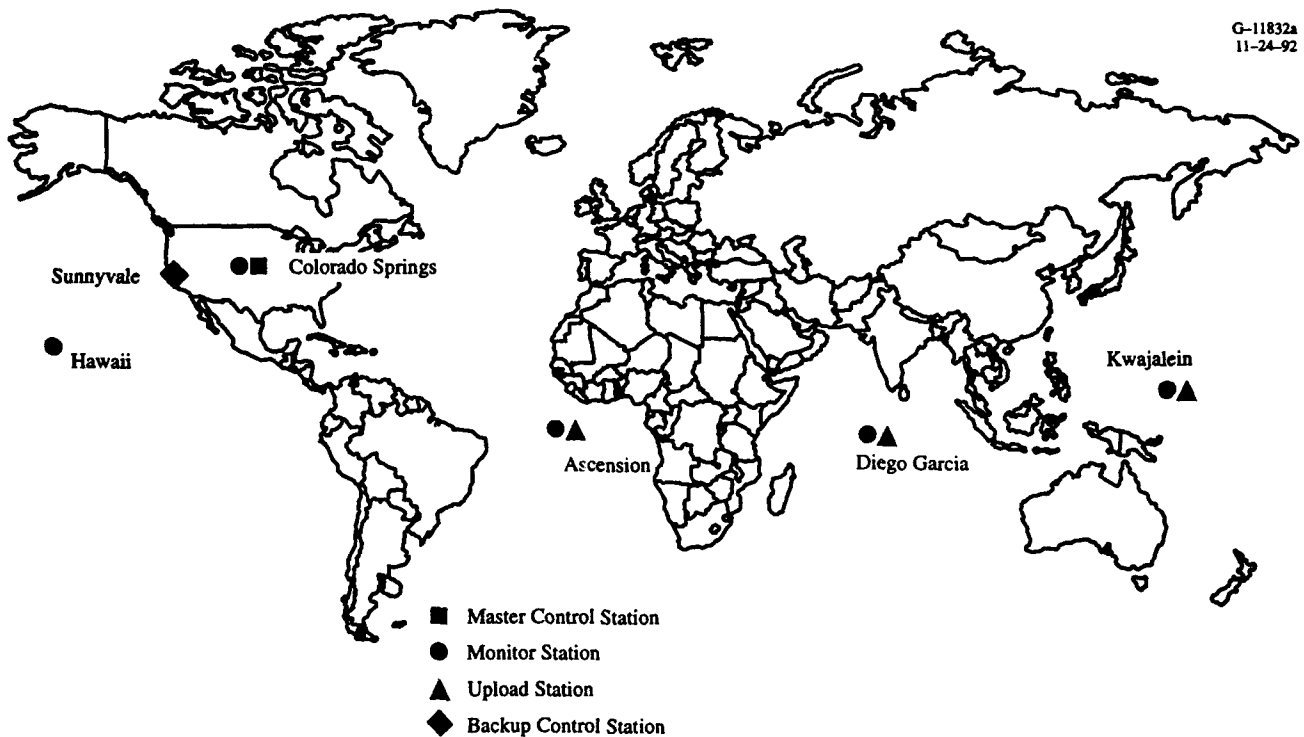
Figure E.2-6 Geographical Location of Control Segment Sites

E-11

between stations is less than 90 deg. Other than the MCS, all locations are within 15 deg latitude of the equator. These factors combine to ensure that satellites are within Monitor Station coverage over 80 percent of their orbital trajectories.

Figure E.2-7 summarizes the major OCS functions and communications links. As shown in the figure, the five remote MS locations continuously collect measurements of the GPS satellite navigation signals at the two GPS broadcast frequencies. These measurements are communicated from the MS
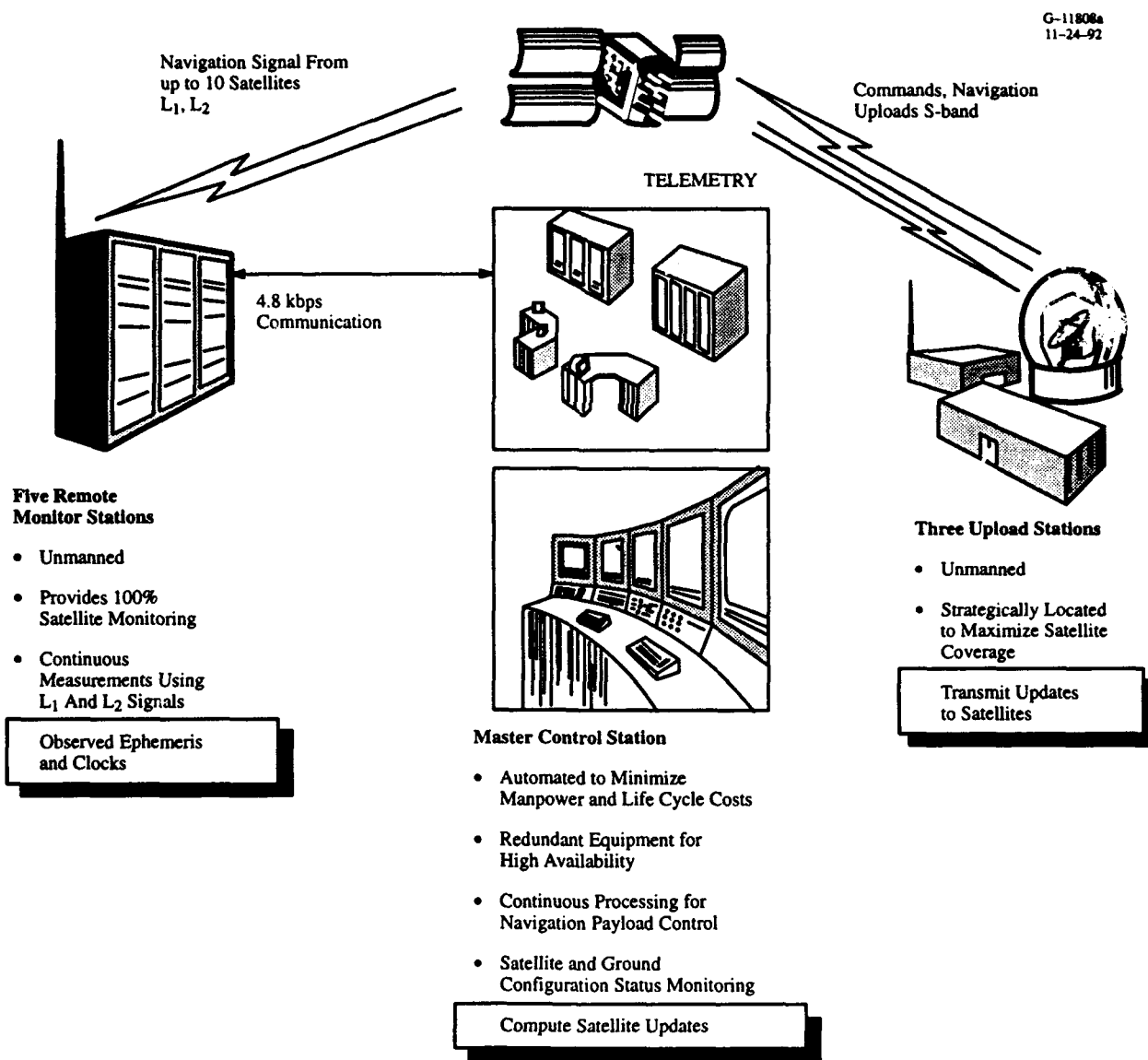
Figure E.2-7   Pictorial of OCS Major Functions

E-12

sites to the MCS site at Falcon AFS. Because the MS positions are known precisely, the accumulated ranging information in the MS measurements can be processed at the MCS to solve the navigation problem in reverse for satellite orbit determination and elimination of systematic errors. Precise orbital data and status information is transmitted from the MCS to the ULS sites, where it is uploaded to the appropriate satellites.

E.2.5 The GPS User Segment

Overview — The GPS User Segment consists of the set of all equipment employed by the users of the system to receive and process the GPS L-band signals. GPS receiver designs differ widely, depending on application and manufacturer, but typically follow the top-level architecture shown in Fig. E.2-8. The preamplifier and front-end functions are similar to those in most radio receivers, providing amplification of the signals and filtering to reject electromagnetic energy outside the GPS bands (refer to Fig. E.2-1). The "heart" of a GPS receiver is composed of the "measurement function" performed by the tracking loops shown in Fig. E.2-8, and "navigation function" performed by the navigation algorithms. These two functions are described in the following paragraphs.

Measurement Function — Two fundamental measurements are performed by a GPS receiver: determination of the "pseudorange" (i.e., actual range to a satellite plus the effect of user clock error)
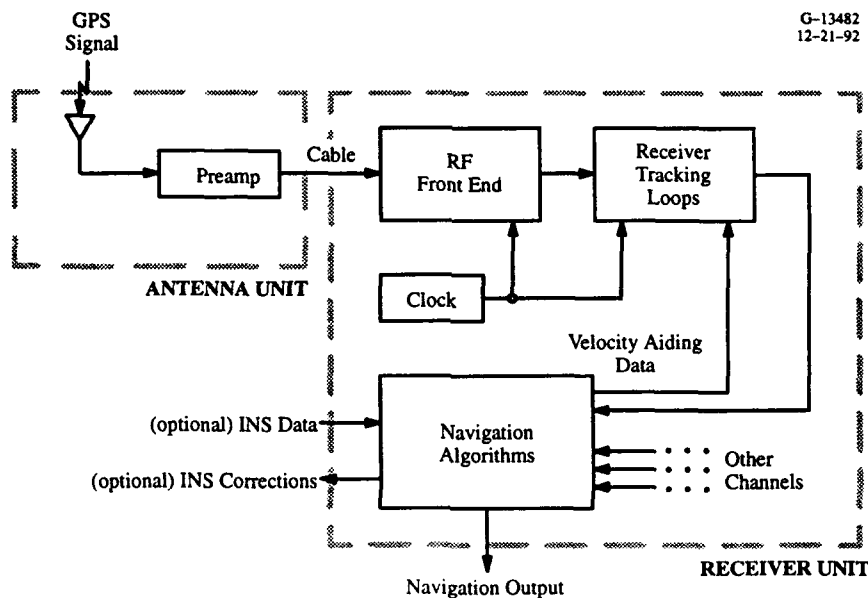
Figure E.2-8   Simplified GPS Receiver Block Diagram

E-13

and "delta range" (change in pseudorange over a short, fixed interval) between the user and a specific satellite. Pseudorange measurements are performed by a "code tracking loop" that measures delay relative to the receiver's internal clock by synchronizing an internally generated replica of the C/A or P code to the received code. Delta range measurements are performed by a "carrier tracking loop" that tracks the instantaneous frequency of the L-band carrier. Using the outputs of the code and carrier tracking loops, the measurement function also demodulates the 50 bits/sec data message carried on both the L_1 and L_2 signals.

Some low-cost receivers, intended primarily for slowly moving or stationary applications, contain only one or two channels (that is, distinct code and carrier tracking loop pairs). This type of receiver must time-share the available channels among the satellites in view, sequencing between the satellites that are used in the navigation solution. For more demanding applications (i.e., where the highest accuracy is required or significant vehicle dynamics are involved) dedicated channels are typically used for each satellite included in the solution. In addition to allowing receivers to maintain code loop lock on GPS signals through high-dynamic maneuvers, the use of dedicated channels improves signal to noise ratio. Receivers with up to 12 tracking channels are in common use today.

Receiver signal processing techniques have been developed in recent years, very significantly improving code tracking accuracy (i.e., reduce the noise in code measurements). Two of the most important of these techniques are "integrated Doppler processing" and the use of "closely-spaced correlators" in the receiver code tracking loops.

GPS receivers that employ integrated Doppler processing determine user range-to-satellite changes (over time spans of a few minutes) by integrating the Doppler frequency shift of the carrier signal. Conceptually, the integrated carrier data are used to create a smooth curve or track of the evolution of user-to-satellite range. The relative accuracy of this curve is high (carrier-derived range changes are accurate to inches). However, the absolute location of this curve cannot be determined from carrier data. At the same time, code tracking provides a measure of absolute pseudorange that is corrupted by high-frequency errors (including quantization errors and the "delta" term of Selective Availability). Integrated Doppler processing receivers adjust the location of the smooth carrier-derived curve to best fit the code-derived pseudoranges. User position is then derived from this adjusted curve.

Most GPS receivers measure pseudorange by correlating received code with (typically) three pre-stored replicas of the code which are staggered in time. A curve is fit to the three resulting correlation coefficients and the desired pseudorange is associated with the peak on the curve. In nearly all current receivers, the pre-stored code replicas are separated by one chip of the code (1.023 MHz rate

for the C/A code). Recently, one receiver manufacturer has reduced the correlator spacing (following signal acquisition) to 5 or 10 percent of a chip width. Whereas some older receivers have exhibited noise levels equivalent to tens of feet of position error, the closely spaced correlator technique reduces the error to approximately 4 inches.

Current generation receiver design makes extensive use of digital circuitry. All code tracking, carrier tracking, and data demodulation processes in most modern receivers are implemented in special-ly-designed digital circuitry and software. These "digital" designs have been made possible through advancements in GaAs Monolithic Microwave Integrated Circuits (MMIC), gate arrays, and Applica-tion Specific Integrated Circuit (ASIC) technologies.

Navigation Function — In the Navigation Function, the quantities provided by the Measure-ment Function are processed to generate three-dimensional position and velocity and GPS time. Per-forming the Navigation Function involves implementation of a set of well-defined mathematical equations. Therefore, it is usually implemented in a microprocessor (as opposed to the type of application-specific integrated circuits used in the Measurement Function).

Figure E.2-9 presents a "flat earth" or two-dimensional example of the basic mathematical problem which the Navigation Function solves. In this example, the user has available the satellite locations (from the ephemeris information in the navigation message) and three pseudoranges (from the Measurement Function), and wishes to find the user location. Geometrically, this could be accom-plished with a map and compass by iteratively modifying the three pseudoranges by a common amount until the three circular "lines of position" intersect. In GPS, the common amount by which the pseudo-ranges must be modified is the receiver clock bias representing the difference between the receiver clock time and GPS time. GPS time can therefore be recovered by subtracting this bias from the receiver clock.

In a practical Navigation Function, three significant "complicating factors" arise: 1) the solution must be found in three dimensions, 2) four or more satellites must be used, and 3) random errors will exist in each pseudorange and will prevent "spheres of position" (i.e., spheres centered at satellites with radii equal to pseudoranges) from intersecting at a single point. Each of these complicating factors is in fact handled easily by formulating the Navigation Function as a least-squares type estimator. In the simplified example of Fig. E.2-8, such an estimator would typically be designed to minimize (in a statis-tical sense) the area of triangle formed by the three lines of position; extension to three dimensions and any number of satellites is straightforward. In most receivers, the position solution obtained from
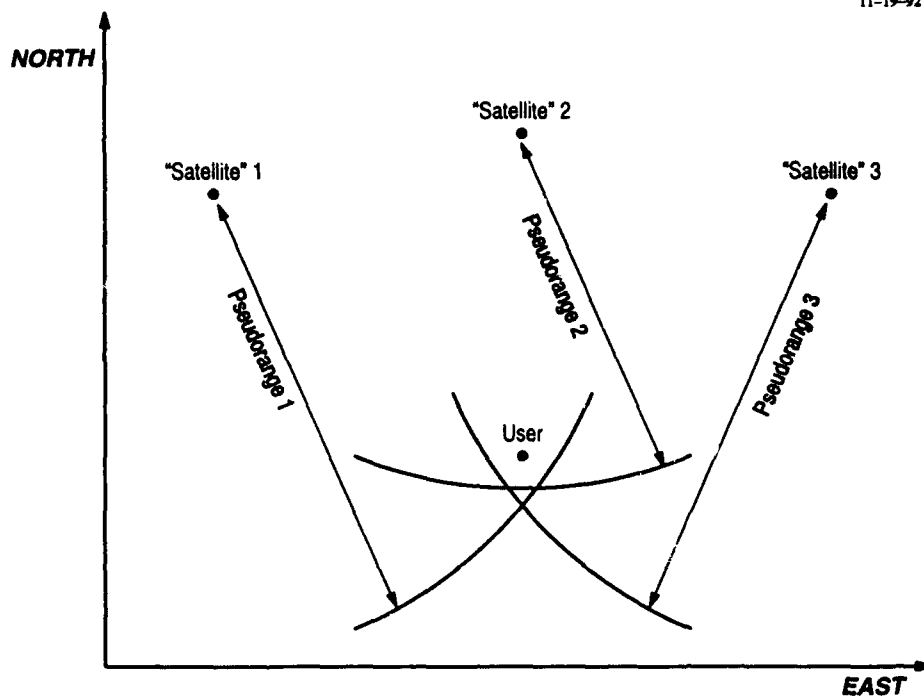
Figure E.2-9 Two-Dimensional Example of Problem
Solved by Navigation Function

current pseudorange measurements is mathematically filtered, i.e., previous solutions are used to re-
duce the impact of errors present in the current observations. The technique for finding the user's veloc-
ity from delta range measurements is almost identical, mathematically, to the position technique.

E.3 GPS ACCURACY PREDICTION

E.3.1 Overview

For planning purposes, it is important to be able to relate the user's navigation errors (i.e., in
latitude/longitude or altitude) to pseudorange errors and the geometrical configuration of satellites as
viewed by the user. Fortunately, to a good approximation, the error in computed navigation quantities
is given by the following simple formula (termed the "error equation" herein):

$$\text{Error in Quantity } X = \text{UERE} \times \text{XDOP} \tag{E.3-1}$$

where

Quantity X:

Navigational quantity of interest, for example, horizontal
position (X=H) or vertical position (X=V)

E-16

UERE (User Equivalent Range Error):
  Error in determining the distance between a user and one satellite

XDOP (Dilution of Precision for Quantity X):
  Scale factor, dependent only on user-to-satellite geometry,
  relating error in quantity X to UERE (e.g., HDOP for
  horizontal position, VDOP for vertical position).

This widely used formula separates the effects of geometry (which only influence XDOP) from equipment and atmospheric errors (which only influence UERE).

In Section E.3.2, the most commonly used XDOPs and the error quantities used in the above error equation are defined precisely. An error budget describing the important components of UERE is then presented in Section E.3.3. The error equation is applied in Section E.3.4 to provide examples of GPS accuracy in typical geometry. Finally, in Section E.3.5, a modified error budget and examples of typical errors are presented for the important special case of differential GPS.

E.3.2   Dilution of Precision (DOP)

In the error equation introduced in the previous section, the dilution of precision (or DOP) term depends entirely on the number of satellites employed in a navigation solution and the geometrical arrangement of satellites relative to the user. The terminology "dilution of precision" derives from the fact that, in virtually all practical cases, the error in the navigation quantity of interest (i.e., the left-hand side of error equation, Eq. E.3-1) is larger than the UERE. Therefore, in the error equation, the satellite geometry is viewed as "diluting" the satellite ranging accuracy given by UERE.

The concept of DOP is illustrated in the simplified examples shown in Fig. E.3-1. In these examples, it is assumed that the user and two satellites lie in a plane and have synchronized clocks. For each satellite, the satellite ranging error is shown in a band about the true range. For the situation labeled "Good HDOP/Good VDOP" the user-to-satellite line-of-site (LOS) vectors meet in a right angle at the user. In this situation, it can be shown that HDOP and VDOP both equal one, i.e., no "dilution" of the satellite ranging accuracy occurs for either horizontal or vertical positioning.
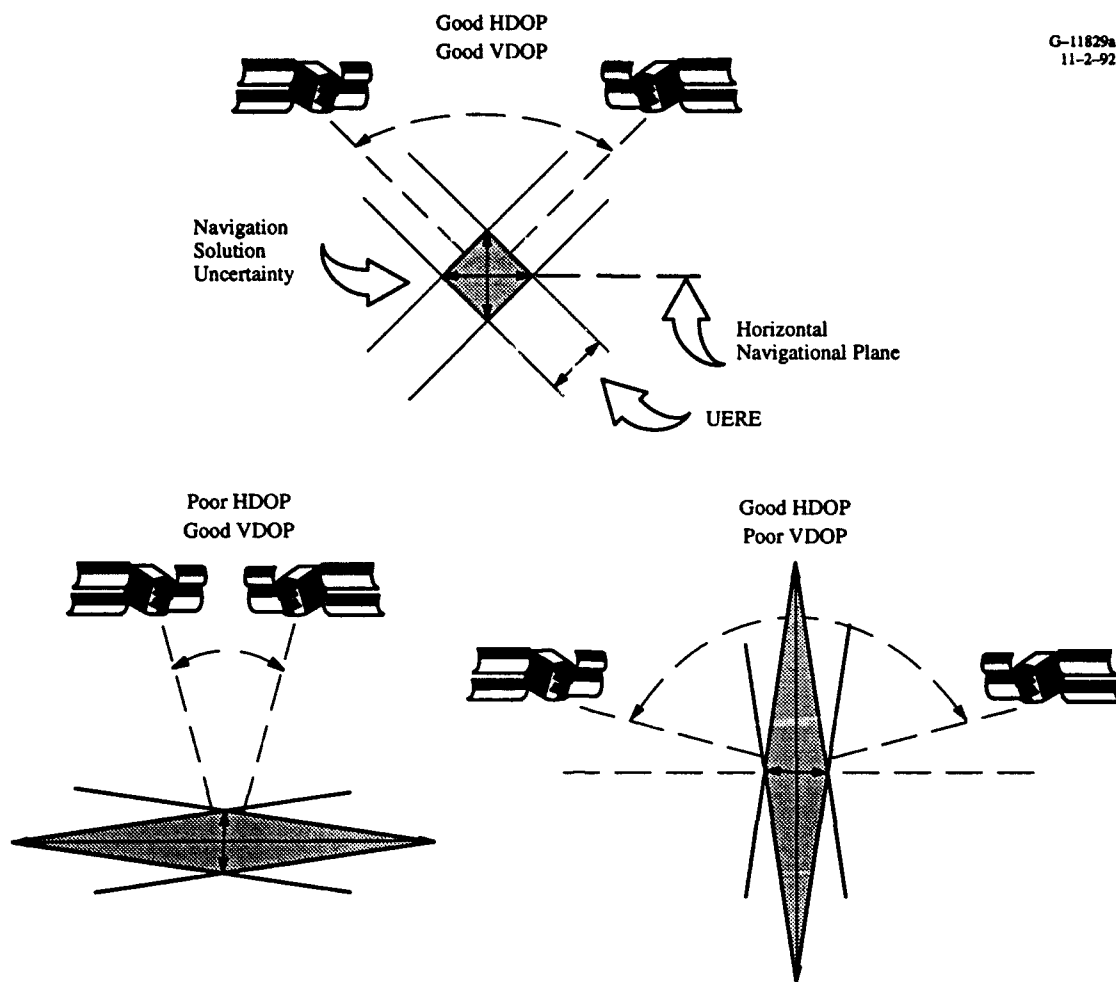
Figure E.3-1 Intuitive Aspects of HDOP and VDOP

When the two satellites are both nearly overhead (the "Poor HDOP/Good VDOP" case in Fig. E.3-1) the user has two measurements near the vertical axis (hence, good VDOP) but no measurements near the horizontal axis (hence, poor HDOP). This result is illustrated qualitatively by the elongated diamond-shaped area of position uncertainty shaded in the figure. For a quantitative example, assume that the LOS for each satellite is 5 deg from the vertical. The resulting VDOP is 0.7, i.e., the vertical position error is 70 percent of the UERE (because, in essence, the two measurements can be averaged). However, the HDOP is 8.1, that is, the horizontal error is over eight times the UERE. An analogous case for satellites placed near the horizon is illustrated at the lower right of Fig. E.3-1.

Mathematically, DOP quantities are defined in terms of range error and navigation error statistics. In the derivation of DOPs, it is assumed that the distributions of ranging errors for all satellites are zero mean and have the same variance; these assumptions are well justified in GPS for large sample sets.

UERE is then defined as the standard deviation (or RMS value) of the ranging errors. The following variance statistics for position and timing error quantities are also defined:

P_x, P_y = variances of horizontal error components along axes selected at right angles (e.g., x=east, y=north)

P_v = variance of vertical error

P_t = variance of timing error (expressed in units of distance).

Then the commonly used GPS DOPs are defined by

$$\text{VDOP} = \sqrt{(P_v)}/\text{UERE} \qquad (E.3\text{-}2)$$

$$\text{TDOP} = \sqrt{(P_t)}/\text{UERE} \qquad (E.3\text{-}3)$$

$$\text{HDOP} = \sqrt{(P_x + P_y)}/\text{UERE} \qquad (E.3\text{-}4)$$

$$\text{PDOP} = \sqrt{(P_x + P_y + P_v)}/\text{UERE} \qquad (E.3\text{-}5)$$

$$\text{GDOP} = \sqrt{(P_x + P_y + P_v + P_t)}/\text{UERE}. \qquad (E.3\text{-}6)$$

Comparison of Eqs. E.3-2 through E.3-6 with Eq. E.3-1 shows that for the "V" and "T" cases, the error equation outputs (i.e., left-hand side of the error equation) are the rms vertical and timing errors, respectively. For the "H" case, the output error is the "distance root mean squared" or DRMS. In many requirements documents and published error analyses, horizontal errors are expressed in terms of the "2 DRMS" which is simply two times the DRMS. The 2 DRMS has a convenient interpretation as the radius of a circle that will contain at least 95 percent of horizontal position measurements (the exact percentage depends on the satellite-to-user geometry). In the "P" case, the output error is the RMS 3-dimensional radial error. In the "G" case, interpretation of the output error is less intuitive. GDOP is typically used simply as a geometry figure of merit when both 3-dimensional position and time are of interest.

E.3.3   GPS Range Error Budget

The UERE is the "sum" of error contributions from many sources. In virtually all of the formulations in common use today, error sources are defined which act independently. Therefore, the UERE may be more precisely defined as the root-sum-square of the individual error source contributions. A tabulation of the individual error sources is termed an error budget. Error budgets will necessarily depend to some extent on the details of receiver and antenna implementation. Also, because the

DoD has not made public the statistics associated with Selective Availability, some uncertainty is associated with the level of its contribution. For these reasons, no single GPS error budget can be considered authoritative. A typical error budget based on minimum-capability user equipment is given in Table E.3-1.

Table E.3-1   GPS UERE Error Budget

GPS SEGMENT	ERROR SOURCE	PPS (ft, 95%)	SPS (m,rms)
SPACE	Clock & Navigation Subsystem ℾ	3.0	3.0
SPACE	Predictability of Satellite Perturʋᴀ ⌐	1.0	1.0
SPACE	Other	0.5	0.5
CONTROL	Ephemeris Prediction Model Implementation	4.2	4.2
CONTROL	Selective Availability	∩	23
CONTROL	Other	0.9	0.9
USER	Ionospheric Delay Compensation	2.3	5-10
USER	Tropospheric Delay Compensation	2.0	2.0
USER	Receiver Noise & Resolution	1.5	7.5
USER	Multipath	1.2	1.2
USER	Other	0.5	0.5
TOTALS	Without Selective Availability	6.6	10.8 – 13.9
TOTALS	With Selective Availability	6.6	25.3 – 26.7

Note from the error budget that, when active, the contribution of Selective Availability to C/A code UERE is larger than that of all the other error sources combined. Aside from Selective Availability, errors associated with the Space and Control Segments primarily address the stability and predictability of satellite clock and ephemeris behavior. User Segment errors are attributed to propagation link time delays and receiver processing mechanisms. The propagation link errors include those effects related to time delays influenced by RF propagation through the earth's ionosphere and troposphere, and mutual interference effects created by multipath reflections. Note that ionospheric and tropospheric effects grow exponentially for elevation angles less than 10 deg.

E.3.4 GPS Accuracy in Typical Geometry

"Typical" GPS geometry is often described by HDOP and TDOP on the order of 1.5 and VDOP on the order of 2.0. As will be seen in Section E.4.3, these values correspond approximately to levels of DOP that are exceeded less than 10 percent of the time at mid-latitude locations. Given these values, and the error budget provided in the previous section, determination of GPS accuracy in typical geometry is easily accomplished by applying the error equation (Eq. E.3-1). The results are presented for both PPS and SPS users in Table E.3-2.

Table E.3-2 GPS Accuracy in Typical Geometry

ERROR CATEGORY	PPS	SPS
Horizontal Error (m, 2 DRMS)	19.8	80.0
Vertical Error (m, 95 percent)	26.4	106.7
Timing Error (nsec, 95 percent)	65	262

E.3.5 Differential GPS

Several contributors to GPS range error vary "slowly," that is, their temporal variation (time in which significant changes occur) is on the order of minutes or longer, and their spatial variation is on the order of 100 nm or more. Thus, if the range error at one location and time were known, it could be transmitted to another location where it could be used to improve navigation accuracy. This is the essence of the differential concept illustrated in Fig. E.3-2.

Implementation of differential GPS (DGPS) involves collection of satellite signals at a fixed location whose coordinates are known accurately, processing of the signals to derive estimates of the range errors for all satellites in view, and transmission of the range error estimates as "differential corrections" to users in the local area. Conceptually, DGPS could also be implemented using differential corrections on the position error level and, in fact, such systems exist. However, for most applications, systems based on corrections at the position level have been found to provide less overall benefit.

In general, the UERE after differential corrections depends on the time and distance between the data collection ground station and the user, the characteristics of the satellite component of UERE (especially Selective Availability), and the signal processing sophistication embodied in the user and

E-21

Correction Message

GPS
Receiver

Datalink
Transmitter

Computer

- Differential Correction Software

- GPS Antenna and
  Receiver
- Datalink Antenna
  and Receiver
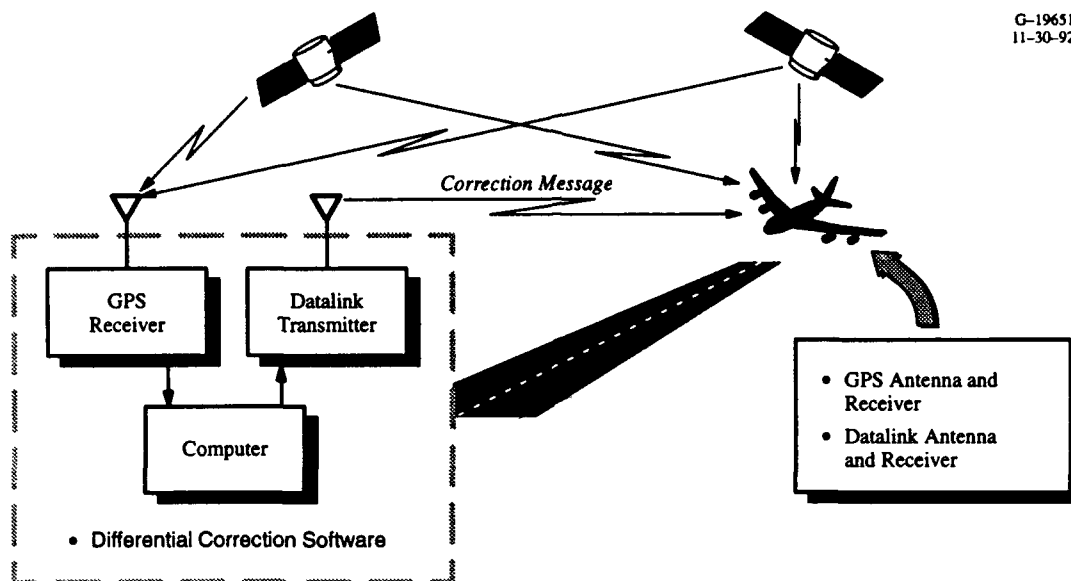
Figure E.3-2   Differential GPS Concept

ground station receivers. The UERE error budget components that are reduced most by differential corrections are satellite position errors, unintentional ephemeris errors, SA-induced ephemeris errors, and ionospheric delay. For a well implemented system involving corrections every 10 to 15 sec, these components can be reduced to less than 1 m (95 percent). Error budgets for DGPS will necessarily depend to some extent on the details of receiver and antenna implementation. Also, because the DoD has not made public the statistics associated with Selective Availability some uncertainty is associated with the level of its contribution. For these reasons, no single DGPS error budget can be considered authoritative. A typical error budget is given in Table E.3-3. This error budget assumes the use of modern signal processing techniques to reduce the impact of receiver noise. It also assumes a baseline (i.e., distance between differential reference station and user) on the order of 100 km or less. Note that under this set of assumptions the difference between PPS and SPS performance is not significant for DGPS.

While in non-differential operation the contributions of receiver noise and multipath are relatively small (especially in comparison to SA and uncompensated ionospheric delays), these are critical errors in DGPS (where SA and ionospheric errors are significantly reduced). Neither receiver noise nor multipath interference is reduced by differential corrections. In fact, noise and multipath experienced at the ground station can be embedded in the differential corrections with the result that the user is subjected to an additional source of error. Advanced receiver signal processing techniques (such as integrated Doppler processing or the use of closely-spaced correlators) to reduce the impact of receiver

noise are therefore commonly used in DGPS applications. Investigation of techniques to reduce the impact of multipath is an active area of current research. Promising techniques have been identified in receiver design (including the use of closely spaced correlators), antenna design, and antenna siting.

Table E.3-3   DGPS UERE Error Budget (Baselines less than 100 km)

GPS SEGMENT	ERROR SOURCE	PPS m, rms	SPS m, rms
SPACE	Clock and Navigation Subsystem Stability	0	0
	Predictability of Satellite Perturbations	0	0
	Other	0	0
CONTROL	Ephemeris Prediction Model Implementation	0.1	0.1
	Selective Availability	0	0.3
	Other	0	0
USER	Ionospheric Delay Compensation	1 – 2	1 – 2
	Tropospheric Delay Compensation	0.5 – 1.0	0.5 – 1.0
	Receiver Noise and Resolution	0.1 – 1.5	0.1 – 1.5
	Multipath	0.8 – 2.4	0.8 – 2.4
	Other	0	0
REFERENCE STATION	Receiver Noise and Reduction	0.1 – 1.5	0.1 – 1.5
	Multipath	0.5 – 1.5	0.5 – 1.5
TOTALS	Without Selective Availability	1.5 – 4.2	1.5 – 4.2
	With Selective Availability	1.5 – 4.2	1.5 – 4.2

Given the DGPS error budget of Table E.3-3, determination of DGPS accuracy in typical geometry is easily accomplished by applying the error equation (Eq. 3-1). Note that this equation remains valid for the DGPS case because differential corrections only impact UERE. The results presented Table E.3-4 are valid for both PPS and SPS users.

Table E.3-4   DGPS Accuracy in Typical Geometry

Horizontal Error (m, 2 DRMS)	4.5 – 12.6
Vertical Error (m, 95 percent)	6.0 – 16.8
Timing Error (nsec, 95 percent)	15 – 41

E.4   GPS AVAILABILITY ESTIMATION

E.4.1   Introduction and Overview

The Federal Radionavigation Plan defines the availability of a navigation system as "the percentage of time that the services of the system are usable." The approach to availability estimation described in this section recognizes that a system is "usable" for a specific application only when it meets the accuracy requirements of that application. For example, at the same instant, the GPS may fail to meet accuracy requirements at a given location for aircraft precision approach, while easily meeting requirements for harbor navigation at the same location. Thus, at this location and instant of time, GPS is usable for harbor navigation (and hence available) but unusable for precision approach (and hence unavailable). GPS availability must therefore always be associated with a level of accuracy. Depending on the application, the level of accuracy may be stated in terms of one-, two-, or three-dimensional position, or time.

Given an accuracy requirement, GPS availability at a given location can be defined as the percentage of time that GPS accuracy as defined by the error equation (Eq. E.3-1) meets the requirement. Given a fixed UERE, defined by building an error budget tailored to the specific application (e.g., accounting for receiver types and DGPS implementation, if any), the error equation allows the accuracy requirement to be restated in terms of a DOP requirement. For example, for aircraft nonprecision approach the accuracy requirement is 328 ft, 2 DRMS (or 164 ft, DRMS). If use of a minimum-capability C/A code receiver is assumed, the error budget of Table E.3-1 specifies a UERE of 83 to 88 ft, RMS. Availability for this application may therefore be stated as the probability that HDOP at the user location is 1.86 or less (1.86 = 164/88), where use of the high end of the specified UERE range ensures conservative results.

In this section, a procedure is described for developing distribution functions for HDOP, VDOP, PDOP, and TDOP at any user location. For HDOP, for example, the distribution function is defined by

$$H(x) = \text{Probability}(\text{HDOP} < x).$$

Given this function, the nonprecision approach example of the previous paragraph can be completed, that is, the probability that HDOP at the user location is 1.86 or less can be computed as

$$A = H(1.86)$$

A is the GPS availability for the example application.

A methodology for developing DOP distribution functions is described in detail in Section E.4.2. A representative set of distribution functions generated using this methodology is presented in Section E.4.3; this set is developed as an average over ten sites in the continental United States. Examples of the use of the distribution functions to develop GPS availability projections are provided in Section E.4.4.

E.4.2   DOP Distribution Function Methodology

The process of developing DOP distribution functions begins with development of approximate DOP "density functions" in the form of histograms. Conceptually, the histograms show the distribution of DOP that a user would experience at a fixed location over a very long period of time, where both satellite motion and satellite off-air time are considered. An example histogram for VDOP at New York City is given in Fig. E.4-1. In this example and in all subsequent availability calculations, the 21 Primary Satellite GPS constellation is assumed to be in place. The distribution functions are easily obtained from the density function histograms by numerical integration. Because most of the distribution functions calculated in practice tend to be clustered very close to one, the usual practice is to display the complement of the distribution function (i.e., one minus the distribution function). The complement of the distribution function for the New York City example is given in Fig. E.4-2.

A top-level logic flow for an algorithm to generate a DOP histogram for a single user location is given in the "pseudocode" fragment shown in Fig. E.4-3. In essence, the algorithm creates all the possible sets of conditions or "states" that a user can be presented with at the given location, where the different states are defined by different selections of:

- Time of day (defining a set of satellite locations)
- Sets of failed satellites

As an example, one specific user state might be defined by "Satellites ABCDE in view with satellite E failed." Given each such specific state, it is possible to calculate 1) the probability that the user is in the state (the "state probability") and 2) the DOP. The DOP level determines which histogram bin should be incremented, and the state probability determines the increment amount.

E-25
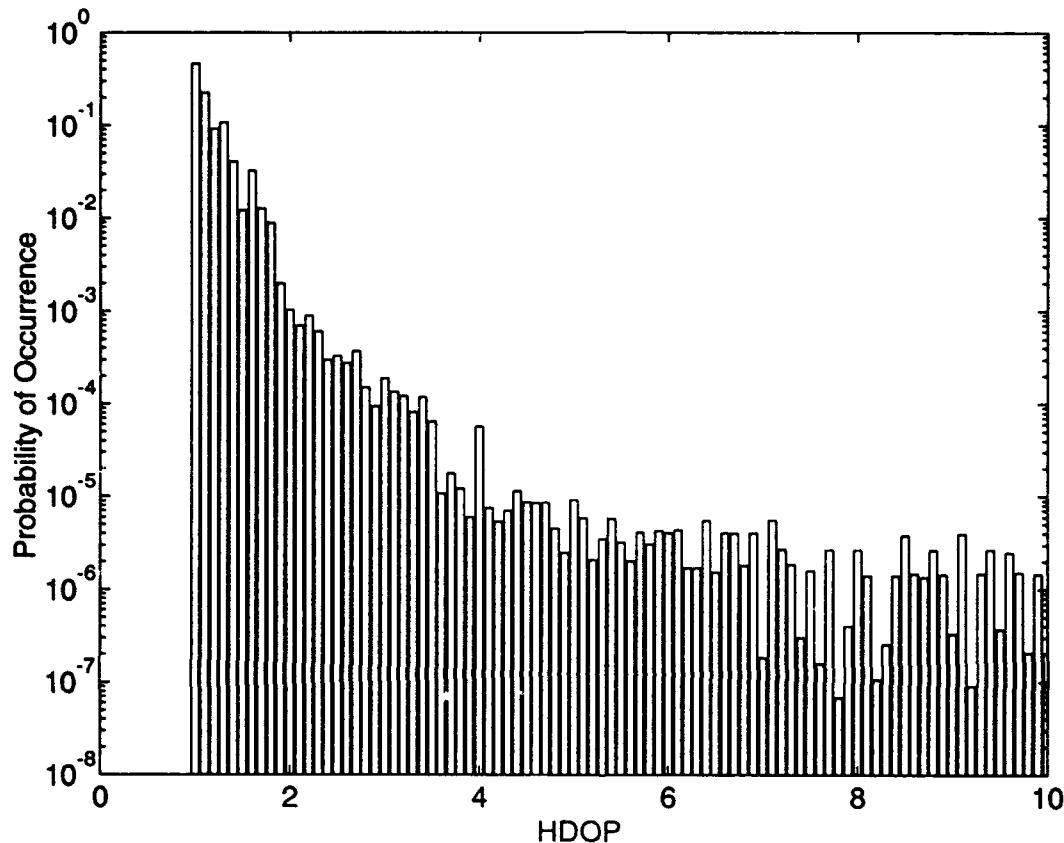
Figure E.4-1   VDOP Histogram for New York City

The key intermediate calculation in the availability of HDOP methodology is calculation of the probability of the appearance of a given set of good and bad satellites, denoted P(S) in Fig. E.4-3. Each P(S) is the probability that one specific set of the satellites in view at a given location and time is out of service. In this context, "in view" satellites are defined to be above mask angle specifications for the application of interest, where the mask angle is defined as the satellite elevation angle below which satellites will not be used.

G-34553
4-21-93
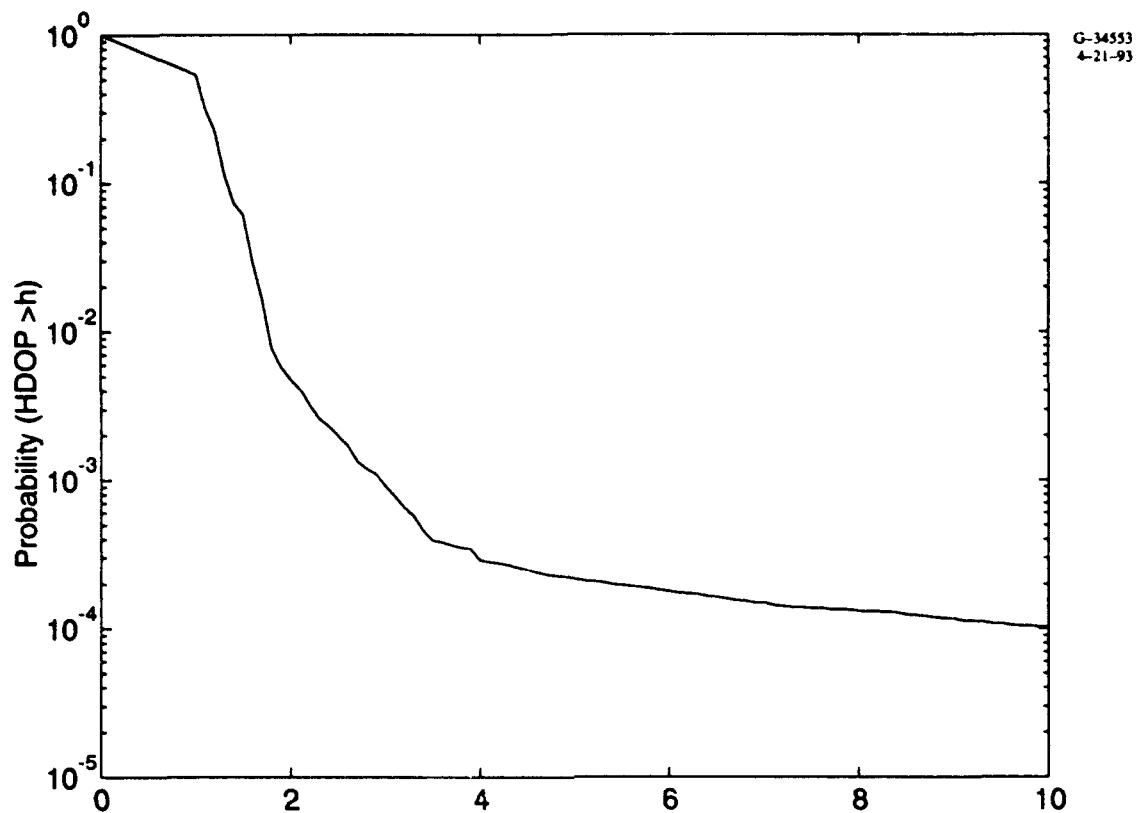
Figure E.4-2   VDOP Distribution Function Complement for New York City

```
Begin
        Loop through times, t, spanning 24 hr
                Calculate satellite positions
                For all out-of-service satellite sets, S
                        Calculate
                        Calculate (HDOP)
                        Increment HDOP bin by P(S)
                Next S
        Next t
End
```
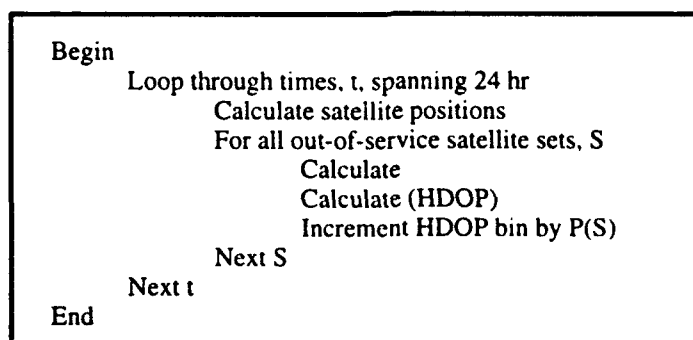
Figure E.4-3   DOP Calculation Algorithm

the application of interest, where the mask angle is defined as the satellite elevation angle below which satellites will not be used.

The methodology used to calculate P(S) is most easily illustrated by a simple example. We consider the case in which five satellites are in view, denoted for convenience ABCDE. One possible "outcome," i.e., specific selection of the set S, is

S = { ABCD good and E bad }.

The probability of the occurrence of S can then be written

P(S) = P(S | 24 good satellites) P(24 good satellites)
 + P(S | 23 good satellites) P(23 good satellites)
 . . .
 + P(S | 0 good satellites) P(0 good satellites)

where the vertical slash ("|") denotes a conditional probability. Methods are therefore needed to calculate probabilities of the forms P(S | i good satellites) and P(i good satellites).

The approach adopted to calculate probabilities of the form P(S | i good satellites) is again most easily illustrated using a simple example. If we take S = { ABCD good and E bad }, then

P(S | 22 good satellites)
 = P(S and 22 good satellites)
    P(22 good satellites)

 = (Combinations where S and 22 good satellites)
    (Combinations where 22 good satellites)

 = (19 1) / (24 2) = .07

where

(19 1) = the number of ways to choose 1 of the 19 out-of-view satellites to be bad (we are only free to choose states for the out-of-view satellites, because the in-view satellites are defined by S)

(24 2) = the number of ways to choose any 2 of 24 satellites to be bad.

This calculation is is based on the assumption that all possible combinations of i good satellites are equally likely to occur.

A methodology for calculating of "constellation state probabilities" of the form P(i satellites good) has been developed by Durand and Caseau, Ref. 1. This methodology models the constellation

state in terms of a Markov chain (described in Ref. 2 and other standard texts). Within the Markov chain, movement between constellation states is dictated by both occurrences of and recovery from:

- Long-term satellite failures (satellite launch needed to repair)

- Short-term satellite failures (repair possible using redundant equipment on board satellites)

- Satellite maneuvers that make the satellite signal unusable.

The failure and restoration processes are described in terms of probability density functions, where the random variables are time to failure and time to restore. The transition between states is constrained such that no more than one satellite is permitted to maneuver at any given time, consistent with assumed DoD policy.

In Ref. 1, published models (i.e., density functions) for long-term failures, short-term failures, and maneuvering are surveyed. In addition, the state probabilities resulting from different combinations of the available models are calculated and compared with state probability estimates provided by DoD. The model combination that provides the best agreement with the DoD state probabilities is summarized in Table E.4-1.

Table E.4-1   Satellite Failure and Maneuver Models (Ref. 1)

PARAMETER	FORM OR VALUE	COMMENTS
Long-term failures[1] MTBF MTTR ($1/\mu$) Failure density Restoration density	 124 months 1 month $0.0006 t^{0.6} \exp[-(t/138.6)^{1.6}]$ $\mu e^{-\mu t}$	NATO Navstar Technical Support Group Meeting
Short-term failures[2] MTBF($1/\lambda$) MTTR ($1/\mu$) Failure density Restoration density	 7300 hours 36 hours $\lambda e^{-\lambda t}$ $\mu e^{-\mu t}$	ICAO FANS, November 1986 Standard models
Maneuvers[3] Frequency Duration	 7 years 3 days	Assumes change to satellite altitude

Notes:
1. Requires satellite launch to repair
2. Repairable by ground control
3. A key assumption is that multiple satellites are never maneuvered simultaneously

The models of Table E.4-1 have been combined and employed to calculate the constellation state probabilities. The result is shown in Table E.4-2 (second column). The third column of Table E.4-2 is the probability that a given number of satellites or more will be operational.

Table E.4-2 Number of Operational Satellites for DoD-Provided Constellationr

NUMBER OF OPERATIONAL SATELLITES	PROBABILITY OF OCCURRENCE	CUMULATIVE PROBABILITY
24	0.703	0.703
23	0.277	0.930
22	0.055	0.985
21	0.012	0.9975
20	0.002	0.9995
19	4.2×10^{-4}	0.9999
18	7.1×10^{-5}	1.0000

E.4.3   Typical DOP Distribution Functions

Figure E.4-4, Fig. E.4-5, and Fig. E.4-6 show distribution function complements for HDOP, VDOP, and TDOP, respectively. The distribution functions are computed over an ensemble of ten United States cities selected to provide geographic diversity: New York, Chicago, Los Angeles, Dallas, Denver, Detroit, St. Louis, Atlanta, Miami, and San Francisco. At each city, time (and the corresponding satellite configuration) is sampled every 5 minutes over a 24-hour period.

E.4.4   Availability Estimation Example

The example of the Coast Guard differential GPS service is used here to illustrate availability estimation using the distribution function complements presented in Section E.4.3. The horizontal accuracy requirement for this service is expected to be set at 10 m, 2-DRMS. For the purpose of this example, assume that the Coast Guard DGPS architecture has been shown to provide UERE near the 1.5 m, rms, level indicated in the error budget of Table E.3-3.

Because the DGPS accuracy requirement is stated in terms of horizontal accuracy, the availability estimation process will focus on HDOP. An acceptable level of HDOP, *h*, is obtained by applying

the accuracy requirement (expressed as a DRMS statistic) and the UERE in the error equation, Eq. 3-1. The result is

$$h = 5/1.5 = 3.3$$

The unavailability associated with this HDOP level may be read directly from Fig. E.4-4, the value is $5 \times 10\text{-}4$. That is, the availability of the HDOP level needed to meet the DGPS accuracy requirement is estimated to be 99.95 percent.
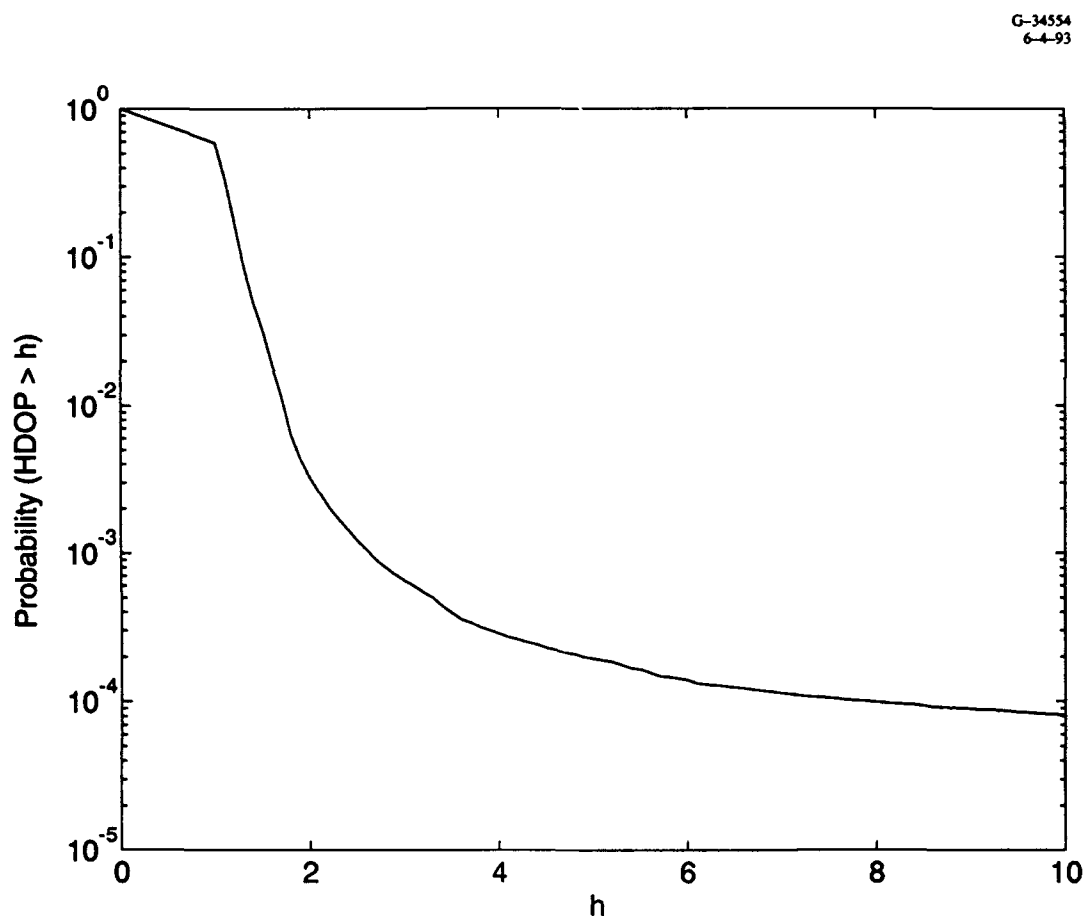
Figure E.4-4 HDOP Distribution Function Complement for Ten Cities
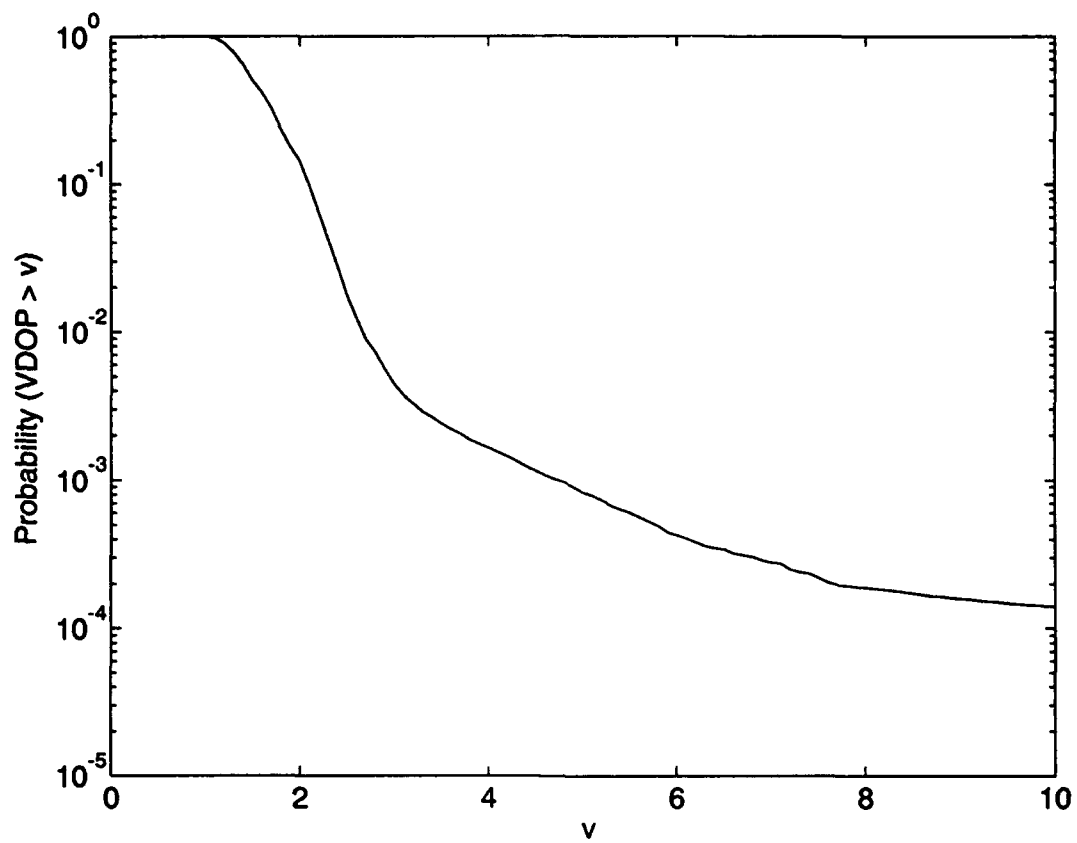
Figure E.4-5   VDOP Distribution Complement for Ten Cities
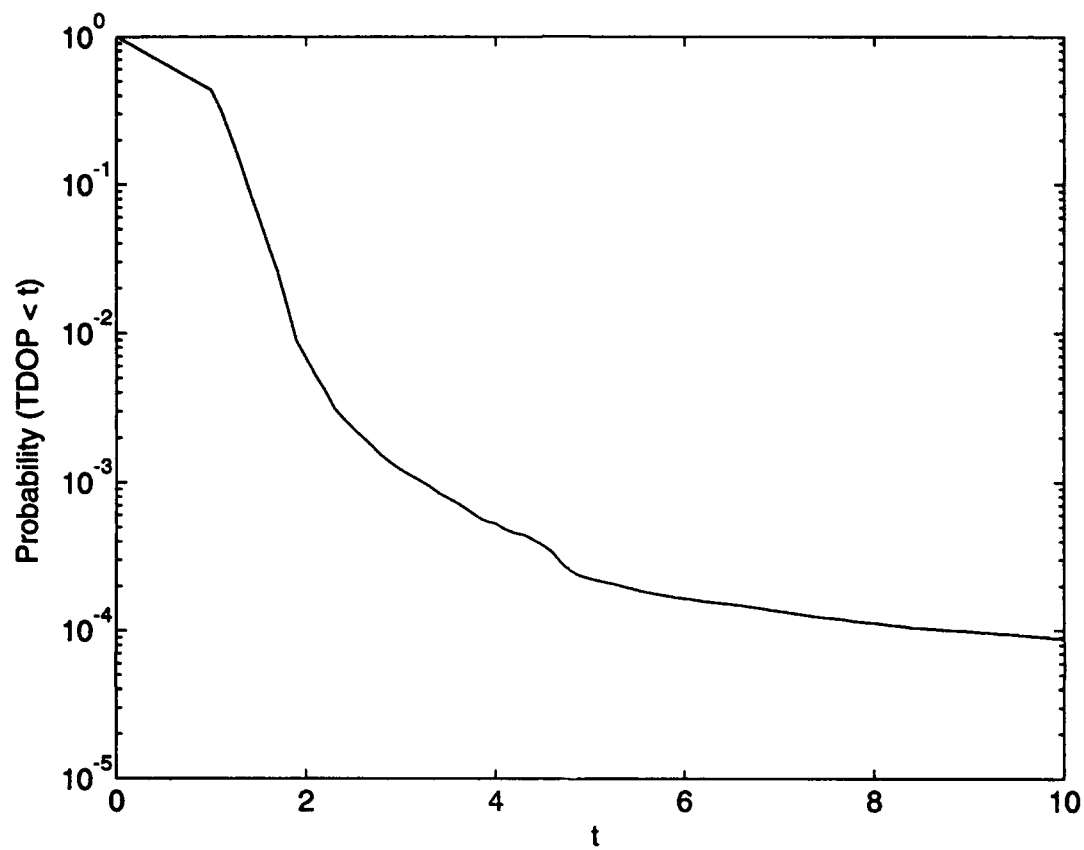
Figure E.4-6   TDOP Distribution Function Complement for Ten Cities

REFERENCES

1. Durand, J.M., and Caseau, A., GPS availability, part II: evaluation of state probabilities for 21 and 24 satellite constellations, *Navigation, Journal of the Institute of Navigation*, vol. 37, no. 3, Fall 1990.

APPENDIX F
GPS USER EQUIPMENT

F.1 INTRODUCTION

The GPS User Segment includes any and all users who receive and process GPS L-band signals for a large variety of applications. In addition to the principal function of general navigation, other applications range from precise tracking of ballistic missiles using all satellites in view, to surveying involving all satellites in view and signals at both L-band frequencies, to precise time transfer that may include single-satellite tracking. The wide variety of potential GPS applications naturally leads to a great diversity in the design of the user equipment available. As the recognized number of commercial applications for GPS has grown, manufacturers of user equipment have become increasingly aware of the potential size of the GPS market. Competition for a slice of this large potential market has led to innovation in GPS receiver designs at a rapid pace. As a result, GPS users are presented with a large number of choices in selecting user equipment for a particular application. It is expected that the number of choices available will only grow as GPS reaches full operational capability.

The intent of this appendix is to provide potential users of GPS with sufficient background to understand the major design choices available today in user equipment. In particular, the following variables are considered:

- Standard Positioning Service (SPS) vs. Precise Positioning Service (PPS); the PPS is only available to military and other DoD approved users

- Single vs. dual frequency; for some applications, benefits may be derived from the use of both L-band frequencies even for civilian (non–PPS) users

- Number of channels; where only a few years ago, multiple channels were only considered appropriate for high-dynamic applications, new technology is providing affordable multichannel benefits to many users

- Code/carrier integration; many receiver manufacturers are deriving significant accuracy improvements through advanced processing of both the code and carrier signals incorporated in the GPS satellite broadcast

- Use of digital technology; increasing use of digital technology in GPS receivers is providing benefits in cost, flexibility, and reliability.

User equipment today is evolving toward maximum use of digital technology and a high degree of code/ carrier integration, especially for civilian applications. This evolution has been driven both by the improved performance available from these technologies, and the potential for lower manufacturing costs in highly digital designs.

This appendix begins, in Section F.2, with an overview of a generic GPS receiver design. Sections F.3 and F.4 then explore some specific GPS receiver designs in the military and commercial worlds, respectively.

F.2   GENERIC RECEIVER DESIGN

GPS receiver design architectures vary considerably. However, these designs are generally partitioned into a *receiver measurement* function and a *navigation and control* function. The receiver measurement function performs pseudorange and delta range processing and measurements along the user-to-satellites lines of sight (LOS). The navigation and control function projects these measurements into the user's navigation coordinate system and performs overall receiver system management. This section presents a general overview of these GPS receiver functional entities.

F.2.1   Basic Receiver Measurements

Two primary forms of measurements are performed by GPS receivers to estimate range and velocity between the user and a given satellite. In both cases, these measurements are related to observed changes in the user-to-satellite LOS range derived from two somewhat independent receiver tracking-loop processes. In the case of LOS distance-related measurements, *pseudorange* (PR) estimates are derived from receiver *code tracking loops* implemented in a variety of *delay-lock loop* (DLL) design configurations. In the case of LOS velocity-related measurements, *accumulated delta range* (DR)* estimates are derived from receiver *carrier tracking loops*. Carrier tracking loops are usually implemented in the form of Costas loops, arc-tangent loops, or other coherent phase-lock-tracking loop configurations. Table F.2-1 presents the inter-relationship among these receiver terminologies for clarity. These tracking loop processes form the basic building blocks of GPS receivers and are discussed in further detail in subsequent subsections of this chapter.

---

*Actually, this is delta pseudorange — however, this appendix uses delta range for conciseness.

Table F.2-1   Relationships Among GPS Receiver Measurement Terminology

MEASUREMENT	MEASUREMENT OBSERVATION	MEASUREMENT IMPLEMENTATION
RANGE	PSEUDORANGE	CODE TRACKING LOOPS [1]
VELOCITY	DELTA RANGE	CARRIER TRACKING LOOPS [2]

[1]For example, Delay Lock Loop (DLL), Coherent DLL, Noncoherent DLL, -Dither DLL, . . .
[2]For example, Phase Lock Loop, Costas Loop, 4th-Power Loop, Arc-Tangent Loop, . . .

The basic operations performed by GPS receiver measurement functions are:

- Code tracking

- Carrier tracking

- Acquisition/reacquisition

- Carrier-to-Noise Power Spectral Density (C/N_o) estimation

- Data demodulation.

Figure F.2-1 presents a highly-generic block diagram of a receiver tracking loop. This diagram will form the basis of subsequent tracking-loop discussions. *The fundamental purpose of the tracking loop is to compare the received signal to a locally generated replica, or estimate, of the received signal,*
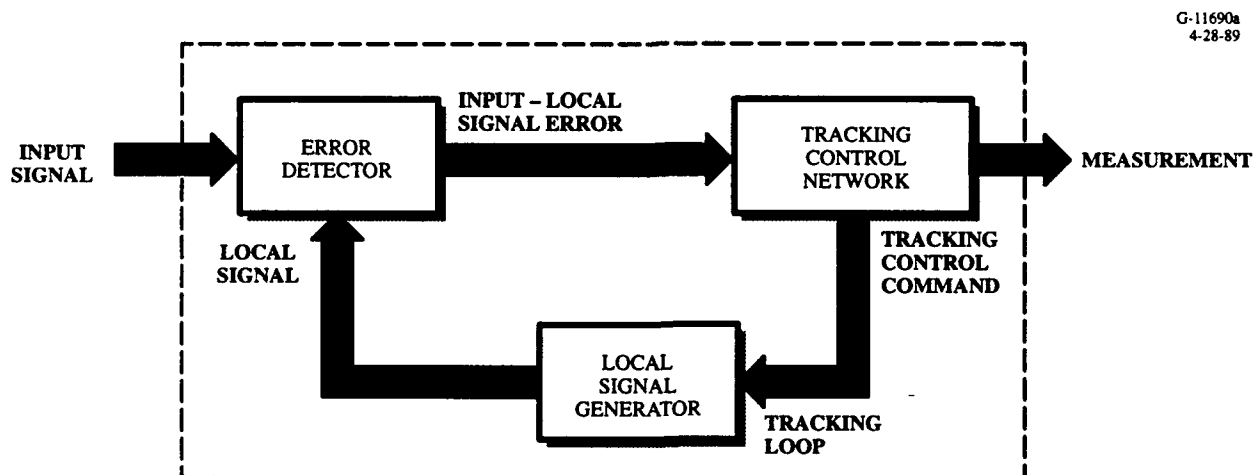
Figure F.2-1   Generic Tracking Loop Functions

F-3

and to minimize the estimate error under closed-loop control. Intuitively, one desires that the local replica signal approximate the received signal as closely as possible. Residual errors determined by the *error detector* are input to the tracking-loop network. The *tracking-loop network* prescribes a control law commensurate with the detected error to generate a tracking control command to the *local signal generator.* The tracking-loop network may contain first, second, and third orders of control using proportional path, integral path, or double-integral path, respectively. Tracking-loop bandwidths are selected so as to accommodate anticipated uncertainties in the received signal related to vehicular dynamics, oscillator errors, and noise sources (interference jammers). This selection process must ensure that the bandwidth is wide enough to handle dynamics and oscillator uncertainties, yet narrow enough to reject noise power levels within the loop-bandwidth relative to the received signal. The local signal generator accepts the tracking-control commands and generates a replica signal based on this command, which in time, produces an estimate of the received signal in both frequency and phase. A closed-loop process is thus formed.

The performance capability of code and carrier tracking loops can be greatly affected by the performance of the receiver's frequency standard used to generate local code and carrier estimates of the code and carrier signals received at the receiver's antenna. These local replica signals are synthesized directly from these receiver frequency standards. A variety of precision crystal oscillators have been implemented as GPS-receiver frequency standards. In addition to temperature-sensitive error terms, the types of crystal oscillators chosen for specific GPS receiver applications are largely driven by the expected vehicle dynamics exciting the oscillator's G-sensitive error sources. Errors in the frequency standard propagate into errors induced in the receiver tracking loops — and thus the receiver's ability to generate stable local code and carrier replica signals. Receiver measurements are ultimately affected. Principal crystal-clock error sources and their relative effects on carrier tracking performance are illustrated in Fig. F.2-2.

In more sophisticated applications, atomic standards, or clocks, may fulfill the receiver's frequency-standard role. Cesium, rubidium, and hydrogen maser clocks — with accompanying costs/performance tradeoffs — have been used in some applications. However, use of atomic clock frequency standards in typical user applications is inappropriate for consideration.

Another measurement function performed by some GPS receivers is the L1/L2 dual-frequency measurements accomplished to correct for time delays encountered by RF propagation through the ionosphere. PR errors may be directly measured — and thus compensated for — by P-code receivers suitably equipped to track the L1 and L2 frequency signals. Since ionospheric effects change rather slowly,
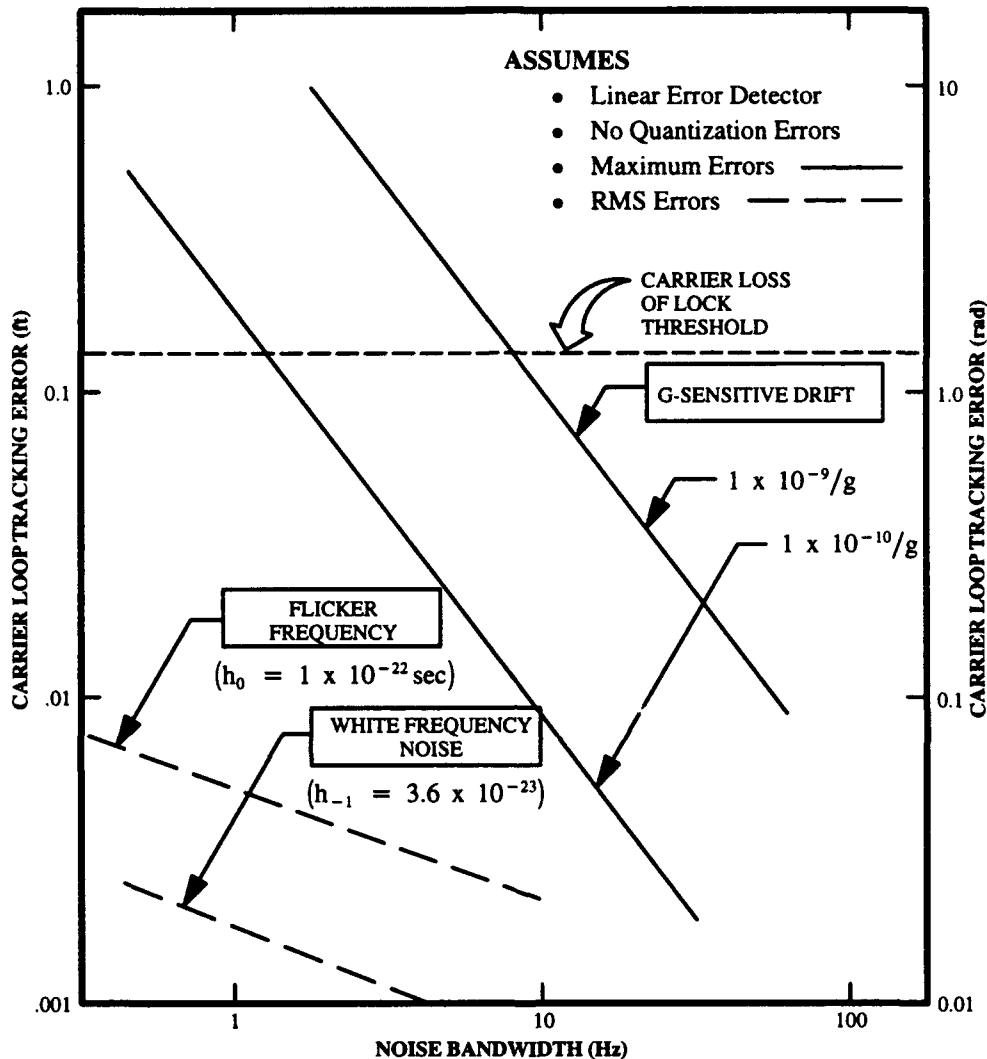
Figure F.2-2   Principal Frequency Reference (Clock) Error Sources and
Their Relative Effects upon Carrier Loop Tracking Performance
vs. Noise Bandwidth

these measurements may be accomplished at rates considerably less than the fundamental PR-measurement rate. A slight penalty is incurred in receiver noise when implementing dual-frequency measurements. However, this additional noise-related error source is considered negligible when compared to the derived benefits of compensating for significant time delays imposed by the ionosphere. Receivers designed without the dual-frequency tracking capability, that is, nearly all commercial receivers, must resort to less accurate ionospheric modeling techniques.

F.2.2   Code Tracking Loops

The primary purpose of the code tracking loop is to compare the incoming PRN code — which is delayed in time by the propagation distance — with the receiver's internally generated replica of the time-delayed PRN code — and to *minimize* the residual difference, or tracking error. The receiver's code estimate is therefore time shifted (or equivalently phase shifted) to match the free-space propagation delay of the received satellite code. The magnitude of code-loop time shift provides the basis for performing pseudorange measurements. The term pseudorange is used since the code loop's time shift includes the actual range plus the receiver clock error relative to GPS system time (and other propagation delays). Changes in code frequency related to Doppler effects are also accounted for in the local code generation process. Figure F.2-3 presents a simplified diagram of the relationship among the time-indexed code transmitted by the satellite, the resultant free-space propagation delay, and the time-shifted, time-indexed PRN code estimate generated internally by the receiver. This time shift is simply scaled by the speed of light, c, to get an uncorrected pseudorange measurement. Corrected pseudo-ranges are produced when the deterministic effects of ionospheric and tropospheric delays are sub-tracted from the uncorrected pseudoranges. Since pseudorange measurements are based upon unique GPS time-of-week code states, they therefore represent *absolute* measures of pseudorange from the user to the satellites.

Figure F.2-4 shows an elementary block diagram of the code-tracking-loop mechanization. At the heart of the code tracking loop is the autocorrelation process. In the upper left corner of this figure,
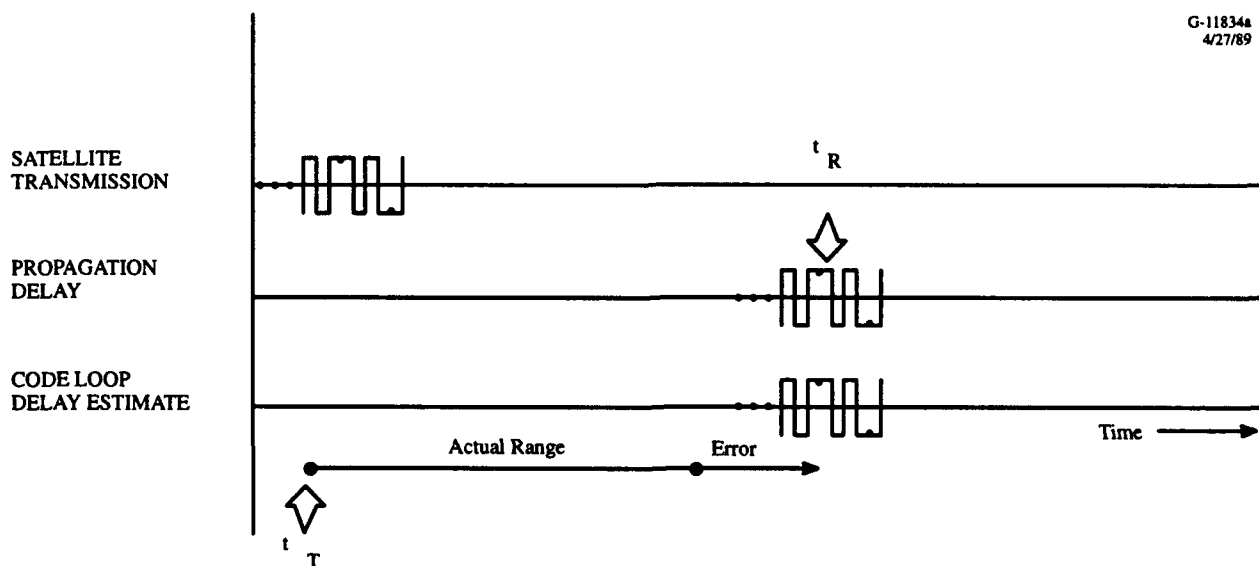
Figure F.2-3   Free-Space Propagation Delay of Transmitted Satellite PRN Code and the Receiver's Delayed Version of the Transmitted PRN Code
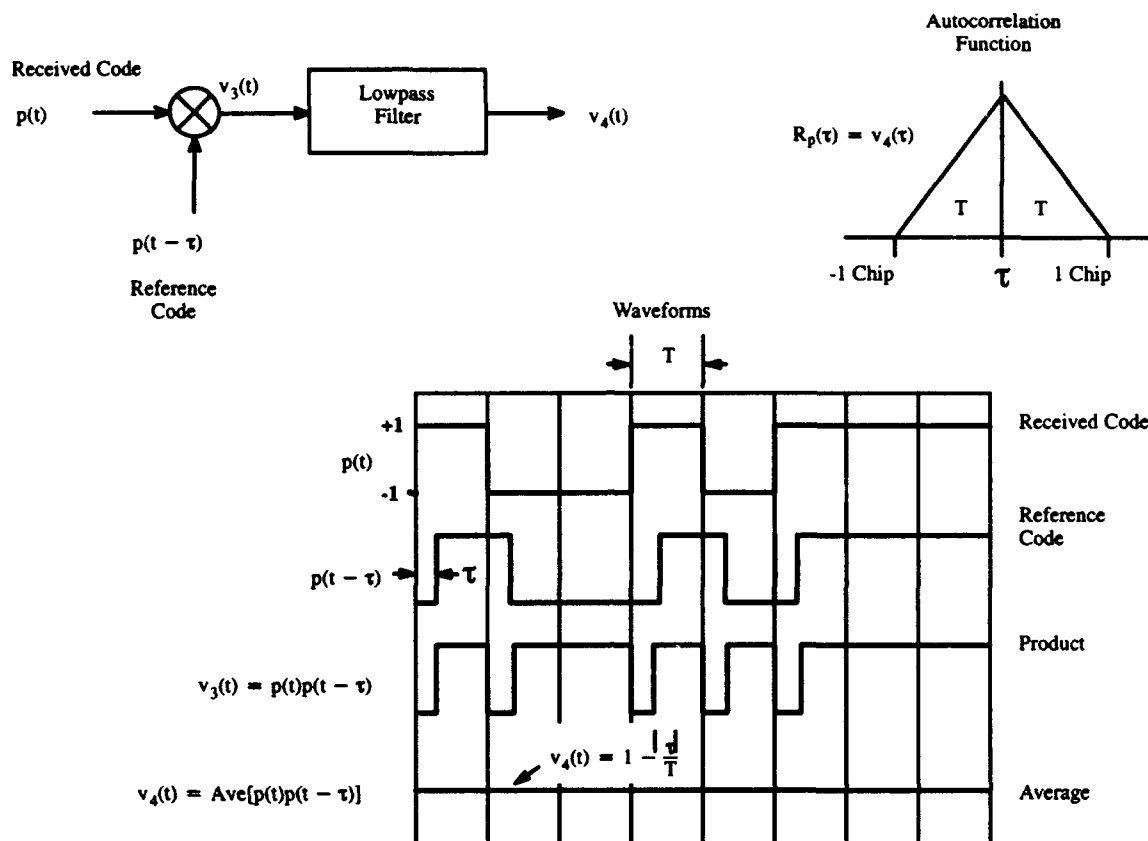
Figure F.2-4   Basic Code Correlation Process

the received code signal, *p(t)*, is compared with a local replica, or reference code, signal, *p(t-τ)*, to pro-
duce an error signal, *p(t)p(t-τ)*. This operation represents the error detector function shown earlier in
the generic tracking loop block diagram. The waveforms shown in the center diagram illustrate this
process whereby the "voltage," v_3 (*t*) is produced. This error "voltage" is then processed through a
low-pass filter to extract the DC component of the error signal, $v_4(t)$, from the actual error, $v_3(t)$. τ
represents the time-mismatch error in the receiver-generated code and the actual received code and is
approximated by this DC value. The autocorrelation function shown in the upper right of this figure
provides a mathematical expression describing the effects of code estimation error (time mismatch) on
the ability to track the received code signal.

Code tracking loops are traditionally implemented in GPS receivers as delay-lock loops (DLL).
Figure F.2-5 portrays the manner by which the autocorrelation process is used to track the received code.
Actual designs of DLLs vary considerably, with state-of-the-art receivers implementing DLLs using
Application Specific Integrated Circuits (ASIC) in hardware and digital signal processing algorithms
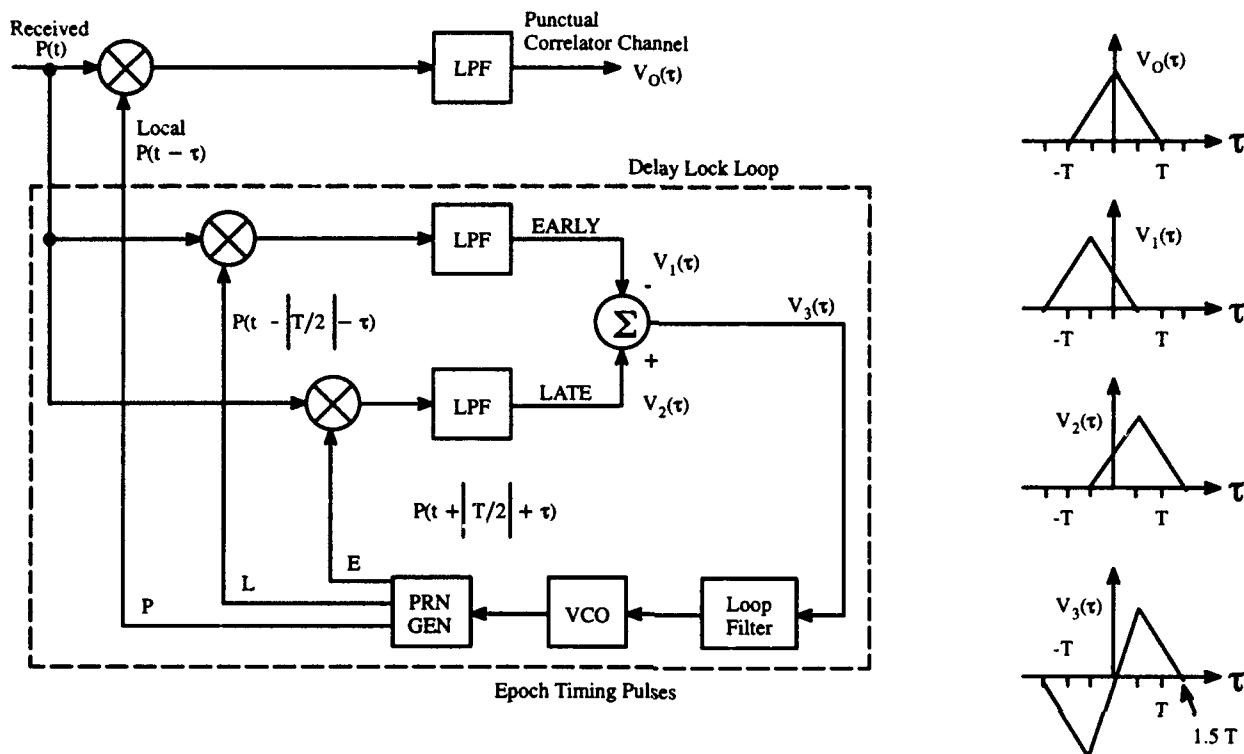
Figure F.2-5   Basic Code Tracking Loop (Delay Lock Loop)

in software. Three correlation processes are accomplished in the DLL — *early* correlation, *late* correlation, and *punctual* (on-time) correlation. The early and late correlators are advanced and retarded, respectively, by half-chip widths as shown within the dash block diagram. This facilitates the means whereby a linear tracking function, v_3 (τ), is realized — within ± 1.5 chip widths — by differencing of these two signals. The linear tracking function reflects the tracking loop network function (consisting of a proportional path only) discussed in the generic tracking loop diagram. The resultant linear tracking function is shown to the right of this figure as v_3 (τ). The punctual signal, v_0 (τ), is used for C/N_0 estimation and is used for code-wipe (PRN despreading) in the carrier tracking loop.

It is incumbent upon the DLL to maintain tracking control within the proportional zone of this DLL tracking function. In fact, the limits of the proportional zone define the maximum loss-of-lock limits for the DLL — i.e., $\pm 1/2$ chip lengths — with stable DLL tracking using only 1% to 10% of this range depending upon design and vehicle dynamics. Code estimation error described by this function

drives a PRN-code generator that advances and retards the early, late, and punctual codes according to the loop estimate code delay error. The first-order nature of the DLL implies that, given significant levels of vehicular dynamics, DLL loss of lock would occur without an external source of aiding. For this reason, the DLL is typically velocity aided by the carrier tracking loop. In the event the carrier tracking loop velocity data is lost or unavailable, then a properly integrated inertial measurement unit (IMU) can readily satisfy the DLL velocity-aiding requirements. First-order DLLs are typically used for code tracking to minimize the loop response time. Given a ramping-velocity input, however, will cause the DLL to lose lock. In unaided receivers, second-order DLLs are sometimes implemented in noncoherent receiver tracking conditions whereby the receiver resorts to AFC tracking thus inhibiting velocity aiding of the code loop. Basic pseudorange measurements are described by Eq. F.2-1.

$$PR = c \, (t_r - t_t) \tag{F.2-1}$$

where:

PR = Pseudorange

c = Speed-of-light constant

t_t = Time of satellite code transmission

t_r = Time of code reception.

Measures of pseudorange are typically updated at one Hertz. These measures are generally produced by averaging pseudorange observations collected at a higher rate, e g., 10 Hz. These observations, or predetection, intervals are selected as integer fractions or multiples of the basic 20-ms Navigation Message data-bit interval depending on the receiver designs.

Equation F.2-2 presents the parametric sensitivities of the tracking loop bandwidth, received carrier power, noise power spectral density, and predetection integration period on overall rms tracking-error response of the code loop. The rms tracking error is the generally accepted measure of the tracking loop's ability to maintain lock. It should be noted that the rms code tracking error is directly proportional to the P-code and C/A-code chip lengths.

$$\sigma_c \geq T_c \left[\frac{NB_L}{2C} \left(1 + \frac{2N}{CT_I} \right) \right]^{1/2} \tag{F.2-2}$$

where:

σ_c = rms code-tracking error (dimensionless)

T_c = Code chip period length (sec)

N = Noise power in one Hertz bandwidth (W/Hz)

C = Received signal power (W)

B_L = Code-loop noise bandwidth (Hz)

T_I = Prediction interval period (sec).

Figure F.2-6 shows the resultant effects of different values of T_I and B_L upon the code loop rms noise given various jammer-to-signal ratios. Code tracking loss-of-lock limit is selected as 0.316 chips in this case. The different curves below Curve A reflect enhanced tracking conditions made feasible by IMU aiding of the code loop, and further by the addition of 50-bps data aiding (using a priori Navigation Message data-bit information).

CURVE	BL	TI
A	1	0.02
B	0.10	0.02
C	0.01	0.02
D	0.01	0.20
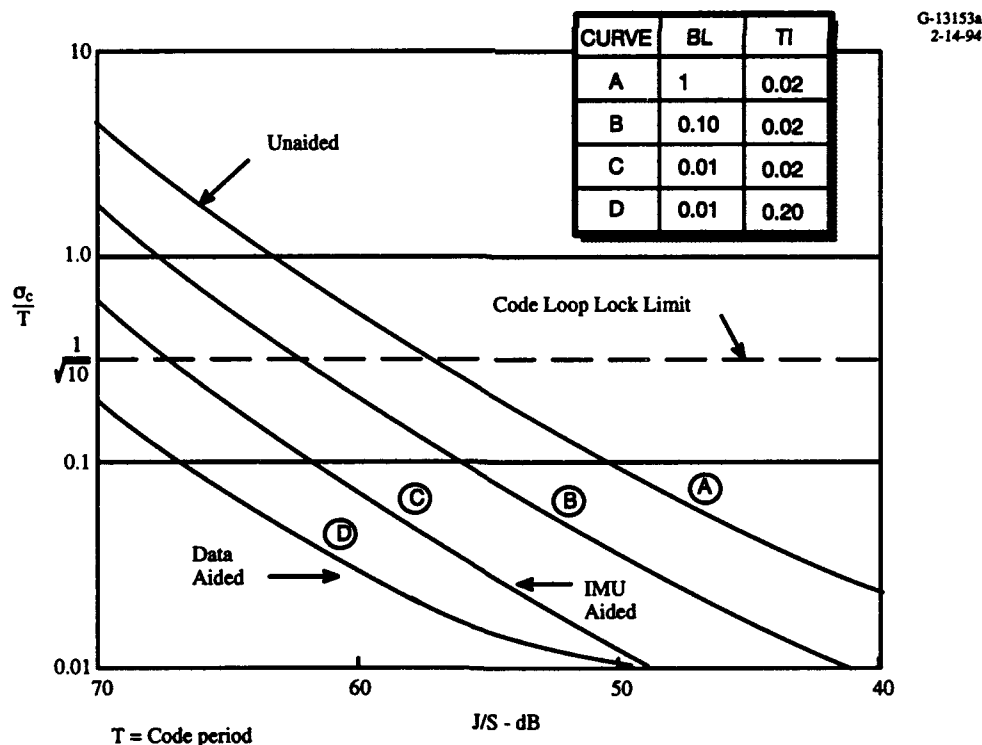
Figure F.2-6   Code Tracking RMS Error for Various Tracking Loop Bandwidths and Predetection Integration Period as a Function of Jammer-to-Signal Ratios

F.2.3   Carrier Tracking Loops

The primary purpose of the carrier tracking loop is to compare the incoming carrier signal — in both phase and frequency — with the receiver's internally generated replica of carrier phase and frequency, and to minimize the residual phase and frequency differences. Phase lock (also known as coherent tracking) is achieved when the receiver's estimate of carrier phase and frequency matches the incoming carrier phase and frequency to within approximately one radian of phase. Within this phase-track limit, errors are relatively linear. Beyond these phase-track limits, nonlinear effects become apparent and the carrier tracking loop is then subject to cycle-slipping or loss of lock.

Accumulated delta range measurements are also measures of range — but in a *relative* sense. Because carrier phase is ambiguous by an integer number of cycles, pseudorange cannot be measured directly for carrier phase. However, a carrier-cycle "count" may be accumulated over a specified time interval and scaled by the carrier wavelength to derive a range measurement for that time interval. In actuality, this "count" is determined by changes in the carrier VCO rate commands (plus delta-phase error measurements at the beginning and end of this interval) over the interval duration. A subsequent carrier-cycle "count" over the following time interval will yield another range measurement over that interval. Differencing these two range measures results in a relative range difference, or delta range, over the second time interval. A rudimentary diagram of the delta range measurement process is presented in Fig. F.2-7. Equation F.2-3 describes a discrete delta range measurement over a delta range measurement interval.

$$DR_k = \lambda \left[\left(n_k + \frac{\phi_k}{2\pi} \right) - \left(n_{k-1} + \frac{\phi_{k-1}}{2\pi} \right) \right] \qquad (F.2-3)$$

where:

DR_k = Delta range measurement for interval t_k - t_{k-1}

λ = Carrier wavelength

n_k = Number of whole cycles during interval t_k

ϕ_k = Phase of 1 at t_k.
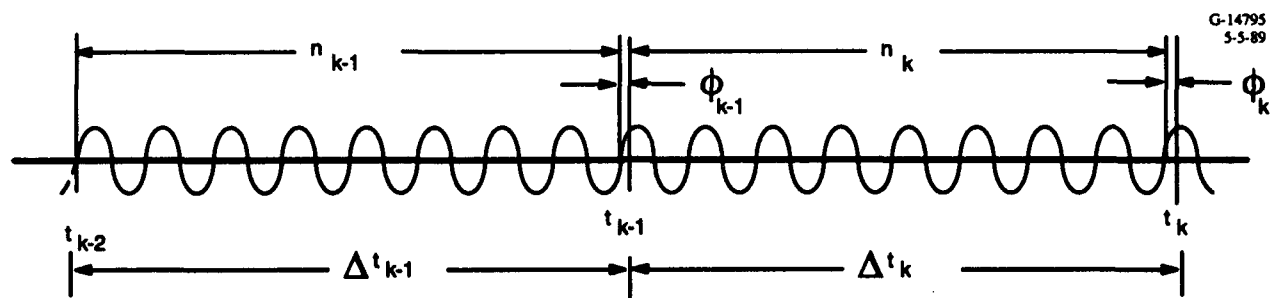
Figure F.2-7   Accumulation of Whole and Fractional Carrier Cycle Counts Over
Adjacent Finite Periods for Determination of Delta Range

This equation shows the whole-cycle and fractional-phase count over the *k-1* interval differenced with a similar count over the *k* interval. This difference is scaled by the carrier wavelength — thus providing a direct measure of range difference between the two intervals. Delta range measurements are typically updated at a 0.1-Hz rate. Like the code tracking loops pseudorange measurements, carrier phase measurements are produced by averaging carrier-phase observations collected at a higher rate. These observation intervals are similarly chosen as integer fractions or multiples of the fundamental 20-ms data-bit period. It should be noted that the DR_k measurement is equal for both P-code and C/A-code receivers with all other factors held constant.

Carrier tracking loops are in some respects more complex than code tracking loops. Since the GPS signal employs BPSK modulation, the carrier component is suppressed and the phase reference signal must be internally reconstructed by the receiver tracking loop. For BPSK modulation, two primary techniques for carrier recovery include frequency-doubling phase-lock loops and Costas loops — or other In-phase/Quadri-phase (I/Q) tracking loop implementations. The carrier estimate is generated by a voltage-controlled oscillator (VCO), or in the case of state-of-the-art digital receivers, as numerically controlled oscillators (NCO). Data demodulation of the 50-bps Navigation Message is also derived via the Costas loop.

Figure F.2-8 presents a *simplified* Costas tracking loop to convey the the principal technical issues associated with coherent phase tracking of BPSK signals. The incoming signal is split — with each branch being mixed with an In-phase (I) and Quadri-phase (Q) tracking loop estimate of the incoming signal. The I-signal component resulting from the mixing process is applied to a low-pass filter (LPF) from which the data-bit sign times the cosine of the loop error is produced. The *loop error* is defined as the received signal phase minus the locally generated phase estimate (matching frequency is implied). Since the loop error is very small under stable carrier phase tracking conditions, then one is able to determine the data-bit polarity at this point as shown in the figure. A similar process occurs for

$$\frac{D(T)}{2} \cos(\theta - \hat{\theta}) -$$

$$-\frac{D(T)}{2} \cos(2\omega_o t + \theta + \hat{\theta})$$

$$+ n(t) \sin(\omega_o t + \hat{\theta})$$

IN-PHASE (I)

LOOP ERROR

$$\theta_E = \theta - \hat{\theta} \approx 0$$

G-11838
6-28-89

DATA

LPF

$$\frac{D(T)}{2} \cos \theta_E$$

$$\approx \frac{D(T)}{2}$$

$\sin(\omega_o t + \hat{\theta})$

$$\frac{D^2(T)}{4} \sin \theta_E \cos \theta_E$$

$$= \frac{D^2(T)}{8} \sin 2\theta_E$$

$D(T) \sin(\omega_o t + \theta) + n(t)$

VCO

LOOP FILTER

$D(T)$ = *Data bit*(+ − 1)

T = *Data period*

ω_o = *Carrier freq.*

θ = *Carrier phase*

$n(t)$ = *Noise term*

90°

$\cos(\omega_o t + \hat{\theta})$

LPF

$$\frac{D(T)}{2} \sin(\theta - \hat{\theta}) -$$

$$\frac{D(T)}{2} \sin \theta_E$$

$$-\frac{D(T)}{2} \sin(2\omega_o t + \theta + \hat{\theta})$$

QUADRI-PHASE (Q)

$$+ n(t) \cos(\omega_o t + \hat{\theta})$$
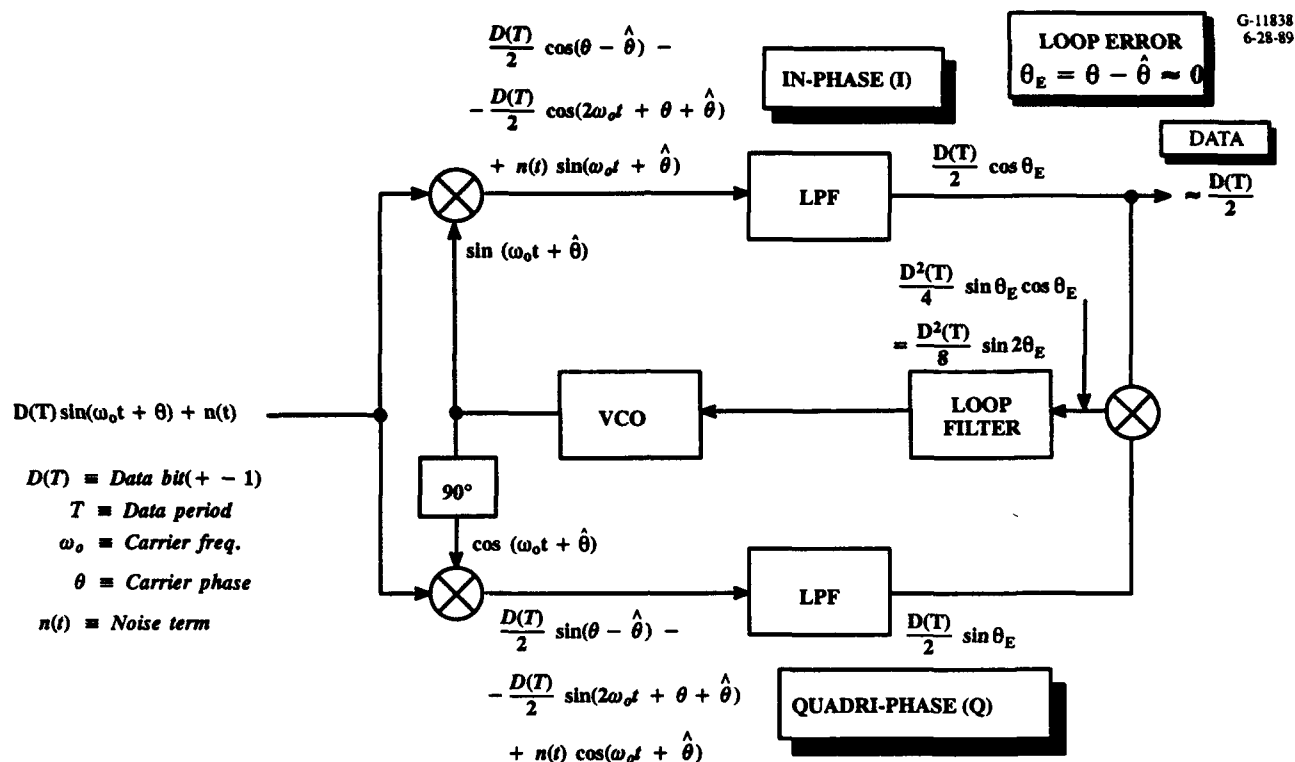
Figure F.2-8   Simplified Block Diagram of a Simplified Costas Loop for
Coherent Phase Tracking

the Q signal resulting in the data-bit sign times the sine of the loop error. The I and Q signals are mixed resulting in a term containing the sine of twice the loop error. Since the loop error is maintained at a small value during stable tracking, small-angle sine approximation of this term results in a direct measure of loop error. This error measure is applied to the tracking-loop network (generally a third-order loop filter while in coherent-phase track) — the output of which generates a tracking control command to the VCO — thus providing a closed-loop estimate of the received carrier signal. This represents the simplest Costas loop implementation. Other Costas loop techniques employ decision-directed data aiding. Many digital receiver use an arc-tangent tracking loop implementation to accomplish coherent phase tracking. Regardless, the function of the carrier tracking loop remains the same.

Carrier-phase rms loop error is described by Eq. F.2-4. Like the code tracking loop, this equation identifies carrier tracking loop sensitivities to carrier tracking-loop bandwidth, received carrier power, noise power spectral density, and predetection integration period in terms of rms phase error. Similarly to code tracking, the rms carrier tracking error is the generally accepted measure of the tracking loop's ability to maintain lock.

$$\sigma_\phi \geq \left[\frac{NB_L}{C} \left(1 + \frac{N}{2CT_I} \right) \right]^{1/2} \tag{F.2-4}$$

where:

σ_ϕ = rms carrier-tracking error (radians)

N = Noise power in one Hertz bandwidth (W/Hz)

C = Received signal power (W)

B_L = Carrier-loop noise bandwidth (Hz)

T_I = Predetection interval period (sec).

Figure F.2-9 shows the resultant effects of carrier loop noise response for the case of the unaided carrier loop in which the tracking loop bandwidth is 20 Hz (to accommodate the dynamics uncertainties), and the case where the tracking loop bandwidth is reduced to 1.0 Hz due to reduced uncertainty in residual vehicular dynamics attributed to IMU-aiding of the carrier tracking loop. Both of these

G-13154a
2-15-94

Curve	BL	TI
A	20	0.02
B	1	0.02

J/S - dB
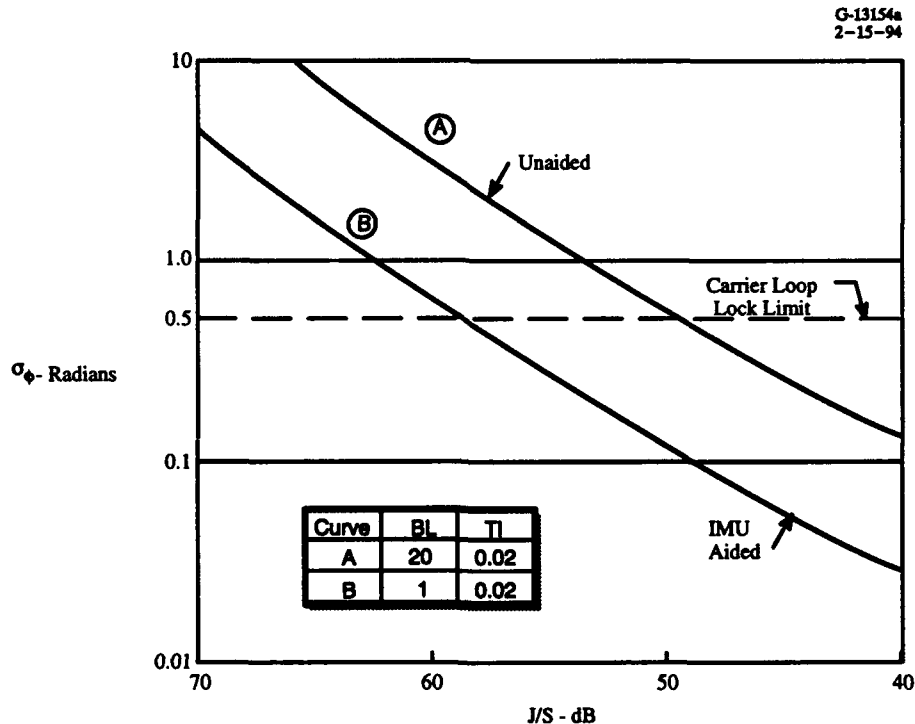
Figure F.2-9 Carrier Tracking rms Error for Various Tracking Loop Bandwidths and Predetection Integration Period as a Function of Jammer-to-Signa' Ratios

curves define the relative tolerance to jamming with the rms-phase error plotted as a function of jammer-to-signal ratio. Carrier loss-of-lock limit is selected as 0.5 radians in this example. Beyond this limit, nonlinear effects dominate and the carrier tracking loop will likely cycle-slip or lose lock.

F.2.4   Acquisition/Reacquisition and Receiver Tracking States

The GPS acquisition process involves a two-dimensional search in *time* (C/A time delay) and *frequency* (discrete Doppler search) for code tracking and AFC/phase tracking. Code search is typically accomplished in half-chip increments. This process continues until a correlation state has been declared when the signal level (determined typically by a noncoherent envelop detector) exceeds a specified code detection threshold. Because of the limited number of chips to search (1023 x 2), this process can occur in a relatively short period of time. Doppler search may continue over a number of intermediate-frequency (IF) Doppler cells until AFC or phase tracking occurs. This search is driven by the Doppler uncertainty resulting from the satellite radial velocities and the user's vehicular dynamics. A typical C/A-code search and acquisition process in a benign environment may take on the order of one or two minutes. Figure F.2-10 presents a conceptualization of the two-dimensional time- and frequency-search cells.

A key point regarding the GPS acquisition process relates to the user and satellite position, velocity, and time uncertainties. Given a frequency uncertainty of 10 kHz, the total number of time-frequency search cells will be approximately 10,000. Assuming that the receiver is able to search
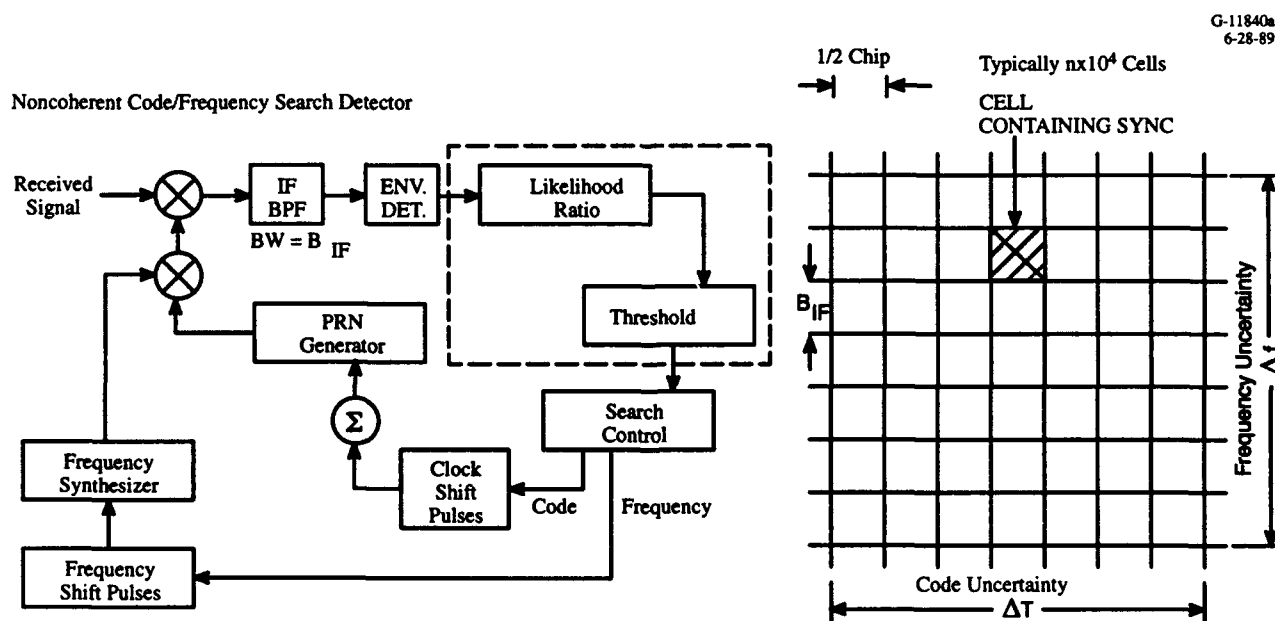
Figure F.2-10 Two-Dimensional Time and Frequency Search for GPS Acquisition

40 chips per second for an acceptable false alarm rate, a 250 sec search would be allocated to a single IF bandwidth alone. A priori or real-time knowledge of satellite and user positions and timing errors can significantly reduce the code search, and therefore the acquisition time. Similar reductions are realized for carrier tracking lock-on when velocity uncertainties are minimized. A priori or real-time information allows the receiver to initialize the time-frequency search cell at the most likely time-frequency window of acquisition. An IMU navigation solution can minimize acquisition/reacquisition search uncertainty and can support direct P-code lock-on. Future receivers will likely employ digital signal processing techniques which implement simultaneous time-frequency searches on a relatively large number of cells to significantly minimize acquisition/reacquisition times.

F.2.5 Basic Receiver Architectures

Up until this point, basic descriptions of the receiver code and carrier tracking loops — along with the acquisition process — have been discussed. This section presents a *top-level* discussion of overall GPS receiver design. A simplified block diagram of a GPS receiver is shown in Fig. F.2-11. This figure ties together many of the concepts discussed up to this stage.

As mentioned earlier, the basic organization of a GPS receiver includes a receiver measurements function and a navigation and control function. The receiver measurement function is facilitated by the code and carrier tracking loops. In early (second-generation) designs, multiple hardware "channel"
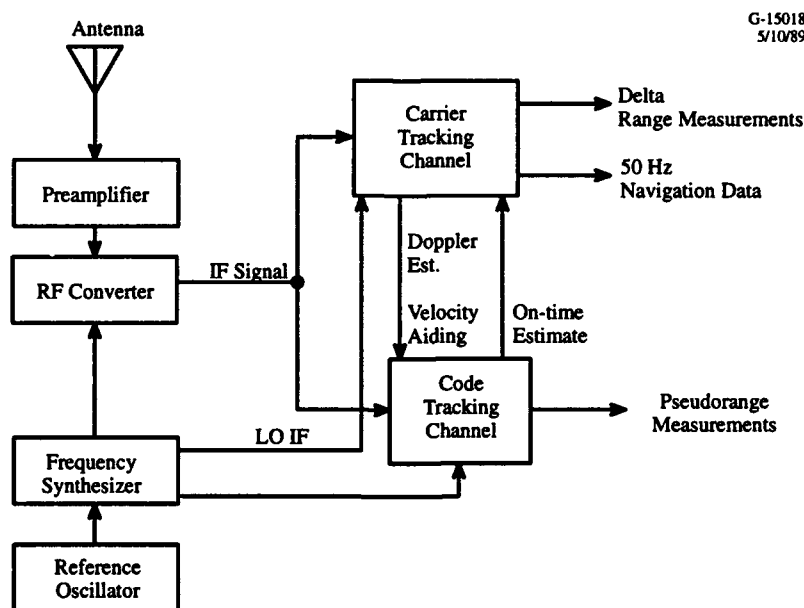
Figure F.2-11 Basic Design of a GPS Receiver

were designed into the receiver to track different satellites simultaneously. To reduce the complexity and size, some receivers implemented sequential tracking designs with inherent dynamics and signal loss penalties. Many of these receivers were highly analog in nature — with basic code tracking, carrier tracking, data demodulation, acquisition/reacquisition, and signal estimation accomplished via analog hardware. Figure F.2-12 presents a simplified block diagram characterizing receiver architectures in this category.

Current-generation receivers are implementing highly digital design architectures. Figure F.2-13 presents a simplified block diagram of digital receivers. The principal characteristic of these designs are that the received wideband signal is simply down-converted via fixed translation frequencies to a lower baseband frequency — thus preserving the embedded wideband characteristics of the received signal (code, Doppler shifts, etc.). This baseband signal is then applied to a high-speed sampling and analog-to-digital convertor (ADC) process. Post-ADC samples are presented to application-specific chips which perform the hardware implementation of the tracking loop functions under software control. All code tracking, carrier tracking, data demodulation, acquisition/reacquisition, and signal estimation processes are implemented in application-specific digital circuitry and software at this point.
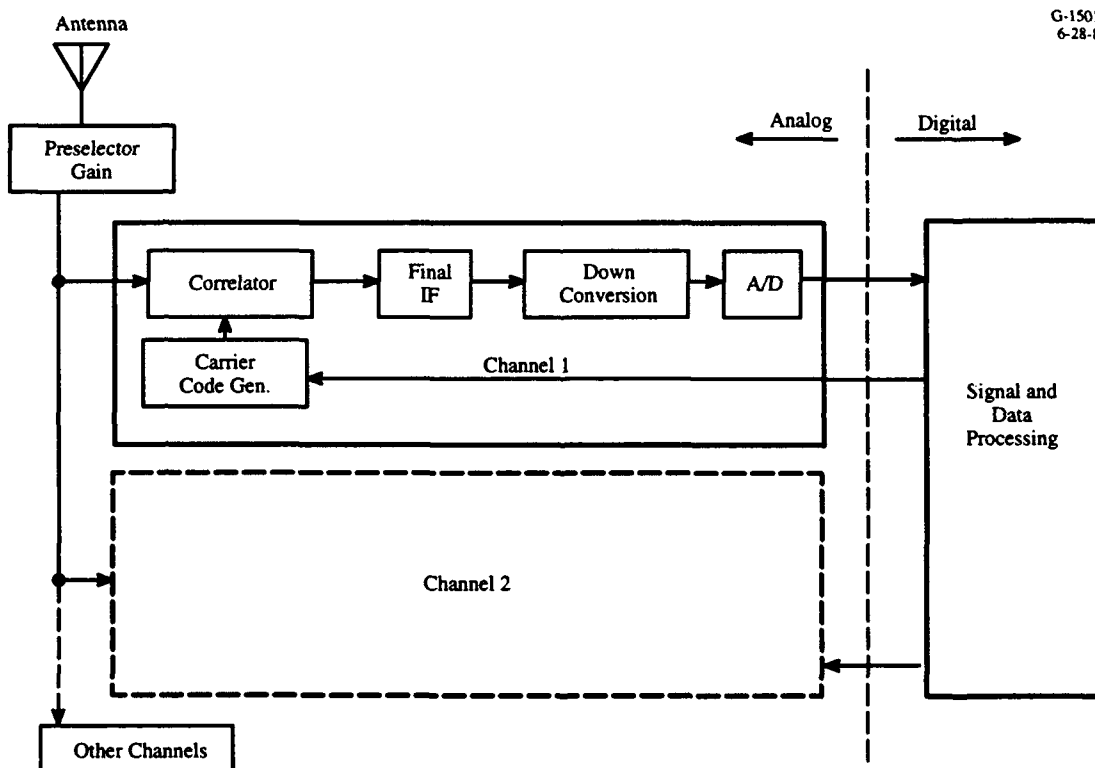
Figure F.2-12   Analog GPS Receiver Basic Architecture
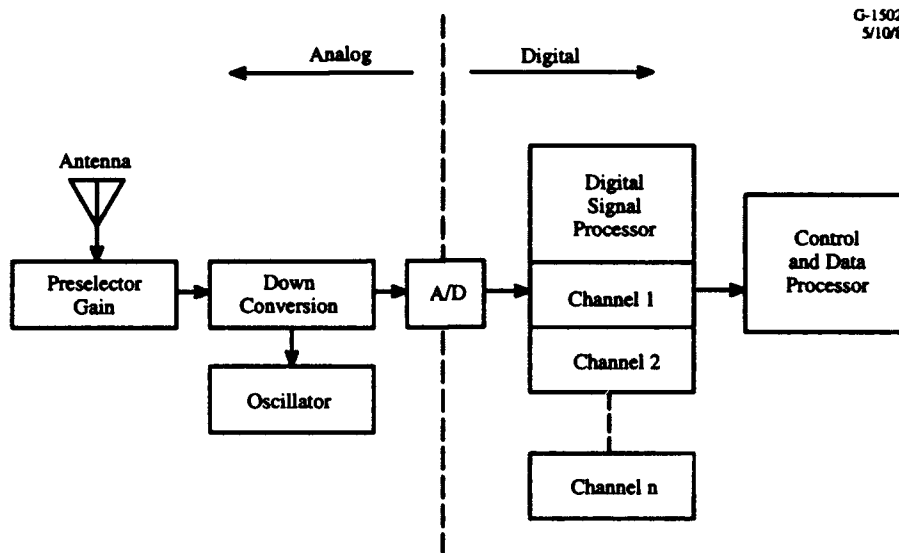
Figure F.2-13 Digital GPS Receiver Basic Architecture

These designs have been made possible through advancements in GaAs Monolithic Microwave Integrated Circuits (MMIC), gate arrays, and Application Specific Integrated Circuits (ASIC) technologies — and in the performance capabilities of high-speed microcomputer technologies. Fourth-generation receiver architectures are combining multiple receiver channels onto single integrated circuit chips promising to greatly enhance GPS receiver size, cost, and performance capabilities.

The navigation and control functions are also implemented in software and perform all computations and decision-making required for generation of the receiver's navigation solution. Highlights of the *fundamental* navigation algorithms and satellite-selection criteria are discussed in the next section.

F.2.6   GPS Navigation Solution and Satellite Selection

This section addresses transformation of the pseudorange and delta range measurements derived from the receiver's code and carrier tracking loops, respectively, into a navigation solution describing the user's position and velocity states. Development of the fundamental navigation equations and satellite selection criteria — based on dilution of precision — are presented.

Figure F.2-14 presents a highly simplified one-dimensional diagram of the vector relationships among the user's position, the satellite's position, and the pseudorange measurement described in the following equation:

$$\mathbf{R_u} = \mathbf{R_i} - \mathbf{D_i}$$ (F.2-5)

USER

D_i

$i^{\underline{th}}$ SV

R_u

R_i

Earth Cross Section
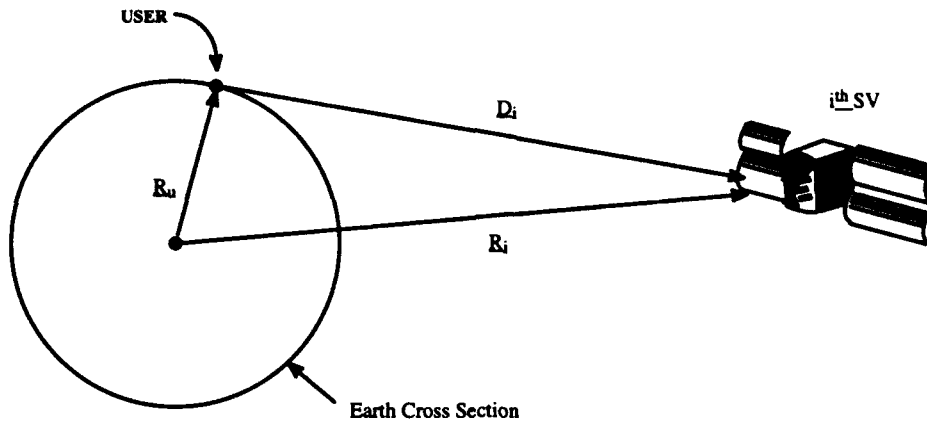
Figure F.2-14 Simplified Diagram Showing the Vector Relationships
for Satellite and User Positions

where:

R_u = User position vector from WGS-84 ECEF Earth center

R_i = Satellite position vector from WGS-84 ECEF Earth center

D_i = User-to-satellite position vector

i = Represents the ith satellite.

Noting that pseudorange measurements are in actuality scalar measurements (magnitude only), then Eq. F.2-5 may be reformulated by multiplying all terms by the user-to-satellite unit vector, e_i, to reflect the scalar pseudorange measurement resulting in:

$$e_i \cdot R_u = e_i \cdot R_i - D_i \qquad\qquad (F.2\text{-}6)$$

where:

e_i = User-to-satellite unit vector containing direction cosine components $[x_i, y_i, z_i]$

D_i = Scalar user-to-satellite distance.

The actual user-to-satellite range may be represented by the pseudorange measurement minus the embedded satellite and receiver clock time-bias error components, the following relationship may be expressed:

$$D_i = PR_i - B_u - B_i \qquad\qquad (F.2\text{-}7)$$

F-19

where:

PR_i = Actual pseudorange measurements

B_u = User's receiver clock bias

B_i = Satellite's clock bias (i[th] satellite).

Combining Eqs. F.2-6 and F.2-7 yields the following equation which characterizes the fundamental navigation equation formulation:

$$\mathbf{e} \cdot (\mathbf{R}_i - \mathbf{R}_u) + T_B = PR_i \qquad \text{(F.2-8)}$$

where:

T_B = The combined *receiver* and *satellite* clock bias errors, $(B_u + B_i)$.

In actuality, the one-dimensional case described by this equation must be expanded into four equations in four unknowns for the point-solution determination of user position error. Three of these unknowns represent the three Cartesian position components, x_u, y_u, and z_u, representing the user ECEF radial position vector. Because the user's receiver has imperfect knowledge of GPS system time, the fourth unknown is included to estimate the receiver clock-bias error. Figure F.2-15 presents a graphical depiction of the four-satellite-tracking quadrilateration technique used to compute the user position vector, $\underline{R}_u$.

Equations F.2-9 through F.2-12 describe the four basic equations used to determine user position and receiver clock bias:

$$PR_1 = \left[(x_1 - x_u)^2 + (y_1 - y_u)^2 + (z_1 - z_u)^2\right]^{1/2} + cT_{B1} + cT_{A1} \qquad \text{(F.2-9)}$$

$$PR_2 = \left[(x_2 - x_u)^2 + (y_2 - y_u)^2 + (z_2 - z_u)^2\right]^{1/2} + cT_{B2} + cT_{A2} \qquad \text{(F.2-10)}$$

$$PR_3 = \left[(x_3 - x_u)^2 + (y_3 - y_u)^2 + (z_3 - z_u)^2\right]^{1/2} + cT_{B3} + cT_{A3} \qquad \text{(F.2-11)}$$

$$PR_4 = \left[(x_4 - x_u)^2 + (y_4 - y_u)^2 + (z_4 - z_u)^2\right]^{1/2} + cT_{B4} + cT_{A4} \qquad \text{(F.2-12)}$$
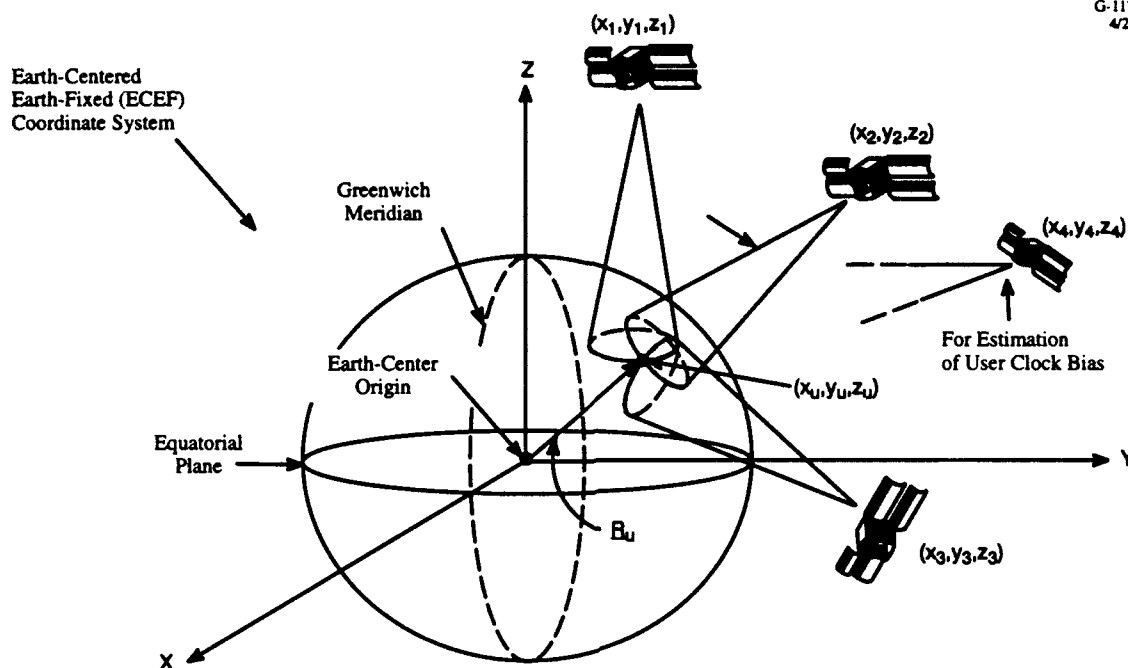
Figure F.2-15 Depiction of GPS Four-Satellite Tracking for Determination of User Position and Receiver Clock Bias

where:

PR_i = User-to-satellite measured pseudorange (i = 1,4)

x_i, y_i, z_i = $ECEF_{x,y,z}$ position of satellite "i" (i = 1,4)

x_u, y_u, z_u = $ECEF_{x,y,z}$ position of user

cT_{Bi} = Combination of *receiver* and *satellite* clock biases times speed-of-light constant (c)

cT_{Ai} = User-to-satellite ionospheric and tropospheric time delays times c

Similarly, a set of four equations characterizing the relationship of delta range measurements to determination of the user's velocity solution and receiver clock drift are listed in Eqs. F.2-13 through F.2-16.

$$DR_1 = \left[(\dot{x}_1 - \dot{x}_u)^2 + (\dot{y}_1 - \dot{y}_u)^2 + (\dot{z}_1 - \dot{z}_u)^2 \right]^{1/2} + c\dot{T}_{B1} \qquad \text{(F.2-13)}$$

$$DR_2 = \left[(\dot{x}_2 - \dot{x}_u)^2 + (\dot{y}_2 - \dot{y}_u)^2 + (\dot{z}_2 - \dot{z}_u)^2 \right]^{1/2} + c\dot{T}_{B2} \qquad \text{(F.2-14)}$$

$$DR_3 = \left[(\dot{x}_3 - \dot{x}_u)^2 + (\dot{y}_3 - \dot{y}_u)^2 + (\dot{z}_3 - \dot{z}_u)^2 \right]^{1/2} + c\dot{T}_{B3} \qquad \text{(F.2-15)}$$

$$DR_4 = \left[(\dot{x}_4 - \dot{x}_u)^2 + (\dot{y}_4 - \dot{y}_u)^2 + (\dot{z}_4 - \dot{z}_u)^2 \right]^{1/2} + c\dot{T}_{B4} \qquad \text{(F.2-16)}$$

where:

DR_i = User to satellite measured delta range (i = 1,4)

$\dot{x}_i, \dot{y}_i, \dot{z}_i$ = ECEF x,y,z velocity of satellite i (i = 1,4)

$\dot{x}_u, \dot{y}_u, \dot{z}_u$ = ECEF x,y,z velocity of user

$c\dot{T}_{Bi}$ = Combination of *receiver* and *satellite* clock drift times c.

Since these equations are nonlinear, a linearized version of the equations is desired to minimize inherent complexities in their implementation into various estimation approaches to the navigation solution (e.g., Kalman filtering). Linear-approximation errors are greatly minimized since the user-to-satellite range is so much greater than incremental variations in the user range. An iterative approach may be developed whereby:

$$x = x_n + \Delta x \qquad \text{(F.2-17)}$$

$$y = y_n + \Delta y \qquad \text{(F.2-18)}$$

$$z = z_n + \Delta z \qquad \text{(F.2-19)}$$

$$T = T_n + \Delta T \qquad \text{(F.2-20)}$$

$$PR_i = PR_{ni} + \Delta PR_i \qquad \text{(F.2-21)}$$

where:

x_n, y_n, z_n, T_n = A priori best (nominal) esitmate of user position and clock bias

$\Delta x, \Delta y, \Delta z, \Delta T$ = Difference between the most recent and the nominal estimate

PR_{ni} = Nominal pseudorange measurement for the ith satellite

ΔPR_i = Difference between the most recent and the nominal pseudorange measurement

Substituting these equations into the general form of Eqs. F.2-9 through F.2-12 yields (ignoring propagation-link correction terms):

$$PR_{ni} + \Delta PR_i = \left[(x_i - (x_n + \Delta x))^2 + (y_i - (y_n + \Delta y))^2 + (z_i - (z_n + \Delta z))^2\right]^{1/2} + cT_n + c\Delta T$$

(F.2-22)

where:

$$T_n = \text{Combination of receiver and satellite clock bias times c.}$$

Expansion and simplification of these equations (ignoring the second-order terms) provides the following expression:

$$\Delta PR_i = \frac{(x_i - x_n)}{PR_{ni} - T_n} \Delta x + \frac{(y_i - y_n)}{PR_{ni} - T_n} \Delta y + \frac{(z_i - z_n)}{PR_{ni} - T_n} \Delta z + \Delta T \qquad \text{(F.2-23)}$$

These linearized equations therefore relate the incremental pseudorange measurements on the left-hand side of the equation to the incremental navigation solution coordinates shown on the right through the coefficient expressions proceeding the incremental navigation coordinates. When formulated in matrix notation for the four incremental navigation solution equations, we have:

$$\begin{bmatrix} e_{x1} & e_{y1} & e_{z1} & 1 \\ e_{x2} & e_{y2} & e_{z2} & 1 \\ e_{x3} & e_{y3} & e_{z3} & 1 \\ e_{x4} & e_{y4} & e_{z4} & 1 \end{bmatrix} \begin{bmatrix} \Delta x \\ \Delta y \\ \Delta z \\ \Delta T \end{bmatrix} = \begin{bmatrix} \Delta PR_1 \\ \Delta PR_2 \\ \Delta PR_3 \\ \Delta PR_4 \end{bmatrix} \qquad \text{(F.2-24)}$$

where:

e_{ij} = Direction cosine component of the user-to-satellite unit vector (i = x, y, z;   j = 1, 4)

Note: Coefficient of DT in Eq. 2.4–23 is unity, thus the "1"s elements in the fourth column

This matrix equation can be simplified into the following forms:

$$H\, x = z \quad or \quad x = H^{-1}\, z \qquad\qquad (F.2\text{-}25)$$

where:

H = Four-by-four-element direction cosine matrix containing unit-vector components

$x = [\varDelta x\ \varDelta y\ \varDelta z\ \varDelta T]^T$

$z = [\varDelta PR_1\ \varDelta PR_2\ \varDelta PR_3\ \varDelta PR_4]^T.$

The linear formulation of the relationship between the pseudorange measurements and the user's navigation solution also allows one to characterize the pseudorange measurement errors, and user position and time errors, using the following expression:

$$\delta x = H^{-1}\, \delta z \qquad\qquad (F.2\text{-}26)$$

where:

δx = Errors in user position and time

δz = Errors in pseudorange measurements.

To characterize the errors associated with the user states and pseudorange measurements, one may formulate the covariance matrix of the expected errors in these entities. The resulting four-by-four matrices characterize the expected values of the squares and products of errors in the user states and pseudorange measurements. The diagonal terms of either covariance matrix reflect the squares of the expected one-sigma errors. The off-diagonal covariances reflect the correlation among the group of pseudorange measurements or user states. Definition of the covariance matrices follows:

$$\text{COV}(z) = E\left\{\delta z\,\delta z^T\right\} \qquad\qquad (F.2\text{-}27)$$

$$\text{COV}(x) = E\left\{\delta x\,\delta x^T\right\} \qquad\qquad (F.2\text{-}28)$$

where:

COV (z) = Pseudorange measurement covariance matrix

COV (x) = User position and time covariance matrix

E $\{\,\bullet\,\}$ = Expectation operator.

Reformulating Eq. F.2-26 with these covariance matrix, the following relationship may be expressed:

$$COV(x) = H^{-1} COV(z)^{-1} H^{T} \qquad (F.2\text{-}29)$$

and applying matrix algebra reformulation, we get:

$$COV(x) = \left[H^{T} COV(z)^{-1} H\right]^{-1} \qquad (F.2\text{-}30)$$

This equation expresses the transformation of pseudorange measurement errors into user position and time errors through the user-to-satellite direction cosine matrix, H — a direct and deterministic reflection of the user-to-satellites relative geometries.

F.3   MILITARY RECEIVERS

The military receivers in current use are dominated by the Phase IIB equipment developed by Rockwell Collins in the early 1980s, and the Phase III equipment for which Collins was awarded the production contract in April of 1985. The Phase IIB family of equipment included one, two, and five channel GPS receivers. The Phase III equipment family primarily differs from the Phase IIB family in its ability to interface with more candidate host vehicles (75 as opposed to 17). The type of architecture employed in these receivers is well represented by the five-channel RCVR-3A, which is described in some detail in the remainder of this section.

A generalized block diagram of the overall Receiver 3A design is illustrated in Fig. F.3-1. Two primary CAPS-7 processors in the Collins Adaptive Processing System (CAPS) microprocessor family perform the bulk of the overall processing tasks. The Receiver Processor CAPS-7 processor function include:

- Controlling the five correlators via the receiver local bus
- Executing the selected Kalman filter mode
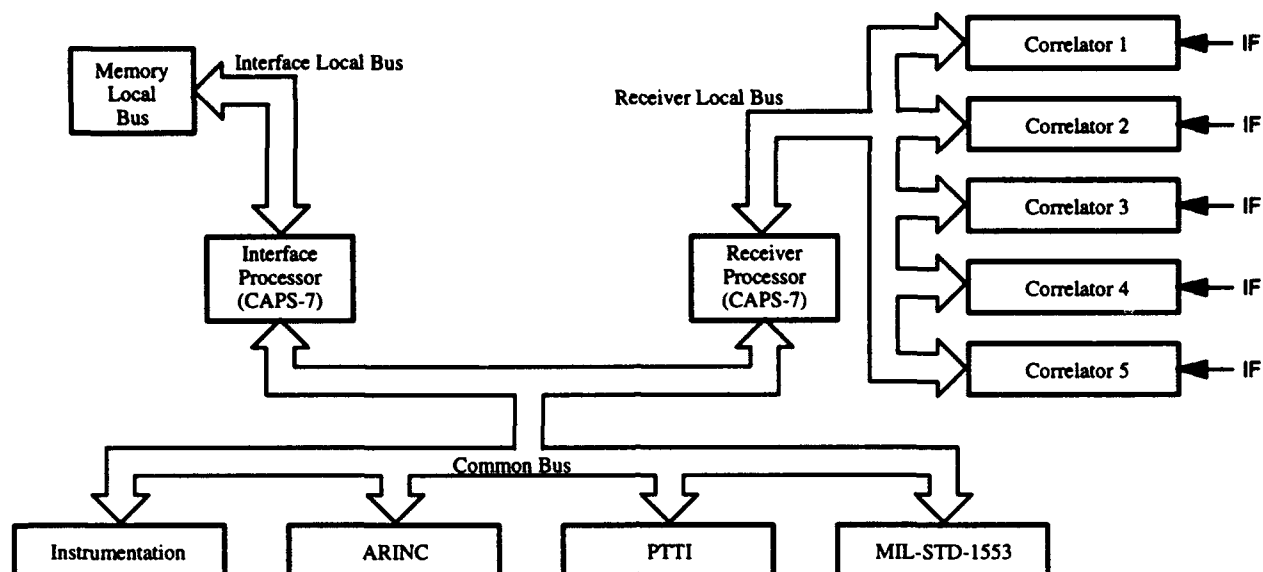
Figure F.3-1 Generalized Block Diagram of the Receiver 3A Architecture

- Computing the navigation solutions

- Using aircraft sensor data (INS, DRS, Baro) to aid in receiver acquisition/reacquisition and (code) tracking loops

- Providing GPS time.

The Interface Processor CAPS-7 processor functions include:

- Controlling all interface functions

- Interfacing with the local bus memory

- Performing the receiver manager functions

- Managing satellite selection/management

- Executing SA/A-S software functions.

The Local Bus Memory contains the EPROM (188K in 32K×8 HCMOS chips), RAM (84K in 8K×8 HCMOS chips), critical memory (8K×8), low-power time source (32.760 kHz crystal), and SA/A-S key-loading interface (KYK-13, KOI-18).

The Common Bus provides communication between the Receiver Processor and the Interface Processor — and routing of all message data to the respective interface options. These options include

the MIL-STD-1553 (five versions currently supported), the ARINC 429/575 serial interfaces, and the Precise Time/Time Interval (PTTI) interface. The PTTI signal can be used to calibrate time sources to within 100 ns, serve as a precision stand-alone time source, or direct P-code acquisition when accompanied by moderately accurate position/velocity data. The instrumentation port support RS-422 data interfaces. Each specific interface is controlled by dedicated microprocessor/LSI circuitry.

T   ceiver 3A design has included a significant level of nuclear hardening to reduce its susceptibility to electromagnetic pulse (EMP) and transient radiation effects.

The basic building blocks of the Receiver 3A design include:

- Antenna Electronics Unit
- IF Processor
- Correlators (5)
- Receiver Processor/Software
- Frequency Standard and Frequency Synthesizer
- Interface Processors/Software.

The Antenna Electronics Unit (AEU) performs the basic functions of limiting, preamplification, and down-conversion of the L1 and L2 frequencies to the first IF frequencies of 173.91 MHz. A local-oscillator (LO) frequency centered between the L1 and L2 frequencies (1401.51 MHz) is used. The frequency down-conversion process allows selection of the interconnecting coax cable to the receiver to be less critical so that the AEU may be colocated with the GPS antenna — a key factor in larger aircraft.

The Frequency Standard design is based upon a temperature-controlled (oven) stress-compensated (SC-cut) crystal for generating the 10.23 MHz principal frequency reference for the receiver. Short-term stability performance on the order of one part in 10^{10} per second is typical for this frequency standard. This reference is inputted to the Frequency Synthesizer for generation of all injection frequencies, digital clocks, and timing signals used throughout the receiver design.

Figure F.3-2 shows a block diagram of the IF Processor. The IF Processor receives the down-converted L1 and L2 173.91 MHz signals and applies 26 MHz bandpass filtering (to more than accommodate the P-code spectrum) prior to automatic gain control (AGC) operation. A key feature of the IF Processor is the two-by-five RF switch (GaAs) which facilitates independent routing of either the L1 or L2 composite down-converted L-band signals to the five correlators. Built-in-test (BIT) functions are also included as shown in the figure.

350 MHz
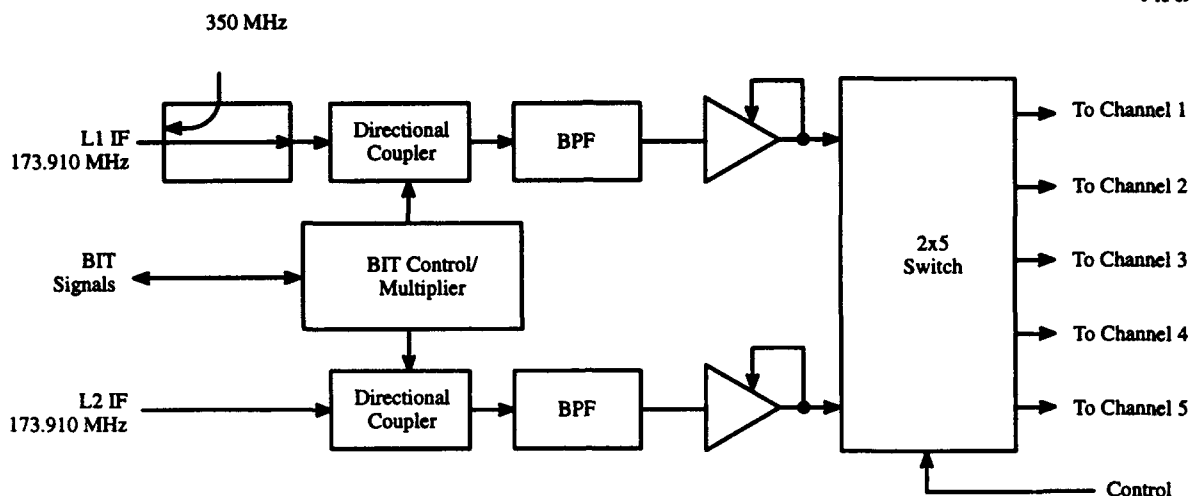
Figure F.3-2   Receiver 3A IF Processor Block Diagram

The Correlator boards perform the basic hardware functions required for code and carrier tracking under direction of the Receiver Processor/Software. Figure F.3-3 presents a detailed block diagram of the correlator design. The 173.91 MHz IF signal is down-converted to 86.316 MHz and then split to accomplish parallel IF paths for carrier (punctual IF path) and code (early/late IF path) tracking functions. The T-code (100 kHz) is also injected at the initial down-conversion stage to inhibit CW-breakthrough effects inherent to analog designs.

The punctual IF path represents the carrier tracking hardware and performs Navigation Message data demodulation and signal power estimation. The punctual code is mixed with the incoming signal at the beginning of this path to despread the DS-SS signal to a narrow spectrum reflecting the carrier frequency and 100 Hz data bit frequency spectrum. Another LO injection frequency of 86.23 MHz down-converts the signal to baseband. This signal is lowpass filtered (40 kHz) and applied to an AGC stage which supports the specified level of jammer-to-signal ratios. Afterwards, the signal is split and the I (0 deg) and Q (90 deg) components produced by the carrier VCO are injected at the last IF stage. Under control of the Receiver Processor/Software command, the (digitally-controlled) VCO-generated signals represent the estimates of the received carrier frequency and phase. The residual low-frequency signal is then passed to eight-bit A/D convertors which produce I and Q digital samples at a 1 kHz sampling rate for use by the preprocessor.
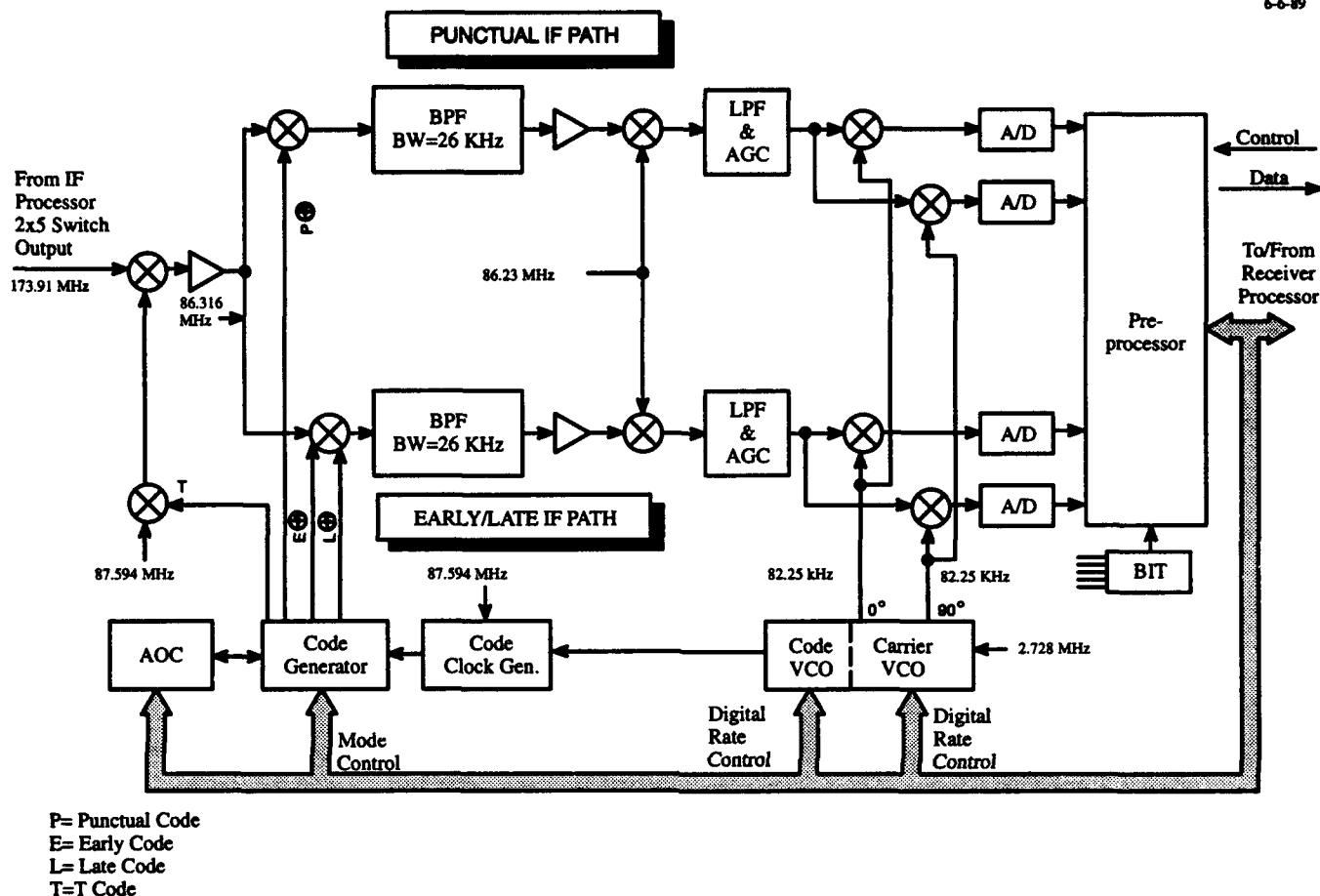
Figure F.3-3 Correlator Board Block Diagram

The early/late IF path performs the basic functions required for code tracking. The early and late codes are introduced to implement the delay-lock loop. From this point, similar processing and signal conditioning functions are performed relative to the upper path. At the end of this path, the I and Q samples are presented to the preprocessor for delay-lock loop processing and control which is likewise performed in the Receiver Processor/Software.

The preprocessor (Z80 microprocessor and LSI) accepts the four parallel I and Q samples every millisecond from the A/D output and processes these samples according to selectable predetection intervals of one-, two-, five-, ten-, or twenty-millisecond intervals. These samples which are synchronized with data-bit transitions — are coherentl ' summed to produce 20 ms sample observables for subsequent processing by the CAPS-7 Receiver Processor. The preprocessor executes signal-power detection, noise-power detection, arc-tangent phase detection (carrier tracking), and code-tracking error detection.

The P- and C/A- coders identified in this figure are incorporated on to a single LSI chip. The Auxiliary Output Chip (AOC) allows Y-code tracking. The code VCO shown at the bottom of the figure operates at a 10.23 MHz nominal frequency — with a code slew range of ∓ 1.245 kHz and a minimum slew resolution of 0.038 Hz. Also, the carrier VCO operates at a nominal frequency of 85.25 kHz — with a slew range of ∓ 21.3 kHz and a minimum slew resolution of 0.65 Hz. The VCOs are implemented on a single gate-array chip. The Receiver Processor/Software controls the code and carrier slew phase and frequencies.

Closure of the tracking loops is implemented digitally in the Receiver Processing/Software. The preprocessor observables are collected as inputs to the digital tracking loops functions performed by the Receiver Processor, and control signals to the code and carrier VCOs are generated as outputs. Digital tracking-loop implementations allows significant flexibility and adaptability in loop-bandwidth and order selection when confronted by jamming and interference conditions.

The carrier tracking loop includes an arc-tangent detector which forms the ratio of the two quadrature observables (I and Q 20-ms samples from the preprocessor) to estimate carrier phase error (θ). Use of the arc-tangent loop in lieu of a Costas loop allows reduction of the required sampling rate from 250 Hz to 50 Hz. The advantages of increased isolation offered by the Costas technique are offset by the arc-tangent loop's accuracy, extended-range-phase-lock capability (which minimizes loop bandwidth requirements), and adaptability to changing dynamics and signal variations.

The early and late preprocessor 20-ms samples form the basis for implementation of the code delay-lock loop tracking. The early-minus-late code error observables are thereby used by the Receiver Processor/Software to generate digital slew commands to the code VCO. Data-bit sign ambiguities are handled by computing the dot product of the punctual signal (hard limited to minimize gain variations between the IF paths) and the early and late signals. Under steady-state tracking, the code-phase delay generated by the DLL — reflecting the satellite-to-user propagation time delay — produces the pseudo-range observables. The code tracking loop is implemented as first-order tracking loops with a tracking loop bandwidth set at 0.5 Hz.

Various interface boards were developed by Collins to allow data communications between the common receiver designs and the unique integration requirements of the host vehicle. A common design architecture was implemented which included a 80C51 microcontroller and 8K dual-port buffer RAM interfacing with the CAPS-7 Interface Processor via the 16-bit-wide Common Bus. Unique protocol processing for transmission and reception of interface-unique data and messages were tailored for each of these dedicated I/O controllers. Figure F.3-4 illustrates the interfaces which are available in the Receiver 3A design.

```
  ┌─────────┐              ┌──────────────┐              ┌──────────────┐
  │  CDU 1  │ ◄═══════════►│              │◄════════════►│   Antenna    │
  └─────────┘              │              │              │ Electronics  │
                           │              │              └──────────────┘
  ┌─────────┐              │              │              ┌──────────────┐
  │  CDU 2  │ ◄═══════════►│              │◄════════════ │     Data     │
  └─────────┘              │    GPS       │              │    Loader     │
                           │              │              └──────────────┘
  ┌─────────┐              │   RCVR       │              ┌──────────────┐
  │  Baro   │ ════════════►│              │◄════════════ │   KYK-13/    │
  │ Altimeter│             │    3A        │              │   KOI-18     │
  └─────────┘              │              │              └──────────────┘
  ┌─────────┐              │              │              ┌──────────────┐
  │ Flight  │ ◄═══════════►│              │◄════════════►│Instrumentation│
  │Instruments│            │              │              └──────────────┘
  └─────────┘              │              │              ┌──────────────┐
  ┌─────────┐              │              │ ════════════►│  Have Quick  │
  │ ARINC INS│◄═══════════►│              │              └──────────────┘
  └─────────┘              │              │              ┌──────────────┐
  ┌─────────┐              │              │◄════════════►│  Time Source │
  │ ARINC INS│◄═══════════►│              │              └──────────────┘
  └─────────┘              └──────┬───────┘

  ┌─────────┐              ┌──┐              ┌──────────────┐
  │   INS   │ ◄═══════════►│  │◄════════════►│     CDU      │
  └─────────┘              │  │              └──────────────┘
  ┌─────────┐              │1 │              ┌──────────────┐
  │ Mission │ ◄═══════════►│5 │════════════► │   Doppler    │
  │Computer │              │5 │              └──────────────┘
  └─────────┘              │3 │              ┌──────────────┐
  ┌─────────┐              │  │              │    Baro      │
  │Time Source│◄══════════►│B │◄════════════►│  Altimeter   │
  └─────────┘              │U │              └──────────────┘
  ┌─────────┐              │S │              ┌──────────────┐
  │ True Air│ ◄═══════════►│  │◄════════════►│     GPS      │
  │  Speed  │              │  │              │   Receiver   │
  └─────────┘              │  │              └──────────────┘
  ┌─────────┐              │  │              ┌──────────────┐
  │  AHRS   │ ◄═══════════►│  │◄════════════►│    Other     │
  └─────────┘              └──┘              └──────────────┘
```
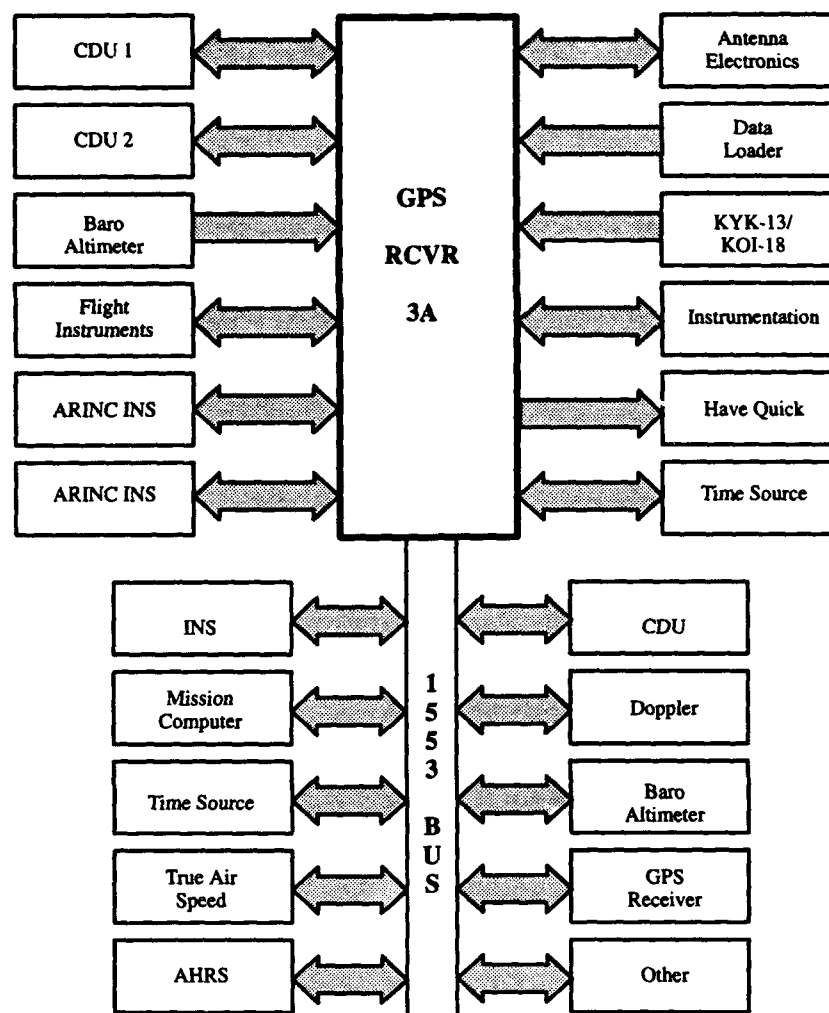
Figure F.3-4   Generalized Block Diagram of the Receiver 3A Interfaces

F.4   COMMERCIAL RECEIVERS

F.4.1   Navigation Receivers

The GPS Report, 1993 GPS Receivers Guide (Ref. 1) lists 81 GPS receiver models classified primarily as navigation receivers (including air, marine, and ground navigation). Prices range from $60,000 for a 10-channel, dual frequency receiver with full P and Y code capabilities, to $695 for a single-channel, single frequency receiver for marine applications. Few available receivers have fewer than 5 channels, and many receivers in the 8- to 12-channel range are available for prices between $1000 and $2000. To remain competitive in both cost and performance, most commercial navigation receivers are employing digital architectures similar to that shown in Figure F.2-13.

F-31

Commercial GPS receivers fall into two major categories according to whether or not they are intended for differential GPS (DGPS) operation. Those receivers that are not intended for DGPS operation typically employ relatively unsophisticated aiding of the code tracking loop by the carrier tracking loop as described in Section F.2; in this case, the only reason for the aiding is to prevent loss of code tracking during dynamic maneuvers. For DGPS operation, where the dominant impact of Selective Availability is eliminated, code tracking noise can be a significant contributor to the overall error budget. In this case, more sophisticated techniques are often employed to significantly reduce code tracking noise. Two of the most important of these techniques are "integrated Doppler processing" and the use of "closely spaced correlators" in the receiver code tracking loops.

GPS receivers that employ integrated Doppler processing determine user range-to-satellite changes (over time spans of a few minutes) by integrating the Doppler frequency shift of the carrier signal. Conceptually, the integrated carrier data are used to create a smooth curve or track of the evolution of user-to-satellite range. The relative accuracy of this curve is high (carrier-derived range changes are accurate to inches). However, the absolute location of this curve cannot be determined from carrier data. At the same time, code tracking provides a measure of absolute pseudorange which is corrupted. Integrated Doppler processing receivers adjust the location of the smooth carrier-derived curve to best fit the code-derived pseudoranges. User position is then derived from this adjusted curve.

As described in Section F.2, most GPS receivers measure pseudorange by correlating three pre-stored replicas of the code which are staggered in time. A curve is fit to the three resulting correlation coefficients and the desired pseudorange is associated with the peak on the curve. In nearly all current receivers, the pre-stored code replicas are separated by one chip of the code (1.023 MHz rate for the C/A code). Recently, one receiver manufacturer has reduced the correlator spacing (following signal acquisition) to 5 or 10 percent of a chip width. Whereas some older receivers have exhibited noise levels equivalent to tens of feet of position error, the closely-spaced correlator technique reduces the error to approximately 4 inches.

F.4.2   Surveying Receivers

The GPS Report, 1993 GPS Receivers Guide (Ref. 1) lists 22 GPS receiver models classified primarily as surveying receivers. Prices range from $60,000 for a 10-channel, dual frequency receiver with full P and Y code capabilities, to $3,000 for a single frequency receiver using a proprietary channel multiplexing scheme. Typical surveying receivers employ 8 to 12 channels and are priced between $6,000 and $30,000. The wide range of costs effectively corresponds to the performance potential of

the receivers. The most expensive receivers offer positioning to the millimeter level. This type of performance requires extremely precise tracking of the carrier phase, typically involving the use of high-quality oscillators. Most high-end surveying receivers also offer built-in capabilities for data storage and postprocessing needed to achieve millimeter-level results. To remain competitive in both cost and performance, most commercial surveying receivers are employing digital architectures similar to that shown in Figure F.2-13.

High accuracy in GPS surveying is achieved by solving for the full carrier cycle counts in all measurements taken over a data collection interval. Use of the L2 frequency in addition to L1 provides effectively double the number of independent measurements for the same time period, and can therefore significantly reduce data collection times. High-end surveying receivers therefore typically use both the L1 and L2 frequencies. An important issue in commercial surveying is the unavailability of the encrypted P code (i.e., the Y code) on the L2 frequency. Receiver manufacturers have developed several techniques to permit the L2 information to be used to advantage without knowledge of the code. The two most commonly used techniques are referred to as "signal squaring" and "cross-correlation."

In signal squaring, the L2 signal is squared, effectively eliminating the Y code (which always multiplies the signal by 1 or −1). Squaring halves the effective wavelength of the L2 carrier to 12 cm. The primary disadvantage of squaring is that noise is squared in addition to the signal, resulting in a reduction of signal to noise ratio. Squaring is generally only successful for stationary receivers.

The cross-correlation techniques takes advantage of the fact that the L1 and L2 Y codes are identical, although they are not necessarily known. Manufacturer-proprietary cross-correlation algorithms estimate the difference in group delay between the L1 and L2 signals. This difference is added to the range derived from the C/A code on L1 to generate an L2 range measurement.

REFERENCE

1. GPS Report, 1993 GPS Receivers Guide, Phillips Business Information, Inc., Washington, D.C., December 1992.

APPENDIX G
STATION OPERATING PARAMETERS

G.1   INTRODUCTION

Many basic "parameters," i.e., types of data and associated values are used to describe the features of the Omega Navigation System. Among the most important of these parameters are those associated with the Omega transmitting stations. These parameters frequently arise in the performance of operational duties associated with the Omega System. This appendix serves as a reference source for some of the most commonly used parameters.

Section G.2 presents the transmitting station "bills," i.e. the specific parameters that either define the station's physical location and structure or its operating requirements/procedures. The basic information in these bills is extracted from Enclosure (1) to Ref. 1, although it has been updated to reflect current information (May 1994). Specifically, each bill provides the following information for the given station:

- Letter Designation

- Location — nearest municipality and geodetic coordinates on a WGS-84 datum

- Signal Transmission Assignment — frequency and antenna current for each of the eight segments in the pattern

- Station Monitor Data — location (nearest municipality/WGS-84 coordinates), computer code, ID number, calibration channel assignment, and station pairs monitored for 10.2 and 13.6 kHz

- Weekly Station Data Message Format — paragraph number, station pair, frequency, and time (UT) or time code; for Loran-C, no station pair is given and the chain identifier is given in place of the frequency; for GPS no station pair or frequency is given

- PCD Assignment — station pair and time code

- Time Codes — UT hour and (approximate) 6-month period to use when directed by Japan's Maritime Safety Agency.

G.2 OMEGA STATION BILLS

G.2.1 Norway

1. **LETTER DESIGNATION**: "A"

2. **LOCATION**:
   a. Geographic: Bratland, Norway
   b. Geodetic: 66.4202° N, 13.1370° E

3. **SIGNAL TRANSMISSION ASSIGNMENT**:

SEGMENT	FREQUENCY (kHz)	ANTENNA CURRENT (amps)	SEGMENT	FREQUENCY (kHz)	ANTENNA CURRENT (amps)
1	10.2	332	5	12.1	282
2	13.6	236	6	11.05	304
3	11⅓	294	7	12.1	282
4	12.1	282	8	12.1	282

4. **MONITOR**:
   a. Geographic: Utskarpen, Norway
   b. Geodetic: 66.2897° N, 13.5502° E
   c. Computer Code: NORW2
   d. I.D. Number: 54
   e. Calibration Assignment: G
   f. Station Pairs: BA, CA, EA, HA

5. **WEEKLY STATION DATA MESSAGE**:

PARAGRAPH	STATION PAIR	FREQUENCY	TIME (UT)
1	B-A	10.2 kHz	1300
2	B-A	13.6 kHz	1300
3	C-A	10.2 kHz	(1)
4	C-A	13.6 kHz	(1)
5	E-A	10.2 kHz	1100
6	E-A	13.6 kHz	1100
7	H-A	10.2 kHz	1800
8	H-A	13.6 kHz	1800
9	(LORC)	(7970X)	1200
10	(GPS)	—	0816

6. PCD ASSIGNMENT: C-A at (1).

    (1) = 0500 for October through March and 1700 for April through September as directed by the Japanese Maritime Safety Agency.

    G.2.2   Liberia

1. LETTER DESIGNATION: "B"

2. LOCATION:

    a. Geographic: Paynesville, Liberia
    b. Geodetic: 06.3036° N, 10.6644° W

3. SIGNAL TRANSMISSION ASSIGNMENT:

SEGMENT	FREQUENCY (kHz)	ANTENNA CURRENT (amps)	SEGMENT	FREQUENCY (kHz)	ANTENNA CURRENT (amps)
1	12.0	351	5	12.0	351
2	10.2	425	6	12.0	351
3	13.6	310	7	11.05	383
4	11⅓	372	8	12.0	351

4. MONITOR:

    a. Geographic: Monrovia, Liberia
    b. Geodetic: 06.3143° N, 10.8172° W
    c. Computer Code: LIBE2
    d. I.D. Number: 43
    e. Calibration Assignment: H
    f. Station Pairs: AB, DB, EB, FB

5. WEEKLY STATION DATA MESSAGE:

PARAGRAPH	STATION PAIR	FREQUENCY	TIME (UT)
1	A-B	10.2 kHz	1300
2	A-B	13.6 kHz	1300
3	D-B	10.2 kHz	1600
4	D-B	13.6 kHz	1600
5	E-B	10.2 kHz	1000
6	E-B	13.6 kHz	1000
7	F-B	10.2 kHz	1500
8	F-B	13.6 kHz	1500
9	(N/A)	—	—
10	(GPS)	—	0846

6. PCD ASSIGNMENT: None

G.2.3 Hawaii

1. LETTER DESIGNATION: "C"

2. LOCATION:

a. Geographic: Haiku Valley, Oahu Island, Hawaii, U.S.A.

b. Geodetic: 21.4047° N, 157.8308° W

3. SIGNAL TRANSMISSION ASSIGNMENT:

SEGMENT	FREQUENCY (kHz)	ANTENNA CURRENT (amps)	SEGMENT	FREQUENCY (kHz)	ANTENNA CURRENT (amps)
1	11.8	389	5	$11\frac{1}{3}$	402
2	11.8	389	6	11.8	389
3	10.2	446	7	11.8	389
4	13.6	333	8	11.05	410

4. MONITOR:

a. Geographic: Wahiawa, Oahu Island, Hawaii, U.S.A.

b. Geodetic: 21.5209° N, 157.9964° W

c. Computer Code: HAWAI

d. I.D. Number: 29

e. Calibration Assignment: F

f. Station Pairs: AC, DC, GC, HC

5. WEEKLY STATION DATA MESSAGE:

PARAGRAPH	STATION PAIR	FREQUENCY	TIME (UT)
1	A-C	10.2 kHz	(1)
2	A-C	13.6 kHz	(1)
3	D-C	10.2 kHz	2000
4	D-C	13.6 kHz	2000
5	G-C	10.2 kHz	2400
6	G-C	13.6 kHz	2400
7	H-C	10.2 kHz	0100
8	H-C	13.6 kHz	0100
9	—	—	—
10	(GPS)	—	0916

6. PCD ASSIGNMENT: A-C at (1).

(1) = 0500 for October through March and 1700 for April through September as directed by the Japanese Maritime Safety Agency.

G.2.4 North Dakota

1. LETTER DESIGNATION: "D"

2. LOCATION:
   a. Geographic: LaMoure, North Dakota, U.S.A.
   b. Geodetic: 46.3659° N, 98.3356° W

3. SIGNAL TRANSMISSION ASSIGNMENT:

SEGMENT	FREQUENCY (kHz)	ANTENNA CURRENT (amps)	SEGMENT	FREQUENCY (kHz)	ANTENNA CURRENT (amps)
1	11.05	381	5	13.6	307
2	13.1	319	6	11⅓	371
3	13.1	319	7	13.1	319
4	10.2	412	8	13.1	319

4. MONITOR:
   a. Geographic: Dickey, North Dakota, U.S.A.
   b. Geodetic: 46.5596° N, 98.6386° W
   c. Computer Code: N$DAK
   d. I.D. Number: 51
   e. Calibration Assignment: E
   f. Station Pairs: BD, CD, FD, HD

5. <u>WEEKLY STATION DATA MESSAGE</u>:

PARAGRAPH	STATION PAIR	FREQUENCY	TIME (UT)
1	B-D	10.2 kHz	1600
2	B-D	13.6 kHz	1600
3	C-D	10.2 kHz	2000
4	C-D	13.6 kHz	2000
5	F-D	10.2 kHz	1700
6	F-D	13.6 kHz	1700
7	H-D	10.2 kHz	(1)
8	H-D	13.6 kHz	(1)
9	(LORC)	(8970Y)	1800
10	(GPS)	—	0946

6. <u>PCD ASSIGNMENT</u>: H-D at (1).

(1) = 1100 for October through March and 2200 for April through September as directed by the Japanese Maritime Safety Agency.

G.2.5 La Reunion

1. <u>LETTER DESIGNATION</u>: "E"

2. <u>LOCATION</u>:

   a. Geographic: Plaine Chabrier, La Reunion Island, France

   b. Geodetic: 20.9741° S, 55.2899° E

3. <u>SIGNAL TRANSMISSION ASSIGNMENT</u>:

SEGMENT	FREQUENCY (kHz)	ANTENNA CURRENT (amps)	SEGMENT	FREQUENCY (kHz)	ANTENNA CURRENT (amps)
1	12.3	373	5	10.1	463
2	11.05	428	6	13.6	332
3	12.3	373	7	$11\frac{1}{3}$	416
4	12.3	373	8	12.3	373

4. <u>MONITOR</u>:

   a. Geographic: Riviere des Pluies, La Reunion Island, France

   b. Geodetic: 20.9086° S, 55.5127° E

   c. Computer Code: REUNI

   d. I.D. Number: 38

   e. Calibration Assignment: D

   f. Station Pairs: AE, BE, FE, GE

5. <u>WEEKLY STATION DATA MESSAGE</u>:

PARAGRAPH	STATION PAIR	FREQUENCY	TIME (UT)
1	A-E	10.2 kHz	1100
2	A-E	13.6 kHz	1100
3	B-E	10.2 kHz	1000
4	B-E	13.6 kHz	1000
5	F-E	10.2 kHz	1800
6	F-E	13.6 kHz	1800
7	G-E	10.2 kHz	0500
8	G-E	13.6 kHz	0500
9	(N/A)	—	—
10	(GPS)	—	0616

6. <u>PCD ASSIGNMENT</u>: None

G.2.6 Argentina

1. <u>LETTER DESIGNATION</u>: "F"

2. <u>LOCATION</u>:

   a. Geographic: Golfo Nuevo, Chubut, Argentina

   b. Geodetic: 43.0536° S, 65.1908° W

3. <u>SIGNAL TRANSMISSION ASSIGNMENT</u>:

SEGMENT	FREQUENCY (kHz)	ANTENNA CURRENT (amps)	SEGMENT	FREQUENCY (kHz)	ANTENNA CURRENT (amps)
1	12.9	306	5	12.9	306
2	12.9	306	6	10.2	394
3	11.05	357	7	13.6	289
4	12.9	306	8	$11\frac{1}{3}$	347

4. <u>MONITOR</u>:

   a. Geographic: El Tehuelche, Argentina

   b. Geodetic: 42.7533° S, 65.1008° W

   c. Computer Code: ARGE2

   d. I.D. Number: 65

   e. Calibration Assignment: A

   f. Station Pairs: BF, DF, EF, GF

5. <u>WEEKLY STATION DATA MESSAGE</u>:

PARAGRAPH	STATION PAIR	FREQUENCY		TIME (UT)
1	B-F	10.2	kHz	1500
2	B-F	13.6	kHz	1500
3	D-F	10.2	kHz	1700
4	D-F	13.6	kHz	1700
5	E-F	10.2	kHz	1800
6	E-F	13.6	kHz	1800
7	G-F	10.2	kHz	0900
8	G-F	13.6	kHz	0900
9	(N/A)	—		—
10	(GPS)	—		0646

6. <u>PCD ASSIGNMENT</u>: G-F at 0900 UT.

G.2.7 Australia

1. <u>LETTER DESIGNATION</u>: "G"

2. <u>LOCATION</u>:

   a. Geographic: Woodside, Victoria, Australia
   b. Geodetic: 38.4812° S, 146.9353° E

3. <u>SIGNAL TRANSMISSION ASSIGNMENT</u>:

SEGMENT	FREQUENCY (kHz)	ANTENNA CURRENT (amps)	SEGMENT	FREQUENCY (kHz)	ANTENNA CURRENT (amps)
1	11⅓	350	5	13.0	310
2	13.0	310	6	13.0	310
3	13.0	310	7	10.2	390
4	11.05	370	8	13.6	290

4. <u>MONITOR</u>:

   a. Geographic: Carrajung, Victoria, Australia
   b. Geodetic: 38.3955° S, 146.6600° E
   c. Computer Code: AUST$
   d. I.D. Number: 22
   e. Calibration Assignment: A
   f. Station Pairs: CG, EG, FG, HG

5. WEEKLY STATION DATA MESSAGE:

PARAGRAPH	STATION PAIR	FREQUENCY	TIME (UT)
1	C-G	10.2 kHz	2400
2	C-G	13.6 kHz	2400
3	E-G	10.2 kHz	0500
4	E-G	13.6 kHz	0500
5	F-G	10.2 kHz	0900
6	F-G	13.6 kHz	0900
7	H-G	10.2 kHz	0400
8	H-G	13.6 kHz	0400
9	(N/A)	—	—
10	(GPS)	—	0716

6. PCD ASSIGNMENT: F-G at 0900 UT

G.2.8   Japan

1. LETTER DESIGNATION: "H"

2. LOCATION:

a. Geographic: Shushi-Wan, Tsushima Island, Japan

b. Geodetic: 34.6156° N, 129.4536° E

3. SIGNAL TRANSMISSION ASSIGNMENT:

SEGMENT	FREQUENCY (kHz)	ANTENNA CURRENT (amps)	SEGMENT	FREQUENCY (kHz)	ANTENNA CURRENT (amps)
1	13.6	269	5	11.05	334
2	11⅓	325	6	12.8	285
3	12.8	285	7	12.8	285
4	12.8	285	8	10.2	360

4. MONITOR:

a. Geographic: Ozaki, Tsushima Island, Japan

b. Geodetic: 34.3247° N, 129.2064° E

c. Computer Code: JAPAN

d. I.D. Number: 33

e. Calibration Assignment: F

f. Station Pairs: AH, CH, DH, GH

5. WEEKLY STATION DATA MESSAGE:

PARAGRAPH	STATION PAIR	FREQUENCY	TIME (UT)
1	A-H	10.2 kHz	1800
2	A-H	13.6 kHz	1800
3	C-H	10.2 kHz	0100
4	C-H	13.6 kHz	0100
5	D-H	10.2 kHz	(2)
6	D-H	13.6 kHz	(2)
7	G-H	10.2 kHz	0400
8	G-H	13.6 kHz	0400
9	(LORC)	(9970Y)	0400
10	(GPS)	—	0746

6. PCD ASSIGNMENT: D-H at (1).

(1) = 1100 for October through March and 2200 for April through September as directed by the Japanese Maritime Safety Agency.

G.3   REFERENCE

1. Department of Transportation/U.S. Coast Guard, Omega Navigation System Operations Manual, COMDTINST M 16566.1A, December 1988.

PROBLEM SOLUTIONS

CHAPTER 1

1. The antipode of a station is, in many ways, the "image" of the station. For example, the near-field modal interference which corrupts a station signal out to a range of about 1000 km is also found within a similar radius at the antipode. A more mundane problem discovered by navigators operating close to the antipode is that the station bearing can change so rapidly within a receiver time constant that the receiver's navigational filter/algorithm may become unstable and fail.

2. Signal 2 attenuates more rapidly since:
    *   daytime attenuation > nighttime attenuation
    *   westerly propagating signal attenuation > easterly propagating signal attenuation
    *   attenuation of signals propagating over low conductivities (e.g., frozen tundra) > attenuation of signals over high conductivities (e.g., seawater)

3. The short-path SNR in a 100 Hz bandwidth is

    $$25dB - 40dB = -15dB > -20dB$$

    and therefore passes the SNR usability test. The S/L is

    $$25dB - 19dB = 6dB \geq 6dB$$

    and thus passes the S/L usability test.

    The M1DM is $8dB \geq 6dB$ so the M1DM usability criterion is satisfied. Thus, all three criteria are satisfied and the signal is considered usable.

4. The conductivity of seawater is higher than that of fresh-water ice since seawater contains salt, a weakly bound ionic compound that is partially dissociated in water. The presence of free ions always increases conductivity since an applied electric field causes motion of the positive and negative charges, resulting in a current.

5. The lane width for a single 13.6 kHz station signal is just the signal wavelength. Since 10.2 and 13.6 kHz signals have the same free-space velocity (c), then

    $$c = f\lambda = (10.2kHz) \times \lambda_{10.2} = (13.6kHz) \times \lambda_{13.6}$$

    where f is the frequency and λ is the wavelength. Thus

    $$\lambda_{13.6} = \left(\frac{10.2}{13.6}\right)\lambda_{10.2} = \frac{3}{4}\lambda_{10.2} = \frac{3}{4} \times 30km = 22.5km$$

    If 10.2 and 13.6 kHz signals (from the same station) have the same phase at some range from the station, then the same phase will occur at an incremental distance over which both signals will develop an integral number of wavelengths. The *minimum* incremental distance over which this occurs is

    $$3\lambda_{10.2} = 4\lambda_{13.6} = 90km$$

6. The atmospheric noise at local summer afternoon is usually larger than at other times since the lightning discharges associated with thunderstorms are the principal source of VLF noise. Thunderstorms occur predominantly at local noon/early afternoon hours so that the VLF energy from the accompanying lightning discharges is propagated, preferentially to the east, toward longitudes at local afternoon/late afternoon hours.

CHAPTER 3

1. Columns 4 and 5 of Table 3.5-2 show that the base voltage-limited current is less than the output power-limited current for the following stations and frequencies:

Station	Frequencies (kHz)
North Dakota	10.2, 11.05, $11\frac{1}{3}$
Argentina	10.2, 11.05, $11\frac{1}{3}$

    The base voltage-limited currents for these stations and frequencies are lower than the others because of the higher base reactance resulting from the lower antenna capacitance (see Table 3.5-1). This is characteristic of stations with insulated tower antennas (except for Japan) where the effective area for capacitive coupling is smaller.

2. For the $11\frac{1}{3}$ kHz North Dakota signal, the pulse rise-time profile is

    $$s(t) = A(1 - e^{-t/19.0})$$

    Where t has units of msec and A is the pulse envelope amplitude when $t \gg 19$ msec. The time required for the pulse envelope to increase from 0 (at $t=0$) to $0.9A$ is found by setting

    $$0.9A = A(1 - e^{-t/19.0})$$

    or

    $$e^{-t/19.0} = 0.1$$

    Taking logarithms of both sides yields

    $$t = 43.7 \text{ msec}$$

CHAPTER 4

1. Determine the crossing angle of the LOPs at each of the candidate fix points. The crossing angle closest to 90° will yield the best accuracy and the crossing angle closest to 0° or 180° will yield the worst fix accuracy. The LOP crossing angle is the same as the included angle formed by the intersection of the two ranges and is easily determined in all cases by calculating the arc tan.
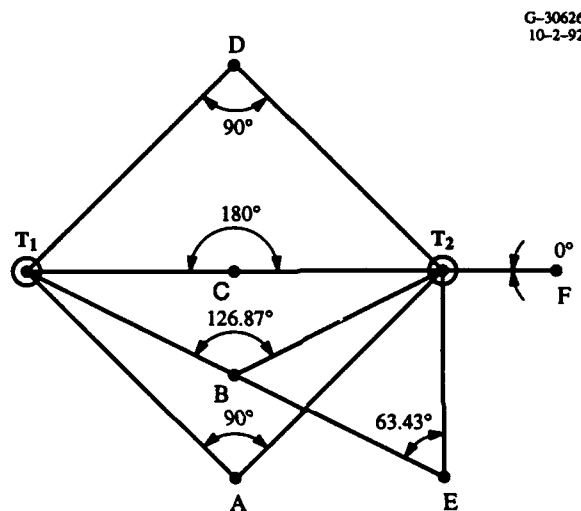
a. Points A and D will have the best, and equal, accuracy because of the 90° crossing angle.

b. Points C and F will have the worst accuracy, and in fact do not support a position fix since C is on the baseline with a 180° crossing angle and F is on the baseline extension with a 0° crossing angle.

c. The accuracy at point E is expected to be slightly better than the accuracy at point B because the crossing angle at E is closer to 90°.

2. a. First determine x_p using geometry and a few construction lines.
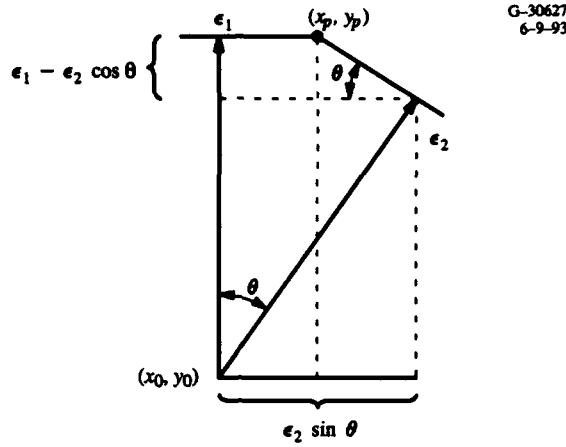
$$x_p = \epsilon_2 \sin\theta - \frac{(\epsilon_1 - \epsilon_2 \cos\theta)}{\tan\theta} = \frac{\epsilon_2 - \epsilon_1 \cos\theta}{\sin\theta}$$

Note that y_p is the offset from y_0 and is given by

$$y_p = \epsilon_1$$

Now, compute the variance of the radial position error:

$$\sigma_p^2 = E\{x_p^2 + y_p^2\} = E\left\{\frac{\epsilon_1^2 \sin^2\theta + \epsilon_1^2 \cos^2\theta + \epsilon_2^2 - \epsilon_1\epsilon_2\cos\theta}{\sin^2\theta}\right\}$$

$$= E\left\{\frac{\epsilon_1^2 + \epsilon_2^2 - \epsilon_1\epsilon_2\cos\theta}{\sin^2\theta}\right\}$$

$$= \frac{\sigma_{\epsilon_1}^2 + \sigma_{\epsilon_2}^2 - 2\rho\sigma_1\sigma_2\cos\theta}{\sin^2\theta}$$

Assuming that $\sigma_{\epsilon_1}^2 = \sigma_{\epsilon_2}^2 = \sigma_\epsilon^2$ and the correlation coefficient (ρ) is zero, σ_p^2 becomes:

$$\sigma_p^2 = \frac{2\sigma_\epsilon^2}{\sin^2\theta}$$

and the GDOP is:

$$\text{GDOP} = \frac{\sigma_p}{\sigma_\epsilon} = \frac{\sqrt{2}}{\sin\theta}$$

S-4

b) Using the range-range GDOP formula, the GDOP for each of the user positions in Problem 1 is:

USER POSITION	GDOP
A	$\sqrt{2}$
B	$1.25\sqrt{2}$
C	∞ *
D	$\sqrt{2}$
E	$1.12\sqrt{2}$
F	∞ *

*Indeterminate

3. a. If you select the in-line geometry, it is necessary to cross a baseline extension for all possible trajectories from point A to point B. Notice that the T_1T_2 baseline is the T_3T_2 baseline extension. Also, the T_2T_3 baseline is the T_1T_2 baseline extension. The hyperbolic fix cannot be computed on a baseline extension. This can be confirmed by computing the GDOP. Notice that when you are on a baseline extension, one or more of the angles goes to zero. Since sin (0) = 0, the GDOP goes to infinity.

If you select the delta station geometry, there is no need to cross a baseline extension with a direct trajectory from point A to point B. The GDOP is well behaved for all points along the direct trajectory. Therefore, the delta station geometry is the best for the assumed mission.

b. To determine the GDOP in the center of the triangle, simply input 120° for each angle in the GDOP formula. The resulting GDOP is $\sqrt{\frac{4}{3}}$.

At the midpoint of the T_1T_2 baseline, $\theta_3 = 180°$ and $\theta_1 = \theta_2 = 90°$. The resulting GDOP is equal to $\sqrt{2}$. This confirms that a hyperbolic fix can be obtained on a baseline.

Determining if the center of the triangle yields the minimum GDOP is easily tested using numerical techniques. We know that the GDOP increases from $\sqrt{\frac{4}{3}}$ to $\sqrt{2}$ as we go from the center of the triangle to the center of a baseline. If

point A is moved to one of the station locations, the resulting GDOP increases to 1.51. If point A is moved from the center location to increase (or decrease) any

two angles by 5°, the resulting GDOP increases from $\sqrt{\dfrac{4}{3}}$ = 1.15 to 1.25. Based

on the symmetry of this geometry, any movement from the geometric center of the tria' results in an increase in the GDOP.

c. The minimum GDOP is smaller for the delta configuration hyperbolic geometry than it is for the range-range fix: 1.15 as compared to 1.41. Also, the GDOP is only 1.41 on a baseline for the hyperbolic case whereas the GDOP goes to infinity on the baseline for the range-range case.

4. The hyperbolic lane width on the baseline is only half as wide as the rho-rho lane width because the phase repeats every $\lambda/2$ in the hyperbolic mode.
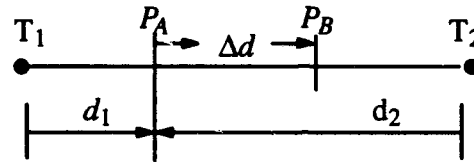
At P_A, the phase difference is

$$\phi_{1A} = \frac{2\pi d_1}{\lambda}; \quad \phi_{2A} = \frac{2\pi d_2}{\lambda}; \quad \phi_{dA} = \phi_{1A} - \phi_{2A} = \frac{2\pi}{\lambda}(d_1 - d_2)$$

At P_B, the phase difference is

$$\phi_{1B} = \frac{2\pi(d_1 + \Delta d)}{\lambda}; \quad \phi_{2B} = \frac{2\pi(d_2 - \Delta d)}{\lambda}; \quad \phi_{dB} = \phi_{dA} + \frac{4\pi\Delta d}{\lambda}$$

The change in the phase difference associated with the change in position is

$$\phi_{dB} - \phi_{dA} = \frac{4\pi\Delta d}{\lambda}$$

which is twice as large as the change in phase associated with a single range measurement. Therefore, the distance associated with a 2π shift in the hyperbolic phase is half as large as in the rho-rho mode.

The hyperbolic lane width is a minimum on the baseline. Therefore, the hyperbolic lane is wider at all other operating points. This can be seen from Fig. 4.2-4.

5. If the receiving antenna is submerged, there will be a significant reduction in the amplitude of the signal as a function of depth below the surface. However, even at depths of 3 m to 10 m, the received signal strength is usually sufficient to support position determination. The primary problem is associated with the signal phase shift introduced by the signal path through the water.

The additional phase shift introduced by the water will tend to be common to each of the received signals. However, the magnitude of the phase shift due to the water will be unknown and a function of depth, i.e., antenna position. Recall from Section 4.2 that the unknown common phase associated with the transmitted signals can be eliminated through the use of phase differences, which is the hyperbolic mode of operation.

The added phase shift due to the water is analogous to a large random clock error and cannot be estimated in the rho-rho mode. Therefore, a rho-rho fix cannot be determined underwater.

The wavelength at 10.2 kHz in seawater is approximately 50 ft, given that the phase shift is 2 cec/ft and a phase shift of 100 cec corresponds to one wavelength.

6. For the rho-rho mode of operation, only two measurements are required to compute a fix. The associated H (see Sections 4.4.6) for this case is

$$H = \begin{bmatrix} h_{11} & h_{12} \\ h_{21} & h_{22} \end{bmatrix}$$

where h_{11} and h_{21} are the latitude partials (Eqs. 4.4-1) for the two measurements and h_{12} and h_{22} are the longitude partials (Eq. 4.4-2). Let A be

$$A = H^T H = \begin{bmatrix} \left(h_{11}^2 + h_{21}^2\right) & \left(h_{11}\,h_{12} + h_{21}\,h_{22}\right) \\ \left(h_{11}\,h_{12} + h_{21}\,h_{22}\right) & \left(h_{22}^2 + h_{12}^2\right) \end{bmatrix} = \begin{bmatrix} a & b \\ b & c \end{bmatrix}$$

Note that A is a symmetric matrix—this is always true, independent of the number of measurements. The determinant of A is

$$|A| = ac - b^2$$

It can be seen from Eq. 4.4-1 and 4.4-2 that if the same station is used for both ranges, or if the receiver is on the baseline extension, then

$$h_{11} = h_{21} \text{ and } h_{12} = h_{22}$$

Why would one be tempted to use the same station for both measurements? Don't fall into the trap of assuming that, because there is more than one frequency available from each Omega station, each frequency can be counted as separate measurement in the fix algorithm. There are good reasons for using measurements at multiple frequencies from a single station, but only when suitable fix geometry is provided by all of the measurements to yield the necessary observability.

Completing the problem, a, b, and c are

$$a = 2\,h_{11}^2, \quad b = 2\,h_{11}h_{22}, \quad c = 2h_{22}^2$$

These values for a, b, and c yield a determinant value of zero for A. Therefore, the least-squares solution cannot be obtained. If the receiver is on the baseline, it can also be shown that the determinant of A is zero and a fix cannot be computed.

The same indeterminate result is obtained if the clock drift state is included in the state vector and any two of the required three range measurements are obtained from the same station, or the receiver is on the baseline or baseline extension. Although the mathematics required to calculate the determinant of the 3×3 matrix is not difficult, it is tedious and is left as an exercise for the student.

CHAPTER 6

1. The problem is not North Dakota but La Reunion, which is often received over the long path in this area. This explanation is easily supported by coverage analysis.

2. The predicted interference boundary is probably wrong. While efforts have been made to locate interference boundaries both accurately and conservatively, uncertainties exist. This is true despite use of full-wave modeling and experimental studies espe~·······~ validation programs. Also, in this particular case, data shows that the boundary seems ......tly from year to year. It is important that a report of this type be archived for use in coverage revision.

3. The predicted long path boundary is probably wrong. The circumference of the world is 40,000 km. An east-west differential error of only 0.1 dB/MM would cause a prediction error of 4 dB — enough to move the boundary about 1,000 km. Long path boundaries are very uncertain.

4. This is not mainly a problem of weak signals; it is high noise. Summer thunderstorms are common in the area. However, the noise is highly impulsive and one would hope a well designed and installed receiver could operate. The situation will, however, be difficult as the signals are also relatively weak. The operational experience of others using similar aircraft in the area should be checked. If others are navigating satisfactorily, the user needs to "clean up" the installation.

CHAPTER 7

1. The first eight states of the system synchronization state vector are $\delta\phi_{X\Omega}$ where $X = A, B, \dots H$. These states are obtained from the $\delta\phi_{XU}$ given in the table for the sample problem as

    $$\delta\phi_{X\Omega} = \delta\phi_{XU} - \delta\phi_{\Omega U}$$

    Where $\delta\phi_{\Omega U}$ is just the mean of the $\delta\phi_{XU}$ given in the table. The offset of Omega system time from UTC, $\delta\phi_{\Omega U}$, also serves as the ninth state. If we are given a similar table for δf_{XU}, then states 10 through 17 can be determined in a similar way, i.e.,

    $$\delta f_{X\Omega} = \delta f_{XU} - \delta f_{\Omega U}$$

    Where $\delta f_{\Omega U}$ is the 18th state and is obtained as an average of the δf_{XU} over the stations, X. Thus, the two tables provide sufficient information to estimate the system state vector. Reciprocal path data are used as additional independent measurements to supplement the external data, which may sometimes be incomplete.

2. We are given that the estimated "frequency" offset of Station B from the Omega System "frequency" is -0.32 µsec/day. The adjustment (or directive) is the negative of this estimate, computed over a 4-hour time period. Thus, the corresponding ACCUM directive for Station B would be

    $$+ 0.32/6 \simeq + 0.05 \text{µsec/4-hours}$$

CHAPTER 8

1. At hour 01, the raw MX1104 phase data value for a given station is 649 and at hour 02 it is 497. These data represent single-path measurements of phase with respect to the reference oscillator, which has a stability of 10^{-7} or better (see Table 8.2-3). A stability of 10^{-7} implies a "drift" of one microsecond (approximately 1 cec of 10.2 kHz) for an Omega format period of 10 seconds. Thus, in an hour, the oscillator with this stability would drift by more than 3.5 lanes. Hence the observations are consistent with a signal whose phase is unchanged and an oscillator with a drift rate of 4.2×10^{-8}. Thus, in the absence of predictions it is impossible to tell whether the phase increased or decreased.

    If predictions *are* available, they can be used to "calibrate" (over a period of several days) the MX1104 reference oscillator, to within the accuracy of the predictions. Suppose this calibration yielded an oscillator drift rate of 4.78×10^{-8}. Thus, over one hour (3600 seconds), this would lead to a phase.change of

    $$4.78 \times 10^{-8} \times 3600 \text{ sec} = 172.1 \text{ } \mu\text{sec}$$

    This change would actually be negative since the displayed/recorded datum is actually $X - R$ where X is the station signal phase and R is the reference oscillator phase.

    Thus, with *no signal phase change*, the datum at hour 02 should read (given that it read 649 at hour 01):

    $$649 - 172 = 477$$

    If an *increase* in phase is predicted, then the observed value of 497 implies a measured increase of 20 cec between hours 01 and 02.

    For phase-difference measurements, no oscillator calibration is needed, since the signals being differenced are assumed to be radiated by their respective stations at the same time (thanks to system synchronization). In these cases, both the lane value (leftmost digit) and the centicycle value (two rightmost digits) are both coherent from *hour* to *hour*. For the lane digit, this coherence is broken only when the receiver is shut down (e.g., due to a power failure) between the hourly measurements.

2. Signals affected by self-interference, such as modal interference or long-path domination, are not Mode 1-dominated signals. The PPC Model only corrects signals that are dominated by the Mode 1 component (see Chapter 9). A user must *de-select* signals with self-interference.

CHAPTER 9

1a. If a transmitting station and receiver have an angular separation of 60° on a spherical earth, then the separation in radians is

$$\frac{2\pi}{360} \times 60 = \frac{\pi}{3} = 1.047 \text{ radians}$$

b. The path length on a spherical earth is $1.047 \, R_E$ where $R_E = 6367$ km is the average earth radius. Thus, path length = 6667.51 km.

c. A 12 kHz signal has a free-space wavelength of $c/(12 \times 10^3 \text{ sec}^{-1})$ where $c = 2.9979 \times 10^5$ km/sec. The wavelength is thus 24.9825 km.

d. The free-space wave number is just the reciprocal of the free-space wavelength, and is thus 0.040028 km^{-1} for 12 kHz signals.

e. In terms of the free-space wave number, k_0, the nominal wave number is given by

$$k_{NOM} = 0.9974 \, k_0$$

Thus, from the results of 1d we have

$$k_{NOM} = 0.039924 \text{ km}^{-1}$$

f. From Eq. 9.2-5, the nominal phase for the path over a spherical earth is

$$\phi_{NOM} = k_{NOM} \, D$$

Where k_{NOM} is given from the results of 1e and D is given by the results of 1b. Thus

$$\phi_{NOM} = 0.039924 \times 6667.51 = 266.193 \text{ cycles}$$

g. If, at a given time, the exact PPC is known to be zero, then, by Eq. 9.2-6, the observed cumulative phase at this time is the same as the nominal phase, i.e.,

266.193 cycles

h. An Omega receiver which is phase-synchronized to the received signal measures the *fractional* part of the cumulative phase, i.e.,

0.193 cycle

2a. Since an SID results from excess X-ray and EUV radiation (originating from certain types of solar flares) on the dayside ionosphere, the sub-models describing the effect of these events on the Omega phase would be defined within the phase velocity domain (mid-path region).

b. The excitation domain lies at the "boundaries" of the phase velocity domain/mid-path region and, thus, the segments encompassed by the excitation domain depend on the extent of the mid-path region. Similarly, the size of the end-path regions constituting the groundwave domain also depends (through the FPII and LPII) on the size of the mid-path region comprising the phase velocity domain.

c. Since the hypothetical SID sub-models are in the phase velocity domain, they are "wave number-like" and therefore have a minus sign attached in the expression for predicted phase (see Eq. 9.5-11).

d. The SID sub-models would apply to day-paths only (see Table 9.5-4) and since they apply only to conductivity levels and 7 and 10, *two* sub-models are required.

CHAPTER 10

1. The short-path and the long-path from a station to a receiver are, respectively, the shorter-arc and the larger-arc of the great circle joining the station and the receiver. The maximum length of the short path is 20 megameters (on spherical earth) as it is half the great-circle circumference.

2. The two GDOPs differ by the signal frequency-dependent scale factor, as described below:

   Non-dimensioned GDOP = λ (Dimensioned GDOP), where λ is the signal wavelength; note, frequency × wavelength = Speed of light.

3. The table below lists the usable signal coverage criteria parameters, their nominal threshold values, and the associated rationale for selecting the threshold values. Note, the most restrictive coverage criteria parameter for determining coverage is M1DM.

Coverage Criteria Parameter	Nominal Threshold Value	Rationale for the Threshold Value
Short-path Signal-to-Noise Ratio (SPSNR)	-20 dB (in 100 Hz Bandwidth)	Minimum SPSNR required for aircraft navigation; consistent with current Omega receivers.
Mode 1 Dominance Margin (M1DM)	6 dB	A reasonable M1DM value which provides sufficient margin for the signal to be a Mode 1-dominated signal as well as to avoid lane slip/jump due to random ionospheric fluctuations.
Ratio of Short-path Signal and Long-path Signal (S/L)	6 dB	A reasonable S/L value which provides sufficient margin for the signal to be a short-path-dominated signal under random ionospheric fluctuations.
Path/Terminator Crossing Angle (PTCA)	5 deg	Minimum PTCA needed to exclude extremely rapid day-to-night transition along a path in which lane slip/jump is likely to occur.
GDOP	3	Maximum GDOP needed to exclude 2-drms position errors exceeding 12 km.

4. The minimum number of Omega stations needed for computing a hyperbolic navigation position-fix is three stations. The minimum number is sufficient, provided the associated GDOP of the fix geometry is below the accepted threshold value. The GDOP of a fix generally decreases with increasing number of usable-signal stations.

5. Stations A and H should be deselected at Boston as the signal paths from these stations to Boston cross geomagnetic polar region.

6. At the southern tip of Australia:

   (1) The SNR (in 100 Hz bandwidth) is between –20 and –30 dB

   (2) The Modal interference-induced phase deviation is less than 20 cec.

7. An Omega signal transmitted by a station has the greatest usable range in the easterly directions; the shortest usable range from the station is along the westerly directions. This is a direct consequence of the facts that: (1) Mode 1 signal attenuation rate is much higher in the westerly than easterly direction, and (2) signals are modal to much longer distances in the westerly directions than easterly directions.

8. The primary source of noise at Omega frequencies is lightning discharges associated with world-wide thunderstorm activity. The noise at a given location is generally highest at the local summer afternoon.

CHAPTER 11

1. Since $1 - P_R = MTTR/MTBF$, it follows that

$$\Delta(1 - P_R) = - \frac{MTTR}{(MTBF)^2} \Delta(MTBF)$$

and

$$\frac{\Delta(1 - P_R)}{1 - P_R} = - \frac{\Delta(MTBF)}{MTBF}$$

Since it is given that $\Delta(MTBF) = -100$ hours it follows that

$$\frac{\Delta(1 - P_R)}{1 - P_R} = \frac{100}{2000} = 0.05$$

Thus, the unreliability of a receiver increases by 5%.

2. Since unscheduled off-air events are independent of all other events, $P(\overline{T}_2^u \overline{T}_6^s) = P(\overline{T}_2^u) P(\overline{T}_6^s)$ Substituting the appropriate off-air probabilities from Table 11.3-1 yields

$$P(\overline{T}_2^u \overline{T}_6^s) = 0.0000023$$

3. The event that at least one of the two stations is in an off-air condition is $\overline{T}_3^u + \overline{T}_5^u$ (recall "+" means "or" when combining events). Thus

$$P(\overline{T}_3^u + \overline{T}_5^u) = P(\overline{T}_3^u) + P(\overline{T}_5^u) - P(\overline{T}_3^u \overline{T}_5^u)$$

The third term arises because $\overline{T}_3^u$ and $\overline{T}_5^u$ are not mutually exclusive and the set intersection is added twice with the first two terms. Thus, the third term is included to subtract the extra contribution. Moreover, since unscheduled off-air events are independent,

$$P(\overline{T}_3^u \overline{T}_5^u) = P(\overline{T}_3^u) P(\overline{T}_5^u)$$

Thus

$$P(\overline{T}_3^u + \overline{T}_5^u) = P(\overline{T}_3^u) + P(\overline{T}_5^u) - P(\overline{T}_3^u) P(\overline{T}_5^u)$$

and substituting the given reliabilities yields

$$P(\overline{T}_3^u + \overline{T}_5^u) = 0.1264$$

4a. Station "A" fails the M1DM criterion; Station "B" passes all criteria; Station "C" fails the PTCA criterion; Station "D" passes all criteria; Station "E" passes all criteria; Station "F" fails the SNR criterion; Station "G" fails the LP/SP criterion; and Station "H" fails the SNR criterion.

The set of stations B, D, and E have GDOP < 6 since the set does not include F or G. Thus, only stations B, D, and E are in the coverage set.

b. The maximal coverage set contains all those signals which satisfy the *deterministic* coverage criteria (i.e., all except the SNR criterion). From the solution to (a), it is seen that stations F and H satisfy the deterministic coverage criteria. Moreover, the set of stations B, D, E, F, and H has a GDOP < 6 since it exceeds four stations in number and does not contain F or G. Thus, the maximal coverage set contains station signals B, D, E, F, and H.

5a. $P(A_1A_2A_3) = 0$ since stations 1 and 2 (A and B) are not in the maximal coverage set.

b. $P(A_2A_4A_5) = 1$ since stations 2, 4, and 5 are in the maximal coverage set and all satisfy the SNR criterion.

c. $P(A_4A_5A_6A_8) = 0$ since stations 6 and 8 fail the SNR criterion.

d. For the random SNR case, $P(A_4A_5A_6A_8) \neq 0$ since there is a finite probability that the SNRs will exceed –20 dB for both signals F and H even though their mean SNR values are both less than –20 dB.

6. First, normalize the weights. Since $w_1 + w_2 + w_3 + w_4 + w_5 + w_6 = 27$, set
$$w_1' = 2/27 \; ; \; w_2' = 4/27 \; ; \; w_3' = 7/27 \; ; \; w_4' = 5/27 \; ; \; w_5' = 2/9 \; ; \; w_6' = 1/9 \; .$$

Compute

$$P_{SA} = \sum_{i=1}^{6} w_i' P_R P_{A_i}$$

$$= 0.9 \left(\frac{2}{27} \times 0.85 + \frac{4}{27} \times 0.80 + \frac{7}{27} \times 0.72 + \frac{5}{27} \times 0.93 + \frac{2}{9} \times 0.78 + \frac{1}{9} \times 0.87 \right)$$

$$= 0.7293$$

7. First construct

$$H = \begin{bmatrix} k_0\cos\beta_1 & k_0\sin\beta_1 & \Delta T \\ k_0\cos\beta_2 & k_0\sin\beta_2 & \Delta T \\ k_0\cos\beta_3 & k_0\sin\beta_3 & \Delta T \\ k_0\cos\beta_4 & k_0\sin\beta_4 & \Delta T \end{bmatrix} = \begin{bmatrix} k_0 & 0 & \Delta T \\ 0 & k_0 & \Delta T \\ -k_0 & 0 & \Delta T \\ 0 & -k_0 & \Delta T \end{bmatrix}$$

Further, calculate

$$\begin{bmatrix} 1/(2k_0^2) & 0 & 0 \\ 0 & 1/(2k_0^2) & 0 \\ 0 & 0 & 1/(4(\Delta T)^2) \end{bmatrix} \qquad H^T = \begin{bmatrix} k_0 & 0 & -k_0 & 0 \\ 0 & k_0 & 0 & -k_0 \\ \Delta T & \Delta T & \Delta T & \Delta T \end{bmatrix}$$

and

$$H^T H = \begin{bmatrix} 2k_0^2 & 0 & 0 \\ 0 & 2k_0^2 & 0 \\ 0 & 0 & 4(\Delta T)^2 \end{bmatrix}; \quad (H^T H)^{-1} = \begin{bmatrix} 1/(2k_0^2) & 0 & 0 \\ 0 & 1/(2k_0^2) & 0 \\ 0 & 0 & 1/(4(\Delta T)^2) \end{bmatrix}$$

$$(H^T H)^{-1} H^T = \begin{bmatrix} 1/(2k_0) & 0 & -1/(2k_0) & 0 \\ 0 & 1/(2k_0) & 0 & -1/(2k_0) \\ 1/(4\Delta T) & 1/(4\Delta T) & 1/(4\Delta T) & 1/(4\Delta T) \end{bmatrix}$$

Thus, Eq. 11.8-7 yields

$$\delta N = (1/2k_0)\delta\phi_1 - (1/2k_0)\delta\phi_3$$

$$\delta E = (1/2k_0)\delta\phi_2 - (1/2k_0)\delta\phi_4$$

$$\delta\gamma = \frac{1}{4\Delta T}(\delta\phi_1 + \delta\phi_2 + \delta\phi_3 + \delta\phi_4)$$

Putting in the particular values yields:

$$\delta N = -0.88\text{km}$$

$$\delta E = -0.15\text{km}$$

$$\delta\gamma = 0.0013\text{cycle/min}$$

8 a. Since the SP/LP lower bound threshold has been decreased to 0 dB, the signal from station G joi..s B, D, and E in the coverage set (see problem 5(a)). Note that F and G do not both occur in the coverage set so that GDOP < 6 as required by the PACE default signal coverage access criterion.

b. The solution to Problem 5(b) indicates that signals B, D, E, F, and H are in the maximal coverage set. In this case, the deterministic LP/SP criterion has been relaxed so that G is also in the maximal coverage set. Hence, the maximal coverage set includes signals B, D, E, F, G, and H. Although both F and G occur, the set contains more than four signals so that GDOP < 6.

c. Since one of the PACE default signal coverage access criteria is *relaxed* and since Problem 9 found that $Q_0 = 1$, then it must also be true that $Q_0 = 1$ in this case.

d. With Station 2(B) off-air, signals D, E, and G are in the coverage set. Moreover, since F and G are no. both in the coverage set, GDOP < 6 (i.e., the GDOP criterion is satisfied) so that

$$Q_{23} = 1$$

e. With stations 2(B) and 8(H) off-air, signals D, E, F, and G remain. The procedure is identical to that carried out in Section 11.7.2 (which also considered four stations in the maximal coverage set). Thus,

$$Q_{128} = P(A_4 A_5 A_6 \overline{A}_7) + P(A_4 A_5 \overline{A}_6 A_7) + P(A_4 \overline{A}_5 A_6 A_7)$$
$$+ P(\overline{A}_4 A_5 A_6 A_7) + P(A_4 A_5 A_6 A_7)$$

Note that the 3rd, 4th, and 5th terms are probabilities of events in which both F and G are accessible (out of 3 total accessible signals for the 3rd and 4th terms; out of 4 total accessible signals for the 5th term). Since, for these cases, GDOP > 6, the coverage criterion is violated and these terms are excluded. Thus,

$$Q_{128} = P(A_4 A_5 A_6 \overline{A}_7) + P(A_4 A_5 \overline{A}_6 A_7)$$

9 a. Problem 10(a) determined that signals B, D, E, and G are in the coverage set. Thus, removing a single station still leaves 3-station coverage (GDOP criterion is satisfied since F is not in the coverage set). Thus

$$Q_1 = Q_2 = \dots Q_8 = 1$$

b. Since the total number of two-station combinations out of 8 stations is $\binom{8}{2} = \frac{8 \cdot 7}{2 \cdot 1} = 28$, it is

easier to compute the number of *zero* Q_{ij}'s. The stations in the coverage set are B, D, E, and G (or 2, 4, 5, and 7), so that an off-air pair involving any 2 of B, D, E, or G, will leave only 2 stations in the

coverage set and the corresponding Q is zero. There are $\binom{4}{2} = 6$ of such pairs so that the total

number of *non-zero* dual outage Q's is $28 - 6 = 22$.

c. $P_{SA} = P_R P_A$ and $P_A = Q_0 P(B_0) + Q_1 P(B_1) + \ldots$ (as given in the text).

Now $Q_0 = 1$ as the result of Problem 1(a) and $Q_1 = Q_2 = \ldots Q_8 = 1$ as the result of Problem 3(a). Also, there are 22 non-zero Q_{ij}'s as the result of Problem 3(b). Since the network reliability factors for 3, 4, and 5 station outages are assumed zero, P_A, is given as follows:

$$P_A = 0.732 + 8 \times 0.010 + 22 \times 0.001 = 0.834$$

10. If concurrent scheduled off-air events for two stations are not allowed, the probability that the stations are concurrently on-air is decreased relative to the case in which scheduled and unscheduled off-air events at different stations are independent. This is shown explicitly in Section 11.6, where the following result is derived:

$$P(T_1 T_2) = P(T_1)P(T_2) - P(\overline{T}_1^s)P(\overline{T}_2^s)$$

This reduction comes about because the scheduled off-airs cannot occur at the same time (where $T_1 T_2$ would not occur anyway) and thus a scheduled off-air at either station is more likely to occur when the other station is on-air. This has the effect of increasing the number of times (or likelihood) that $T_1 T_2$ does not occur.

11. Create a new reliability set with a non-zero probability of annual maintenance off-air (say 0 33) for both stations A and B. Compute three scenarios using the best, nominal, and worst case SRM selections. Compare the three scenarios.

12. Create a reliability set with zero probability of scheduled, unscheduled, and maintenance off-airs for all stations for all months (this removes the random effects from the P_{SA} computation an reduces it to simply coverage). Compute a P_{SA} scenario using this reliability set and a P_{SA} threshold of 0.5 and nominal values for the other parameters.

13. Compute a P_{SA} scenario with all stations off-air except A, E, and H, and with relaxed values for all parameters except GDOP (e.g., SPSNR = –99 dB, LPSNR = –99 dB, M1DM = 0 dB, PTCA = 0 degrees, GDOP = 6). Choose the minimum reporting method and all hours/months. The bad GDOP areas will show up as red on the cell display.

CHAPTER 12

1a. The duty cycle for any common Omega frequency is about 10 percent since this is the fraction of time the signal is being transmitted. Since the time constant is 150 seconds, the effective averaging time is

$$150 \text{ sec}/10 = 15 \text{ seconds}$$

b. The unique frequency signal at any given station is transmitted in four segments during every time frame. Thus, the duty cycle is 4/10 and the effective averaging time is

$$0.4 \times 150 \text{ sec} = 60 \text{ seconds}$$

c. The noise equivalent bandwidth for the common frequency Omega signals is

$$1/(4 \times 15 \text{ sec}) = 0.017 \text{ Hz}$$

Thus the processing gain relative to the input noise is

$$100/0.017 = 6000$$

or

$$10 \log_{10} 6000 = 37.8 \text{ dB}$$

d. The noise equivalent bandwidth for the unique frequency Omega signals is

$$1/(4 \times 60 \text{ sec}) \ 0.004 \text{ Hz}$$

and the processing gain is

$$100/0.004 = 24000$$

or

$$43.8 \text{ dB}$$

2. If the signal power to noise power ratio is 12 dB, then

$$10 \log_{10}\left(\frac{P_s}{P_N}\right) = 12$$

so that

$$\frac{P_s}{P_N} = 15.85$$

Thus, according to Eq. 12.2-3, the corresponding phase error is

$$\Delta\phi = 1/\sqrt{(2 \times 15.85)} = 0.178 \text{ radian}$$

If the frequency is $f = 13.6$ kHz then this phase error (in μsec) is

$$0.178 \text{ radian} \times \frac{1 \text{ cycle}}{2\pi \text{ radians}} \times \frac{(1/f)\text{sec}}{1 \text{ cycle}} \times \frac{10^6 \mu \text{sec}}{1 \text{ sec}}$$

or

$$2.1 \ \mu \sec$$

3. Using the expression for the signal power-to-noise power ratio estimate,

$$\left(\frac{S}{N}\right)_{estimate} = \frac{1}{4(1 - <\cos\phi>)}$$

we find the following SNR estimates:

Station A: 1.39 (1.43 dB)
Station B: 1.09 (0.04 dB)
Station G: 0.64 (−1.93 dB)
Station H: 4.17 (6.20 dB)

The sum of the SNRs is 7.29 so that the weights for each signal are

$w_A = 0.191$
$w_B = 0.150$
$w_G = 0.088$
$w_H = 0.571$

INDEX

data driven, 9-6

data indicators, 9-29

data link, 9-2

data presentation, 8-19

data processing procedure, 8-22

day and night time constants, 9-58

day linear model coefficients, 9-30

day phase velocity variation, 9-48

day wave number, 9-56

day/night coefficients, 9-33

day/night terminator, 5-50, 10-11, 10-32

daytime evolution function, 9-58

daytime ionospheric response time, 9-58

daytime path, 9-30, 9-37

daytime phase profile, 9-58

daytime phase value, 6-14

day-to-day diurnal changes, 6-32

day-to-day variation, 2-7, 6-32, 9-30, 9-35, 9-55, 11-59

dead reckoning, 4-1, 12-24

dead reckoning mode, 12-18

dead reckoning procedures, 2-10

decibels per megameter, 5-18

decorrelation, 6-34

decorrelation time, 12-29

dedicated aircraft, 8-9

de-excitation, 6-4

de-excitation region, 9-21, 9-50

dehydrator, 3-23

delay time, 8-18

depth of penetration, 5-69

derivative composition, 12-21

derivatives of a vector, 5-54

deselect, 6-15, 6-25

deselection data, 12-26

deselection guidance, 12-18

desynchronized, 8-21

detection circuitry, 2-23

detection stage, 8-18, 12-11

detector, 12-9

deterministic (non-random) events, 3-11

deterministic coverage component, 11-51

deterministic coverage parameters, 11-32

de-weighting, 6-15, 12-8

diagnostic error codes, 8-20

diagonal weighting matrix, 9-33

difference frequencies, 6-32

difference frequency system, 9-17

Differential Omega, 4-41, 9-2, 13-5

differential operator, 5-55

differential proton flux, 6-30

digital matched filters, 12-11

digitized maps, 12-17

dimensionless functional form, 9-48

dip angle, 5-9, 9-44, 9-53, 10-5

dipole model, 9-44

direct phase measurement, 6-9

direct ranging, 1-7, 4-4

direction of arrival, 6-1, 6-3

directives, 7-16, 7-18

discrete spectrum, 9-41

disk recording system, 8-19

dispersive correlation, 6-33

displacement current, 5-6

displayed phase-difference values, 12-2

disturbed polar regions, 12-18

diurnal, 2-30

diurnal behavior, 2-11, 6-37, 8-14, 8-16, 9-26, 9-27

diurnal changes, 6-4, 9-18

diurnal function, 9-56, 9-58

diurnal irregularities, 6-26

diurnal phase behavior, 8-15

diurnal phase corrections, 9-18

diurnal phase variation, 6-22, 6-34, 8-23

diurnal plots, 9-29

diurnal rate of change, 6-4

diurnal sampling intervals, 9-38

diurnal shift, 9-15, 9-56

diurnal variation, 6-26, 9-2

divergence, 4-40, 5-54, 5-58

DMA, 2-29, 2-30

dominant mode, 9-5

Doppler measurements, 2-27, 12-2

double diurnal effect, 6-14

downlead, 3-26, 3-27

down-sampling, 9-31

Draco, 2-10

D-region, 5-7, 5-23, 9-15, 9-20, 9-43, 10-4

drift rate, 3-16, 12-22

driver amplifier, 2-17, 3-23

driving function, 9-57

dry soil, 5-36

D-station, 2-20

dual Omega receivers, 6-25

dummy load, 3-23

dump schedules, 9-58

duty cycle, 11-58, 12-12

dynamic diurnal function, 9-56

E

E-field antennas, 10-5, 11-13, 12-7

E-region, 5-8

e-wave, 5-11, 5-71

earth ionosphere medium, 1-1, 1-3

earth's magnetic field, 5-23, 10-5

earth's surface, 5-6, 9-22

earth-ionosphere (EI) waveguide, 5-2, 5-3, 5-4, 5-10, 5-22, 5-70, 5-71, 6-26, 9-21, 9-44, 10-4

earth-ionosphere electromagnetic environment, 9-40

east is easy, 5-50

inhomogeneous waveguide, 5-39, 5-40, 5-41

initial frequency covariance, 7-14

initial phase covariance, 7-14

initialization, 12-29

inner or dot product, 5-53

input amplifier, 2-17, 3-21

input data preprocessor, 7-13

INS-derived position, 8-40

insertion times, 7-18

instantaneous winds, 12-24

Institute of Electrical and Electronics Engineers, 2-35

Institute of Navigation, 2-35

insulated tower, 1-3, 2-18, 3-2, 3-27

integer part, 9-11, 9-23, 9-32

integrated basis, 12-28

integrated navigation systems, 2-27, 4-1, 12-2, 12-27, 12-29

integration contour, 9-15

integrity, 13-1, 13-4

interaction point, 9-51

inter-channel measurement noise coupling, 12-24

interference, 6-16

interfering mode (IM), 6-22, 11-21

interfering noise, 12-28

intermediate states, 9-55

intermodulation products, 8-18, 12-10

internal methods, 9-2

internal oscillator drift, 8-19

internal synchronization, 7-3

internal synchronization data, 7-4

internal time constants, 8-19

International Navigation Association (INA), 2-34, 9-8

International Omega Association (IOA), 2-34, 9-8

International Omega Technical Commission (IOTC), 1-2, 2-4, 3-5

international partnership, 3-6

interoperable, 2-27

interoperable navigation systems, 12-2, 12-27

interoperable receiving systems, 3-18, 7-6

interplanetary magnetic field, 6-32

interpolation function, 9-56

inter-station propagation times, 2-11

intrinsic attenuation constant, 5-67

intrinsic impedance, 5-65

intrinsic phase constant, 5-67

intrinsic stability, 3-15

IOA/INA annual meetings, 2-35

ionization profiles, 9-55

ionosphere, 1-4, 2-7, 5-7, 9-22

ionosphere hardening, 9-6

ionospheric conductivity, 5-2, 5-8

ionospheric conductivity gradient, 5-8, 10-5, 10-12

ionospheric contribution, 9-52

ionospheric disturbances, 6-1, 12-18

ionospheric D-region, 9-41, 9-57

ionospheric effects, 5-38

ionospheric fluctuations, 12-28

ionospheric height, 6-19, 9-55

ionospheric ionization, 6-28

ionospheric parameters, 9-52, 10-5

ionospheric physics, 2-7

ionospheric processes, 9-18

ionospheric profiles, 6-39, 6-40

ionospheric reflection height, 5-41, 10-5, 10-12

ionospheric response, 6-28, 6-31

ionospheric variations, 6-2

IPP, 10-28, 10-44

isotropic medium, 5-23

isotropic/linear, 5-60

isotropic/planar waveguide, 5-10, 5-19

J

Japan, 10-29

Japan Maritime Safety Agency (JMSA), 1-2, 2-5, 3-5, 3-7, 7-4, 7-24

Japan station, 2-21

joint phase error probability density function, 11-60

K

k, 5-62

Kailua, 2-19

Kalman estimation algorithm, 2-24

Kalman estimation technique, 7-5

Kalman filter, 4-7, 4-30

Kalman gain, 7-12

Kennelly, 2-7

Kennelly-Heaviside layer, 2-7

keying pulses, 3-19

L

La Reunion, 2-20

lane, 1-7, 9-11, 12-19

lane ambiguity, 2-9, 2-10, 2-14, 3-35, 12-19

lane assignment, 9-32

lane changes, 8-23

lane count, 1-7, 2-23

lane counter, 4-20

lane determination, 4-1, 4-20

lane identification, 2-12, 2-14, 2-24

lane number, 9-32

lane number difference relationship, 8-30

lane resolution, 2-24

lane slip/jump, 4-43

lane value, 8-23

laned, 8-7, 8-30

laning, 4-41

laning algorithm, 9-32

Laplace's operator, 5-55

Laplacian operator, 5-62

large phase errors, 9-7

last point of ionospheric interaction, 9-42

latitude, 1-7, 4-26

latitude/longitude readout, 2-24

lattice tables, 2-28

launch angle, 9-42

leading edge, 3-12

leap seconds, 3-4

least-squares algorithm, 4-1, 4-30

least-squares estimate, 9-25

least-squares fix, 4-32

left-handed, 5-66

LF, 2-6

LF beacon, 9-2

L-flag, 8-28

Liberia, 2-18

Liberia Station, 10-29

lightning, 6-16

lightning discharges, 2-23, 9-35, 12-5

limiter, 2-24, 8-17

limiter level, 12-6, 12-10, 12-12

limiting, 6-11

limiting device, 2-23

line of position (LOP), 1-1, 1-8, 2-22, 4-4, 6-21, 8-27, 9-12, 9-13, 11-61

linear, 2-23

linear electron loss dependence, 9-57

linear estimate of signal-to-noise ratio, 8-19

linear model coefficients, 9-5, 9-6, 9-17, 9-23, 9-27, 9-33, 9-47

linear polarization, 5-66

linear PPC model coefficients, 8-7

linear scale, 8-24

linearization error, 9-23, 9-47

linearized, 12-20

linearized range equations, 11-62

linearly polarized, 8-17

linearly polarized wave, 5-66

line-of-position error, 6-25

lobe structure, 12-9

local coverage elements, 11-27

local day, 9-15

local illumination condition, 9-15, 9-55

local ionosphere, 9-5

local maximum day, 9-5, 9-23, 9-33, 9-55, 9-56

local maximum night, 9-5, 9-23, 9-33, 9-55, 9-56

local night, 9-15

local noise, 6-2

Local Notices to Mariners, 2-29

local station bearing, 12-23

local summer noon, 2-33, 10-27

local tangent, 9-42

local time, 9-51

local wave number behavior, 9-53

local winter midnight, 2-33, 10-27

locally generated interference, 6-2

locus, 6-22

logistic support, 3-6

Lognormal distribution, 12-6

long great-circle path, 6-2

long keying pulses, 3-21, 3-24

long path, 1-5, 5-50, 6-21, 8-6, 10-14, 10-16, 10-22, 12-21

longer arc, 6-20

longitude, 1-7

long-path boundaries, 6-41

long-path interference, 6-2, 6-16

long-path limitations, 6-21

long-path propagation, 10-14

long-path signal dominance, 6-40, 8-37, 12-17

long-path signal propagation, 8-14

long-path signals, 6-37

long-path SNR, 10-21

long-term ground sites, 8-9

Long-term Omega Monitor Program, 8-1, 8-9

long-term Omega signal monitor, 8-9, 8-20

long-term time dependence, 9-34

long-term year-dependent sub-model, 9-6, 9-51

long-term year-dependent variation, 9-7

loop (H-field) antenna, 2-24, 5-26

loop error, 8-19, 12-12

loop filter, 12-11

loop steering, 12-24

loop steering switch, 12-9

loran (LOng RAnge Navigation), 2-2

Loran-A, 8-8, 8-41

Loran-C, 3-8, 4-41, 7-4, 7-5

Loran-C timing equipment, 7-19

Lord Kelvin, 2-7

loss tangent, 5-61

lossy medium, 5-67

low conductivity, 6-17

low ground conductivity, 6-40

low SNR, 8-7

low-conductivity regions, 2-15

lower-boundary parameter, 9-46

lowest phase velocity TM mode, 9-42

low-stability reference mode, 8-16, 8-21

low-stability reference oscillator, 8-23

M

magnetic equator, 6-6

magnetic field, 1-6, 5-63, 5-65, 5-74, 6-5, 10-5

magnetic poles, 6-31

magnetized plasma, 5-73

magnetospheric "hiss", 12-6

major functional subsystems, 3-4, 3-19

malfunctioning oscillator, 8-36

manual plotting, 9-12

manual synchronization, 2-23, 12-2

Marconi, 2-7

marginal coverage, 8-8

marine receivers, 2-27, 11-12, 12-2

marine users, 2-22, 12-2

Master Data File, 8-30

Master Data File block, 8-32

master/secondary mode, 2-12, 6-28, 7-4

master/secondary procedure, 2-10

master/slave mode, 2-3

MASTERFILE, 8-12

matched filters, 12-11

matrix database, 10-24, 10-48

matrix diagram, 10-24, 10-25, 10-43, 10-46

matrix format, 2-34

matrix inversion, 9-33

matrix norm, 7-13

maximal coverage set, 11-29, 11-49, 11-54

maximum antenna current, 3-33

maximum effective reflection height, 9-5

maximum error, 6-29

maximum output power, 3-35

maximum path solar zenith angle, 9-32

maximum phase deviation, 6-6

maximum solar zenith angle, 9-30

Maxwell's Equations, 5-2, 5-57

mean epoch, 1-3

mean error, 9-36

mean time between failures (MTBF), 11-11

mean time to repair (MTTR), 11-11

measurement matrix, 7-12, 9-25, 9-30, 11-64, 12-23

measurement noise vector, 7-12

measurement path-times, 7-16

measurement times, 3-8

measurement vector, 4-34, 7-12

Mediterranean, 8-43

Megatek model, 9-37

Mercator diagram, 10-32

Mercator Projection, 5-36, 10-36

meteor showers, 6-31

meteorological balloons, 2-28, 12-3, 12-6

MFE cassette tape recorders, 8-2

microprocessors, 2-23

mid-latitude ionosphere, 5-9

mid-path illumination, 6-4

mid-path region, 6-4, 9-20, 9-22, 9-42, 9-53

mid-path segments, 9-43

minimization function, 9-24

minimum coverage fraction, 11-8

minimum effective reflection height, 9-5

minimum phase, 6-11

minimum shift keying (MSK), 2-26, 12-25

minimum solar zenith angle, 9-30

mis-synchronized, 8-36

mixed illumination, 6-10

mixed illumination path, 5-44, 10-11

MKSC system, 5-51

modal, 1-5, 5-44, 5-47, 10-7, 10-13, 10-34, 10-42

modal "maps", 12-17

modal components, 9-43

modal exclusion products, 12-18

modal interference, 5-3, 5-42, 5-44, 6-11, 6-16, 6-18, 6-21, 6-34, 6-37, 6-40, 8-6, 8-7, 8-14, 8-37, 10-11, 10-25, 12-17

modal interference effects, 10-7

modal interference region, 6-21, 9-5

modal phase excursions, 12-26

modal predictions, 8-8

modal structure, 6-17

modally disturbed, 5-44

mode, 5-10, 10-5, 10-14

Mode 1, 2-15, 5-3, 5-29, 6-9, 9-5, 9-42, 10-6, 10-7, 10-9, 10-12

Mode 1 component, 9-5

Mode 1 dominance, 5-36, 5-42, 5-44, 6-22, 9-16, 10-6, 10-8, 10-14, 10-21

Mode 1 Dominance Margin (M1DM), 1-5, 10-22, 10-49

Mode 1 electric field, 8-17

Mode 1 frequency dependence, 5-38

Mode 1 model, 12-16

Mode 1 phase velocity, 9-47

Mode 1 signal behavior, 5-44

Mode 1 signal phase behavior, 9-5

Mode 1/Mode 3 inteference, 6-40

Mode 1-launched wave, 9-51

Mode 2, 5-42, 6-18, 6-22, 6-37, 10-6, 10-11

Mode 2 dominance, 6-22

Mode 2-dominant signal, 6-25

Mode 2 interference, 6-40

Mode 3, 5-44, 6-18, 10-7, 10-11

mode conversion, 5-40, 5-45, 6-19, 10-12

mode equation, 5-13, 5-15

mode parameters, 5-28, 5-31, 5-36

mode signal characteristics, 5-31

mode signal field components, 5-16

mode theory, 5-2, 5-3, 5-25

mode-sum, 10-11

time/frequency multiplex, 2-15, 3-2

Timing and Control Room, 3-8

Timing and Control subsystem, 3-4, 3-19

top-hat elements, 3-33

top-loaded monopole, 3-27

top-loading radials, 3-27

total duration, 6-30

total electromagnetic field, 9-43

total error, 9-36, 9-39

total geometric path, 6-4

total phase variation, 9-5, 9-47

total signal behavior, 9-5

total signal field, 3-29

total signal phase delays, 3-30

total system performance, 11-7

tower antennas, 3-24

trailing edge, 3-12

trans-arctic path, 6-35

trans-equatorial signals, 6-40

TRANSIT, 2-25, 2-27, 10-26, 12-2, 12-27, 13-8

TRANSIT-derived position, 8-40

transition, 1-4, 6-19, 6-22, 9-56

transition ionosphere, 6-39, 9-57

transition onset time, 6-4, 9-7

transition paths, 9-7, 9-30, 9-38

transition phase data, 9-7

transmission coefficient, 5-71

transmitted signal, 5-39, 5-40

transmitted wave, 5-23, 5-70

transmitter output, 3-33

transmitter subsystem, 3-4, 3-21

transmitter-receiver path, 9-5, 9-10

transmitting source, 5-74

transmitting station performance, 8-10

transmitting station reliability/availability, 11-3

transmitting station reliability/availability component, 11-14

transmitting stations, 3-1

transmitting system, 1-1

trans-polar paths, 2-29, 6-30

trans-polar signal, 6-31

transverse electric (TE), 6-18, 10-6

transverse electric (TE) wave, 5-11, 5-71

transverse electromagnetic (TEM) mode, 5-19

transverse magnetic (TM), 5-49, 6-18, 10-6, 10-12

transverse magnetic (TM) wave, 5-11, 5-71

transverse magnetic mode, 9-5

trapezoidal diurnal phase change, 6-14

traveling wave, 5-63, 5-65

triangular filter, 8-19, 8-22, 8-25

Trinidad, 2-3, 2-16

true air speed and heading, 2-24

Tsushima, 2-21

tuned RF, 12-10

Tuve, 2-7

Type 1 data, 8-15, 8-16, 9-26

Type 1 monitor sites, 9-26

Type 2 data, 8-15, 8-16, 9-26

Type 3 data, 8-15, 9-26

U

U.S. Defense Mapping Agency, 2-28

U.S. Naval Communication Stations (NAVCOMMSTAs), 13-7

U.S. Naval Observatory (USNO), 7-5, 13-8

U.S. Naval Observatory Master Clock (USNO MC), 3-17

U.S. Naval Oceanographic Office, 2-28

U.S. Navy, 13-7

U.S. Navy VLF Communications System, 1-8

U.S.-France bilateral agreement, 2-20

underlying geophysical parameter, 9-55

unflagged daily measurements, 9-34

uniform ionization levels, 6-30

uniform plane wave, 5-65

unique (station-specific) frequencies, 2-15, 3-2

unit position vectors, 12-23

unit vectors, 5-14, 5-52

United States Coast Guard Omega Navigation System Center (USCG ONSCEN), 3-5

units and dimensions of electromagnetic quantities, 5-50

unmodulated VLF signals, 2-10

unpredictability, 6-28

unscheduled off-air, 11-5

unscheduled station off-air, 3-9, 11-5, 11-14

unstable, 9-34

updated position estimate, 12-24

upper-boundary parameter, 9-46

usable signal, 10-1

usable signal criteria, 10-21

useful phase characteristics, 6-2

useful signals, 6-1

user associations, 2-34

user geographic priority, 11-3, 11-6

user geographic regional priority component, 11-22, 11-33

user information support products, 2-31

user operating area distribution, 11-10

USNO measurements, 7-19

USNO Series 4 Bulletin, 7-20

UTC, 8-15

UTC epoch, 3-3, 7-3